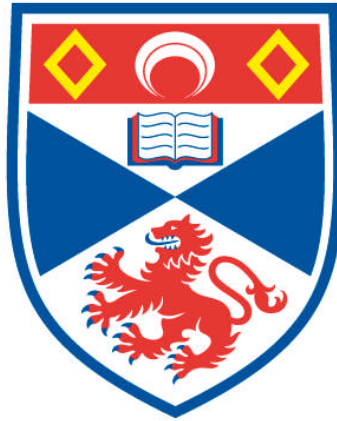


**THE IMPACTS OF CLIMATE CHANGE ON ESTUARINE ECOSYSTEMS:
A CASE STUDY ON THE EDEN ESTUARY, FIFE, SCOTLAND**

Melanie Chocholek

**A Thesis Submitted for the Degree of PhD
at the
University of St Andrews**



2013

**Full metadata for this item is available in
Research@StAndrews:FullText
at:**

<http://research-repository.st-andrews.ac.uk/>

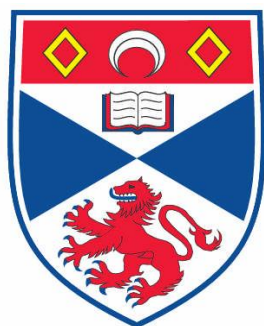
Please use this identifier to cite or link to this item:

<http://hdl.handle.net/10023/3625>

This item is protected by original copyright

THE IMPACTS OF CLIMATE CHANGE ON ESTUARINE ECOSYSTEMS:

A CASE STUDY ON THE EDEN ESTUARY, FIFE, SCOTLAND.



Melanie Chocholek

School of Geography and Geosciences

This thesis is submitted in partial fulfilment for the degree of
PhD at the University of St Andrews

March 2013

Dedicated to my daughter Bridget

Abstract

The Eden Estuary is a small, coastal inlet situated in Fife between the Tay and Forth Estuaries on the east coast of Scotland. A multidisciplinary case study of the estuary was conducted over a three year period observing the dynamic responses of biotic and abiotic behaviour to long term patterns of climate variability. Historical Trend Analysis (HTA) was combined with autocorrelation and spectral density analysis to identify trends, patterns and periodicity in natural cycles. River flow and wind direction data were cross-correlated with the North Atlantic Oscillation Index (NAOI) to link local responses to patterns of northern hemisphere circulation, and with Wolfe Sunspot Numbers representing variable solar activity as a potential driving mechanism for climate driven change. Assessment of the current state of 'estuary health' used a proxy analysis of ecosystem function, combining Bray-Curtis similarity nMDS of macrofaunal community diversity with species functional traits. The observed estuary responses were subsequently projected onto the forecasted climate change scenarios reported by the IPCCAR4, UKCIP09 and to modelled projections of solar activity to propose future trajectories of change for the estuary.

Autocorrelation analysis of river flow and wind direction data identified significant (95%) correlations corresponding to solar, lunar, planetary and volcanic events. Spectral density analysis similarly identified significant (>95%) frequencies corresponding to known periods of solar activity, lunar cycles and Bruckner climatic cycles. Formal cross-correlation revealed significant (95%) relationships between both river flow and wind data with the NAOI, and using a longer times series, between river Thames annual flow and Wolfe sunspot numbers; correlating solar maximums with high flow. Periods consistent to Schwabe and Hale solar cycles were evident in the wind and river data however the NAOI only displayed Hale periodicity, inferring the river and wind data are not solely influenced (or potentially driven) by the NAO. No detrimental impact of estuary change was observed in the biotic responses inferring maintenance of estuary health.

This study identifies potential driving mechanisms of estuary perturbation and whilst causal mechanisms can only be proposed, these observations form a baseline for future targeted modelling, monitoring and management.

Declaration

Candidate's declarations:

I, Melanie Chocholek, hereby certify that this thesis, which is approximately 68,500 words in length, has been written by me, that it is the record of work carried out by me and that it has not been submitted in any previous application for a higher degree I was admitted as a research student in September 2008 and as a candidate for the degree of PhD in September 2009; the higher study for which this is a record was carried out in the University of St Andrews between 2008 and 2012.

Date signature of candidate

Supervisor's declaration:

I here by certify that the candidate has fulfilled the conditions of the Resolution and Regulations appropriate for the degree of in the University of St Andrews and that the candidate is qualified to submit this thesis in application for that degree.

Date signature of supervisor

Permission for electronic publication

In submitting this thesis to the University of St Andrews I understand that I am giving permission for it to be made available for use in accordance with the regulations of the University Library for the time being in force, subject to any copyright vested in the work and not being affected thereby. I also understand that the title and the abstract will be published, and that a copy of the work may be made and supplied to any bona fide library or research worker, that my thesis will be electronically accessible for personal or research use unless exempt by award of an embargo as requested below, and that the library has the right to migrate my thesis into new electronic forms as required to ensure continued access to the thesis. I have obtained any third-party copyright permissions that may be required in order to allow such access and migration, or have requested the appropriate embargo below.

The following is an agreed request by candidate and supervisor regarding the electronic publication of the thesis;

Access to all of printed copy but embargo of all electronic publication of thesis for a period of 2 years on the following grounds as publication would preclude future publication.

Date

Signature of candidate

Signature of supervisor

Acknowledgements

I would like to thank NERC for providing the funding for this PhD.

I owe immeasurable thanks to Dr. Richard Bates for his continued patience and support (professionally and personally) throughout the duration of my PhD studies. I'd also like to thank Richard for the generous loan of a wide array of equipment & the wealth of knowledge he has given me along with it; all of which made this thesis possible. A big thank you also to Richard's daughter Rhiannon for her assistance in the field and to the rest of his family for allowing me to drag him away to survey at weekends.

I would like to thank Dr Jack Jarvis who has similarly provided considerable support and advice throughout my studies.

To Prof. Dave Paterson, for his supportive role as my second supervisor, offering advice and guidance and the use of the SERG lab facilities.

To Irv Davidson (SERG Technician) for helping collect macrofauna cores and sharing a wealth of his knowledge.

To Beccy Aspden & Claire Goll ty (SERG lab managers) for their time, support and advice.

To my fellow PhD students who have provided continual moral support and biscuits.

To the members of SERG, Emma Defew, Birgit Weinmann, Niki Khanna, Christina Wood, Pamela Cramb and Wan Mohd Rauhan Hussin who have all given their moral support, tea and biscuits.

To Dr Ruth Robinson for her advice and support.

To Dr Jason Matthiopoulos for his advice on time series analysis.

To Andy Mackie for helping build field equipment and for his assistance with M.V Envoy.

To Graham Johnstone for his time and the use of his aeroplane for aerial photography of the Eden estuary.

To Colin Cameron for all his IT assistance.

To Ranald Strachan (Fife Countryside Ranger for the Eden Estuary), for his continued support.

To Solinst for the loan and maintenance of their CTD Troll logger.

Thank you also to: BADC, RCHAMS, SEPA, NRFN and CEH for access to environmental data.

Finally, thank you to my family for their continued support.

Table of Contents

1.	CHAPTER 1: INTRODUCTION.....	1-1
1.1.	Rational and Aims	1-1
1.2.	Thesis layout	1-2
1.3.	Study site	1-4
1.4.	Estuaries: An overview, including their ecological importance	1-5
1.5.	Overview of climate reports	1-7
1.6.	Possible causal drivers to climate variability	1-8
1.6.1.	External forcing mechanisms	1-8
1.6.2.	Internal forcing mechanisms	1-9
1.7.	Potential ecosystem impacts to the Eden estuary.	1-11
1.7.1.	Implications to Eden estuary physicochemical conditions	1-11
1.7.2.	Implications to Eden estuary biological conditions	1-12
1.8.	Analytical Considerations	1-13
1.8.1.	Resolution & data issues; data confidence for climate change records	1-13
1.8.2.	Considerations with respect to current climate information;	1-15
1.9.	Summary	1-20
1.10.	References	1-23
2.	CHAPTER 2: HISTORICAL TREND ANALYSIS.....	2-31
2.1.	River Inflow.....	2-32
2.1.1.	Introduction & rationale	2-33
2.1.2.	Methodology	2-34
2.1.3.	Results	2-37
2.1.4.	Discussion	2-55
2.1.5.	Summary	2-60
2.2.	Wind Direction	2-61
2.2.1.	Introduction & Rationale.....	2-61
2.2.2.	Methodology	2-62
2.2.3.	Results	2-64
2.2.4.	Discussion	2-78
2.2.5.	Summary	2-82
2.3.	Spatial Data	2-83
2.3.1.	Introduction & rationale	2-83
2.3.2.	Channel migration of the river Eden.....	2-83
2.3.3.	Shoreline changes	2-92
2.3.4.	Morphological change analysis.....	2-99
2.3.5.	Species distribution patterns	2-111
2.4.	Chapter discussion.....	2-129
2.5.	Chapter summary	2-131
2.6.	Chapter 2: Appendices	2-133
2.7.	References	2-139
3.	CHAPTER 3: ABIOTIC ANALYSIS.....	3-155
3.1.	Tidal Asymmetry Analysis	3-157
3.1.1.	Tidal Instrumental Data.....	3-159
3.1.2.	Estuary volume	3-166
3.2.	Sediment Transport: Bedload.....	3-171
3.2.1.	Time lapse hypsometry	3-177
3.2.2.	Time lapse Bathymetry	3-185
3.3.	Salinity	3-197
3.3.1.	Introduction.....	3-197
3.4.	Chapter Discussion	3-204
3.5.	Chapter summary	3-205
3.6.	Chapter 3: Appendices	3-207
3.6.1.	References	3-225

4.	BIOTIC RESPONSES	4-231
4.1.	Ecosystem Function, Community Composition and Species Diversity	4-232
4.2.	Biotic Responses	4-253
4.2.1.	Species Adaptation / Acclimatisation	4-253
4.3.	Chapter Discussion	4-262
4.4.	Chapter summary	4-263
4.5.	Chapter 4: Appendices	4-265
4.6.	References	4-277
5.	THESIS DISCUSSION & FUTURE IMPLICATIONS	5-283
5.1.	Discussion	5-283
5.2.	Future implications for the Estuary	5-287
5.3.	References	5-291

List of Figures

Chapter 1

- Figure 1-1:** Location of the Eden estuary within East Fife, Scotland. Image ©2012 Google & ©2012 Digital Globe. _____ 1-5
- Figure 1-2:** Monthly mean temperature trends, Vertical scale is the temperature anomaly in degrees Celcius (°C). Seasonal changes have been removed by subtracting the long-term monthly averages. Red - Millport (records commence in 1953), Green - Fair Isle (records commence in 1979), Blue - Peterhead (records commence in 1976). Fisheries Research Services (2007). _____ 1-15

Chapter 2

- Figure 2-1:** River Eden mean flow (ms^{-1}) and total annual flow in cumecs. _____ 2-38
- Figure 2-2:** Regression analysis between monthly rainfall and river flow to identify catchment residence time. _____ 2-38
- Figure 2-3:** Anomaly data for river Eden annual mean flow (cumecs), highlighting periods of above and below average flow conditions. _____ 2-39
- Figure 2-4:** River Eden exceedance data for the period 1968 – 2009. _____ 2-39
- Figure 2-5:** Decomposition analysis of the Eden flow time series. The rectangular scale bars represent equal vertical scale between plots. Y scales are all the log of flow in cumecs. _____ 2-40
- Figure 2-6:** Decomposition trend components for the rivers Eden, Tay and Thames, with Loess regression trend line (dashed blue). _____ 2-41
- Figure 2-7:** Autocorrelation, partial autocorrelation and spectral density analysis of river Eden flow (cumecs). Data is a monthly time series from 1968-2009. (R Statistical software). _____ 2-42
- Figure 2-8:** Autocorrelation, partial autocorrelation and spectral density analysis of river Tay flow (cumecs). Data is a monthly time series from 1968-2009. (R Statistical software). _____ 2-43
- Figure 2-9:** Autocorrelation, partial autocorrelation and spectral density analysis of river Thames flow (cumecs). Data is a monthly time series from 1968-2009. (R Statistical software). _____ 2-44
- Figure 2-10:** The proportion of river Eden winter flow relative to the total annual flow (1968 – 2010). _____ 2-45
- Figure 2-11:** Percentage of river Eden ‘winter’ river flow (January to March & October to December) expressed as anomaly data. _____ 2-46
- Figure 2-12:** Proportion of river Tay winter flow relative to the total annual flow from 1953 – 2009. _____ 2-46
- Figure 2-13:** Percentage of river Tay ‘winter’ river flow (January to March & October to December) expressed as anomaly data. _____ 2-47
- Figure 2-14:** River Eden December to February river flow (cumecs) plotted with the preceding September to November NAO index (smoothed). _____ 2-48
- Figure 2-15:** Cross correlation between the de-trended December to February (D.F) river flow (cumecs) and the previous Autumn NAO index September to November (S.N). _____ 2-49
- Figure 2-16:** River Tay October to March river flow plotted alongside the October to March NAO index (smoothed). _____ 2-49
- Figure 2-17:** Cross correlation between the de-trended October to March river Tay flow (cumecs) and the de-trended October to March NAO index (1954-2008). _____ 2-50
- Figure 2-18:** Autocorrelations and spectral density analysis of the sunspot time series (1970-2011). _____ 2-51
- Figure 2-19:** Autocorrelation, partial autocorrelation and spectral density analysis of ‘Sunspots’. Data is an annual time series from 1749-2011 (R Statistical software). _____ 2-52
- Figure 2-20:** A comparison between pattern in the smoothed annual mean flow data for the rivers Eden and Thames, with the sunspot numbers (Wolfe number). From 1953-2008. _____ 2-53
- Figure 2-21:** A comparison between the smoothed and lagged Thames annual flow data (cumecs) and the Wolfe sunspot time series. _____ 2-53

Figure 2-22: Cross-correlation between the smoothed and lagged Thames annual flow data (cumecs) and the Wolfe sunspot time series. Top left & bottom right are the individual autocorrelations. Top right shows the sunspots 'controlling for river flow' and bottom left shows the river flow 'controlling for sunspot activity'

2-54

Figure 2-23: Interpretation of the significant autocorrelation peaks for the rivers Eden, Tay and Thames.

2-55

Figure 2-24: Harmonic periods. For each of the three rivers, the significant (95%) frequencies identified from the spectral density analyses are given, below each are arrows which show either the second or fourth order harmonic.

2-56

Figure 2-25: Wind counts for cardinal directions; North, South, East & West only.

2-64

Figure 2-26: Decomposition analysis of monthly wind direction counts. The data are truncated at 1981 due to missing values after this period. The vertical scales are logged counts, the rectangular bars to the right signify equal scale across the 4 panels and the horizontal scale is time in years.

2-65

Figure 2-27: Autocorrelation partial autocorrelation and spectral density analysis of the first difference residuals output from the decomposition analysis. The time series range is 1936-1980.

2-67

Figure 2-28: The percentage Contribution of each cardinal direction to overall total number of counts.

2-68

Figure 2-29: Actual cardinal direction counts (N, S, E & W), presenting the relationship between east and west winds.

2-68

Figure 2-30: Trend and first difference data of east and west wind direction counts. Rectangular bars to the right represent equal scale between the displays for the pairs of displays.

2-69

Figure 2-31: Autocorrelation, partial autocorrelation and spectral density analysis for west wind count data.

2-70

Figure 2-32: Autocorrelation, partial autocorrelation and spectral density analysis for east wind counts.

2-71

Figure 2-33: Decomposition analysis: monthly NAO indices from 1936 – 2010.

2-72

Figure 2-34: Decomposition trend components: NAOI 1936-1980 (top) and 1825-2010 (bottom).

2-73

Figure 2-35: Spectral density analysis of the NAOI, top is the 1936-1980 data range (compatible to the wind analyses) and bottom is the extended NAO monthly indices (1825 – 2010). Frequencies above the annual interval are highlighted by the respective inserts.

2-73

Figure 2-36: Visual assessment of the relationship between the % of westerly winds and the September to November NAOI.

2-74

Figure 2-37: Autocorrelation: de-trended September to November NAOI (4 year running mean) cross-correlated to the % of west winds (4 year running mean) for the period 1937 – 2010. Bottom left displays the S-N NAOI controlling for westerly winds.

2-75

Figure 2-38: Spectral density analysis for the two cross-correlated time series. Left is the spectrum for the two series (westerly wind in red & NAOI in black), right is the same data re-plotted with frequency converted to time in years (westerly wind top & NAOI bottom). Significant frequencies exceed the red dashed 95% significance line.

2-76

Figure 2-39: Predicted future sunspot cycles, based on data from Mausumi Dikpata of the National Center for Atmospheric Research and NASA solar physicist David Hathaway. Cycle 24 was estimated to reach its maximum in 2012.

2-76

Figure 2-40: SIDC monthly sunspot indices (annual means), showing variable periodicity over long time scales (1749-2009).

2-77

Figure 2-41: Comparison between the total number of annual counts & the sunspot cycle indices (mean annual). Cycle 24 in red & the following cycle 25 are created from the predicted values.

2-77

Figure 2-42: Interpretation of the autocorrelations for east and west winds direction counts.

2-79

Figure 2-43: Map of the historical positions of the Eden channel. The back ground image is from the Quickbird satellite and is dated August 2002 (copyright 2001 -2010 Satellite Imaging Corporation). The coloured sections mark the area (m^2) between equal lengths of river channel over sequential periods of time

2-87

Figure 2-44: The rate of migration for the different time periods, as anomaly data (difference from the overall mean).	2-88
Figure 2-45: Regression analysis between monthly mean river flow for the period, against the rate of lateral movement of the channel.	2-89
Figure 2-46: Mean NAO Index plotted against the time periods ordered by increasing rate of migration.	2-89
Figure 2-47: The percentage of West winds (of total wind recordings, 1936 - 2010) plotted with the September – November NAO index (both de-trended as anomaly data). The West winds lag behind the NAO by roughly 5 years	2-90
Figure 2-48 Proposed model to explain the differing rates of channel migration exhibited by the river Eden. (The model is designed principally around the availability of river flow data: 1968-2010).	2-90
Figure 2-49: Shoreline dune front positions on the southern outer estuary shore. The area is known as Outhead and is part of the St Andrews Golf Course.	2-94
Figure 2-50: Cardinal wind direction counts. (Chapter 2, section 2.2.3)	2-95
Figure 2-51: Detrended NAO Index values (raw data source :	2-95
Figure 2-52: Proposed conceptual model for shoreline development (Eden Estuary, seaward south shore).	2-96
Figure 2-53a: LiDAR DEM: 2002, horizontal units are meters and vertical units are millimetres.	2-104
Figure 2-53b: LiDAR DEM: 2009, horizontal units are meters and vertical units are millimetres.	2-105
Figure 2-54: A difference plot, showing elevation changes from 2002 to 2009. The LiDAR data is binned to a 2m resolution. Net gain (deposition) is shown in red and net loss (erosion) is shown in blue.	2-105
Figure 2-55: 2009 LiDAR merged with channel bathymetry (top left), showing the positions of cross-sectional transects. In each of the four displays the earlier time point is shown in colour (legend on right applies to all colour displays) Where the coloured initial time point extent is less than the second, the earlier data is bound by a brown perimeter line. The second time point is shown in greyscale and the limit of the data is shown by the solid black line. Where the colour shows through, this indicates erosion or no deposition, whilst the presence of greyscale indicates deposition. (Note March 2011 bathymetry begins only at transect 3 and extend out of the estuary to the right).	2-107
Figure 2.56: Transects 1 and 2, bathymetry cross-sectional profiles located within the middle estuary between the tidal flats.	2-108
Figure 2.57: Transect 3 and 4, cross-sectional bathymetry profiles in the sand dominated outer estuary channel.	2-108
Figure 2-58: Remnant salt-marsh, which is located along the north shore of the outer estuary.	2-116
Figure 2-59: Aerial photograph 1947 copyright RCHAMS (1946 left), showing where the salt-marsh (remnant in light green) in Figure 2-58 used to exist before the sand spit migrated over the top of the marsh post 1947.	2-117
Figure 2-60: The old north shore marsh following the migration of Sanctuary spit over the Saltmarsh. The background images are aerial photographs (1958-1994) and satellite imagery (Quickbird 2002). The remnant marsh is at approximately 2m elevation ODN.	2-118
Figure 2-61: Inner estuary Edenside salt-marsh 1894-2002 (south shore Kincaple Bay). The marsh exhibits approximately a 1% reduction in extent.	2-119
Figure 2-62: Middle estuary salt-marsh showing erosion	2-119
Figure 2-63: All base maps displayed are the 1895 Ordnance survey. Overlain on these are mapped areas of later extents to show changes since 1895 to 2002. Salt-marsh was digitized from historical Ordnance survey maps, apart from 1947 and 2002, which were from an aerial photograph and Quickbird satellite imagery respectively. The Westerly 2002 marsh is displayed as two separate sections, the most westerly is an addition of artificially planted marsh as is not included in the area calculations.	2-120
Figure 2-64: Aerial photograph from 1943, showing the position of the remnant marsh, both have approximately the same seaward extent and are landward of the 1895 marsh frontage.	2-121

Figure 2-65: Remnant Saltmarsh (East Kincaple Bay) displayed with historical shoreline positions. The elevations of the remnant marsh are shown as meters above datum Newlyn. The insert on the left, is an enlargement of the location of the two most seaward remnant marsh patches. _____	2-122
Figure 2-66: The distribution of <i>Zostera</i> species within the Eden estuary, mapped in 1977 by Johnston for a breeding bird survey, and again in 2009 for this research. _____	2-123
Figure 2-67: Aerial photograph from 1940, showing the presence of the pre-existing main channel position along the shoreline at Tentsmuir. The inserts show the various stages of the channel position from 1920 (Ordnance Survey) through to 1975 (aerial photographs). _____	2-125
Chapter 2 appendix 1 Figure 1 LiDAR transect locations, for quantifying the change observed between the two time periods. _____	2-133
Chapter 2 appendix 1 Figure 2: LiDAR transects 1 through to 4. _____	2-134
Chapter 2 appendix 1 Figure 3: LiDAR transects 5 through to 8 _____	2-135
Chapter 2 appendix 1 Figure 4: LiDAR transects 9 through to 12 _____	2-136
Chapter 2 appendix 1 Figure 5: LiDAR transect 13. _____	2-137

Chapter 3

Figure 3-1: Location of the Valeport Model 106 current meter within the Eden Estuary. _____	3-159
Figure 3-2: Valeport Model 106 current meter, housed in 1m weighted cube frame, recovered following relocation during stormy conditions. _____	3-160
Figure 3-3: Analysis of particle size at the two current meter locations. _____	3-161
Figure 3-4: left, illustration of the _____	3-161
Figure 3-5: Neap tidal elevation plot, illustrating Tidal height over the cycle, near bed current velocities and the durations of critical erosion and deposition periods for modal particle size at the location of the instrument (220um). _____	3-162
Figure 3-6: Spring tidal elevation plot, illustrating Tidal height over the cycle, near bed current velocities and the durations of critical erosion and deposition periods for modal particle size at the location of the instrument (220um). Heights are in meters above Ordnance Datum Newlyn. _____	3-163
Figure 3-7: Velocity stage plots (Neap & Spring respectively). The ebb tide is to the left of the plot, falling anticlockwise and rising to the right as the flood. _____	3-163
Figure 3-8: Digital elevation model of the estuary (meters above ODN), presenting the proportion of the estuary filled at mean high water. This data is used in conjunction with Figure 3-9, to calculate the tidal prism by subtracting river flow from the difference between high and low water estuary volume. _____	3-168
Figure 3-9: Digital elevation model of the estuary (meters above ODN), presenting the proportion of the estuary filled at mean low water. _____	3-168
Figure 3-10: Modified Hjulström-Sundborg diagram (Blatt et al., 1981) to present the inter-relationship between particle size, motion and current velocity. (Velocity is on a log scale). _____	3-174
Figure 3-11: Presents the locations of the two hypsometry bed-form surveys (marked by red rectangles) which were undertaken on the inter-tidal zone, exposed at low water. Also highlighted, are the extents of historical and contemporary ebb and flood orientated bed-form complexes. _____	3-177
Figure 3-12: Photograph of a flood bed-form in the study area, which lies to the north of the Eden channel, forming part of the Flood Bed-form Zone identified in Figure.3-11. (sea-ward to left, landward to right). _____	3-178
Figure 3-13: Diagram to illustrate the descriptive terminology of bed-forms. _____	3-178
Figure 3-14: Tidal heights during the period 05/07/11 to 18/07/11. _____	3-183
Figure 3-15: Screen image of data acquisition using Systems Engineering Software (SEA swath real time acquisition version 3.07.10). _____	3-186
Figure 3-16: DEM of the study area, showing numbered profile transects orthogonal to bed-forms. _____	3-187
Figure 3.17: Area 1 DEM; bed-forms were clearly defined for 19/03/11 and three cross-sectional profiles extracted. _____	3-188

<i>Figure 3-18: Cross-sectional profiles for March 2011; orientated left to right SW-NE, landward to sea-ward.</i>	3-189
	3-191
<i>Figure 3-19: Orthogonal profile 1 taken from the flood bed-form field (19-03-11 & 28-03-11). Horizontal distance is in meters increasing seaward. The profile runs SW –NE from landward to sea-ward.</i>	3-191
<i>Figure 3-20: Locations of cross-sectional profiles used to calculate mean estuary-wide bed-form characteristics for estimation of net sediment transport.</i>	3-193
<i>Figure 3-21: Predicted tidal heights, A are September 1990 tides and B are November 1990 tides (Neptune.Tides, 2011)</i>	3-198
<i>Figure 3-22: Annual data for salinity and temperature at Guardbridge (2010). Salinity - extreme of the lower whisker, the lower hinge, the median, the upper hinge and the extreme of the upper whisker 0.16, 0.69, 2.71, 10.79 and 25.94 respectively. Similarly the statistics for temperature are 0.42, 6.85, 12.66, 15.26 and 22.76.</i>	3-199
<i>Figure 3-23: 2010 Salinity and tidal height profile for comparison with Loutit (1991) September 20th profile.</i>	3-200
<i>Figure 3-24: 2010 Salinity and tidal height profile for comparison with Loutit (1991) November 14th profile.</i>	3-201
<i>Figure 3-25: River Eden, Kembeck gauged data, presented as deviation from mean discharge conditions.</i>	3-203
<i>Chapter 3 appendix 1 Figure 1: Neap tidal elevation plot 09/03/10 Eden Outer Channel.</i>	3-207
<i>Chapter 3 appendix 1 Figure 2: Spring tidal elevation plot 16/03/10 Eden Outer Channel.</i>	3-207
<i>Chapter 3 appendix 1 Figure 3: Neap & Spring Velocity stage plots for the above elevation analyses.</i>	3-208
<i>Chapter 3 appendix 1 Figure 4: Neap tidal elevation plot 05/08/10 Eden Outer Channel.</i>	3-208
<i>Chapter 3 appendix 1 Figure 5: Spring tidal elevation plot 14/08/10 Eden Outer Channel.</i>	3-208
<i>Chapter 3 appendix 1 Figure 6: Neap & Spring Velocity stage plots for the above elevation analyses.</i>	3-209
<i>Chapter 3 appendix 1 Figure 7: Neap tidal elevation plot 08/06/11 Kincaple Bay Channel.</i>	3-209
<i>Chapter 3 appendix 1 Figure 8: Spring tidal elevation plot 16/06/11 Kincaple Bay Channel.</i>	3-210
<i>Chapter 3 appendix 1 Figure 9: Neap & Spring Velocity stage plots for Figure 8 elevation analyses.</i>	3-210
<i>Chapter 3 appendix 1 Figure 10: Neap tidal elevation plot 12/07/11 Kincaple Bay Channel.</i>	3-210
<i>Chapter 3 appendix 1 Figure 11: Spring tidal elevation plot 03/07/11 Kincaple Bay Channel.</i>	3-211
<i>Chapter 3 appendix 1 Figure 12: Neap & Spring Velocity stage plots for the above elevation analyses.</i>	3-211
<i>Chapter 3 appendix 2 Figure 1: Location of the cross-sectional profiles for March 2011.</i>	3-212
<i>Chapter 3 appendix 2 Figure 2: Cross-sectional profile 1 for March 2011, showing the ambiguity between corresponding bed-forms. Left-right is SW-NE and landward to sea-ward respectively.</i>	3-212
<i>Chapter 3 appendix 2 Figure 3: Cross-sectional profile 2 for March 2011. Not used due to ambiguity.</i>	3-213
<i>Chapter 3 appendix 2 Figure 4: Cross-sectional profile 3 for March 2011. Showing reversal in movement (data 28/03/11).</i>	3-213
<i>Chapter 3 appendix 2 Figure 5: Location of the cross-sectional profiles for 25/04/11 to 12/05/11.</i>	3-214
<i>Chapter 3 appendix 2 Figure 6: Cross-sectional profile 1 for April/May 2011.</i>	3-214
<i>Chapter 3 appendix 2 Figure 7: Cross-sectional profile 2 for April/May 2011.</i>	3-215
<i>Chapter 3 appendix 2 Figure 8: Cross-sectional profile 3 for April/May 2011.</i>	3-215
<i>Chapter 3 appendix 2 Figure 9: Cross-sectional profile 4 for April/May 2011.</i>	3-216
<i>Chapter 3 appendix 2 Figure 10: Cross-sectional profile 5 for April/May 2011.</i>	3-216
<i>Chapter 3 appendix 2 Figure 11: Location of the cross-sectional profiles for 12/05/11 to 25/05/11.</i>	3-217
<i>Chapter 3 appendix 2 Figure 12: Cross-sectional profile 1 for 12/05/11 to 25/05/11.</i>	3-217
<i>Chapter 3 appendix 2 Figure 13: Cross-sectional profile 2 for 12/05/11 to 25/05/11.</i>	3-218
<i>Chapter 3 appendix 2 Figure 14: Cross-sectional profile 3 for 12/05/11 to 25/05/11.</i>	3-218
<i>Chapter 3 appendix 2 Figure 15: Location of the cross-sectional profiles for 19/03/11 to 28/03/11</i>	3-219
<i>Chapter 3 appendix 2 Figure 16: Cross-sectional profile 1 for 19/03/11 to 28/03/11.</i>	3-219
<i>Chapter 3 appendix 2 Figure 17: Cross-sectional profile 2 for 19/03/11 to 28/03/11.</i>	3-220

Chapter 3 appendix 2 Figure 18: Cross-sectional profile 3 for 19/03/11 to 28/03/11.	3-220
Chapter 3 appendix 2 Figure 19: Location of the cross-sectional profiles for 25/04/11 to 25/05/11.	3-221
Chapter 3 appendix 2 Figure 20: Cross-sectional profile 1 for 19/03/11 to 28/03/11.	3-221
Chapter 3 appendix 2 Figure 21: Cross-sectional profile 2 for 19/03/11 to 28/03/11.	3-222
Chapter 3 appendix 2 Figure 22: Cross-sectional profile 3 for 19/03/11 to 28/03/11.	3-222
Chapter 3 appendix 2 Figure 23: Cross-sectional profile 4 for 19/03/11 to 28/03/11.	3-223
Chapter 3 appendix 2 Figure 24: Cross-sectional profile 5 for 19/03/11 to 28/03/11.	3-223
Chapter 3 appendix 2 Figure 25: Cross-sectional profile 5 for 19/03/11 to 28/03/11.	3-224
Chapter 3 appendix 2 Figure 26: Cross-sectional profile 5 for 19/03/11 to 28/03/13	3-224

Chapter 4

Figure 4-1: Eden estuary macrofaunal core sampling sites.	4-234
Figure 4-2: Dendrogram resulting from the cluster analysis of square root transformed species abundance data. The matrix used the s17 Bray–Curtis similarity index at the 5% level of significance. Samples are prefixed by the year in which they were surveyed. Dashed lines represent group structure for which the SIMPROV test has found no evidence of dissimilarity. Conversely solid black lines have been identified as statistically similar by SIMPROV.	4-236
Figure 4-3: 2D nMDS (Minimum stress: 0.15), with overlays of Bray Curtis similarity of 46% and 50% (blue dashed line) (slack 70%) identified by the SIMPROV analysis and displayed in the dendrogram.	4-237
Figure 4-4: Bubble plot species ‘overlays’ of <i>Nephtys hombergii</i> and <i>Eteone</i> sp. The bubble size represents the scale for the number of individuals within each sample.	4-237
Figure 4-5: Bubble plot ‘overlays’ of <i>Cerastoderma edule</i> , <i>Corophium volutator</i> , total <i>Oligochaetes</i> and <i>Hydrobia ulvae</i> .	4-238
Figure 4-6: 2D nMDS ordination for the normalised environmental variables (stress 0.11). Overlain are the 46% and 50% Similarity divisions which were identified through SIMPROV for the biological data, thus showing that the distinction between the two survey periods observed in the biological data is not explained by the environmental variables.	4-239
Figure 4-7: Mud content nMDS; the percentage of <63 µm particle size retained in sieve.	4-239
Diversity	4-240
Figure 4-8: Diversity indices composite for ‘between’ survey comparison. Error bars are 1 standard deviation.	4-241
Figure 4-9: Dendrogram resulting from the cluster analysis of square root transformed species abundance data. The matrix used the s17 Bray–Curtis similarity index at the 5% level of significance. Samples are prefixed by the year in which they were surveyed. Dashed lines represent group structure for which the SIMPROV test has found no evidence of dissimilarity. Conversely solid black lines have been identified as statistically similar by SIMPROV.	4-242
Figure 4-10: 2D MDS of species data (2-d: Minimum stress: 0.11 occurred 32 times), with overlays of Bray Curtis similarity at 20% and 25% (slack 70%) identified from the Dendrogram.	4-242
Figure 4-11: Overlay ‘Bubble plots’ representing defining species for the 25% Bray Curtis similarity partition.	4-243
Figure 4-12: Overlay ‘Bubble plots’ representing defining species for the 25% Bray Curtis similarity partition;	4-244
Figure 4-13: 2D MDS ordination for the normalised environmental variables (stress 0.11).	4-244
Figure 4-14: nMDS of the environmental variables; % Organic content and Particles retained in 0.125 mm sieve.	4-245
Figure 4-15: Diversity indices composite for ‘between’ survey comparison. Error bars are 1 standard deviation.	4-246
Figure 4-16: <i>Nereis diversicolor</i> feeding (left) on a <i>Tubificoides benedii</i> and (right) on organic debris, found within the 2009 samples.	4-249

Figure 4-17: <i>Zostera noltii</i> sample locations (August 2009).	4-254
Figure 4-18: <i>Zostera noltii</i> blades laying over a centimetre scale graticule (small divisions are mm) used to calibrate the 'measurement tool'.	4-254
Figure 4-19: <i>Zostera noltii</i> patch and 0.0625m ² quadrat for evaluation of stem density.	4-255
Figure 4-20: Eden estuary <i>Zostera noltii</i> mean density expressed per m ²	4-256
Figure 4-21: <i>Zostera noltii</i> blade width (mm).	4-257
Figure 4-22: Eden estuary <i>Zostera noltii</i> blade length (cm).	4-258
Figure 4-23: Surface water ammonium (NH ₄ ⁺) levels recorded against mean salinities for the inner, middle and both outer estuary locations.	4-258
Figure 4-24: Principal component analysis of <i>Zostera noltii</i> morphometrics and environmental attributes.	4-259
Figure 4-25: Principal component analysis output statistics.	4-260
Chapter 4 appendix 1 Figure 1: Evenness diversity indices for the individual samples, error bars are 1 standard deviation of the survey total.	4-265
Chapter 4 appendix 1 Figure 2: Richness diversity indices of the individual samples, error bars are 1 standard deviation of the survey total	4-266
Chapter 4 appendix 1 Figure 3: Total number of individual counts and total number of species counts for the individual samples, error bars are 1 standard deviation of the survey total.	4-267
Chapter 4 appendix 1 Figure 4: Interstitial / pore water salinity. Comparison between values recorded by Johnston (1977) and the present survey (2010).	4-268
Chapter 4 appendix 1 Figure 5: Evenness diversity indices for the individual samples, error bars are 1 standard deviation of the survey total.	4-269
Chapter 4 appendix 1 Figure 6: Richness diversity indices for the individual samples, error bars are 1 standard deviation of the survey total.	4-270
Chapter 4 appendix 1 Figure 7: Total number of individual counts and total number of species counts for the individual samples, error bars are 1 standard deviation of the survey total.	4-271
Chapter 4 appendix 1 Figure 8: BIOPTIS survey species matrix.	4-272
Chapter 4 appendix 1 Figure 9: BIOPTIS survey environmental variables matrix.	4-273
Chapter 4 appendix 1 Figure 10: SNH survey species matrix.	4-274
Chapter 4 appendix 1 Figure 11: SNH survey environmental variables matrix.	4-275

List of Tables

Table 2-1: The rate of channel migration between sequential periods, calculated from digitized positions of channel centres from aerial and satellite imagery and multibeam bathymetry. _____	2-87
Table 2-2: Attributes to investigate the migration rate of the Eden Channel. The upper half of the table is sorted by time periods (grey) and the lower part of the table is the same data sorted by increasing migration rate. Normalised extreme flows were calculated by dividing the number of extreme flows by the number of months in the period and multiplying by twelve. _____	2-88
Table 2-3: Acquisition system setup summary. _____	2-102
Table 2-4: Identification attributes of the <i>Zostera</i> species (Butcher 1941b; Ukmpa 2001; Wyer et al. 1977). _____	2-113
Table 2-5: Changes to the area of salt-marsh (m^2), here the 1895 and 1914 areas were digitized from the historical ordnance survey maps, whilst aerial photographs/satellite imagery were used for 1947, 1958 and 2002. _____	2-121
Table 2-6: Summary of the principal influences identified from this chapter as impacting on estuarine tidal asymmetry dynamics and leading to consequential spatial changes. In brackets are the additional influences which combine to amplify the principal driving mechanism. _____	2-129
Table 2-7: Summary of the frequencies identified through spectral density analysis. The most dominant frequency per data series is displayed in red. Some notable shared periods have been highlighted to help with identifying shared frequencies. _____	2-130
Table 3-1: Attributes from four Spring and four Neap tidal phases. The range given is for ebb and flood respectively. _____	3-163
Table 3-2: Instrument data sorted by Neap and Spring cycle, with mean values for certain attributes. _____	3-165
Table 3-3: Attributes derived from the DEM's for use in calculating the asymmetry ratio. _____	3-169
Table 3-4: Attributes derived from the DEM's for calculation of the tidal prism _____	3-169
Table 3-5: Summary data for the pilot study pin survey on the flood bed-form field. _____	3-181
Table 3-6: Summary data calculated from the bed-form migration equation. _____	3-181
Table 3-7: Summary data which are representative of both spring and neap cycle current velocities. _____	3-182
Table 3-8: Net migration rate calculated following the methods of Bates and Oakley (2004). _____	3-182
Table 3-9: Bed-form migration rates ($m/tide$), to be used in quantifying the volume and mass of the sediment being transported per tidal cycle. _____	3-183
Table 3-10: Volume and mass of sediment being transport per tidal cycle through the West Sands channel. _____	3-184
Table 3-11: Summary data for area 1, for both neap and spring cycles. Additionally the March Spring data are shown (included as total mean data). Rate is $m/tide$ and heights are meters. _____	3-189
Table 3-12: Calculation of sediment transport. (Data exclusive of March). _____	3-190
Table 3-13: Calculation of sediment transport inclusive of March data. (March had wave activity & flattened bed-forms). _____	3-190
Table 3-14: Sediment transport for area 1 using velocity data methods (excluding March data). Rate (C) is expressed as $m/tide-1$ _____	3-190
Table 3-15: Summary data for migration rate ($m/tide$) and bed-form height (m) extracted from the orthogonal profiles over the two survey periods for area 2. _____	3-192
Table 3-16: Volume of sediment transported for area 2, calculated using equation (6). _____	3-192
Table 3-17: Migration rate $m/tide$ (using Bates and Oakley 2004), _____	3-192
Table 3-18: Average bed-form height (m) and wavelengths (m) measured from cross-profile transects. _____	3-193
Table 3-19: Volume of sediment transport calculated using bed-form equation (6) combined with average estuary wide measurements of height (Table 3-18) and migration rates calculated for area 1 and area 2 analyses. _____	3-194
Table 3-20: A quantitative estimate of sediment transport in the Eden estuary (per tidal cycle). Left includes the new channel which cuts across West Sands spit, right is with this zone excluded. _____	3-194
Table 3-21: A comparison of bed-form migration rates (data from Wever, 2004). _____	3-196

Table 3-22: <i>Guardbridge annual summary data on salinity and temperature (2010).</i>	3-200
Table 3-23: <i>River Eden monthly total flow (cumecs) (Centre for Ecology & Hydrology, 2010)</i>	3-201
Table 4-1: <i>Particle size categories. Modal size class is shown in red and missing data as N/A.</i>	4-240
Table 4-2: <i>Particle size categories. Modal size class is shown in red.</i>	4-245
Table 4-3: <i>Eden river flow: statistics for 5 years preceding each survey (Johnston 1978 – salinity measurements were taken in August)</i>	4-250
Table 4-4: <i>Zostera noltii mean density expressed per m²</i>	4-256
Table 4-5: <i>Tabulated data used for as input to the PCA</i>	4-259

CHAPTER 1

1. INTRODUCTION

This thesis is a multidisciplinary study of the impacts of climate change on an estuarine ecosystem. It utilizes empirical data from both historical records and contemporary analyses to measure abiotic and biotic estuary responses in relation to global climate change driving mechanisms. The responses and associated drivers are then used together with forecasted climate change scenarios to anticipate future trends within the estuary.

1.1. Rational and Aims

Estuaries are highly productive spatially and temporally complex transitional ecosystems, valuable for their biodiversity, ecosystem services and socio-economics. Estuary dynamics are driven largely by variability in river flow, tidal regime and predominant wind direction (effecting waves and currents); with environmental pressures being delivered from both landward and seaward directions they are especially vulnerable to climate change. Their ecological and anthropogenic importance coupled with their vulnerability creates an important need to understand how these ecosystems will respond to the projected changes to global climate.

The Intergovernmental Panel on Climate Change (IPCC) was established in 1988 and given the mandate by its joint founders 'to assess scientific information related to climate change and to evaluate the environmental and socio-economic consequences of climate change' (Houghton *et al.* 1990). This multidisciplinary approach has led to an increase in the number of holistic approaches to ecosystem management based on policy requirements, however there remains a paucity of 'whole ecosystem' based research investigating climate driven change, despite the continued integrated approaches to legislation e.g. Habitats Directive (1992), Water Framework Directive (2000), Marine and Coastal Access Act (2009) and more recently the Marine (Scotland) Act (2010).

Many individual aspects of estuary processes and species responses have been investigated with respect to the changing climate e.g. river discharge (Wikner and Andersson 2012), food web response to temperature changes (Freitas *et al.* 2007), re-alignment, sea level rise and sediment budgets (Nicholls *et al.* 2000), etc, however the interrelationship between the complex feedback mechanisms is difficult to up-scale for an ecosystem response. Although an individual response can be lost when broadening research to whole ecosystems the breadth covered to reveal the combined interactive responses is valuable to gain an overview of expected change predicted by the IPCC07 and the UK Climate Impacts Programme (UKCIP).

For UK estuaries, historically there has been a wealth of research undertaken based on discrete flood frequency analysis (Black and Anderson 1994; Black and Werritty 1997; Horner and Walsh 2000; Lane 2008; Macdonald 2006; Macdonald and Black 2010; Macdonald *et al.* 2006; Marsh 2008; Mcewen 2006; Werritty 2002; Werritty and Leys 2001; Werritty *et al.* 2006). This work has largely been driven by the economic consequences of flooding but few studies focus on the patterns or cycles of climate driven hydrological change over longer time periods. Globally, focus has shifted towards identifying patterns of cyclical behaviour to aid the sustainable management of water resources (e.g. Daniels 2007; Mundo *et al.* 2012; Rai *et al.* 2010) and more recently on climate links to identify periodicity corresponding to climate circulation patterns (De Vita *et al.* 2012; Jury and Melice 2000; Laignel *et al.* 2010) for the improvement of model predictions. Following this new time series frequency approach, periodicities found within hydrological data series have drawn potential links with global driving mechanisms such as variability in solar activity (Tomasino and Dalla Valle 2000; Yousef 2000), lunar nodal orbit (Ling *et al.* 2011; Miller and Eriksson 1997) and with climate mode oscillations (e.g. Rubio-Alvarez and Mcphee 2010; Switanek and Troch 2011). These approaches mark a broadening of concepts from local climate patterns impacting on the hydrology towards more global drivers of change.

Based on the afore mentioned research gaps and the connections to potential causal drivers of global climate change, this study has the following aims;

Aims

- Empirically evaluate historical data for the Eden estuary to identify pattern or trend over decadal-centennial time scales, using traditional monotonic trend and spectral/ frequency analysis methodologies.
- To identify key abiotic influences to an estuary from empirical contemporary analyses which may be used as indicators of climate driven change.
- To capture a relative trajectory of 'estuary health' through an estimation of ecosystem function and evaluation of the adaptive/acclimatisation response of the keystone species/habitat *Zostera noltii* to environmental stress.

1.2. Thesis layout

Each chapter is a composite of individual sections which cover a distinct facet of estuary processes; each section is introduced, results are given and discussed individually. The chapters are then collated to form chapter discussions integrating the findings from each section. Finally these discussions are integrated to form a concluding chapter with recommendations.

Chapter 1 (this chapter) is presented as eight main sections: it begins by outlining the rationale behind the study, introduces the study area and outlines the thesis layout. The chapter continues

with an overview of estuaries and their ecological importance, presents a summary of the current climate observational data provided by the UKCIP and IPCC07-AR4 (fourth assessment report), together with future climate projections and introduces potential candidates as drivers of global climate change. Having identified the future climate scenarios, an overview of how the predicted changes to climate will impact on an estuary ecosystem is given. Finally, the last section outlines analytical considerations regarding data quality, length of records and their interpretation.

Chapter 2 uses 'Historical Trend Analysis' (HTA) to investigate the presence of pattern and trend within selected chronologies. The data series chosen were the available time series for the primary drivers of estuary dynamics (river flow and wind regime) and data for the resulting spatial changes to the estuary (channel and shoreline alignment and the spatial distribution of key species). The analysis of these data enabled assessment of the estuary's response to climate variability between multi-decadal and centennial time scales. Patterns and trends in data are analysed in order that in the following chapters contemporary data can be placed in context with long term change. These regional univariate analyses were cross-correlated with potential climate drivers to link regional responses to global responses and to potential causal mechanisms.

Chapter 3 is an empirical analysis of more contemporary data; it aims to identify key abiotic influences to an estuarine ecosystem that may be applied as indicators of climate driven change. Data series were chosen that reflected the 'state' of equilibrium dynamics i.e. the balance between river inflow and the tidal volume reflecting the erosional or depositional stage of the estuary. Data that were chosen for analysis were tidal asymmetry dynamics, tidal prism changes, residual bedload transport and the salinity regime. The patterns present in these data and the net rates and direction of change enabled the current 'state' of equilibrium dynamics to be placed in a long term trend context within the HTA results.

Chapter 4 investigates the biotic responses to climate variability in terms of the relative 'estuary health'. This chapter is composed of two sections, the first uses community macrofaunal diversity as a proxy for ecosystem functioning. Comparison is made with two previous studies to identify a trajectory of change. The second section investigates the response of the keystone species *Zostera noltii* to existing conditions within the estuary. In particular adaptation/ acclimatisation of *Zostera noltii* is assessed through the morphological changes they display growing at key locations along the landward-seaward environmental gradient. Understanding the resilience of *Zostera noltii* to different environmental stresses gives an indication of potential maintenance of biodiversity through change.

Chapter 5 brings together the results of the previous chapters integrating the findings across the different lines of investigation to present an up-scaled estuary response to climate change with reference to scenarios from the IPCC07 and UKCIP climate reports. Finally this chapter discusses the relative contributions from various proposed driving mechanisms on a global scale and their links to the local responses observed in the estuary.

1.3. Study site

The Eden estuary is a relatively small estuary extending to approximately 8km². It drains 307.4 km² of low lying North Fife (Figure 1-1), of which 76% is agricultural land (NRFA 2011). The Eden estuary is currently protected by five legislative designations of which 3 are international, one is national and one regional. It was first given a national designation in 1971 as a Site of Special Scientific Interest (SSSI) under the 1949 Countryside Act and later re-notified under section 28 of the Wildlife and Countryside Act 1981 when the area of site coverage was extended in 1990. By 1978, the estuary was given a regional designation under Section 21 of the National Parks and Access to the Countryside Act 1949 as a Local Nature Reserve (LNR). The first international designation was awarded in early 2000 under the terms of the European Community Directive 79/409/EEC on the Conservation of Wild Birds, as a Special Protection Area (SPA). The second international designation was awarded in the same year, with the estuary forming a part of the Eden Estuary, Tentsmuir Point and Abertay Sands Ramsar, designated as a wetland site of international importance under the Ramsar Convention on July 28th, 2000. The latest international designation was awarded in 2005, with the Firth of Tay and Eden estuary being designated as a Special Area of Conservation (SAC) under the European Commission Conservation of Natural Habitats and of Wild Flora and Fauna/ Habitats Directives 92/43.

Similar to many British rivers, the Eden owes much of its physical character to the events during and subsequent to Last Glacial Maximum at approximately 20kYr. The river occupies a drowned valley, which was scoured, eroded and partially infilled by gravel sequences and clays during phases of ice sheet advancement and retreat throughout the late Devensian (ca. 26,000-10,000 years ago) and into the early post glacial Holocene (Flandrian) periods (10,000-8,000 years ago). (Ferentinos and Mcmanus 2009; Price 1983) Glacio-isostatic and eustatic adjustment throughout these periods resulted in changes to relative sea level, causing continual shoreline displacement. In the late Holocene uplift of the land outpaced sea level rise, leading to the development of characteristic raised beaches, links and dune features formed from reworked glacial material out-washed into the off-shore zone. This lowering of relative sea level also allowed the emergence of the estuarine tidal flats and growth of the marginal saltmarshes (Price 1983).

The basement geology of the surrounding area to the estuary is dominated by Devonian Lower Old Red Sandstones to the north younging southwards into the Upper Old Red Sandstones bordering the north of the Eden at Tentsmuir. Younging continues south into Lower Carboniferous Dinantian sequences of calciferous sandstones beneath St Andrews. The superficial deposits are remnants from the last phase of glaciation (Flandrian) and are largely sands, silts and clays, which overlie peat layers at Tentsmuir and Carse clays in the estuary. It is thought that the sands within St Andrews bay, which form the marine source to the estuary, are reworked outwash deposits following the retreat of the Flandrian ice sheet (Hansom, 1999; Ferentinos & McManus, 1981).

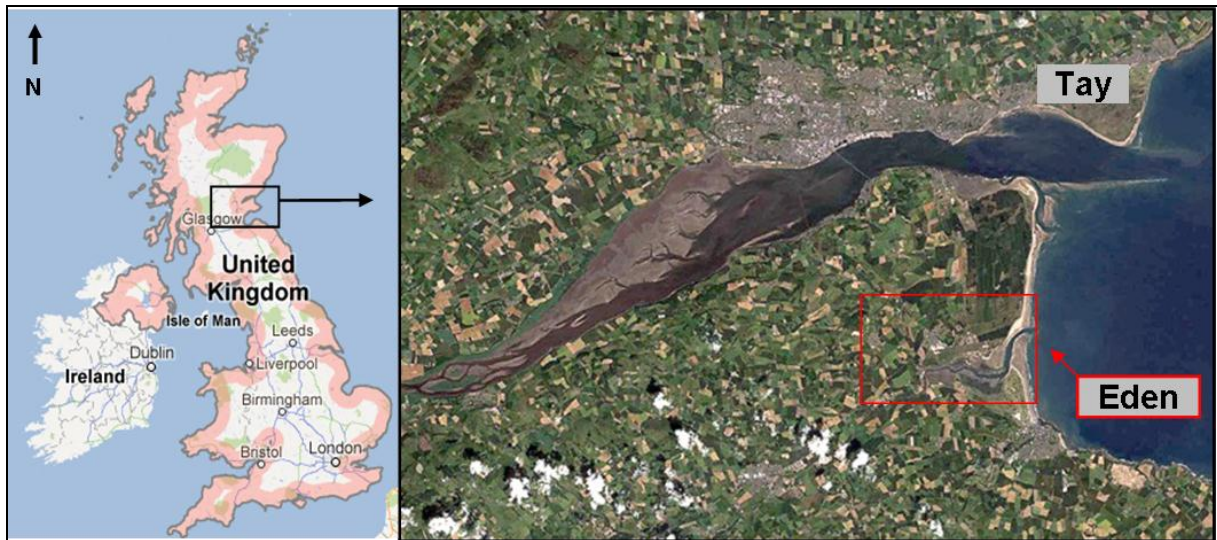


Figure 1-1: Location of the Eden estuary within East Fife, Scotland. Image ©2012 Google & ©2012 Digital Globe.

Freshwater inflow to the estuary is supplied by the rivers Eden and Motray Water. In 2010 the average mean daily flow for the Eden was $3.98 \text{ m}^3/\text{s}$; mean total monthly flow 10.78 m^3 and the total annual flow was 129.34 m^3 .

Much of the extensive intertidal flats, extending to 7.9 km^2 , are exposed at low tide leaving only the channel filled with water. The tidal range in 2011 was 2.40m and 4.78m for neap and spring tides respectively. The duration of the ebb exceeds that of the flood, hence the estuary is ebb dominated. The estuary sediments are represented by sands at the mouth and towards the middle estuary, grading to finer sand and mud towards the upper reaches. Using the classification of Boyd & Dalrymple (1992), the estuary is also described as being wave dominated, especially at the mouth, where littoral transport has formed a barrier, partially enclosing the estuary, leading it to be classified as a bar-built estuary (Eastwood 1977; Mcmanus and Green 1977).

1.4. Estuaries: An overview, including their ecological importance

An estuary is defined as semi enclosed coastal body of water with a free connection to the sea, within which saltwater is diluted by river inflow, allowing a continuous exchange of water between the two (Pritchard 1967).

Estuaries are ecotones (transitional habitats) with fresh water input from a river in the upper estuary and saline water input from the lower estuary. Animals that move across and interact with the ecotone are referred to as vectors and are responsible for transporting nutrients and organic matter between the interfaces.

Estuaries are ephemeral features on geological (millennia) timescales, however they are thought to oscillate between erosive and depositional conditions on much shorter multi-decadal to perhaps centennial timescales (Pethick 1994). The oscillation is driven by morphological feedbacks; deep

estuaries tend to show ebb-asymmetry¹ i.e. stronger tidal ebb velocities which may remove sediment from the estuary and shallow estuaries have a tendency towards flood-asymmetry (with a net import of sediment by the tidal currents) (Lanzoni and Seminara 1998; Lanzoni and Seminara 2002). The morphological influence is by modifying the flow velocities through frictional drag in shallow water especially over tidal flats. Changes to either sea level or erosion of tidal flats, alters the average water depth and may force a change in flood or ebb dominance (Brown and Davies 2010).

This oscillatory behavior lead to the classification scheme designed by Pethick (1994) where an estuary is described by its evolutionary stage and tidal asymmetry; an early forming (post Holocene) estuary is described as wide, deep and with dominant flood transport. These estuaries are thought to rapidly infill, developing a central channel and intertidal flats and thus forming a Type I estuary with flood dominated asymmetry. Continued accretion of the tidal flats eventually leads to a reversal of asymmetry, to ebb dominated conditions and forming a Type II estuary. Erosion of the tidal flats under ebb dominated conditions returns the estuary to being more Type I in character and hence feedbacks between the morphology and tidal asymmetry drive the estuary back and forth between Type I and Type II stages.

Traditionally estuaries may be classified by geomorphology, based on their water mixing, by hydrodynamics and by water balance (between evaporation and fresh water input). The latter example is more appropriate for tropical estuaries where evaporation is more dominant. Classification based on geomorphology separates estuaries by their physical mode of formation, thus categories include drowned river valleys, bar-built estuaries or lagoons, fjord-type estuaries, and tectonically created estuaries. Classification by water mixing defines estuaries by the salinity giving the following categories; salt wedge, weakly stratified, strongly stratified and well mixed (Pritchard 1967). This classification is based on the relative competition between river inflow and tidal forcing, which depending upon the relative balance (and often coupled with morphology) may lead to density driven mixing. Classification by hydrodynamics combines the stratification with the ratio of surface to near bed flow velocities (Hansen and Rattray 1966). Well-mixed estuaries with unidirectional net outflow, i.e. seaward flows with no vertical structure are termed Type 1 estuaries, Type 2 estuaries show flow reversals at depth, and include most temperate estuaries. These are generally well mixed or weakly stratified estuaries. Type 3 estuaries e.g. fjords, display a strong vertical structure with gravitational circulation giving strong surface outflow and very small depth-averaged flows, thus are moderately to strongly stratified. Lastly there are Type 4 estuaries, which exhibit seaward flows with a weak vertical structure and highly stratified conditions e.g. a salt-wedge estuary.

Historically estuaries have been and continue to be centres of settlement and trade, as a consequence population is normally densely concentrated around associated port areas. With increases to population and greater industrialization estuaries played a greater role in the provision

¹ Asymmetry is inequality in the duration of incoming & outgoing tide. The shorter period tends to have greater current velocities, which may induce net sediment transport in that direction.

of services; providing a source for industrial and agricultural water, and a sink for waste water, sewage and surface drainage. The addition of both nutrients and pollutants to estuaries restricts their use for commercial aquaculture and shell fisheries, however they have been increasingly used for leisure pursuits. The physio-biological interactions within estuaries make them very effective at retaining dissolved and particulate matter as such estuaries are often described as buffers or filters, however their efficiency as a trap leads them to be susceptible to pollution.

Estuaries and coastal ecosystems form some of the most highly productive ecosystems (Costanza *et al.* 1998), due to their ability to retain organic and particulate matter, which drives both primary and secondary productivity, biogeochemical cycling and storage. Being open systems, estuaries also serve as important connections between rivers and the sea, exchanging water, nutrients and sediment with the shelf seas driving productivity.

As diverse habitats, estuaries provide sheltered refugia and important feeding grounds for migrating and overwintering birds, nursery grounds for juvenile commercial fish and sources of food and shelter for seals and porpoise. Peripheral saltmarshes often line the middle and upper estuary, which not only have a role as habitat for a wealth of diversity but also provide a buffer to erosion. In addition they are thought to be one of the largest carbon sinks of all soil ecosystems (because of higher sequestration rates under saline conditions, inhibiting production of CH₄ & N₂O due to abundant sulphate in saline conditions).

It is the socio-economic and ecological service provision that reflects the value of estuaries and drives the protective legislation responsible for their management, and forms the basis of increased research into climatic perturbation.

1.5. Overview of climate reports

Empirical evidence presented by the UKCIP09 (Jenkins 2009) reveals air temperatures for Scotland have risen by about 0.8°C since 1980. All regions of the UK have experienced an increase in heavy winter precipitation over the past 45 years and a decrease in summer rainfall (except NE England and N Scotland). Severe windstorms have become more frequent around the UK, however not above those observed in the 1920s. Sea-surface temperatures have risen around the UK by about 0.7°C and sea level has risen by about 1mm/yr for the 20th Century, however at a higher rate since the 1990s and 2000s.

The IPCC07 AR4-WG1 (IPCC 2007c) climate projections for medium emissions scenarios for the 2050s are as follows;

- The central estimate for the increase in winter mean temperature is 1.7°C
- The central estimate for the increase in summer mean temperature is 2.3°C
- The central estimate for the increase in summer mean daily maximum temperature is 3°C

- The central estimate for the increase in summer mean daily minimum temperature is 2.5°C
- The central estimate for the change in annual mean precipitation is 0%
- The central estimate for the change in annual winter mean precipitation is 10%
- The central estimate for the change in annual summer mean precipitation is -13%

The IPCC report the “Warming of the climate is unequivocal, as is now evident from observations of increases in global average air and ocean temperatures, widespread melting of snow and ice and rising global average sea level” (IPCC 2007c), continuing “that eleven out of the last twelve years (1995-2006) rank among the twelve worst years in the instrumental records’ and that the 100 year linear trend (1906-2005) of 0.74 [0.56 to 0.92] °C, is larger than the corresponding 0.6 [0.4 to 0.8] °C (1901-2000) in the TAR²” (IPCC 2007c).

1.6. Possible causal drivers to climate variability

The latest reports from the IPCC (IPCC 2007a; IPCC 2007b) state ‘the Earth’s climate is changing as a result of increasing anthropogenic emissions of greenhouse gases’, however considerable controversy continues to be debated regarding the relative contributions of anthropogenic and natural variability to the observed climate change trajectories. Despite the controversy it is widely accepted that there are both internal and external contributions of various scales.

1.6.1. External forcing mechanisms

Solar activity provides energy for the Earth’s climate; in the short term cycles of approximately 11 years are observed, these are referred to as Schwabe cycles and are named after Heinrich Schwabe who discovered cyclical patterns of activity in 1843 (Hoyt and Schatten 1997). Over the ~11 year cycle the solar constant which is approximately 1366 W/m² varies by approximately 1 W/m² (Foukal *et al.* 2006) which is ~0.07% increase above the ~240 W/m² globally averaged non reflected component (Shaviv 2008). An index to measure the level of activity was designed by Rudolf Wolf in early 1849; the method recorded visible activity as a number of sunspots on the photosphere of the sun, becoming known as the Wolfe Number (Hoyt and Schatten 1997) and this methodology continues today as the International Sunspot Number. Whilst the long term average of a cycle is ~11 years, cycles may vary from 9 to 13 years. Cycles of ~22 years are also observed these are referred to as Hale cycles, named after George Hale, and reflect solar magnetic polar reversals i.e. every ~22years the magnetic field returns to its original polarity.

Cycles of ~90 years are also present, these are referred to as Gleissberg cycles and are named after Wolfgang Gleissberg following the publishing of considerable material regarding the cycle in

² TAR is the Third Annual IPCC Report i.e the preceeding report to the 2007 AR4

1938 (Hoyt and Schatten 1997). Smoothing the ~11 year Schwabe cycles with an approximate 18 year running mean reveals these longer period modulations (Yousef and El Raey 1995).

Planetary configurations, particularly those of Jupiter and Saturn with the Sun, have also been found to have associations to climate patterns (Scafetta 2010). It has been postulated that alignment of the Jovian planets with the Sun apply a mass driven gravitational torque that influences the Sun's processes, and in turn the Earth's atmospheric circulation patterns (Mazzarella and Scafetta 2012; Scafetta 2010; Scafetta 2012a; Scafetta 2012b; Scafetta 2012c). Jupiter, having the largest mass and magnetic field of all of the Solar System planets is the most influential planet with a sidereal orbital period of 11.86 years. Saturn has an orbital period of 29.46 years. Synodic orbital alignments (between two planets) with respect to Jupiter reveal periodicities of 12.78 years Jupiter-Neptune, 13.8 years for Jupiter-Uranus, 19.87 years Jupiter-Saturn, 11.18 years Jupiter-Mars, 12.01 years Jupiter-Earth, 11.68 years Jupiter-Venus and 11.8 years Jupiter-Mercury. Tri-synodic periods between the Sun, Jupiter and Venus, Earth and Mars all approximate to 44.7 years. The tri-synodic between the Sun, Jupiter and Saturn occurs every 59.58 years. The Sun's orbit around the barycentre (centre of mass between the Sun and the planets) reveals cycles ranging from ~14 to ~26 years, averaging ~20 years (Camuffo 2001). These are a few examples of periodicities which may be manifest in climate and environmental data. Many are quite similar in duration, which makes it difficult to attribute the origin of a particular periodicity.

Lunar Orbital Cycles influence the oceans tides on various temporal scales, from diurnal to ~ multi-decadal. One of the longer period cycles is the lunar nodal cycle; it was observed by Bradley in 1728 as being determined by the relative movement of the plane within which the moon orbits the Earth (Haigh *et al.* 2011; Yndestad 2004). It is a gravitational driven cycle lasting 18.6 years where over the course of 9.3 years the moon travels in an increasingly elliptical path and at its closest pass to the earth it exerts a gravitational pull on the oceans causing a 3.7% increase in tidal heights (Pugh 2004). A second cycle that has been observed in tidal records is the Lunar Perigee; the duration of the cycle is 8.85 years. This cycle is a consequence of the variation in distance from the Earth to the Moon, due to the orbit of the Moon around the Earth-Moon centre of mass not being circular, and gives rise to apogee (furthest from the Earth) and perigee (closest to the Earth). The influence of the perigee is manifest as a quasi 4.4 year cycle, giving rise to larger tidal ranges particularly at the equinox (Haigh *et al.* 2011).

1.6.2. Internal forcing mechanisms

Internal influences which contribute to climate variability come from both natural and anthropogenic sources. The IPCC07 (IPCC 2007b) have attributed the increase in greenhouse gasses (GHG's) over the past 250 years to three main causes; fossil fuels, land use and agriculture (through changes to land use i.e. deforestation or change of practices and through drainage changes). The GHG anthropogenic emissions are mainly from Carbon dioxide (CO₂), Methane (CH₄), Nitrous oxide (N₂O) and Halocarbons e.g. Fluorine, Bromine and Chlorine etc) which are emitted from both

industrial and individual usage; “in the UK, 40 per cent of CO₂ emissions are caused by individuals, mostly from energy used in the home, driving and air travel” (IPCC 2007b). However many natural processes also produce a number of GHG’s such as CH₄ released from wetland carbon sequestration, CO₂ through decomposition of organic matter and volcanic emissions, N₂O from bacterial nutrient cycling in temperate and tropical soils, Sulphur dioxide (SO₂) as volcanic aerosols, Ozone (O₃) which is continually produced and destroyed in the atmosphere by photo-chemical reactions, and water vapour, which is perhaps the most abundant GHG, occurring in the atmosphere largely through evaporation and transpiration.

GHG’s have an effect on the Earth’s climate through alteration of the energy balance between the incoming solar radiation and the outgoing thermal (infrared) radiation.

Volcanism effects the climate through three mechanisms 1) by ash resident in the lower stratosphere reflecting back solar radiation and causing cooling of the lower atmosphere 2) by absorption of solar radiation by silicic ash particles in the lower stratosphere causing local heating and thermally driven circulation and 3) by the injection of gases into the lower stratosphere which drive the chemical destruction of ozone, which then lowers UV absorption and hence the radiative heating in the lower stratosphere (Cole-Dai *et al.* 2000; McCormick *et al.* 1995; Rampino *et al.* 1988; Robock 2000).

The impact volcanism can have on climate perturbation is dependent on the latitude and the type of eruption. To have a lasting global forcing, the aerosols and or ash particles from an eruption must be injected into the lower stratosphere, which is higher at the mid latitudes than at the poles due to the oblateness of the atmosphere. Generally the larger ash particles fall out of the atmosphere relatively quickly (6-12 months) and hence have a limited impact on global temperatures, however SO₂ is converted to sulphate aerosols residing in the atmosphere for 2 to 3 years, which may drive a net global cooling from the blocking of incoming solar radiation (Fischer *et al.* 2007; Robock 2000).

The latitude of the volcanic eruption also influences the nature of climatic perturbation; low latitude stratospheric eruptions cause circulation patterns that resemble positive phases of the North Atlantic Oscillation (NAO), whilst the high latitude stratospheric eruptions mimic negative phases of the NAO (Fischer *et al.* 2007; Robock 2000).

The North Atlantic Oscillation (NAO) The NAO forms a part of the Northern Annular Mode, which is the pattern of climatic variability for the northern hemisphere (previously called the Arctic Oscillation). The NAO represents a large scale atmospheric pressure gradient between the subtropical anticyclone (high pressure zone) near the Azores and the sub-polar cyclonic (low pressure zone) system near Iceland. The relative strengths and positions of these systems vary continually and from year to year, however the NAO is more pronounced during winter months (Stenseth *et al.* 2003).

The NAO is recorded as the NAO index (NAOI); when there is a large pressure differential between the two systems, this is denoted by a positive NAOI and when there is a low difference in pressure between the two systems this is denoted by a negative NAOI. In NAOI positive years generally there are more frequent and stronger westerly winds accompanied by cool summers and mild wet winters, in contrast NAOI negative years are characterized by fewer westerlies and much colder winters (Hurrell *et al.* 2003).

The NAO is one of the major large scale climate controls in Europe (Dickson *et al.* 2000; Hurrell 1995), with Western Europe predominantly being controlled by westerly airflows and particularly through the passage of depressions (Hurrell *et al.* 2003). During strongly NAOI positive phases, not only are there more and stronger westerly winds, but the passage of the depressions leads regionally to a rise in sea level due to the reduction in atmospheric pressure (Pugh 2004). Conversely, in NAOI negative years, higher atmospheric pressure may lead to a regional lowering of sea level.

“There appear to be no ‘significantly’ dominant periodicities in the NAO” (Ottersen *et al.* 2001), however, there have been extended periods that have displayed persistence in a particular phase (Hurrell 1995; Trigo *et al.* 2002).

1.7. Potential ecosystem impacts to the Eden estuary.

The observational trend data (UKCIP09) highlights that greatest changes for the UK have been from increased heavy winter precipitation over the past 45 years and a decrease in summer rainfall (except NE England and N Scotland) and from the occurrence of more frequent severe windstorms. Sea level has risen by a rate of ~1mm/yr for the 20th Century and sea-surface temperatures have been observed to have risen around the UK by ~ 0.7°C, which is consistent with the reported increase in global mean air temperature by the IPCC (IPCC 2007a), contributing to the thermal expansion of the oceans.

The climate report predictions (IPCC 2007c) for medium emissions scenarios highlight the likelihood of most global change to be from increased mean air temperatures (and concomitant sea level rise), and from greater seasonality and increased winter precipitation.

1.7.1. Implications to Eden estuary physicochemical conditions

Changes to physicochemical conditions may be driven by increased precipitation, runoff and river flow, air temperature and sea temperatures, to associated relative sea level rise and to increased winds and changes to the dominant wind direction.

River inflow, tides, currents and prevailing wind direction play a pivotal role in estuary dynamics; collectively they determine the asymmetry between the flood and ebb tidal dominance and hence

estuarine sediment transport and morphodynamics. Increased precipitation will cause increased river flow, shifting the asymmetry seaward. Depending upon the hydrodynamics, a seaward shift in the salinity regime may be observed or an increase in stratification through density separation. If sea level rise, primarily through thermal expansion, causes the tidal wedge to shift landwards and balances the increased river inflow, the estuary mixing may remain constant. However with the increase in water volume, despite the equality of water input, ebb current velocities are likely to increase driving a shift towards a more erosional environment, with re-suspension, followed by mobilization of sediment and at times associated pollutants.

Increased river inflow may drive a shift in nutrient and suspended sediment levels within the estuary, through increased runoff within the agricultural catchment however residence times may decrease in response to the increased water volume in the estuary. With increased fresh water input to the estuary a seaward shift in PH and gas exchange may be observed (with increased solubility of CO₂ at lower salinities and temperatures).

The predicted increase in winds are likely to assist either in driving ebb tidal currents (offshore winds), or flood currents (onshore winds) thus helping to perturb the asymmetry dynamics. Strong winds blowing in opposition to the tides are likely to cause an increase in wave heights (Pugh 2004), which in shallow water will re-suspend sediments. At high water winds are likely to drive cliffing erosion, widening the estuary to accommodate the increased water volume. At low water strong winds are likely to drive an increase in aeolian transport either into or out of the estuary depending on the dominant wind direction, however onshore transport by wind typically dominates over offshore, partly because winds blowing over the sea are stronger (due to them being less affected by friction).

1.7.2. Implications to Eden estuary biological conditions

Forcing factors that operate on short time scales are likely to impact more dramatically on estuarine ecosystems (since they are driven by both landward and seaward change) potentially changing conditions faster than the ecosystem can adapt (Day *et al.* 2008). Such changes modify hydrological conditions and regimes that play a major role in structuring the biotic diversity that maintains ecosystem function. Sea level rise and to a slightly lesser extent, salinity and Sea surface temperature will change relatively slowly over time scales that will largely allow the ecosystem to adapt, this has been observed with saltmarshes for the Thames estuary (Van Der Wal and Pye 2004), leading to spatial migration of habitats and spatial species compositional changes, reflecting changing morphology and sediment distribution under new hydrodynamic conditions.

With the predicted increase in precipitation, and hence river flow, nutrient inputs from the largely agricultural catchment are likely to increase which may drive an increase in primary productivity. This is due to the strong empirical relationship between bacterial abundance and Chlorophyll a (Chla) concentration (Bird and Kalff 1984) where increased primary production may drive increased

secondary production. However nutrient loading may also lead to the dominance of macro-algae (Cfas 2007; Clelland 1997) causing loss of diversity through changing anoxic conditions.

Increased seasonality in precipitation often can lead to extremes of desiccation and exposure, especially of the higher intertidal flats. For these cases 'within year' regime shifts (temperature, salinity and exposure) may therefore cause loss or re-distribution of species that are living close to their ecological limits especially for species with limited mobility or dispersal. Stochasticity in community assemblages leads to higher biodiversity and more productivity (Chase 2010), therefore loss of species may alter the β -diversity (spatial variability in species composition) shifting community composition towards becoming less even (Daily *et al.* 2000) and more dominated by certain resilient species, driving feedback loops that lead to increased loss of diversity and lower utilization of available nutrients. Similarly with predicted increases to sea level, strong winds and energy levels within the estuary, community compositions may change both temporally and spatially. The implications for reduced evenness are impacts to ecosystem stability and function through a lowering of functional redundancy and having fewer species that may respond differently to different environmental perturbations (Hooper *et al.* 2005).

Predicted increases to sea level, strong winds and energy levels within the estuary may cause loss or fragmentation of habitat through increased erosional conditions. Habitat size is important for persistence of populations; fragmentation leads to small and isolated populations which are vulnerable due to loss of connectivity, restricting the ability to re-establish and expand. Diversity of habitat also promotes ecosystem stability; with loss of variability in habitat type, there is likely to be a reduction in the number of available niches and thus resource usage.

1.8. Analytical Considerations

1.8.1. Resolution & data issues; data confidence for climate change records

There are numerous modelling & research organizations that record & collate data on climate change; UK Climate Impacts Programme (UKCIP), Intergovernmental Panel on Climate Change (IPCC), Marine Climate Change Impacts Partnership (MCCIP), Scotland & Northern Ireland Forum For Environmental Research (SNIFFER), Scottish Climate Change Impacts Partnership (SCCIP), Met Office Marine Data Bank (MDB), Comprehensive Ocean-Atmosphere Data Set (COADS now ICOADS) Fisheries Research Services (FRS, now Marine Scotland Science), Permanent Service for Mean Sea Level (PSMSL), Proudman Oceanographic Laboratory (POL, now the National Oceanographic Centre - NOC), National Climatic Data Centre (NCDC) & British Oceanographic Data Centre (BODC) to name a few. Data collected by different systems and potentially with different temporal sampling through history require caution in their interpretation, for the 'noise' that they may contain. For example, the widely used HadISST dataset, held by the Meteorological

Office, runs from 1870 onwards and is a composite of data from several sources; records pre 1980's being supplied by COADS. The HadISST_1.1_SST is a set of SST data in monthly 1° area grids of *In situ* sea surface observations and satellite derived estimates. Whilst this is an invaluable dataset in terms of its length, it potentially contains inconsistencies from different modes of capture.

In terms of scales of variability, caution should also be taken for interpretation of data series that may not fully capture natural periodicity. Time series of at least 50 years are recommended for climate impact studies (CEH and UKMO 2001; Douglas 1992). Recorded data held by many organizations listed above are largely from the mid 1950's or early 1960s and are commonly used as baseline data. Statistical analyses based upon these relatively short records should also be assessed with care, due to the large natural variability within the UK climate where many trends found in short time series are no longer significant when considered in a longer term context (Dawson *et al.* 2001; Wilby *et al.* 2008).

The frequency of natural variability periodicity affecting the Earth ranges from diurnal tidal cycles, to longer events such as the Atlantic multi-decadal oscillation (AMO) and to probably the lowest frequency cycle of orbital eccentricity lasting 100,000 & 400,000 years respectively. Sampling to capture relevant periodicity is critical in accurately assessing climate impact trends.

Periodicity also interacts with other feedback mechanisms which alter the earth's climatic regime. For example, cycles of eccentricity impact on the absolute received solar insolation (Beer *et al.* 2006), although mean global insolation only varies by $<2.5\text{Wm}^{-2}$ throughout the cycle. In contrast, the 11 year solar sunspot cycle effects a mean global forcing of 0.25Wm^{-2} (taking account of 30% albedo) (Beer *et al.* 2006). Whilst this seems quite small, the changes that occur in the UV spectrum cause further perturbations of 1-5% in the Ozone layer, the main heat source of the upper stratosphere (Langematz *et al.* 2005), leading to radiative coupling and heating of the lower stratosphere. This in turn changes and weakens the positions of both the sub-tropical jet stream and meridional circulations. Such stratospheric heating at low latitudes results in a poleward migration of circulation patterns, whilst the converse is true where heating is more uniform (Haigh and Blackburn 2006). The IPCCAR4 report (IPCC 2007c) incorporates a global solar radiative forcing of $0.12 [0.06 \text{ to } 0.30] \text{W/m}^2$.

Palaeovolcanic events have been incorporated as chemical atmospheric perturbations in climate studies since the 1990's (Chenet *et al.* 2005; Dawson *et al.* 1997; Savarino *et al.* 2003) yet their signatures are not generally removed from the widely used modelling datasets. The extent of these perturbations depends largely on the volume of sulphur rich gasses and fine ash released into the stratosphere, the latitude at which they are injected and the volume of hydrous components (Savarino *et al.* 2003). Whilst the stratosphere becomes progressively lower in the higher latitudes enabling smaller eruptions to have greater climate impacts, at the lower latitudes the effects are spread globally and more quickly because of the equatorial wind systems. Generally, bigger eruptions produce fewer, larger aerosol particles, which are heavier and settle out of the atmosphere more quickly. Thus, residence time in the W/m^2 atmosphere is critical which is also

regulated by the rate of oxidation. The entire stratospheric production of sulphate is attributed to the oxidation of SO₂ by OH, due to the lack of liquid water in the stratosphere (Savarino *et al.* 2003).

1.8.2. Considerations with respect to current climate information;

Sea Surface Temperature

Data recorded by the Fisheries Research Services (FRS) is used by many organizations for environmental research & climate modelling. There are three coastal monitoring sites which represent Scotland (Fair Isle, Millport and Peterhead) where FRS have been able to obtain records of coastal sea surface temperature that extend back more than 20 years. FRS (2000) reported at all of these stations a general trend of warming at a rate of between 0.2 and 0.6°C per decade since 1980 with the trend appearing to be strongest on the west coast of Scotland. The difficulty for interpretation of relatively short time series is demonstrated in Figure 1-2. The longer record for Millport shows three clear anomalies which are discussed in detail later with respect to salinity. Dawson *et al* (2001) places short term records from 1977 to 1997, (which show temperature range increases from 0.05 and 0.120C/yr), in a longer term context which captures the natural variability of the data, using a 100yr COADS dataset. Analysis of these data however does not appear to show any clear trend of increased SST.

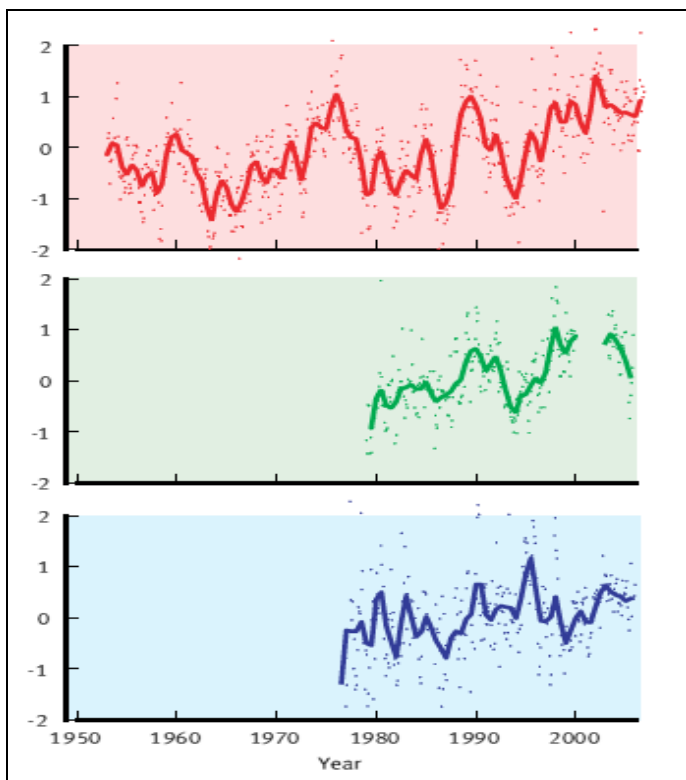


Figure 1-2: Monthly mean temperature trends, Vertical scale is the temperature anomaly in degrees Celcius (°C). Seasonal changes have been removed by subtracting the long-term monthly averages. Red - Millport (records commence in 1953), Green - Fair Isle (records commence in 1979), Blue - Peterhead (records commence in 1976). Fisheries Research Services (2007) © Crown Copyright..

UKCIP08 (Jenkins 2008) reports a UK annual mean averaged SST increase of 0.7°C over the past three decades. The report uses a long term dataset (1870-2006), sub-selected for UK coastal data from the global gridded HadISST1, expressed as anomalies to the baseline 1961-90 average of 11.3°C, after Rayner *et al* (2003). The emphasis reported is in terms of recent change for the past 30 years and not the long term regression coefficient or periods of above or below long term average conditions. In doing so the focus overlooks the periodicity captured by the relatively long time series.

MCCIP (2008) report a trend for general warming of the eastern North Atlantic between 0.5°C and 1°C per decade during the last 20 years, which they recognize may be influenced by the periodicity of the Atlantic Multi-decadal Oscillation (AMO) (Knight *et al.* 2005). Further reporting that UK sea surface temperatures (SST) have been increasing since the 1980s at a rate of 0.2–0.6 °C per decade, but with strong regional variations with warming occurring more quickly in the English Channel and southern North Sea compared to Scottish continental shelf waters. Datasets used are the HadISST (Rayner *et al.* 2003) and also the BODC Argo Float data, the latter has poor coverage of Scottish waters. MCCIP confidence in the UK assessments is moderate due to the distribution of observations and the poor sampling of seasonal cycles. Interpretation of the HadISST includes consideration of the distribution of sampling and to multi-decadal periodicity. Similar to UKCIP, the data is plotted as deviations from the 1961-1990 baseline average observations. This reference baseline will be discussed later with respect to salinity.

Wind, Storm Surge & Wave height

SNIFFER (Barnett 2006) report average annual wind speed for three representative Scottish stations (Lerwick, Tiree and Leuchars) over the time series 1957 to 2004 (with values estimated from Turnhouse before 1969). Both Tiree and Leuchars show a trend of decreasing average wind speeds in the last forty years. For all three stations, gale days show no clear trends.

UKCIP08 (Jenkins 2008) reports severe windstorms around the UK have become more frequent over the past few decades, but not exceeding those seen in the 1920s. Trends are difficult to identify, due to low frequency of storms, decadal variability and by the unreliability and lack of representative direct wind speed observations. Alexander *et al.* (2005) presented an analysis shown within the UKCIP08 report, whereby a severe storm event is characterized by a rapid change in mean sea-level pressure (MSLP). They identified a significant increase in the number of severe storms over the UK as a whole since the 1950s. Periodicity from their analysis is apparent, with a correlation between the stormiest periods in the 1920s and 1990s with decades of sustained positive NAO index as apposed to the 1960's (the least stormy decade) when the smoothed NAO index was most negative.

MCCIP (2008) report a trend for greater incidence of severe winds and larger mean wave heights in western and northern UK waters are being observed. No other trends are noted. A study by

Dawson (2001) of gale frequency for Edinburgh with respect to high magnitude volcanic eruptions using the Mossman-Hickey chronology (1780-1988), reveals a significant and persistent trend in declining gale day frequency, at a rate of 0.11 gale days per year over the 200 year record. These findings support the data from Leuchars in terms of general trends.

Sea Level change

UKCIP08 (Jenkins 2008), uses composite datasets from AR4-WG1 shoreline tidal gauges & satellite altimetry ocean surface measurements. The shoreline datasets are sparsely distributed and vary in their time series with Aberdeen representing eastern mainland Scotland and being one of the longest UK records. Base line data are taken as 1961-1990. Reported corrected sea level rise around the UK is approximately 1mm/yr for the 20th century. The rate for the 1990's and 2000's was reported to be higher. The UK national network of tide gauges is maintained by the Proudman Oceanographic Laboratory, Liverpool.

MCCIP (2008), report global average sea level to have risen by 1-2mm per year during the 20th century. The Aberdeen tidal gauge records extend from 1862 and show an increasing trend of 0.69 mm yr⁻¹ (+- 0.06 SE). Satellite altimetry measurements for the period 1993-2003 revealed higher annual increases of around 3 mm. However it is unclear whether the gauge data for this period reflected these higher increases, or if the change in recording system with the launch of the Topex/Poseidon satellite in 1992 explains the trend change. Chen *et al.* (2006) gives a precision of 1 mm/yr or better. Interpretation of the Topex/Poseidon data alone should be viewed with caution due to the relative short time series not fully capturing longer term variability and periodicity.

Corrections to the raw data time series for datum are based upon averaged national data for eustatic & isostatic relative changes following deglaciation since last glacial maximum 20,000 BP. Such averaging coupled with sparse distribution of representative stations, makes interpretation of local sea level changes difficult. However, UK records are sufficiently long to incorporate inter-annual and decadal variability.

Discontinuities in global mean data for both sea level and SST relate to corresponding ENSO and NAO events, Tsimplis *et al.* (2006), found sea surface temperature sensitivity to the NAO to be approximately 0.85 °C per unit of NAO, resulting in a thermosteric sea-level change of about 1-2 cm per unit NAO (additional to those due to winds and air pressures), clearly showing the relevance of thermal expansion as a component of sea level rise, however, heterogeneity within the world's oceans leads to variable contributions of thermal expansion to global sea level rise.

Antonov *et al.* (2005) found for the period 1955-2003 thermal expansion contributed 0.33 mm/year to global sea level rise and approximately half of this thermosteric trend due to differential warming of the Atlantic Ocean. The IPCC (2001) attribute 50% of global sea level rise to thermal expansion, locally however, the thermosteric contribution for the northern North Sea has a more minor role. Dawson (2001) demonstrates this using the COADS long series of SST data, showing whilst there

is inter-annual variability and evidence of longer term periodicity, the regression slope is much lower than elsewhere around the UK coastline, reflecting the northern North Sea as strongly influenced by variability in the Northern Atlantic.

Further consideration should also be given to rates of differential re-alignment around the coast of Scotland corresponding to spatial heterogeneity of ice loading, rock properties and crustal thickness; rates for Aberdeen are approximately 0.5 mm a^{-1} and locally for the Tay & Eden area $1-1.9 \text{ mm a}^{-1}$. (May and Hansom 2003).

Salinity

Fisheries research services (Now Marine Scotland Science - MSS) collect salinity data from four full coastal monitoring sites around Scotland located at Loch Maddy, Loch Ewe, Orkney and Shetland. Data have been collected since 1999, with the addition of a sampling site at Fair Isle which began in 2003. An ecosystem monitoring site also lies 5km offshore from Stonehaven in 50m water depth, having weekly records extending back to 1997. The longest dataset held comes from the Faroe-Shetland channel, which dates back to 1900.

FRS report salinity data that exhibit seasonality with lows in late spring and highs in autumn matching similar trends in temperature. They further report salinity changes over the past 20 years within North Sea waters having similar trends to those in the Atlantic, although on a greater scale. In particular a salinity minima was recorded in 2000 and 2001 showing the lowest values since 1997. For the North Atlantic during this period salinity was reported as increasing following a period of very low values.

In the northern North Sea the salinity is heavily influenced by inflowing north-east Atlantic water which exhibits multi-decadal periodicity from several sources; the time series for most of the recorded FRS salinity data, is too short to fully capture this variability and hence interpretation of the data is difficult.

MCCIP (2008) use datasets from Coastal and shelf sea monitoring stations maintained around Scotland by the FRS, Marine Laboratory Aberdeen (MARLAB), the Scottish Association for Marine Science (SAMS) Oban, and in the Irish Sea by the Government Laboratory of the Isle of Man. From this data they report surface waters to the north and west of the UK and in the northern North Sea becoming relatively more saline since the 1970s, with no clear trends in the shallow coastal waters of the Irish Sea, southern North Sea and western Scotland. The deep waters of the North Atlantic are reported to have freshened over the past 40 years. The MCCIP also noted a decadal-scale cyclical pattern of change around the UK reflecting mean North Atlantic and Nordic Sea conditions, which have evolved from a salinity maximum during the early 1960's and a minimum in the mid 1990's.

Belkin (2004) describes a series of decadal salinity and concomitant temperature anomalies occurring in the northern North Atlantic from the 1950's onwards, which correspond to the findings of FRS & MCCIP. Three major salinity anomalies (Great Salinity Anomalies – GSA) have now been identified; GSA'70s, GSA'80s and more recently GSA'90s. Great Salinity Anomalies are areas of water with low salinity propagating around the North Atlantic sub-polar gyre. A comparison of propagation speeds of the three GSA's indicates long-term intensification of the Subarctic Gyre circulation (Belkin 2004) which may be part of longer wavelength periodicity driving circulation. Controversy over the propagation and causal mechanisms has led to continued research, Wadley & Bigg (2004) first questioned whether these anomalies could be “a response to global warming, or part of the natural variability of the climate system”. Using the coupled climate simulation HadCM3 pre-industrial model, Bigg & Wadley (2007) found the model generated events which originated in both the Greenland and Labrador Seas forming GSA's with similar periodicities to those observed. Their investigations inferred that coupled ocean-atmosphere feedback interactions were not responsible for the GSA's, rather some causal mechanism within the ocean.

Sunby and Drinkwater (2007), describe a number of high salinity anomalies in addition to the low salinity anomalies from the Faroe-Shetland Channel time series. They maintain these anomalies represent “two different and opposing events of volume flux variations occurring at two different time periods” (displacements along salinity gradients), with high salinity anomalies occurring in the northeast Atlantic at the same time as low salinity anomalies occur in the northwest Atlantic and vice versa. These generally opposing signals are reported to travel at velocities within the greater gyre system at speeds consistent with the sub-polar gyre velocity.

The close interrelationship between salinity and temperature signatures in the ocean and the presence of the multi-decadal high and low salinity anomalies suggests that the variability seen within the short UK SST data should be viewed in terms of a snap shot within a cyclical system. The phase of the snapshot within the cyclical pattern is critical for the interpretation of the trend. Base line data commonly used in the UK extends over the period from 1961-1990; the location of the anomalies within this snapshot time series will impact on the trend seen. The bias in interpretation is not only important for SST, but also for the thermosteric contribution to sea level rise estimates.

Precipitation

UKCIP08 & 09 - (Jenkins 2008; Jenkins 2009) report a greater contribution of heavy precipitation to winter rain fall for all regions of the UK and for summer all regions except NE England and N Scotland show decreases.

SNIFFER (Barnett 2006) report a clear upward trend in winter precipitation since 1961, with an increase of almost 70% in winter precipitation in North Scotland. Average precipitation was also reported to be increasing with Scotland becoming 20% wetter between 1961 and 2004. They report longer term trends from 1914-2004 of a reduction in summer precipitation in East Scotland and an

increase in spring precipitation in West Scotland. Average precipitation was reported to have increased across most of Scotland since 1914, apart from a slight reduction in both average annual and winter precipitation in East Scotland, an opposing trend to the period 1961 to 2004. The largest changes were reported to have taken place in winter months across all but the most eastern areas of Scotland. Autumnal rather show eastern areas being the only region to become wetter, with increases of more than 20%. In summer, northern areas of Scotland, and in particular the north-west have become drier since 1961. The reduction in summer precipitation is greater than 20% in some areas. Further reported is a trend of increasing rainfall intensity in both East and West Scotland.

From the SNIFFER (Barnett 2006) report, it is clear there is much short term variability which, when taken in terms of the 1961+ time series, gives rise to different conclusions. Consideration should also be given to the role of the spatial distribution of rain gauge stations to the patterns of data recorded.

Information on gauge inflow and changes in snowfall and retention is required to fully understand the contribution precipitation makes to the catchments of the river Tay and river Eden. However, long UK river flow and precipitation series (1861-1971), have shown variability in high and low flood periods, but no clear trend in rainfall maxima, volume or flood peaks (Robson 2002; Wilby *et al.* 2008). None the less local consideration should be given to by pass flows during flood events, which may lead to under estimates of overall flow.

1.9. Summary

Estuaries are highly productive transitional ecosystems providing a wealth of socio-economic and ecological ecosystem services; valuable for erosion and pollution buffering, nutrient cycling and storage, as a water resource for agriculture and energy provision, as an outlet for drainage, and providing a diverse array of habitats and food sources for both resident and visiting species.

Observational data reported by UKCIP09 (Jenkins 2009) identify an increase in air temperatures of ~0.8°C since 1980, increased seasonality in precipitation over the past 45 years with heavy winter rainfall, more frequent severe windstorms, however not above those observed in the 1920s. Sea-surface temperatures were reported to have risen around the UK by about 0.7°C and sea level to have risen by about 1mm/yr for the 20th Century, however at a higher rate since the 1990s and 2000s. The IPCC07 AR4-WG1 (IPCC 2007c) UK climate projections for medium emissions scenarios for the 2050s identify the mean temperatures for both winter and summer to increase (1.7°C and 2.3°C respectively) and for no increase in total precipitation, however greater seasonality with a 10% increase in mean winter precipitation and a 13% reduction in summer precipitation.

Estuary dynamics are largely driven by variability in river flow, tidal regime and predominant wind direction (effecting waves and currents), thus predicted climate change which impacts on these drivers is likely to re-shape the estuary dynamics with consequential impacts to morphology, the spatial distribution of habitats and to community compositions. Species which are close to their ecological limits, especially those with low dispersal ranges and the less motile, are most vulnerable to regime shifts and may not be able to adjust in pace with the rate of climate driven change.

Analysis and interpretation of observational data should take into consideration the periodicity of known natural cycles, which vary in length from semi-diurnal to centennial (or greater) time scales. Time series of at least 50 years are recommended for climate impact studies (CEH and UKMO 2001; Douglas 1992), however with our current knowledge of associations to external forcing mechanisms, for greater confidence in long term trends, time series of greater than 90 years are perhaps more appropriate.

1.10. References

- Alexander, L. V., S. F. B. Tett, and T. Jonsson. 2005. Recent observed changes in severe storms over the United Kingdom and Iceland. *Geophysical Research Letters* **32**.
- Antonov, J. I., S. Levitus, and T. P. Boyer. 2005. Thermosteric sea level rise, 1955-2003. *Geophysical Research Letters* **32**: 4.
- Barnett, C., J. Hossell, M. Perry, C. Procter and G. Hughes. 2006. A handbook of climate trends across Scotland. SNIFFER project CC03. Scotland & Northern Ireland Forum for Environmental Research, 62pp.
- Beer, J., M. Vonmoos, and R. Muscheler. 2006. Solar variability over the past several millennia. *Space Science Reviews* **125**: 67-79.
- Belkin, I. M. 2004. Propagation of the "Great Salinity Anomaly" of the 1990s around the northern North Atlantic. *Geophysical Research Letters* **31**.
- Bigg, G. R., and M. R. Wadley. 2007. Simulation of "great salinity anomalies" in coupled climate models. *Journal of Geophysical Research-Oceans* **112**: 9.
- Bird, D. F., and J. Kalf. 1984. Empirical Relationships between Bacterial Abundance and Chlorophyll Concentration in Fresh and Marine Waters. *Canadian Journal of Fisheries and Aquatic Sciences* **41**: 1015-1023.
- Black, A. R., and J. L. Anderson. 1994. The Great Tay Flood of January 1993. Institute of Hydrology Tay Purification Board.
- Black, A. R., and A. Werritty. 1997. Seasonality of flooding: A case study of North Britain. *Journal of Hydrology* **195**: 1-25.
- Boyd, R., R. Dalrymple, and B. A. Zaitlin. 1992. Classification of Clastic Coastal Depositional Environments.. *Sedimentary Geology* **80**: 139-150.
- Brown, J. M., and A. G. Davies. 2010. Flood/ebb tidal asymmetry in a shallow sandy estuary and the impact on net sand transport. *Geomorphology* **114**: 431-439.
- Camuffo, D. 2001. Lunar influences on climate. *Earth Moon and Planets* **85-6**.
- CEH, and UKMO. 2001. To What Degree can the October/November 2000 Flood Events be Attributed to Climate Change? Defra FD2304. Department for Environment, Food and Rural Affairs: London; 40 pp.
- CFAS. 2007. OSPAR eutrophication assessments: SEPA comprehensive procedure 2008 - Eden. DEFRA: Environment Agency, Marine Environmental Research.
- Chen, J. L., C. R. Wilson, B. D. Tapley, and X. G. Hu. 2006. Thermosteric effects on interannual and long-term global mean sea level changes. *Journal of Geodesy* **80**: 240-247.
- Chenet, A. L., F. Fluteau, and V. Courtillot. 2005. Modelling massive sulphate aerosol pollution, following the large 1783 Laki basaltic eruption. *Earth and Planetary Science Letters* **236**: 721-731.
- Clelland, B. E. 1997. The Eden estuary: a review of its ecological and conservation interest, with particular reference to water quality. *The estuaries of central Scotland*.

- Cole-Dai, J. H., E. Mosley-Thompson, S. P. Wight, and L. G. Thompson. 2000. A 4100-year record of explosive volcanism from an East Antarctica ice core. *Journal of Geophysical Research-Atmospheres* **105**: 24431-24441.
- Costanza, R. and others 1998. The value of the world's ecosystem services and natural capital (Reprinted from *Nature*, vol 387, pg 253, 1997). *Ecological Economics* **25**.
- Daily, G. C. and others 2000. Ecology - The value of nature and the nature of value. *Science* **289**: 395-396.
- Daniels, J. M. 2007. Flood hydrology of the North Platte River headwaters in relation to precipitation variability. *Journal of Hydrology* **344**.
- Dawson, A., D. Smith, and S. Dawson. 2001. Potential impacts of climate change on sea levels around Scotland. *Scottish Natural heritage, Research , Survey and Monitoring Report*. No 178.
- Dawson, A. G., K. Hickey, J. Mckenna, and I. D. L. Foster. 1997. A 200-year record of gale frequency, Edinburgh, Scotland: possible link with high-magnitude volcanic eruptions. *Holocene* **7**: 337-341.
- Day, J. W. and others 2008. Consequences of climate change on the ecogeomorphology of coastal wetlands. *Estuaries and Coasts* **31**: 477-491.
- De Vita, P., V. Allocca, F. Manna, and S. Fabbrocino. 2012. Coupled decadal variability of the North Atlantic Oscillation, regional rainfall and karst spring discharges in the Campania region (southern Italy). *Hydrology and Earth System Sciences* **16**.
- Dickson, R. R. and others 2000. The Arctic Ocean response to the North Atlantic oscillation. *Journal of Climate* **13**: 2671-2696.
- Douglas, B. C. 1992. Global Sea-Level Acceleration. *Journal of Geophysical Research-Oceans* **97**: 12699-12706.
- Eastwood, K. M. 1977. *Some Aspects of the Sedimentology of the Superficial Deposits of the Eden Estuary, Fife, Scotland*. University of St Andrews.
- Ferentinos, G., and J. Mcmanus. 1981. Nearshore Processes and shoreline development in St Andrews Bay, Scotland, U.K., p. 161-174. Special Publication of the International Association of Sedimentologists.
- Ferentinos, G., and J. Mcmanus. 2009. *Nearshore Processes and Shoreline Development in St Andrews Bay, Scotland, U.K.* Blackwell Publishing Ltd.
- Fischer, E. M., J. Luterbacher, E. Zorita, S. F. B. Tett, C. Casty, and H. Wanner. 2007. European climate response to tropical volcanic eruptions over the last half millennium. *Geophysical Research Letters* **34**.
- Foukal, P., C. Frohlich, H. Spruit, and T. M. L. Wigley. 2006. Variations in solar luminosity and their effect on the Earth's climate. *Nature* **443**: 161-166.
- Freitas, V., J. Campos, M. Fonds, and H. W. Van Der Veer. 2007. Potential impact of temperature change on epibenthic predator-bivalve prey interactions in temperate estuaries. *Journal of Thermal Biology* **32**.

- FRS. 2000. Ocean Climate Status Report 1999. Fisheries Research Services Report, 06/00. Aberdeen.
- . 2007. Scottish Ocean Climate Status Report 2004 and 2005. Hughes S.L. (ed.). Fisheries Research Services Aberdeen. 40pp.
- Haigh, I. D., M. Eliot, and C. Pattiaratchi. 2011. Global influences of the 18.61 year nodal cycle and 8.85 year cycle of lunar perigee on high tidal levels. *J. Geophys. Res.* **116**: C06025.
- Haigh, J. D., and M. Blackburn. 2006. Solar influences on dynamical coupling between the stratosphere and troposphere. *Space Science Reviews* **125**: 331-344.
- Hansen, D. V., and M. Rattray. 1966. New Dimensions in Estuary Classification. *Limnology and Oceanography*. **Vol. 11**: 319-326.
- Hansom, J. D. 1999. The coastal geomorphology of Scotland: understanding sediment budgets for effective coastal management. In: Baxter, J., Duncan, K., Atkins, S. and Lees, G., Editors., p. 34-44. *Scotland's Living Coastline*.
- Hooper, D. U. and others 2005. Effects of biodiversity on ecosystem functioning: A consensus of current knowledge. *Ecological Monographs* **75**: 3-35.
- Horner, M. W., and P. D. Walsh. 2000. Easter 1998 floods. *Journal of the Chartered Institution of Water and Environmental Management* **14**: 415-418.
- Houghton, J. T., G. J. Jenkins, and J. J. Ephraums. 1990. The IPCC Scientific Assessment, p. 410 pp. Report prepared for Intergovernmental Panel on Climate Change by Working Group I.
- Hoyt, D. V., and K. Schatten. 1997. *The Role of the Sun in Climate Change*. Oxford University Press.
- Hurrell, J. W. 1995. Decadal trends in the North-Atlantic Oscillation -Regional temperatures and precipitation. *Science* **269**: 676-679.
- Hurrell, J. W., Y. Kushnir, G. Ottersen, and V. M. 2003. The North Atlantic Oscillation: Climate Significance and Environmental Impact, p. 279. *Geophysical Monograph Series*.
- IPCC. 2001. *Climate Change 2001: The Scientific Basis*. Contribution of Working Group I to the Third Assessment Report of the Intergovernmental Panel on Climate Change, p. 881pp. In J. T. Houghton, Y. Ding, D.J. Griggs, M. Noguer, P.J. van der Linden, X. Dai, K. Maskell, and C.A. Johnson [ed.].
- . 2007a. *Climate Change 2007 - The Physical Science Basis*. Contribution of Working Group I to the Fourth Assessment Report of the IPCC. Intergovernmental Panel on Climate Change (IPCC).
- . 2007b. *Climate Change 2007 – Impacts, Adaptation and Vulnerability*. Contribution of Working Group II to the Fourth Assessment Report of the IPCC. Intergovernmental Panel on Climate Change (IPCC).
- . 2007c. *Climate Change 2007: Synthesis Report*. Contribution of Working Groups I, II and III to the Fourth Assessment Report of the Intergovernmental Panel on Climate Change, p. 104. In R. K. Pachauri and A. Reisinger [eds.]. IPCC, Geneva, Switzerland.

- Jenkins, G. J., Perry, M.C., and Prior, M.J. 2008. The climate of the United Kingdom and recent trends. Met Office Hadley Centre, Exeter, UK.
- . 2009. The climate of the United Kingdom and recent trends. Met Office Hadley Centre, Exeter, UK.
- Jury, M. R., and J. L. Melice. 2000. Analysis of Durban rainfall and Nile river flow 1871-1999. *Theoretical and Applied Climatology* **67**.
- Knight, J. R., R. J. Allan, C. K. Folland, M. Vellinga, and M. E. Mann. 2005. A signature of persistent natural thermohaline circulation cycles in observed climate. *Geophysical Research Letters* **32**.
- Laiguel, B., N. Massei, A. Rossi, J. Mesquita, and S. Slimani. 2010. Water resources variability in the context of climatic fluctuations on both sides of the Atlantic Ocean. *Global Change: Facing Risks and Threats to Water Resources* **340**.
- Lane, S. N. 2008. Climate change and the summer 2007 floods in the UK. *Geography* **93**: 91-97.
- Langematz, U., K. Matthes, and J. L. Grenfell. 2005. Solar impact on climate: modeling the coupling between the middle and the lower atmosphere, p. 868-875. *In* I. Ermolli, J. Pap and P. Fox [eds.], *Conference on Solar Variability and Earths Climate*. Soc Astronomica Italiana.
- Lanzoni, S., and G. Seminara. 1998. On tide propagation in convergent estuaries. *Journal of Geophysical Research-Oceans* **103**: 30793-30812.
- . 2002. Long-term evolution and morphodynamic equilibrium of tidal channels. *Journal of Geophysical Research*.
- Ling, H., H. Xu, W. Shi, and Q. Zhang. 2011. Regional climate change and its effects on the runoff of Manas River, Xinjiang, China. *Environmental Earth Sciences* **64**.
- MacDonald, N. 2006. An underutilized resource: historical flood chronologies a valuable resource in determining periods of hydro-geomorphic change. *Sediment Dynamics and the Hydromorphology of Fluvial Systems* **306**: 120-126.
- MacDonald, N., and A. R. Black. 2010. Reassessment of flood frequency using historical information for the River Ouse at York, UK (1200-2000). *Hydrological Sciences Journal- Journal Des Sciences Hydrologiques* **55**: 1152-1162.
- MacDonald, N., A. Werritty, A. R. Black, and L. J. Mcewen. 2006. Historical and pooled flood frequency analysis for the River Tay at Perth, Scotland. *Area* **38**: 34-46.
- Marsh, T. 2008. A hydrological overview of the summer 2007 floods in England and Wales. *Weather* **63**: 274-279.
- May, V. J., and J. D. Hansom. 2003. *Coastal Geomorphology of Great Britain*. Geological Conservation Review Series, GCR Volume No. 28. Joint Nature Conservation Committee, Peterborough, 754 pp.
- Mazzarella, A., and N. Scafetta. 2012. Evidences for a quasi 60-year North Atlantic Oscillation since 1700 and its meaning for global climate change. *Theoretical and Applied Climatology* **107**.
- MCCIP. 2008. *Marine Climate Change Impacts Annual Report Card 2007–2008*. (Eds. Baxter JM, Buckley PJ and Wallace CJ), Summary Report, MCCIP, Lowestoft, 8pp.

- McCormick, M. P., L. W. Thomason, and C. R. Trepte. 1995. Atmospheric effects of the Mt Pinatubo eruption. *Nature* **373**: 399-404.
- McEwen, L. J. 2006. Flood seasonality and generating conditions in the Tay catchment, Scotland from 1200 to present. *Area* **38**: 47-64.
- McManus, J., and C. Green. 1977. Report on Pilmour Links beaches and the eastern part of the Eden estuary(Contractor: University of Dundee). Unpublished report to Fife Regional Council, Glenrothes.
- Miller, D. J., and K. A. Eriksson. 1997. Late Mississippian prodeltaic rhythmites in the Appalachian basin: A hierarchical record of tidal and climatic periodicities. *Journal of Sedimentary Research* **67**.
- Mundo, I. A. and others 2012. Multi-century tree-ring based reconstruction of the Neuquén River streamflow, northern Patagonia, Argentina. *Climate of the Past* **8**.
- Nicholls, R. J., A. Dredge, and T. Wilson. 2000. Shoreline change and fine-grained sediment input: Isle of Sheppey Coast, Thames Estuary, UK. *Coastal and Estuarine Environments: Sedimentology, Geomorphology and Geoarchaeology* **175**.
- NRFA. 2011. National River Flow Archive: © NERC - Centre for Ecology & Hydrology.
- Ottersen, G., B. Planque, A. Belgrano, E. Post, P. C. Reid, and N. C. Stenseth. 2001. Ecological effects of the North Atlantic Oscillation. *Oecologia* **128**: 1-14.
- Pethick, J. 1994. Estuaries and Wetlands - Function and Form. *Wetland Management*: 75-87.
- Price, R. J. 1983. Scotland's environment during the last 30,000 years. Scottish Academic Press.
- Pritchard, D. W. 1967. "What is an estuary: physical viewpoint". p. 3-5. *In* G. H. Lauf [ed.], *Estuaries*. A.A.A.S.
- Pugh, D. T. 2004. Changing sea levels. Effects of tides, weather and climate. Cambridge University Press: 280 pp.
- Rai, R. K., A. Upadhyay, and C. S. P. Ojha. 2010. Temporal Variability of Climatic Parameters of Yamuna River Basin: Spatial Analysis of Persistence, Trend and Periodicity. *The Open Hydrology Journal* **4**: 184-210.
- Rampino, M. R., S. Self, and R. B. Stothers. 1988. Volcanic Winters. *Annual Review of Earth and Planetary Sciences* **16**: 73-99.
- Rayner, N. A. and others 2003. Global analyses of sea surface temperature, sea ice, and night marine air temperature since the late nineteenth century. *Journal of Geophysical Research-Atmospheres* **108**.
- Robock, A. 2000. Volcanic eruptions and climate. *Reviews of Geophysics* **38**: 191-219.
- Robson, A. J. 2002. Evidence for trends in UK flooding. *Philosophical Transactions of the Royal Society of London Series a-Mathematical Physical and Engineering Sciences* **360**: 1327-1343.

- Rubio-Alvarez, E., and J. Mcphee. 2010. Patterns of spatial and temporal variability in streamflow records in south central Chile in the period 1952-2003. *Water Resources Research* **46**.
- Savarino, J., S. Bekki, J. H. Cole-Dai, and M. H. Thiemens. 2003. Evidence from sulfate mass independent oxygen isotopic compositions of dramatic changes in atmospheric oxidation following massive volcanic eruptions. *Journal of Geophysical Research-Atmospheres* **108**.
- Scafetta, N. 2010. Empirical evidence for a celestial origin of the climate oscillations and its implications. *Journal of Atmospheric and Solar-Terrestrial Physics* **72**: 951-970.
- . 2012a. A shared frequency set between the historical mid-latitude aurora records and the global surface temperature. *Journal of Atmospheric and Solar-Terrestrial Physics* **74**.
- . 2012b. Does the Sun work as a nuclear fusion amplifier of planetary tidal forcing? A proposal for a physical mechanism based on the mass-luminosity relation. *Journal of Atmospheric and Solar-Terrestrial Physics* **81-82**.
- . 2012c. Multi-scale harmonic model for solar and climate cyclical variation throughout the Holocene based on Jupiter-Saturn tidal frequencies plus the 11-year solar dynamo cycle. *Journal of Atmospheric and Solar-Terrestrial Physics* **80**.
- Shaviv, N. J. 2008. Using the oceans as a calorimeter to quantify the solar radiative forcing. *Journal of Geophysical Research-Space Physics* **113**.
- Stenseth, N. C. and others 2003. Studying climate effects on ecology through the use of climate indices: the North Atlantic Oscillation, El Nino Southern Oscillation and beyond. *Proceedings of the Royal Society of London Series B-Biological Sciences* **270**.
- Sundby, S., and K. Drinkwater. 2007. On the mechanisms behind salinity anomaly signals of the northern North Atlantic. *Progress in Oceanography* **73**: 190-202.
- Switanek, M. B., and P. A. Troch. 2011. Decadal prediction of Colorado River streamflow anomalies using ocean-atmosphere teleconnections. *Geophysical Research Letters* **38**.
- Tomasino, M., and F. Dalla Valle. 2000. Natural climatic changes and solar cycles: an analysis of hydrological time series. *Hydrological Sciences Journal-Journal Des Sciences Hydrologiques* **45**.
- Trigo, R. M., T. J. Osborn, and J. M. Corte-Real. 2002. The North Atlantic Oscillation influence on Europe: climate impacts and associated physical mechanisms (vol 20, pg 9, 2002). *Climate Research* **22**: 97-97.
- Tsimplis, M. N., A. G. P. Shaw, R. A. Flather, and D. K. Woolf. 2006. The influence of the North Atlantic Oscillation on the sea-level around the northern European coasts reconsidered: the thermosteric effects. *Philosophical Transactions of the Royal Society a-Mathematical Physical and Engineering Sciences* **364**: 845-856.
- Van Der Wal, D., and K. Pye. 2004. Patterns, rates and possible causes of saltmarsh erosion in the Greater Thames area (UK). *Geomorphology* **61**: 373-391.
- Wadley, M. R., and G. R. Bigg. 2004. "Great Salinity Anomalies" in a coupled climate model. *Geophysical Research Letters* **31**: 4.

- Werritty, A. 2002. Living with uncertainty: climate change, river flows and water resource management in Scotland. *Science of the Total Environment* **294**: 29-40.
- Werritty, A., and K. F. Leys. 2001. The sensitivity of Scottish rivers and upland valley floors to recent environmental change. *Catena* **42**: 251-273.
- Werritty, A., J. L. Paine, N. Macdonald, J. S. Rowan, and L. J. Mcewen. 2006. Use of multi-proxy flood records to improve estimates of flood risk: Lower River Tay, Scotland. *Catena* **66**: 107-119.
- Wikner, J., and A. Andersson. 2012. Increased freshwater discharge shifts the trophic balance in the coastal zone of the northern Baltic Sea. *Global Change Biology* **18**.
- Wilby, R. L., K. J. Beven, and N. S. Reynard. 2008. Climate change and fluvial flood risk in the UK: more of the same? *Hydrological Processes* **22**: 2511-2523.
- Yndestad, H. 2004. The Lunar nodal cycle influence on the Barents Sea. Norwegian University of Science and Technology.
- Yousef, S. 2000. Nile Flood Forecast, p. 263-266. ICEHM2000.
- Yousef, S. M., and M. El Raey. 1995. Major Solar Episodes Reconstructed Using Records of The River Nile, Tree-Ring Indices and Sunspots., p. 76. *Bulletin De L'Institut D'Egypte*.

CHAPTER 2

2. HISTORICAL TREND ANALYSIS

Chapter aim

- To identify trends or pattern evident within the historical time series of selected driving mechanisms of change (river inflow to the estuary, morphology and local wind regime).
- To identify the consequential responses to these driving mechanisms with respect to spatial changes in channel and shoreline alignment and additionally to the spatial distribution of selected key biological habitats.

Historical trend analysis (HTA) is a method commonly used to look for persistent long term pattern and trend within a data time series. HTA is a valuable tool which can utilize both qualitative and quantitative data to understand long period (multi-decadal) variable behaviour, identifying the direction and also rate of change. HTA is ideally used for periods of at least 50 years (CEH and UKMO 2001; Douglas 1992), which capture the longer frequency cycles known to exist within climatic data. Many of the UK environmental time series available for analysis are relatively short and reflect the fact that the importance for accurate environmental chronologies for future climate modelling was largely only recognised during the mid twentieth century for the UK. This is reflected in the current use of the 1961-1990 long term mean as the baseline for many of the UK climate reports.

Standard methods for HTA range from direct analysis of historical instrumental chronologies via decomposition to the component trend and seasonality fractions (Cryer and Kung-Sik 2008), fourier/spectral analysis (Broersen 2006) to identify signal periodicity over time and temporal-morphological change analysis, looking at how spatially morphology responds to climatic forcing (Emphasys-Consortium 2000). Limitations for these methods vary, however availability of data is the most restrictive factor which together with data quality have the greatest effect on the level of confidence in quantifying change over time.

HTA is used in this chapter to understand climate signals that are manifest over a range of timescales. The chronologies chosen are river flow, wind direction counts and spatial responses in terms of river channel migration, shoreline changes, estuary basin analysis and the distribution of key species. The analysis of these data enables assessment of the estuary response to climate variability forced by background long-period natural cycles. This long-period analysis provides the background to the shorter term responses investigated in later chapters. Additionally, the regional univariate analyses is cross-correlated with more global indices (NAOI) and potential driving mechanisms (orbital & solar cycles) in order to link regional to global responses with potential

natural drivers of climate change. Identifying and understanding the responses to natural cycles of variability may help to separate the natural from superimposed anthropogenic change.

2.1. River Inflow

There are many hydrological-climate studies for the UK that largely focus on discrete extreme events through history, changes to catchments or with flow trends motivated by the need for flood prevention and control (Black and Werritty 1997; Horner and Walsh 2000; Macdonald and Black 2010; Marsh 2008; Werritty and Leys 2001). Modelling of future scenarios often use General Circulation Models (GCM's) combined with the 'long term mean data', for which model outputs are then downscaled to regional or catchment level for mitigation efforts. However, few studies investigate the multidecadal patterns within continuous river flow data, the causal mechanisms of these patterns or potential links to climate indices (Pattison and Lane 2011). Equally few studies have been conducted to investigate change driven by external mechanisms, such as solar or orbital forcing. None the less, investigating hydro-meteorological data to explain climatic variability is not a new concept. In the late 1800's Eduard Bruckner, who was subsequently described by Huntington (1915) as 'one of the chief European authorities on climate', first put forward a possible link between weather conditions and water levels. In 1890 Bruckner proposed hypothetical sequences of long and shorter period climate fluctuations which were associated to alternating cold-wet and warm-dry weather, with frequencies from 10 to 35 years and to much longer frequencies of a few hundreds years. These sequences were derived from northern hemisphere meteorological data, Caspian Sea levels, and on temporal variations in Alpine glaciers. He associated these alternating periods with above and below average agricultural productivity in Europe (warm dry, cold wet respectively) following characteristic 35 year patterns, showing possibly for the first time the socioeconomic implications of climate change (Stehr and Storch 2000) and also the presence of periodic pattern in hydrological data. Latterly the cyclicity of the Bruckner frequency has been interpreted as resulting from "the non linear effect of solar activity on atmospheric processes"(Raspopov *et al.* 2004; Raspopov *et al.* 2000).

There is increasing research that focuses on the relationship between the transient (inter-cycle) and long term variations in solar activity (manifest as sunspots) and the consequential impacts to climate variability (Herman and Goldberg 1978; Hoyt and Schatten 1997; Love *et al.* 2011; Mufti and Shah 2011; Serre and Nesme-Ribes 2000; Shaviv 2008; Zhao and Han 2012). Sunspots (the were historically observed by eye as early as A.D 829 by the an Arabic astronomer Giaafar (Hoyt and Schatten 1997); by the early 1600s observations were made by telescope, but it was not until the 19th century, when Heinrich Schwabe discovered cyclical patterns of activity in 1843, that more detailed records were compiled. A measure of the solar magnetic activity was devised to investigate the cyclic variations in activity by Rudolph Wolfe in 1849; the method recorded visible activity as a number of sunspots on the photosphere of the sun, becoming known as the Wolfe Number (Hoyt and Schatten 1997) and this methodology continues today as the International Sunspot Number.

These cycles exhibit variety in period length from between approximately 9 and 13 years, however the normal contemporary length is 10.5 years and overall long term average length is 11.1 years. The importance of sunspot numbers lies in them being the only continuous solar observations that span over centuries, providing a chronology of solar activity with which to investigate the solar-climate relationship, where it is postulated that variability in incoming solar radiation drives structural changes in atmospheric circulation, giving rise to patterns of warmer and wetter and colder drier climatic periods with consequential impacts to river flows. The influence of long-term solar activity on river flow has been demonstrated through a number of recent studies; Prokoph (2012) identified an ~ 11 year cyclicity, consistent with solar activity, within hydrological records for the Southern Canada, Fu (2012) identified periodicities of approximately 11 and 22 years (in accordance with solar activity), and additional shorter term periodicities consistent with El Nino (2-7 years) within stream flow records from across southern Canada, Hajian (2010) identified long-range cross-correlation between sunspot numbers and stream-flow records for the rivers Daugava, Holston, Nolichucky and French Broad and in several recent studies by Mauas America (Mauas and Flamenco 2006; Mauas *et al.* 2011; Mauas *et al.* 2008) significantly correlating the stream flow of one of the largest rivers in the world, the Paraná in South America, with sunspot numbers.

Modulations, harmonics and combinatory frequencies of the approximate 11 year cycle, the 22 year polar magnetic field (Raspopov *et al.* 2004) and of the 18.6 lunar nodal cycle (Yndestad 2006) have been identified, which may explain some of the longer period variability in hydrological records.

2.1.1. Introduction & rationale

A review of observed climate trends for the UK can be summarised by the following; the UKCIP09 (Jenkins 2009) reports observed trends for an increased contribution of heavy precipitation to winter rain fall for all regions of the UK in the preceding 45 years, and for summer all regions except NE England and N Scotland show decreases. SNIFFER (Barnett 2006) similarly report a clear increase in winter precipitation since 1961, with a maximum increase of 70% in winter precipitation in North Scotland. Average precipitation was also reported to be increasing, becoming 20% wetter between 1961 and 2004, but no clear trend for summer precipitation was seen in this period. In the longer term context (1914-2004) however, patterns are less clear, with a reduction of summer rainfall in East Scotland and increasing rainfall to the West. Average precipitation was reported to have increased across most of Scotland since 1914, apart from a slight reduction in both average annual and winter precipitation in East Scotland, an opposing trend to the period 1961 to 2004. The SNIFFER (Barnett 2006) report, highlights much variability which, when viewed over different time scales (1914-2004 or 1961-2004), gives rise to different conclusions, suggesting there may be a requirement to view the data in a different way to the traditional monotonic trend analysis.

The Eden Estuary is, unlike the larger estuaries in the UK, sparse in information that could be used for flow analyses. The relatively small size however is ideally suited to flow studies for climatic signatures as it has relatively little catchment management which may mask natural climate signals.

Freshwater inflow to the estuary is principally supplied by the river Eden for which there is flow data from 1968 to 2010. Since this represents a relatively short chronology, additional information has been used in this study for the adjacent and much longer studied river Tay, a record from 1953 to 2010. In addition, in order to test the longest possible sampling periods a comparison is also made to the river Thames, the longest chronology for the UK.

The river Tay has the highest flow of all UK rivers (Marsh and Lees 2003), despite not being the longest nor having the largest catchment. Following the Great Tay Flood in 1993, the largest on UK record since 1814, the economic impact prompted research into historical flood frequency. Black & Anderson (1994) identified 3 major flood years that preceded 'The Great Tay Flood of January 1993'. From analysis of historical data from 1814, they noted the presence of clusters of flood rich and poor periods and made reference to favoured climate change scenarios reported at that time that predict increased rainfall in the catchment. McEwen (2006) built upon this previous research by specifically investigating flood rich and poor years and recognized the need to include explanatory environmental and climatic variables as contributory causal factors to flooding events. In further trying to predict future risk, McDonald *et al.* (2006) used HTA coupled with probability density functions to calculate return periods for the 1993 'Great Tay Flood'. Their results gave a return period of be between 220 and 250 years. These estimates were further refined by Werritty *et al.* (2006) who worked on an improvement flood risk estimation using sediment core data that revealed 50, 100 and 200 year floods predicted to reach 1875, 2250 and 2050 m^3s^{-1} respectively.

The research literature for the Tay all share a common theme; that of a pattern of flood rich and poor periods at defined frequencies with links to long periodicity (as return periods) in repeated events with contributory climatic and environmental variables as factors determining magnitude and frequency of flood events. These findings provide the motivation for the aims of this section on river flow analysis.

Aims

- Investigate general patterns, trends and periodicity within continuous river flow time series for the Eden and Tay estuaries.
- Investigate changing seasonality of flow with respect to observed climate trends.
- Investigate links between flow patterns and climate indices (NAOI) to establish any causal relationships.
- Investigate cross-correlation with solar activity, as a potential driving mechanism for change.

2.1.2. Methodology

Data was sourced from the National River Flow Archive (NFRA) (Centre for Ecology & Hydrology 2010), copyright of the material is owned by the Natural Environment Research Council (NERC) and is used here for research purposes only.

Data was acquired for the following gauging stations; river Eden Kembeck station (NO415158), with a data range 1968-2010 and the river Tay Ballathie station (NO147367), with a data range from 1952-2010. Additionally data was obtained for the river Thames Kingston station (TQ177698) with a data range 1883-2010. These rivers have catchment areas of; 307.4 km², 4587.1 km² and 9948 km² respectively.

Identifying the presence of general trend and patterns

Exploratory data analysis (EDA) used annual and monthly flow (cumecs / m³s⁻¹) summary data, plotted in Microsoft Excel (2003), displaying the data as a time series to identify general trends. Monotonic trend was further investigated via the non parametric Mann-Kendall test using R statistical software (Cran 2011).

Understanding the time delay between precipitation and the transfer of runoff as river flow is important for the interpretation of the flow data in relation to climate patterns. This relationship was investigated by plotting the linear regression between the two variables in Microsoft Excel (2003). In determining the R² correlation coefficient between precipitation & river flow, a low R² infers residence time within the catchment and conversely a large R² infers a more direct transfer of runoff, thus providing a guide to runoff buffering by the catchment.

Standardized annual flow (difference from the long term mean values) was plotted to identify the variability of above or below average conditions, to detect pattern rather than monotonic trend.

Exceedance (the percentage percentile for which flow in ms⁻¹ was equalled or exceeded for the flow record) provides a guide to trend in more extreme high or low flow conditions. These data were pre calculated by NRFA and the downloaded data were plotted in Excel to identify trend or pattern.

Trend was investigated in further detail using R (Cran 2011) software through decomposition analysis and comparison was made with the longer river time series of the Tay and Thames to give a longer term perspective.

The stationary de-trended data which were calculated in the decomposition analysis were then passed through autocorrelation (ACF) & partial autocorrelation (PACF) to determine if significant cycles were present. The ACF and PACF are time domain methodologies and rely on serial correlation, thus additionally a frequency domain methodology (spectral density analysis) was applied using R statistical software (Gamiz-Fortis *et al.* 2011; Sengul and Can 2011). Both methods effectively give the same result as they are transforms of each other however autocorrelation is generally used to examine serial dependence, whilst spectral analysis examines periodic behaviour that is not necessarily related to regular cyclical changes. Using both methods allows identification of differing characteristics of the variable behaviour in the time series.

Identifying changes to seasonality

Exploratory data analysis used Microsoft Excel (2003) to graph the percentage contribution of flow during winter months with respect to total annual flow over the time series, for both the river Eden and the river Tay, to investigate whether winters were wetter and summers drier. The year was split in half between summer months (April to September) and winter months (January- March & October-December) giving the within year seasonality. Monotonic trend in the percentage of winter flow over time was investigated via the non parametric Mann-Kendall test using R statistical software (Cran 2011).

Variability of the percentage of winter flow over time was displayed by plotting the standardized annual flow (difference from the long term mean values as anomaly data) against time, to highlight periods of above or below average conditions, to identify any pattern present.

Identifying links to Climate indices

The climate of Scotland is strongly influenced by the oceanic waters of the North Atlantic; prevailing south-westerly winds pick up heat from the North Atlantic Current (a powerful warm ocean current continuing the Gulf Stream northeast)(Colling and Team 2001) as they move eastwards giving Scotland it's distinctly mild and wet climate. Changes in the strength of the Atlantic Ocean circulation may therefore impact on the patterns of precipitation experienced over time. The North Atlantic Oscillation (NAO) describes the changes in both the latitude and speed of the jet stream (Woollings and Blackburn 2012) and is one of the major large scale climate controls in Europe (Dickson *et al.* 2000; Hurrell 1995), with Western Europe predominantly being controlled by westerly airflows and particularly through the passage of depressions. Hence the NAO has been chosen here as an appropriate index for cross-correlation with river flow in attempting to link patterns of river flow with regional and possibly global climate change.

The NAO climate index used here was downloaded from KNMI Climate Explorer (2011), as monthly values. The monthly time series for both data were investigated for similarities in trend using Microsoft Excel (2003), from these data the December to February flow displayed a similar pattern and trend to the preceding September to November NAO index (NAOI).

Formal cross correlation of the December to February flow and preceding September to November NAOI were tested by multiple time series autocorrelation & partial autocorrelation using R statistical software (Cran 2011).

Identifying potential driving mechanisms

The NAO lies within the lower part of the North Annular Mode (NAM) and similarly provides a measure of the manifestation of the north-south shifts in atmospheric mass between the polar region and mid latitudes. Some evidence points towards external factors as contributing to the

behaviour of the NAO e.g. volcanic aerosols (Robock 2000; Shindell *et al.* 2001) and silicic ash (Gerstell *et al.* 1995) injected into the stratosphere and also fluctuations in solar activity (Haigh and Blackburn 2006; Hoyt and Schatten 1997; Rind *et al.* 2008; Swingedouw *et al.* 2011). The link between the NAO and solar activity lies through the NAM which has been significantly correlated to solar variability (Ruzmaikin and Feynman 2002), thus changes to the NAM will be reflected in the NAO and hence the climate of Europe, with consequences to river flow. Sunspot indices (as an indicator of the magnitude of solar activity) are used here in cross-correlation with river flow to link patterns of flow with external drivers through the NAO.

Sunspot indices were downloaded as monthly data from the Solar Influences Data Center (SIDC) (2011) for the time series 1749 – 2011. Exploratory data analysis used R statistical software to plot autocorrelations (ACF), partial autocorrelations (PACF) and spectral density analyses to identify the length of periodic or quasi periodic cycles present within the sunspot data. This methodology was important to first establish what cycles may be expected to manifest in the river flow and was an initial step in linking, via cross correlation with the river flow series, locally driven variability to external forces.

Microsoft Excel (2003) was used to investigate which monthly data displayed the solar signal and by what approximate time lag the river data responded to the signal. Following this, the strength of the relationship between sunspot cycles and river flow data was investigated by formal cross-correlation by multiple time series autocorrelation & partial autocorrelation using R statistical software (Cran 2011).

2.1.3. Results

Identifying the presence of general trend and pattern

The river Eden annual flow (Figure 2-1) exhibited an apparent trend for a gradual increase in both total flow and mean flow (cumecs) over the time series. Investigating this apparent trend further using the nonparametric Mann-Kendall monotonic trend test, based on the null hypothesis of no trend present, returned a 2 sided p value of 0.014. On this evidence, the null hypothesis may be rejected. This robust simple test shows strong evidence for a change in the long term mean between 1968 and 2010.

The linear regression for Figure 2-1 has a gradient which gives a rate of change per year as 0.71 cumecs averaged over the whole time series; the R^2 value for the regression is low, resulting from the variability in the time series and hence confidence in the regression is low.

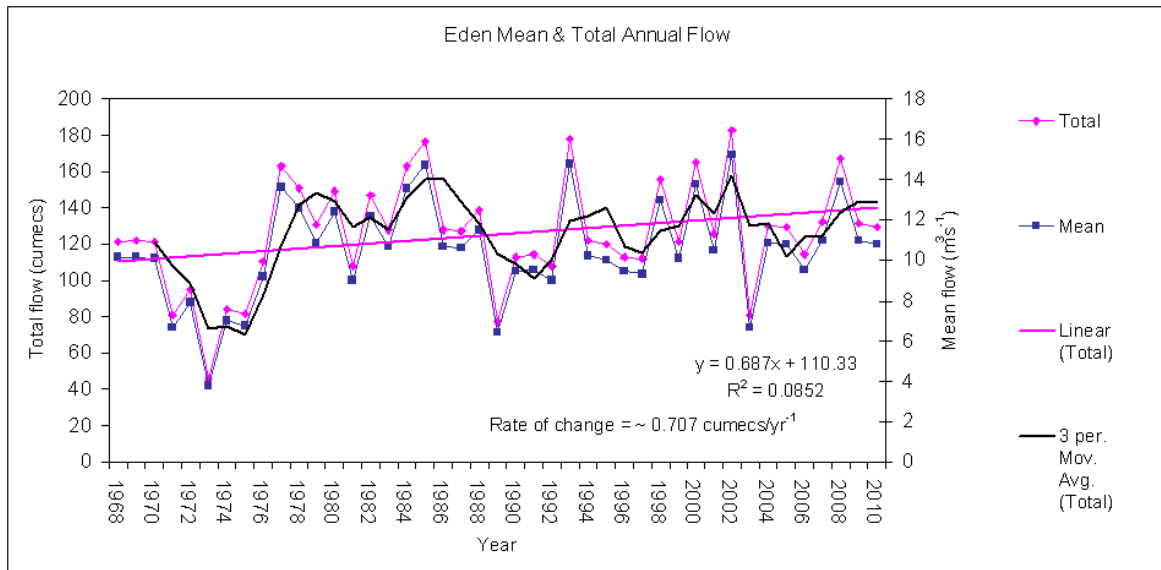


Figure 2-1: River Eden mean flow (ms^{-1}) and total annual flow in cumeecs.

Linear regression between precipitation (mm) and river flow (cumeecs) (Figure 2-2) returned an R^2 value of 0.87, providing evidence of a good correlation between the two variables and inferring the majority of precipitation leaves the catchment as runoff rather than being retained within the catchment.

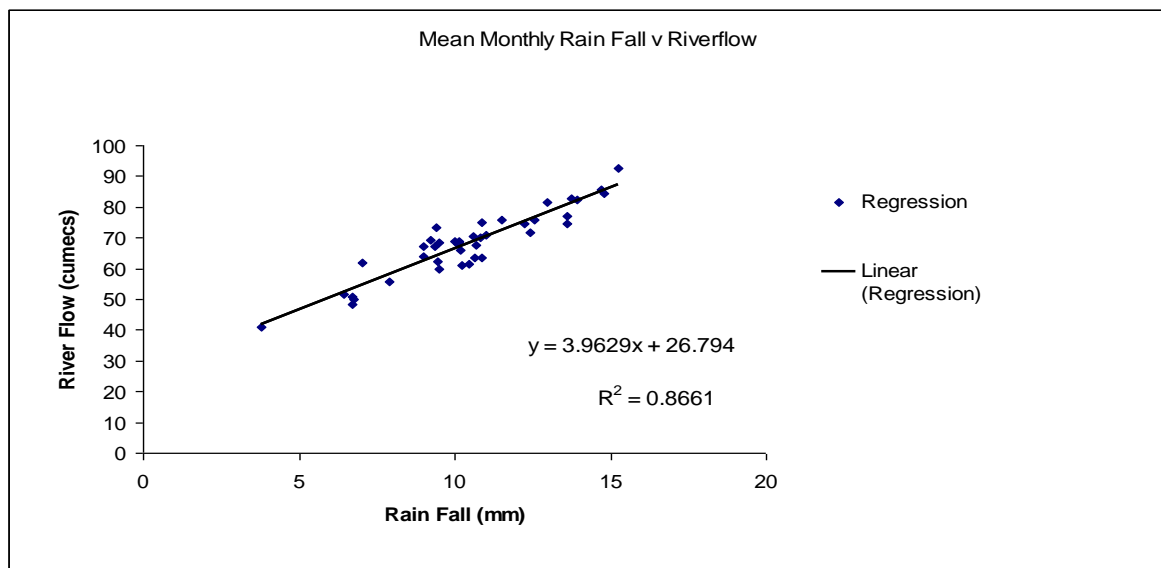


Figure 2-2: Regression analysis between monthly rainfall and river flow to identify catchment residence time.

The variability in flow is presented in Figure 2-3; here the data are expressed as anomalies deviating from the long term mean, clearly there are periods of above average and below average flow, with 1968-1976 exhibiting for example as flow below the long term mean and 1977-1988 above the long term mean. There is some evidence that there may be quasi-periodic behaviour in the time series.

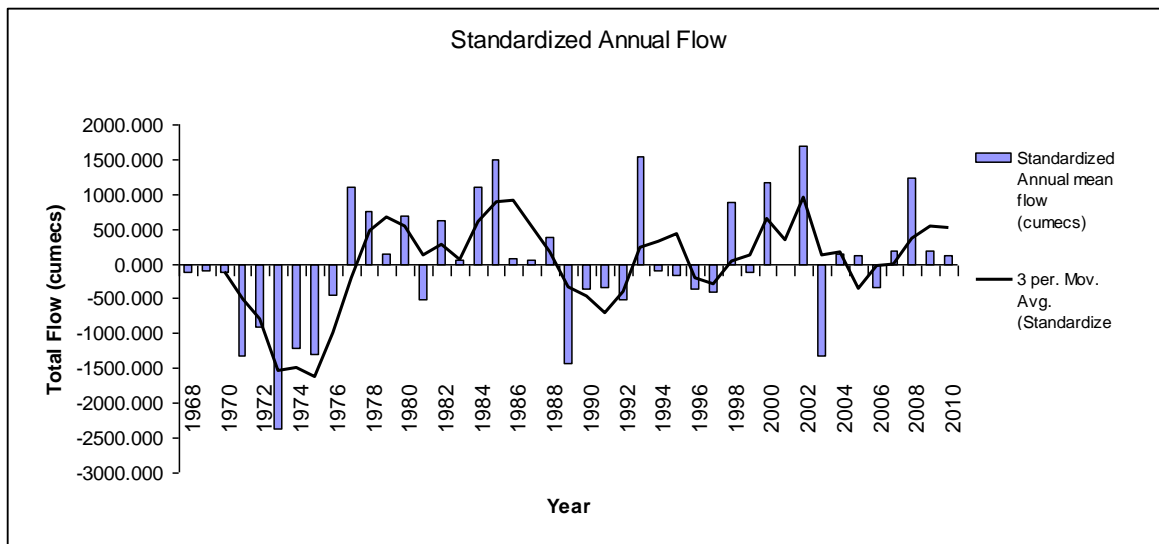


Figure 2-3: Anomaly data for river Eden annual mean flow (cumecs), highlighting periods of above and below average flow conditions.

Extreme flow (either high or low) is investigated in Figure 2-4, where a general upward trend in all three series is observed. A similar pattern to the de-trended anomaly data in Figure 2-3 is evident particularly in the 10% exceedance for extreme high flows.

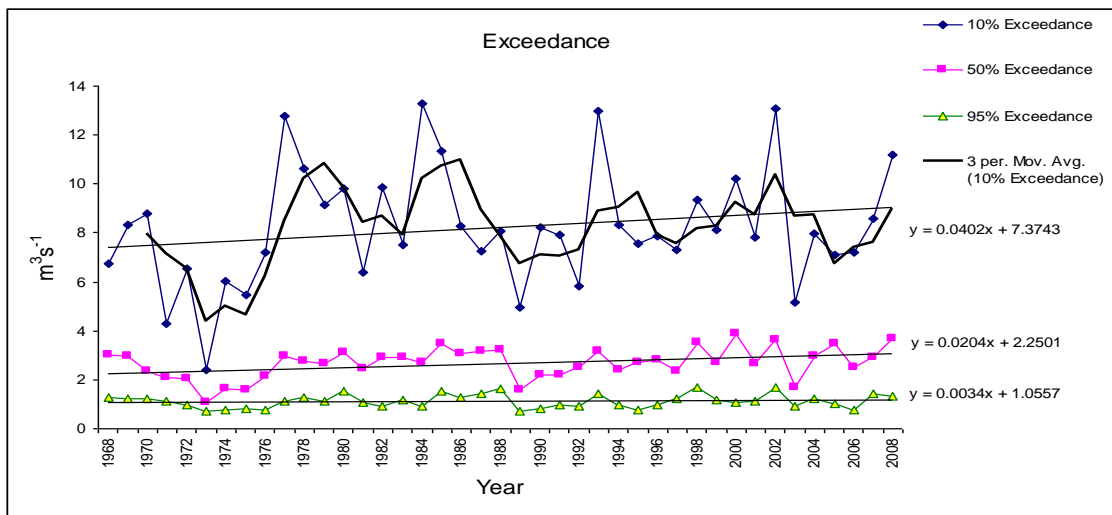


Figure 2-4: River Eden exceedance data for the period 1968 – 2009.

Long term trend is investigated in further detail (Figure 2-5), by deconvolving the various components of seasonality, trend and the remaining irregular portion, which is the ‘first difference’ stationary data. The trend component appears to display some pattern from 1976-1990 and again 1990-2004 (both periods of 14 years). The time series for the river Eden is quite short, thus to place these results in perspective the trends for the rivers Tay and Thames have been plotted (Figure 2-6).

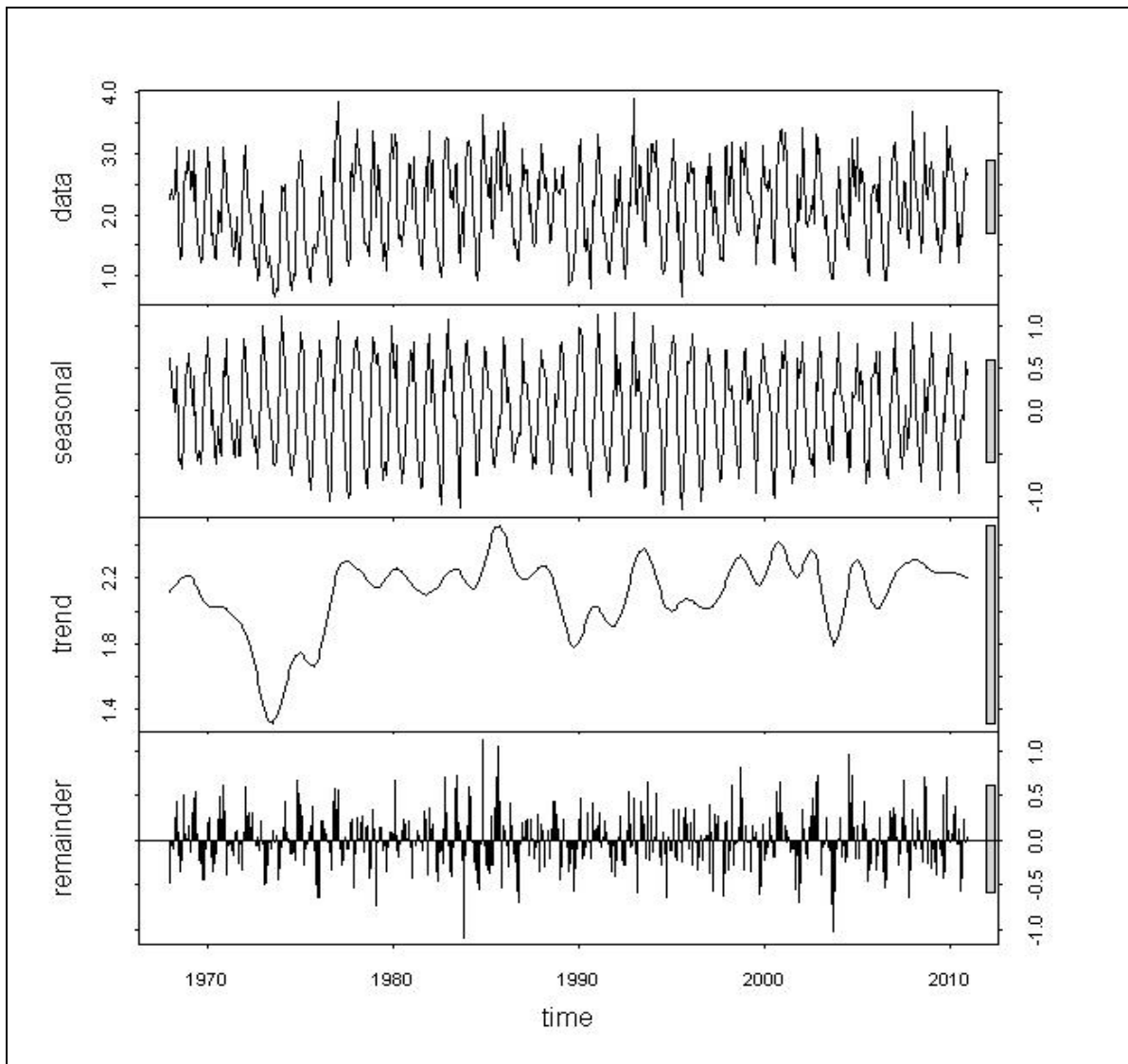


Figure 2-5: Decomposition analysis of the Eden flow time series. The rectangular scale bars represent equal vertical scale between plots. Y scales are all the log of flow in cumecs.

For all three time series the mean is non stationary, giving an upward variably positive trend, the Mann-Kendall trend test for the Tay and Thames ($p=0.002$ and $p= 3.28 \text{ e-}06$ respectively) reveals >95% significance for a positive trend.

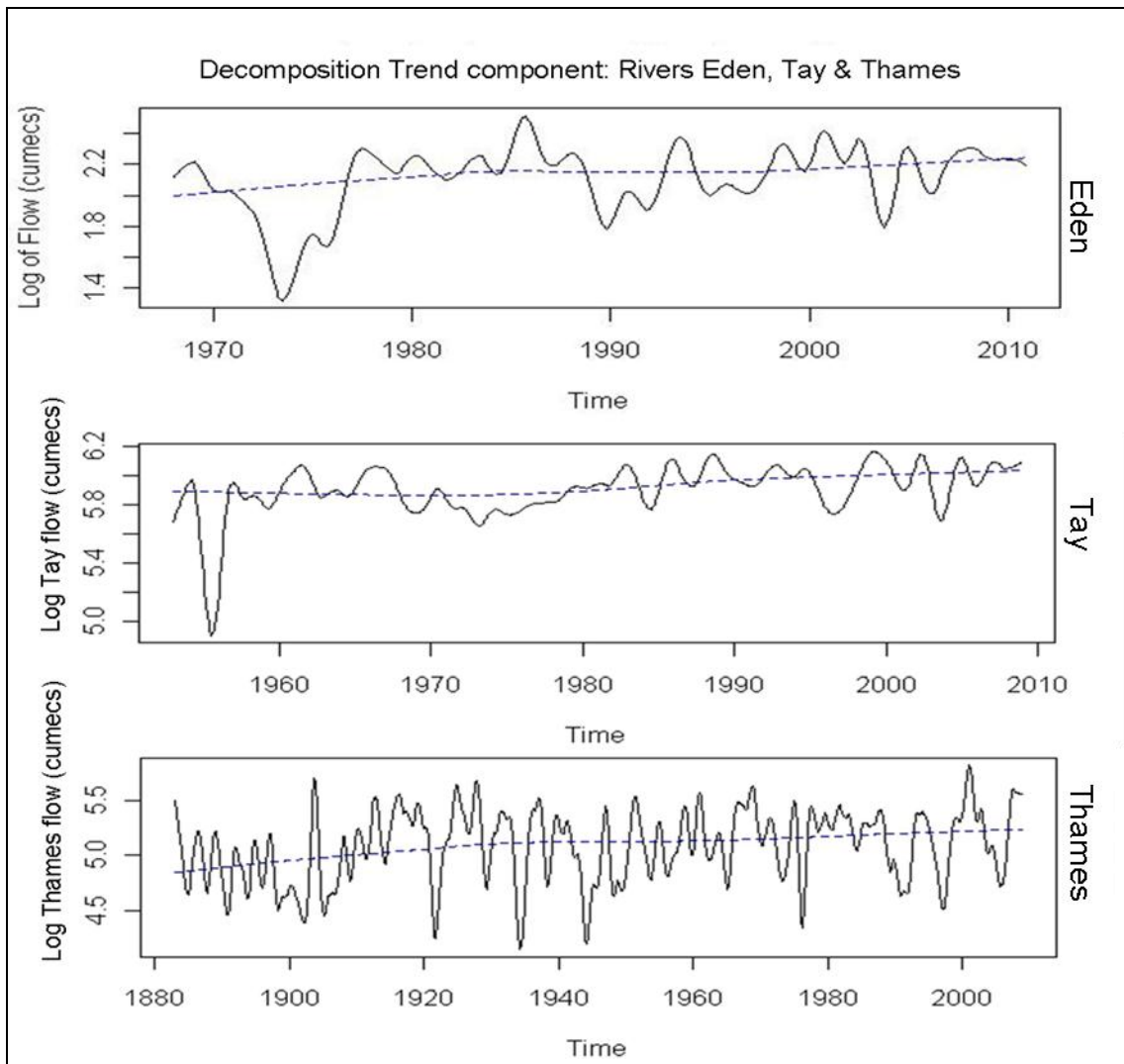


Figure 2-6: Decomposition trend components for the rivers Eden, Tay and Thames, with Loess regression trend line (dashed blue).

Investigation of the residual component from the decomposition analysis explores potential periodicity in the time series (Figure 2-7), the residual component is used here as it represents the first difference stationary data with seasonality and trend removed. Two methods are applied auto and partial autocorrelation (ACF, PACF) and spectral density analysis. The ACF has lag intervals of 10 years and the data are input as a monthly time series from 1968-2009, thus adding the lag to the beginning of the time series enables identification of a particular peak within the series. The first lag at zero is ignored as it does not represent real data. The red dashed line represents the 95% significance level. In general, distinct cycles are not seen, inferring there is a lack of serial dependence despite the presence of some large peaks. However there is evidence for dampened irregular oscillations being present with ACF values which are significant corresponding to the following dates; 1969, 1970, 1971, 1972, 1973, 1975, 1976, 1978, 1982, 1986, 1987, 1991, 1992, 1996, 1997 and 1999.

The partial autocorrelation (which shows significance once the dependence on previous cycles has been accounted for) similarly reveals a lack of obvious cycles. The significant peaks are presented in dominance order showing strongest influence and correspond to the following dates; 1969, 1973, 1970, 1972, 1976, 1975 and 1974 respectively. From the PACF, 1973 now stands out as a strongly significant lag, where previously its dominance was masked by other lags.

For both autocorrelations no singular cyclical periodicity is evident throughout the time series, however there are a number of significant (>95%) peaks at variable periodicity that persist and clearly have an influence over the time series. The relevance of these dates will be discussed later.

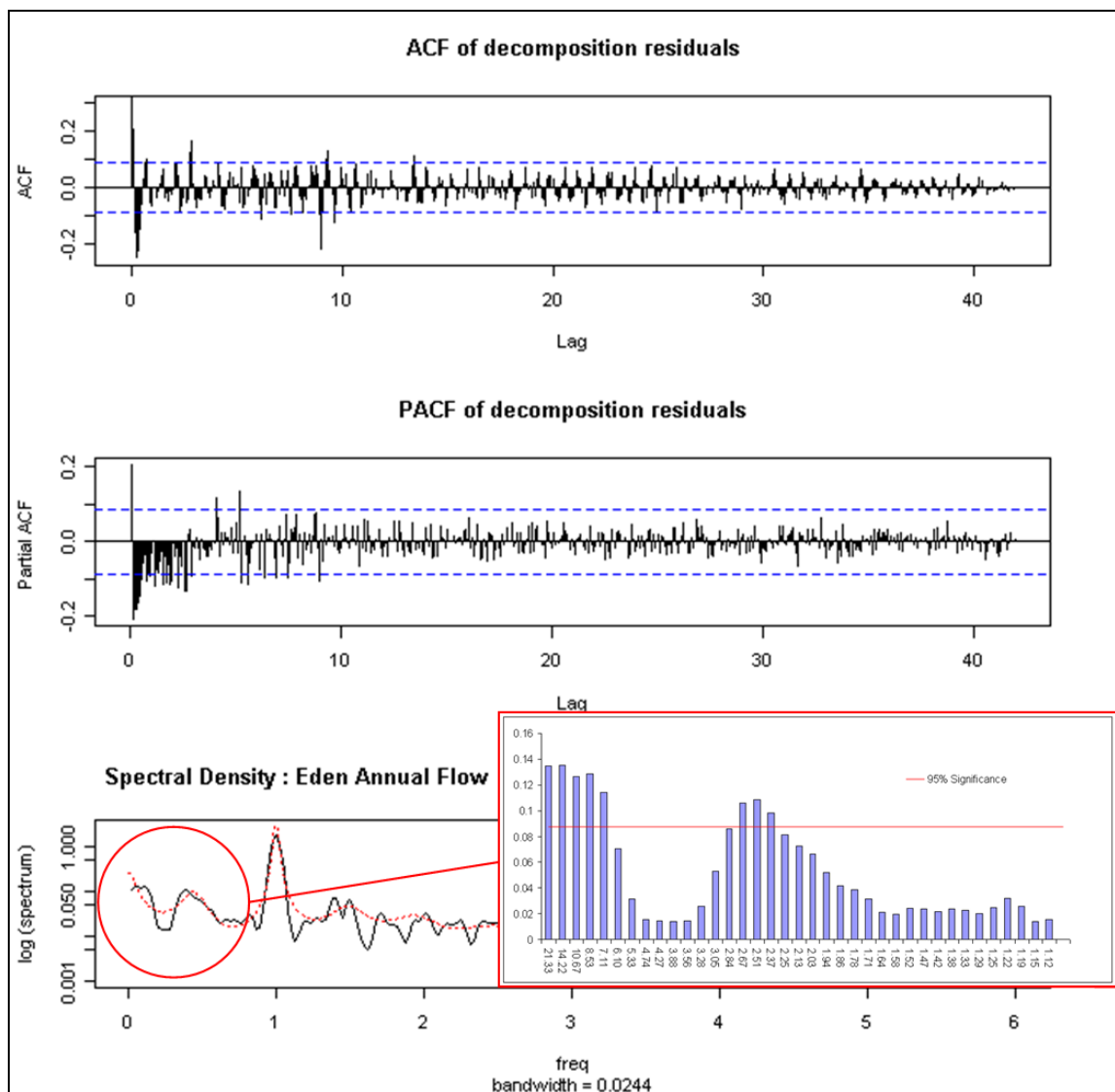


Figure 2-7: Autocorrelation, partial autocorrelation and spectral density analysis of river Eden flow (cumecs). Data is a monthly time series from 1968-2009. (R Statistical software).

In Figure 2-7 (bottom) the spectral density analysis identifies periodicity in the frequency domain; values exceeding the annual cycle are to the left of the main peak (at frequency 1) and are in

decreasing order, this zone has been enlarged to reveal more detail (highlighted red), the periodicity in years is taken from the reciprocal of the frequency. Significant (95%) periodicity is present where values exceed the red line and here reveal the presence of significant period lengths of 21.33, 14.22, 10.67, 8.53, 2.67, 2.51 and 2.37 years. Again the relevance of these period lengths will be discussed later.

The same analyses were repeated for the river Tay (Figure 2-8), having a longer time series and hence potentially able to reveal longer serial events.

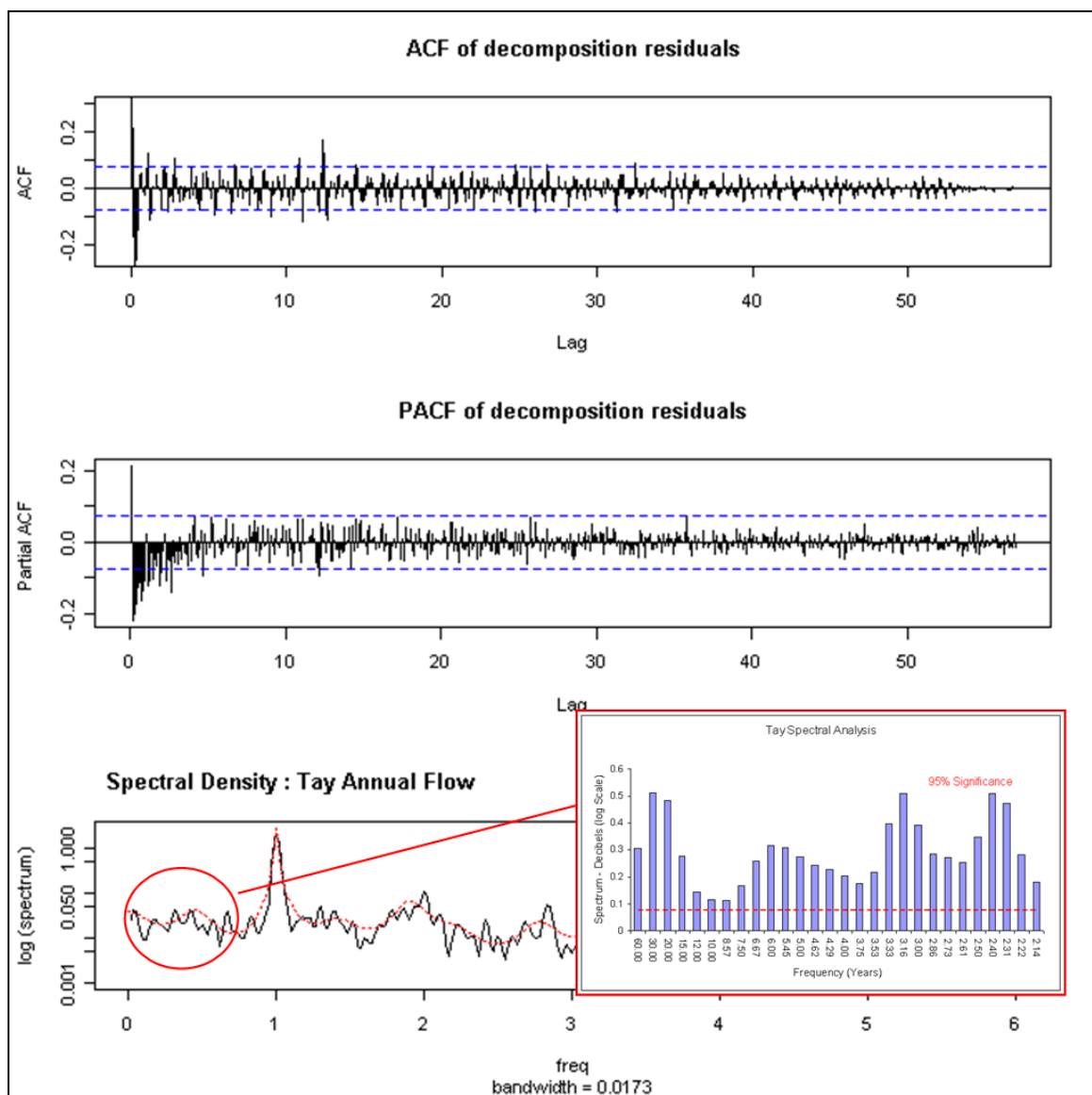


Figure 2-8: Autocorrelation, partial autocorrelation and spectral density analysis of river Tay flow (cumecs). Data is a monthly time series from 1968-2009. (R Statistical software).

Despite the longer record the ACF for the river Tay similarly reveals a lack of distinct serial cycles. Though once again there is a presence of significant peaks throughout the time series. ACF values

which are significant correspond to the following dates; 1953, 1954, 1955, 1957, 1959, 1961, 1963, 1964, 1965, 1967, 1969, 1971, 1977, 1978, 1979, 1983 and 1986.

The PACF for the river Tay displays significant peaks, in order of dominance, for the following dates; 1954, 1955, 1957 and 1965. The spectral density analysis for the river Tay reveals significant frequencies corresponding to period lengths of; 30, 20, 15, 12, 10, 8.57, 7.5, 6.67, 6, 3.16 and 2.4 years.

Analysis of the river Thames (Figure 2-9) also gave various significant oscillatory peaks which dampen out throughout the time series. ACF values which are significant correspond to the following dates; 1883, 1885, 1889, 1893, 1895, 1896, 1900, 1901, 1904, 1911, 1912, 1913, 1916, 1922, 1923, 1929, 1933 and 1960. After which the peaks dampen out below the significance level.

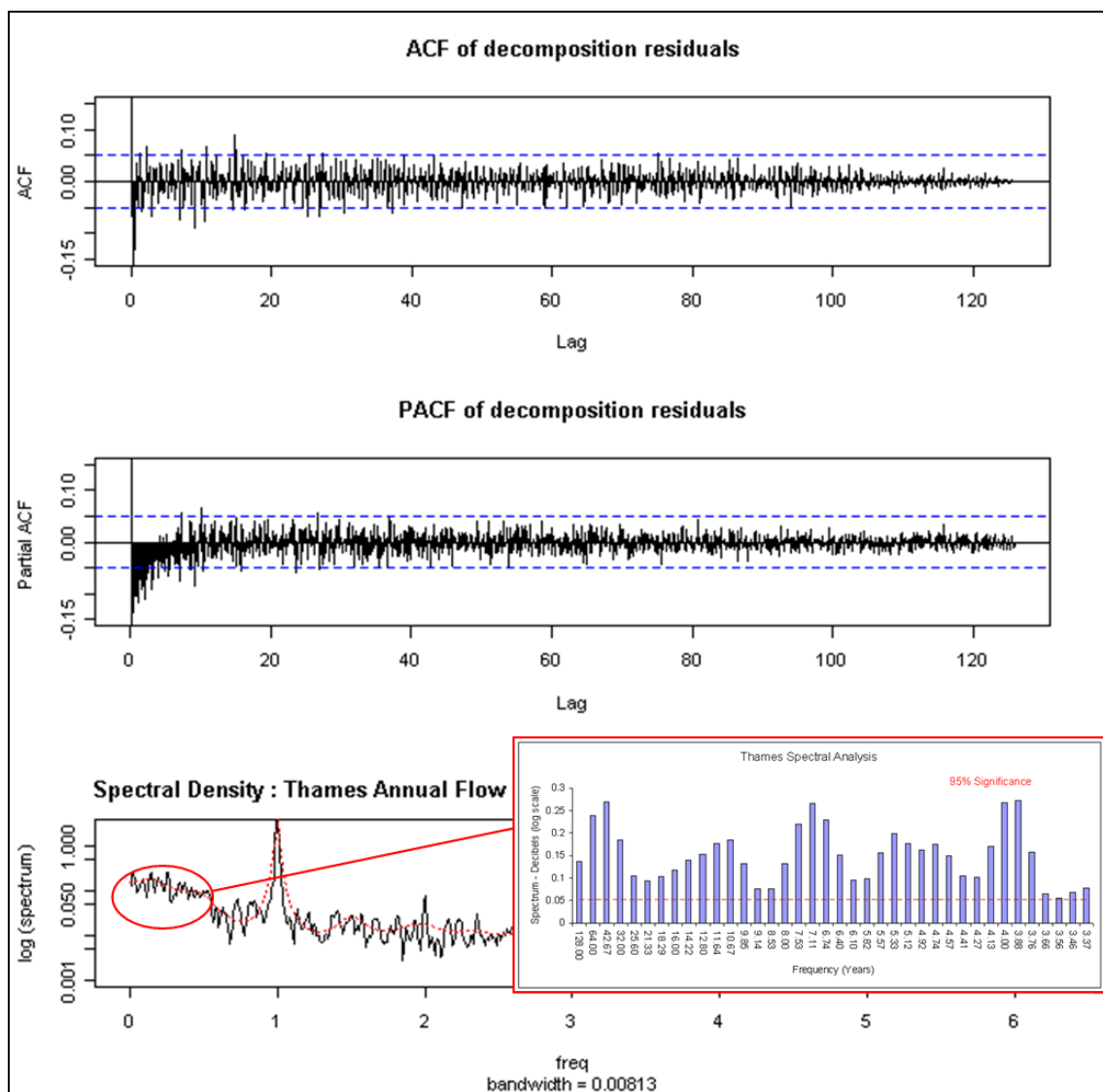


Figure 2-9: Autocorrelation, partial autocorrelation and spectral density analysis of river Thames flow (cumecs). Data is a monthly time series from 1968-2009. (R Statistical software).

The PACF has significant peaks which correspond to the following date; 1883, 1885, 1889, 1892, 1893, 1898, 1906, 1909 and 1919.

The spectral density analysis for the river Thames reveals many significant frequencies corresponding to period lengths of; 64, 42.67, 32, 25.6, 21.3, 18.29, 16, 14.22, 12.8, 11.64, 10.67, 9.85, 7.11, 5.33, 4.7, 4 and 3.88 years respectively. Of these the most dominant peaks are 42.67, 10.67, 7.11 and 3.88 years.

Despite the differences in catchment properties, the spectral density analyses for all three time series share certain similar significant frequencies, particularly between the Eden and the Thames sharing 21.33, 14.22, 10.67 and 7.11 year significant frequencies. The spectral density analysis for the Tay exhibits approximately similar frequencies of 20, 15, 10 and 7.5 years. Additionally the Tay and Eden share a ~ 8.5 year significant frequency.

Identifying changes to seasonality of flow

Using traditional basic long term mean trend analysis, the percentage of annual flow occurring during winter months for the river Eden (Figure 2-10) presents a positive linear regression, inferring some positive trend ($0.08\%/yr^{-1}$). The R^2 value is very low, reflecting high variability and little confidence in the regression. Investigating the trend formally using the simple non-parametric Mann-Kendall trend test, reveals no evidence for a positive trend ($\tau = 0.004$, 2-sided p value = 0.886).

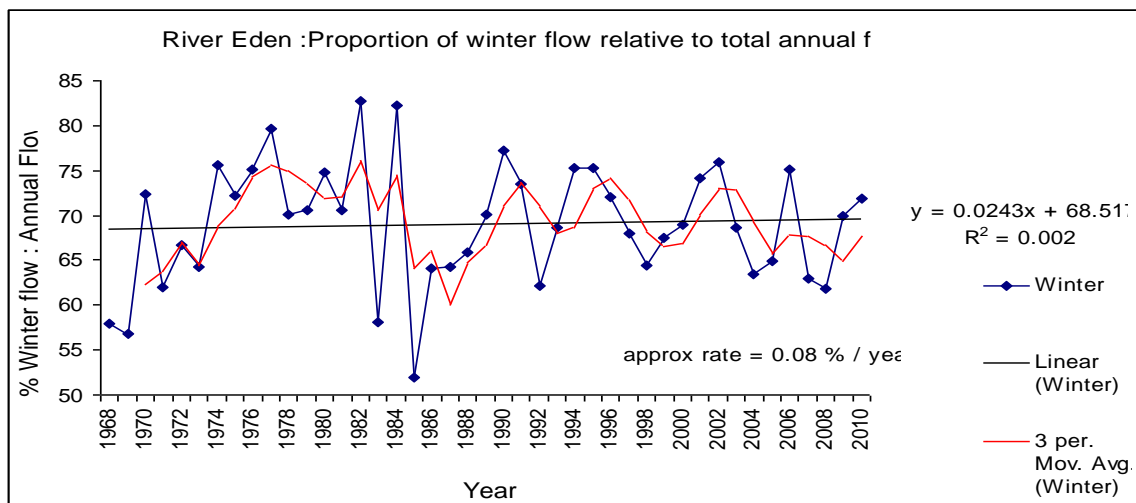


Figure 2-10: The proportion of river Eden winter flow relative to the total annual flow (1968 – 2010).

Displaying the percentage of ‘winter’ flow as anomaly data (Figure 2-11) highlights further the variability of flow over time; cycling between distinct periods of above (e.g. 1974-1994) and below average (e.g. 1995-1998) winter flow, however without regular cyclical periodicity as inferred from the autocorrelation analyses. From figures 2-10 and 2-11, it is difficult to discern if there may be

potential monotonic trend over a longer time frame, or whether the hint of trend is figment result of sampling a particular section of variable flow (i.e. from a trough to a peak).

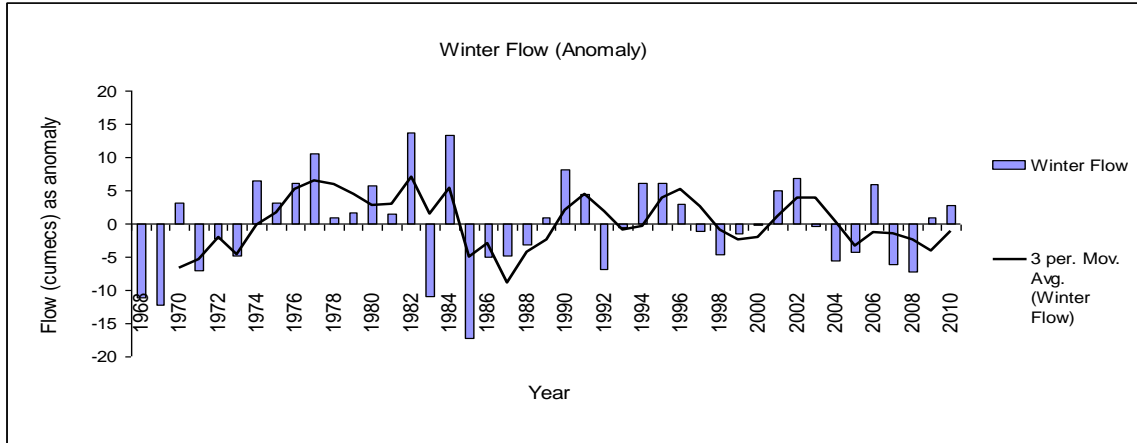


Figure 2-11: Percentage of river Eden ‘winter’ river flow (January to March & October to December) expressed as anomaly data.

Using the longer timer series for the neighbouring river Tay to further explore potential monotonic trend (Figure 2-12) in the percentage of winter flow; the simple linear regression inferred some positive trend ($0.08\%/yr^{-1}$) however the R^2 value is similarly low reflecting high variability and little confidence in the regression. Investigating the trend more formally with the non parametric Mann-Kendall trend test reveals some evidence for an increase in winter flow ($\tau = 0.153$, 2-sided p value = 0.094).

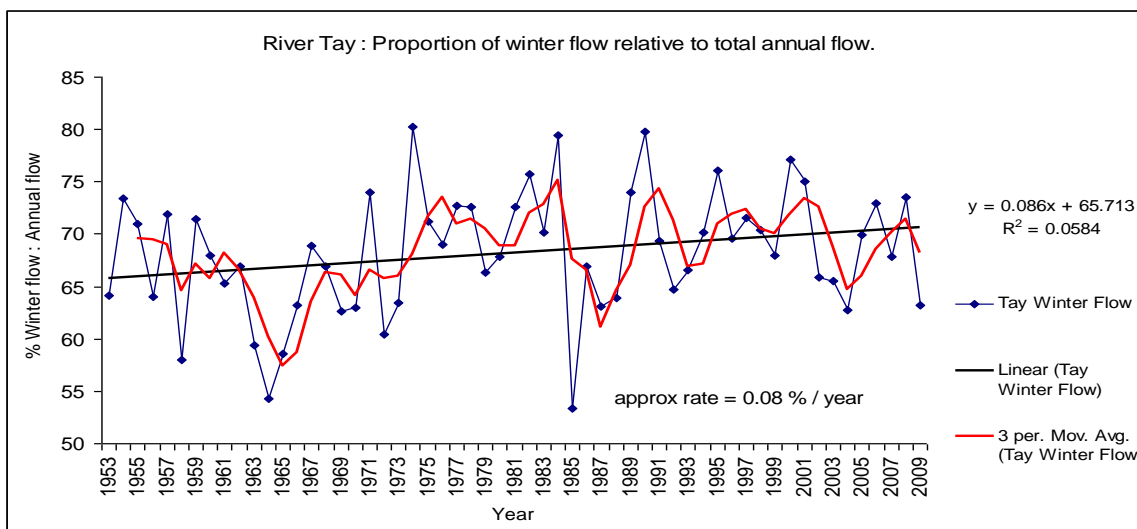


Figure 2-12: Proportion of river Tay winter flow relative to the total annual flow from 1953 – 2009.

The anomaly data for the Tay (Figure 2-13) presents very similar patterns of distinct periods of above and below average winter flow (e.g. 1974-1994 as positive anomalies and 1995-1998 as negative anomalies).

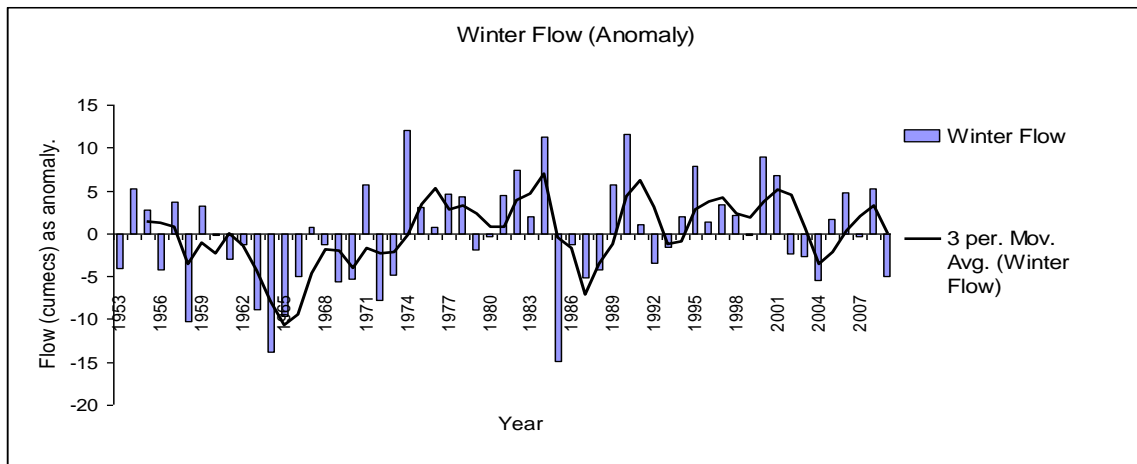


Figure 2-13: Percentage of river Tay 'winter' river flow (January to March & October to December) expressed as anomaly data.

The Thames data were not plotted here for comparison as it is difficult to compare the Thames seasonality to the Tay & Eden due to the differences in regional weather, in part driven by the local topography. However, the Mann-Kendall trend test for the river Thames identifies evidence of trend, but as a negative one ($\tau = -0.141$, 2-sided p value = 0.020).

Identifying links to the NAO

The NAO exerts its greatest influence particularly during the winter months, shaping northern hemisphere precipitation and temperatures (Hurrell 1995; Hurrell and Deser 2010). Hence, here the December to February flow for the river Eden was compared for similarity in trend and variability with the preceding September to November NAOI (Figure.2-14). Reasonable similarity is apparent, with distinct pattern in both time series for above and below average conditions.

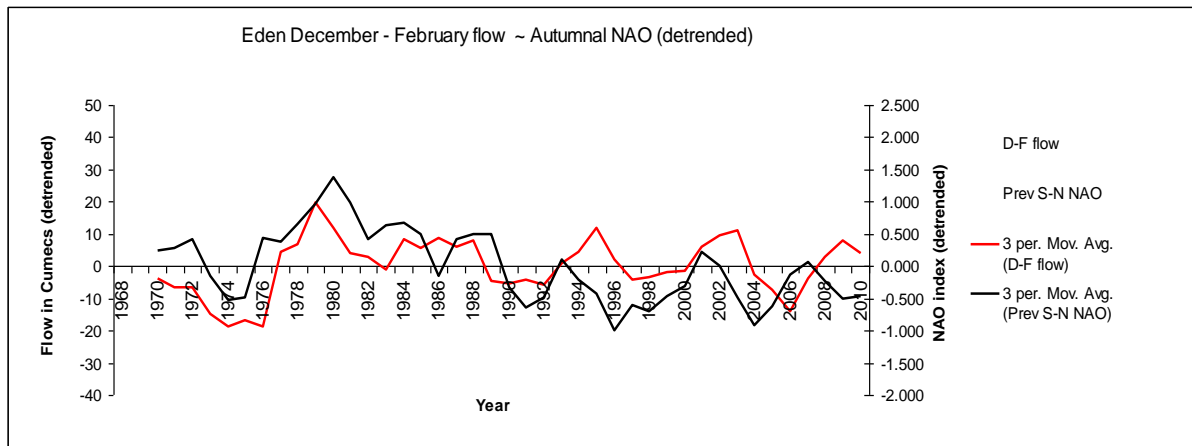


Figure 2-14: River Eden December to February river flow (cumecs) plotted with the preceding September to November NAO index (smoothed).

The relationship between the two time series was formally investigated using cross-correlation (Figure.2-15) where data were input as de-trended anomaly data (1969-2010). The figure presents the individual autocorrelations (top left for the winter river flow, and bottom right for the autumnal NAOI) and also the cross-autocorrelations with 'flow' being controlled by the NAO (top right) and also for the opposite condition of the NAO being controlled by 'flow'. The dashed blue line represents the threshold for 95% significance with peaks that reach beyond the dashed lines represent significant values. The cross-correlation of the NAO controlling for river flow indicates there is a significant relationship between the two time series.

For the individual December-February river flow autocorrelation, a 95% significant peak is seen at lag 4 and at a lower significance of 90% at lag 12. The individual autocorrelation for the NAO similarly has a 95% significant peak at lag 4 and further 90% significant peaks at lags 1 and 8.

In the cross-correlation, with the NAO controlling for river flow (Figure 2-15 top right), lag 1 corresponds to the year 1969 and is significant at 95%. The NAO also correlates to river flow at >90% significance at lags 8 and 13, which correspond to the years 1981 and 1983 respectively. Additionally lag 8 lies just below the 90% significance threshold for the NAO controlling river flow and corresponds to the year 1976.

These analyses were repeated for the river Tay winter months, which held most similarity between October and March.

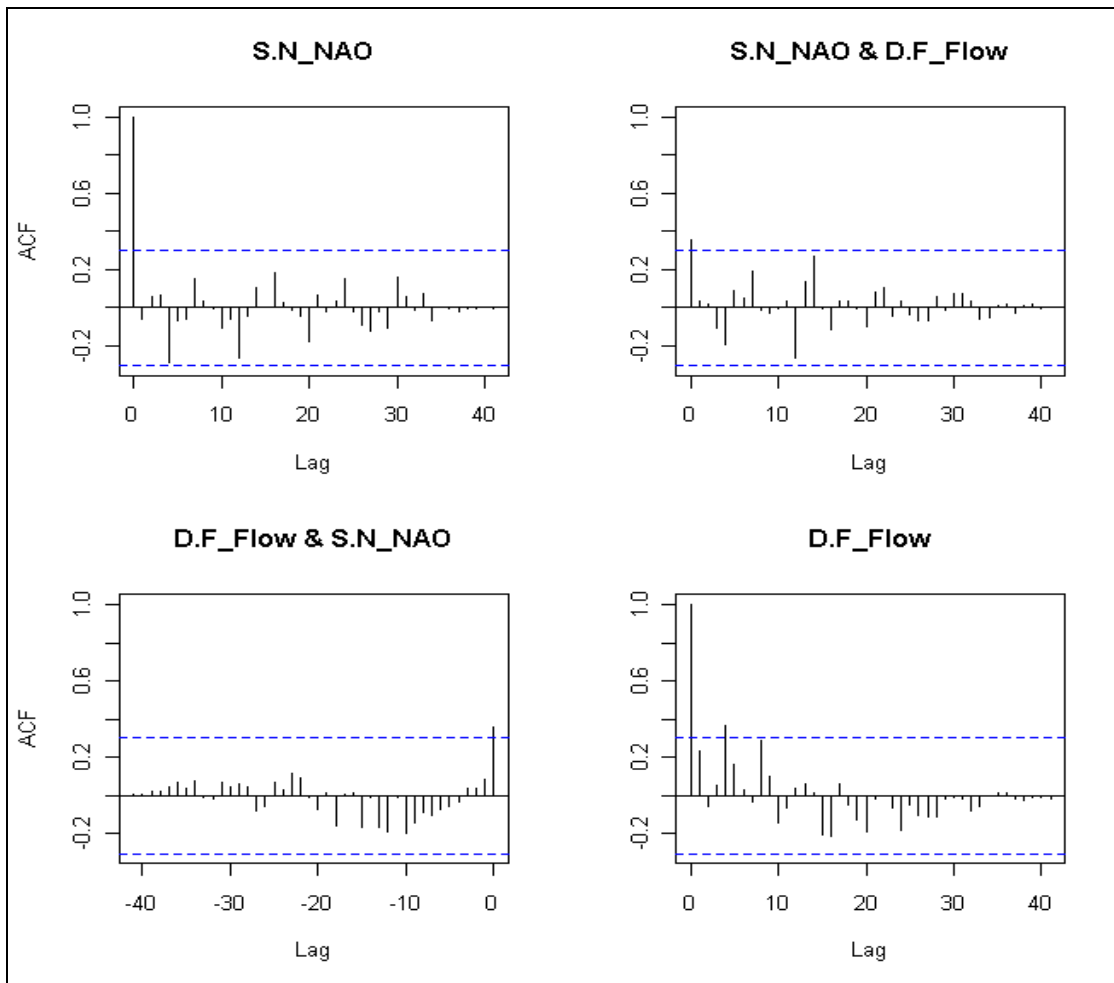


Figure 2-15: Cross correlation between the de-trended December to February (D.F) river flow (cumecs) and the previous Autumn NAO index September to November (S.N).

The general pattern of both October to March river flow and the NAOI (Figure 2-16) are once again very similar when smoothed over several years

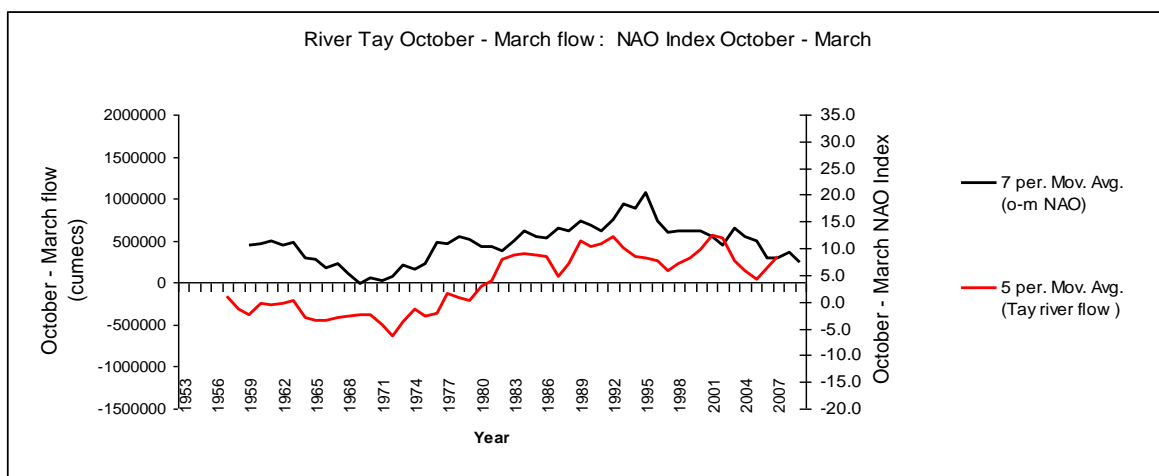


Figure 2-16: River Tay October to March river flow plotted alongside the October to March NAO index (smoothed).

. The time series displays a 'low' around 1970 and a 'high' around 1994, before descending again towards 2008, thus showing a long period oscillation with a wave length of approximately 40 years.

The cross-correlation analysis, with the 'NAO controlling for river flow' (Figure 2-17 top right), reveals significance (>95%) over multiple lags; lag 1, 8, 9 and 11 corresponding to the years 1954, 1961, 1962 and 1964 respectively. Bottom left, 'Flow controlling for the NAO', displays an ~35 year period which is not significant. The partial autocorrelation failed to identify any further significant lags.

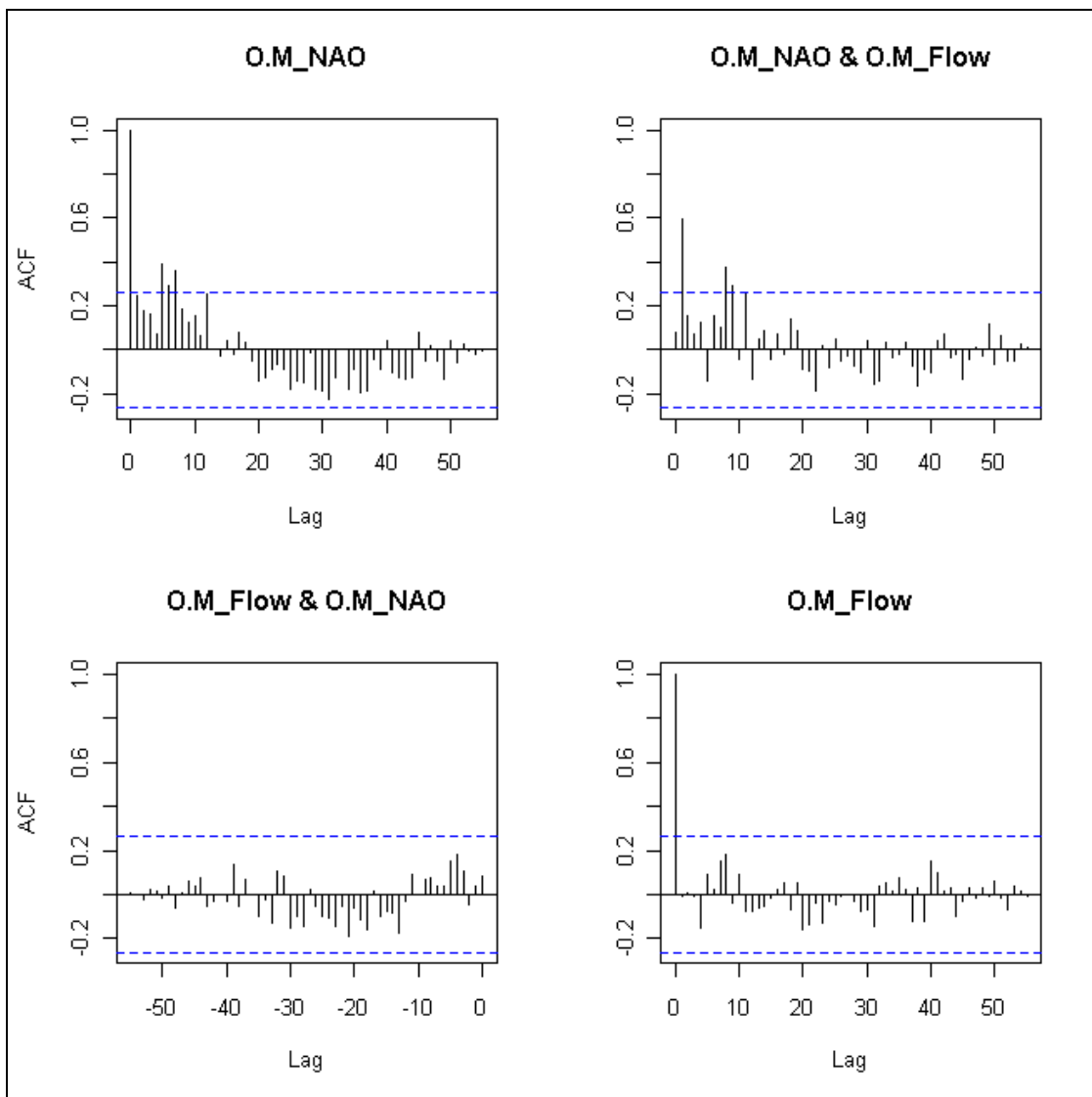


Figure 2-17: Cross correlation between the de-trended October to March river Tay flow (cumecs) and the de-trended October to March NAO index (1954-2008).

Identifying the relationship to sun spot activity

Initially the shortened times series, 1970 - 2011 of sunspot numbers (Wolfe number) was used to identify the dominant Schwabe cycle length, since cycle length varies through time, thus for comparison with the shorter river time series mean period length was required. Figure 2-18 displays the autocorrelations and spectral density analysis, lag intervals represent 10 years and the 95 % significance thresholds are shown as the blue dashed lines (red for the spectral density insert).

The ACF identifies clear significant cycles, which approximate to 10-11 years in length. The partial autocorrelation displays the strength of the first cycle and revealing lags 1, 2, 3 and 9 as significant.

The Spectral density analysis for this shortened time series reveals the dominant cycle to be 10.8 years (Figure 2-18, bottom right insert).

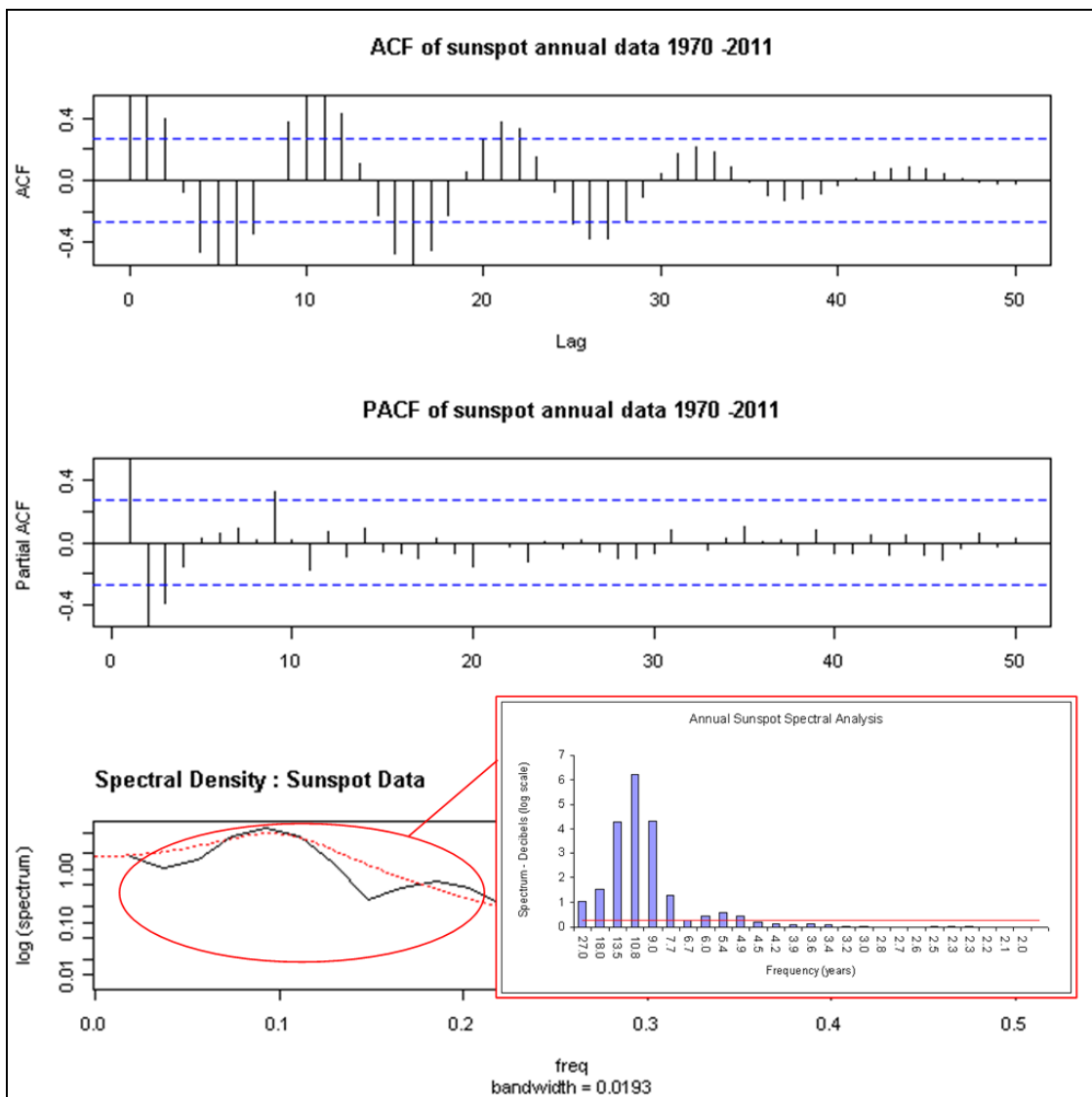


Figure 2-18: Autocorrelations and spectral density analysis of the sunspot time series (1970-2011).

Investigating higher order periodicity within the entire sunspot record (Figure 2-19) the autocorrelations display lag intervals of 50 years and similarly the thresholds for 95% significance are shown as blue dashed lines (red for the spectral density insert).

The ACF shows two levels of oscillations which dampen out along the time series. Dominant periods are at approximately 11 years and 90-100 years. The PACF reveals a strong significant (95%) cluster of peaks around 1757, followed by lone peaks at 1766, 1806, 1834, 1869, 1894 and 1962 (90% sig). The spectral density analysis (Figure.2-18 bottom) identifies the dominant periods present as 11.25, 10.8, and a longer periodicity of 90, 67.5, 135 and 54 years (in dominance order).

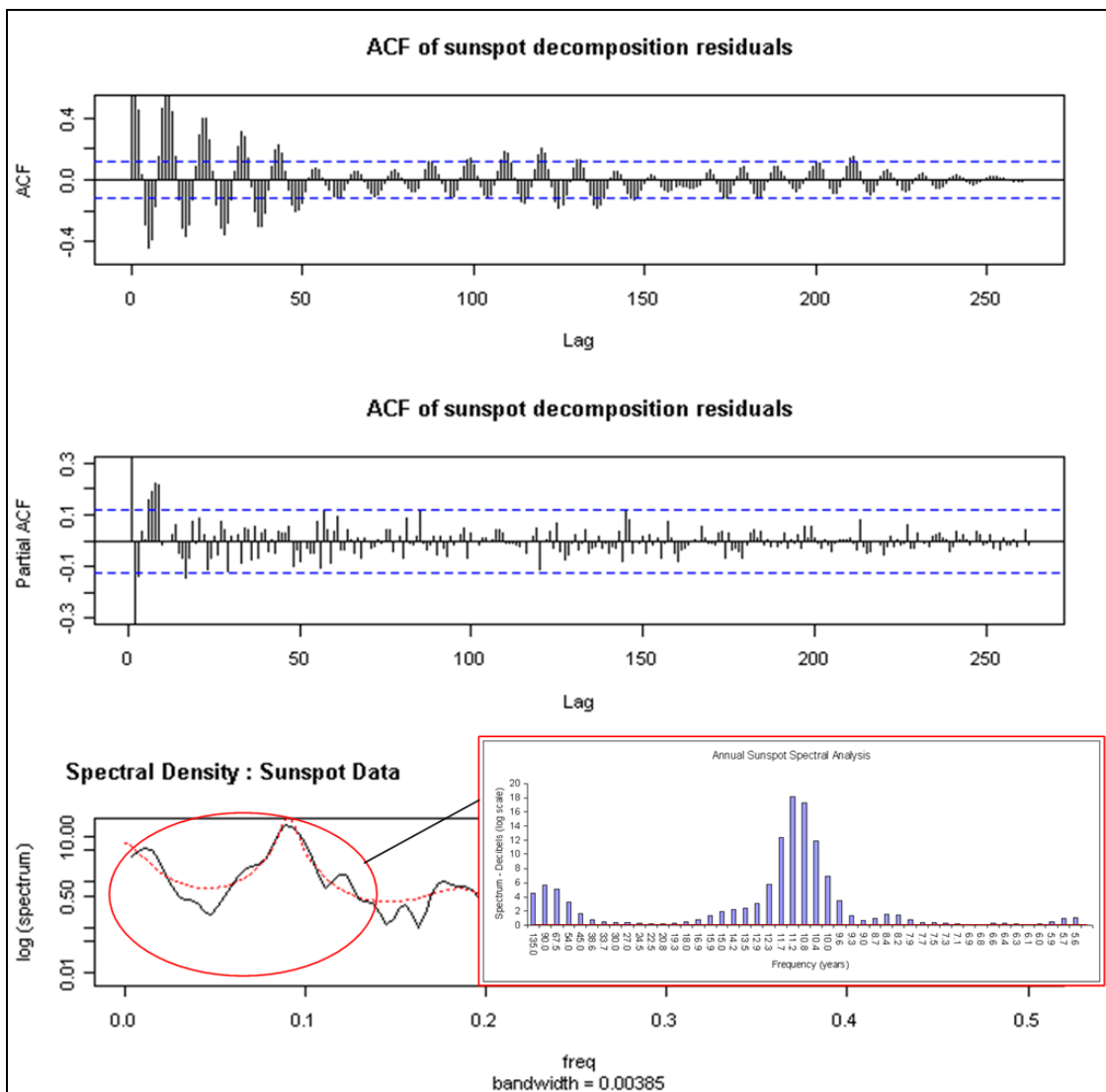


Figure 2-19: Autocorrelation, partial autocorrelation and spectral density analysis of 'Sunspots'. Data is an annual time series from 1749-2011 (R Statistical software).

Figure 2-20, displays the similarity in pattern between the rivers Eden and Thames smoothed mean annual flow in cumecs (as anomaly data), alongside the annual sunspot time series. Despite the catchment differences between the Eden and the Thames, there is reasonably similarity in pattern of flow. However, the Eden series is too short to identify long wavelength signals, thus the Thames data having similar trend, was used for cross correlation with the sunspot data to link flow pattern to sunspot activity.

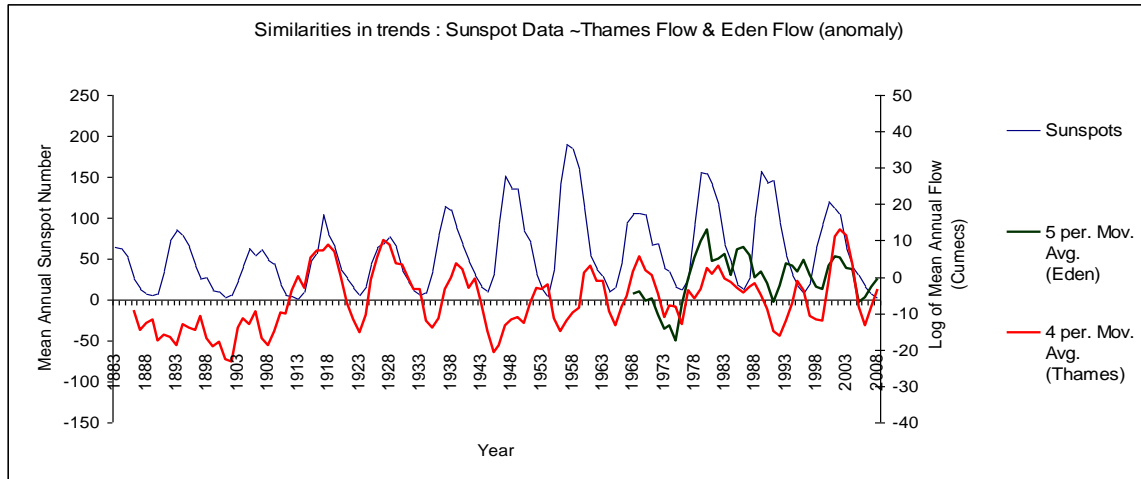


Figure 2-20: A comparison between pattern in the smoothed annual mean flow data for the rivers Eden and Thames, with the sunspot numbers (Wolfe number). From 1953-2008.

For a visual assessment for cross correlation, the Thames data was adjusted for a lag of 9 years and plotted against the Wolfe sunspots (Figure 2-21). This shows a match between flow peaks and solar maximums equating to the Schwabe approximate 11 year cycles. The general upward trend of the Thames data, infers a match to the longer frequency periods present in the sunspot data. The two series were then formally tested for cross-correlation to reveal any shared periodicity (Figure 2-22)

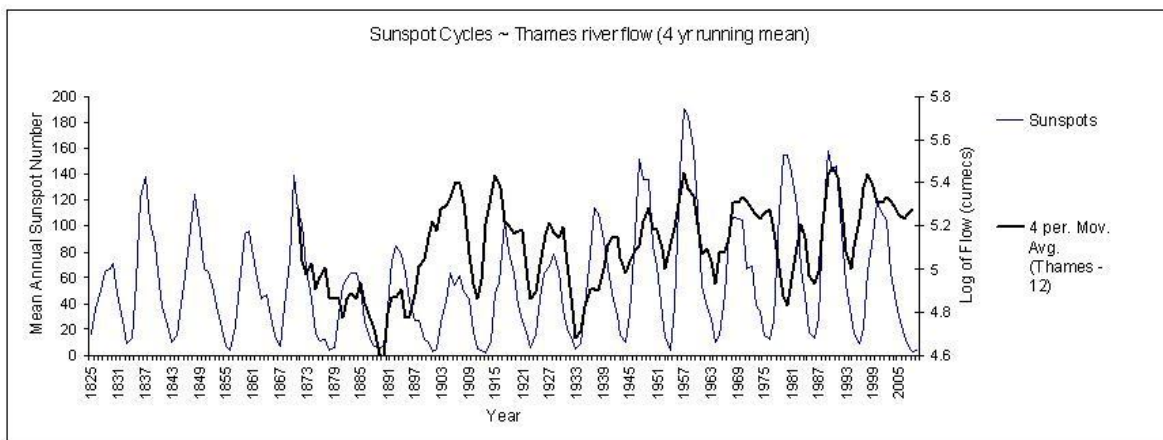


Figure 2-21: A comparison between the smoothed and lagged Thames annual flow data (cumecs) and the Wolfe sunspot time series.

The cross-correlation analysis, with the 'sunspots' controlling for river flow (Figure 2-22 top right), reveals a significant relationship (>95%) over multiple lags; the interval between clusters of lags represents the approximate 10-11 years Schwabe sunspot cycles, however there is also evidence for a longer period influence.

Clearly river flow cannot influence sunspot activity (Figure 2-22, bottom left) hence the correlations reflects the periodicity received from the sunspot cycle (again the interval between clusters is ~11 years)

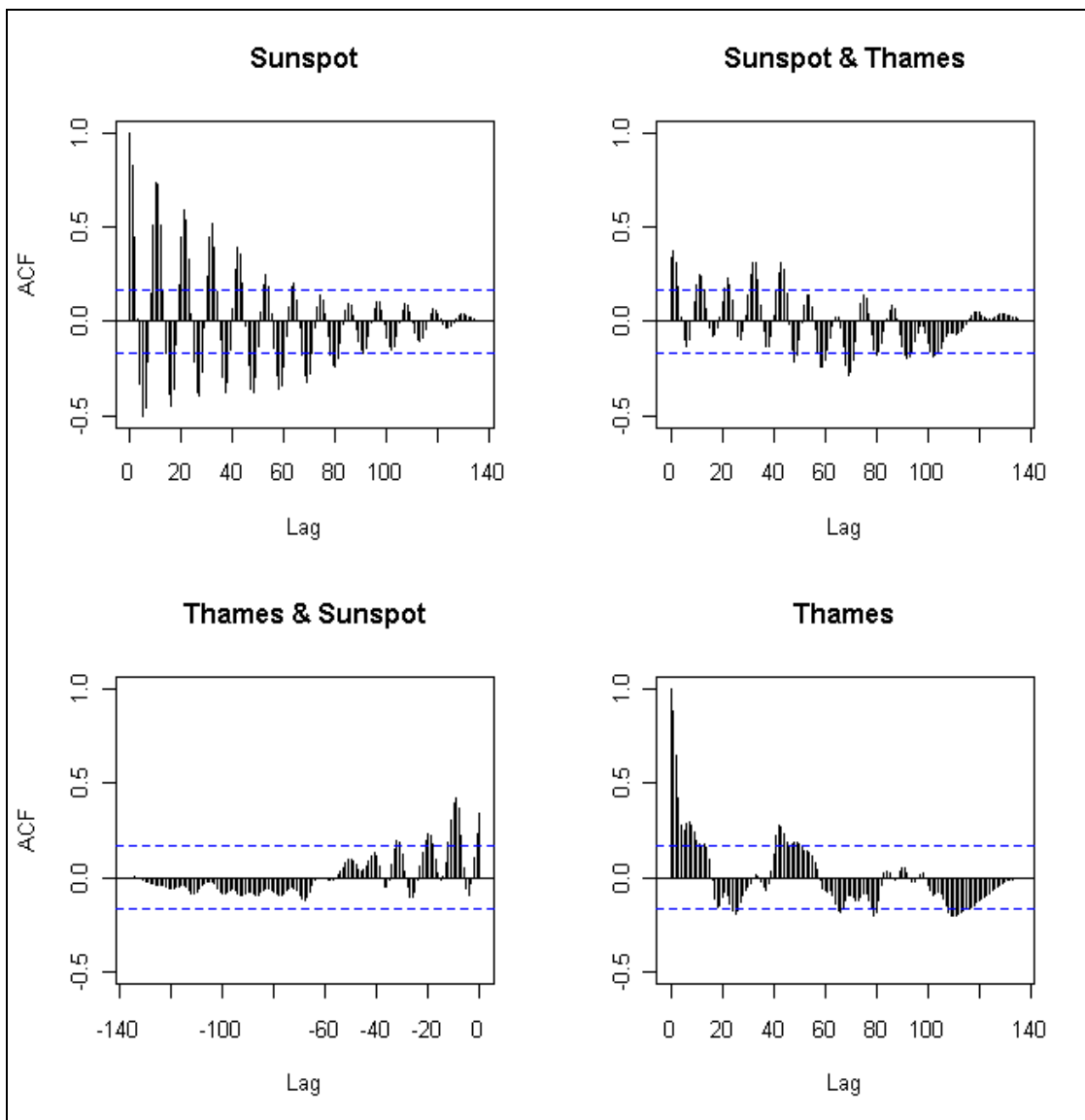


Figure 2-22: Cross-correlation between the smoothed and lagged Thames annual flow data (cumecs) and the Wolfe sunspot time series. Top left & bottom right are the individual autocorrelations. Top right shows the sunspots 'controlling for river flow' and bottom left shows the river flow 'controlling for sunspot activity'.

Figure 2-22 gives clear evidence for a significant (95%) relationship between the smoothed river Thames flow and the Schwabe solar sunspot cycles and provides reasonable evidence for a higher order periodicity influencing the flow time series also.

2.1.4. Discussion

Identifying the presence of general trend and pattern via EDA

The EDA identified significant (95%) positive trend in total annual river flow for all three times series and indicated potential patterns to be present, however no clear cyclical dependency was identified by the autocorrelations. Significant peaks (95% & 90%) were present, exceeding the long term mean variability. Re-plotting the autocorrelations and labelling the significant peaks (Figure 2-23) with potential external forcing mechanisms enables an understanding of why no singular serial periodicity (or sinusoidal behaviour) was identified by the autocorrelation.

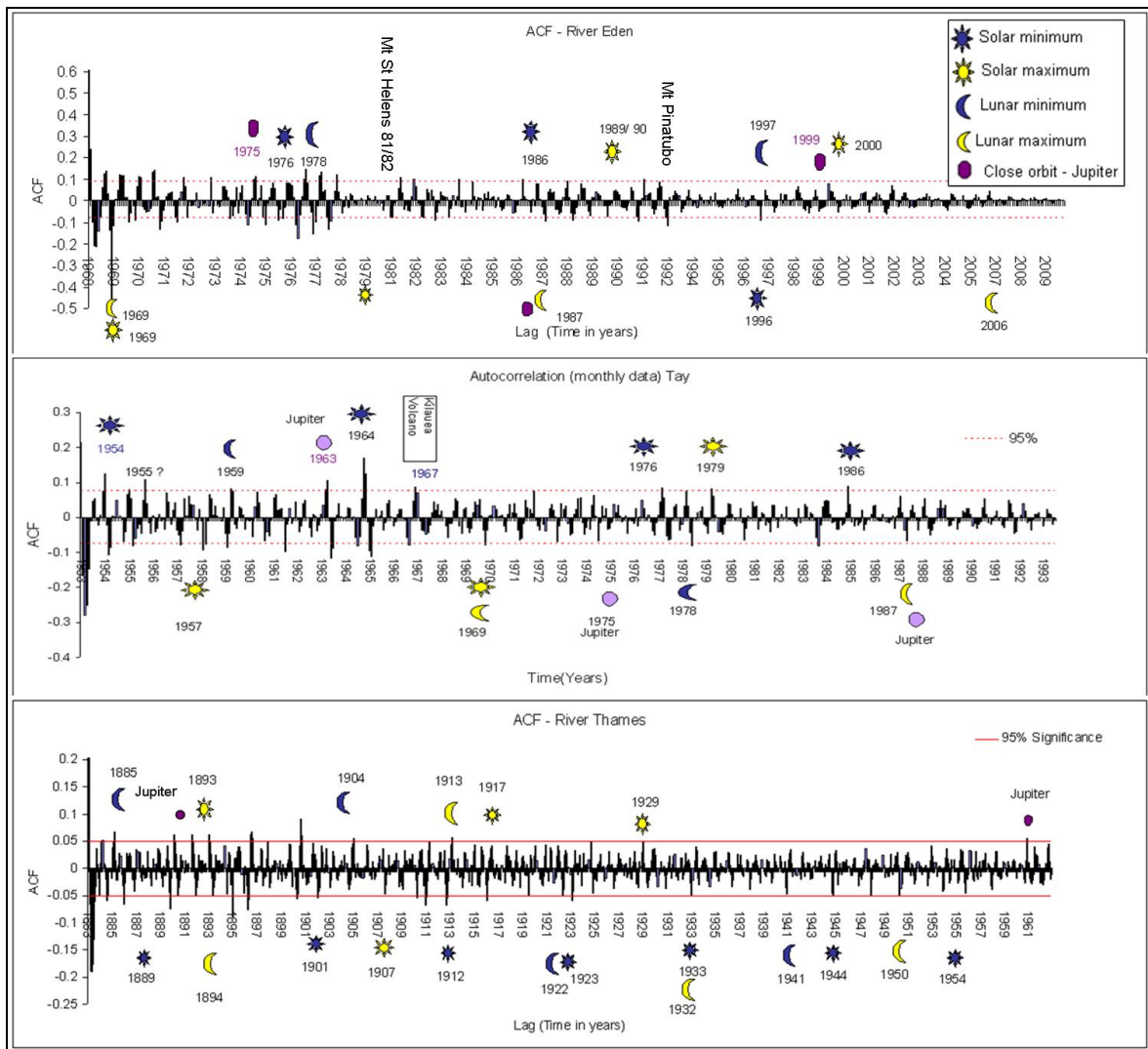


Figure 2-23: Interpretation of the significant autocorrelation peaks for the rivers Eden, Tay and Thames.

Convolving several cycles with differing phase and amplitude is likely to result in a non regular wave form, very similar to what is observed from the river flow time series. Clearly there is a strong influence from several internal and external sources that have either directly or indirectly caused significant variability to the river flows. It is known that volcanic eruptions have caused climate perturbations e.g. Mt St Helens (Hobbs *et al.* 1982), El Chichon (Gerstell *et al.* 1995; Labitzke *et al.* 1983) and Pinatubo (McCormick *et al.* 1995) and depending upon their latitude and type of eruption, their impacts can mimic different phases of the NAO in the northern hemisphere (Robock 2000) and thus cause changes to precipitation and consequential river flow. Increasing recent research has also refocused on the solar control of climate (Ineson *et al.* 2011; Mufti and Shah 2011; Rumaikin 2007; Scafetta 2010; Swingedouw *et al.* 2011) and with linking modulation of the NAO to solar cycles (Alvarez-Ramirez *et al.* 2011; Kodera 2002). Similarly, lunar and planetary orbital influences have also been shown to impact on climate variability (Davis and Brewer 2011; Haigh *et al.* 2011; Yndestad 2006) with consequences to river flows (Prokoph *et al.* 2012).

The spectral density analyses for all three time series share certain similar significant frequencies (despite the differences in catchment, river management and regional topography) particularly between the Eden and the Thames sharing 21.33, 14.22, 10.67 and 7.11 year significant frequencies. The 21.33 period stands out as approximate to the Hale magnetic cycle and the 10.67 within the range of the Schwabe sunspot cycle. The significant frequencies for the Tay are ambiguous and may reflect modification by abstraction & usage for hydroelectric operations, though exhibiting approximately similar frequencies of 20, 15, 10 and 7.5 years. Additionally the Tay and Eden share a ~ 8.5 year significant frequency, which corresponds approximately to the lunar perigee.

Only by viewing the collective time series do the periodicities present begin to show clarity; the Eden's highest frequency is 21.33, halving this we find the third frequency present 10.67. Similarly taking 14.22 and halving this we get 7.11, it is possible then that some of the identified frequencies may be harmonics. Figure 2-24 presents some of the identified harmonics for the three river flow series.

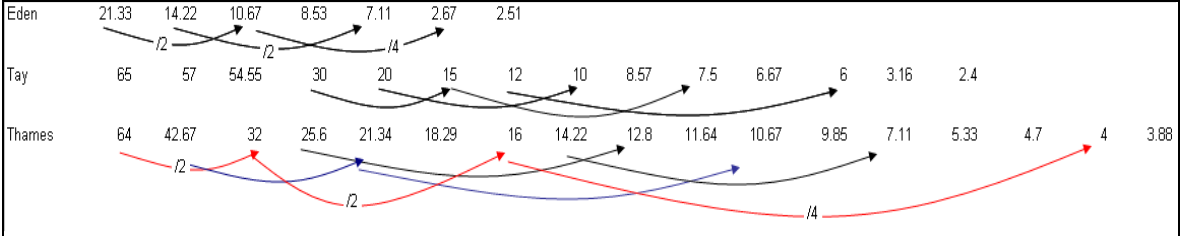


Figure 2-24: Harmonic periods. For each of the three rivers, the significant (95%) frequencies identified from the spectral density analyses are given, below each are arrows which show either the second or fourth order harmonic.

Some of these shared frequencies have been identified in other times series, for example Kondrashov (2005) found the following frequencies; 64, 19, 12, 7, 4.2 and 2.2 in the extended Nile river records (A.D 622-1922), of these frequencies he remarks that the 7 year period is 'most striking'. Similarly the 7 year period is identified in the North Atlantic sea surface temperature instrumental records (Moron *et al.* 1998), in sea surface pressures (Da Costa and De Verdiere 2002), within the NAOI (Berger 2008; Wunsch 1999) and in combined solar influences with El Nino in stream flow across southern Canada (Fu *et al.* 2012). Berger (2008) proposes the approximate 7 year period "to be a result of energy capture from internal oscillations into periods resulting from interference of solar and tidal cycles near 11 years", however looking closely at figures 2-23 and 2-24 the 7 year period is evident as the interval between the solar maximum and the following solar minimum. The 14.22 years period present in both the Thames and the Eden may therefore be the harmonic frequency of the 7.11 primary period. The 10.67 periodicity equates to the common length of the Solar Schwabe cycle and it is postulated that this gives rise to the harmonic frequency of 21.33 in both the Thames and the Eden, however this cycle may also be interpreted as approximate to the 22 year (Hale magnetic) double sunspot cycle. The 8.53 period (8.57 Tay) remains unidentified however it is a close approximation to the lunar perigee of 8.85 years.

The river Thames data show higher order periodicity of 18.29, 32, 42.67 and 64 years; two of these frequencies (18 and 33 years) have been found in a 300 year tree ring time series at the Kola Peninsula Russia (Raspopov *et al.* 2000) and were attributed to combinatory frequencies of the solar cycle, contributing to the Bruckner climatic cycle (fundamental climatic oscillations of 30-45 years). The Bruckner climatic cycle has also been identified within instrumental air temperature data for Padua Italy (Camuffo and Bertolin 2012) at a period of 35.8 years. Similarly Hernandez (2010) through spectral analyses of the diatom oxygen isotope ratios of a sedimentary record in northern Chile found "significant ENSO frequencies of 7-9 years and 15-17 years, and periodicities of the solar activity cycles such as 11 years (Schwabe), 23 years (Hale) and 35 years (Bruckner)". Whether the 32 and 42.67 Thames frequencies are attributed to the Bruckner climatic cycle remains unclear, as too with the origin of the 64 year period. There is also ambiguity regarding the ~18 year periodicity identified by Raspopov *et al.* (2000) as a 'combinatory frequency', since the cycle length may also be interpreted as derived from the lunar nodal period of 18.6 years, which plays an important role in affecting weather (Camuffo 2001; Cervený and Shaffer 2001; Yamazaki *et al.* 2012), impacting on atmospheric (and ocean) tides potentially affecting the spatial distribution of pressure systems and thus rainfall.

Identifying changes to seasonality

No evidence in significant (95%) positive trend for increased river flow occurring more seasonally (i.e. during the more wintery months of January-March and October–December) was observed for the river Eden ($p=0.886$), however the river Tay data provided some evidence of positive trend ($p=0.094$). Conversely a negative trend was presented by the Thames data ($p=0.020$), although it is difficult to compare between the Thames seasonality and the Tay and Eden, due to the differences in regional weather, in part driven by the local topography.

The combined data from these analyses give uncertainty in trend in seasonality of flow; this may be a result of the methodology used being inadequate to capture potential trend, or to the length of the time series indicating apparent trend by not fully capturing long period oscillations. Certainly the anomaly data identified distinct periods of above and below average winter flow, which points towards oscillatory behaviour, however whether the oscillations are about a constant or non constant mean remains ambiguous and requires further investigation.

Identifying links to Climate indices

Similarity in both trend and variability was apparent when comparing the smoothed time series between the River Eden December to February annual flow and the preceding September to November NAOI; formal cross-correlation of these time series identified significant shared lags corresponding to 1969 (>95%), 1981 & 1982 (>90%) and 1976 (~90%). Although the cross-correlation is testing for one input controlling for the other, here the NAOI is indicating a climate pattern which is itself driven externally. The shared significant lags correspond to specific events; 1969 is both the Schwabe solar maximum and also the lunar nodal maximum, each have been found to modulate the North Atlantic Oscillation (Alvarez-Ramirez *et al.* 2011; Koderá 2002) and lunar cycles in influencing tidal levels (Eliot 2012; Haigh *et al.* 2011). The peaks for 1981 and 1982 are likely resulting from climatic perturbation by two sequential volcanic eruptions which injected large volumes of ash and sulphur dioxide into the lower stratosphere; Mt St Helens in 1981 and El Chichon in 1982, causing cooling of the northern hemisphere (McGuire 1999). The final significant lag period corresponds to 1976, this was a Schwabe solar minimum and also a close orbit by Jupiter, which would have similar impacts to the lunar maximum.

Similarly the smoothed October to March time series for both the River Tay annual flow and the NAOI presented the same general pattern of trend and variability to each other; cross-correlation of these two series identified 4 significant (>95%) shared lag periods corresponding to the following dates; 1954, 1961, 1962 and 1964 respectively. Of these, 1954 and 1964 are both solar minima, though interestingly the 1957 solar maximum is not seen, perhaps not showing in the winter records so well due to the Earth's inclination from the Sun at this time of year. The periods for 1961 and 1962 remain unidentified though may be attributed to Hawaiian eruptions of Halemaumau and Kilauea at this time.

Both the Rivers Eden and Tay have significant cross-correlations with the NAOI, linking regional weather to northern hemisphere climate patterns with periods that are consistent with solar and lunar cycles and additionally from the influence of major volcanic eruptions altering stratospheric/tropospheric circulation.

Identifying potential driving mechanisms

The most influential potential driving mechanism consistently present in the data analyses so far, seems to be the Schwabe solar cycles and thus these were further investigated for their periodicity and cross-correlated with the Thames annual river flow data, being the longest flow record. The length of the Schwabe sunspot cycles varies widely through time, but averages over the total record approximately 11 years. The variability is important and matching the length of the sunspot time series with that of the flow record enables the identification of shared periodicity. Here both long and short sunspot time series were investigated for period length. Spectral density analysis of the short (1970-2011) time series revealed the dominant frequency to be 10.8 years, which is consistent with the periodicity found in the Eden river flow data. The autocorrelations presented clear significant oscillations, which dampened out towards the end of the time series. This dampening is probably the result of the irregular nature of the cycle lengths weakening serial dependency in the autocorrelation and does not reflect the strength of the cycles. The partial autocorrelation revealed a masked frequency corresponding to 1978, which marks the lunar nodal minimum however a lack of literature for the impact of the lunar nodal cycle on the solar Schwabe cycles exists, although perhaps at lunar minima the gravitational attraction from the moon would impact less on the Sun.

Spectral density analysis of the full sunspot time series revealed two dominant frequencies; the Schwabe sunspot cycle period changed to 11.25 years (second commonest frequency 10.8 years) and a higher order frequency of 90 years was present. Three other high order frequencies corresponding to 135, 67.5 and 54 years were also identified; of these a harmonic is seen as $135/2$ being 67.5 years, which may be in turn the 5th harmonic of the 11.25 solar period. The 90 year frequency is identified as the Wolf-Gleissberg cycle, with nominal periodicity of 80-100 years (Hoyt and Schatten 1997; Yousef 2000), this cycle has also been identified in dendroclimatological Lapland tree spectra as a 90 year period (Burroughs 2003). Uncertainty remains as to the 54 year frequency seen in the full sunspot time series however this was also seen in the River Tay data. It too may represent a harmonic, as the lunar nodal period is a factor of both 90 and 54.

The autocorrelations clearly show the Schwabe and Wolf-Gleissberg cycles and additionally in the partial autocorrelation a significant (95%) frequency at approximately lag 146 corresponding to 1894, which was the lunar nodal maximum and again showing the influence of the moon on the solar sunspot cycle.

Whilst it could be argued that both solar and lunar cycles are not persistent throughout the autocorrelations and therefore may not be the primary driving mechanism for long term trend and

variability, the overall variation in the presence or strength of cycle impact on the river flow time series is dependent on the relative strength and timing of the cycle within the seasons, as well as in the actual magnitude of the cycle itself. For example, the successive lunar nodes start 0.3 years later on each cycle and therefore cause the cycle to slide from season to season. Similarly the irregularity of the solar sunspot cycles is such that their impact may too be dependent upon the season they occur in.

Further investigation of the relationship between the solar influence on river flow through plotting the smoothed annual flow of the rivers Eden and Thames alongside the solar Schwabe cycles displayed similarity in both pattern and trend over the short and long term. Shifting the Thames data for a 9 year lag improved the similarity further giving a good match between peak river flows and solar maximums; this relationship is broadly consistent with the findings of Ineson (2011), where the minimum phase of the Schwabe sunspot cycle correlated with winter climate patterns resembling negative patterns of the NAO. Accordingly solar maximums would therefore present more positive NAO phases with concomitant precipitation and river flow.

Formally cross-correlating the smoothed Thames annual river flow with the solar sunspot data provided evidence for a significant relationship over multiple lags; with significant positive correlations corresponding to solar maximums and high river flow and vice versa.

Clearly solar and lunar cycles play an important role in determining climate and in shaping the patterns of river flow observed for the UK. Whilst these analyses did not identify clear evidence of increased seasonality they highlighted the importance of the occurrence of the solar and lunar modes within the seasons, which may lead to apparent changes in seasonality. In terms of long term positive trend, it is perhaps too early to determine with the length of instrumental flow records available in light of the identification of high order periodicity of ~90 years. This study did not attempt to quantify any anthropogenic component of driven change; only by fully understanding the natural driving mechanisms can any valid estimation of human influence be made.

2.1.5. Summary

Exploratory data analysis investigated potential trend for both increased river flow and increased seasonality of flow; no significant trend was observed for the river Eden annual flow, however both the rivers Tay and Thames displayed significant (95%) positive trend using the Mann-Kendall trend analysis. Evidence for increased seasonality of flow was inconclusive, with the river Eden data displaying no trend, the river Tay data displaying some trend and the Thames data a negative trend (Mann-Kendall 95%). Further investigating the three time series for periodicity using autocorrelations and spectral density analysis identified significant influence from solar, lunar and planetary sources and additionally potentially from high magnitude volcanic eruptions. Changes to seasonality of flow may hence be due to the occurrence of the orbital influence or combined influences within different seasons, year on year.

Significant trend and pattern was observed through formal cross-correlation between the autumnal NAOI and winter river flow for both the rivers Tay and Eden over multiple lags, giving strong evidence for a relationship between the climate index and winter river flow. Similarly, a significant relationship was also found through formal cross-correlation between the smoothed lagged (-9yrs) river Thames annual flow and the Wolfe solar sunspot numbers; correlating solar maximums with high river flow. The presence of long period cyclical events in the order of ~90 years gives uncertainty to understanding the presence of monotonic trend without a much longer time series and thus in understanding the proportion of anthropogenic influence to trend and variability about the long term mean.

2.2. Wind Direction

2.2.1. Introduction & Rationale

There are relatively few studies that explore the regional wind climate for the East coast of Scotland or place the regional wind climate conceptually with respect to large-scale atmospheric circulation. Determination of trend and pattern within the wind direction time series is important in understanding regime shifts within estuaries in terms of the impact dominant wind direction can have on tidal asymmetry, current velocities, waves and aeolian transport.

HR Wallingford (1995) studied wind data from RAF Leuchars for the period 1987 – 1991, whilst evaluating coastal erosion impacts at Montrose. Their findings revealed a reduction in the occurrence of onshore winds that exceeded force 5, during the five year study period. A follow up shoreline management study at Montrose by Halcrow (1998), revealed the increasing occurrence of onshore wind and wave conditions for the period 1992 – 1996. These two studies highlight the potential for pattern within the directional wind time series, however being such short time scales they give little insight into much longer period patterns.

Dawson (Dawson *et al.* 2001; 1997), later used the longest record of gale frequency in Scotland (Edinburgh Mossman-Hickey chronology) to identify changing patterns of storminess since 1780 AD. Comparison of gale frequencies with NAO indices from 1824 onwards revealed broad agreement in periods of strongly positive NAO indices being accompanied by increased storminess around the Scottish coastline. These findings confirmed those of Hurrell (1995), who maintained that during winter periods with a more positive NAOI, the westerlies over Europe were 8 m s^{-1} stronger on average than during more negative NAO winters, he additionally identified decadal variability within the indices.

Dawson (Dawson *et al.* 2001; 1997) also highlighted the role of increased volcanic activity in triggering tropospheric cooling as contributory to episodes of increased gale frequency. At first this

seems counter intuitive, as positive NAO indices are generally associated with warmer conditions, however the Tambora example given states that the 3 months following the eruption experienced slackening of westerlies and strengthening of north easterlies and easterlies. These climatic conditions are typical of patterns exhibited by negative phases of the NAO. Recent studies (Ineson *et al.* 2011) have demonstrated that a modelled reduction in direct incoming solar irradiance gave rise to patterns of surface temperatures and pressures similar to the negative NAO, so it is interesting to note that the three identified periods by Dawson (1997) of above average number of gale days coincided with periods of lower solar irradiance as recognised in the sunspot cycles.

The aim of this section of chapter 2 is to;

- Identify the presence of general patterns and trends within the directional wind count data.
- Verify if the dominant periods of east and west winds found by Wallingford (1995) and Halcrow (1998) are present and if this pattern persists over the times series.
- Confirm if any east-west pattern in the data could be linked to phases of the NAO.
- Explore potential relationships between wind patterns and solar irradiance.

2.2.2. Methodology

To maintain compatibility with historic direction data, daily direction summaries were tabulated at 03:00, 09:00,15:00 & 21:00 hrs, these were sorted according to sector (N,NE,E,SE,S,SW & NW) and the number of recordings per sector was then used for analysis. Data were recorded at RAF Leuchars with the copyright belonging to the British Atmospheric Data Centre (BADC) and the Meteorological Office, and are used here under the terms & conditions for NERC PhD research.

Identifying the presence of general trend and pattern via EDA

Exploratory data analysis used Microsoft Excel (2003) to graph wind summary data against time. The summary data were then analyzed for component trend, seasonality and periodicity through decomposition analysis using R software (Cran 2011); the stationary first difference de-trended data were then further passed through autocorrelation, partial autocorrelation and spectral density analysis in R to determine the presence of significant periodicity. The time series analysis program

for decomposition requires a continuous data record and thus the time series processed here was truncated at 1981 to provide a continuous time series 1936 – 1981.

Identifying the presence of east – west pattern

Exploratory data analysis used Microsoft Excel (2003) to graph the percentage contribution of each cardinal wind direction to the number of total counts to identify pattern. Cardinal directions only were used, as inclusion of intermediate directions confused interpretation. Cardinal direction here is defined as inclusive of winds $\pm 22.5^\circ$ of the compass cardinal directions (N, NE, E, SE, S, SW, W & NW). Using percentages can often lead to apparent pattern, thus to confirm if true patterns were present the actual direction counts for each cardinal direction was additionally displayed, to determine if the change in number of counts in easterly winds was related to the number of counts in westerly winds.

Periodicity in the two series was investigated by autocorrelation and partial autocorrelation using R statistical software (Cran 2011).

Identifying links to the NAO

The NAO climate indices used here were downloaded from KNMI Climate Explorer (2011), as monthly values. The monthly time series were scaled (to eliminate negative values) then analyzed for trend, seasonality and periodicity via decomposition analysis using R software (Cran 2011). Two time ranges were investigated, firstly from 1936-1980 to match the wind data time series and secondly, over the length of the full NAOI (1825-2010) to identify longer period periodicity and to place the shorter time series in context. The trend data were displayed along side each other with Loess regression to aid visual assessment. The first difference stationary data output from the decomposition analysis was then passed through to spectral density analysis to identify significant frequency in periodicity over the two sample intervals.

Microsoft Excel (2003) was used to investigate similarities in trend between the percentage of directional westerly wind counts and the NAOI, displaying the two smoothed times series along side each other for a visual assessment of their relationship. Formal cross correlation between the % westerly wind counts and the September-November de-trended NAOI was tested by multiple time series autocorrelation & partial autocorrelation (Cran 2011) as 4 year running mean data.

Identifying the relationship to sun spot activity

Sunspot indices were downloaded as monthly data from SIDC (2011) for the time series 1749 – 2010 as a representation of solar activity and hence the amount of radiation emitted by the Sun which potentially can heat the Earth's atmosphere and differentially drive circulation (thus wind

patterns). Using predicted values of future sunspot cycles (Smeter.Net 2006), a combined time series was created to capture long period cyclical variability which was then displayed in Microsoft Excel (2003).

To assess the relationship between solar activity through sunspot cycles and total wind direction counts, the two time series were displayed alongside, using Microsoft Excel (2003) to give an overview prior to cross correlation. Formal cross-correlation was not undertaken since the potential pattern seen appeared to follow cycles equal to, or in excess of Wolf-Gleissberg (80-90 yr) cycles, and thus longer than the time period for the data.

2.2.3. Results

Identification of general pattern within the data series:

The relative contributions of the principle cardinal point wind directions are displayed (Figure 2-25) as total counts per year. The greater number of direction counts comes from the West, after which the easterlies are the next dominant. North and south winds have approximately similar counts.

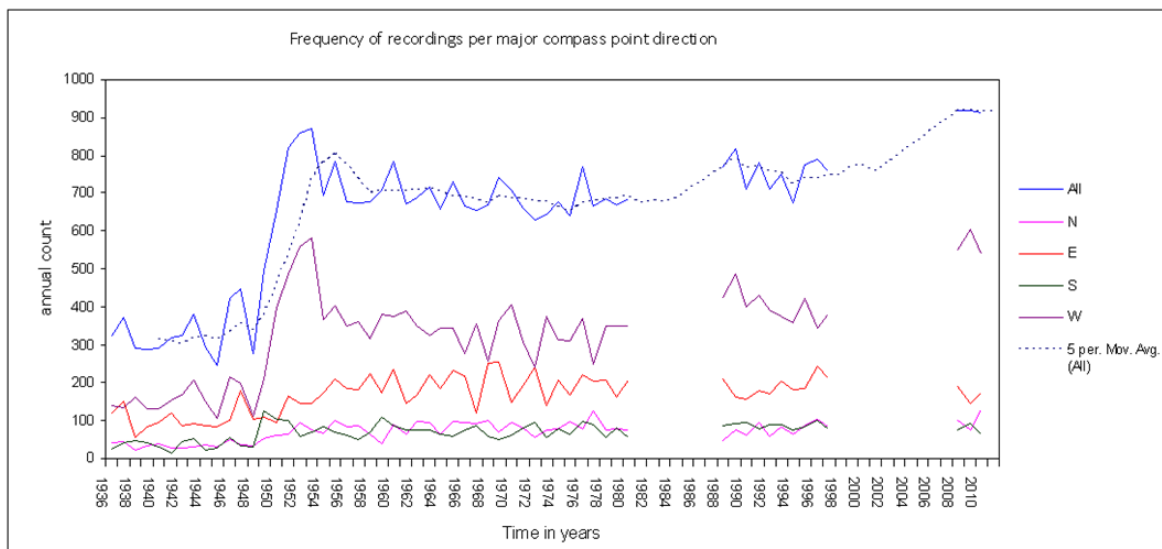


Figure 2-25: Wind counts for cardinal directions; North, South, East & West only.

Of note is the large increase in the number of wind counts per year between the early 1940s and the early 1950s. The change in number of counts is seen most dramatically in the westerly wind component of total number of counts.

Mean monthly total wind counts (1936-1981) were investigated for trend, seasonality and periodicity in the residual components through decomposition analysis (Figure 2-26) using R (Cran 2011). The data were truncated at 1981, as the software is unable to handle null and missing values. The decomposition display is split into four sections; the top section is the original input data, below which is the seasonal component, followed by the trend component and finally the first difference residual data (remainder following the removal of seasonal and trend components).

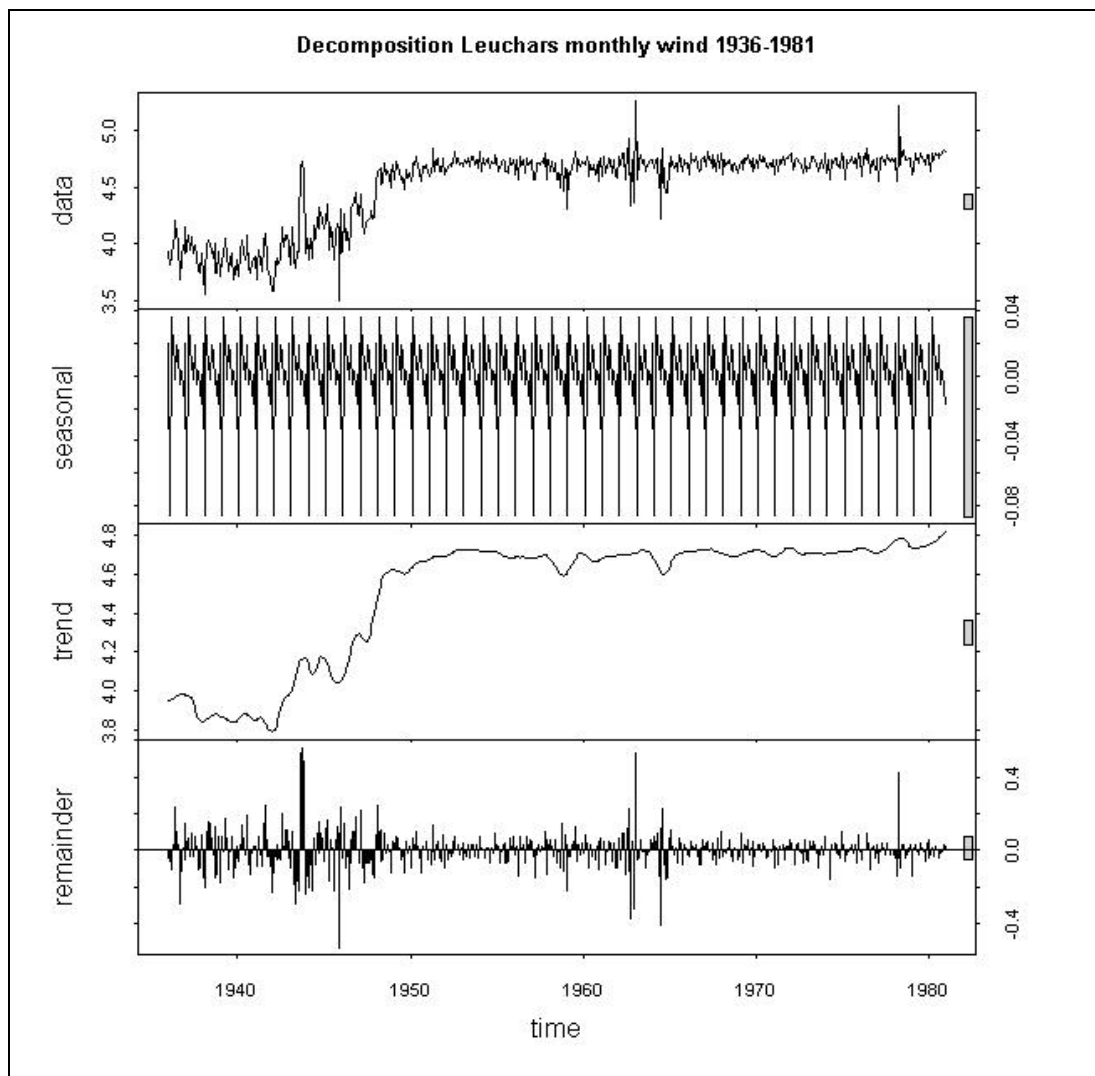


Figure 2-26: Decomposition analysis of monthly wind direction counts. The data are truncated at 1981 due to missing values after this period. The vertical scales are logged counts, the rectangular bars to the right signify equal scale across the 4 panels and the horizontal scale is time in years.

Again, the most distinctive feature in the trend component is the stepped increase in wind counts which occurs between 1940 and 1950. The first difference residual component additionally identifies potential periodicity of ~15-20 years, with distinct peaks in the number of counts in the early and mid 1940s and again in the early and mid 1960s, with a final peak in the late 1970s.

The first difference de-trended data (remainder) were then passed through autocorrelation, partial autocorrelation and spectral density analysis to quantify significant periodicity (Figure 2-27).

The autocorrelation and partial autocorrelation displays (Figure 2-27) have lag intervals of ten years; the data range is from 1936-1981, thus lag 10 corresponds to 1945 etc. Blue dashed lines represent 95% significance and peaks which exceed these lines in either direction are significant. No single cyclical period is identified by the autocorrelations however a number of significant peaks are present. The significant peaks in the autocorrelation correspond to the following years; 1936, 1937, 1938, 1939, 1940, 1941, 1943, 1946, 1954 and 1955. The partial autocorrelation (which describes the relationship between the current counts and those at lag t once the correlations for all successive years between the current time and lag t have been accounted for) identifies the following significant peaks; 1936, 1937, 1938, 1940, 1946 and reveals a further peak at 1948.

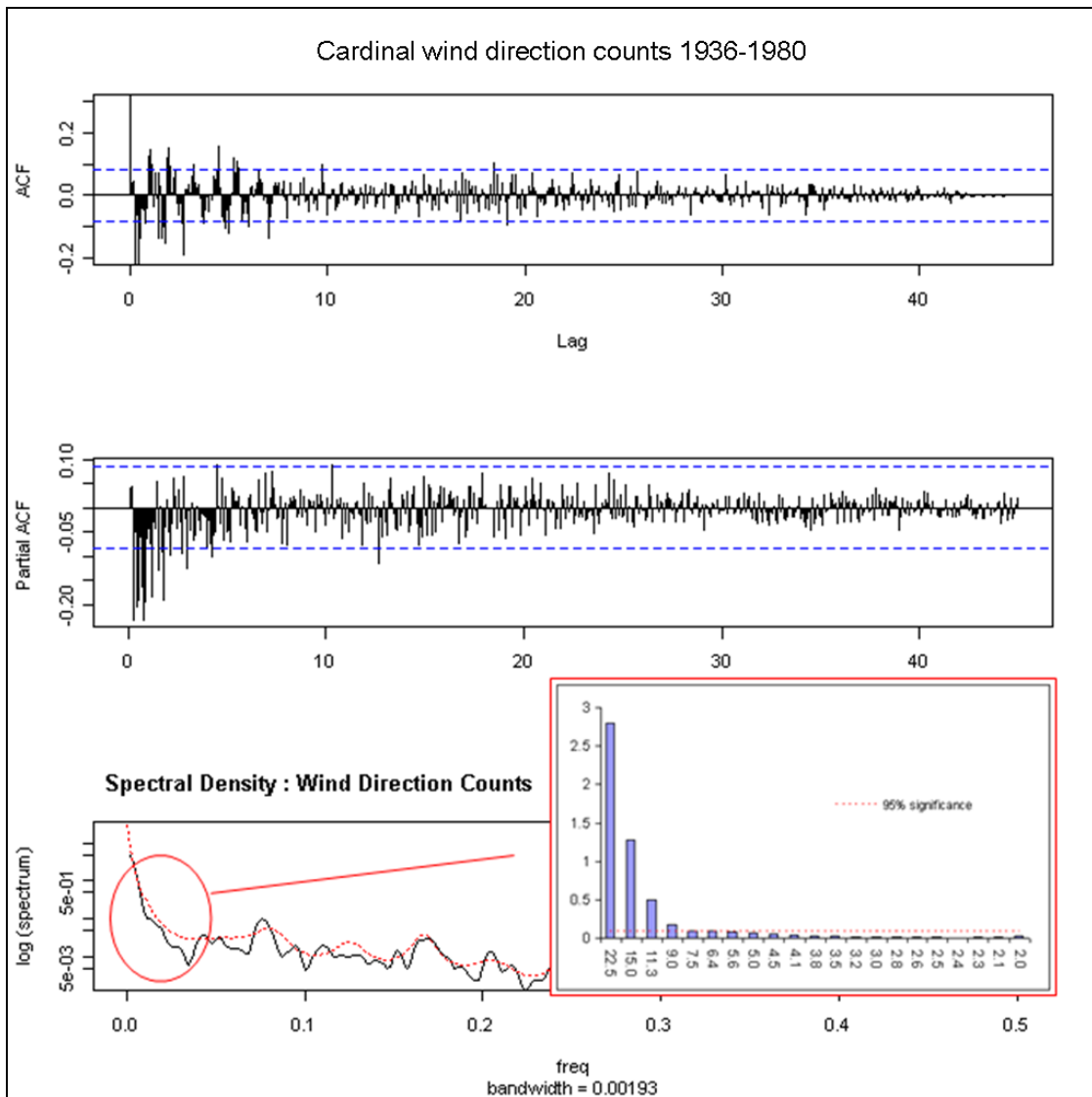


Figure 2-27: Autocorrelation partial autocorrelation and spectral density analysis of the first difference residuals output from the decomposition analysis. The time series range is 1936-1980.

The spectral density analysis (Figure 2-27, bottom) displays the dominant frequencies present in order from left to right; since the input data are monthly, the annual frequency is at 0.083' and is the reciprocal of the frequency (i.e. $1/0.083'$). Values to the left of the annual peak are higher order periodicity than the annual cycle and are highlighted in the insert. Significant (>95%) frequencies identified by the spectral density analysis are; 22.5, 15, 11.3 9 and 7.5 years respectively.

Identification of east – west pattern found by Wallingford (1997) and Halcrow (1998):

Figure 2-28 is an analysis of the different percentage contributions that each cardinal direction makes to the total number of counts recorded. From this analysis, the north and south winds show only a small variation over time and appear not to be directly related to each other. However, the % of north winds follows a similar trend to the % west winds and the % south wind follows a similar

pattern to the % east winds. The percentage of east and the percentage of west wind appear to have an opposing relationship, however this may be accentuated by the methodology of using percentages.

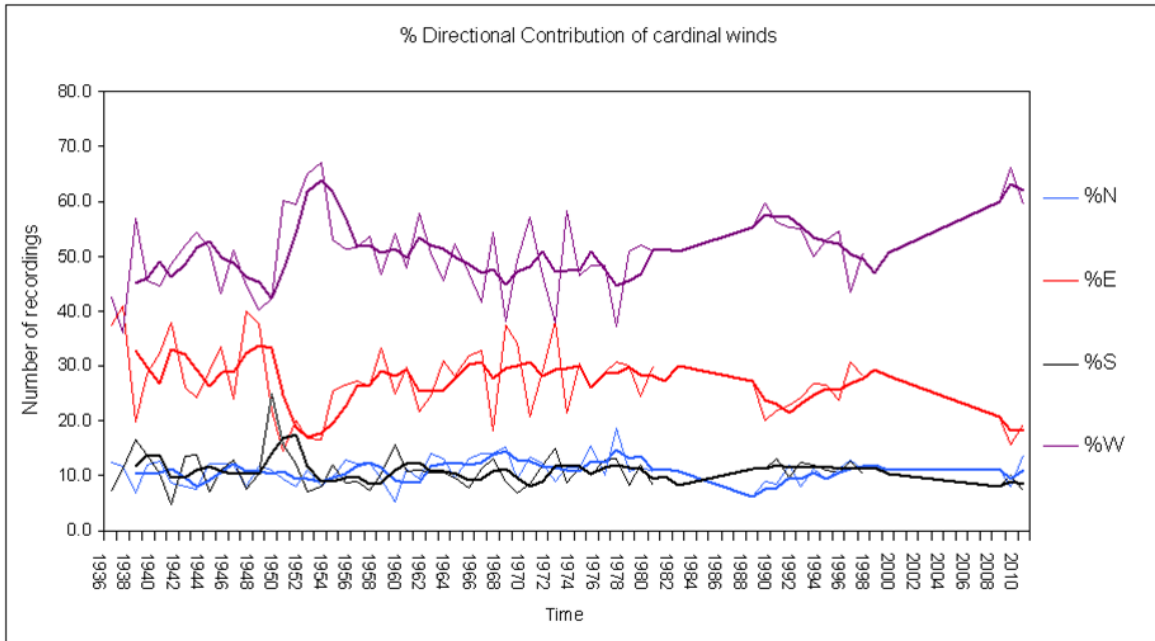


Figure 2-28: The percentage Contribution of each cardinal direction to overall total number of counts.

Further investigating this apparent relationship; Figure 2-29 presents the actual counts for each cardinal direction and verifies indeed this is the case, particularly post 1950s.

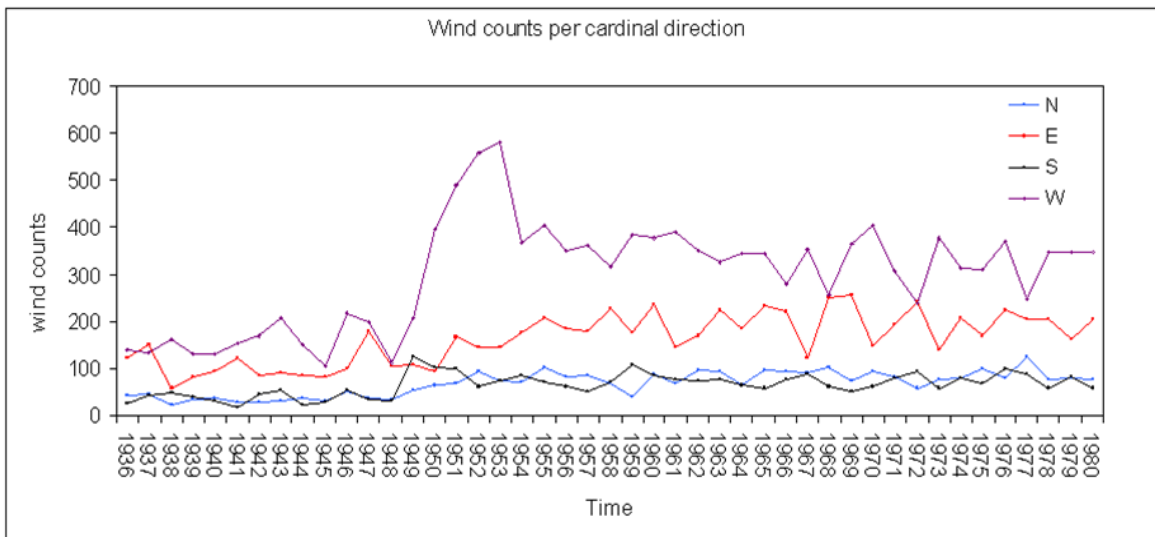


Figure 2-29: Actual cardinal direction counts (N, S, E & W), presenting the relationship between east and west winds.

The trend data for the easterly winds (Figure 2-30) displays more variability than the westerly winds and although the first difference data (remainder, Figure 2-30) identifies a periodicity of approximately 15 years in both time series, the easterly wind data display additional periods of approximately 5-7 years which are less clear in the westerly winds.

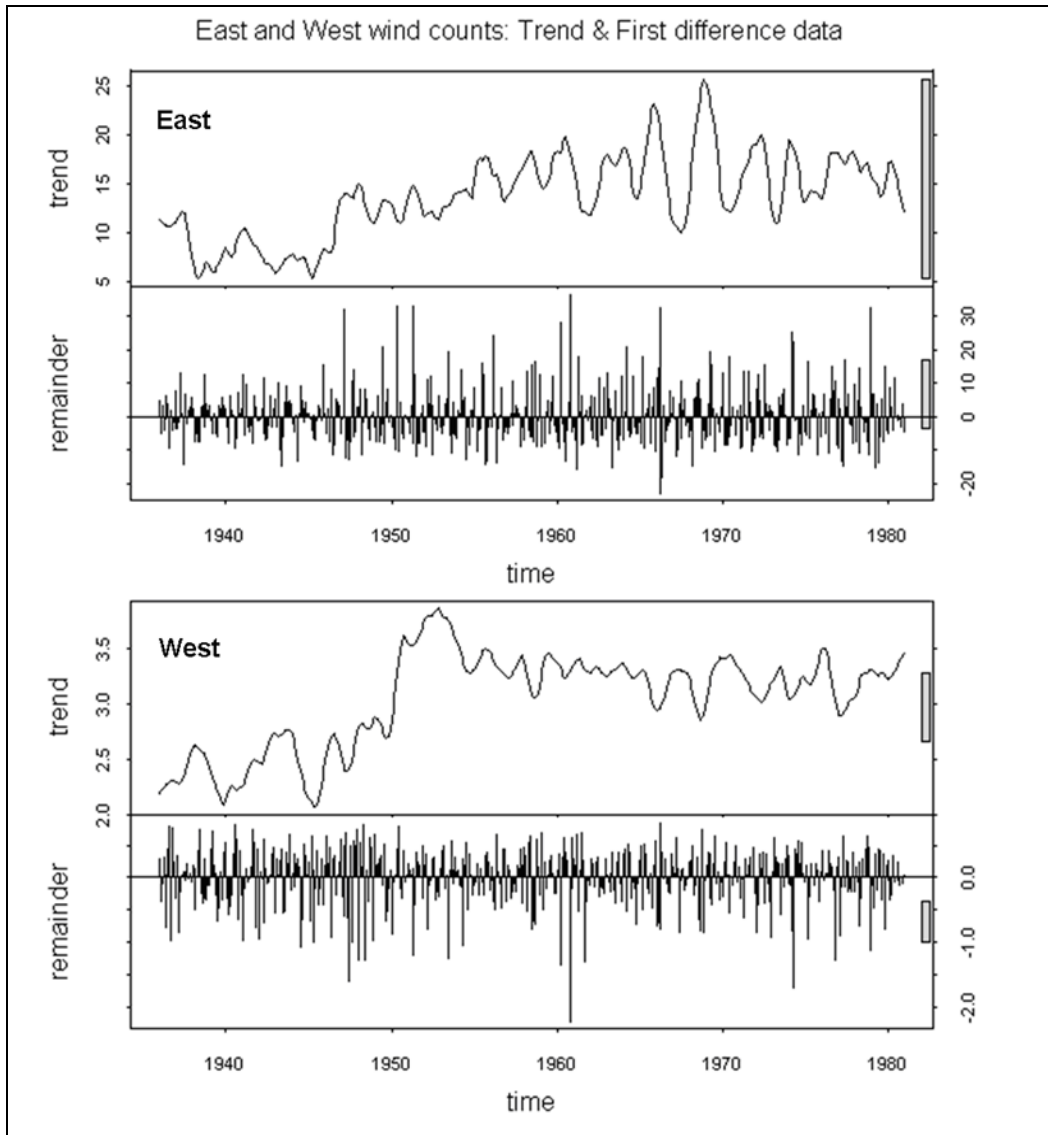


Figure 2-30: Trend and first difference data of east and west wind direction counts. Rectangular bars to the right represent equal scale between the displays for the pairs of displays.

The first difference data for the west winds were analysed for autocorrelation (Figure 2-31) to identify the potential cyclical events suggested by the time series represented in Figure 6. The lag intervals are 10 years and the data range is 1936-1980, thus lag 10 corresponds to 1946 etc.

For the autocorrelation significant peaks corresponded to the following dates; 1936, 1937, 1939, 1940, 1943, 1946, 1948, 1949, 1953, 1956 and 1957. The partial autocorrelation identifies significant peaks which correspond to the following dates; 1936, 1938, 1943, 1948 and additionally 1954.

The spectral density analysis of the westerly winds (Figure 2-31 bottom & insert) identifies the following significant (95%) frequencies; 22.5, 15, 11.3, 9 and 7.5 years, of these 22.5 years was the strongest frequency.

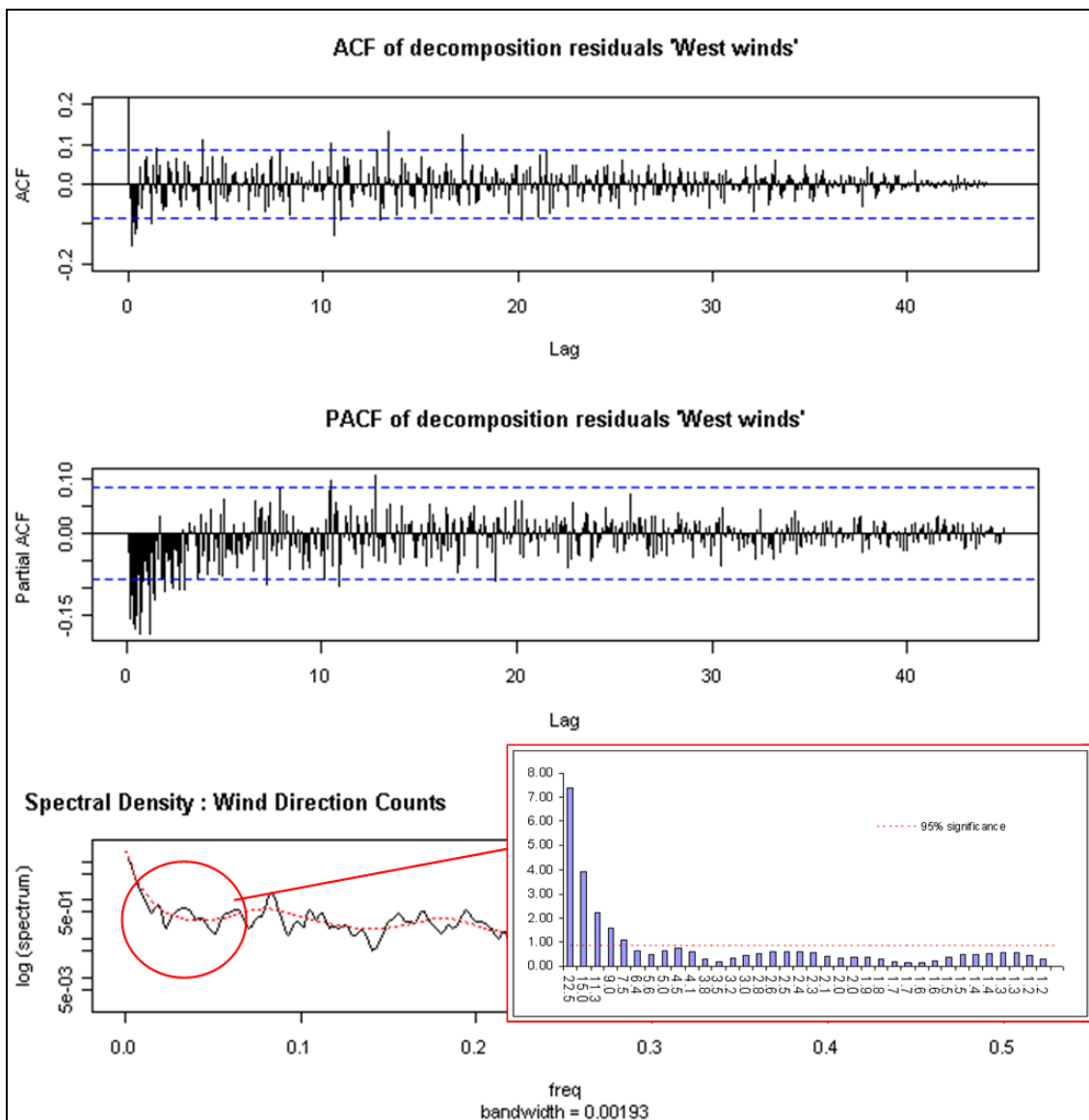


Figure 2-31: Autocorrelation, partial autocorrelation and spectral density analysis for west wind count data.

The same analyses were repeated for the easterly winds (Figure 2-32), with the autocorrelation identifying significant (95%) peaks corresponding to the following dates; 1936, 1939, 1940, 1941, 1944, 1946, 1951 and 1954.

The partial autocorrelation identified significant (95%) peaks corresponding to the following; 1936, 1938, 1944, 1945, 1950, 1951 and 1955 and the spectral density analysis identified many significant (95%) frequencies; 22.5, 15, 4.5, 4.1, 3.8, 3.5, 3.2, 3, 2.8, 2.6, 2.5 and 1.4 years. Of these 2.8 and 22.5 were strongest.

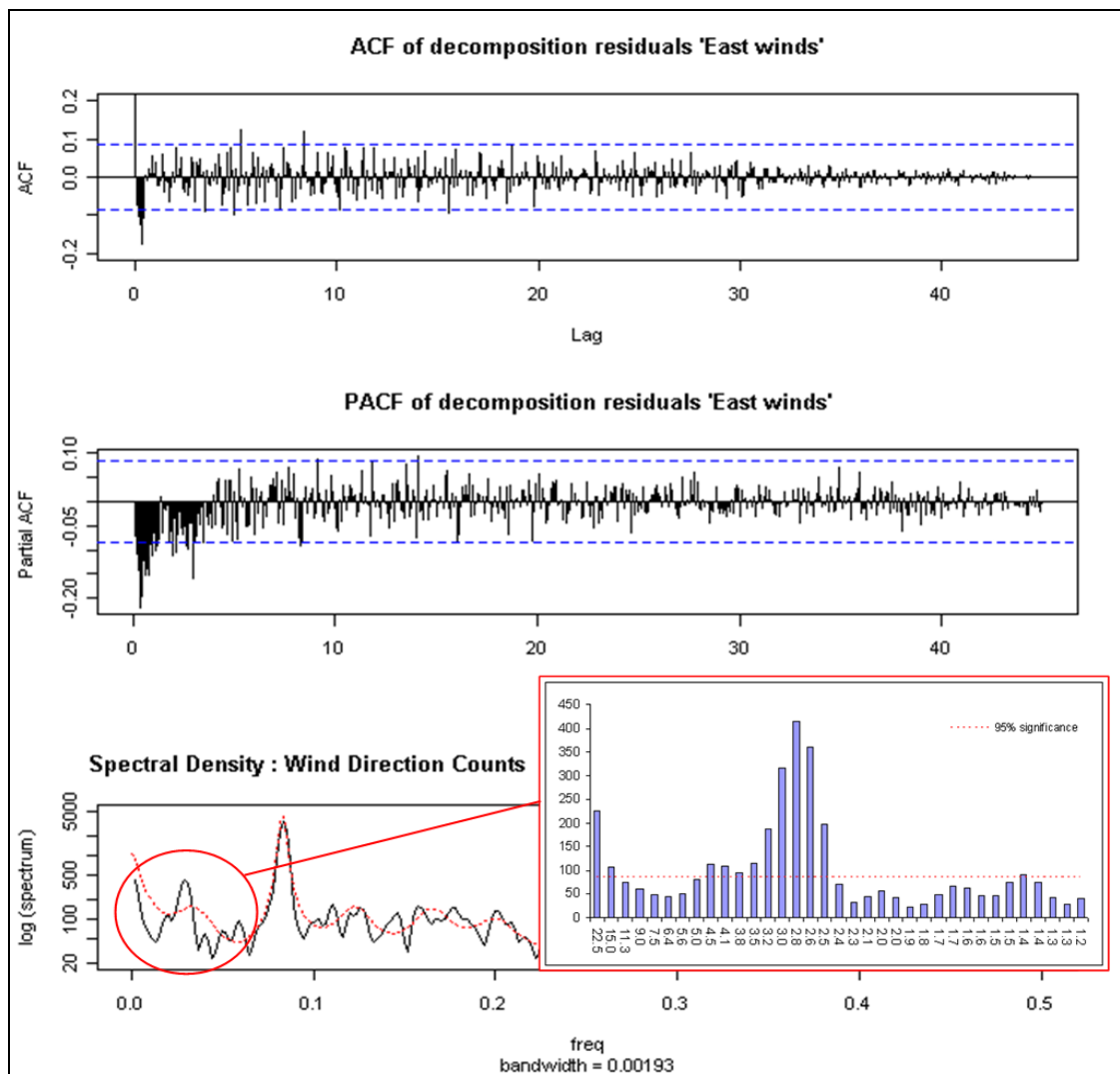


Figure 2-32: Autocorrelation, partial autocorrelation and spectral density analysis for east wind counts.

Identification of any links to the NAO;

To understand potential links with the NAO the same temporal range of NAOI was investigated to match the wind data (1936-1980). The trend component of the decomposition analysis (Figure 2-33)

identifies a slight positive trend from the 1930s up to the early 1950s, after which there is a more negative trend descending towards 1980. The first difference data ('remainder', Figure 2-33) display potential periodicity at approximately decadal and 6-7 year time scales.

Using the extended time series (1825 – 2010), the data were similarly investigated for trend through decomposition analysis, giving a better understanding of longer term variability. Figure 2-34 presents the extracted trend components of both time series (long & short) with a Loess trend-line overlain. In the extended time series, there appears to be a low amplitude parabolic trend, with the turning point centred in the early 1900's.

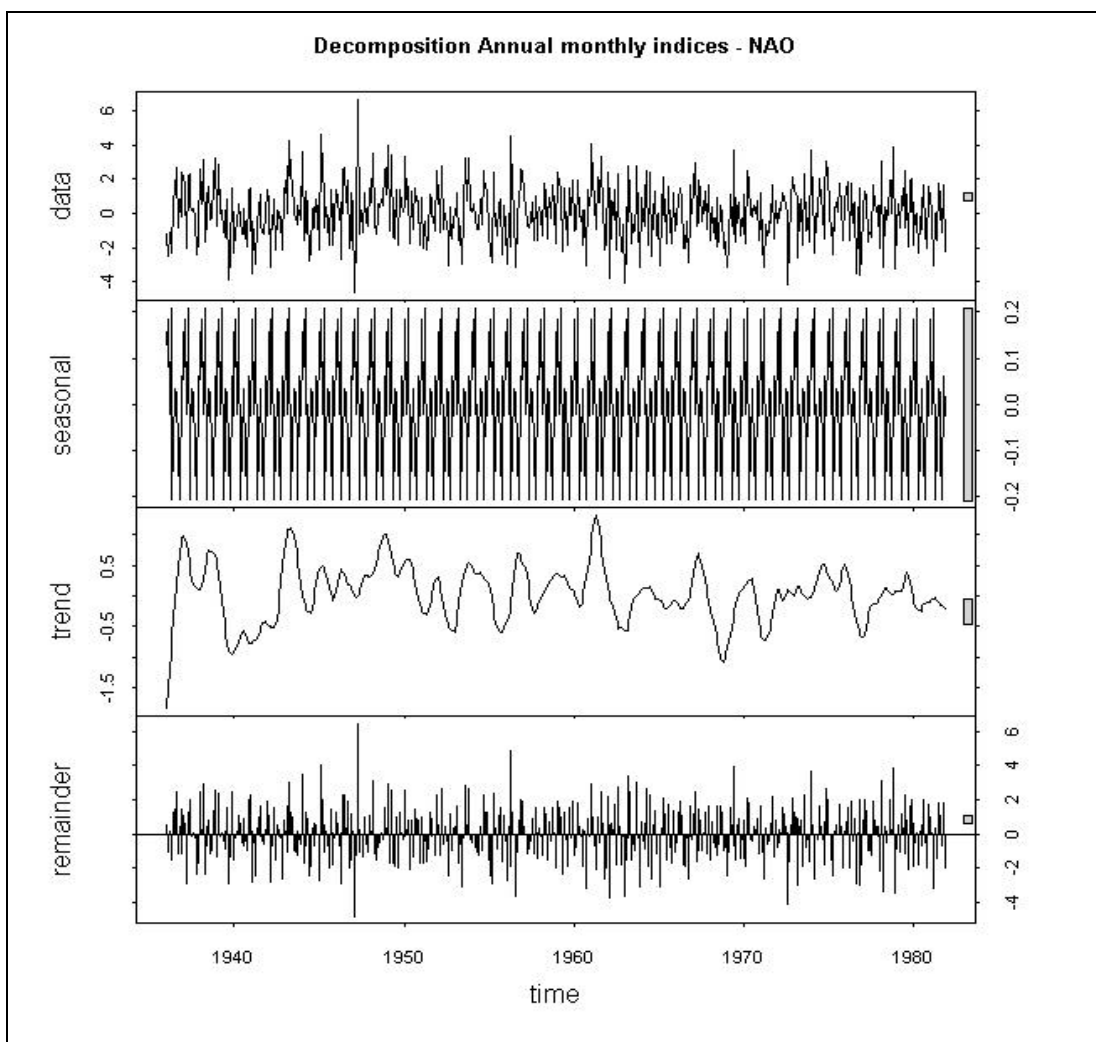


Figure 2-33: Decomposition analysis: monthly NAO indices from 1936 – 2010.

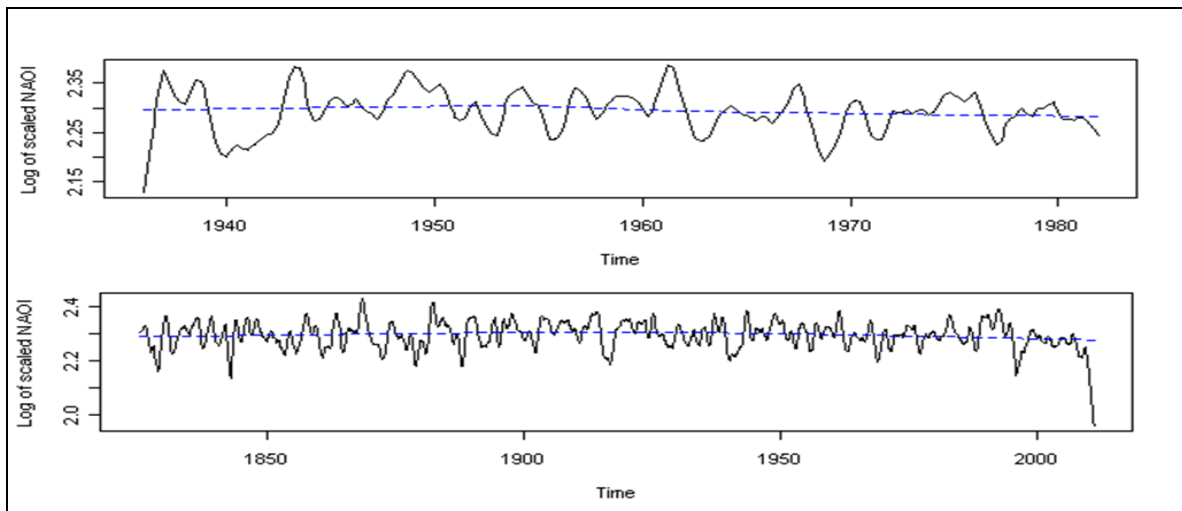


Figure 2-34: Decomposition trend components: NAOI 1936-1980 (top) and 1825-2010 (bottom).

Analysing the spectral density analysis of the first difference stationary data (Figure 2-35) for the two NAOI time series identifies different significant frequencies in periodicity over the two sample intervals. The significant (95%) frequencies for the 1936-1980 data were identified as 16, 12, 6, 2.67, 2.18, 1.50 years and 1.2 years. The most dominant frequency was 2.67 years. Significant frequencies identified for the extended times series data were; 93.75, 37.50, 15.63, 13.39, 7.81, 5.86, 4.93, 3.99, 30.7 and 2.68 years and the most dominant frequency was 7.81 years (followed by 2.68).

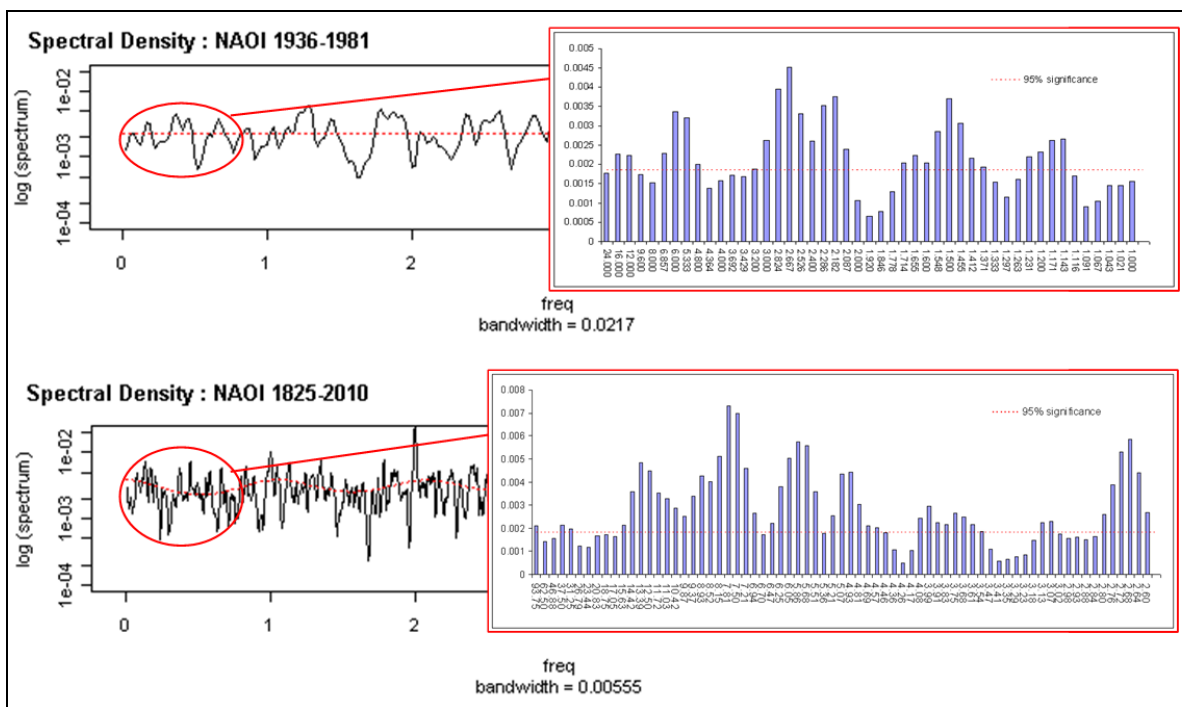


Figure 2-35: Spectral density analysis of the NAOI, top is the 1936-1980 data range (compatible to the wind analyses) and bottom is the extended NAO monthly indices (1825 – 2010). Frequencies above the annual interval are highlighted by the respective inserts.

Comparison between the westerly wind counts and the NAOI (Figure 2-36), reveals the two smoothed times series share similar pattern and general trend, however the wind data is lagging the NAO by roughly 3-5 years.

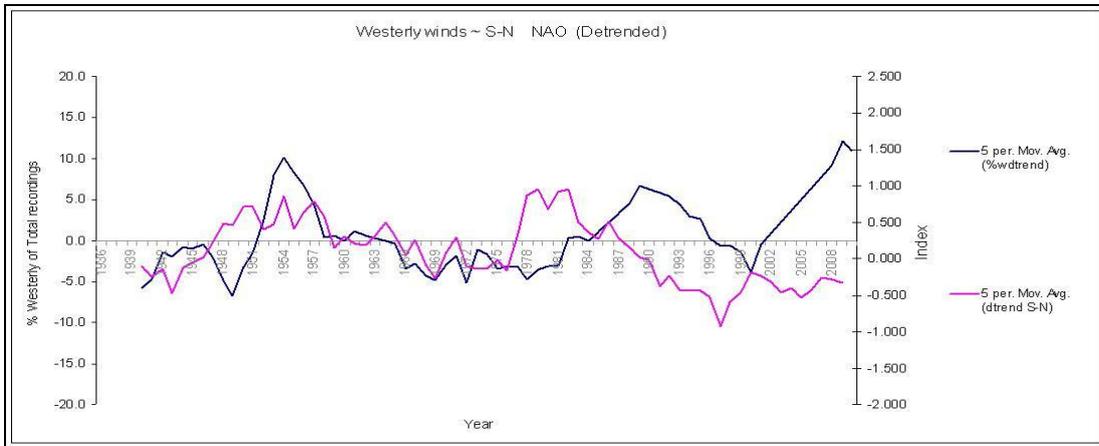


Figure 2-36: Visual assessment of the relationship between the % of westerly winds and the September to November NAOI.

Formal cross-correlation between the two time series is presented in Figure 2-37. The autocorrelations for the two individual cases are displayed top left and bottom right; cross-correlation with the September-November NAOI controlling for westerly wind is shown bottom left and the converse situation top right. The cross-correlation identifies that the September-November NAOI controls for the westerly winds over multiple significant (95%) lags. The shared periodicity is approximately 35 years. Although significant lags are observed for the westerly winds controlling for the NAOI (top right), this likely reflects the pattern imparted from the NAOI, though could also indicate a shared driving mechanism.

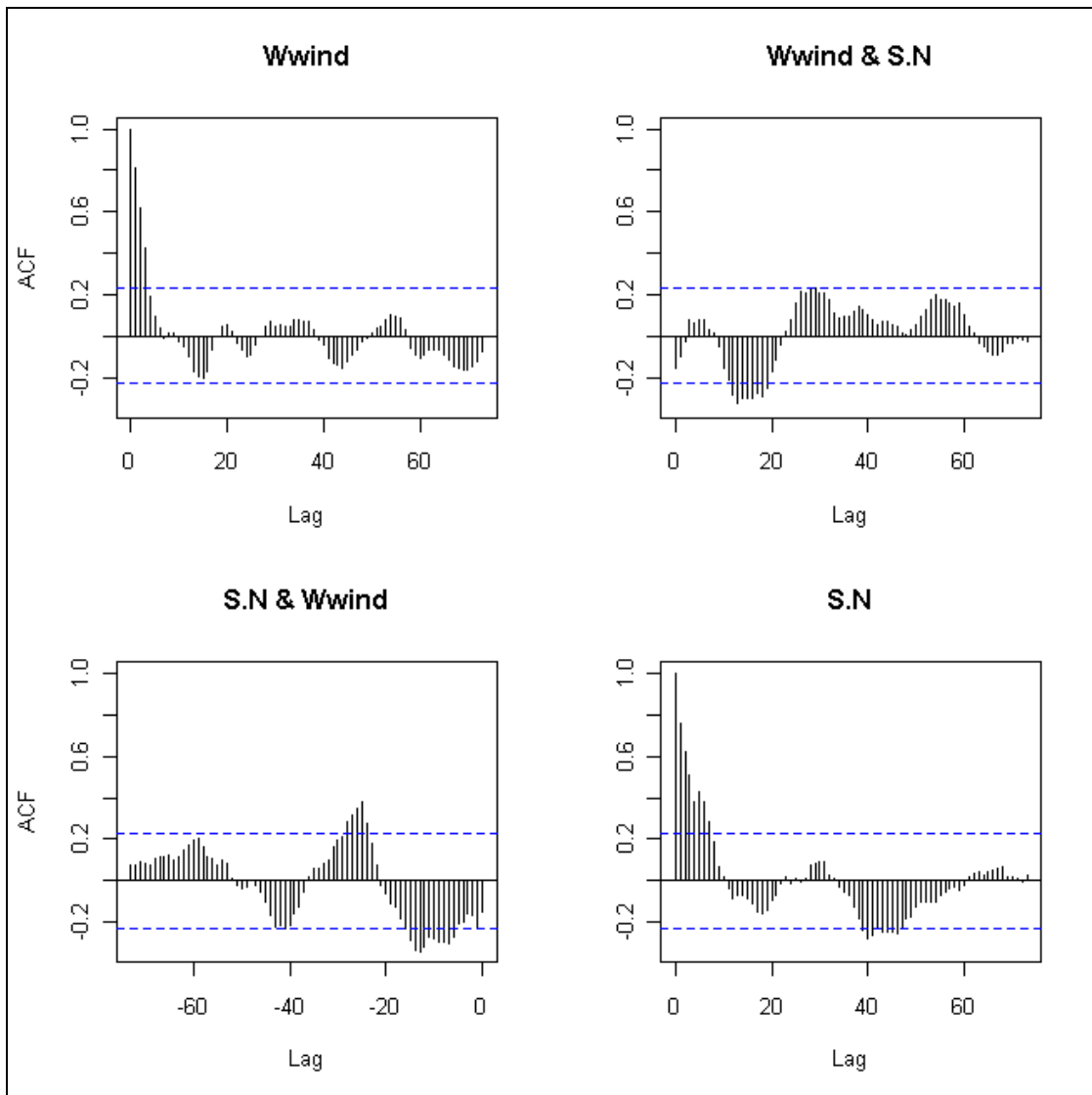


Figure 2-37: Autocorrelation: de-trended September to November NAOI (4 year running mean) cross-correlated to the % of west winds (4 year running mean) for the period 1937 – 2010. Bottom left displays the S-N NAOI controlling for westerly winds.

Further investigation of the approximate shared 35 year cycle through spectral density analysis (Figure 2-38) reveals significant (95%) frequencies for the westerly wind data as; 37.50, 25.00, 18.75, 9.37, 12.50, 10.71 and 8.33 years respectively in dominance order. Significant (95%) frequencies identified in the S-N NAOI were; 25.00, 37.50, 7.50, 15.00 and 10.71 years respectively in dominance order. Thus there are two common frequencies of 37.5 and 25 years.

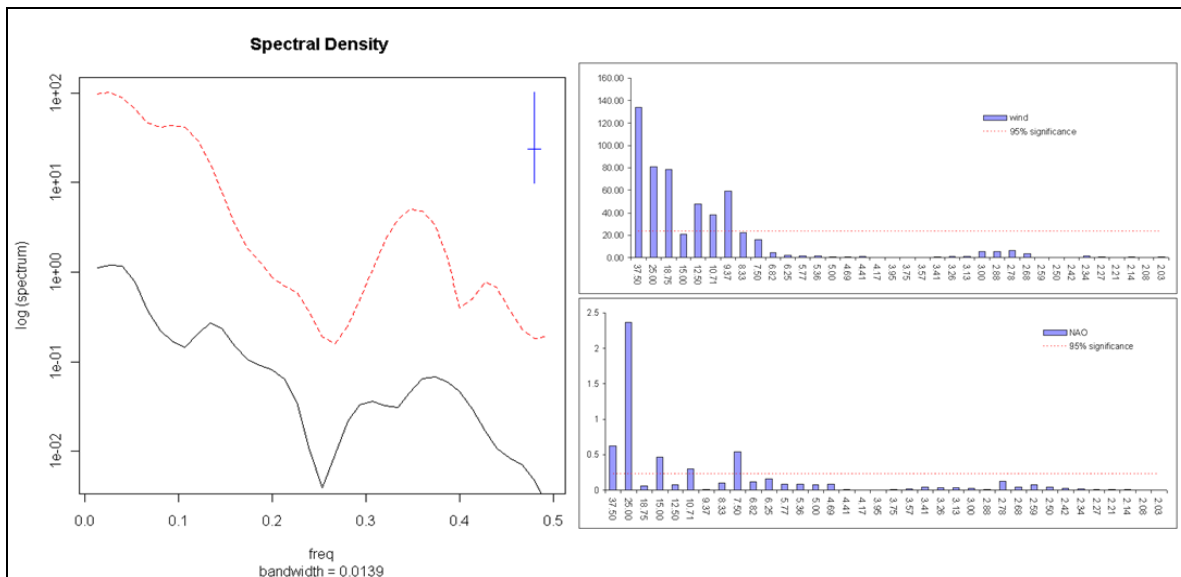


Figure 2-38: Spectral density analysis for the two cross-correlated time series. Left is the spectrum for the two series (westerly wind in red & NAOI in black), right is the same data re-plotted with frequency converted to time in years (westerly wind top & NAOI bottom). Significant frequencies exceed the red dashed 95% significance line.

Identification of any links to sunspot cycles:

Using downloaded monthly sunspot indices (SIDC 2011) and predicted future indices from smeter.net (2006) (Figure 2-39), a combined sunspot times series was compiled spanning from 1749 to 2009. Using this time series, correlation between total wind counts and the sunspot data was investigated.

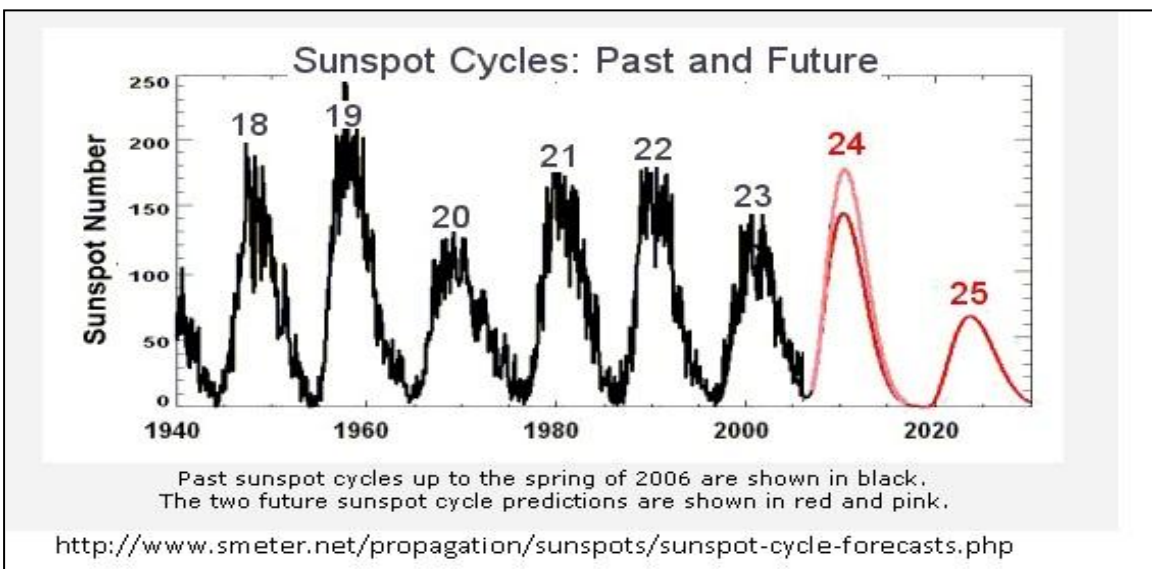


Figure 2-39: Predicted future sunspot cycles, based on data from Mausumi Dikpata of the National Center for Atmospheric Research and NASA solar physicist David Hathaway. Cycle 24 was estimated to reach its maximum in 2012.

Plotting the compiled sunspot data as annual values and superimposing the 10 year running mean (Figure 2-40) enables longer period cycles of approximately 80 years to be identified.

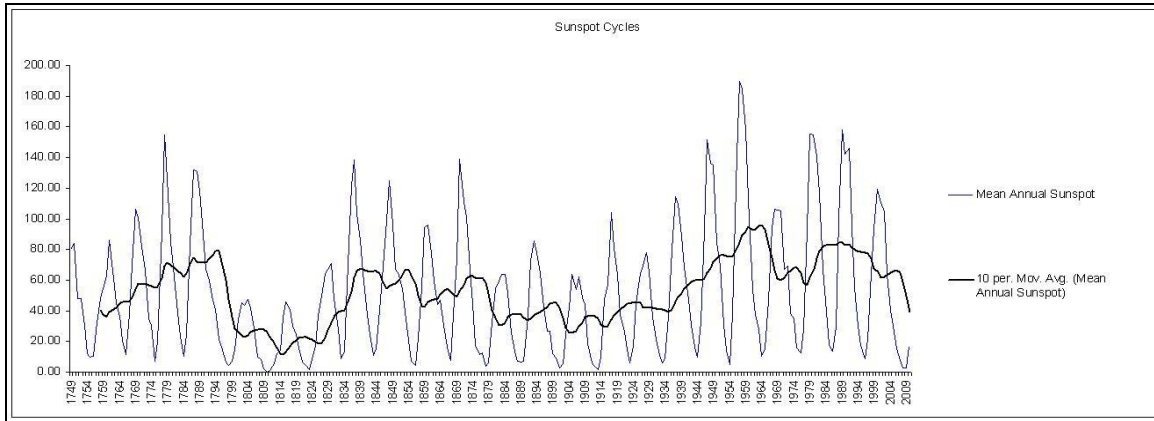


Figure 2-40: SIDC monthly sunspot indices (annual means), showing variable periodicity over long time scales (1749-2009).

Using the predicted values and the historic recorded sunspot indices, the ‘total number of wind counts’ were plotted alongside the sunspot data (Figure 2-41). The sunspot cycles increase in magnitude to a maximum at cycle 19, this trend is matched by a similar increase in the number of wind counts, however with a lag period. The average cycle maximum for the following 5 cycles remains relatively high, matching the sustained level of wind direction counts. The data range for the wind records in Figure 2-41 is too short at present to suggest more than a potential relationship with long term variability in solar activity.

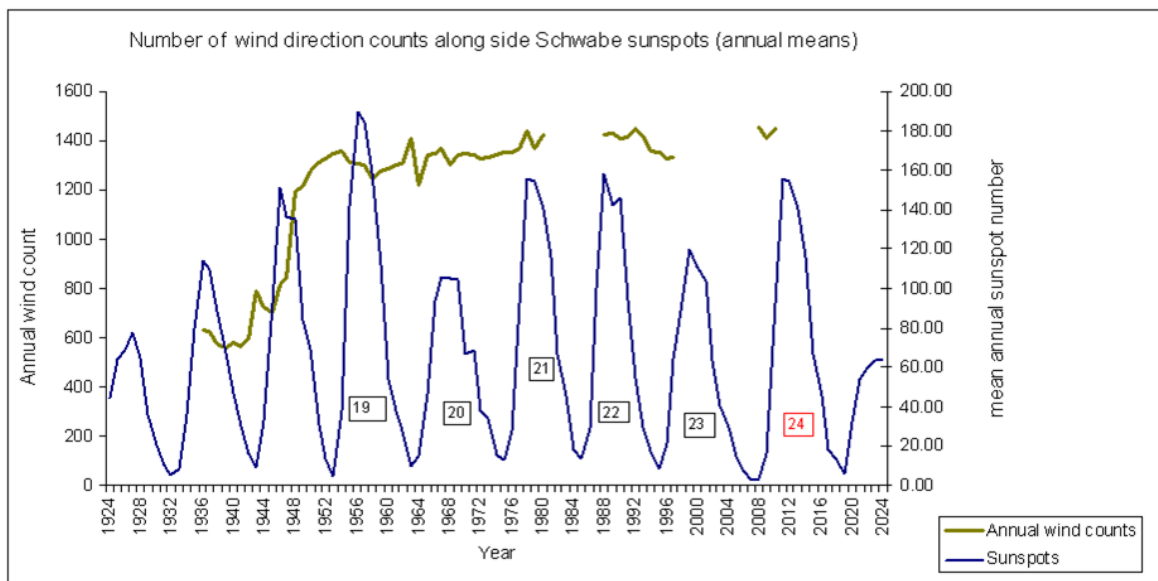


Figure 2-41: Comparison between the total number of annual counts & the sunspot cycle indices (mean annual). Cycle 24 in red & the following cycle 25 are created from the predicted values.

2.2.4. Discussion

The prevailing wind direction for the UK is from the Southwest and is determined by the relative high latitude of the UK and also the proximity between opposing anticlockwise sub-polar lows & clockwise subtropical highs drawing Tropical Maritime air north-eastwards (Colling and Team 2001). However, there is variability in wind direction caused by changes to the positions and magnitude of the pressure gradient between the Icelandic low and Azores high and regionally by differences in topography.

Exploratory analysis of the wind direction data identified a rapid and considerable increase in the number of wind counts between the 1940's and 1950's, the greatest contribution to this change was observed to be from the westerly wind contribution. Although autocorrelation and partial autocorrelation of the data failed to identify a cyclical behaviour, there were significant (95%) peaks corresponding to influence from solar maximum and minimums and orbital influences from the Moon and Jupiter. With the recorded variability in the length of solar cycles from 9 to 13 years, giving an average of ~11years, and also with variability in the magnitude of the cycles themselves, coupled with interaction between planetary orbital variations, it is perhaps not surprising that the autocorrelations (which rely on serial dependency) failed to identify significant cyclical behaviour. Spectral density analysis did reveal significant frequencies of 22.5, 15, 11.25, 9 and 7.5 years. Within these frequencies factors are present; 7.5 is a factor of 15 and 11.25 a factor of 22.5. These shorter periods therefore likely represent the half cycle, with 11.25 being half of the ~22 year (Hale) solar magnetic polarity reversal (the half period is also called the Schwabe sunspot cycle) and 7.5 is the half cycle of 15, and may also be related to the solar magnetic cycle as $22.5/3$. The ~7.5 year frequency is also found in a number of other records; Feliks and Ghil (2007; Feliks *et al.* 2010) found a 7-8 year significant period in Jerusalem precipitation data, Northern Israel tree ring widths and also in the NAOI. Da Costa and De Verdiere (2002) similarly identified 7.7 year periods between sea surface temperatures and sea level pressures. The 9 year frequency is ambiguous, it may represent the shorter durations of the Schwabe sunspot cycle (ranging from 9-13 years) however it is also very close in length to the lunar nodal half cycle (9.3 yrs). Feliks and Ghil (2007; Feliks *et al.* 2010) identified a 9.2 year significant cycle in both Beirut precipitation data and northern Israel tree ring widths.

Overall the range of spectral frequencies identified in the wind direction data are similarly found in many other physical and biological data, for example central England temperature data (1700–1950) as 76, 23, 14.5, 11.5, 7.6, 5.2 and 3.1 years (Burroughs 1992), Lapland tree rings data at 90, 30, 23, 18 and 11.3 years (Lamb 1972) and in air pressure data (O'Brien and Currie 1993) as the 18.6 year lunar nodal cycle.

Although the autocorrelations are difficult to interpret, due to serial dependency and the magnitude of the peaks deteriorates over time; the westerly winds differed slightly from those of the east winds (Figure 2-42) in that the westerlies displayed a weaker influence from lunar periods. The westerly

winds were largely influenced by unidentified significant peaks at the following dates; 1936, 1949, 1946, 1953 and 1943 respectively in order of influence.

The spectral density analyses differed also, west winds displayed the same spectral frequencies as 'all wind' data and were dominated by the 22.5 year frequency, whilst the east winds were dominated by the shorter 2.8125 year frequency (which is the 8th harmonic of 22.5). This latter frequency has been identified as a significant oscillatory mode through spectral analysis of sea surface temperature data by Feliks (2011) who found a good synchronization between observed and simulated ocean data and the NAO.

Whilst both west and east wind spectral analysis revealed 22.5 and 15 year significant frequency peaks, the 11.3 sunspot and the 9 year frequency were not significant in the east winds suggesting differences in their driving mechanisms. However of interest was a 4.5 year peak corresponding to 9/2 and also 3.75 years corresponding to the difference between the solar minimum and maximum (4th harmonic of 15 years).

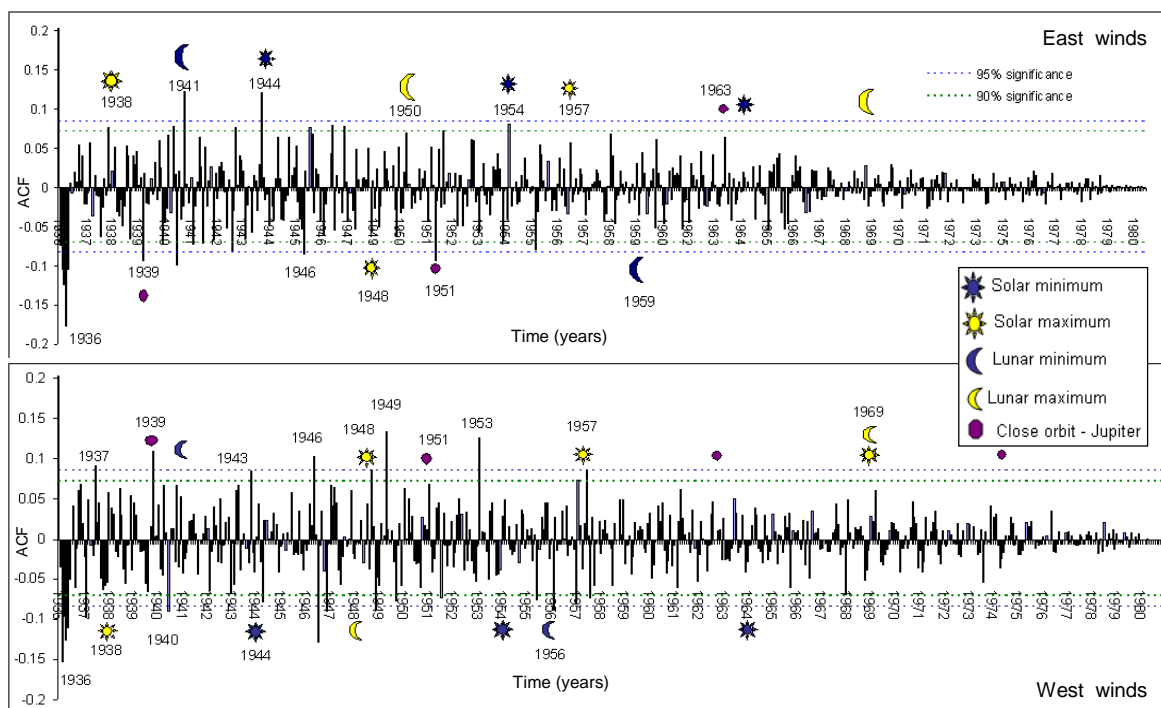


Figure 2-42: Interpretation of the autocorrelations for east and west winds direction counts.

In recent years there has been increasing research linking the orbital resonance between the Sun and the Jovian planets (Juckett 2003; Scafetta 2012a; Wilson *et al.* 2008), to cyclical climate periods (Scafetta 2010; Scafetta 2012b). Studying cycles of the Earth's climate and those of the Sun's barycentric motion, Scafetta (2012b) found a good correlation over multiple frequencies corresponding to the orbits of Jupiter and Saturn. Additionally, alignment between Venus–Earth–

Jupiter and Mercury–Venus gave resonance cycles of 11.05-11.10 years equating to the observational mean Schwabe sunspot cycle length and inferring the “planets are driving solar variability that then drives the Earth's climate”. Focussing on higher periodicity, Jose (1965) identified a 178.7 year periodicity in the Sun's barycentric motion, where the angular momentum correlated to the ~11 year Schwabe and ~22 year Hale cycle. Wilson (2008) further noted a relationship between the torque exerted to the sun by the synodic period of Jupiter and Saturn (19.858 years) and the Hale ~22 year magnetic polarity reversal; whereby a 9:8 ratio resulted in one

$$\text{Jose cycle of 178.7 years} \frac{22.34 \times 19.858}{22.34 - 19.858} = 178.7 \text{ years}$$

Investigating this further, the period of time for the 3 largest planets to realign with Jupiter approximates to 44.7 years, which is the quadrature of 178.7 and coincidentally is double the hale magnetic polarity cycle. Referring back to the 15 year cycle found in all 3 spectral analyses, this time period appears to equate to the Jose cycle divided by the orbital period of Jupiter (178.7/11.86=15.07) and hence infers a link between particularly west winds and orbital forcing.

In linking patterns found within the wind data to variability in climate, the NAOI was investigated for trend and periodicity. The NAO is deterministic controlling the position of the mid latitude jet streams and hence one of the major controls of climate in Europe (Dickson *et al.* 2000; Hurrell 1995; Moberg and Jones 2005). Negative phases of the NAO result in the jet stream moving southwards leading to slackening of westerlies and colder drier weather over northern Europe, whilst positive phases push the jet stream more northwards giving rise to warmer wetter and windier conditions (Kidston *et al.* 2010; Woollings and Blackburn 2012; Woollings *et al.* 2011). The NAOI was investigated through decomposition analysis over two different time series, one compatible to the wind data series and the other to identify longer frequency trend. A potential 6-7 year cycle was identified over the shorter range and a much longer ~90 -100 year period over the extended time series. Quantifying the potential periodicity present, spectral density analysis revealed a number of significant (95%) frequencies, the most dominant in the short temporal range was 2.67 years and in the longer range 7.81-7.5 and also 2.68. These frequencies were also present in the wind data and infer either shared periodicity or the NAO as a driving mechanism.

Investigating this relationship further, the smoothed annual de-trended data for both the September to November NAOI and westerly winds were visually compared and displayed similar pattern and trend, though the wind data lagged by approximately 3-5 years, which may infer different response times to a shared driving mechanism. Formal cross-correlation revealed significant shared cyclical behaviour of approximate 34 years. Quantifying the periodicity through spectral density analysis, the data for westerly winds was dominated by a 37.50 spectral peak and a secondary 9.37 year peak, whilst the NAOI data was dominated by 25.0 years and 7.5 years respectively. Whilst the cross-correlation identifies a close relationship between the NAO and the westerly winds, linking regional wind regimes to hemispheric circulation, differences in the dominant frequencies suggest that the

westerly winds reflect more clearly higher order periodicity on the scale of the Bruckner cycle (30–45 a).

The exploratory data analysis identified significant influence on the wind data from solar Schwabe and Hale cycles. Although there has been increasing recent research investigating the solar influence on climate, the idea is not a recent one. As early as A.D 807, the Arabic astronomer, Abu Alfadhli Giaafar, observed sunspot activity (Hoyt and Schatten 1997), but it was not until the mid 1840's until Rudolf Wolf constructed a record of historical data and noticed an 11 year cyclical pattern and also the presence of a long period, 83 yr, cycle (later known as the Gleissberg Cycle). Links to the role of solar strength variability on the Earth's climate were first speculated by Herschel (1801) and have continued by many authors more recently (Haigh and Blackburn 2006; Hoyt and Schatten 1997; Ineson *et al.* 2011; Langematz *et al.* 2005; Scafetta 2012b).

Ineson *et al.* (2011) identified weaker westerly winds in winters at the minimum phase of the 11-year sunspot cycle; comparing Figures 2-29 and 2-41 a similar pattern is seen, with westerly winds increasing approaching the solar maximums. Comparison between the total number of wind counts and the Wolf's sunspot cycle (Figure 2-41) reveals a tentative positive link between the two, or perhaps an indication of a shared driving mechanism. Despite the limited nature of the wind data in relation to the long term periodicity of the sunspot data, and since atmospheric tides are thermally driven it seems reasonable, in light of the exploratory data analysis and the NAO data, to propose a link between regional wind patterns and variable insolation (recorded as the sunspot cycle indices). Irradiance driven climate change remains controversial science, global insolation is recorded to only vary by $< 2.5\text{Wm}^2$ throughout the Schwabe cycle and thus the magnitude of change thought to be insufficient to drive observed global surface air and sea temperatures. (Foukal 2012; Foukal *et al.* 2006; Frohlich and Lean 1998). It is this 'bottom up' approach which has dominated research and climate models until more recently, when spatial stratospheric responses to spectral variation and photo chemistry began to be included as 'top down' forcing (Gray *et al.* 2010; Haigh *et al.* 2010; Oberlaender *et al.* 2012), identifying differential heating responses and coupled stratosphere-troposphere interactions (Haigh and Blackburn 2006; Langematz *et al.* 2006). More recently however, it has been postulated that the solar impact on climate may be more complex than total solar irradiance (TSI)(Veretenenko and Ogurtsov 2012), based on findings that “ the total radiative forcing associated with solar cycle variations is 5 to 7 times larger than those associated with TSI variations” (Shaviv 2008).

The trend shown by the total wind direction counts (Figure 17), may provide evidence for the longer period Greissberg cycle, which has been reported in other natural systems for example the river Nile as an 80 cycle (Yousef 1995b; Yousef 2000), in the nitrate content of the Tibetan ice plateau as an 88.1 year cycle (Wang *et al.* 2000) and in tree ring data from the Koala Peninsula Scandinavia (Raspovov *et al.* 2000).

Linking the regional responses of climate change to more global indices and orbital variability will help to develop understanding of patterns of long term climate change and enable a better separation of anthropogenic driven responses from natural system behavior.

2.2.5. Summary

Wind regime data for the East Coast of Scotland revealed general patterns with an abrupt increase in the total directional wind counts during the 1940's -1950's, which corresponds to a period of increasing magnitude of the solar activity as marked by an increase in sunspot activity during this time. The greatest contribution of wind counts was from westerly winds. The significant (95%) periodicity within the total counts and those of the west winds were the same; 22.5, 15, 11.25, 9, and 7.5 years, corresponding to primary and harmonic periods of largely solar activity, with additional periods from orbital influences of the moon and Jupiter. East winds displayed similar significant periodicity at 22.5 and 15 years but these were dominated by frequencies about the main peak at 2.8 years, inferring a different driving mechanism. In general over the sampling interval, as west winds increased, east winds decreased and vice versa.

Analysis of NAO data also revealed the presence of significant frequencies dominated by 2.67 years over a sample interval 1936-1981 and by 7.5/ 7.8 and 2.68 over the interval 1825-2010. Cross-correlating the September-November NAO with the percentage contribution of westerly winds revealed a significant relationship (>95%) over multiple lags displaying cycles of approximately 34 years. Individual periodicity for the westerly wind cross-correlation input was dominated by a 37.50 spectral peak and a secondary 9.37 year peak, whilst the NAOI data was dominated by 25.0 years and 7.5 years. The cross-correlation identified a close relationship between the NAO and the westerly winds, linking regional wind regimes to hemispheric circulation with differences in the dominant frequencies suggesting that the westerly winds reflect more clearly higher order periodicity on the scale of the Bruckner cycle (30–45 a).

Evidence for the presence of orbital and solar cycles was found consistently throughout these analyses, suggesting that orbital forcing has a major control not only on the Earth's climate but also likely on solar activity. It is further postulated that with a deeper understanding of the coupling between these systems it may be possible to make more comprehensive predictions to the impact of future climate change.

2.3. Spatial Data

Section 2.3 investigates the directional trends and gross morphological changes that the estuary has undergone over long timescales. The analyses aim to capture change that transgresses decades to almost centennial scales to identify any potential pattern in variability that may link environmental responses to climate drivers.

2.3.1. Introduction & rationale

Four selected 'areas' of study were chosen that would display different representative responses by the estuary to climate variability on multi-decadal timescales.

- The migration of the seaward section of the river Eden channel. Whilst channels are known to migrate in response to dynamic natural processes, in assessing the differential rates of movement, patterns present may be directly linked to climate variability.
- Changes to the shoreline dune frontal positions
- The analysis of changes to topographical elevations to identify directional trends in erosional or depositional phases of evolution.
- Trends in the spatial extents of particular key species as proxies for ecosystem health.

2.3.2. Channel migration of the river Eden

Historical aerial photographs, satellite imagery and sequential bathymetry datasets (1946 – 2010) have been used here to quantify movement of the seaward end of the river Eden channel, which has been observed to move in a gradual north-westwards direction over many decades by a process of lateral migration. Channel migration is the lateral shifting of a river channel, fundamentally driven by dynamic natural gravitational and topographical processes that include Coriolis & centrifugal forces, flow, bank erosion and aggradation (Castelle *et al.* 2007; 2007; Morales *et al.* 2001). These processes allow the release of energy, which in turn effects the distribution of sediment in a feedback mechanism. Of these drivers, it is yet unknown exactly which is the dominant process for the Eden.

First reference to migration of the seaward end of the Eden channel was made by Keith Eastwood (1977) who noted an important phase of shifting to have taken place between 1895 and 1919, when some 880m of northward movement was observed. A repositioning of the channel seen in the 1949 aerial photographs also revealed a relic 1919 channel, Eastwood describes this rapid movement to the new position to have occurred from an avulsion rather than gradual movement, since there was an absence of intermediary positions. The Eden channel was also described as shoaling seawards

towards the delta, with river flow continuing to exit via a narrow channel cutting the crest of the delta. Such shoaling may be evidence of aggradation and could have conceivably have contributed to the avulsion.

Ferentinos & McManus (1981) also mapped changes in the position of the Eden channel over time using historical maps & aerial photographs to digitize the channel positions. Their study revealed a gradual change in position between the period 1855 and 1981, with rates of movement calculated latterly, between 1949 and 1981, as 10 my^{-1} . Ferentinos & McManus concurred with Eastwood regarding a probable avulsion causing the southerly repositioning of the channel. However in their analysis of migration of the river Tay channel, they observed both gradual northward & southerly movements together with changes to the depth of the channel. It seems likely though that the cause of the gradual southerly Tay movements may have been due to dredging (as channel maintenance) however no specific reference is given to this.

Aims

- Identify rates of migration for the periods available.
- Investigate potential causal mechanisms for changing rates.
- Link patterns in rates of movement with observed climate trend patterns.

2.3.2.1. Methodology

Identifying rates of migration

Aerial photographs were acquired from the Royal Commission on the Ancient and Historical Monuments of Scotland (RCHAMS) as digital format (Crown Copyright, for use only within this thesis). These were imported into GIS and rectified using EDINA ordnance survey 1:10,000 base map, linking permanent features visible on the photographs to the same features present on the base map (e.g. roads, field boundaries, buildings, etc). The photographs were then saved as rectified TIFF images containing spatial information (British National Grid, OSGB_1936 Datum). Where photographs were not available, satellite imagery was used in the form of Quickbird, LANDSAT-7 and Ortho-SPOT and also bathymetry data, which was obtained as swathe sidescan twice per year during the PhD.

Error estimation: in using different sources of spatial data, it was unavoidable to collate a dataset with different spatial resolutions. The LANDSAT-7 and Ortho-SPOT data have a relatively coarse horizontal resolution of 23m (with additional panchromatic band at 15m spatial resolution). The Quickbird data have a much finer resolution of 0.6m panchromatic and 2.6m for multispectral. Bathymetry data has the highest spatial resolution, being cm scale acquisition, binned to 1m. The

aerial photographs are rectified in GIS with a maximum rms error <25m, however the final accuracy is highly dependent upon having sufficient points visible on the photographs to rectify the image.

Using ArcGIS 9.3 (Esri) shape files (polylines) were built for channel centre positions, as this was considered the most feasible way of determining movement of the channel (contours were only available for bathymetric data). To calculate the area of migration, the most accurate repeatable method for estimating the rate of channel migration took into consideration the differing shapes / sinuosity of the channel, i.e. from year to year movement was rarely at the same location along the channel section and hence a simple linear transect at selected locations wasn't possible. The most robust method was found to be by measuring equal lengths of channel section from a common hinge point and calculating the area in meters² between the measured lengths. Using the measuring tool, a 2250m length for each channel centre line (shape file) was measured from a common 'hinge point' and the area between successive periods was then digitized (polygon shapefile). Using the 'calculate geometry' functionality within the attribute table options, the area in m² was calculated. The rate of migration was calculated by dividing the area by the number of months in the period and then multiplying by twelve to give m²y⁻¹.

Using Microsoft Excel (2003) a table of migration rates for the time periods was constructed.

The channel centre positions & relative areas of migration were displayed in GIS as a 1:12,000 map, for visual assessment of sinuosity and relative migration rate. Finally Microsoft Excel (2003) was used to plot the rate of migration as anomaly data (difference from group mean) for the time periods.

Identifying potential causal mechanisms

Various environmental data were collated for investigation to potential drivers of channel migration. Analysis of river data was undertaken to explore either a direct relationship with respect to point erosion at low tides, or indirectly by interrupting long-shore drift. The NAO was also explored, as an indicator of phases of particular weather conditions (i.e groups of positive / negative years), impacting on wind and wave provinces, potentially altering tidal asymmetry and again altering long-shore drift.

River flow data (1968-2010) sourced from the National River Flow Archive (NRFA), is Copyrighted to the Natural Environment Research Council (NERC) and is used here for research purposes only. Mean monthly flow (cumecs) was calculated for the relevant periods.

The NAO climate index used here was downloaded from KNMI Climate Explorer (2011), as monthly values (1946 – 2010). Following the previous results for river flow analysis in section 2.1, the mean monthly values were also expressed as the mean September to November de-trended index.

A table of attributes was constructed as exploratory analysis, for which the data was sorted by period & also by rate of migration for ease of assessing increasing or decreasing trends. The data in

the table is limited by the river flow time series (1968-2010). Extreme flows were defined here as flow that exceeded two three standard deviations from the mean monthly values for the time series. These were then normalised by dividing the number of extreme flows divided by the number of months in the period.

Microsoft Excel (2003) was used to plot the regression of migration rate against the mean monthly river flow, to assess the role of flow in contributing to differential migration rates.

Microsoft Excel (2003) was also used to plot anomaly data (departure from mean conditions) for the mean NAO index against the different time periods (September to November NAO wasn't plotted based on the results from the table of attributes). This analysis was done to understand if regional or more hemispheric (Global?) climatic conditions were contributing to patterns of channel migration.

Identifying links to Climate indices

Data: the NAO climate index (KNMI 2011) expressed as the mean September to November de-trended index (deviation from mean conditions) was used here, as it was previously found in section 2.2 to correlate well with the percentage of westerly winds, which are known to impact on estuarine circulation and asymmetry (Burchard 2009; Geyer 1997; Li and Li 2011; Scully *et al.* 2005; Whitney and Codiga 2011). The Wind data (BADC & Meteorology Office) were expressed as the percentage of westerly winds (as per section 2.2), presented as de-trended data (deviation from mean conditions).

Microsoft Excel (2003) was used for exploratory data analysis; plotting the percentage of westerly winds and September - November NAO index against time. To identify similarities in trend between these and the differential migration periods, the time frames were overlain as shaded blocks. Observations from the former plot, lead to the development of a proposed schematic model for climate links.

2.3.2.2. Results

Identifying the rate of migration

Migration of the river channel (Figure 2-43) has not followed a uniform pattern giving rise to varying sinuosity from period to period. The area between sequential years was used as a way to measure the rate of lateral shift and varies from approximately 8000 m² to 14,000 m² per year (Table 2-1).

Table 2-1: The rate of channel migration between sequential periods, calculated from digitized positions of channel centres from aerial and satellite imagery and multibeam bathymetry.

Date Range	Rate of Migration (m ² /yr)
1946 - 1948	11250.40
1948 - 1958	13110.84
1958 - 1968	11395.40
1968 - 1975	11159.25
1975 - 1988	12379.17
1988 - 1994	14052.20
1994 - 2000	7804.55
2000 - 2002	10262.88
2002 - 2009	12631.36
2009 - 2010	13382.07

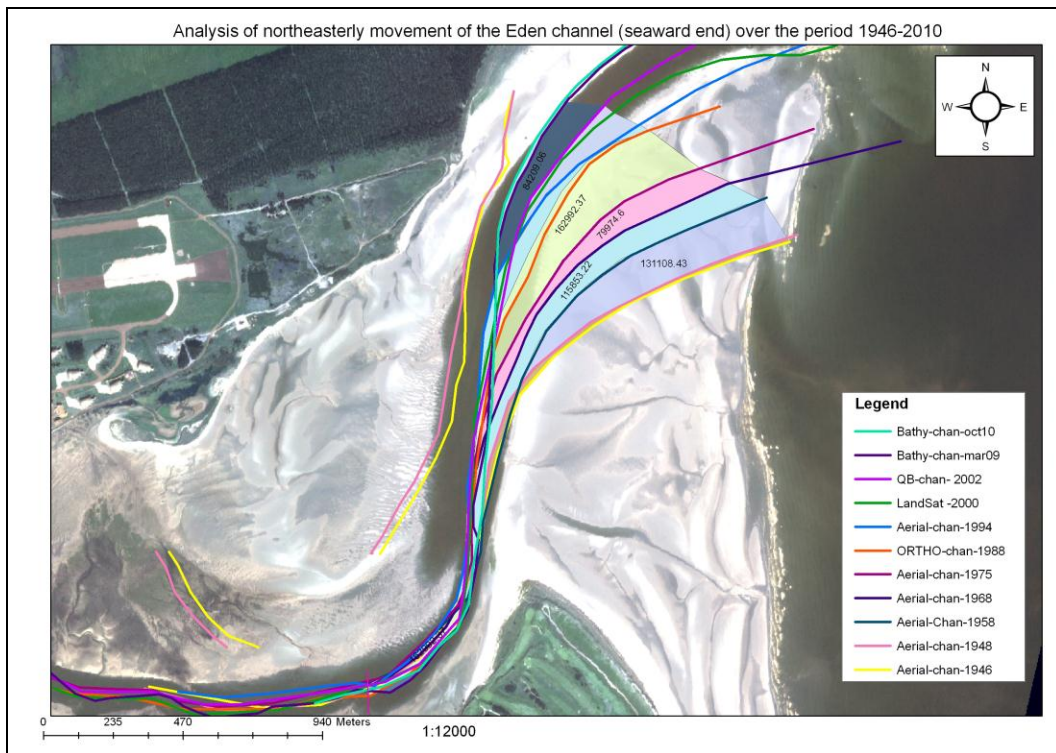


Figure 2-43: Map of the historical positions of the Eden channel. The back ground image is from the Quickbird satellite and is dated August 2002 (copyright 2001-2010 Satellite Imaging Corporation). The coloured sections mark the area (m²) between equal lengths of river channel over sequential periods of time

Presenting the deviation from the mean rate of migration for the different periods (Figure 2-44); the periods 1958-1968 and 1994-2000 are seen to differ the greatest over an approximate time span of 30- 35 years, this period length may be interpreted as approximate to the Bruckner cycle.

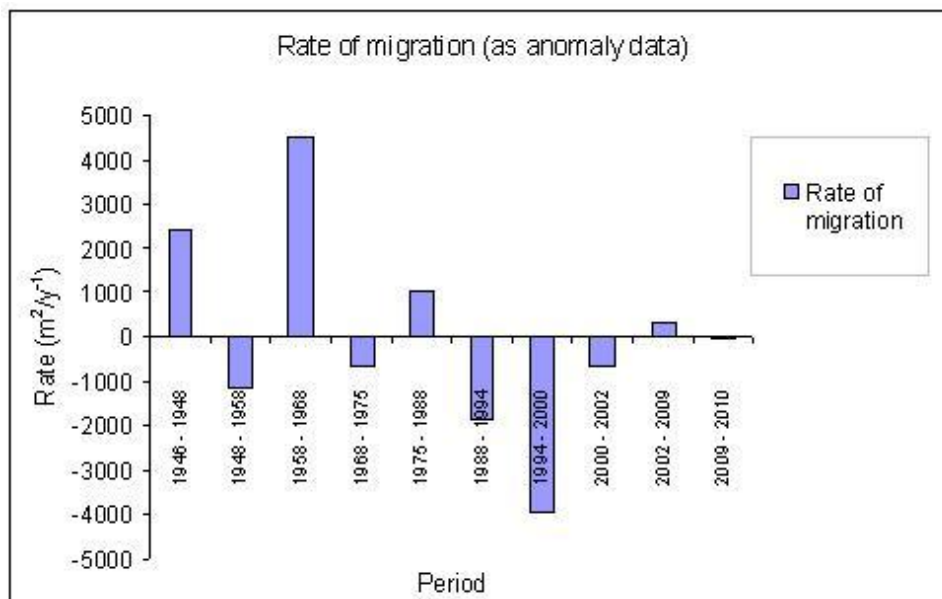


Figure 2-44: The rate of migration for the different time periods, as anomaly data (difference from the overall mean).

Identifying potential causal mechanisms

To identify potential causal driving mechanisms a table of attributes (Table.2-2) for the time periods was used for a quick visual assessment. From the attributes used, the table shows there is no clear single driving mechanism that explains the variability in the rates of migration.

Table 2-2: Attributes to investigate the migration rate of the Eden Channel. The upper half of the table is sorted by time periods (grey) and the lower part of the table is the same data sorted by increasing migration rate. Normalised extreme flows were calculated by dividing the number of extreme flows by the number of months in the period and multiplying by twelve.

Date Range	Mean Flow / Period (Cumecs)	Flows > 2 std. Deviations	> 2 std Normalised/yr	Flows > 3 std. Deviations	> 3 std. Normalised/yr	Rate of Migration (m ² /yr)	Mean S-N NAO	Mean NAO
1968 - 1975	8.150	10	1.390	1	0.140	11159.247	-0.110	-0.110
1975 - 1988	11.338	40	3.038	17	1.290	12379.167	0.004	0.004
1988 - 1994	10.217	14	2.333	6	1.000	14052.198	0.690	0.690
1994 - 2000	10.050	9	1.500	4	0.666	7804.545	-0.248	-0.248
2000 - 2002	12.720	20	9.600	7	3.360	10262.880	-0.052	-0.052
2002 - 2009	11.032	23	3.450	8	1.200	12631.359	-0.371	-0.371
2009 - 2010	10.078	4	2.530	2	1.630	13382.072	-1.188	-1.188
1994 - 2000	10.050	9	1.500	4	0.666	7804.545	-0.248	-0.248
2000 - 2002	12.720	20	9.600	7	2.360	10262.880	-0.052	-0.052
1968 - 1975	8.150	10	1.390	1	0.140	11159.247	-0.110	-0.110
1975 - 1988	11.338	40	3.038	17	1.290	12379.167	0.004	0.004
2002 - 2009	11.032	23	3.450	8	1.200	12631.359	-0.371	-0.371
2009 - 2010	10.078	4	2.530	2	1.630	13382.072	-1.188	-1.188
1988 - 1994	10.217	14	2.333	6	1.000	14052.198	0.690	0.690

Plotting the mean monthly flow (cumecs) against the rate of movement (Figure 2-45) as a regression and calculating the R² value, shows extremely poor evidence for any correlation in mean

monthly flow to increased rate of movement. However, plotting mean NAO index against the rate of migration (Figure 2-46) does show a very general trend for increased migration in more NAO positive periods. The September to November NAO was not plotted, as this was seen to be an approximate proxy for river flow (based on the findings in section 2.1).

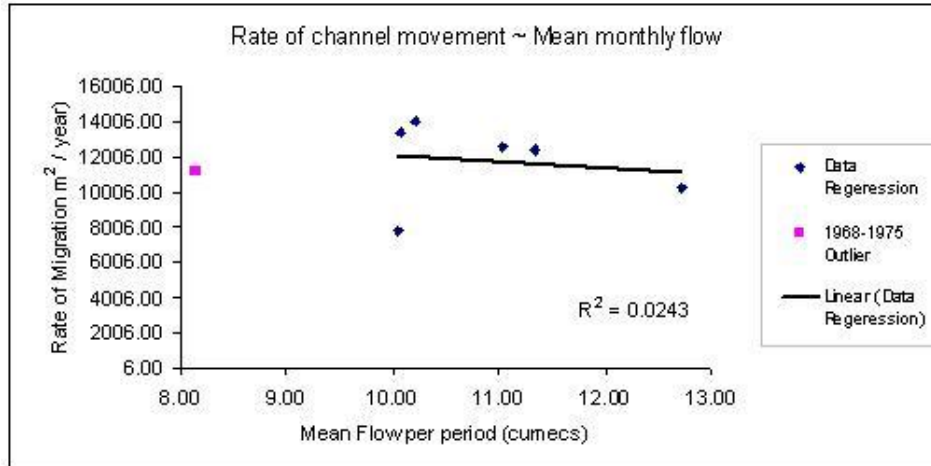


Figure 2-45: Regression analysis between monthly mean river flow for the period, against the rate of lateral movement of the channel.

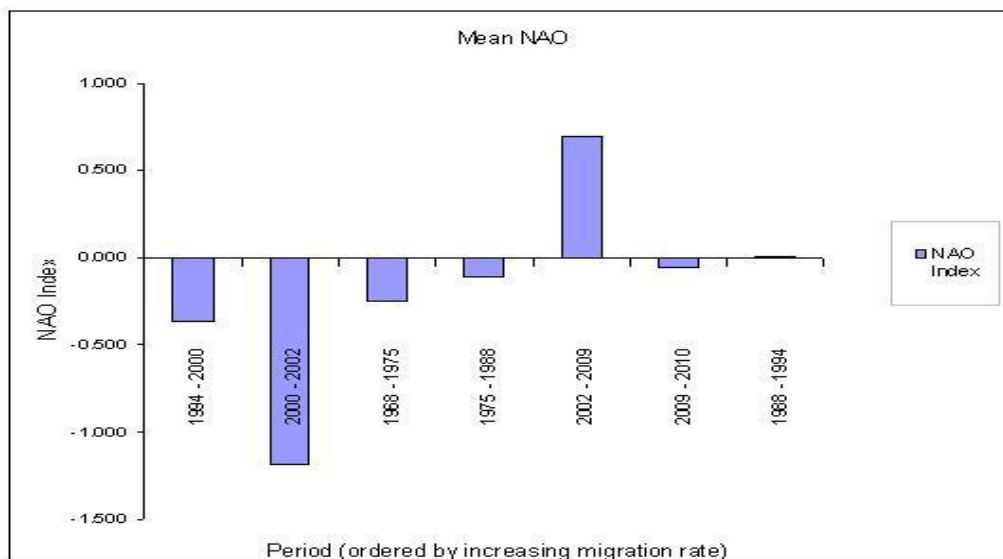


Figure 2-46: Mean NAO Index plotted against the time periods ordered by increasing rate of migration.

Identifying links to Climate indices

Since there was a very general visual correlation between the rate of migration and the mean NAO Index, and it is known that westerly winds slacken during periods of positive NAO indices, the relationship was further investigated by comparing periods of migration with the % of westerly winds (Figure 2-47) to see if the correlation was robust. Figure 2-47, below shows the different migration rates broadly fit into categories of relatively lower westerlies and higher westerlies. Following this

hypothesis, a proposed model for linking migration rate to climate as a driving mechanism is given in Figure 2-48.

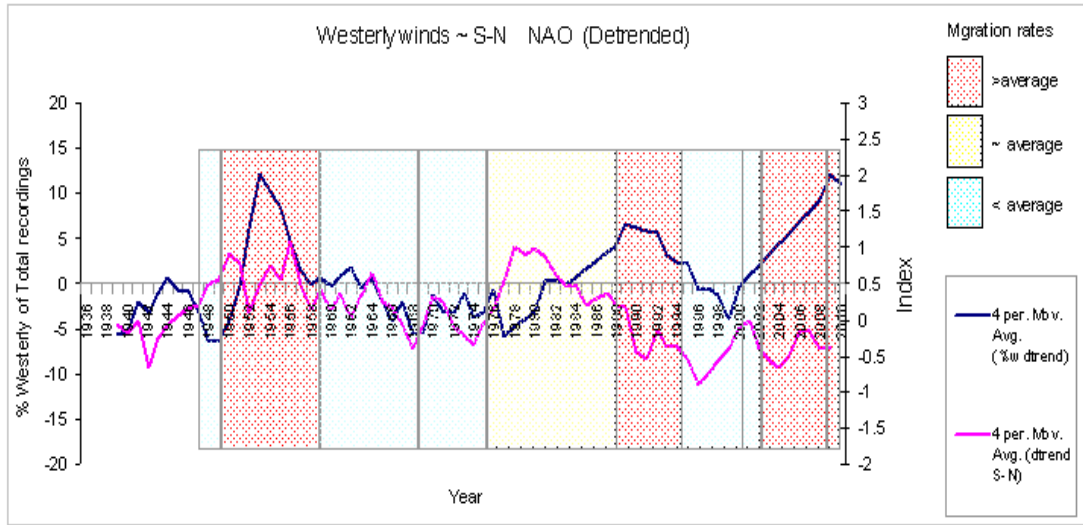


Figure 2-47: The percentage of West winds (of total wind recordings, 1936 - 2010) plotted with the September – November NAO index (both de-trended as anomaly data). The West winds lag behind the NAO by roughly 5 years. Time periods with relatively higher or lower than mean westerly conditions are identified by coloured shading.

The generalized model (Figure 2-48) was formed based on the interaction between the percentage of offshore winds in a particular period of migration and the feedback between the length of the ebb / flood tides and current velocities strengthening / weakening the Coriolis Effect.

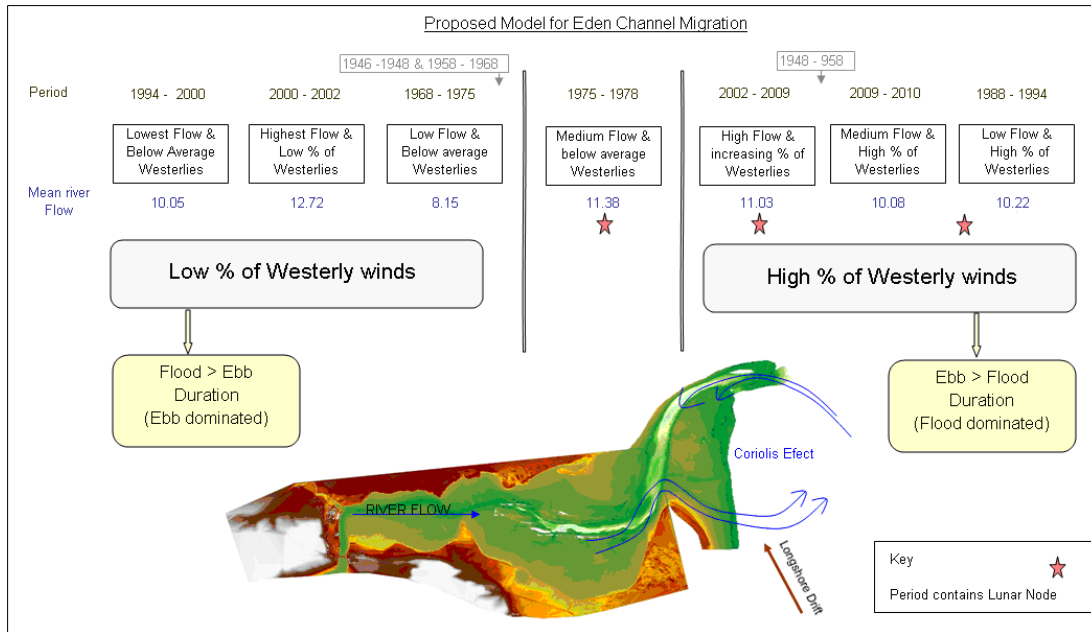


Figure 2-48 Proposed model to explain the differing rates of channel migration exhibited by the river Eden. (The model is designed principally around the availability of river flow data: 1968-2010).

A broad association of relatively below average westerly winds with periods of lower migration rates and vice versa are observed from Figure 5. Sorting the time periods by migration rate, enabled a grouping of similar migration rates with similar percentages of westerly winds, however perfect ordering wasn't accomplished, probably due to errors resultant from rectifying the images and subjective placement of channel centre positions. Despite this three groupings were identified as; 'below average westerlies & slower migration', 'average westerlies & average migration' & 'higher than average westerlies & faster migration'. No linear relationship is directly seen with mean river flow, however lunar nodal maximums also occur in periods of higher migration, which would increase the flood volume further. The model is underpinned by having sustained westerly (offshore) winds altering the tidal asymmetry, consistent wind causing a shorter flood duration. In doing so, following the laws of conservation, the flood velocities become increased and combined with the Coriolis Effect in the outer estuary give rise to stronger northerly erosive currents entering the estuary. Conversely Coriolis force and centrifugal force influencing the ebb tidal currents may be strong enough to cause horizontal flow separation, giving rise eventually to ebb and flood dominated channels respectively. This is possibly already beginning to happen, where a new channel is starting to cut across the bar at West Sands and ultimately may lead to an avulsion.

This model does not take account of Aeolian transport or surface wave erosion, both of which may have a role in altering particularly the intertidal zone.

2.3.2.3. Discussion

Ferentinos & McManus (1981), described the Eden as a drift aligned inlet, with the dominant driver in the positioning of the channel being long-shore drift. This general rationale is consistent with several authors (Ashton and Murray 2006; Lichter *et al.* 2011; Morales *et al.* 2001). However under this hypothesis, one would expect that during periods of higher percentages of onshore winds, long-shore drift would be enhanced and therefore channel migration rates would be higher. The findings of this study are not consistent with increased migration being associated with dominance in onshore winds in fact the contrary appears to be the case. Whilst long-shore drift rates are likely to be enhanced by onshore wind (weakened westerly / Negative NAO conditions) the shortened ebb duration will have increased velocities (under the law of conservation). Therefore currents leaving the estuary under Coriolis and gravitational forces are likely to interact with the northward drift, displacing it more eastward onto the spit in the area of the river mouth. Conversely, relatively weaker ebb velocities occur under more offshore winds, such that long-shore drift continues less interrupted in a northwardly direction contributing to the channel migration process.

The role of dominant wind directions has been seen to have a major role in the mixing and stratification of estuaries (Burchard 2009; Chen and Sanford 2009; Chen *et al.* 2009), with offshore (onshore) winds leading to increased (reduced) circulation and reduced (increased) mixing. Li and

Li (2011) experimented on the effects of prevailing wind on the stratification and circulation in estuaries with and without Coriolis Effects. They found that in the presence of Coriolis induced rotational currents, down estuary wind gave rise to counter-clockwise lateral circulation and vice versa. These findings seem consistent with the proposed model (figure 6.) and when viewed in context with observed trends in the NAO, the model may viably explain the higher and lower rates of migration exhibited by the Eden channel.

2.3.2.4. Summary

The seaward end of the river Eden channel was observed to laterally migrate at rates between 8000 and 14000 m²y⁻¹ (over a 2250m measured section). The movement is not linear and appears to follow a pattern similar to the NAO. The time span between the highest and lowest migration rate is approximately 30-35 years and may possibly be associated to the Bruckner cycle period, however without a longer time series this is just speculative. In terms of causal mechanisms, the most likely mechanism was found to be a feedback between offshore (onshore) winds and tidal asymmetry coupling with the Coriolis Effect and long-shore drift to drive the channel northwards. Patterns of migration rates broadly correspond to trends in the percentage of westerly winds, which similarly correlate to the September – November NAO index (as anomaly data). Therefore linking channel migration responses to more global (or northern hemisphere) climate provinces; it may hence be possible model future channel movements.

2.3.3. Shoreline changes

In section 2.3.2, a conceptual model was proposed for the migration of the Eden channel, this model was underpinned by the prevalence of both onshore and offshore winds. Here this concept is further investigated to suggest a mechanism for the oscillatory behaviour of the shoreline dune frontage on the southern shore of the outer estuary. Whilst it has been previously shown that both the bordering northern and southern shorelines show similar oscillatory behaviour in response to variability in wind and wave conditions (Ferentinos and McManus 1981; May and Hansom 2003; Wal and Mcmanus 1993), the focus here is on the southern shore since it represents a pre-cursor to the migratory channel system. The southern shore also has a more extensive catalogue of historical imagery for analysis.

The accretion along the fore-dune face is dependent upon a sustainable supply of sediment to the beach; a long dry fetch across which sand may be mobilized by wind (Bauer and Davidson-Arnott 2003; Davidsonarnott and Law 1996) and the frequency of erosive tide and wave conditions. The interaction of these controls determines the rates of change and dominance in the direction of change.

2.3.3.1. Methodology

Historical Ordnance Survey maps, aerial photographs (RCHAMS) and Satellite imagery (Satellite Imaging corporation) used in section 2.3.2, were used here to digitize the fore-dune positions in ArcGIS to produce a series of 'polyline' shapefiles. The map of historical shorelines from 1885 to 2009 was then used to determine patterns of shoreline movement over the period. Some caution has been considered in the interpretation of the historical map derived shorelines, as it is known that during the updates of these maps, not all data is re-evaluated and much of the spatial information is carried through from the previous versions.

2.3.3.2. Results

Two patterns can be seen in the development of the shorelines (Figure 2-49). Firstly looking along the seaward shoreline, the dune frontage has accreted significantly since 1855, however the shorelines do not appear as increasing chronologically. There has been considerable accretion in a north easterly direction between 1895 and subsequent years, after which the shorelines are more closely spaced and show both advancement and retreat over the various periods. Secondly, a less obvious pattern is seen at the northern tip of the shore (Outhead), where the tip either points slightly into the estuary, or slightly out seaward.

Figure 2-50, presents the directional contribution of the cardinal wind direction counts, with the dates of the historical shoreline positions overlain. The two shoreline periods with a low percentage of westerlies (offshore winds) and higher percentage of easterlies (onshore wind) are 1968 and 1975 respectively. On Figure 2-49 these two shorelines lie landward of the earlier 1946 shoreline and hence must represent a period of coastline retreat. 1988 falls within a period of sustained onshore winds until the mid 1980's after which offshore westerlies become dominant, which appears to have lead latterly to a slight progradation of the shoreline. The next sequential shoreline is 2002, again following a period of increasingly more negative NAO indices, accompanied by relatively increased onshore winds.

The three periods, 1968, 1975 and 1988 and the baseline 1855 shoreline give rise to an inward facing coastal tip at Outhead, whilst 2002 has a more intermediate position. These periods all lie within or after a sustained period of low or more negative NAO indices (Figure 2-51) and accompanied by more onshore wind conditions (Figure 2-50).

There are limited wind data available for the period preceding 1946, however given the known relationship between westerly winds and phases of the NAO (Hurrell 1995; Hurrell and Deser 2010; Ottersen *et al.* 2001; Trigo *et al.* 2002), Figure.9 shows a sustained period of strongly positive NAO indices from 1895 through to the early 1930's, inferring offshore westerly wind conditions prevailed. This may provide an explanation for the dramatic change in the shoreline advancement between 1895 and 1946, a distance of approximately 250 metres. The 1958 shoreline position lies seaward of later years; it also succeeds a period of strongly positive NAO indices (Figure 2-51) with a

concomitant high percentage of westerly offshore winds and infers a period of shoreline accretion. Similarly, 1994 follows a strongly NAO positive period, with an above average westerly winds (Figure 2-51 and Section 2.2 Figure 2-36).

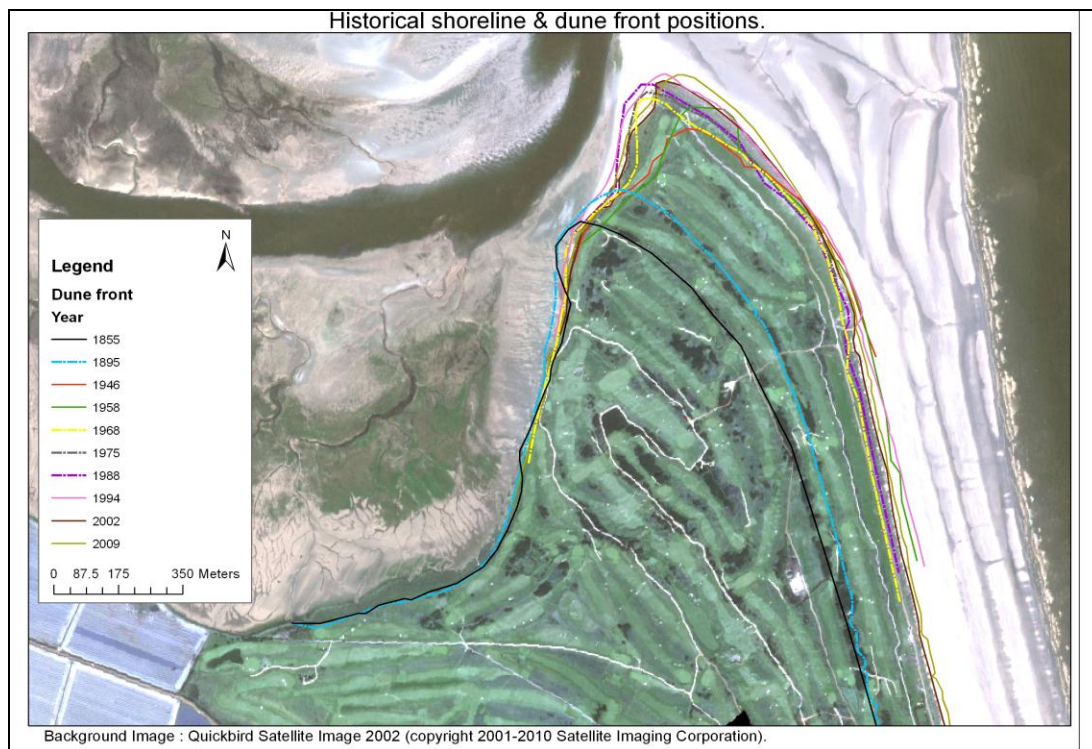


Figure 2-49: Shoreline dune front positions on the southern outer estuary shore. The area is known as Outhead and is part of the St Andrews Golf Course.

The time point 2009 is within a generally more negative NAO period, though following a more positive NAO peak around 2005, the proportion of westerly winds (Figure 2-50) is far higher than 2002 leading to the advancement of the shoreline towards the 1946 position. Interestingly the proportion of westerly winds seems disproportional to the magnitude of the change in the NAO index, which seems to suggest that there may be additional contributory factors.

The 1895 shoreline is seen to be seaward of the 1855 position, developing through a period of generally more positive NAO indices (particularly in the late 1860's and mid 1880's), reflected in the advancement of the shoreline from the 1855 location.

The more out ward pointing shorelines (1895, 2009, 1994, 1958 and 1946) seem to develop following a period of more strongly positive NAO indices accompanied by a higher contribution of offshore westerly winds.

Following the identification of periods of accretion / erosion being associated with dominance of predominantly offshore / onshore winds respectively, a conceptual model (Figure 2-52) was derived to explain the relative positions that the historical shoreline occupy.

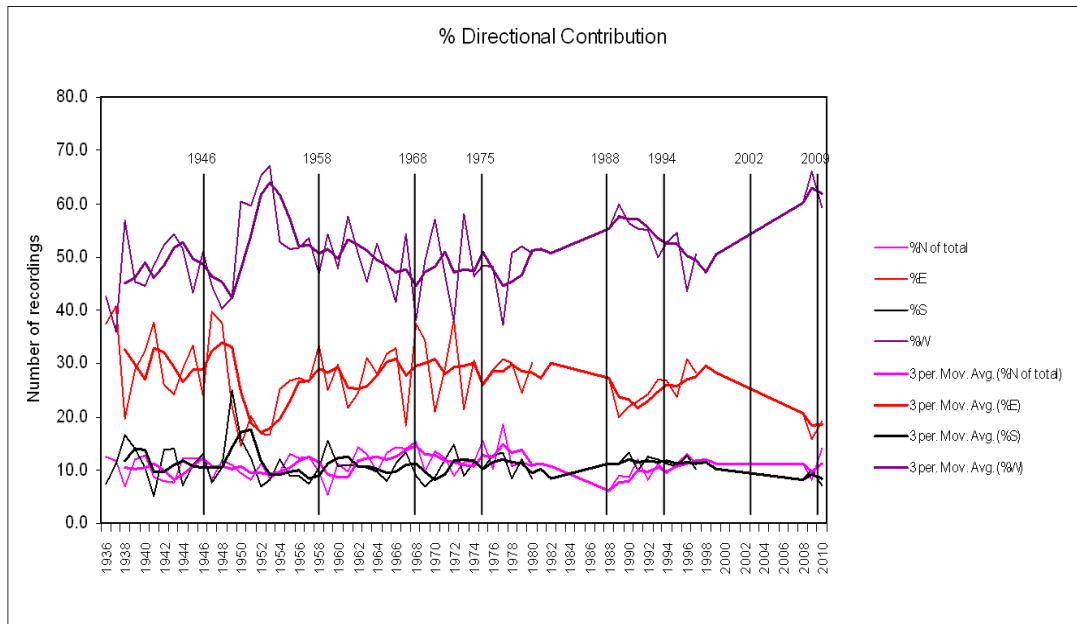


Figure 2-50: Cardinal wind direction counts. (Chapter 2, section 2.2.3)

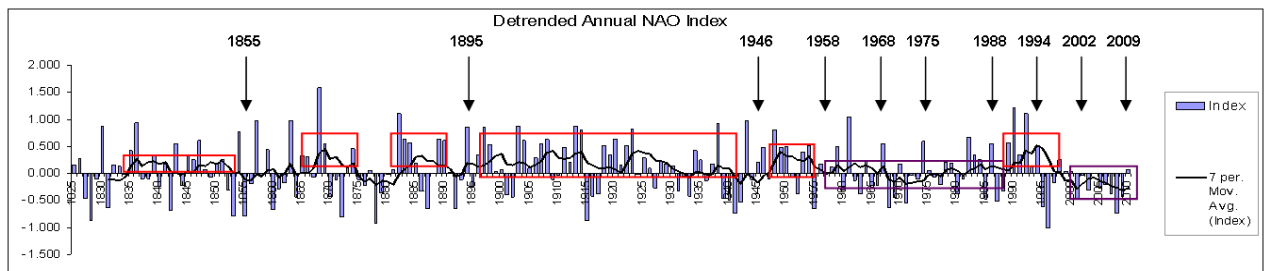


Figure 2-51: Detrended NAO Index values (raw data source : <http://www.cru.uea.ac.uk>)

Figure 2-52 shows the proposed conceptual model to explain the differential development of the shoreline positions between 1855 and 2009. The model is driven by the relationship between phases of the NAO and prevalence of either offshore or onshore wind conditions. While the model is displayed as being dipolar, a continuum of conditions would exist between the two end points.

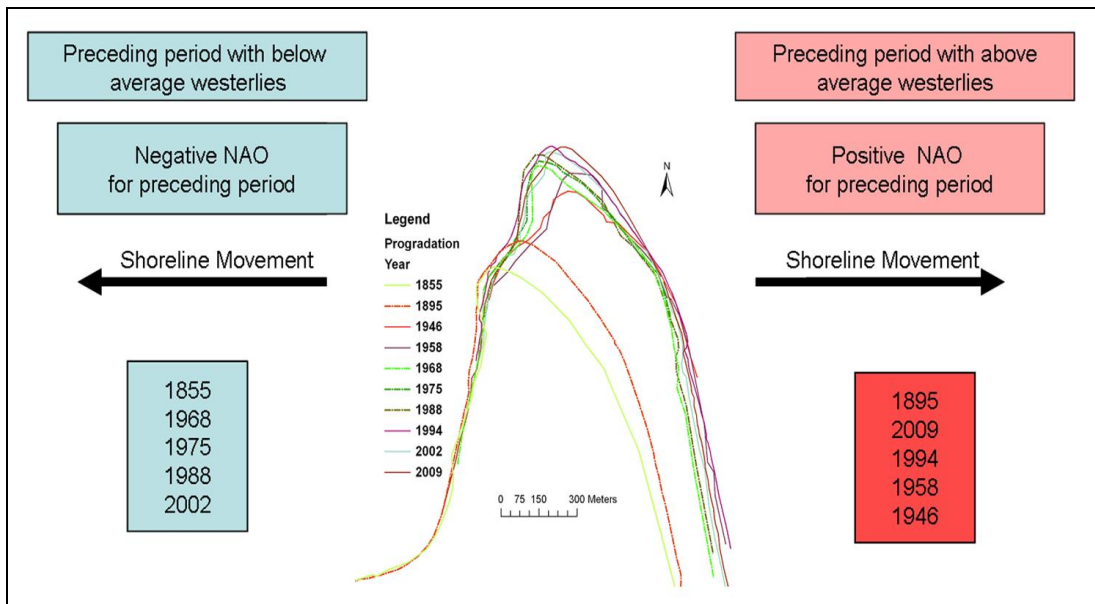


Figure 2-52: Proposed conceptual model for shoreline development (Eden Estuary, seaward south shore).

2.3.3.3. Discussion

From the above data and the conceptual model, two patterns in the spatial development of shorelines emerge; an inward facing coastal tip at Outhead accompanied by seaward dune recession occurs during periods within or after a sustained period of low or more negative NAO indices coupled with largely onshore wind conditions. A second opposing pattern is seen as a more outward pointing coastal tip at Outhead developing following a period of more strongly positive NAO indices accompanied by a higher contribution of offshore westerly winds. The principal factors that determine the spatial pattern are wind and wave activity, however, the way that they interact with the shore is not straightforward.

The progradation of the shorelines under offshore westerly winds might appear counterintuitive, especially considering that longshore drift in St Andrews bay is strengthened by wave refraction driven by onshore winds (Ferentinos and Mcmanus 1981). However Wal & McManus (1993) noted during studies along the Tentsmuir shoreline (to the north of the Eden mouth) that a greater frequency of offshore wind lead to the development of wind-shadow foredunes at the upper beach, in the form of barchans. When persisting through the spring tides, the dunes further accreted aided by pioneer vegetation to form a foredune ridge. The offshore winds can also help to deliver dune grass seed seaward to the embryo dunes, where they become entrained in the newly forming barchans. Similarly, Lynch (2009; Lynch *et al.* 2010) found offshore wind to be an important driver in beach–dune evolution and that dune topography influenced offshore wind flow causing secondary flows in the lee of the dunes, becoming deflected or reversed resulting in sediment

movement alongshore or onshore. Under positive NAO conditions, with prevailing south westerly winds, this may explain the greater advancement under aeolian longshore drift at the northern end of the shoreline compared to the more southerly end.

Wind forms and also modifies the character of waves, changing their impact on the beach and shoreline. Due to the low angled nature of the beach, waves that occur along this stretch of coastline are largely spilling or plunging breakers. The latter are normally generated from long swell waves generated out in the North sea and as they approach the shore the base of the wave is slowed by frictional drag, the crest curls over and plunges downwards dissipating energy over a short area of the beach; as such they tend to have strong erosive power (Wright *et al.* 1999) and may contribute to the movement of sediment up the beach, as well as contributing to erosion of the dune face on higher tides, this is particularly enhanced by lunar nodal tides which at their maximum increase by 3.7% of the tidal range (Pugh 2004). Swell waves may persist after the wind that generates them has subsided, due to the transference of energy over such long distances, thus their impact may be proportionally greater than the local direct wind influence and may contribute the discrepancy in rates between dune recession and accretion. Offshore winds are likely to stall approaching swell waves, through surface friction and on the gently sloping beach causes the waves to break further up the beach in shallower water with more power, surging sediment up towards the higher shore (Paola 2000). During sustained offshore winds the high water may also be lower than predicted as the sea is pushed away from the shore (Pugh 2004), limiting wave erosion of the dune face and providing accommodation space for dune advancement. Onshore winds conversely cause waves to break earlier and in deeper water with less disturbance of the bottom sediment and so providing little nourishment to the mid beach sediment store. At low water the onshore winds move mobile sand from the middle beach to the upper beach and dune face (Hansom 1999; Wal and Mcmanus 1993) and under sustained onshore conditions the mid beach becomes depleted, which may restrict further foredune accretion. The high water level is increased due to water piling against the coast (Pugh 2004) making the dune front susceptible to wave erosion and removal of sediment via increased longshore transport.

Differing rates of accretion are seen in Figure 2-49 which do not appear to linearly correlate to the number of winds recorded (as seen in Figure 2-50), which may suggest other factors are involved in determining the rate of movement. Also the difference between the proportion of westerly winds and the relative magnitude of the positive phases of the NAO similarly infers additional drivers may be contributing to the changes seen, for example the difference between 1994 and 2009 NAO conditions & the percentages of westerly winds.

In the case of the large shoreline changes seen between 1895 and 1946; it is known that dune stabilization was undertaken during the early 1900's with the planting of Lyme grass to help reduce the impacts of erosion (Wilson 1910). This may account for the some of the rapid accretion up to 1946, after which the shoreline seems to be in a more stable equilibrium and oscillates back and forth at relatively similar rates. The addition of the municipal rubbish dump in the 1940's, occupying the end 900m of the shoreline, may also have contributed to expansion and stabilisation of the

dunes up to the 1946 shoreline position, with the inclusion of inert building material acting as a hard defence.

The discrepancy between the expected percentage of westerly winds, as inferred from the NAOI for the period, and the actual recorded winds, may possibly be explained by climatic perturbations caused by a strengthening of the polar vortex leading to an increased pole to equator temperature gradient altering the strength and position of the jet stream (Robock 2000). The years 2008 and 2009 were periods of high incidence of volcanic activity; particularly important was the plinian rhyolitic eruption of Chaiten in Chile, which emitted between 5 and 10×10^{11} kg of tephra between May 2008 & January 2009.(Alfano *et al.* 2011). With the assumption that 20-50 wt% total particle mass was less than 63 μ m, this eruption contributed to between 40 and 290 wt% of the total global average annual ash emissions for 2008 (Durant *et al.* 2011) based on a 1000 year average eruption frequency.

It is known that injection of aerosols to the lower stratosphere can substantially perturb the radiative balance, causing simultaneous stratospheric warming and tropospheric cooling (Fischer *et al.* 2007; Jones *et al.* 2003; Robock 2000). Regardless of the latitude of the eruption, the impacts can be global, depending upon the eruptive characteristics. Despite the relative low levels of sulphur dioxide emitted by Chaiten, the large volumes of silicic fine ash injected into the stratosphere would have caused radiative forcing similar to the silicic El Chichon eruption of 1982, which gave estimated stratospheric heating 20 times the background net levels (Gerstell *et al.* 1995). In August 2008 another explosive volcanic event occurred at Kasatochi, in the Aleution Islands, injecting a mass of 1.6×10^7 kg of ash and 1.5 Mt of SO₂ into the stratosphere (Prejean and Brodsky 2011). These two and a further eruption at Sarycher (NE of Japan) in June 2009 emitting 1.2 Mt of SO₂, through clustering may represent climate forcing that could span decades (eg Crowley 2000). The impact of higher latitude eruptions to European climate, is in mimicking negative phases of the NAO and cold winters, with strong jet stream winds forcing cold air west from Siberia and on to Europe (Robock 2000), which may help to explain the greater percentage of westerly winds within a generally more negative phase of the NAO.

2.3.3.4. Summary

At the seaward extent of the Eden estuary, the bordering northern and southern shorelines show similar oscillatory behaviour, with variable rates of accretion and recession. Further investigation in the pattern of movement highlighted periods of seaward accretion to be associated with increased westerly offshore wind conditions and more positive phases of the NAO and the development of a more outward pointing tip at Outhead. Conversely, coastal recession was associated with more easterly onshore winds, more negative phases of the NAO and a more inward pointing tip at Outhead. Indirect effects from the dominant winds upon wave activity, was likely to have impacted on sediment supply and the relative amount of direct erosion of the shorelines at high water,

contributing to the patterns seen. It is also speculated that the lunar nodal cycle may exacerbate erosion during more negative phases of the NAO contributing to higher tides and dune cliffing.

Anomalies in rates of accretion are seen, particularly between 1895 and 1946, which may be due to dune stabilization with the deliberate planting of pioneer Lyme grass to abate erosion along the shore and also with the development of a municipal rubbish dump towards to end of this period, within the end 900m section of the shore. A further anomaly exists in the difference between 1994 and 2009 NAO conditions & the percentages of westerly winds recorded; 2009 seems to have abnormally high westerly winds than would be expected from the value of the NAOI. This may be explained by the incidence of several large volcanic eruptions occurring in 2008 and 2009, which injected significant amounts of silicious ash & SO₂ into the stratosphere which would be expected to cause global cooling, generally negative NAO conditions and strong westerly cold winds over Europe.

Whilst the relative rates of change are difficult to quantify, due the heterogeneity in response along the shoreline, it is clear that patterns present arise from dominant climatic provinces; such knowledge is of great value in developing management strategies within ecologically and economically valuable coastlines.

2.3.4. Morphological change analysis

Whilst estuaries are ephemeral features in terms of geological timescales, in the relative short term (decades), they are thought to oscillate in a dynamic equilibrium between erosional and depositional phases, resulting from complex feedback relationships between morphology, inflow and current velocities (Dronkers 1986; 1994). By evaluating the current stage that the Eden estuary is experiencing, comparison to previous stages enables predications of future changes in the estuary and thus potentially provides valuable information for the planning and provision of management strategies.

A classification based on the morphological relationship between the development of tidal flats and channel depth causing tidal asymmetry has been proposed by Pethick (1994), this classification is used in this thesis to identify the oscillatory stage within which the Eden estuary is currently in. Type I estuaries were defined as being wide deep estuaries with low lying intertidal flats, displaying flood asymmetry with a net import and deposition of sediment. Type II estuaries are defined as having high intertidal flats (exposed for the majority of the tidal cycle), with a central slot channel, ebb asymmetry giving rise to a net export of sediment. Changes to the hydrodynamics of an estuary through natural or anthropogenic forcing mechanisms may alter the balance between river inflow & the tidal volume (asymmetry) leading to either flood or ebb dominance. Such changes to the length of either the flood or ebb duration will impact on the length of time the current velocities (critical sediment threshold) for residual sediment transport are maintained (Prandle *et al.* 2006), leading to either net import or export of sediment. The morphological influence on asymmetry results from the

modification of flow velocities through frictional drag in shallow water, especially over tidal flats (Lanzoni and Seminara 1998; Lanzoni and Seminara 2002). Since asymmetry in tidal velocity is a fundamental component of estuary classification, 'Asymmetry Analysis' is used here as a tool for evaluating flood or ebb dominance of the estuary, to gain a qualitative understanding of the potential net sediment transport regime, thus enabling the identification of the oscillatory stage and the trajectory of change. This knowledge is valuable in the prediction of how the estuary and its biotic diversity will respond to changes in sediment supply and the vulnerability to erosion and changes to ecosystem function.

'Asymmetry Analysis'; for estuaries with shallow central channels, the mean depth at low water is often less than at high water giving a flood dominated asymmetry with a net import of sediment into the estuary. As the tidal flats become higher following deposition and the central channel deepens, the mean depth at low water eventually exceeds that at high water, giving rise to ebb dominant asymmetry and a net export of sediment (Dronkers 1986; Friedrichs and Aubrey 1988; Friedrichs and Madsen 1992; Pethick 1994; Scully *et al.* 2005). Erosion or deposition dominance may also be determined by the relative lengths of the slack water periods, controlling the morphological development of the tidal flats. Longer high water slack periods enable greater deposition on the higher tidal elevations, whilst longer low water slacks may lead to deposition within and on the channel margins leading to wider and shallower estuaries (Brown and Davies 2010). Changes to either sea level or erosion of the tidal flats, alters the average water depth and may therefore force a change in flood or ebb dominance.

In the absence of historical instrumental tidal data to assess tidal asymmetry, morphological elevations in the form of Light Detection and Ranging (LiDAR) data and contemporary bathymetry surveys (acquired for this Phd) are being considered here to identify morphological changes over the past decade to infer relative ebb or flood dominance and hence potential directions of change that could allow classification of the estuary in terms of an erosional or depositional phase. The earliest LiDAR dataset was acquired for the SNH commissioned report No.007 (2004) and a second LiDAR dataset which was collected in 2009 was made available by SEPA. Bathymetric data sets were acquired in March 2009, November 2009, April 2010, July 2010 and March 2011.

Aims

- Identify gross changes in surface elevation within the estuary.
- Determine the stage of estuarine development in terms of Pethick's (1994) classification and speculate on possible direction and overall rate of change .

2.3.4.1. Methodology

Identifying change

LiDAR

LiDAR is an optical remote sensing technique, acquired here by aircraft, providing highly accurate 3D elevation data over large areas. It uses a narrow beam of short wavelength light to image the ground surface, with each high resolution data point assigned an X,Y and Z coordinates within a geographic coordinate system. The point data are normally used to build Digital Elevation Models (DEM's) to give a surface representation of the point data.

LiDAR data for 2002 was acquired from the National Centre for Environmental Data & Surveillance (NCEDS) by the University as a part of the designation of the Tay and Eden estuary SAC designation. A second 2m raster digital elevation model (DEM) dataset was provided courtesy of the Scottish Environment Protection Agency (SEPA) for 2009 for use within this PhD.

Cross calibration of the two LiDAR datasets was performed to check for 'between survey error', using static elevations measured with RTK dgps. The static elevations used here were stone bridges at Guardbridge and over the Motray water; multiple points were measured at each location and cross referenced by the BNG coordinate with the two LiDAR datasets. The mean error difference from the RTK elevations resulted in a bulk shift of -11.15cm to the 2009 LiDAR survey.

The 2009 LiDAR dataset was imported into ArcGIS (Esri © 1995–2008) as a DEM surface raster dataset in millimetre SI units. The 2002 LiDAR was available as point data which had undergone data reduction for ease of processing and was in meter SI units. The point data were imported into ArcGIS (Esri) and rastered to 1m resolution using the inverse distance weighted solution within spatial analyst. The 2002 raster was then converted to millimetre SI units using the raster calculator in spatial analyst. Having the two DEM's now in matching units, the difference between the two time series was evaluated using the cut/fill option in spatial analyst. This routine identifies the relative change between both data sets

Cross-profile transects were extracted from each of the LiDAR DEM's (See Appendix) using the 'interpolate line' and 'create graph profile' functions on the 3D Analyst toolbar. The data points were then exported from the graph profile in ASCII format. The data were subsequently imported into Excel (Microsoft 2003) to allow both time series to be displayed on the same graph for ease of interpretation.

Contemporary bathymetry datasets were used to extend the time series, as any directional trend cannot be inferred with only two time sampling points, however overlap between the LiDAR and bathymetry is limited to the channel edges. Despite this, channel depth is useful to infer directional change, following the reasoning of Pethick (1994) regarding asymmetry of tidal flow and net sediment transport.

Swath Bathymetry

The bathymetry data were also cross calibrated between surveys, using a long section of scaffold war time tank barrier which was mapped with RTK DGPS. Acquisition survey positioning was sufficiently accurate such that no static corrections were required. The vertical error between the sequential surveys varied between approximately 10 and 20cm.

The Bathymetry data collection began in March 2009, mapping the accessible channel area of the Eden estuary using Swath bathymetry, on the MV Envoy. Surveys were conducted at least twice per year for the main channel area. Line spacing was dependent upon water depth and allowed 50% swath overlap. To optimise swath width / area of ensonification, surveys were undertaken approaching high water. Line positioning was maintained using Hypack software (Hypack.Inc) on the navigation computer at the helm. Acoustic data were continually monitored on the acquisition computer to ensure swath coverage and the data quality was maintained. Table 2-3 outlines the acquisition setup.

Table 2-3. Acquisition system setup summary.

system	Description
vessel	MV Envoy
sonar system	Submetrix 2000
transducer	SEA High Frequency 468 kHz (30 pings per sec) footprint <5cm
Motion Reference Unit	TSS DMS-02 / 05 Mounted directly above the transducers. (TSS inc, Watford, Hertfordshire, UK).
Gps (vessel position)	Vector GPS – Model : Trimble DSM212L , Trimble Ltd, Hook, Hampshire, UK / DGPS input MAX CSI, Calgary, Alberta, Canada.
Heading	Compass: Aximuth 1000 (KVH Industries)
SVP	Applied Microsystems MicroSV .Mounted at the sonar head.
tidal correction	not necessary - as real time RTK DGPS was input to MRU
Navigation software	Hypack Max Survey software version (Coastal Oceanographics Inc.)
Recording software	Swathplus (SEA Ltd.) version 3.07.10.00
survey speed	4 knts approx average.

Survey system calibration: to enable consistency of data quality between surveys, the system geometry was calibrated for Roll, Skew and Pitch

Roll calibration – using a flat area of sea bed, multiple short lines were recorded in opposite directions, with a 50% swath overlap. Data was then processed using SeaSwath (Sea.Ltd 1998-2011) and imported to Swathplus Grid Processor (Sea.Ltd) to calculate the adjustment for transducer angles deviating from the setup geometry.

Skew – Multiple short lines were recorded in opposing directions over a known object at different offsets. Similarly the data was processed using SeaSwath (Sea.Ltd) and imported to Swathplus Grid Processor (Sea.Ltd) to calculate the correction for horizontal deviation of the transducers from the setup geometry.

Pitch - Multiple short lines were recorded in opposing directions up and down a uniform slope. Data was then processed using SeaSwath (Sea.Ltd) and imported to Swathplus Grid Processor (Sea.Ltd) to calculate the adjustment for the deviation in the vertical plane of transducer angles from the setup geometry.

The survey data were then replayed using the corrected acquisition geometry in SeaSwath (Sea.Ltd), filtered for spurious points and noise in the nadir region, before being imported to Swathplus Grid Processor (Sea.Ltd) for further editing and noise reduction. The processed gridded data was then exported as X,Y,Z format at 1m horizontal bin resolution data as a text file. (Analysis is directed toward vertical changes, thus 1m horizontal resolution was thought to be sufficient and would capture horizontal change that has been observed during the period of this study at rates of 40 m a^{-1} in the outer channel)

The data were recorded in coordinate system UTM zone 30 and was converted to OSGB36 using Grid InQuest file conversion software (Geodetic Software Solutions Ltd.) before being loaded into ArcGIS (Esri ; Esri) for analysis.

In ArcGIS the point data was interpolated using the IDW method in spatial analyst, giving a digital elevation model (DEM) for comparison with the LiDAR elevation data and was also displayed for a 3D visual analysis in ArcScene (Esri © 1999–2008). Using the 3D Analyst toolbar function in ArcGIS, cross-sectional profiles were taken at intervals along the channel, the data were output to Excel (Microsoft 2003) for display.

2.3.4.2. Results

Identifying change

LIDAR: Figure 2-53 a, presents the 2002 dataset and Figure 2-53 b, the 2009 dataset. Both share the same colour scheme representing surface elevation. These were used to quantify change between the two time periods, by subtracting one from the other to give a difference plot. The

difference plot between 2002 and 2009 LiDAR is presented in Figure 2-54. Zones where the 2009 data is lower than the 2002 data are coloured blue and zones where 2009 are higher elevations by red. Small difference artefacts are apparent as some E-W banding with small undulations in the along track direction. This is due to small errors in the acquisition positioning. In general, the estuary shows more erosion (blue areas) than deposition (red areas). The deposition is patchy and mostly occurs on the northern outer section of the estuary, with deposition having occurred largely on the channel edges further up channel. The peninsular edges, on the southern shore, show increased elevation however this may be an apparant change due to vegetative growth of *Salicornia* (Glass wort) that grows prevalently here, since the LiDAR can not discriminate between vegetation and sediment elevations.

The difference between the mean elevations of each original raster datasets is 3.8cm (because of differing water levels, the channel area was excluded from these calculations). Calculating the difference between the sums of the binned 'net loss' & 'net gain' volumes in the difference plot, gave a mean vertical difference of 4.7cm (Standard error 3.6 cm) over the 8 year period between 2002 and 2009. The change represents an approximate volume difference of between 173238.8 m³ and 209710.1 m³ (3.8 - 4.7cm vertical change). Assesment of LiDAR transect profiles reveal a gradient of change (Chapter 2 Appendix 1, Figures 1-5), with the upper estuary having a smaller degree of vertical change than the lower estuary and the north shore displaying slightly more change than the south shore. The majority of change is also approximately below the mean neap high water.

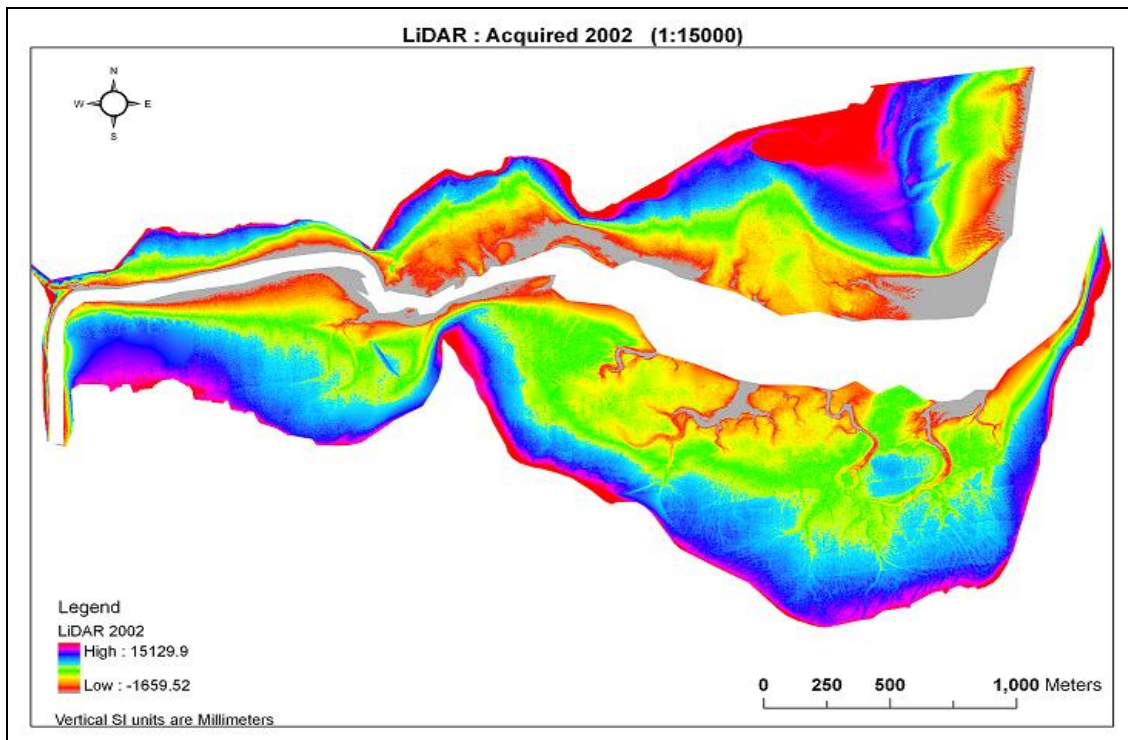


Figure 2-53a: LiDAR DEM: 2002, horizontal units are meters and vertical units are millimetres.

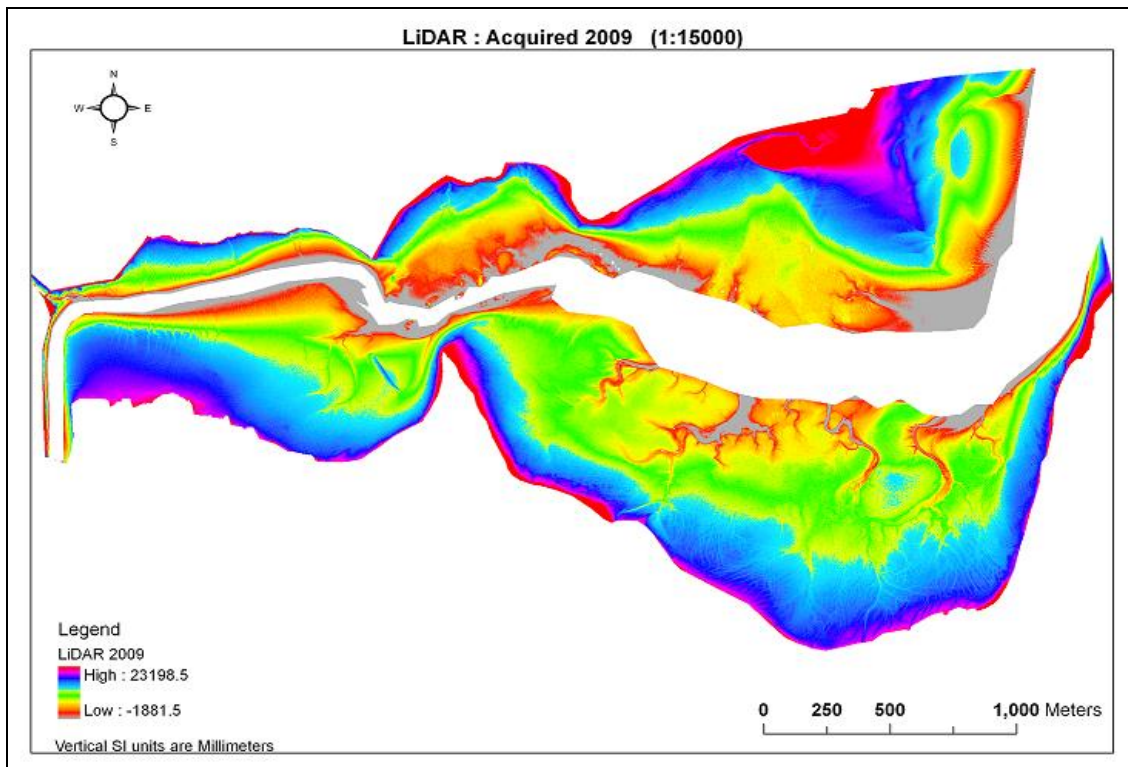


Figure 2-53b: LiDAR DEM: 2009, horizontal units are meters and vertical units are millimetres.

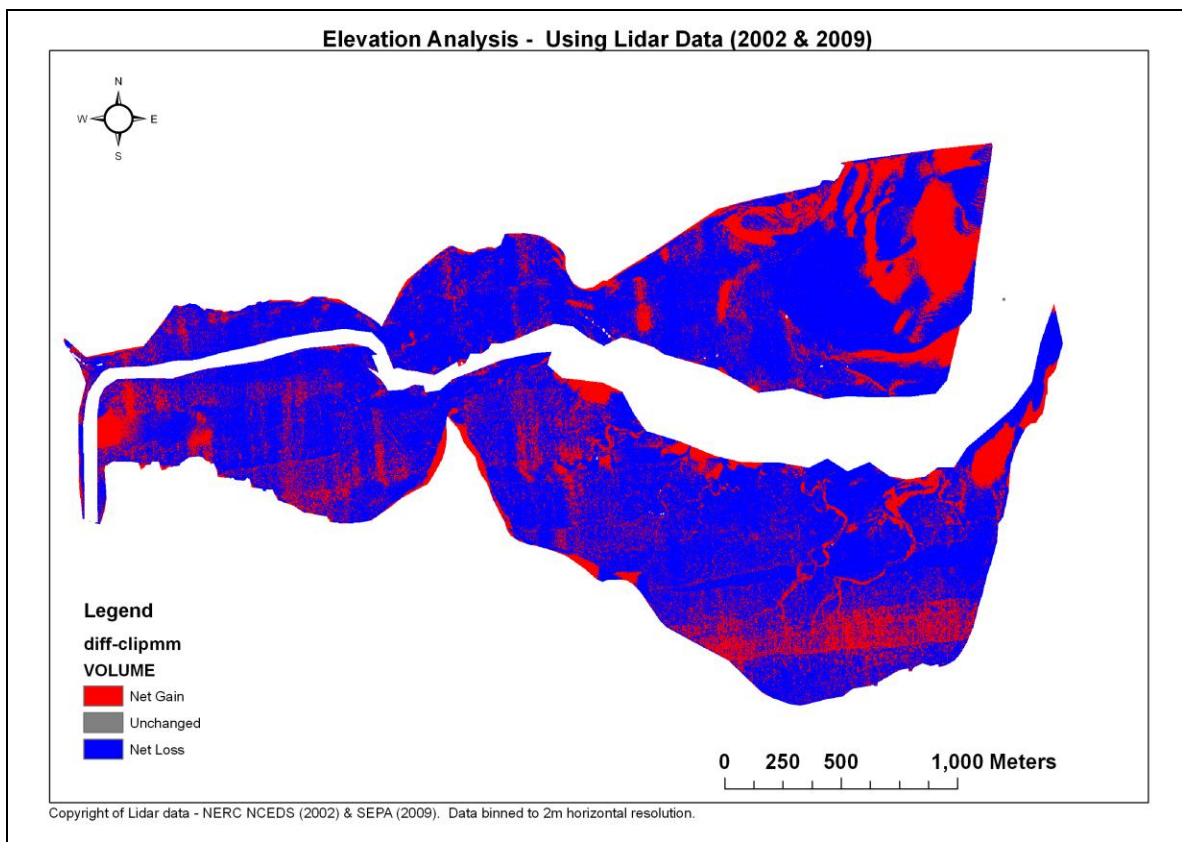


Figure 2-54: A difference plot, showing elevation changes from 2002 to 2009. The LiDAR data is binned to a 2m resolution. Net gain (deposition) is shown in red and net loss (erosion) is shown in blue.

Based on the results of this comparison between two data sets alone it is difficult to understand if there has just been an erosive phase between the sample intervals, or if the system reverted at some time to being depositional. In order to test this and potentially to identify directional trends, the time series was extended using bathymetry data.

Bathymetry: Figure 2-55 shows four 3D datasets; top left combines the March 2009 bathymetry with the 2009 LiDAR data, the following November bathymetry data are overlain in greyscale, to show changes between the two time periods. The further three displays show bathymetry for the channel, in each case the earlier sampling point is displayed in colour and the subsequent sample point is displayed in greyscale. For all displays the same colour legend is used for continuity and is shown on the right. On each of the 3D displays, four cross-sectional transects are marked, to identify change in terms of deposition or erosion and the data for the transects shown in Figures 2-56 and 2-57. The cross-sectional transects are described from the north to the south along the profile and from the inner to outer estuary (T1-T4). The bathymetry datasets are not identical in coverage, thus care must be taken in interpretation when viewing the channel as a whole in Figure 2-55 to appreciate the spatial heterogeneity of erosion and deposition

Between each sequential dataset there has been differing amounts of patchy deposition, the most notable of which was between March 2009 and November 2009. The November data were acquired at the end of the spring tidal cycle, whilst the April, July and March 2011 datasets were following the neap cycle.

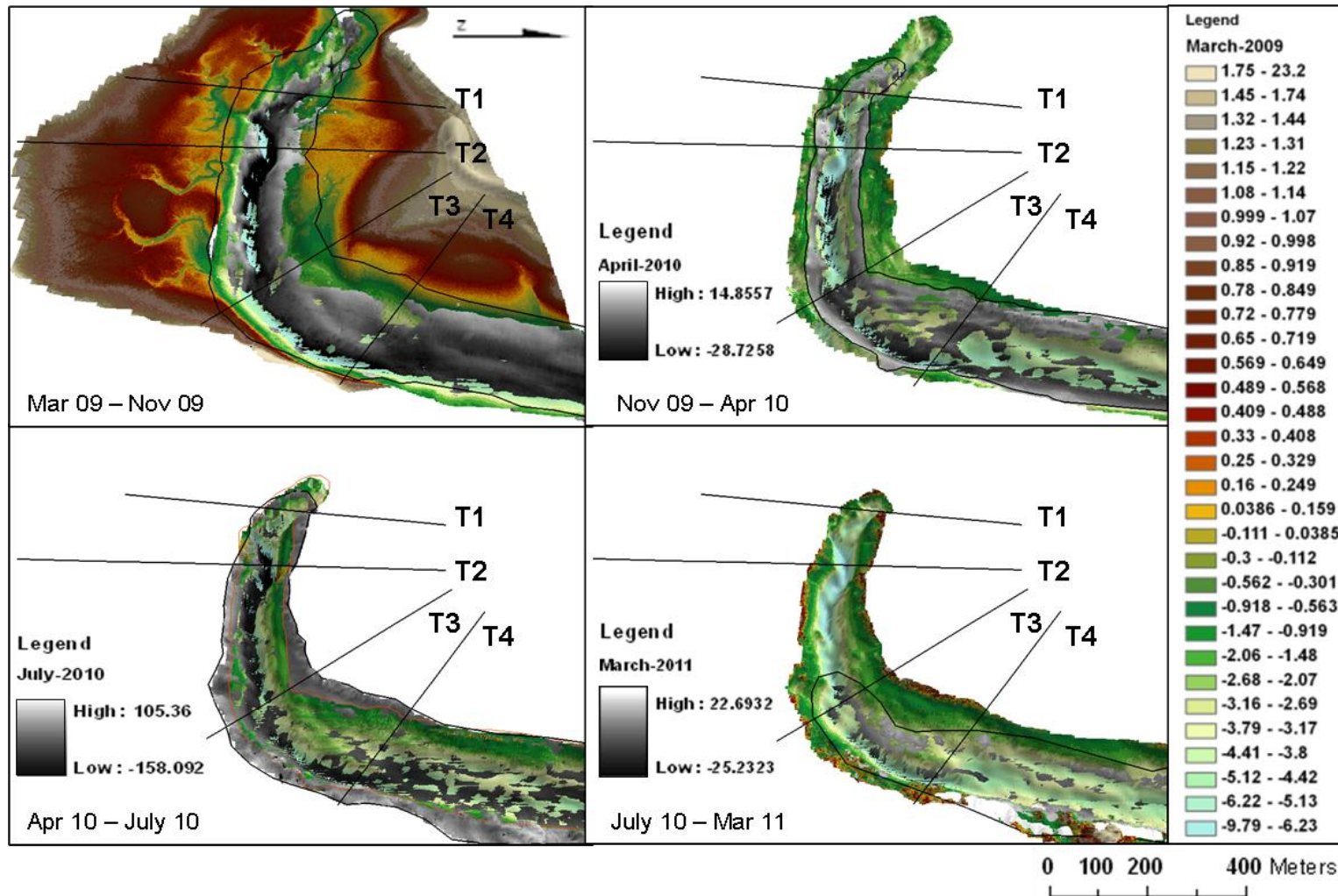


Figure 2-55: 2009 LiDAR merged with channel bathymetry (top left), showing the positions of cross-sectional transects. In each of the four displays the earlier time point is shown in colour (legend on right applies to all colour displays) Where the coloured initial time point extent is less than the second, the earlier data is bound by a brown perimeter line. The second time point is shown in greyscale and the limit of the data is shown by the solid black line. Where the colour shows through, this indicates erosion or no deposition, whilst the presence of greyscale indicates deposition. (Note March 2011 bathymetry begins only at transect 3 and extend out of the estuary to the right).

Figure 2-56 shows the middle estuary transects (T1 & T2) that lay between the tidal flats. Both of these transects, show a general pattern of the central channel becoming more shallow and also elevation increase on the channel edge. Transects three and four (Figure 2-57) are bordered by a sand bar to the south and sand bank to the north. Here a northward movement of the channel and again a general pattern of becoming more shallow over time is apparent.

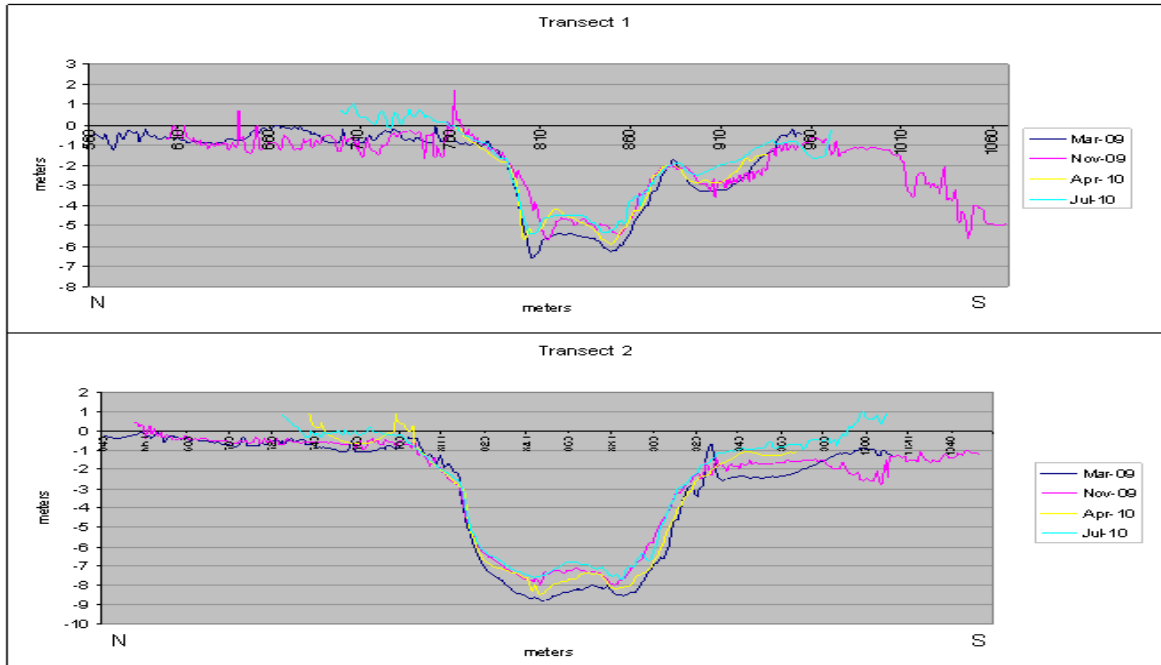


Figure 2.56: Transects 1 and 2, bathymetry cross-sectional profiles located within the middle estuary between the tidal flats.

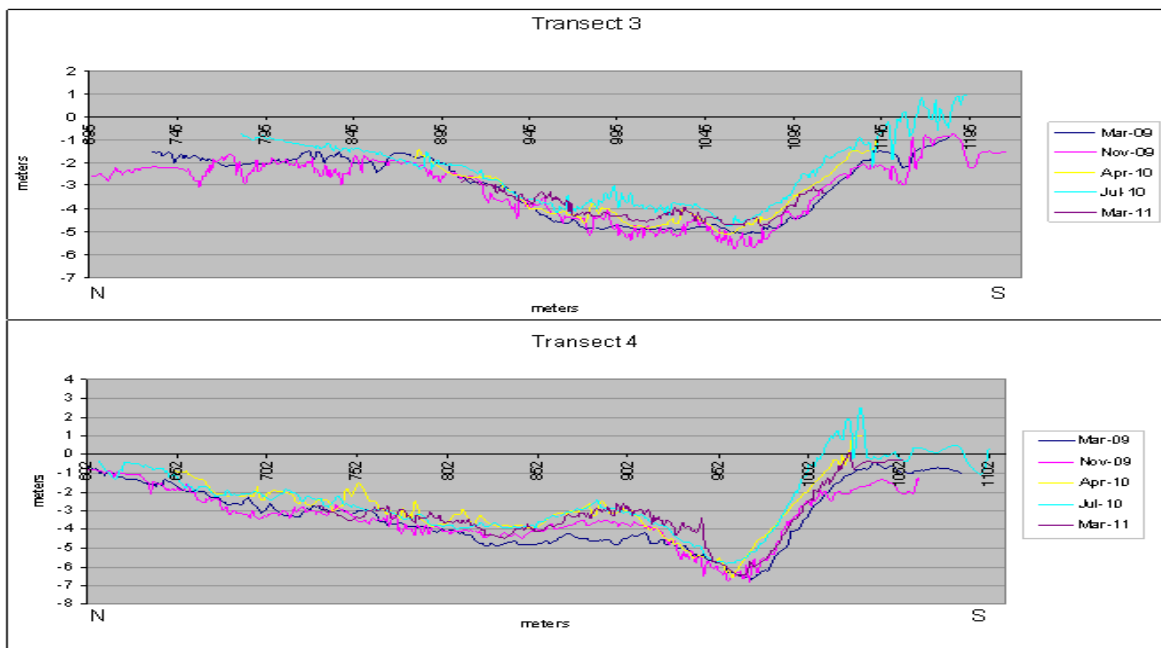


Figure 2.57: Transect 3 and 4, cross-sectional bathymetry profiles in the sand dominated outer estuary channel.

2.3.4.3. Discussion

The LiDAR elevation data indicates that the majority of the estuary has lost sediment between 2002 and 2009 with small areas of deposition towards the outer estuary and on the channel margins. The bathymetry data acquired along the channel between March 2009 and March 2011 extend the LiDAR results and demonstrate that the middle and outer estuary channel had become shallower over time and the outer section migrated northwards. The differences in the scale of change between sampling intervals may be explained by variation in the acquisition timing within the spring-neap cycle, whereby the tidal volume difference impacts on the tidal asymmetry altering the net sediment transport.

While the combined data sets provide more information they still might be inadequate to fully determine long-term trends in cycles of erosion and deposition however they do provide the opportunity to make infer possible interpretations. 1. There has been continued erosion of the tidal flats with the eroded sediment being deposited within and on the channel margins from where a proportion of it may be exported from the estuary. 2. The system no longer displays ebb-dominant asymmetry and is now in a more depositional phase.

The profiles taken across the estuary at different positions demonstrate that both ebb and flood-dominance is seen at different places in the estuary. Ebb- or flood-dominance has been elsewhere reported to change along the length of an estuary, with dominance varying according to morphology / topography based on water depths; the outer deeper water section of the estuary being generally more ebb-dominated and becoming progressively flood-dominated towards the inner estuary (Friedrichs and Aubrey 1988). Robins & Davies (2010) maintain that an increase in mean sea level will result in the shifting of the flood/ebb dominance further up the estuary in a landward direction; with a reduction in velocities leading to a reduction in sediment transport in the lower estuary, but increases in the upper estuary due to frictional resistance.

Both LiDAR datasets were acquired at the opposite phases of the lunar nodal cycle; 2002 was a lunar minimum (almost circular orbit), whereas 2009 was close to the lunar maximum (an eccentric orbit, causing greater gravitational influence). The impact of the lunar maximum is to increase the tidal height by 3.7% of the tidal range (Pugh 2004). At maximum eccentricity the mean tidal range (3.3m) would be increased by 12cm (13mm year^{-1} over the 9.3 years of lunar movement) and may therefore impact on the flood/ ebb dominance. The Eden estuary resembles a Type II estuary, with extensive intertidal flats bordering a central slot style channel. Under Pethick's (1994) classification, one would expect to see largely ebb asymmetry, and with increasing mean sea level the ebb dominance would shift up estuary (Robins and Davies 2010) leading to a proportionally more ebb dominated and erosional environment. If ebb velocities were sufficient enough, the channel may become wider and shallower and eventually may reverse the estuary to a more Type I character.

However, ebb velocities alone may not be sufficient to reduce the tidal flats by the amount observed (particularly at the higher shore), though combined with the more sustained periods of offshore winds (sections 2.2 & 2.3) waves generated within the estuary may have been sufficient to cause

resuspension of sediment (Green 2011) particularly significant at high water (Anderson 1972). With increased water depth the wave heights would also increase and similarly their velocity and erosion capability would increase. Under sustained offshore winds, the tidal durations would also alter, with an increase in the ebb and a reduction in flood duration. Such a reduction in flood duration would likely give rise to higher flood velocities causing an import of sediment. It could therefore be that the enhanced ebb velocities induced by a change in mean sea level, may be offset by the strengthening of flood velocities under sustained offshore wind conditions. The situation is further complicated by fresh water inflow from the Eden and Motray, for which the discharge has increased over the period by 5 cumecs for mean winter flow. Upstream the impact is to strengthen the ebb and weaken the flood velocities. Down estuary (seaward), the opposite occurs as the low water becomes more protracted resulting in a shorter and faster flood (Godin 1985). The protracted low water is exacerbated by the increasing offshore winds, leading to deposition within the channel, whilst the shorter high water slack allows for less deposition to occur on the higher flats.

The bathymetry profiles seem to indicate sediment is being deposited in and on the sides of the channel, which is consistent with longer low water slacks, however from the data available, the source of the sediment is not known. Potentially the sediment may be eroded material from the tidal flats which is redistributed over the tidal cycle within the channel zone. Conversely the source may be sediment brought in from the bar under longshore transport or from offshore under wave activity during the flood tide.

Of all the controls on deposition, erosion and transport of sediment within an estuary, wind waves theoretically would have the larger impact on erosion and re-suspension (Dolphin and Green 2009). Within the Eden estuary, fine sediment eroded and transported during the flood tide may remain in suspension at the short high water slack, under turbulent wind-wave conditions, and is consequently transported seaward by the following ebb currents. Similarly the coarser sediment may also be transported seaward, but over shorter distances, depending on the duration for which the critical sediment transport velocity is maintained. Thus wind-waves within the estuary may act to counteract landward residual transport (Dronkers 1986) and give rise to the spatial heterogeneity of erosion and deposition observed in the estuary..

Although sufficient data are not available to definitively place the estuaries' developmental stage within Pethick's (1994) classification, the evidence accumulated places it most likely within a Type II erosional phase. Since 2011, mean sea level is falling, with respect to the lunar node gravitational influence, potentially shifting the tidal asymmetry seaward and increasing the dominance of the flood tides towards the outer estuary, coupled with a reduction in the frequency of westerly (offshore) winds under the current more negative NAO period, it is likely that toward the lunar minimum, the tidal flats may be replenished under more Type 1 conditions. It was not possible to estimate a rate of change with the data available.

2.3.4.4. Summary

The morphology of the Eden estuary has many inter-related controls that determine whether it is largely in an erosional or depositional phase. From the data it was observed that the estuary had undergone an erosive phase during the period 2002 -2009; bathymetry profiles show since 2009 the channel has become shallower and slightly narrower. A number of discrete drivers are proposed for this change: 1 increased mean sea level driven by the lunar nodal cycle causing a shift in the asymmetry up estuary leading to a more ebb dominated and erosive environment; 2 sustained offshore winds during the period enabling greater erosion within the estuary by wind waves, the erosional material being carried seaward by the ebb currents and deposited more seaward depending upon particle size; 3 increased river flow during the period contributing to a longer ebb duration and strengthening ebb velocities; 4 lowering of the tidal flats caused by internally generated wind waves under a period of higher frequency of westerly (offshore) winds. Following Pethick's (1994) classification, the estuary is therefore classified as Type II ebb dominated with the possibility of future loss of the central slot channel due to infilling by sediment resulting in a reversal in asymmetry to a more Type I flood character.

2.3.5. Species distribution patterns

A decline in local biodiversity often leads to a concomitant reduction in the provision of ecosystem-level processes (Hooper *et al.* 2005; Solan *et al.* 2006). However, the loss of some species may have a particularly strong impact because of their importance as ecosystem engineers and their role in mediating the environment that helps support their habitat. The effects of disturbance on habitats can be difficult to assess and so changes to the extent and spatial distribution of selected taxa (such as ecosystem engineers and keystone species) may be used to indicate a relative measure of ecosystem health. A reduction or fragmentation of habitat may not necessarily impact on diversity (Yaacobi *et al.* 2007), although patch size may be critical to the number of individuals it can support (Herbener *et al.* 2012). In order to examine potential changes in habit and related function, two biotopes were chosen here for spatial analysis, namely, marginal salt-marsh and intertidal eel grass beds.

Marginal salt-marsh was chosen for its importance as a species diverse habitat, for coastal protection properties (Moller 2006) and as an important sink for atmospheric carbon (Chmura *et al.* 2003; Choi and Wang 2004). Eel grass beds were chosen as a habitat with an important keystone species (*Zostera spp*) supporting a hierarchy of dependent organisms and having an critical role in engineering the immediate environment by modifying tidal velocities (Fonseca *et al.* 1982; Fonseca and Koehl 2006) thus enabling the trapping of organic and sediment particles, which improves nutrient availability, and through binding and stabilizing sediment.

Salt-marsh : salt-marsh systems amount to approximately 44,370 ha in Britain (Allen and Pye 1992), they represent transitional habitats occupying the interface between the land and the sea. This habitat is dominated by swards of halophytic (salt-tolerant) plants characterised by regular flushing by tidal flow, delivering sediments, nutrients and moisture to the marsh. Salt-marsh tends to develop on sheltered coasts, largely occurring within estuaries (Allen 2000), where there is protection from strong wave action. Due to their position between the land and sea, they are particularly susceptible to climate change (Simas *et al.* 2001) from both sides in terms of fragmentation by fresh water runoff and species competition from the landward side and altered salinity (through precipitation or evapotranspiration), altered wind-wave climate, sea level rise (Pethick 1993) and sediment supply from the seaward side.

Further, climate change susceptibility is manifest by the relatively low plant species diversity within salt-marshes, as having fewer species weakens the potential to buffer against perturbations. However, despite low plant diversity salt marshes are extremely productive habitats (Pye 2000). Salt-marshes provide a number of ecosystem services; acting as a buffer to wave erosion, providing a habitat to many species of resident and migratory birds, a source of food for a range of organisms and as a medium for the cycling of nutrients. Salt-marshes also represent an extremely valuable sink for atmospheric carbon where decaying vegetative matter accumulates and is decomposed within the marsh under both aerobic and anaerobic conditions. During this process there is an abundance of bacterial sulphate that inhibits the production of other climate impacting gasses, such as CH₄ (methane) and NO₂ (nitrous oxide) (Chmura *et al.* 2003; Giani *et al.* 1996). This discriminates saline marshes from other wetland soils as carbon sinks making them potentially the most valuable of all carbon sinks per unit area (Choi and Wang 2004; Whiting and Chanton 2001). It is proposed that wetland marshes may store as much as 498 Pg of carbon worldwide, which represents roughly one third of the world's soil storage (Eswaran *et al.* 1995). Decline of coastal salt-marsh has been attributed to both natural forcing, through sea level rise, changes to the wave / wind climate and thus supply of sediment, and to anthropogenic forcing through land claim, embankment construction and channel dredging (the latter two increasing the tidal range and current velocities) (Van Der Wal and Pye 2004; Van Der Wal *et al.* 2008). The fate of the eroded salt-marsh material in terms of whether the carbon is released back to the atmosphere or retained within the marine environment is presently not known (Choi and Wang 2004).

Eelgrass: eelgrass (*Zostera sp.*) is a member of the angiosperms (flowering plants), which is often found within estuaries. They are a highly dynamic species, able to acclimatize to a range of environmental conditions often resulting in a fragmental spatial structure (Duarte *et al.* 2006). In appearance they resemble grasses, with long green narrow blade like leaves. The different *Zostera* species may be differentiated by their leaf size and the number of leaf veins (see Table 2-4).

Table 2-4: Identification attributes of the *Zostera* species (Butcher 1941b; Ukmpa 2001; Wyer et al. 1977)

Species	Length	Width	Veins
<i>Zostera marina</i>	20-50 cm	4-10 mm	5-11
<i>Zostera angustifolia</i>	15-30 cm	1-3 mm	3-5
<i>Zostera noltii</i>	10-22cm	0.5-1.5	3

Three species are typically found in the UK, the largest of which is *Zostera marina* (common eelgrass) which was the more common species up until approximately 1917, after which *Zostera angustifolia* (narrow-leaved eelgrass) became more commonly found (Butcher 1934). Both of these species usually occupy more saline conditions and are found submerged in runoff channels or grow below mean low water neaps (Wyer *et al.* 1977). The smallest *Zostera* species is *Z. noltii* (dwarf eelgrass), which favours lower salinities than *Z. marina* or *Z. angustifolia* and ranges from the mid to high shore and tolerates exposure (Davison and Hughes 1998). Although the *Zostera* species are seed producing, they largely spread through vegetative propagation via clonal creeping rhizomes (Duarte *et al.* 2006) leading to low genetic diversity within patches (Larkum *et al.* 2006). Having low genetic diversity reduces resilience to disease (Adams *et al.* 1971), which may have led to the large pre-1920s UK loss in extent of *Zostera* through the fungal wasting disease *Labyrinthula zosterae*. The slime mould appears to cause disease under higher salinities affecting *Z. marina* more than *Z. angustifolia* (Davison and Hughes 1998), which may explain why *Z. marina* is now less common, however under Annex 1 of the UK Habitats Directive all *Zostera* species are considered nationally scarce..

Although low in genetic diversity, the greatest attribute of *Zostera* is perhaps the ability to display morphological and physiological variation in response to changing environmental conditions and available resources, enabling them to persist where other species are at their ecological limits. *Zostera* are defined as a keystone species, a species that plays a critical role in maintaining and structuring the diversity of their ecological communities and whose impact is also disproportional to abundance (Mills *et al.* 1993; Paine 1969).

In terms of ecosystem services, *Zostera* provides a low energy habitat with ecological niches that gives rise to a highly species rich community of primary and secondary producers. The *Zostera* blades support a large number of epiphyte algal species, some of which live solely on *Zostera* (Davison and Hughes 1998). They are also a direct food source for Brent geese, Wigeon and Whooper swans in the estuary. Within the patches, a wealth of invertebrate species cycle organic matter providing nutrients for a heterotrophic food chain. Below the sediment, the network of roots bind and stabilize the sediment, whilst in the water column the leaf blades reduce local current

velocities and trap sediment particles. *Zostera* are susceptible to severe wave action, flooding and also frost damage. All of which can lead to change in patch density or spatial dynamics (Duarte *et al.* 2006)

Both taxonomic groups are represented by a range of different species; salt-marsh typically shows a spatial zonation of parallel vegetation extending from mean high water neaps to the interface with terrestrial plants, for historical extent analysis it is only feasible to map the perennial mid and higher marsh zones and not the annual pioneer species that occur on the lower marsh intertidal areas (i.e. *Salicornia* sp.) as these generally do not appear on historical maps. Similarly, not all of the *Zostera* species present in the estuary were selected in this study for practical reasons. *Zostera angustifolia* tends not to grow in distinct patches, but as individual plants spaced along the runoff channels and is therefore difficult to map, thus *Zostera noltii* was chosen as an indicator species. Being generally found in the lower salinities, it was also thought that *Z. noltii* may indicate if there had been any shift in the salinity regime.

A scarcity of literature exists on the spatial extents of salt-marsh and *Zostera* species under consideration. The historical ordnance survey maps, whilst valuable for the information they provide, often carry outdated information through from previous versions to the updated maps, leading to uncertainty as to when changes occurred. Aerial photographs are thus preferable for their greater temporal accuracy, however these can be limited by their coverage or availability. The earliest mention of both salt-marsh and *Zostera* is from Wilson (1910) who wrote an extensive narrated inventory of the biota of the Eden. He described the estuary as being 'fairly well clothed' in what looked like long grass and was referring to *Zostera marina* (though more likely it was *angustifolia*). He continues to describe the presence of 'salt-grass flats' being almost composed of a single species, *Puccinellia maritima* (common salt-marsh grass) zoning into the terrestrial *Festuca ovina* (Sheep's fescue / links grass) landward.

Eastwood (1977) describes the migration of Sanctuary spit between 1948 and 1973 over the vegetative remains of a stand of salt-marsh, which previously lay in the lee of the spit on the northern shore of the Eden. Following seaward exposure the marsh was described as being eroded into discoidal blocks that were subsequently transported some distance along the shore onto West Sands beach. In 1978/ 1979 Johnston (1979) wrote, in respect to available historical information at the time, highlighting the virtual disappearance of *Zostera*, however from his maps of *Zostera* species in 1978, clearly a presence was still evident (Figure .8).

By 2003, a survey undertaken just east of Martin's point (Coble shore) revealed a single small stand of *Zostera* sp., which was reported to be 15-20% in cover (Bates *et al.* 2004). The report indicated that several beds were known to exist; *Zostera noltii* on the open flats on the north side, whilst *Zostera angustifolia* and *marina* were confined to the drainage channels on the south, however due to the scale of the survey, detailed mapping of these areas appears not to have been possible at the time.

The scarcity of surveys continued through to 2007, when Fife Coast & Countryside Trust produced their annual report (Strachan 2007) which included a *Zostera* survey at Coble shore, carried out in July of that year. The survey noted only 8 plants were found, however this was probably not representative of the whole estuary, but reflected the availability of sampling effort. From the location, these were likely *Z. angustifolia* at the mid shore stand. Most recently Maynard *et al* (2011) describes the once extensive size of both *Spartina* and *Puccinellia* stands within the estuary to be still apparent some 20m seaward of their present location.

A clear record of the distribution and extent of the two taxa is difficult to establish due to the almost anecdotal nature of much of the records and to the constraints on time and sampling effort for both Ordnance Survey map updates and for the broad scale general surveys. Despite these limitations, valuable information pertaining to the relative health and direction of change for the estuary may be gained, which is not only useful in terms of predicting the potential health of the estuary in the future, but also to plan management and conservation action where required.

2.3.5.1. Methodology

Identifying historical Saltmarsh extents

Rectified aerial photographs and historical ordnance survey maps are used in conjunction with RTK DGPS positions of historical Saltmarsh frontages. (eg Cox *et al.* 2003; Greensmith and Tucker 1965) to identify any change to the extent of cover.

The seaward extent of remnant patches of historical salt-marsh were mapped using RTK DGPS to record the X,Y & Z positions (British National Grid ODN) along the perimeter of the old marsh. The coordinate point file was then imported into ARCGIS (Esri © 1995–2008), from where they were displayed with respect to various historical Ordnance Survey Maps.

Aerial photographs were acquired from the Royal Commission on the Ancient and Historical Monuments of Scotland (RCHAMS) as digital format (Crown Copyright). These were imported into GIS and rectified using DIGIMAP (Edina 2012) ordnance survey 1:10,000 base map, linking permanent features visible on the photographs to the same features present on the base map (e.g. roads, field boundaries, buildings, etc). The photographs were then saved as rectified TIFF images containing spatial information (British National Grid, OSGB_1936 Datum). Where photographs were not available Quickbird satellite imagery was used (S.I.C. 2002). The estimated error for the aerial photographs rectified in GIS approximates to a maximum rms error <15m, however the final accuracy is highly dependent upon having sufficient points visible on the photographs to rectify the image. The Quickbird data have a much finer resolution of 0.6m panchromatic bands and 2.6m multispectral bands.

For each time sample point, the area of salt-marsh was digitized as a shapefile in ARCGIS (Esri © 1995–2008) . Using the ruler tool from the main menu, lengths of sections were measured. Whilst

within the shapefile table, a new column was added using the options menu from which the area of the shape was calculated using the 'calculate geometry' column option.

Historical extents of *Zostera* sp.

A scanned map of the historical 1977 extent of *Zostera* species (Johnston *et al.* 1979) was imported into GIS and rectified using DIGIMAP (Edina 2012) ordnance survey 1:10,000 base map, linking the estuary perimeter shape and features to the base map. The extents of the *Zostera* species were then digitized from the rectified 1977 map and shapefiles created. Within the shapefile table, a new column was added using the options menu from which the area of the shape was calculated using the 'calculate geometry' column option.

During the summer of 2009, patches of *Zostera noltii* were mapped using RTK DGPS to record with X,Y & Z positions (British National Grid ODN) along the perimeter of the *Z. noltii* patches. The coordinate point file was then imported into ARCGIS (Esri © 1995–2008) and converted to a shapefile. Within the shapefile table, the area of the *Zostera* was calculated in the same way as for the historical data.

2.3.5.2. Results

Identifying historical Saltmarsh extents

An exposed section of remnant salt-marsh (Figure 2-58) at an elevation of approximately 2m ODN lies along the north shore of the outer estuary. This marsh was also seen in the 1947 aerial photograph (Figure 2-59), at which time the extent was approximately 6640m² where it is protected behind Sanctuary spit. Since this section of coast is at present located in front of the spit, the spit must have migrated over the top of the marsh (in accordance with Eastwood (1977)).



Figure 2-58: Remnant salt-marsh, which is located along the north shore of the outer estuary.



Figure 2-59: Aerial photograph 1947 copyright RCHAMS (1946 left), showing where the salt-marsh (remnant in light green) in Figure 2-58 used to exist before the sand spit migrated over the top of the marsh post 1947.

An analysis of the sequential aerial photographs (Figure 2-60), indicated that the marsh persisted through the 1960s and 1970s as Sanctuary spit develops. Between 1975 and 1988, the length of the section of marsh reduces from 350m to 250m, with the reduction being on the seaward side. By 1994, the spit has migrated south-westwards and over the majority of the marsh, leaving only a small section enclosed between the spit and the land. By 2002 the spit has largely become static and the area enclosed in filled with sediment, probably washed over from the seaward side and also from finer material brought in from the landward runoff drainage channel from Tentsmuir.

The marsh existing behind the spit today is largely is dominated by *Phragmites australis* (Common reed) and *Bolboschoenus maritimus* (previously also known as *Scirpus maritimus*- Sea clubrush). This marsh obtains its nutrients, particulate matter and required sediment for vertical accretion from landward runoff by a stream from Tentsmuir and also tidally from seaward into the semi-enclosed area behind the spit.

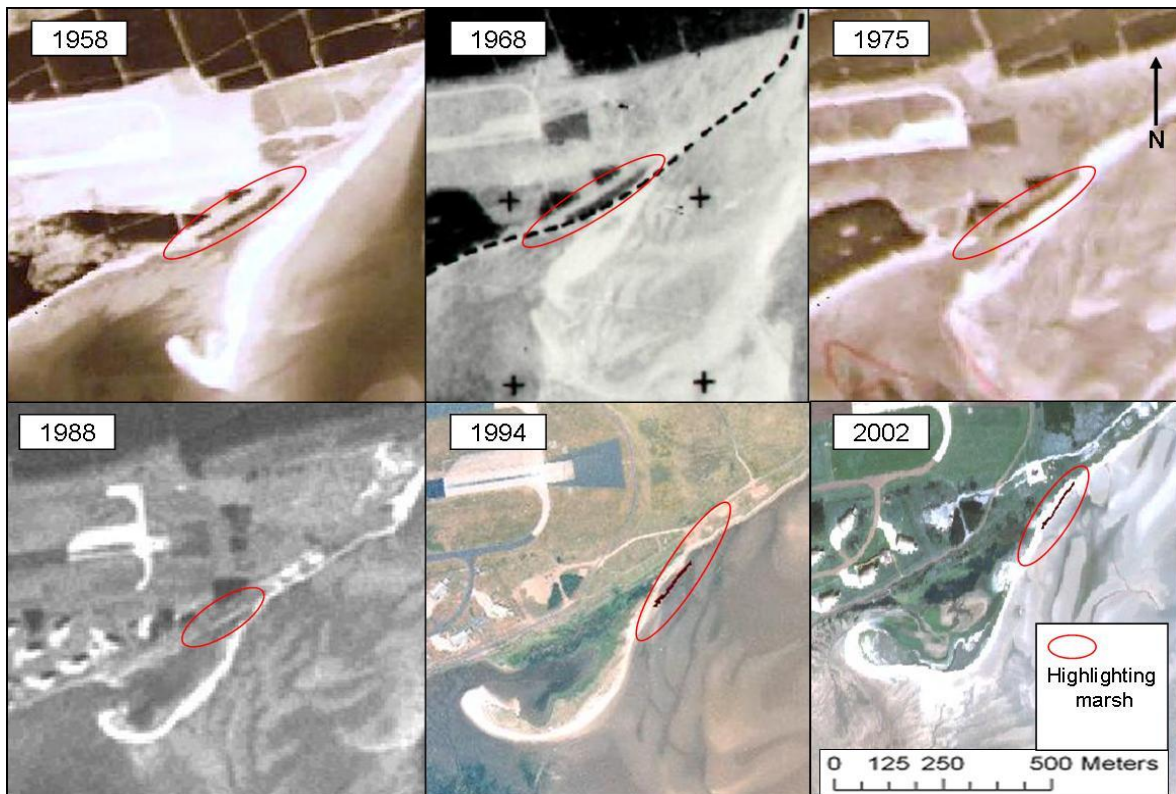


Figure 2-60: The old north shore marsh following the migration of Sanctuary spit over the Saltmarsh. The background images are aerial photographs (1958-1994) and satellite imagery (Quickbird 2002). The remnant marsh is at approximately 2m elevation ODN.

Towards the middle and inner estuary, existing stands of marsh appear to have changed little in extent over the period studied (1855-2009) (Figure 2-61 and Table 2-5),. Calculating the percentage change via the relative areas digitized, the marsh has reduced by approximately 1.3 percent (1 dec. pl), suggesting the inner estuary marsh has been relatively stable over the study period.

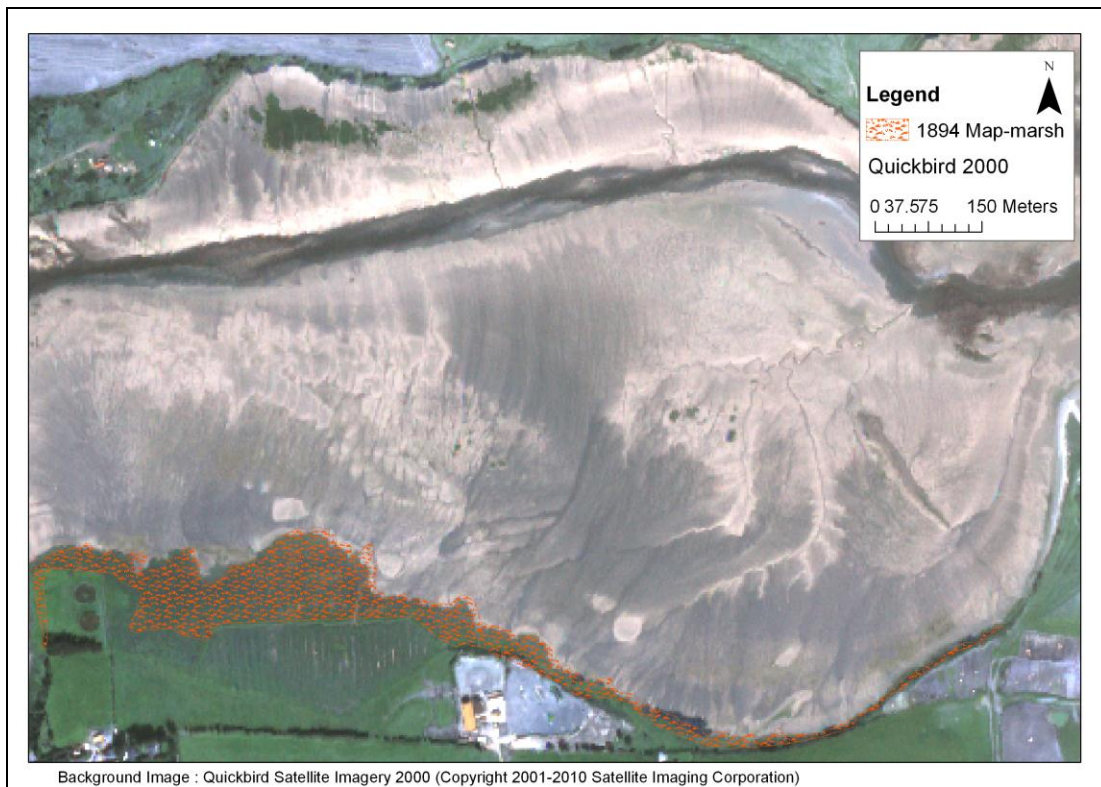


Figure 2-61: Inner estuary Edenside salt-marsh 1894-2002 (south shore Kincaple Bay). The marsh exhibits approximately a 1% reduction in extent.

The middle estuary salt-marsh has two main stands (Figure 2-62 and Table 2-5), one to the west and one to the east littoral margin of Kincaple bay. In the period, from 1855 up to 1947 both marshes show a slight reduction in area towards the outer limits (edge of the bay), although overall the change is relatively small approximating to a 12 percent reduction for both marshes. By 1958 the westerly marsh shows a much greater reduction of 23 percent, whilst the easterly marsh has receded by only a further 10 percent. The pattern of greater recession of the westerly marsh continues up to 2002, at which time there is a 13 percent reduction on the west compared to a slight increase on the east, due to artificial planting in Marsh 2000 (Maynard *et al.* 2011).



Figure 2-62: Middle estuary salt-marsh showing erosion.

The pattern of change for the two marshes was very similar, with the seaward side receding consistently but slowly between 1855 and 2002 (Figure 2-63). The greatest change was found to occur on the outer edges of the marshes and in particular between 1947 and 1958.

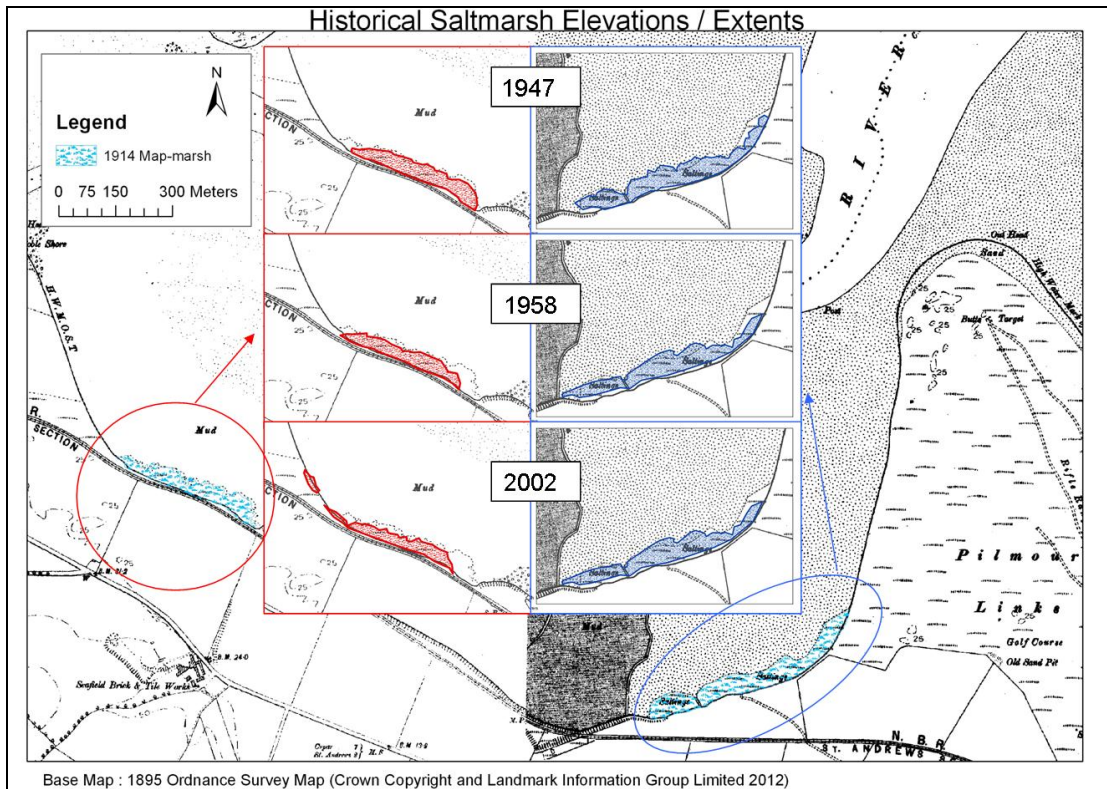


Figure 2-63: All base maps displayed are the 1895 Ordnance survey. Overlain on these are mapped areas of later extents to show changes since 1895 to 2002. Salt-marsh was digitized from historical ordnance survey maps, apart from 1947 and 2002, which were from an aerial photograph and Quickbird satellite imagery respectively. The Westerly 2002 marsh is displayed as two separate sections, the most westerly is an addition of artificially planted marsh as is not included in the area calculations.

The relatively small changes that occurred are not equal in magnitude on the two stands; the eastern marsh has undergone greater retreat than the western marsh. Post 1958 both stands of marsh show a reduction in size, the greatest change shown was in the westerly marsh, with a net loss of -6124 m^2 approximating to a 41 percent reduction between 1895 and 2002. The easterly stand of marsh changed by -3810 m^2 , equating to approximately a 14 percent reduction during the period.

Table 2-5: Changes to the area of salt-marsh (m²), here the 1895 and 1914 areas were digitized from the historical ordnance survey maps, whilst aerial photographs / satellite imagery were used for 1947, 1958 and 2002.

Year	Edenside	K'Bay (W)	K'Bay (E)
1895	58815	14855	27212
1914	N/A	14604	26764
1947	N/A	13099	23755
1958	58869	10092	21354
2002	58030	8730	23402

On the south side of the estuary, remnant patches of salt-marsh were also present, in accordance with Maynard (2011), protruding from the sediment (Figures 2-64 and 2-65). South of Coble shore remnant marsh was noted seaward of the present day extent of salt-marsh. The remnant marsh extent appears to coincide with the seaward extent of the mid 1940's marsh in the same location in Kincaple Bay, (Figure 2-64).

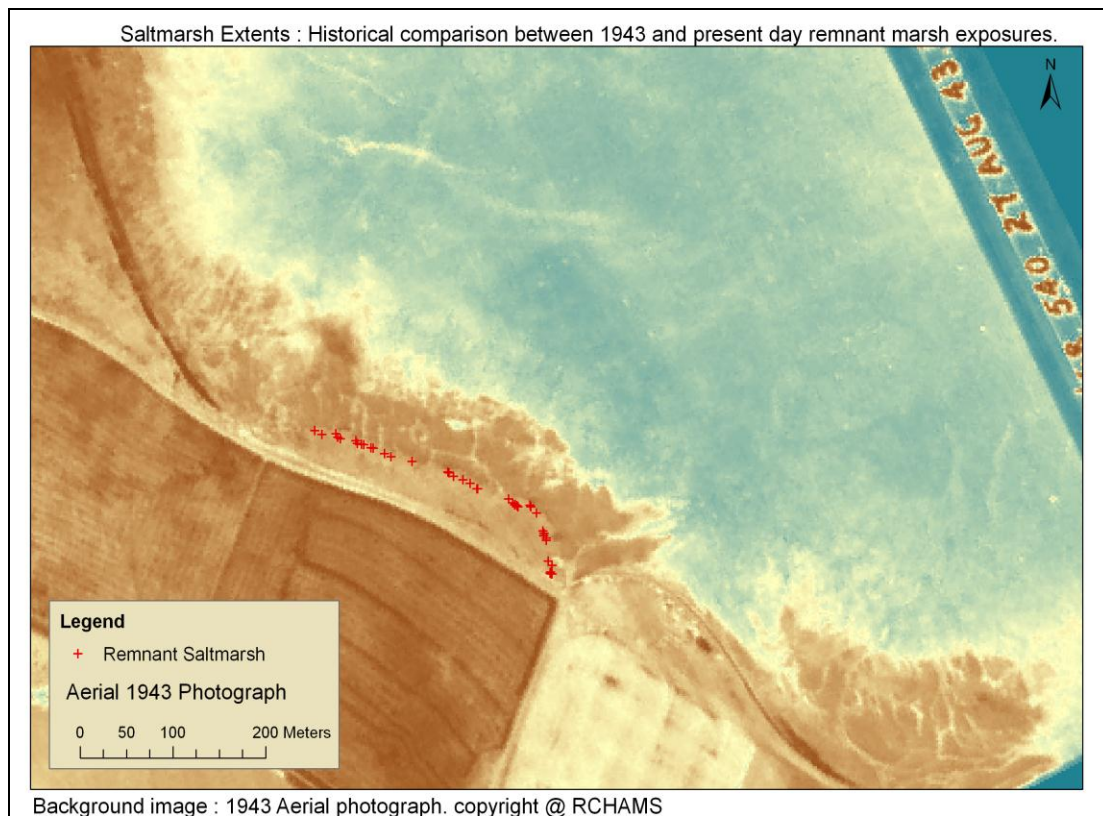


Figure 2-64: Aerial photograph from 1943, showing the position of the remnant marsh, both have approximately the same seaward extent and are landward of the 1895 marsh frontage.

The rate of recession, calculated by the reduction in area over the time interval (1943 and 2002), was approximately 73 m²a⁻¹. This loss of marsh equates to a linear recession of the seaward side by approximately 13 m along the full length of the marsh.

Further east (seaward) along the littoral margin, more remnant marsh was visible (Figure 2-65); these may be interpreted as 3 previous stands at approximately 1.4m, 1.2m and 1m elevation ODN,

or as stages in the recession of a single stand. The proximity of the marsh at 1.4m ODN to that of the easterly main stand (towards the centre of the Kincaple Bay shoreline) suggests it may, before 1895, have been part of a continuous feature.

Further seaward towards Pilmour Spit two further remnant stands of marsh at 1.2m and 1m elevation ODN were noted. These lie seaward of the 1855 shoreline, however straddle the 1895 shoreline. The successive shorelines all lie behind the remnant marsh patches. It is not clear from these results when or why these marshes declined and eventually disappeared.

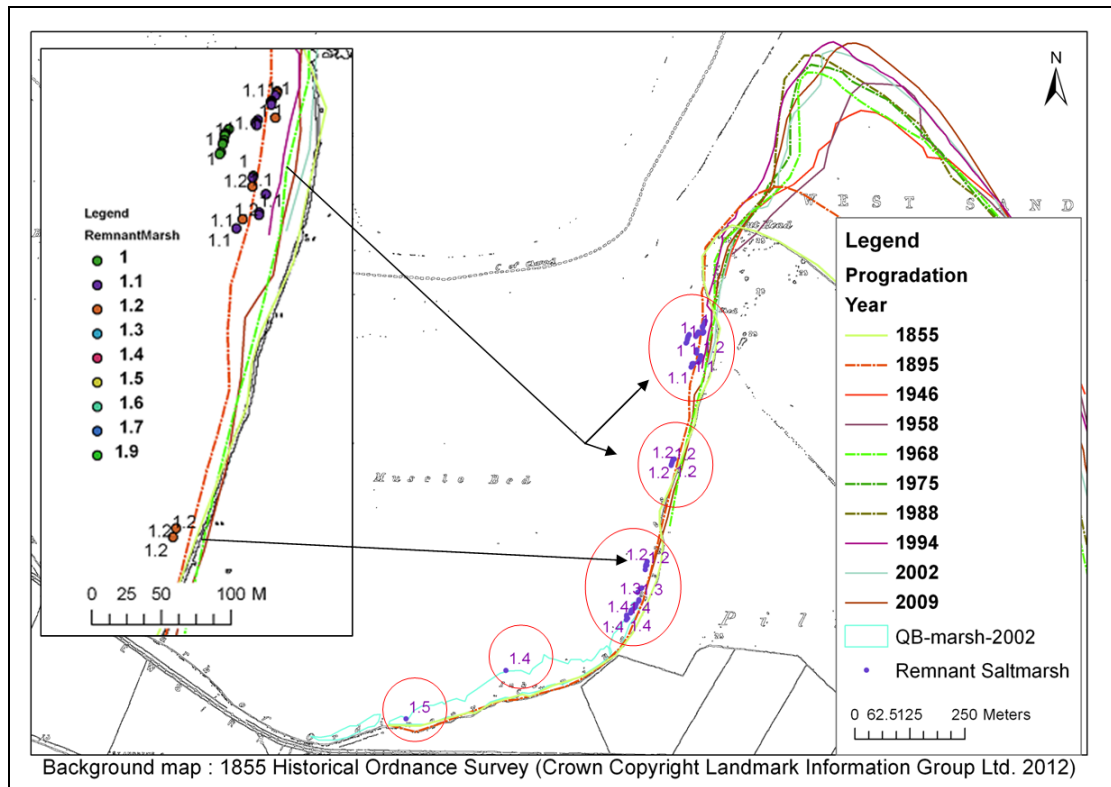


Figure 2-65: Remnant Saltmarsh (East Kincaple Bay) displayed with historical shoreline positions. The elevations of the remnant marsh are shown as meters above datum Newlyn. The insert on the left, is an enlargement of the location of the two most seaward remnant marsh patches.

Identifying historical *Zostera* extents

The extents of the mapped 1977 marsh (Johnston *et al.* 1979) and the RTK DGPS 2009 mapped *Z. noltii* were recorded (Figure 2-66). In the original report, no differentiation between the species of *Zostera* was given in terms of which stands were either *Z. noltii* or *Z. angustifolia*, thus it is difficult to compare relative patch area or distribution changes over the time. From the position of the *Zostera* sp. along the high littoral to sub-tidal gradient and with knowledge of the location of *Z. angustifolia* beds in Kincaple Bay today, it would be reasonable to assume that some of the patches mapped by Johnston (1979) are in fact *Z. angustifolia* rather than *Z. noltii*. The area of the remaining patches (which are more likely to be *Z. noltii*) amounts to a total of 63,169 m². When

compared to the data acquired in 2009, which has a total combined area of 18,458 m², a reduction in total area of -44711 m² of *Z.noltii* is observed.

The accuracy of Johnston's mapped data in 1977 is not known; colonised areas may well have been grouped, rather than patches being individually surveyed giving the impression of a greater extent than was really the case. However, it can also be seen (Figure 2-66) that *Z. noltii* has very actively colonised the southern shore in the inner estuary, where previously there were no patches present or at least none recorded. The plants were also noted to be spreading seaward towards Sanctuary Spit on the northern shore, where previously no stands were known. Similarly along the high littoral margin of Coble shore and further round in to Kincaple Bay patches of *Z.noltii* had colonised by 2009.

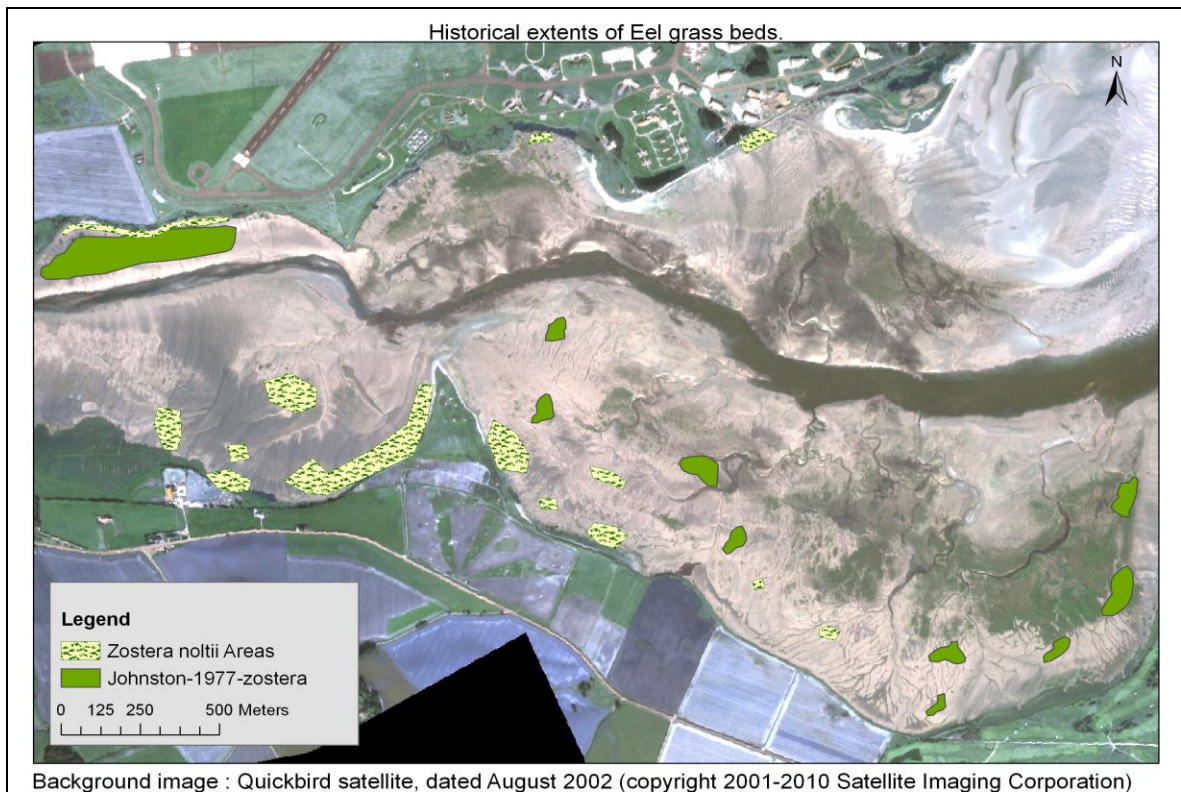


Figure 2-66: The distribution of *Zostera* species within the Eden estuary, mapped in 1977 by Johnston for a breeding bird survey, and again in 2009 for this research.

2.3.5.3. Discussion

Identifying spatial changes to salt-marsh over historical timescales has proven difficult, particularly as intertidal detail from historical Ordnance survey maps was inconsistent between updated versions and also likely shaped by access or time constraints. For the Eden estuary early maps show no evidence for any salt-marsh existing on the northern shore. For the southern shore, there

is variable quality in the accuracy from map to map; this is perhaps because the southern shore underwent more change in terms of development, such as railway embankment construction and development of the golf courses. Access to the southern shore is far easier and thus may explain the more accurate surveys that were undertaken along this shoreline.

Eastwood (1977), Ferentinos and McManus (1981; 2009) and Jarvis & Riley (1987), have all documented the accretion and recession of the northern shoreline at the entrance to the Eden estuary, in the vicinity of the remnant salt-marsh. The marsh clearly declined due to the lateral migration of Sanctuary Spit, which was probably initiated towards the end of the 1800s and developed through to the 1980s, due to localized wave refraction at the estuary mouth (Eastwood 1977; Mcmanus 2008). At high water wave refraction was believed to have driven south westerly long-shore currents, which transported sediment into the estuary forming and sustaining Sanctuary Spit. Cessation in spit growth in the 1980s was thought to have resulted from sediment starvation, with the implementation of Rip Rap defences put in place at the seaward end of the main RAF Leuchars runway (Ahmad and Mcmanus 1994).

The 1920 Ordnance survey map shows not only the early developmental stage of the spit, but also the proximity of the channel to the shore (Figure 2-67). Through the sequence of aerial photographs from 1940 to 1975, not only was the spit shown to lengthen and alter in shape, but the channel position gradually moved away from the shoreline. By the 1950s the northerly channel was no longer the main route for both flow and sediment transport and by the mid 1970s the northerly channel has become largely in-filled.

It is proposed that initiation of Sanctuary Spit and its developmental cessation was associated with the northerly channel development and its later closure. Through the lateral migration of the channel towards the northern shoreline; source material for the spit was probably made available through erosion of the channel edge. This process occurred following considerable accretion of the Tentsmuir dune system in the late 1800s, prior to planting of the forest. Despite the current channel position being not far off the 1940s location, sediment does not appear to be added to the spit in the same way. This may be because dune accretion rates are inhibited by interruption of the westerly offshore winds by the forest plantation, thus the current channel is further from the fore dunes than in the early 1920s. Whilst the RIP RAP defences, located at the high water zone near the end of RAF Leuchars runway, may inhibit longshore drift into the estuary on the north shore, sediment starvation was more likely caused by channel proximity. Following cessation in growth, the spit changed in shape towards the tip displaying an inward curvature during periods of above average offshore winds (e.g. Figure 2-67, 1958) and rotation seaward during periods of more onshore conditions (e.g. Figure 2-67, 1975).

Determining the cause of changes to the extent of the salt-marshes on the southerly shore of the estuary is less straight forward. No large scale morphological changes have occurred during the period, with the exception of the accretion of the seaward side of Pilmour Spit. The existing salt-marsh in the inner estuary has changed only marginally between 1895 and 2002, however in

Kincaple Bay the stands have changed and appear to be more vulnerable on the west shore. The greatest period of change was between 1947 and 1958, with a 23 percent reduction in the western marsh area. During this time period the coast would have experienced increasing relative sea levels (under lunar nodal influence), with a 3.7 percent increase in tidal range (Pugh 2004). Although during this period the coast experienced both above and below average westerly winds, in the years leading up to the nodal maximum (1950) onshore winds began to dominate. Under such conditions the high water duration becomes protracted, exposing the westerly marsh to onshore wave activity for a longer period. With the flood tide exceeding the ebb in duration, the consequential ebb velocities would theoretically be greater in magnitude and thus any eroded material kept in suspension under wave activity at high water, would be exported seaward (Anderson 1972; Green 2011).

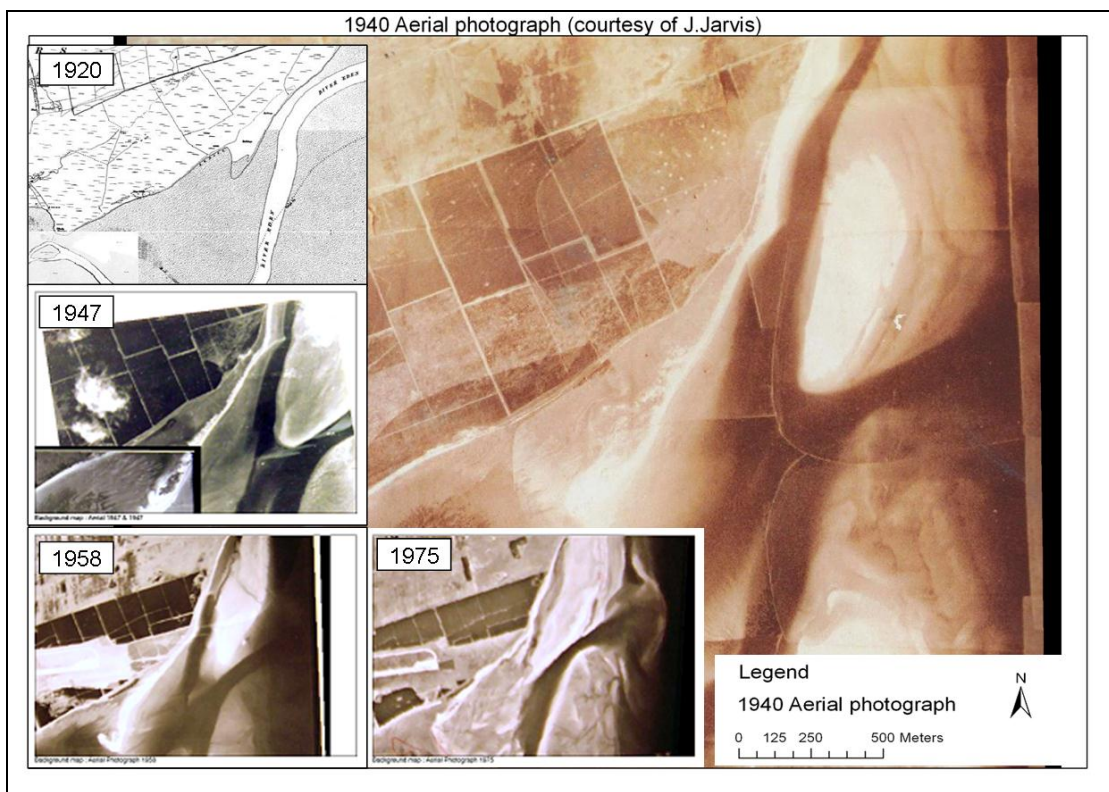


Figure 2-67: Aerial photograph from 1940, showing the presence of the pre-existing main channel position along the shoreline at Tentsmuir. The inserts show the various stages of the channel position from 1920 (Ordnance Survey) through to 1975 (aerial photographs).

Similar marsh erosion events for the North Sea coast have been identified as causing rapid retreat of coasts in the 1950s through to the 1970s but with the greatest retreat between 1973 and 1988 (Van Der Wal and Pye 2004), corresponding with an increase in North Sea wave heights from about the 1960s, peaking in the early 1980s (Bacon and Carter 1991; Jelliman *et al.* 1991). The more easterly marsh lies towards the centre of Kincaple bay and is therefore less prone to either direct

onshore or offshore wind-waves, particularly as the marsh is protected to seaward by Pilmour Spit. This may explain why there was a difference in the magnitude of erosion between the two stands.

Two more lunar nodal maxima occur prior to 2002, one in 1969 which was similarly a period of more onshore wind conditions (although the change to the westerly marsh at this time is not recorded) and again in 1987 which follows a decade of increasing offshore winds. Under sustained offshore winds the low tide becomes protracted resulting in a stronger flood tide, which may explain the reduced erosion of the westerly and slight accretion of the easterly marsh as sediment was brought to the littoral margin.

To the rear of the westerly marsh is an artificial embankment, thought to have been built around the early 1800s by Napoleonic prisoners of war (pers. Comm. C. Maynard, SERG). Such embankments restrict the available space for marshes to adjust to sea level changes, increase reflected wave energy and in retaining higher level ground are often sources of runoff water dissecting the back marsh. Further along the shoreline and beyond the easterly marsh, there was a section that has endured a history of erosion. Wilson (1910) describes a need to protect the High Hole from wave erosion during stormy weather and recounts memories of when the steep bank adjoining the 11th hole required protecting with timber. Here Sea Lyme-grass (*Elymus arenarius*), which was experimentally planted in 1847 on the links, was planted from the estuary round to the sands to stabilize the dunes.

Despite the soft engineering measure, Wilson (1910) continues to describe a 70 yard eroded and undermined section “to the west of the groyne which was recently” emplaced (early 1900s) to protect the course; the groyne was located at what was then the end of the spit and whilst protecting the shoreline from wave attack from seaward, may also have reduced the long-shore drift, that runs seaward from Kincaple Bay northeast along Pilmour shore (Eastwood 1977). During the 1920s 10 groynes were put in place and subsequently augmented with wooden sleepers, by the 1970s concrete blocks were added (Duck *et al.* 1995). In 1978 erosion continued to be a problem as the groynes fell into disrepair, leading the installation of welded mesh gabions (Maccaferri.Ltd. 2005). These welded mesh gabions failed 15 years later due to their inability to flex and were replaced by more extensive woven gabions, revetment mattresses and sand recharge in 2000. Despite the mitigation measures, much of the recharged sand was removed following a trend for strong easterlies combined with high tides in 2006 (Strachan 2007) which were lunar nodal maximum tides, resulting in the requirement for subsequent sand recharge, which was completed in 2008.

It is not known when the two remnant stands of marsh along the shore of Pilmour Spit declined, though from observation (Figure 2-65) the shoreline seems to have retreated landward from the back of the marsh, under what were more onshore (easterly) conditions. Elsewhere in the bay, the Salt-marsh has accommodated changes to sea level hence sea level rise alone is unlikely to be the cause of total decline. It was observed that further into the estuary (landward) the magnitude of

marsh change is lessened and timing delayed, suggesting that wind-wave and circulation drivers are more likely to be causal, affecting the outer estuary to a greater extent (Figure 2-64, Table 2-5)

Under offshore wind conditions, whilst direct wind and wave erosion potentially may impact on the Pilmour shoreline, flood tidal velocities would exceed ebb velocities following a protracted low water duration and hence would work against long-shore drift. Eroded sediment would therefore be more likely to remain redistributed along the shoreline. Under onshore conditions, although the shoreline is protected from direct wind erosion, refracted waves may enter the mouth of the estuary (Eastwood 1977); suspended sediment would hence be exported under enhanced long-shore drift, driven by the protracted high water causing a dominance in ebb velocities. It is therefore likely that the two remnant stands probably suffered under a period of sustained onshore conditions, where sediment was removed from the area restricting spatial adjustment. The position of the Eden channel and the proximity of the beach shoal spit area may also have played a role causing surging waves to break.

Additional to the natural stands of marsh, artificially planted areas of salt-marsh were successfully established by Maynard (2011) on both the southern and northern shores of the middle estuary, however in later trials comparative growth differences between transplanted plugs of *Bolboschoenus maritimus* and *Puccinellia maritima* were evident with *P. maritima* showing “extremely limited” growth (Maynard in Prep.). *Puccinellia* sp. enter into symbiotic relationships with mycorrhizal fungi (Wilde *et al.* 2009), which aid in the acquisition of nutrients, particularly nitrogen. Initial establishment of *Puccinellia* may therefore be dependent upon the presence of arbuscular mycorrhiza. The southern shore Kincaple Bay *Puccinellia* marshes are located in front of both agricultural and amenity golf course land; possible decline in these marshes speculatively may partly be due to the use of fungicide and herbicide applications, reducing the ability of the marsh to withstand environmental change.

From the original mapped extent of *Zostera* (Figure 2-67), changes to the total extent of plant cover were difficult to establish given the records available and similar to the problems encountered with the historical mapping of salt-marsh, records have been dependent upon access and sampling effort. What is clear is that *Z. noltii* has spread to more diverse habitats (higher energy and salinities) inferring an ability to accommodate and embrace the environmental change that has occurred since the mid 1970s.

2.3.5.4. Summary

Scarcity of updated and estuary wide data between 1855 and 2002, has made it difficult to accurately evaluate the changes undergone by the Eden estuary salt-marsh and eelgrass *Zostera noltii* and to attribute the change to specific causes.

From the information available however, the following conclusions are drawn.

Saltmarsh;

The inner estuary marsh has changed very little during the time interval, with a reduction in area of approximately 1 percent.

Along the north shore at the estuary mouth a remnant stand of marsh remains. This marsh declined to its current extent due to the migration of Sanctuary Spit, which was probably initiated by the proximity of the Eden channel to the shoreline, providing sediment for spit development. The spit migrated over the marsh between 1988 and 1994.

The middle estuary marsh in Kincapple Bay shows more change than the inner estuary marsh, increasing post 1914. The greatest change was apparent between 1947 and 1958 during which time there was a 23 percent reduction in area of the westerly stand. The increase in rate of change appears to be resulting from increased tidal range (under the lunar nodal maximum in 1950) associated with sustained long periods of onshore wind conditions, leading to protracted high water durations followed by increased ebb velocities.

Further along the bay to seaward, on Pilmour Spit, two remnant patches of salt-marsh remain. With the information available it is not clear when these declined. It is likely however that added anthropogenic pressures from groynes, bank reinforcement and gabion baskets altered hydrological conditions impacting on energy levels, sediment supply and accommodation space, inhibiting the marsh from adjusting to environmental pressures.

Zostera noltii;

Since 1977, *Z. noltii* has colonised the southern shore of the inner estuary where previously no stands were present.

In the middle estuary *Z. noltii* has spread seaward along both shores. No records exist for any previous stands on the north shore. On the south shore there are 6 relatively large stands, where it is thought only two existed previously (however records are unclear).

The combined area of *Z. noltii* stands is less now than in 1977, however it is not known if individual patches were mapped or the area containing the patch was mapped. Despite this, the species has spread to more areas of the estuary.

Evaluation of the two taxa has shown the following; for salt-marsh, environmental change during the analysis period has had a detrimental impact, which may have been exacerbated by anthropogenic pressures to mitigate for the erosion pressures, particularly in the outer estuary. Artificial marsh planting has been successful in the middle estuary (Maynard *et al.* 2011) which contributes towards replenishing the 3 hectares lost in the years up to 2002. For *Z. noltii*, it was observed that environmental change during the analysis period have not been detrimental, perhaps due to *Z. noltii* growing more landward towards the inner estuary. In terms of estuary health and functioning;

clearly the loss of salt-marsh must have reduced the estuaries buffering capacity for change. The seaward colonisation of *Z. noltii* infers that this species is not at its ecological limit and not suffering from insurmountable environmental pressures.

2.4. Chapter discussion

This chapter aimed to identify trends or patterns within 3 selected driving mechanisms controlling estuary asymmetry dynamics and additionally to the consequential spatial changes in channel position, shoreline alignment and to selected key biological habitats. Throughout this chapter common threads linked the individual sections, with observed patterns of change displaying associations to solar & orbital influences and to patterns within the northern hemisphere circulation expressed through the NAOI, these associations have been summarised in Table 2-6.

Table 2-6: Summary of the principal influences identified from this chapter as impacting on estuarine tidal asymmetry dynamics and leading to consequential spatial changes. In brackets are the additional influences which combine to amplify the principal driving mechanism.

Estuary Driving mechanism	Influenced by
River flow	Solar, Lunar and Planetary, NAO
Wind regime	Solar and Planetary, (Lunar?), NAO
Morphology	Lunar nodal cycle, (wind regime and river flow)
Consequential impacts to	Influenced by
Channel migration	NAO & wind regime (lunar nodal cycle)
Shoreline alignment	NAO & wind regime (lunar nodal cycle)
Key biological habitats	Lunar nodal cycle & wind regime

Both the river flow and the wind count data displayed evidence of a significant 'cross-correlation' relationship with the autumnal NAOI however the strengths of the relationships differed, with a stronger multi-decadal signature more evident with the west wind counts, as an approximate cyclical period of 34 years. Although the river flow data displayed significant relationships over several lags with the NAOI, some of the significant lag periods corresponded to solar minimum and maximum cycle activity, others are suspected to be volcanic in origin, overall however an underlying weak (non significant) periodicity of approximately 35 years was also present, inferring multiple perturbing influences for the river flow data. This approximate 35 year period shared by both the wind count and river flow data is consistent with the Bruckner cycle, similarly identified within air temperature data in Italy (Camuffo and Bertolin 2012), tree ring data from the Koala Peninsula Russia (Raspopov *et al.* 2004) and in the nitrates of the Tibetan ice plateau (Wang *et al.* 2000).

What remains unclear is why the association with the NAOI is stronger with the wind data than with the river flow data, as it may be expected that precipitation would closely follow the NAO (with prevailing south-westerly winds picking up heat and moisture from the North Atlantic Current) however it is perhaps explained by wind being more directly influenced, whilst river flow requires additional processes (evaporation and precipitation).

Spectral analysis of the monthly data for 'wind direction counts' and 'river flow' (three observed datasets) revealed several similar frequencies present (Table 2-7), although with slight variation due to different time ranges for the input data, coupled with the irregularity in cycle lengths. Despite this, frequencies consistent with the Schwabe sunspot and Hale magnetic pole reversal are easily identifiable together with a number of other periods for which the identity remains ambiguous (15, ~8, 7-7.5 and 2.7-2.8). The asymmetry of the solar Schwabe cycle approximates to duration from maximum to minimum of 7 years and 3 years to return to maximum activity and thus may account for the latter two frequency ranges.

Table 2-7: Summary of the frequencies identified through spectral density analysis. The most dominant frequency per data series is displayed in red. Some notable shared periods have been highlighted to help with identifying shared frequencies.

System	Dates	Frequencies present																						
Eden	1968 - 2009	21.33	10.7	8.53	7.11	2.67	2.51	2.37																
Tay	1953 - 2009	65	57	54.4	30	20	15	12	10	8.57	7.5	6.67	6	3.16	2.4									
Thames	1883 - 2008	64	42.7	32	25.6	21.3	18.3	16	14.2	12.8	11.6	10.7	9.85	8.53	7.11	5.33	4.7	4	3.88	2.72	2.67			
All winds	1936 - 1981	22.5	15	11.3	9	7.5																		
West wind	1936 - 1981	22.5	15	11.3	9	7.5																		
East wind	1936 - 1981	22.5	15	4.5	4.1	3.8	3.5	3.2	3	2.8	2.6													
NAO (long)	1825 - 1980	93.8	37.5	31.3	15.6	14.4	12.5	11.7	11	8.93	8.52	8.15	7.81	7.5	7.21	5.85	4.93	3.99	3.13	2.68				
NAO (short)	1936 - 1980	16	12	6.86	6	5.33	4.8	3	2.83	2.67	2.18	1.5	1.1											
Sunspots (long)	1749 - 2011	135	90	67.5	54	45	38.6	33.7	30	27	24.5	22.5	19.3	18	15.9	15	14.2	13.5	12.9	12.3	11.7	11.2	10.8	10.4
	contd.																							
Sunspots (short)	1970 - 2011	27	18	13.5	10.8	9	7.7	6	5.4	4.9														

What is interesting from Table 2-7 is that the Hale (~22.yrs) is absent from the NAOI data despite being present within the wind and river data series, inferring that the NAO and the wind/ river data series are perhaps co-driven rather than the NAO having an intermediary role. Table 2-7 also highlights the dominant periods for each system do not overlap and that more corresponding frequencies are observed between the sunspot data, wind data and the river flow data, compared to the NAOI, which displays only frequencies 14-16 and ~8.5 years which are shared across all data. The origin of the ~15 and ~8.5 years is not fully understood, however they have been identified by Scafetta (2012) and Yamaguchi (2010) investigating sunspot data and climate interactions.

The third driving mechanism of estuary dynamics, morphology, was concluded to be most likely driven by changes to the tidal range under the influence of the lunar nodal cycle, with the change in tidal volume causing a shift in the tidal asymmetry, driving an either erosional or depositional phases. Additionally both river flow and wind regime were also believed to contribute, accentuating shifts in asymmetry.

Of the three selected estuary driving mechanisms (Table 2-6) it is the wind regime, with its close associations to the NAO and solar activity, which has been identified here as driving the 'consequential responses' augmented by the lunar nodal tidal range variability.

This chapter has demonstrated the close interrelationship between patterns of change observed within the Eden estuary with those present in the local climate (through wind and river flow as vectors of change) and the wider northern hemisphere circulation. Additionally significant relationships were identified with external forcing mechanisms, as orbital influences and as correlations to Wolfe sunspot numbers, representing variability in solar irradiance. Although a number of influential variables have been identified, the nature of the relationships is not fully understood; without modelling the hypothesized causal mechanism against the proposed dependant variable it is not possible to propose them driving mechanisms. It is also likely that patterns present in the Eden data are the consequence of several coupled non linear interactions and thus modelling to identify specific driving mechanisms would require more time than is available within the scope of this study.

2.5. Chapter summary

Historical Trend Analysis was used to investigate pattern and trend within the data for three selected potential driving mechanisms controlling tidal asymmetry dynamics. River flow, wind regime (direction counts) and morphological elevation analyses identified common threads linking the data, with observed patterns of change displaying associations to solar & orbital influences and to patterns within the northern hemisphere circulation expressed through the NAOI. Data were also analysed for the consequential spatial changes in channel position, shoreline alignment and to selected key biological habitats resulting from the perturbation of the tidal asymmetry; these data all exhibited trends associated with the wind regime, the NAOI and additionally by changes to the tidal range through the gravitational influence of the lunar nodal cycle.

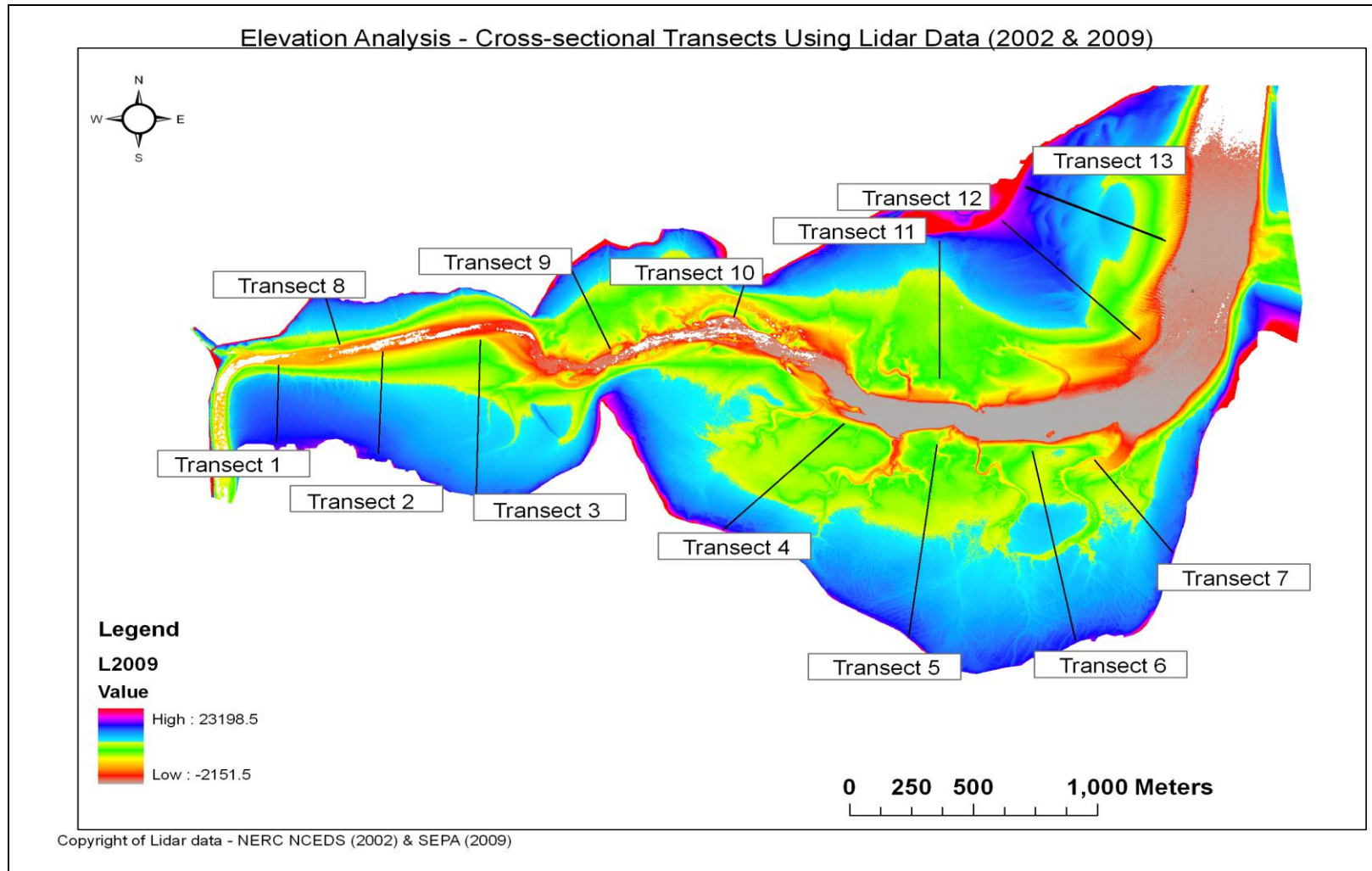
Both the river flow and the wind count smoothed annual data displayed evidence of a significant 'cross-correlation' relationship with the autumnal NAOI as an approximate cyclical period of 34 years, with a stronger multi-decadal signature more evident within the west wind counts. Spectral density analysis of the monthly individual data revealed significant (95%) relationships with periods consistent with the solar Schwabe and Hale cycles in both wind and river data however the Hale cycle was not present in the NAOI; in addition frequencies of ~15 years ~8.5 and 7-7.5 years were present in the monthly NAOI, wind direction count and river flow data. Not all frequencies were shared across all the data (river flow, wind direction counts and the NAOI), suggesting a range of perturbing mechanisms acting on the systems or the presence of feedback causing additional cycles to the external influences.

The third selected driving mechanism of estuary dynamics, morphology, is believed to be driven by a combination of the lunar nodal cycle impacting on the tidal volume and by both the river flow and sustained on or offshore wind regimes causing a shift in the tidal asymmetry, towards either an erosional or depositional phase.

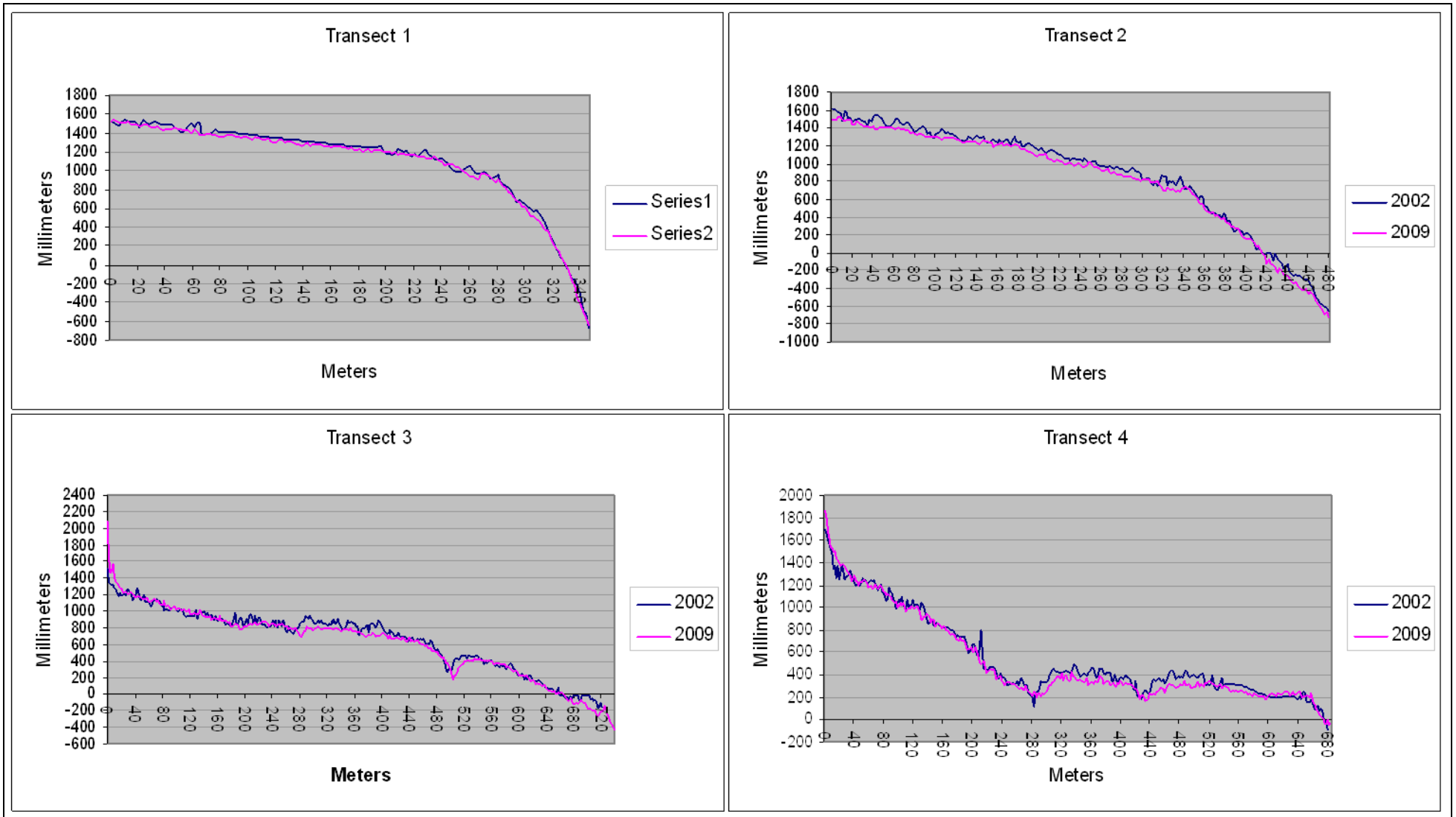
The wind regime, with its close associations to the NAO and solar activity, was proposed here as the main driving mechanism for the 'consequential responses' i.e. the spatial changes observed in channel position, shoreline alignment and with the spatial extents of key biological habitats. In addition tidal range changes, driven by gravitational lunar nodal forces, was believed to contribute to the impacts of sustained wind directions, particularly to erosion at high water when coupled with wave activity.

This chapter aimed to identify climate signals present within the chronologies of selected drivers for tidal asymmetry dynamics and to assess the estuarie's response to perturbation in terms of shoreline alignment and to the spatial extents of key biological habitats. A close interrelationship was identified between patterns of change observed within the Eden estuary and with those present in the local climate and the wider northern hemisphere circulation as significant cross-correlations with the NAOI. Significant relationships were also identified between external forcing mechanisms, as orbital influences and as correlations to Wolfe sunspot numbers, representing variability in solar irradiance. This chapter focused on exploratory analysis and was limited to identifying associations to potential driving mechanisms, without further research to model these proposed drivers against responses, speculation can only be made as to the relationships found.

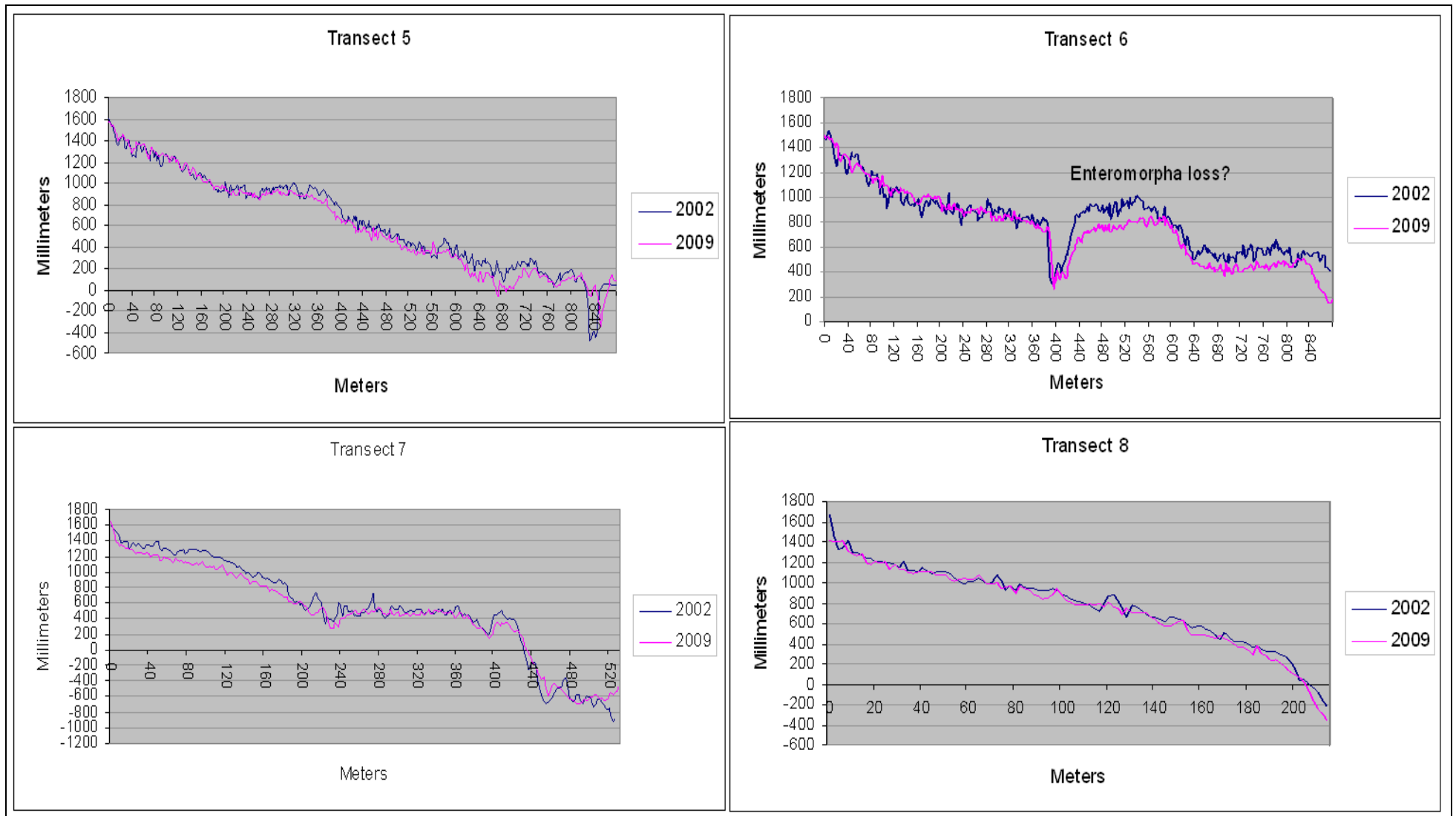
2.6. Chapter 2: Appendices



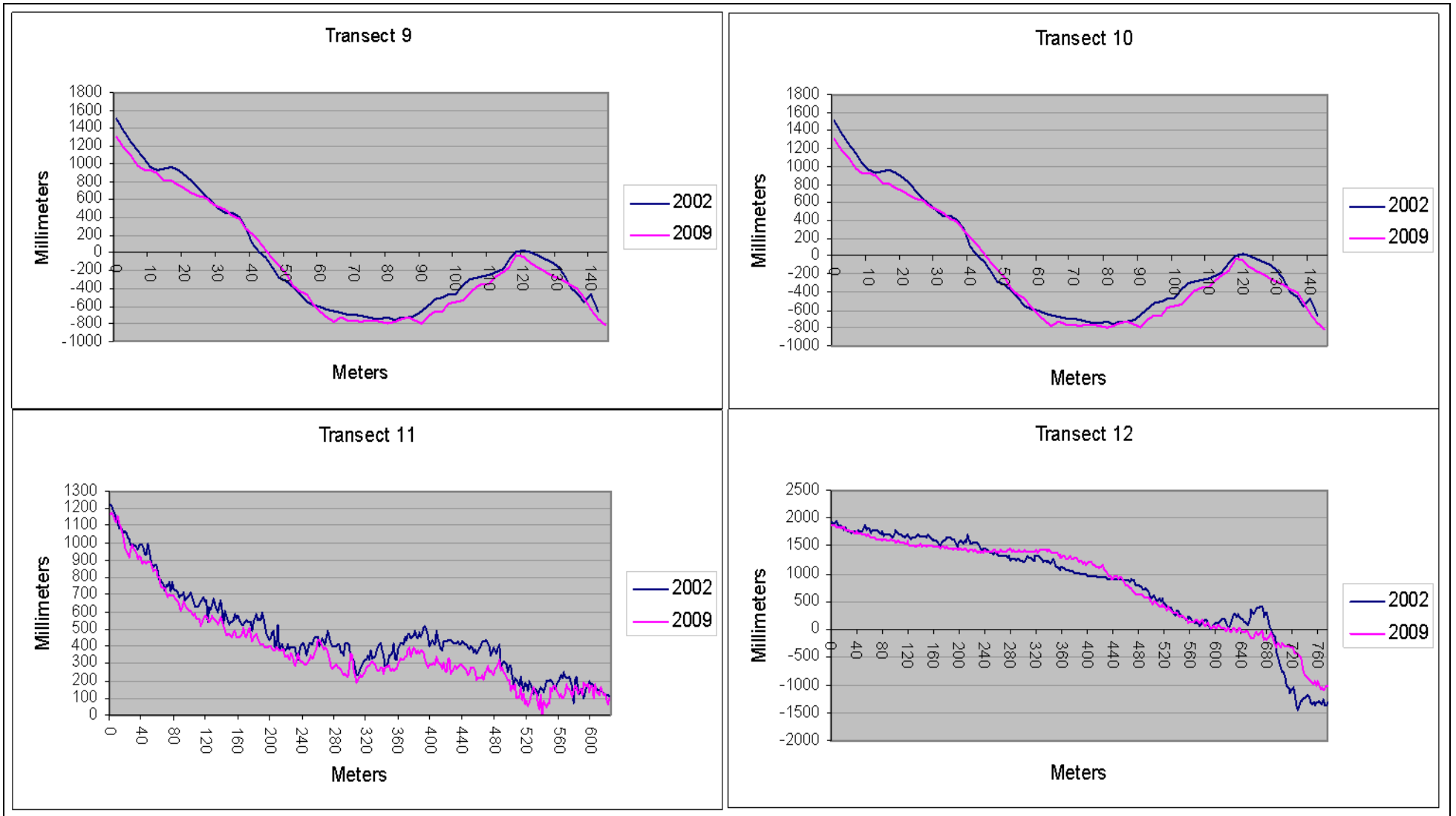
Chapter 2 appendix 1 Figure 1 LiDAR transect locations, for quantifying the change observed between the two time periods.



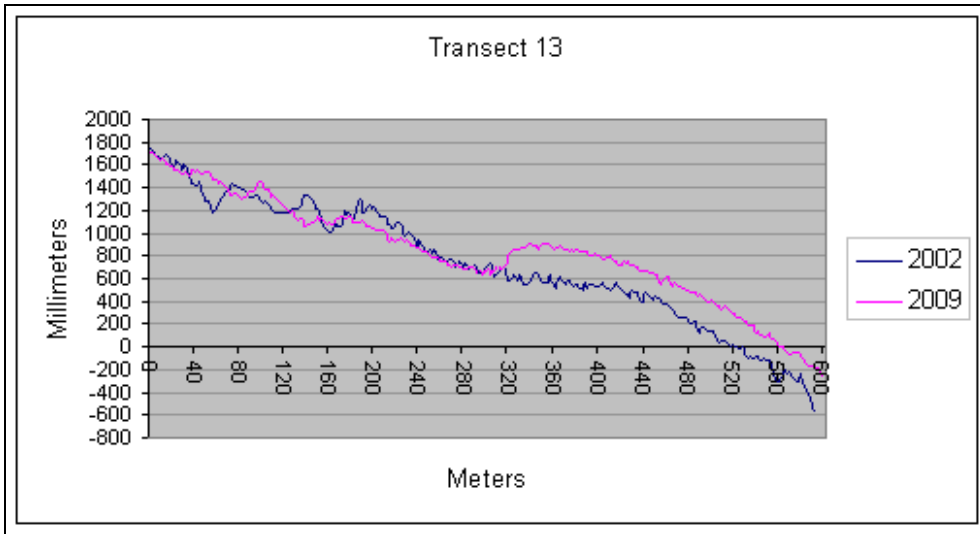
Chapter 2 appendix 1 Figure 2: LiDAR transects 1 through to 4.



Chapter 2 appendix 1 Figure 3: LiDAR transects 5 through to 8



Chapter 2 ppendix 1 Figure 4: LiDAR transects 9 through to 12



Chapter 2 appendix 1 Figure 5: LiDAR transect 13.

2.7. References

Section 2.1 River Flow

- Alvarez-Ramirez, J., J. C. Echeverria, and E. Rodriguez. 2011. Is the North Atlantic Oscillation modulated by solar and lunar cycles? Some evidences from Hurst autocorrelation analysis. *Advances in Space Research* **47**: 748-756.
- Barnett, C., J. Hossell, M. Perry, C. Procter and G. Hughes. 2006. A handbook of climate trends across Scotland. SNIFFER project CC03. Scotland & Northern Ireland Forum for Environmental Research, 62pp.
- Berger, W. H. 2008. Solar modulation of the North Atlantic Oscillation: Assisted by the tides? *Quaternary International* **188**: 24-30.
- Black, A. R., and J. L. Anderson. 1994. The Great Tay Flood of January 1993. Institute of Hydrology Tay Purification Board.
- Black, A. R., and A. Werritty. 1997. Seasonality of flooding: A case study of North Britain. *Journal of Hydrology* **195**: 1-25.
- Broersen, P. M. T. 2006. *Automatic Autocorrelation and Spectral Analysis*. Springer.
- Burroughs, W. J. 2003. *Weather Cycles: Real or Imaginary?* Cambridge University Press.
- Camuffo, D. 2001. Lunar influences on climate. *Earth Moon and Planets* **85-6**.
- Camuffo, D., and C. Bertolin. 2012. Recovery of the early period of long instrumental time series of air temperature in Padua, Italy (1716-2007). *Physics and Chemistry of the Earth* **40-41**: 23-31.
- CEH, and UKMO. 2001. To What Degree can the October/November 2000 Flood Events be Attributed to Climate Change? Defra FD2304. Department for Environment, Food and Rural Affairs: London; 40 pp.
- Centre for Ecology & Hydrology. 2010. NERC. National River Flow Archive: 18011- Forth at Craigforth.
- Cervený, R. S., and J. A. Shaffer. 2001. The moon and El Niño. *Geophysical Research Letters* **28**.
- Colling, A., and O. U. O. C. Team. 2001. *Ocean Circulation*. Butterworth-Heinemann.
- Cran. 2011. R Statistical Software <http://cran.r-project.org/>.
- Cryer, J. D., and C. Kung-Sik. 2008. *Time Series Analysis With Applications in R*, Second ed. Springer.
- Da Costa, E. D., and A. C. De Verdiere. 2002. The 7.7-year North Atlantic oscillation. *Quarterly Journal of the Royal Meteorological Society* **128**: 797-817.
- Davis, B. A. S., and S. Brewer. 2011. A unified approach to orbital, solar, and lunar forcing based on the Earth's latitudinal insolation/temperature gradient. *Quaternary Science Reviews* **30**: 1861-1874.

- Dickson, R. R. and others 2000. The Arctic Ocean response to the North Atlantic oscillation. *Journal of Climate* **13**: 2671-2696.
- Douglas, B. C. 1992. Global Sea-level Acceleration. *Journal of Geophysical Research-Oceans* **97**: 12699-12706.
- Eliot, M. 2012. Sea level variability influencing coastal flooding in the Swan River region, Western Australia. *Continental Shelf Research* **33**: 14-28.
- Emphasys-Consortium. 2000. Modelling Estuary Morphology and Process. Final Report. Estuaries Research Programme, Phase 1 MAFF Contract CSA 4938.
- Fu, C., A. L. James, and M. P. Wachowiak. 2012. Analyzing the combined influence of solar activity and El Nino on streamflow across southern Canada. *Water Resources Research* **48**.
- Gamiz-Fortis, S. R., J. M. Hidalgo-Munoz, D. Argueso, M. J. Esteban-Parra, and Y. Castro-Diez. 2011. Spatio-temporal variability in Ebro river basin (NE Spain): Global SST as potential source of predictability on decadal time scales. *Journal of Hydrology* **409**: 759-775.
- Gerstell, M. F., J. Crisp, and D. Crisp. 1995. Radiative Forcing of the Stratosphere by SO₂ Gas, Silicate Ash and H₂SO₄ Aerosols Shortly After the 1982 Eruptions of El Chichon. *Journal of Climate* **8**: 1060-1070.
- Haigh, I. D., M. Eliot, and C. Pattiaratchi. 2011. Global influences of the 18.61 year nodal cycle and 8.85 year cycle of lunar perigee on high tidal levels. *J. Geophys. Res.* **116**: C06025.
- Haigh, J. D., and M. Blackburn. 2006. Solar influences on dynamical coupling between the stratosphere and troposphere. *Space Science Reviews* **125**: 331-344.
- Hajian, S., and M. S. Movahed. 2010. Multifractal Detrended Cross-Correlation Analysis of sunspot numbers and river flow fluctuations. *Physica a-Statistical Mechanics and Its Applications* **389**.
- Herman, J. R., and R. A. Goldberg. 1978. Sun, weather, and climate. Scientific and Technical Information Office, National Aeronautics and Space Administration : for sale by the Supt. of Docs., U.S. Govt. Print. Off.
- Hernandez, A., S. Giralt, R. Bao, A. Saez, M. J. Leng, and P. A. Barker. 2010. ENSO and solar activity signals from oxygen isotopes in diatom silica during late glacial-Holocene transition in Central Andes (18A degrees S). *Journal of Paleolimnology* **44**: 413-429.
- Hobbs, P. V., J. P. Tuell, D. A. Hegg, L. F. Radke, and M. W. Eltgroth. 1982. Particles and Gases in the emissions from the 1980-1981 Volcanic Eruptions of Mt St Helens. *Journal of Geophysical Research-Oceans and Atmospheres* **87**: 1062-1086.
- Horner, M. W., and P. D. Walsh. 2000. Easter 1998 floods. *Journal of the Chartered Institution of Water and Environmental Management* **14**: 415-418.
- Hoyt, D. V., and K. Schatten. 1997. *The Role of the Sun in Climate Change*. Oxford University Press.
- Huntington, E. 1915. *Civilization and climate*. Yale University Press, Newhaven.
- Hurrell, J. W. 1995. Decadal Trends in the North-Atlantic Oscillation - Regional Temperatures and Precipitation. *Science* **269**: 676-679.

- Hurrell, J. W., and C. Deser. 2010. North Atlantic climate variability: The role of the North Atlantic Oscillation. *Journal of Marine Systems* **79**: 231-244.
- Ineson, S. and others 2011. Solar forcing of winter climate variability in Northern Hemisphere. *Nature Geoscience* **4**: 753-757.
- Jenkins, G. J., Perry, M.C., and Prior, M.J. 2009. The climate of the United Kingdom and recent trends. Met Office Hadley Centre, Exeter, UK.
- Knmi. 2011. Climate Explorer NAO indices 1821 -2011 <http://climexp.knmi.nl/data/inao.dat>.
- Kodera, K. 2002. Solar cycle modulation of the North Atlantic Oscillation: Implication in the spatial structure of the NAO. *Geophysical Research Letters* **29**.
- Kondrashov, D., Y. Feliks, and M. Ghil. 2005. Oscillatory modes of extended Nile River records (AD 622-1922). *Geophysical Research Letters* **32**.
- Labitzke, K., B. Naujokat, and M. P. McCormick. 1983. Temperature Effects on the Stratosphere of the April 4, 1982 Eruption of El Chichon, Mexico. *Geophysical Research Letters* **10**: 24-26.
- Love, J. J., K. Mursula, V. C. Tsai, and D. M. Perkins. 2011. Are secular correlations between sunspots, geomagnetic activity, and global temperature significant? *Geophysical Research Letters* **38**.
- MacDonald, N., and A. R. Black. 2010. Reassessment of flood frequency using historical information for the River Ouse at York, UK (1200-2000). *Hydrological Sciences Journal- Journal Des Sciences Hydrologiques* **55**: 1152-1162.
- MacDonald, N., A. Werritty, A. R. Black, and L. J. McEwen. 2006. Historical and pooled flood frequency analysis for the River Tay at Perth, Scotland. *Area* **38**: 34-46.
- Marsh, T. 2008. A hydrological overview of the summer 2007 floods in England and Wales. *Weather* **63**: 274-279.
- Marsh, T. J., and M. L. Lees. 2003. Hydrological Data UK: hydrometric register and statistics 1996-2000 Centre for Ecology and Hydrology, Wallingford.
- Mauas, P., and E. Flamenco. 2006. Solar activity and the streamflow of the Parana River. *In* I. Ermolli, J. Pap and P. Fox [eds.], *Solar Variability and Earth's Climate*. Memoire Della Societa Astronomica Italiana - Series.
- Mauas, P. J. D., A. P. Buccino, and E. Flamenco. 2011. Long-term solar activity influences on South American rivers. *Journal of Atmospheric and Solar-Terrestrial Physics* **73**.
- Mauas, P. J. D., E. Flamenco, and A. P. Buccino. 2008. Solar Forcing of the Stream Flow of a Continental Scale South American River. *Physical Review Letters* **101**.
- McCormick, M. P., L. W. Thomason, and C. R. Trepte. 1995. Atmospheric effects of the Mt-Pinatubo eruption *Nature* **373**: 399-404.
- McEwen, L. J. 2006. Flood seasonality and generating conditions in the Tay catchment, Scotland from 1200 to present. *Area* **38**: 47-64.
- M^cGuire, B. 1999. *Apocalypse: A natural history of global disasters*. Cassell & Co. London.

- Microsoft. 2003. Microsoft Office Professional Edition Excel SP3.
- Moron, V., R. Vautard, and M. Ghil. 1998. Trends, interdecadal and interannual oscillations in global sea surface temperatures. *Climate Dynamics* **14**: 545-569.
- Mufti, S., and G. N. Shah. 2011. Solar-geomagnetic activity influence on Earth's climate. *Journal of Atmospheric and Solar-Terrestrial Physics* **73**: 1607-1615.
- Pattison, I., and S. N. Lane. 2011. The relationship between Lamb weather types and long-term changes in flood frequency, River Eden, UK. *International Journal of Climatology*.
- Prokoph, A., J. Adamowski, and K. Adamowski. 2012. Influence of the 11 year solar cycle on annual streamflow maxima in Southern Canada. *Journal of Hydrology* **442**: 55-62.
- Raspopov, O. M., V. A. Dergachev, and T. Kolstrom. 2004. Periodicity of climate conditions and solar variability derived from dendrochronological and other palaeoclimatic data in high latitudes. *Palaeogeography Palaeoclimatology Palaeoecology* **209**: 127-139.
- Raspopov, O. M., O. I. Shumilov, E. A. Kasatkina, E. Turunen, and M. Lindholm. 2000. 35-year climatic Bruckner cycle - Solar control of climate variability?, p. 517-520. *In* A. Wilson [ed.], *Proceedings of the 1st Solar and Space Weather Euroconference on the Solar Cycle and Terrestrial Climate*. Esa Special Publications.
- Rind, D., J. Lean, J. Lerner, P. Lonergan, and A. Leboissitier. 2008. Exploring the stratospheric/tropospheric response to solar forcing. *Journal of Geophysical Research-Atmospheres* **113**.
- Robock, A. 2000. Volcanic eruptions and climate. *Reviews of Geophysics* **38**: 191-219.
- Rumaikin, A. 2007. Effect of solar variability on the Earth's climate patterns. *Advances in Space Research* **40**: 1146-1151.
- Ruzmaikin, A., and J. Feynman. 2002. Solar influence on a major mode of atmospheric variability. *Journal of Geophysical Research-Atmospheres* **107**.
- Scafetta, N. 2010. Empirical evidence for a celestial origin of the climate oscillations and its implications. *Journal of Atmospheric and Solar-Terrestrial Physics* **72**: 951-970.
- Sengul, S., and I. Can. 2011. Stochastic modelling of mean monthly flows of Karasu River, in Turkey. *Water and Environment Journal* **25**: 31-39.
- Serre, T., and E. Nesme-Ribes. 2000. Nonlinear analysis of solar cycles. *Astronomy and Astrophysics* **360**: 319-330.
- Shaviv, N. J. 2008. Using the oceans as a calorimeter to quantify the solar radiative forcing. *Journal of Geophysical Research-Space Physics* **113**.
- Shindell, D. T., G. A. Schmidt, R. L. Miller, and D. Rind. 2001. Northern Hemisphere winter climate response to greenhouse gas, ozone, solar, and volcanic forcing. *Journal of Geophysical Research-Atmospheres* **106**: 7193-7210.
- SIDC. 2011. <http://sidc.oma.be/DATA/monthssn.dat>.
- Stehr, N., and H. V. Storch. 2000. *Eduard Bruckner: The Sources and Consequences of Climate Change and Climate Variability in Historical Times*. Springer.

- Swingedouw, D., L. Terray, C. Cassou, A. Voltaire, D. Salas-Melia, and J. Servonnat. 2011. Natural forcing of climate during the last millennium: fingerprint of solar variability. *Climate Dynamics* **36**: 1349-1364.
- Werritty, A., and K. F. Leys. 2001. The sensitivity of Scottish rivers and upland valley floors to recent environmental change. *Catena* **42**: 251-273.
- Werritty, A., J. L. Paine, N. Macdonald, J. S. Rowan, and L. J. McEwen. 2006. Use of multi-proxy flood records to improve estimates of flood risk: Lower River Tay, Scotland. *Catena* **66**: 107-119.
- Woollings, T., and M. Blackburn. 2012. The North Atlantic Jet Stream under Climate Change and Its Relation to the NAO and EA Patterns. *Journal of Climate* **25**: 886-902.
- Wunsch, C. 1999. The interpretation of short climate records, with comments on the North Atlantic and Southern Oscillations. *Bulletin of the American Meteorological Society* **80**: 245-255.
- Yamazaki, Y., A. D. Richmond, and K. Yumoto. 2012. Stratospheric warmings and the geomagnetic lunar tide: 1958-2007. *Journal of Geophysical Research-Space Physics* **117**.
- Yndestad, H. 2006. The influence of the lunar nodal cycle on Arctic climate. *Ices Journal of Marine Science* **63**: 401-420.
- Yousef, S. 2000. Nile Flood Forecast, p. 263-266. ICEHM2000.
- Zhao, J., and Y. Han. 2012. Sun's total irradiance reconstruction based on multiple solar indices. *Science China-Physics Mechanics & Astronomy* **55**: 179-186.

Section 2.2 Wind direction

- Burroughs, W. J. 1992. *Weather cycles real or imaginary*. Cambridge University Press.
- Colling, A., and O. U. O. C. Team. 2001. *Ocean Circulation*. Butterworth-Heinemann.
- Cran. 2011. R Statistical Software <http://cran.r-project.org/>.
- Da Costa, E. D., and A. C. De Verdiere. 2002. The 7.7-year North Atlantic oscillation. *Quarterly Journal of the Royal Meteorological Society* **128**: 797-817.
- Dawson, A., D. Smith, and S. Dawson. 2001. Potential impacts of climate change on sea levels around Scotland. *Scottish Natural heritage, Research, Survey and Monitoring Report*. No 178.
- Dawson, A. G., K. Hickey, J. McKenna, and I. D. L. Foster. 1997. A 200-year record of gale frequency, Edinburgh, Scotland: possible link with high-magnitude volcanic eruptions. *Holocene* **7**: 337-341.
- Dickson, R. R. and others 2000. The Arctic Ocean response to the North Atlantic oscillation. *Journal of Climate* **13**: 2671-2696.

- Feliks, Y., and M. Ghil. 2007. Interannual, synchronized oscillations over the North Atlantic, Eastern Mediterranean and Ethiopian Plateau. Geophysical Research Abstracts, European Geosciences Union.
- Feliks, Y., M. Ghil, and A. W. Robertson. 2010. Oscillatory Climate Modes in the Eastern Mediterranean and Their Synchronization with the North Atlantic Oscillation. *Journal of Climate* **23**.
- . 2011. The Atmospheric Circulation over the North Atlantic as Induced by the SST Field. *Journal of Climate* **24**.
- Foukal, P. 2012. A New Look at Solar Irradiance Variation. *Solar Physics* **279**.
- Foukal, P., C. Frohlich, H. Spruit, and T. M. L. Wigley. 2006. Variations in solar luminosity and their effect on the Earth's climate. *Nature* **443**: 161-166.
- Frohlich, C., and J. Lean. 1998. The Sun's total irradiance: Cycles, trends and related climate change uncertainties since 1976. *Geophysical Research Letters* **25**.
- Gray, L. J. and others 2010. SOLAR INFLUENCES ON CLIMATE. *Reviews of Geophysics* **48**.
- Haigh, J. D., and M. Blackburn. 2006. Solar influences on dynamical coupling between the stratosphere and troposphere. *Space Science Reviews* **125**: 331-344.
- Haigh, J. D., A. R. Winning, R. Toumi, and J. W. Harder. 2010. An influence of solar spectral variations on radiative forcing of climate. *Nature* **467**.
- Halcrow Crouch. 1998. Montrose Bay Shoreline Management Study. Unpublished report to Angus Council and Glaxo Wellcome.
- Herschel, W. 1801. Observations tending to investigate the nature of the sun, in order to find the causes or symptoms of its variable emission of light and heat:with remarks on the use that may possibly be drawn from solar observations. *Philos. Trans. R Soc. London* **92**: 265-318.
- Hoyt, D. V., and K. Schatten. 1997. *The Role of the Sun in Climate Change*. Oxford University Press.
- Hurrell, J. W. 1995. Decadal trends in the north-Atlantic Oscillation - Regional temperatures and precipitation. *Science* **269**: 676-679.
- Ineson, S. and others 2011. Solar forcing of winter climate variability in Northern Hemisphere. *Nature Geoscience* **4**: 753-757.
- Jose, P. D. 1965. Sun's motion and sunspots. *Astronomical Journal* **70**,: 193-200.
- Juckett, D. 2003. Temporal variations of low-order spherical harmonic representations of sunspot group patterns: Evidence for solar spin-orbit coupling. *Astronomy & Astrophysics* **399**.
- Kidston, J., D. M. W. Frierson, J. A. Renwick, and G. K. Vallis. 2010. Observations, Simulations, and Dynamics of Jet Stream Variability and Annular Modes. *Journal of Climate* **23**.
- KNMI. 2011. Climate Explorer NAO indices 1821 -2011 <http://climexp.knmi.nl/data/inao.dat>.

- Lamb, H. H. 1972. *Climate -Past, Present and Future*. Methuen.
- Langematz, U., K. Matthes, and J. L. Grenfell. 2005. Solar impact on climate: modeling the coupling between the middle and the lower atmosphere, p. 868-875. *In* I. Ermolli, J. Pap and P. Fox [eds.], *Conference on Solar Variability and Earths Climate*. Soc Astronomica Italiana.
- . 2006. Solar impact on climate: modeling the coupling between the middle and the lower atmosphere. *Solar Variability and Earth's Climate* **76**: 868-875.
- Microsoft. 2003. *Microsoft Office Professional Edition Excel SP3*.
- Moberg, A., and P. D. Jones. 2005. Trends in indices for extremes in daily temperature and precipitation in central and western Europe, 1901-99. *International Journal of Climatology* **25**: 1149-1171.
- Oberlaender, S. and others 2012. The influence of spectral solar irradiance data on stratospheric heating rates during the 11 year solar cycle. *Geophysical Research Letters* **39**.
- O'Brien, D. P., and R. G. Currie. 1993. Observations of the 18.6-Year Cycle of Air-Pressure and a Theoretical-Model to explain Certain Aspects of this Signal. *Climate Dynamics* **8**: 287-298.
- Raspopov, O. M., O. I. Shumilov, E. A. Kasatkina, E. Turunen, and M. Lindholm. 2000. 35-year climatic Bruckner cycle - Solar control of climate variability?, p. 517-520. *In* A. Wilson [ed.], *Proceedings of the 1st Solar and Space Weather Euroconference on the Solar Cycle and Terrestrial Climate*. Esa Special Publications.
- Scafetta, N. 2010. Empirical evidence for a celestial origin of the climate oscillations and its implications. *Journal of Atmospheric and Solar-Terrestrial Physics* **72**: 951-970.
- . 2012a. Does the Sun work as a nuclear fusion amplifier of planetary tidal forcing? A proposal for a physical mechanism based on the mass-luminosity relation. *Journal of Atmospheric and Solar-Terrestrial Physics* **81-82**.
- . 2012b. Multi-scale harmonic model for solar and climate cyclical variation throughout the Holocene based on Jupiter-Saturn tidal frequencies plus the 11-year solar dynamo cycle. *Journal of Atmospheric and Solar-Terrestrial Physics* **80**.
- Shaviv, N. J. 2008. Using the oceans as a calorimeter to quantify the solar radiative forcing. *Journal of Geophysical Research-Space Physics* **113**.
- SIDC. 2011. <http://sidc.oma.be/DATA/monthssn.dat>.
- Smeter.Net.2006. <http://www.smeter.net/propagation/sunspots/sunspot-cycle-forecasts.php>.
- Veretenenko, S., and M. Ogurtsov. 2012. Regional and temporal variability of solar activity and galactic cosmic ray effects on the lower atmosphere circulation. *Advances in Space Research* **49**: 770-783.
- Wallingford, H. M. 1995. *Montrose Bay coastal Erosion Study - Phase II Tidal Modelling of Montrose and Lunan Bays*. H R Wallingford. Wallingford.
- Wallingford, H. R. 1997. *Coastal Cells in Scotland*. Scottish Natural Heritage Research, Surveying & Monitoring Report No.56.

- Wang, N., T. Yao, and L. G. Thompson. 2000. Nitrate concentration in the Guliya ice core and solar activity, p. 11. PAGES Newsletter.
- Wilson, I. R. G., B. D. Carter, and I. A. Waite. 2008. Does a spin-orbit coupling between the Sun and the Jovian planets govern the solar cycle? Publications of the Astronomical Society of Australia **25**.
- Woollings, T., and M. Blackburn. 2012. The North Atlantic Jet Stream under Climate Change and Its Relation to the NAO and EA Patterns. Journal of Climate **25**: 886-902.
- Woollings, T., J. G. Pinto, and J. A. Santos. 2011. Dynamical Evolution of North Atlantic Ridges and Poleward Jet Stream Displacements. Journal of the Atmospheric Sciences **68**.
- Yousef, S. 1995b. The Possibility of Forecasting Nile Floods During the Coming Forty Years. The First Scientific Congress on Science In Service of Sustained Development of Nile Basin Countries. 22-24 May.
- . 2000. Nile Flood Forecast, p. 263-266. ICEHM2000.

Section 2.3.2 Spatial Data- River Eden Migration

- Ashton, A. D., and A. B. Murray. 2006. High-angle wave instability and emergent shoreline shapes: 1. Modeling of sand waves, flying spits, and capes. Journal of Geophysical Research-Earth Surface **111**.
- Burchard, H. 2009. Combined Effects of Wind, Tide, and Horizontal Density Gradients on Stratification in Estuaries and Coastal Seas. Journal of Physical Oceanography **39**: 2117-2136.
- Castelle, B., J. Bourget, N. Molnar, D. Strauss, S. Deschamps, and R. Tomlinson. 2007. Dynamics of a wave-dominated tidal inlet and influence on adjacent beaches, Currumbin Creek, Gold Coast, Australia. Coastal Engineering **54**: 77-90.
- Chen, S.-N., and L. P. Sanford. 2009. Axial Wind Effects on Stratification and Longitudinal Salt Transport in an Idealized, Partially Mixed Estuary. Journal of Physical Oceanography **39**: 1905-1920.
- Chen, S.-N., L. P. Sanford, and D. K. Ralston. 2009. Lateral circulation and sediment transport driven by axial winds in an idealized, partially mixed estuary. Journal of Geophysical Research-Oceans **114**.
- Eastwood, K. M. 1977. Some Aspects of the Sedimentology of the Superficial Deposits of the Eden Estuary, Fife, Scotland. University of St Andrews.
- Esri. Copyright © 1995–2008. ArcGIS. Environmental Systems Research Institute, Inc. California. USA.
- Ferentinos, G., and J. Mcmanus. 1981. Nearshore Processes and shoreline development in St Andrews Bay, Scotland, U.K., p. 161-174. Special Publication of the International Association of Sedimentologists.

- Geyer, W. R. 1997. Influence of wind on dynamics and flushing of shallow estuaries. *Estuarine Coastal and Shelf Science* **44**: 713-722.
- Knmi. 2011. Climate Explorer NAO indices 1821 -2011 <http://climexp.knmi.nl/data/inao.dat>.
- Li, Y., and M. Li. 2011. Effects of winds on stratification and circulation in a partially mixed estuary. *Journal of Geophysical Research-Oceans* **116**.
- Lichter, M., M. Klein, and D. Zviely. 2011. Dynamic morphology of small south-eastern Mediterranean river mouths: a conceptual model. *Earth Surface Processes and Landforms* **36**: 547-562.
- Morales, J. A., J. Borrego, I. Jimenez, J. Monterde, and N. Gil. 2001. Morphostratigraphy of an ebb-tidal delta system associated with a large spit in the Piedras Estuary mouth (Huelva Coast, Southwestern Spain). *Marine Geology* **172**: 225-241.
- Scully, M. E., C. Friedrichs, and J. Brubaker. 2005. Control of estuarine stratification and mixing by wind-induced straining of the estuarine density field. *Estuaries* **28**: 321-326.
- Whitney, M. M., and D. L. Codiga. 2011. Response of a Large Stratified Estuary to Wind Events: Observations, Simulations, and Theory for Long Island Sound. *Journal of Physical Oceanography* **41**: 1308-1327.

Section 2.3.3 Spatial Data – Shoreline Changes

- Alfano, F. et. al. 2011. Tephra stratigraphy and eruptive volume of the May, 2008, Chaiten eruption, Chile. *Bulletin of Volcanology* **73**: 613-630.
- Bauer, B. O., and R. G. D. Davidson-Arnott. 2003. A general framework for modeling sediment supply to coastal dunes including wind angle, beach geometry, and fetch effects. *Geomorphology* **49**: 89-108.
- Crowley, T. J. 2000. Causes of climate change over the past 1000 years. *Science* **289**: 270-277.
- Davidson-Arnott, R. G. D., and M. N. Law. 1996. Measurement and prediction of long-term sediment supply to coastal foredunes. *Journal of Coastal Research* **12**: 654-663.
- Durant, A. J., G. Villarosa, W. I. Rose, P. Delmelle, A. J. Prata, and J. G. Viramonte. 2011. Long-range volcanic ash transport and fallout during the 2008 eruption of Chaitén volcano, Chile. *Physics and Chemistry of the Earth, Parts A/B/C*.
- Ferentinos, G., and J. Mcmanus. 1981. Nearshore Processes and shoreline development in St Andrews Bay, Scotland, U.K., p. 161-174. Special Publication of the International Association of Sedimentologists.
- Fischer, E. M., J. Luterbacher, E. Zorita, S. F. B. Tett, C. Casty, and H. Wanner. 2007. European climate response to tropical volcanic eruptions over the last half millennium. *Geophysical Research Letters* **34**.

- Gerstell, M. F., J. Crisp, and D. Crisp. 1995. Radiative forcing of the stratosphere by SO₂ gas, silicate ash and H₂SO₄ aerosols shortly after the 1982 eruptions of El Chichon. *Journal of Climate* **8**: 1060-1070.
- Hansom, J. D. 1999. The coastal geomorphology of Scotland: understanding sediment budgets for effective coastal management. In: Baxter, J., Duncan, K., Atkins, S. and Lees, G., Editors,, p. 34–44. *Scotland's Living Coastline*.
- Hurrell, J. W. 1995. Decadal Trends in the North-Atlantic Oscillation - Regional Temperatures and Precipitation. *Science* **269**: 676-679.
- Hurrell, J. W., and C. Deser. 2010. North Atlantic climate variability: The role of the North Atlantic Oscillation. *Journal of Marine Systems* **79**: 231-244.
- Jones and others 2003. Surface climate responses to explosive volcanic eruptions seen in long European temperature records and mid-to-high latitude tree-ring density around the Northern Hemisphere. American Geophysical Union.
- Lynch, K., D. W. T. Jackson, and J. A. G. Cooper. 2009. Foredune accretion under offshore winds. *Geomorphology* **105**: 139-146.
- . 2010. Coastal foredune topography as a control on secondary airflow regimes under offshore winds. *Earth Surface Processes and Landforms* **35**: 344-353.
- May, V. J., and J. D. Hansom. 2003. Coastal Geomorphology of Great Britain. Geological Conservation Review Series, GCR Volume No. 28. Joint Nature Conservation Committee, Peterborough, 754 pp.
- Ottersen, G., B. Planque, A. Belgrano, E. Post, P. C. Reid, and N. C. Stenseth. 2001. Ecological effects of the North Atlantic Oscillation. *Oecologia* **128**: 1-14.
- Paola, C. 2000. Sedimentology and sedimentary basins: From turbulence to tectonics. *Nature* **405**: 123-123.
- Prejean, S. G., and E. E. Brodsky. 2011. Volcanic plume height measured by seismic waves based on a mechanical model. *J. Geophys. Res.* **116**: B01306.
- Pugh, D. T. 2004. Changing sea levels. Effects of tides, weather and climate. Cambridge University Press: 280 pp.
- Robock, A. 2000. Volcanic eruptions and climate. *Reviews of Geophysics* **38**: 191-219.
- Trigo, R. M., T. J. Osborn, and J. M. Corte-Real. 2002. The North Atlantic Oscillation influence on Europe: climate impacts and associated physical mechanisms (vol 20, pg 9, 2002). *Climate Research* **22**: 97-97.
- Wal, A., and J. Mcmanus. 1993. Wind regime and sand transport on a coastal beach-dune complex, Tentsmuir, eastern Scotland, p. 159-171. Geological Society.
- Wilson, J. H. 1910. Nature Study Rambles Around St andrews. St Andrews University Press.
- Wright, J., A. Colling, D. Park, and O.U.O.C. Team. 1999. Waves, tides, and shallow-water processes. Butterworth-Heinemann, in association with the Open University.

Section 2.3.4 Spatial Data- Morphological Change analysis

- Anderson, F. E. 1972. Resuspension of Estuarine Sediments by Small Amplitude Waves. *Journal of Sedimentary Petrology* **42**: 602-&.
- Bates, C. R., C. G. Moore, T. Malthus, J. M. Mair, and E. Karpouzli. 2004. Broad scale mapping of habitats in the Firth of Tay and Eden Estuary, Scotland. Scottish Natural Heritage Commissioned Report No. 007 (ROAME No. F01AA401D).
- Brown, J. M., and A. G. Davies. 2010. Flood/ebb tidal asymmetry in a shallow sandy estuary and the impact on net sand transport. *Geomorphology* **114**: 431-439.
- Dolphin, T. J., and M. O. Green. 2009. Patterns of Wave-orbital Speed and Skin Friction Under Estuarine (Fetch-limited) Waves. *Journal of Coastal Research*: 178-182.
- Dronkers, J. J. 1986. Tidal asymmetry and estuarine morphology. *Journal of Sea Research* **20(2/3)**:.
- Esri. Copyright © 1995–2008. ArcGIS. Environmental Systems Research Institute, Inc.California. USA.
- . © 1995–2008. Environmental Systems Research Institute (ESRI), Inc.California. USA. ARCMAP Version 9.3.
- . © 1999–2008. Environmental Systems Research Institute (ESRI), Inc.California. USA. ARCScape Version 9.3.
- Friedrichs, C. T., and D. G. Aubrey. 1988. Non-Linear Tidal Distortion in Shallow Well-Mixed Estuaries - A Synthesis. *Estuarine Coastal and Shelf Science* **27**: 521-545.
- Friedrichs, C. T., and O. S. Madsen. 1992. Nonlinear Diffusion of the Tidal Signal in Frictionally Dominated Embayments. *Journal of Geophysical Research-Oceans* **97**: 5637-5650.
- Godin, G. 1985. Modification of River Tides by the Discharge. *Journal of Waterway Port Coastal and Ocean Engineering-Asce* **111**: 257-274.
- Green, M. O. 2011. Very small waves and associated sediment resuspension on an estuarine intertidal flat. *Estuarine Coastal and Shelf Science* **93**: 449-459.
- Hypack.Inc. 56, Bradley St, Middletown, CT06457, USA. Copyright 2010.
- Lanzoni, S., and G. Seminara. 1998. On tide propagation in convergent estuaries. *Journal of Geophysical Research-Oceans* **103**: 30793-30812.
- . 2002. Long-term evolution and morphodynamic equilibrium of tidal channels. *Journal of Geophysical Research*.
- Microsoft. 2003. Microsoft Office Professional Edition Excel SP3.
- Pethick, J. 1994. Estuaries and Wetlands - Function and Form. *Wetland Management*: 75-87.

- Prandle, D., A. Lane, and A. J. Manning. 2006. New typologies for estuarine morphology. *Geomorphology* **81**: 309-315.
- Pugh, D. T. 2004. *Changing sea levels. Effects of tides, weather and climate.* Cambridge University Press: 280 pp.
- Robins, P., and A. Davies. 2010. Morphological controls in sandy estuaries: the influence of tidal flats and bathymetry on sediment transport. *Ocean Dynamics* **60**: 503-517.
- Scully, M. E., C. Friedrichs, and J. Brubaker. 2005. Control of estuarine stratification and mixing by wind-induced straining of the estuarine density field. *Estuaries* **28**: 321-326.
- Sea.Ltd. 1998-2011. SEA Swath Real Time Acquisition System. Copyright © Systems Engineering & Assessment Ltd. (SEA). Version 3.07.10.00.
- . 2001-2011. SEA Grid Processor. Copyright© Systems Engineering & Assessment Ltd. Version 3.07.9.00.

Section 2.3.5 Spatial Data- Species Distribution

- Adams, M. W., Ellingbo.Ah, and E. C. Rossman. 1971. Biological Uniformity and Disease Epidemics. *Bioscience* **21**: 1067-&.
- Ahmad, A., and J. Mcmanus. 1994. Comparisons of intertidal sediments in two coastal embayments in eastern Scotland using remote sensing techniques., p. 327-335. *In* R. Vaughan [ed.], *Remote sensing from research to operational applications in the new Europe.* Springer Hungarica.
- Allen, J. R. L. 2000. Morphodynamics of Holocene Salt marshes: a review sketch from the Atlantic and Southern North Sea coasts of Europe (vol 19,pg 1155, 2000). *Quaternary Science Reviews* **19**: 1839-1840.
- Allen, J. R. L., and K. Pye. 1992. Coastal saltmarshes: Their nature and importance.
- Anderson, F. E. 1972. Resuspension of Estuarine Sediments by Small Amplitude Waves. *Journal of Sedimentary Petrology* **42**: 602-&.
- Bacon, S., and D. J. T. Carter. 1991. Wave Climate Changes in the North-Atlantic and North-Sea. *International Journal of Climatology* **11**: 545-558.
- Bates, C. R., C. G. Moore, T. Malthus, J. M. Mair, and E. Karpouzli. 2004. Broad scale mapping of habitats in the Firth of Tay and Eden Estuary, Scotland. Scottish Natural Heritage Commissioned Report No. 007 (ROAME No. F01AA401D).
- Butcher, R. W. 1934. *Zostera.* Report on the Present Condition of Eel Grass on the Coasts of England, based on a Survey during August to October, 1933. *Journal du Conseil* **9**: 49-65.
- . 1941b. Notes on the variation of the species British of *Zostera.*, p. 592-597. Report of the Botanical Society and Exchange Club of the British Isles. 10 (3).

- Chmura, G. L., S. C. Anisfeld, D. R. Cahoon, and J. C. Lynch. 2003. Global carbon sequestration in tidal, saline wetland soils. *Global Biogeochemical Cycles* **17**.
- Choi, Y. H., and Y. Wang. 2004. Dynamics of carbon sequestration in a coastal wetland using radiocarbon measurements. *Global Biogeochemical Cycles* **18**.
- Cox, R., R. A. Wadsworth, and A. G. Thomson. 2003. Long-term changes in salt marsh extent affected by channel deepening in a modified estuary. *Continental Shelf Research* **23**: 1833-1846.
- Davison, D. M., and D. J. Hughes. 1998. *Zostera Biotopes (Volume I). An overview of dynamics and sensitivity characteristics for conservation management of marine SAC's*. Scottish Association for Marine Science (UN Marine SACs Project).
- Duarte, C. M., J. W. Fourqurean, D. Krause-Jensen, and B. Olesen. 2006. Dynamics of seagrass stability and change. *Seagrasses: Biology, Ecology and Conservation*: 271-294.
- Duck, R. W., J. Mcmanus, and J. J. Diez. 1995. Comparative study of two largely infilled estuaries: The Eden estuary (Scotland) and the Ria de Foz (Spain). *Netherlands Journal of Aquatic Ecology* **29**: 203-210.
- Eastwood, K. M. 1977. *Some Aspects of the Sedimentology of the Superficial Deposits of the Eden Estuary, Fife, Scotland*. University of St Andrews.
- Edina. 2012. DIGIMAP Ordnance Survey Products © Crown Copyright/database right 2012. An Ordnance Survey/EDINA supplied service.. Causway House, Edinburgh, Scotland. U.K. University of Edinburgh.
- Esri. © 1995–2008. Environmental Systems Research Institute (ESRI), Inc. California. USA. ARCMAP Version 9.3.
- Eswaran, H., E. Van Den Burgh, P. Reich, and J. Kimble. 1995. Global soil carbon resources, p. 27-43. *In* R. Lal [ed.], *Soils & Global Change*. CRC Lewis, Boca Raton Fla.
- Ferentinos, G., and J. Mcmanus. 1981. Nearshore Processes and shoreline development in St Andrews Bay, Scotland, U.K., p. 161-174. Special Publication of the International Association of Sedimentologists.
- . 2009. *Nearshore Processes and Shoreline Development in St Andrews Bay, Scotland, U.K.* Blackwell Publishing Ltd.
- Fonseca, M. S., J. S. Fisher, J. C. Zeman, and G. W. Thayer. 1982. Influence of the Seagrass, *Zostera-Marina* on Current Flow. *Estuarine Coastal and Shelf Science* **15**: 351-&.
- Fonseca, M. S., and M. A. R. Koehl. 2006. Flow in seagrass canopies: The influence of patch width. *Estuarine Coastal and Shelf Science* **67**: 1-9.
- Giani, L., K. Dittrich, A. Martsfeldhartmann, and G. Peters. 1996. Methanogenesis in saltmarsh soils of the North Sea coast of Germany. *European Journal of Soil Science* **47**: 175-182.
- Green, M. O. 2011. Very small waves and associated sediment resuspension on an estuarine intertidal flat. *Estuarine Coastal and Shelf Science* **93**: 449-459.
- Greensmith, J. T., and E. V. Tucker. 1965. Salt marsh erosion in Essex. *Nature* **206**: 606-607.

- Herbener, K. W., S. J. Tavener, and N. T. Hobbs. 2012. The distinct effects of habitat fragmentation on population size. *Theoretical Ecology* **5**: 73-82.
- Hooper, D. U. and others 2005. Effects of biodiversity on ecosystem functioning: A consensus of current knowledge. *Ecological Monographs* **75**: 3-35.
- Jarvis, J., and C. Riley. 1987. Sediment transport in the mouth of the Eden estuary. *Estuarine, Coastal and Shelf Science* **24**: 463-481.
- Jelliman, C. E., P. J. Hawkes, and A. H. Brampton. 1991. Wave climate change and its impact on UK coastal management. HR Wallingford Report SR 260.
- Johnston, J. P., J. L. S. Cobb, and B. Bell. 1979. Survey of Shorebird Feeding Distribution and Movements on the Eden Estuary NE Fife, Including a Study of the Invertebrate Food Source. Report for the Nature Conservancy Council,. South East Scotland Region.
- Larkum, A. W. D., R. J. Orth, C. M. Duarte, K. Moore, and F. Short. 2006. *Zostera: Biology, Ecology, and Management. Seagrasses: Biology, Ecology and Conservation*, p. 361-386. Springer Netherlands.
- Maccaferri.Ltd. 2005. St Andrews Royal & Ancient Golf Club: Erosion Protection Case History. Maccaferri Ltd. River View House, Friarton Road, Perth Scotland. Consultancy HR Wallingford.
- Maynard, C., J. Mcmanus, R. M. M. Crawford, and D. Paterson. 2011. A comparison of short-term sediment deposition between natural and transplanted saltmarsh after saltmarsh restoration in the Eden Estuary (Scotland). *Plant Ecology & Diversity* **4**: 103-113.
- Mcmanus, J. 2008. Trends of change in coastal landforms and processes. Scottish Natural Heritage, Commissioned Report No: XXX
- Mills, L. S., M. E. Soule, and D. F. Doak. 1993. The Keystone-Species Concept in Ecology and Conservation. *Bioscience* **43**: 219-224.
- Moller, I. 2006. Quantifying saltmarsh vegetation and its effect on wave height dissipation: Results from a UK East coast saltmarsh. *Estuarine Coastal and Shelf Science* **69**: 337-351.
- Paine, R. T. 1969. A Note on Trophic Complexity and Community Stability. *American Naturalist* **103**: 91-&.
- Pethick, J. 1993. Shoreline Adjustments and Coastal Management - Physical and Biological Processes Uunder Accelerated Sea-Level Rise. *Geographical Journal* **159**: 162-168.
- Pugh, D. T. 2004. Changing sea levels. Effects of tides, weather and climate. Cambridge University Press: 280 pp.
- Pye, K. 2000. Saltmarsh erosion in southeast England: mechanisms, causes and implications, p. pp. 359-396. *In* B. R. Sherwood, Gardiner, B.G. and Harris, T. [ed.], *British Saltmarshes*. Westbury Publishing, Yorkshire.
- Solan, M., D. G. Raffaelli, D. M. Paterson, P. C. L. White, and G. J. Pierce. 2006. Marine biodiversity and ecosystem function: empirical approaches and future research needs - Introduction. *Marine Ecology-Progress Series* **311**: 175-178.

- Strachan, R. 2007. Eden Estuary LNR Annual Report. Fife Ranger Service, Fife Coast & Countryside Trust.
- S.I.C. 2002. Quickbird. Copyright 2001-2012. Satellite Imaging Corporation. All Rights Reserved. 36842, Meados Creek Court, Magnolia, Texas. USA
- Simas, T., J. P. Nunes, and J. G. Ferreira. 2001. Effects of global climate change on coastal salt marshes. *Ecological Modelling* **139**: 1-15.
- UKMPA 2001. UK Marine SAC's Project, Communities, Zostera. Scottish Association for Marine Science (SAMS). www.ukmarinesac.org.uk/communities/zostera/z9.htm#a1.
- Van Der Wal, D., and K. Pye. 2004. Patterns, rates and possible causes of saltmarsh erosion in the Greater Thames area (UK). *Geomorphology* **61**: 373-391.
- Van Der Wal, D., A. Wielemaker-Van Den Dool, and P. M. J. Herman. 2008. Spatial patterns, rates and mechanisms of saltmarsh cycles (Westerschelde, The Netherlands). *Estuarine Coastal and Shelf Science* **76**: 357-368.
- Whiting, G. J., and J. P. Chanton. 2001. Greenhouse carbon balance of wetlands: methane emission versus carbon sequestration. *Tellus Series B-Chemical and Physical Meteorology* **53**: 521-528.
- Wilde, P., A. Manal, M. Stodden, E. Sieverding, U. Hildebrandt, and H. Bothe. 2009. Biodiversity of arbuscular mycorrhizal fungi in roots and soils of two salt marshes. *Environmental Microbiology* **11**: 1548-1561.
- Wilson, J. H. 1910. *Nature Study Rambles Around St Andrews*. St Andrews University Press.
- Wyer, D. W., L. A. Boorman, and R. Waters. 1977. Studies on Distribution of *Zostera* in the Outer Thames Estuary. *Aquaculture* **12**: 215-227.
- Yaacobi, G., Y. Ziv, and M. L. Rosenzweig. 2007. Habitat fragmentation may not matter to species diversity. *Proc. R. Soc B* **274**: 2409-2412.

Section 2.4 Discussion

- Camuffo, D., and C. Bertolin. 2012. Recovery of the early period of long instrumental time series of air temperature in Padua, Italy (1716-2007). *Physics and Chemistry of the Earth* **40-41**: 23-31.
- Raspopov, O. M., V. A. Dergachev, and T. Kolstrom. 2004. Periodicity of climate conditions and solar variability derived from dendrochronological and other palaeoclimatic data in high latitudes. *Palaeogeography Palaeoclimatology Palaeoecology* **209**: 127-139.
- Scafetta, N. 2012. Multi-scale harmonic model for solar and climate cyclical variation throughout the Holocene based on Jupiter-Saturn tidal frequencies plus the 11-year solar dynamo cycle. *Journal of Atmospheric and Solar-Terrestrial Physics* **80**.
- Wang, N., T. Yao, and L. G. Thompson. 2000. Nitrate concentration in the Guliya ice core and solar activity, p. 11. *PAGES Newsletter*.

Yamaguchi, Y. T., Y. Yokoyama, H. Miyahara, K. Sho, and T. Nakatsuka. 2010. Synchronized Northern Hemisphere climate change and solar magnetic cycles during the Maunder Minimum. *Proceedings of the National Academy of Sciences of the United States of America* **107**.

CHAPTER 3

3. ABIOTIC ANALYSIS

Chapter aim

- To identify key abiotic influences to an estuarine ecosystem that may be applied as indicators of climate driven change.

Introduction

Historically estuaries have been classified by their abiotic attributes; geomorphology, tidal characteristics and level of stratification. However, further to these, additional abiotic factors contribute to the complexity of gradient conditions that exist along the length of an estuary and play vital roles in estuary morphological development and the structuring of ecological diversity (Little, 2000; FSBI, 2007; Mucha and Costa, 1999; Attrill and Rundle, 2002). These additional core factors include salinity, dissolved oxygen, temperature, water depth, nutrients, turbidity, pH and energy levels, all of which not only vary spatially along the estuary, but also temporally within the tidal duration and from season to season. One of the important ecological roles an estuary fulfils is to provide feeding areas and nursery grounds for marine organisms, and wildfowl, providing a highly nutrient rich environment with shallow turbid niches giving protection throughout their development (Elliott *et al.*, 2007). Whilst the organisms that reside within estuaries are adapted to occupy particular niches within the extreme abiotic gradients, transient species may be restricted by tolerance limits and thus patterns of more mobile organisms may change with regime shifts related to climate variability.

Recent UK Climate reports (UKCIP, MCCIP, SNIFFER etc), suggest the East coast of Scotland will experience increases in the seasonality of precipitation, with concomitant increase in seasonality of river flow, also changes in relative sea level and a decrease in average wind speeds, accompanied by increased storminess & wave surges. From Chapter 2, such changes are expected to follow climate index patterns i.e. periods reflected by prolonged positive NAO indices will be accompanied by increased precipitation and potentially a lowering of estuary salinity under increased river discharge. The prolonged mild weather leading to increases in sea surface temperature (SST) with impacts to thermal expansion (thus sea level rise), evaporation and circulation/ stratification. Wind driven waves and circulation will be influenced by generally more offshore conditions. Prolonged periods of negative NAO indices will likely be accompanied by drier summers, potentially leading to desiccation of the inter-tidal areas, a landward shift in estuarine salinity, greater dominance of onshore wind waves and circulation and a lowering of SST under colder conditions.

Changes between sustained NAO phases will impact primarily on the equilibrium between river flow and the tidal prism; shifts in this equilibrium will be reflected in the tidal asymmetry and thus

direction of net sediment transport, leading to either a largely depositional or erosional environment. Dominance in either river flow or tidal prism, will also impact on water temperature, which is recognized as having a major influence particularly on fish ecology, directly controlling metabolic processes and consequently growth rates (Magnuson *et al.*, 1979). Similarly changes to salinity driven by greater prism intrusion, will also affect metabolic processes, influencing oxygen consumption and osmoregulation. A close interrelationship exists between the vertical distribution of temperature density and salinity (decrease in temperature being associated with a dramatic increase in salinity and density), with feedbacks to levels of dissolved oxygen and PH. Temperature exerts the primary control on dissolution of gasses, reducing solubility with increasing temperatures and decreasing solubility as salinity increases (Al-Anezi *et al.*, 2008, Mosley *et al.*, 2010). Thus moving from river to full saline conditions in an estuary, both CO₂ (hence PH) (Mosley *et al.*, 2010) and dissolved oxygen become less saturated along the gradient.

The preceding paragraphs identify the key roles abiotic variables play along the estuarine continuum and how shifts in their regime may be driven by the predicted climate perturbation. The interrelationship between variables allows some to be used as relative proxies for others (i.e. temperature or salinity for approximate PH etc), thus the following have been chosen as indicators of change;

Tidal asymmetry analysis

Aim

- Identify the estuary as being largely depositional or erosional in phase.

Tidal asymmetry analysis is used here to complement the historical trend analysis of morphological change in the previous chapter, giving supporting evidence to the present directional trend in erosional or depositional character and to further postulate upon the future changes. Tidal curve data, particularly analysis of velocities, provide information relating to bedload sediment transport and larger particles in the region of the instrument, however for a more complete understanding of general conditions the 'Dronkers (1986) asymmetry ratio' is calculated to give a γ value indicating again a dominance in either flood or ebb duration and takes into consideration the morphology of the estuary. The relative contribution of tidal and river flow to the asymmetry reflects approximate temperature regimes; with river water often dropping much lower in temperature and with greater variability than seawater which generally remains stable, seasonally and over long timescales. The relative river/ seawater contributions have further implications to the availability of particulate matter and nutrients. Changes to the tidal prism and volume of river flow are thus valuable as proxy temperature and salinity regime shifts.

Bed-form transport

Aim

- Quantify the net rate and direction of sediment transport (bed-load).

Assessment of bed-form transport is used to complement the tidal asymmetry analysis, to quantify a relative rate and the volume of net sediment transport, through the lateral migration of mega-ripples.

Salinity

Aim

- Identify regime shifts in salinity.

Contemporary data were used to elucidate present conditions, with the additional use of limited recent historical data to identify potential directional trends of change, correlating spatial changes with regime shifts. Salinity was chosen as it represents the transition regime between fresh and marine conditions, indicative of temperature, dissolved oxygen and PH conditions with respect to the contribution of river to seawater.

3.1. Tidal Asymmetry Analysis

Tidal asymmetry is the modification of the tidal wave as it propagates within the estuary, giving rise to unequal flood and ebb phases which principally drive the direction of net sediment transport. The nature of wave propagation is influenced by the interaction of river discharge, tidal range, tidal current velocities, wind direction & strength, morphology and channel geometry (Dyer, 1995, Dronkers, 1986, Friedrichs and Aubrey, 1988). Thus, climate driven changes to estuary hydrodynamics, though modification of tidal volume (either from relative sea level changes or from sustained meteorological conditions) and changes to river discharge will impact with morphological feedback mechanisms on the asymmetry of flood or ebb tidal dominance.

Ebb or flood dominance may refer either to an inequality in the durations of the ebb or flood phases or to inequality in the current velocities between the two phases. These two different types of dominance are often referred to as horizontal (velocity) and vertical (duration) asymmetry and are interrelated by non-linear conditions due to the changing interaction with morphology and cross-sectional area with tidal level (Dronkers, 1986, Wang *et al.*, 1999).

Vertical asymmetry is said to be ebb dominant if the duration of the falling ebb tidal phase exceeds that of the rising flood and similarly vice versa. This inequality is important for the residual transport of suspended fine particles. Horizontal asymmetry is characterised by two conditions; 1. The

duration of critical erosion/ transport velocities, where flood velocity duration exceeds that of the ebb, asymmetry is flood dominant and net sediment transport will be on the flood phase and under the opposite conditions asymmetry is in favour of the ebb. This residual net transport reflects the movement of bed-load and larger suspended particles. 2. Asymmetry in slack water durations, where the inequality between high and low water slack durations gives a relative indication of the direction of net transport of finer suspended particles. Subtracting the 'slack before flood' (SBF) duration from the 'slack before ebb' (SBE) duration to give positive values for flood dominance and negative values for ebb dominance (Dronkers, 1986).

Before analysis of tidal asymmetry it is first important to understand the natural variability in tidal conditions throughout the year; from this information a choice can then be made to minimise acquisition effort against which tide or tides are most representative of "average" conditions.

Tidal constituents: The principal tidal constituents in the Eden estuary are mixed semidiurnal tides over approximately a 12.4 hour period, these are referred to as M_2 lunar constituents (the subscript denotes two tides per lunar tidal day) and give rise to two unequal high water and two unequal low water tides for the majority of the time. The range (elevation change between high water and low water) also varies over a two week cycle in relation to the proximity of the Moon and Sun with the Earth. When all three are in alignment (new or full moon) this configuration gives rise to the maximum tidal ranges, which are the spring tides. As the Moon and Sun approach a 90 degree separation, the tidal ranges are at their minimum and are referred to as neap tides. The changes to the range of the tides are driven by the gravitational forces exerted by both the Sun and the Moon; when in alignment their forces are combined and cause both very high and very low tides. Conversely, when the Sun and Moon are separated by 90 degrees, their gravitational forces work in opposition to each other resulting in both smaller high and low water tidal ranges. Intermediate tidal conditions occur between phases of the lunar cycle (Pugh, 2004)

Distance – The Earth and Sun follow an elliptical orbit around their common centre of mass, as the Earth passes close to the sun (perihelion) the gravitational forces cause above average tides with larger ranges, conversely as the Earth becomes further from the Sun (aphelion), gravitational forces become weaker and below average tidal forces occur (Pugh, 2004)

A further lunar constituent which impacts on the tidal range is the distance between the Moon and the Earth during the Moon's orbital path. When the Moon is at its furthest distance (apogee) it exerts less gravitational influence, however at its closest (perigee) there is a strong gravitational force exerted, causing larger than average or a greater difference between high and low tides. Maximum semidiurnal tides occur when perigee coincides with the spring tides, which occurs approximately three times per year. Additionally on much longer time scales (18.61 years full cycle) (Pugh, 2004) the orbital path of the moon changes from being almost circular to being more strongly elliptical, when the gravitational influence is at its strongest.

Declination - The axial tilt of the Earth, which with the proximity to the Sun determines the seasons, also contributes to the extent of the tidal range. Maximum inclination either towards or away from the Sun (aphelion, perihelion), results in solstice tides when the moon's declination is also at a maximum. This occurs twice per year on the winter and summer solstices and exerts low gravitational forces on the tides. Three months following on from the solstice the Earth's axial tilt is perpendicular to the Sun and thus at zero declination; towards the equinox, the moon also enters a phase of zero declination, the combined gravitational affect causes equinoctial tides (Pugh, 2004).

It is therefore preferable to select a tide where the phase of the interacting tidal components is at a minimum. Ensuring that the tidal elevations are relatively equal minimises any asymmetry in the vertical and consequently through non-linear relationships, to the horizontal tide.

3.1.1. Tidal Instrumental Data

Data were collected from 2 channel locations in the estuary (Figure 3-1) representing outer and middle estuary conditions. The survey was limited by having only one current meter and also by water depth for the instrument and boat access. The design for mounting the current meter took into consideration protection from tangling by the marker buoy rope during lower tides and minimising the modification of tidal currents through the mounting system. The data collection programme suffered from seasonal barnacle encrustations, tangling with algal mats and other debris being carried down the Eden, with consequent loss of meter readings. The current meter was relocated on a number of occasions by floating debris and required replacement following loss during 2010.

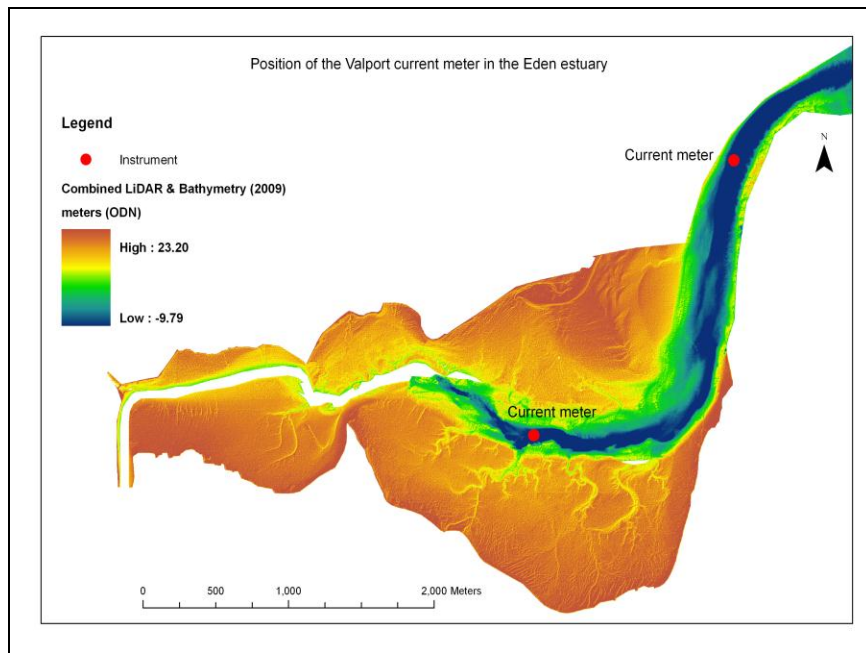


Figure 3-1: Location of the Valeport Model 106 current meter within the Eden Estuary.

3.1.1.1. Methodology

Current meter data were acquired between March 2010 and August 2011, capturing scales of diurnal to seasonal variability.

The current velocity and tidal elevations were recorded using a Valeport lightweight Model 106 current meter, hung mounted within a meter cube of weighted aluminium frame, which allowed free rotational movement of the instrument (Figure 3-2).



Figure 3-2: Valeport Model 106 current meter, housed in 1m weighted cube frame, recovered following relocation during stormy conditions.

Data were downloaded using Valeport's DataLog™ software and imported into Excel (Microsoft, 2003) for graphical analysis. Tidal elevation plots and Velocity stage plots were built, for spring and neap tidal cycles respectively, based upon the following definitions with respect to Hjulstrom's diagram of erosion, transportation and deposition (Blatt *et al.*, 1981);

- Slack water velocities defined as $= > 0.02 \text{ ms}^{-1}$
- Critical erosion velocities (U_{cr}) based upon modal particle size 220um $= > 0.2 \text{ ms}^{-1}$
- Critical deposition velocities (V_{cr}) based upon modal particle size 220um $= < 0.1 \text{ ms}^{-1}$
- Vertical tide is defined by the time-interval between two adjacent high waters
- Horizontal tide is defined as the time interval between adjacent flood and ebb slack waters

During the deployment of the current meter Van Veen grab samples were taken of the sediment in the location of the instrument to calculate the critical velocities for erosion and deposition throughout the tidal cycle. Particle size analysis was carried out using a Coulter Counter LS230. A small sub-

sample replicate of raw sediment from each ground truth location was mixed with water and added to the LS230 machine through a 2mm sieve until the obscuration reached approximately 12%. Each sample was sonicated for 30 seconds before a run commenced. Each run lasted approximately 5 minutes and the output of the two samples is seen in Figure 3-3.

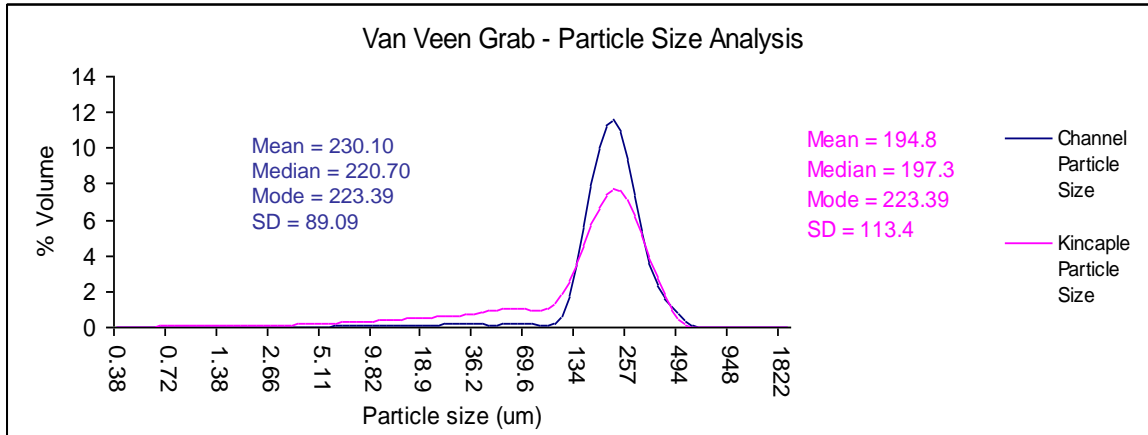


Figure 3-3: Analysis of particle size at the two current meter locations.

The choice of representative tide was investigated by analysing the relationship between the elevation range and the duration of the tidal phase (ebb or flood, Figure 3-4). Approaching maximum tides the ebb range is always less than flood and vice versa following maximum tide. The flood range increases as the duration decreases approaching maximum tide, whilst both range and duration increase for the ebb.

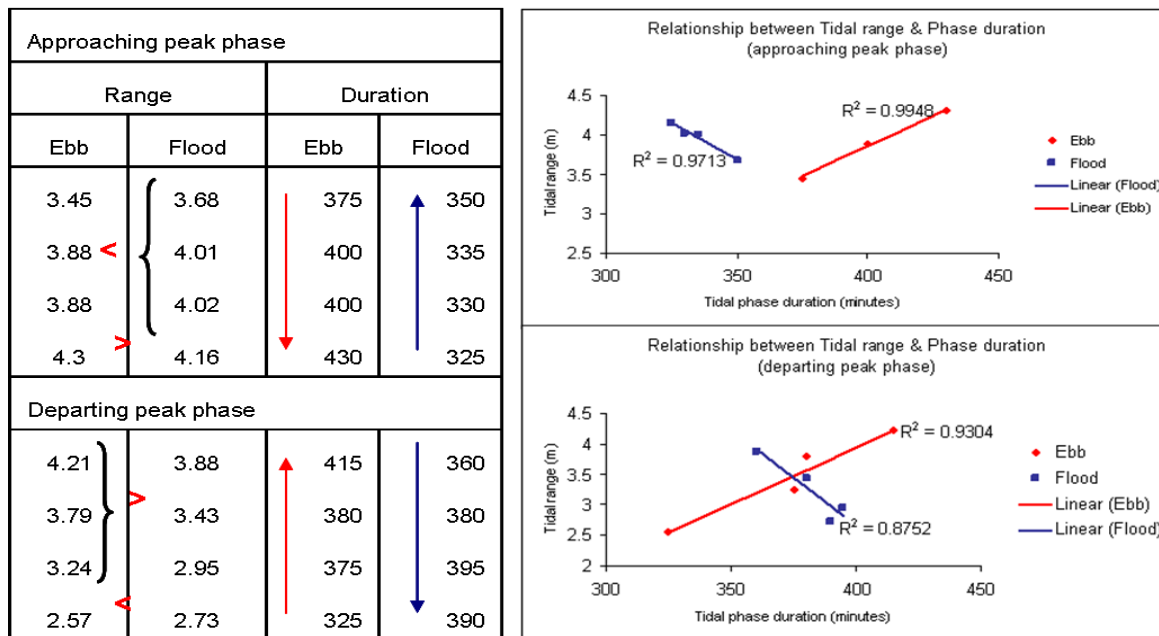


Figure 3-4: left, illustration of the relationship between tidal range and the duration of cycle phase. Right, The relationship between tidal range; approaching (above) or departing (below) from the peak of the tidal phase.

Departing from maximum tides the flood range decreases as duration increases, whilst both range and duration decrease for the ebb. Thus, for asymmetry analysis the maximum tidal range for each selected spring and neap cycles was chosen to minimise variation due to inequality of range.

3.1.1.2. Results

Due to problems with data acquisition and the restriction in selecting only maximum tidal elevations per tidal phase (spring or neap group of tides) where the inequalities in range are minimised, 8 tidal curves were analysed over the two locations. For each, a tidal elevation plot and a velocity stage plot were produced to give a visual appraisal of the asymmetry in both vertical and horizontal tide.

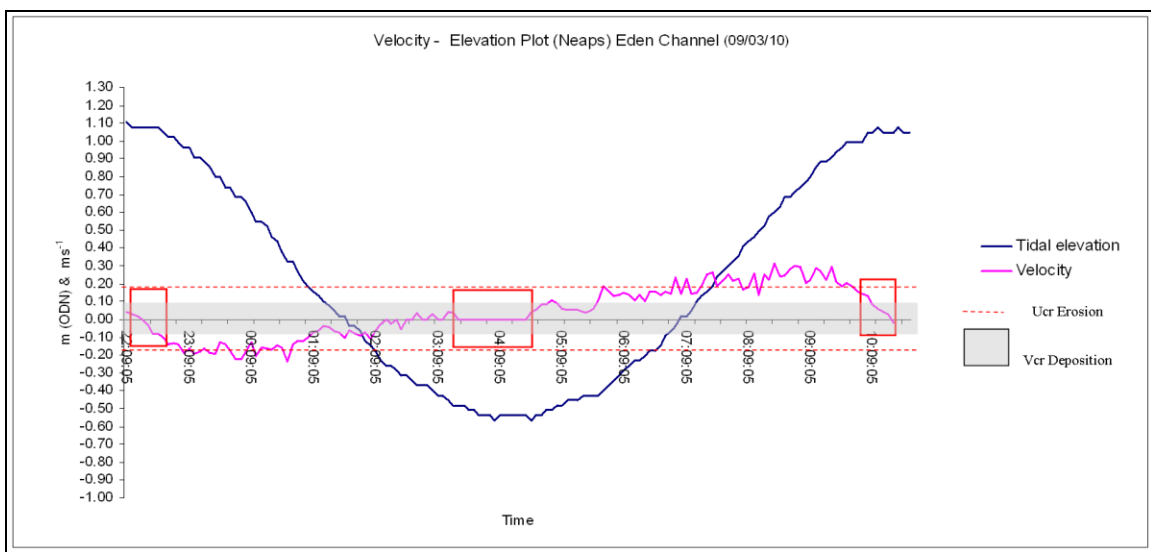


Figure 3-5: Neap tidal elevation plot, illustrating Tidal height over the cycle, near bed current velocities and the durations of critical erosion and deposition periods for modal particle size at the location of the instrument (220 μ m).

The plots are particularly useful for estimating the horizontal tide in terms of velocities and the times of the slack water duration, which combine to give an overview of bedload and suspended sediment transport. Figures 3-5, 3-6 3-7 and Table 3-1 present the tidal data for the spring and neap tides (09/0310 & 16/03/10 respectively) for the outer channel. The remaining analyses are found in Appendix 3-1.

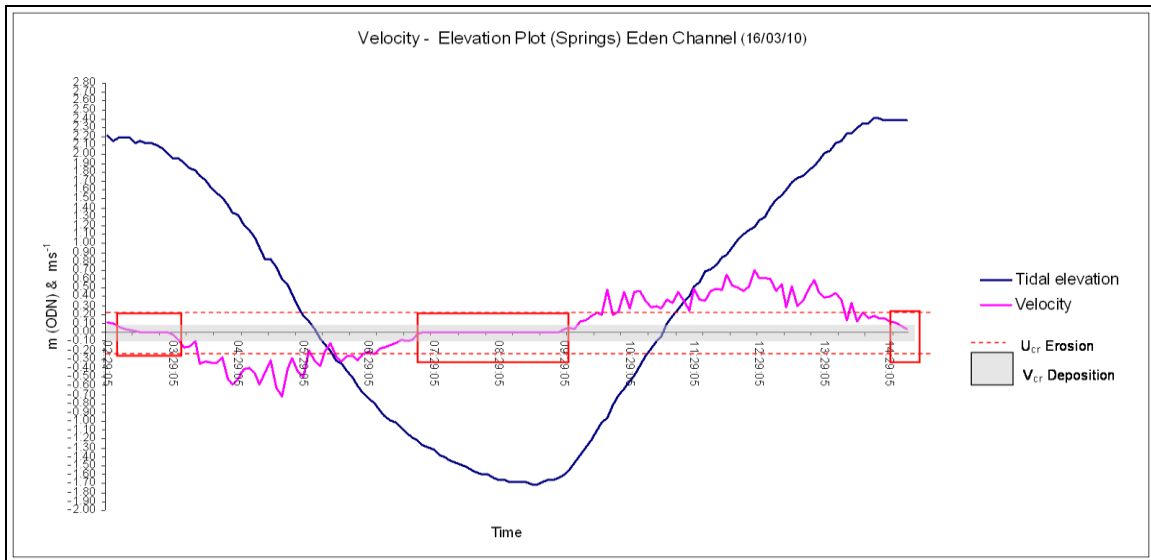


Figure 3-6: Spring tidal elevation plot, illustrating Tidal height over the cycle, near bed current velocities and the durations of critical erosion and deposition periods for modal particle size at the location of the instrument (220um). Heights are in meters above Ordnance Datum Newlyn.

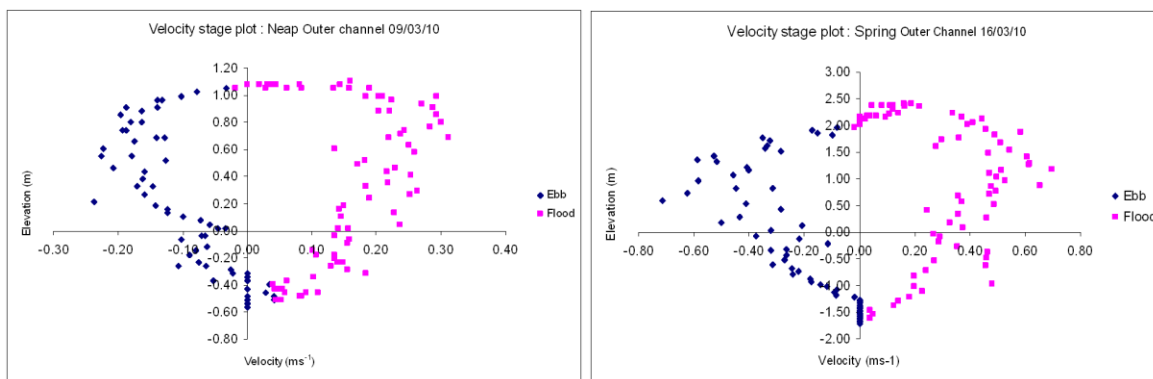


Figure 3-7: Velocity stage plots (Neap & Spring respectively). The ebb tide is to the left of the plot, falling anticlockwise and rising to the right as the flood.

Table 3-1, presents the tidal attributes from the selected tidal curves.

Table 3-1: Attributes from four Spring and four Neap tidal phases. The range given is for ebb and flood respectively.

Location	Date	Phase	Duration	Ebb Time	Flood Time	Diff	U_{cr} Ebb	U_{cr} Flood	V_{cr} HW	V_{cr} LW	HW Slack	LW Slack	Range (m)
Channel	09/03/2010	Neap	12:40:00	05:45:00	06:55:00	01:10:00	00:25	02:05	00:35	04:30	00:10	01:30	1.64 /1.61
Channel	16/03/2010	Spring	12:20:00	06:30:00	05:50:00	00:40:00	02:40	03:55	01:05	02:45	00:40	02:15	3.92 /4.10
Channel	05/08/2010	Neap	13:00:00	06:15:00	06:45:00	00:30:00	00:45	01:30	01:45	05:45	00:45	03:30	2.06 /2.06
Channel	14/08/2010	Spring	11:30:00	06:00:00	05:30:00	00:30:00	02:00	02:15	01:30	03:00	01:00	01:45	4.17 /4.26
Kincaple	08/06/2011	Neap	12:20:00	05:35:00	06:45:00	01:10:00	01:45	02:40	01:45	03:05	01:00	02:35	3.01 /3.01
Kincaple	16/06/2011	Spring	12:20:00	07:15:00	05:05:00	02:10:00	02:20	02:45	01:00	02:35	00:15	01:10	4.30 /4.32
Kincaple	12/07/2011	Neap	12:40:00	06:40:00	06:00:00	00:40:00	00:50	01:50	02:40	06:20	02:30	06:40	3.32 /3.32
Kincaple	03/07/2011	Spring	12:10:00	07:05:00	05:05:00	02:00:00	02:05	03:15	01:35	04:25	01:10	04:25	4.32 /4.32

From the table five main observations are evident;

- Generally the neap tides have flood phase durations exceeding the ebb phase and the spring tides are vice versa.
- The critical erosion velocity duration of the flood phase always exceeds that of the ebb. Though mean erosion velocities may be greater on the ebb phase during springs. Maximum ebb velocities occur, 2.6-2.8 hrs after HW and peak flood velocities 1.5-1.8 hrs before HW.
- The duration of low water deposition is always shorter on the spring cycles.
- The duration of the critical velocity for deposition during low water always exceeds the duration for deposition during high water.
- The low water slack duration (slack before flood -SBF) always exceeds the high water slack (slack before ebb -SBE).

Additionally, an influence from overtides is seen in the Kincaple Bay data towards the middle of the ebb cycle and closer to high water on the flood.

3.1.1.3. Discussion

The data from this analysis are limited very much by only have a single current meter and not being able to investigate how the tidal asymmetry varies along the length of the estuary. It is however expected from model outcomes that the asymmetry becomes more flood dominated moving landwards into shallower water due to the frictional influence (Robins and Davies, 2010). Comparison between the two locations is limited and thus the data have been combined to give an overall perspective of the middle-outer estuary conditions.

With reference to the vertical tide, the data show that the mean ebb durations (06:23:07) over the two sites exceed mean flood durations (05:59:23), giving a net ebb asymmetry in vertical tide. This net value is derived from mean ebb spring durations exceeding mean ebb neap durations and mean flood springs being less than mean flood neap durations (Table 3-2). The implications are important for the transport of finer particles (Dronkers, 1986, Wang *et al.*, 1999) and infer an export of sediment from the estuary.

Data for the horizontal tide reveal the duration of critical erosion/ transport velocities; for the modal particle size in the vicinity of the instrument the flood phase always exceeds those of the ebb tide. The implication for bedload and coarser suspended sediment transport is for a net import of sediment to the estuary (Wang *et al.*, 1999, Dronkers, 1986). The duration of critical velocities for the deposition of the modal particle size is always longer at low water, thus the majority of deposition is likely to occur on and within the channel area. Analysis of the elevation plots for Kincaple Bay suggests that the influence of the overtide greatly increase the durations of low velocity time periods

Table 3-2: Instrument data sorted by Neap and Spring cycle, with mean values for certain attributes.

Date	Phase	Duration	Ebb Time	Flood Time	Diff	U _{cr} Ebb	U _{cr} Flood	Mean U _{cr}	V _{cr} HW	V _{cr} LW	HW Slack	LW Slack	Range (m)
09/03/2010	Neap	12:40:00	05:45:00	06:55:00	01:10:00	00:25	02:05	.22 & .25	00:35	04:30	00:10	01:30	1.64 /1.61
05/08/2010	Neap	13:00:00	06:15:00	06:45:00	00:30:00	00:45	01:30	.21 & .26	01:45	05:45	00:45	03:30	2.06 /2.06
08/06/2011	Neap	12:20:00	05:35:00	06:45:00	01:10:00	01:45	02:40	.34 & .37	01:45	03:05	01:00	02:35	3.01 /3.01
12/07/2011	Neap	12:40:00	06:40:00	06:00:00	00:40:00	00:50	01:50	.34 & .35	02:40	06:20	02:30	06:40	3.32 /3.32
Mean			06:03:45	06:36:15		00:56	02:01		01:41	04:55	01:06	03:33	
16/03/2010	Spring	12:20:00	06:30:00	05:50:00	00:40:00	02:40	03:55	.38 & .42	01:05	02:45	00:40	02:15	3.92 /4.10
14/08/2010	Spring	11:30:00	06:00:00	05:30:00	00:30:00	02:00	02:15	.57 & .32	01:30	03:00	01:00	01:45	4.17 /4.26
16/06/2011	Spring	12:20:00	07:15:00	05:05:00	02:10:00	02:20	02:45	.45 & .39	01:00	02:35	00:15	01:10	4.30 /4.32
03/07/2011	Spring	12:10:00	07:05:00	05:05:00	02:00:00	02:05	03:15	.42 & .44	01:35	04:25	01:10	04:25	4.32 /4.32
Mean			06:42:30	05:22:30		02:16	03:02		01:17	03:11	00:46	02:23	

. Spring tidal deposition durations are seen to be shorter than neap durations, thus the future implications with respect to increasing sea level is that with increased hydraulic depth there will be a shortening period of deposition and thus increased export of suspended particles.

The second important component of the horizontal tide is the duration of slack water. Inequality in the durations gives an indication of the net transport of finer particles. If the duration of the slack water before the flood (SBF) exceeds that of the slack before ebb (SBE), then an export of fine suspended sediment occurs (thus ebb-dominance) and vice versa (Dronkers, 1986). Subtracting t_{LW} slack (SBF) from t_{HW} ,slack (SBE) enables a relative measure of net directional transport of finer particles, where negative values indicate ebb driven transport and positive values flood driven transport. The data in Table 3-1 reveal that the SBF > SBE giving a negative value and thus an export of fine suspended sediment is to be expected.

Over the spring tides, the asymmetry of the vertical and horizontal components tends to be shifted from neap tidal values, resulting from a strengthening of the non-linear interactions. The increased water depth during the spring cycle shifts the asymmetry towards being ebb orientated, which is consistent with Robins & Davies (2010). The spring–neap differences in horizontal tide show increased durations of critical velocities accompanied by increased magnitude of critical velocities on the spring tides and both slack durations are also reduced. Whilst the durations and magnitudes of velocities are increased, the asymmetry changes to being less flood dominant. The implications from this neap–spring change in asymmetry, with respect to increasing sea levels, is that in the future there may be an up-estuary shift in asymmetry with increased ebb dominance and concomitant increase in net export of finer particles and a reduction in flood driven coarser particle transport, giving a largely more erosional environment. This conclusion is not necessarily transferable to all estuaries and each requires careful appraisal, as circulation may be geometry or bathymetry affected resulting in different responses to sea level rise. In a study by Friedrichs *et al* (1990) examining the impact of sea level rise under the Lunar nodal 18.6 year influence, it was concluded that an estuary’s response was dependent on the local geometry, with some systems showing greater flood dominance importing sediment with increased sea level and other systems becoming more ebb dominant.

There are little historical data on recorded near bed velocities within the estuary to compare for changes in asymmetry, however Eastwood (1977) noted a net mean residual flow velocity of 0.0336 ms^{-1} landward. The data in this analysis revealed variability between the two sites with an overall net 0.02 ms^{-1} seaward residual. Eastwood's (1977) data were recorded on the flood delta towards the channel edge and thus is not directly comparable, but may suggest greater flood asymmetry during the 1970's. The timing of the peak velocities given by Eastwood are; 1.5-1.8 hrs before HW and 3-4 hrs after HW. In this analysis maximum flood velocities occur, 1.5-1.8 hrs before HW and peak ebb velocities 2.6-2.8 hrs after HW. There is little change in the flood velocities however the ebb velocities are peaking earlier, with consequences to the intertidal area.

3.1.1.4. Summary

A difference in asymmetry between neap and spring tidal cycles has been recorded with an overall net ebb asymmetry in the vertical tide leading to the expectation of export of finer particles.

Critical velocities for erosion/transport of modal particle sizes on the flood tide exceed those of the ebb tide, favouring a net import of coarser sediment, whilst asymmetry in the slack water durations favour a net ebb transport, in agreement with the vertical tide. With low water slack periods exceeding those at high water, deposition is likely to be along the channel edges and within the channel. In terms of future predicted sea level rise (Jenkins, 2009) it is likely that the asymmetry will be shifted landward accompanied by a change in the vertical tide towards being more ebb dominated with increased export of finer particles. The horizontal tide will show less asymmetry shifting to less strongly flood orientated, likely resulting in reduced import of coarser material. The slack duration will similarly show less asymmetry giving rise to reduced export of finer particles.

3.1.2. Estuary volume

The tidal curve data in the previous section yield valuable information on coarser particle transport in the channel region and inferred export of the finer fraction, however to confirm that the results from the channel instrument data reflect the estuary wide conditions in response to basin morphology, the 'Dronkers (1986) asymmetry ratio' has been calculated. Dronkers (1986) derived an equation (equation 1) to calculate the 'asymmetry ratio' under the hypothesis that a uniform tide reflects morphological equilibrium.

$$\gamma = \left(\frac{h+a}{h-a} \right)^2 \cdot \frac{S_{lw}}{S_{hw}} \quad (1)$$

The equation is parameterized as follows;

- h is the mean hydraulic depth (m) of the estuary given by $h = a + V_{lw} / S_{lw}$

S_{lw} is the surface area (m^2) at low water and V_{lw} is the volume at low water.

- a is the tidal amplitude i.e. half the tidal range (m).
- S_{lw} and S_{hw} are the surface areas at low and high water respectively (m^2).

Where the tides are uniform, the ratio gives a value of $\gamma = 1$ (however considering Stokes drift this is more likely to be 1.1 (DEFRA, 2008)) in the Eden because asymmetrical tides values greater than 1 reflect flood velocity dominance and values less than 1 reflect ebb velocity dominance.

Furthermore, the volume of the tidal prism (the volume of seawater entering the estuary over the tidal cycle) is calculated and compared with historical estimates to gain an understanding of any directional trend in dominance and thus a proxy for possible temperature and salinity regime shifts within the estuary.

3.1.2.1. Methodology

Data used for this analysis (LiDAR and swath bathymetry) were taken from Chapter 2, section 2.3.2. The 2m LiDAR raster digital elevation model (DEM) dataset (SEPA) for 2009 was merged with the March 2009 acquired swath bathymetry to form a mosaic. In the ArcGIS (ESRI, © 1995–2008) toolbox the ‘mosaic to new raster’ option was selected in the ‘data management-raster’ tools. From the mosaic DEM two new rasters were created, cut below the elevation of mean low water and mean high water respectively, based on tidal elevations given for the Tay Bar (adjusted to ODN). The DEM’s were imported to Fledermaus V7 interactive 3D geo-spatial processing and analysis software to calculate the raster statistics. Using the computed statistics, the Dronkers asymmetry ratio was calculated.

Additionally from the raster statistics, the volume of the tidal prism was calculated for comparison with limited historical information. A basic calculation to determine the tidal volume used the difference between low water and high water volume and further subtracted the river volume (excluding the Motray) over the average tidal period, which was taken as 370 minutes.

3.1.2.2. Results

Figure 3-8 (and 3-9 below) present the two DEM’s for high and low water volumes respectively, from which the attributes required for calculating the asymmetry ratio (Table 3-3) were calculated in Fledermaus V7.

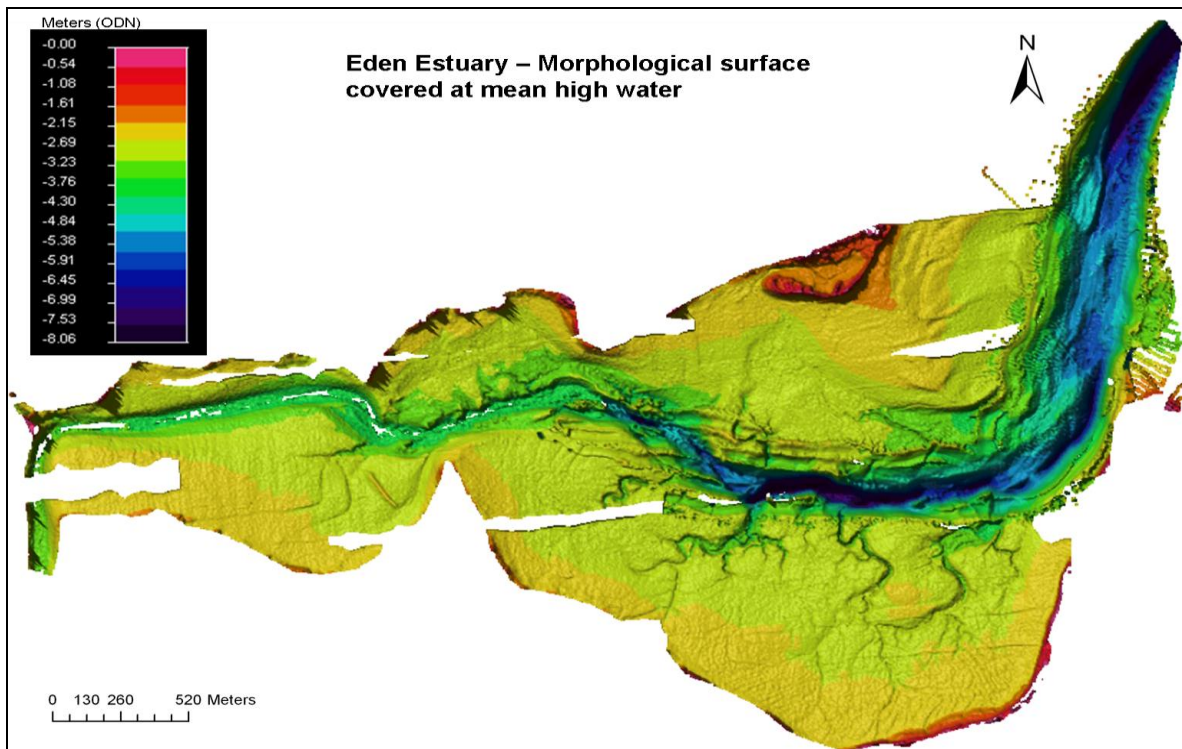


Figure 3-8: Digital elevation model of the estuary (meters above ODN), presenting the proportion of the estuary filled at mean high water. This data is used in conjunction with Figure 3-9, to calculate the tidal prism by subtracting river flow from the difference between high and low water estuary volume.

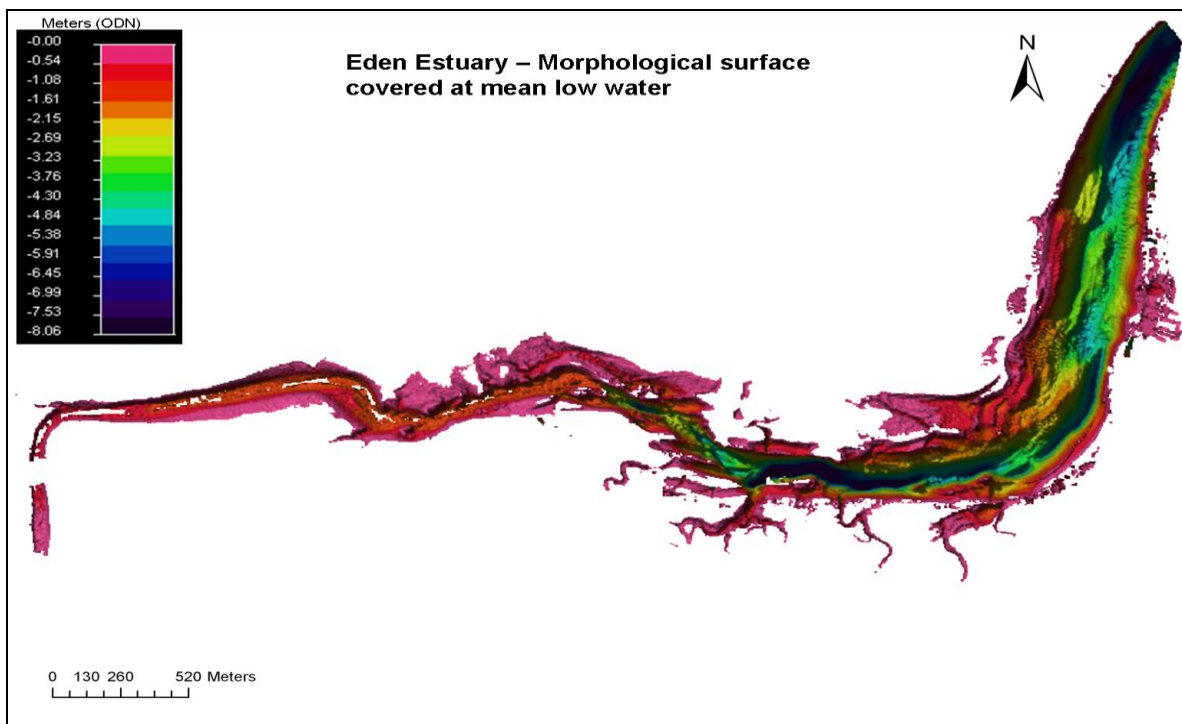


Figure 3-9: Digital elevation model of the estuary (meters above ODN), presenting the proportion of the estuary filled at mean low water.

Table 3-3: Attributes derived from the DEM's for use in calculating the asymmetry ratio.

a (m)	V_{lw} (m ³)	S_{lw} (m ³)	S_{hw} (m ³)	h (m)	γ
1.66	3394436.44	1914480.00	5858940.00	3.44	2.70

Using Table 3-3, the asymmetry ratio was calculated in equation 2, to give a value of $\gamma = 2.70$.

$$\gamma = \left(\frac{3.44 + 1.66}{3.44 - 1.66} \right)^2 \cdot \frac{1914480.00}{5858940.00} = 2.70 \quad (2)$$

Furthermore the statistics taken from the DEM's were also used to determine the volume of the tidal prism (Table 3-4), calculating the difference between low water and high water volume and further subtracting the river volume (excluding the Motray) over the tidal period.

Table 3-4: Attributes derived from the DEM's for calculation of the tidal prism

V_{hw} m ³	V_{lw} m ³	flow ms ⁻¹	flow/tide m ³	Total Volume m ³	Prism m ³
28592763	3394436	4.3	95460	25198326	25102866

The approximate tidal prism was estimated by Eastwood (1977) to be 7,923,000 m³ (under average flow conditions) based on an area of 8×10^6 m², an average water depth of 1m and a combined river discharge (Eden & Motray) of 7.7×10^4 m³. The depth estimate is stated as conservative at 1m however, estimation in the mid 1980s reported 3m (M^cKie, 1985). Using 3m as the mean depth at high water and the present area calculation (5.86 km²), Eastwood's volume is re-calculated to be 17,499,820 m³. This new value, when compared with the current analysis is 7,603,046 m³ less in volume for the tidal prism.

3.1.2.3. Discussion

The Dronkers asymmetry ratio was calculated to be $\gamma = 2.70$, indicating an asymmetrical tide and flood velocity dominance favouring coarser sediment landward transport. Whilst there was a later modification of the Dronkers ratio equation, which included an extra term to accommodate the non prismatic geometry of estuaries, this term incorporated the difference between the surface areas of the channel area at high and low waters. For the Eden, the channel area filled at both high and low water are the same such that the addition of the extra term, would not have contributed the

outcome. The calculated asymmetry ratio is consistent with the current meter data for the horizontal tide and shows that although there were spatial differences between the two instrument locations, overall they reflected estuary wide conditions driven by the relationship between mean hydraulic depth and the estuarie's spatial morphology.

The re-calculated Eastwood tidal prism volume at $17,499,820 \text{ m}^3$, when compared to the current analysis, is $7,603,046 \text{ m}^3$ less in volume. Confidence in comparing these two values is weak, since the accuracy of the historical data is questionable. However Jarvis (1987) refers to a spring tidal volume of $15 \times 10^6 \text{ m}^3$ for the Eden during the '80s, which is not dissimilar to the recalculated Eastwood volume. The size of a tidal prism is related to the basin size, frictional forces and the range of the tide. In section 3.1, comparison with Eastwood's (1977) net mean residual flow velocity of 0.0336 ms^{-1} landward, suggested greater flood asymmetry than at present. If the hydraulic depth of 3m (M^cKie, 1985) is correct, then $a/h = 0.55$ (where a is half the tidal range, and h is the hydraulic depth), which is greater than the present value of 0.48. Friedrichs and Aubrey (1988) maintain that values of a/h greater than 0.3 are seen in flood dominant estuaries, thus the 1970's value infers more flood dominance during that time. It is postulated that the tidal prism during the '70s was less than at present due to a smaller hydraulic depth resulting from a shallower basin under more flood dominant conditions.

The river input per tide in 1977 was reported by Eastwood (1977) to be $7.7 \times 10^4 \text{ m}^3$, the present mean fresh water input from the River Eden per tide is calculated to be $9.5 \times 10^4 \text{ m}^3$ (based on 2005-2009 daily mean ms^{-1}). Changes to the volume of fresh water entering the estuary, has consequences not only to species distribution based on regime shifts, but also to particle transport through density changes and to the concentration of dissolved gasses in the water column (Al-Anezi *et al.*, 2008, Mosley *et al.*, 2010). Assessing the change in river flow volume can only give a speculative insight into the impact of regime shifts, however species distribution towards the inner estuary in relation to salinity changes is explored further in chapter 4.

3.1.2.4. Summary

The Dronkers asymmetry ratio was calculated as $\gamma = 2.70$, indicating a flood asymmetry velocity dominance, which is consistent with the instrument data for the horizontal tide in section 3.1 and infers the estuary is in a depositional phase.

A re-calculated Eastwood (1977) tidal prism volume of $17,499,820 \text{ m}^3$, infers that the basin was probably shallower during the 1970s than today reflecting more flood dominant overall conditions.

3.2. Sediment Transport: Bedload

Sediment transport within estuaries results from complex inter-relationships between physical, chemical and biological processes. Both fine and coarse particles are delivered (as individual particles or bound aggregates) to the estuary from the river catchment in variable quantities dependent mainly upon river flow volume under prevailing climatic conditions. Seaward at the estuary mouth, larger particles are typically transported landward as tidally driven bedload. Within the estuary, flows are typically non linear and are modified by the morphology; strong tidal currents meet with river currents causing much of the coarser sediment to be deposited as the flow velocities rapidly drop. Seaward of this turbidity maxima, tidal currents mobilize, rework and re-suspend sediments preventing the development of a river delta.

Many empirical formulae, numerical models, analytical theories and methodologies exist to directly measure sediment transport; these have largely been developed from linear studies on fluvial environments with predominantly steady state flow conditions. Applying these for marine environments requires modification to account for the different directional components of tidal environments, as well as for the effects of waves and superimposed wind driven currents (Besio *et al.*, 2006). Quantifying the volume of sediment transported into or out of an estuary, is thus a complicated task, with transport rates varying both temporally and spatially in response to morphology and variable water depths within the estuary. To capture average suspended and bedload transport rates, many direct samples may be required (Dinehart, 2002), however since tidal flow dominates over river flow in the Eden estuary and suspended sediment is assumed to be tidally flushed seawards (following a period of residence) two methods have been proposed to approximate sediment bedload transport. The first proposed, follows the methodology of Sternberg (1972) Wewetzer and Duck (1996) and Bates and Oakley (Bates and Oakley, 2004, Oakley, 2003) and is formed from a combination of the bedload transport formula together with near bed velocity data. A second method combines the conservation of mass equation, with the kinetic equation for undisturbed propagation of bed-forms (with the assumption of no sediment by-passing) (Engel and lau, 1980, Jinchi, 1992, Ten Brinke *et al.*, 1999). Both methods are used in this study and applied using data collected through time lapse bathymetry for the sub-tidal bed-forms and by direct measurement of the bed-form geometry for inter-tidal bed-forms, in order to quantify the depositional or erosive phase of the estuary.

Aim of bedload study

- To verify the inferred direction of larger particle transport by the near-bed current velocity measurements which were identified in section 3.1 (Tidal Asymmetry Analysis), through the analysis of migrating bed-forms.

- Quantify a rate and volume of net transport, through time lapse bathymetric analysis, of migrating bed-forms and compare these with current velocity based transport equations, using recorded velocity data (described in section 3.1). Further, to compare the migrations with historical data for direction trend.
- Apply relative directional rates of larger particle sediment transport derived zones of flood or ebb dominated bed-forms to estimate an estuary wide net rate of transport.

Sediment Transport Theory

Sediments that are transported as bedload are generally larger than cohesive particles (> 0.2mm) and move along the bed by rolling, sliding or saltating. Bedload is distinguished from suspended sediment transport by the amount of contact the particle has with the bed. However, it is difficult to differentiate bedload from suspended sediment transport, since particles may travel by both methods during the tidal cycle with changing tidal current velocities.

Bed-forms may be considered as moving objects under tidal flow velocities and hence their movement can be described by the kinetic equation for the speed of movement of a given mass. Similarly, the movement of the sediment particles under steady state flow (without mass accumulation) may be described by the continuity equation. Combining these two equations and integrating over the length of the feature allows an average sediment transport rate to be calculated. The principal hydrodynamic parameter controlling transport is hence velocity, for a given mass, and is determined by the following;

Shear stress: As currents flow over the sea bed they are slowed down by friction caused by the roughness of the sediment. Sediment particles begin to move when the shear stress at the bed becomes strong enough to overcome the friction with neighbouring particles, gravity and the weight of the overlying water column. The point at which motion is initiated is called the critical shear stress (τ_{cr})

This frictional shear stress (or boundary shear stress) is proportional to the product of the density of the water and the square of the time averaged current speed (equation 1).

$$\tau_0 \propto \rho \bar{u}^2 \quad (1)$$

where τ_0 is the shear stress (Nm^{-2}), ρ is the water density (Kgm^{-3}) and \bar{u} is the time averaged velocity (ms^{-1}).

Shear velocity: The time averaged current velocity exerts a frictional force on the sediment. Theoretical studies have demonstrated shear velocity to be directly dependent on water viscosity and the velocity gradient in the water column, this relationship is illustrated in equation (2);

$$\tau_0 = (\mu + \eta) \times \frac{d\bar{u}}{dz} \quad (2)$$

Where τ_0 is the shear stress (Nm^{-2}), μ is the molecular viscosity of seawater (Nm^{-2}) i.e. the resistance to laminar flow, η is the eddy viscosity (Nm^{-2}) and $\frac{d\bar{u}}{dz}$ is the time averaged velocity gradient above the seabed (ms^{-1}). The eddy viscosity is the amount of turbulent flow caused by increased roughness or by development of bed-forms, which cause parcels of water to interact with one another.

Shear velocity is a derived term and cannot be measured directly. The relationship between shear velocity & shear stress however is given by the following (equation 3):

$$\tau_0 = \rho U_*^2 \quad (3)$$

Again, the shear stress is proportional to the square of the velocity.

It is worth noting that sediment may also be transported by shallow water waves in the outer reaches of estuaries and therefore sediment transport may be a combination of current & wave induced movement. Whilst wave transport is more complicated, shear stress is similarly proportional to the square of the orbital velocity. For this study, combined wave and current motion is not pursued, due to time limitations, but is worth noting for interpretation of results.

Velocities leading to erosion, transport and deposition may be empirically estimated from particle diameter and shear velocity (for a given particle and water density) and typically are displayed graphically in the form of a Hjulstrom-Sundborg diagram (Figure 3-10). Sandy sediments require lower velocities to set them in motion, when compared with smaller (cohesive) or larger particles.

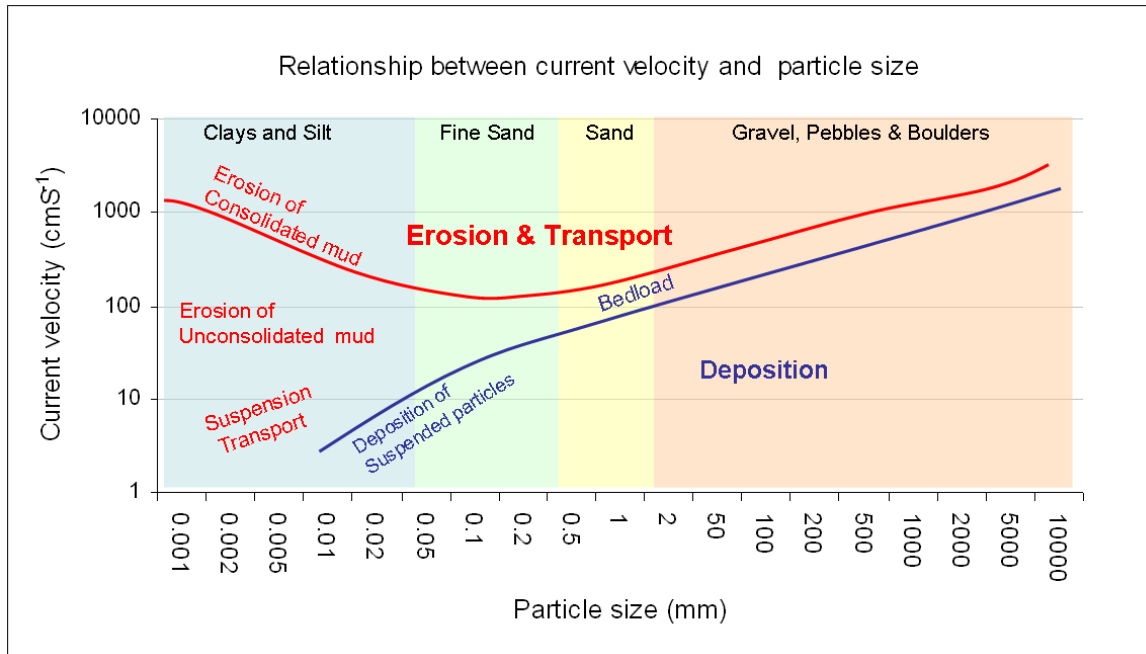


Figure 3-10: Modified Hjulström-Sundborg diagram (Blatt et al., 1981) to present the inter-relationship between particle size, motion and current velocity. (Velocity is on a log scale).

Experiment and theory have shown that bed-load sediment transport is proportional to the cube of shear velocity and since shear velocity is also related to average current velocity, the rate of bed-load transport therefore is also proportional to the cube of the average current velocity measured at a fixed height above the bed (Dinehart, 2002). The interrelationship between the power of the current and bed shear is important, as small changes in either the roughness or in the power of the current can have significant impacts to the bed-load transport.

In combining the conservation of mass, with the kinetic equation, Simons *et al* (1965) found a relationship between sediment transport and the bed-form migration rate, whereby the amount of bed-load transport per metre is related to bed-form migration and could be estimated by the formula (equation 4)

$$s = \alpha * c_b H (m^2 / s) \quad (\text{assuming the bed-form migrates one wavelength undisturbed}). \quad (4)$$

Here C_b is the migration rate (or celerity), H is the height of the bed-form (trough to crest) and α is a shape factor. Bed-form shape is assumed to approximate a triangular cross section, however this is not always the case (Hoekstra *et al.*, 2004) and thus α can vary from 0.48 – 0.6 (triangular = 0.5)

The correct shape factor, α , (equation 5) is critical for accurate quantification of bed-load, as transport is generally restricted to the higher parts of the bed-forms (Hoekstra *et al.*, 2004).

The shape factor is calculated by, $\alpha = \frac{V}{H\lambda}$ (5)

Where V is the bed-form cross-sectional area m^2 measured in a vertical plane parallel to the transport direction, H is the height and λ is the interval distance between successive bed-forms.

Bed-form definition & description

Once the bedload sediment begins to move, a range of bed-forms begin to develop with increasing flow velocity; initially under relatively quiescent conditions the sediment forms a flat bed, but with increasing flow velocity bed-form structures develop. The presence, geometry and dynamics of bed-forms depend largely upon current velocity, water depth and sediment grain size (Rubin and McCulloch, 1980, Flemming, 2000). The size of smaller bed-form features is dependent upon particle size, however for larger bed-forms such as dunes and sandwaves, feature height becomes not only dependent upon particle size, but also proportional to water depth.

Bed-forms are usually present orthogonal to the dominant flow direction and migrate in response to a residual current (Engel and Lau, 1980, Besio *et al.*, 2004, Nemeth *et al.*, 2002), which may result from unequal ebb & flood tidal velocities, wind induced current (Idier *et al.*, 2002) or wave-induced flow (Besio *et al.*, 2008). Tidal induced migration may also occur due to the interaction of the M_4 shallow water harmonic component (Knaapen *et al.*, 2005), which may lead to a modulation of the tidal amplitude and tidal duration.

Bed-forms are classified by wavelength, height and also their shape. Further classification can be made on the superposition of features and orientation. Bed-forms which are present in the outer reaches of the estuary exist usually as three types; small ripples, mega-ripples and sandwaves. Small ripples are believed to be distinct from mega-ripples and hence do not grade in to them (Boyd *et al.*, 1992). Small ripples are often less than 0.3m in wavelength, whilst mega-ripples range in wavelength from 0.6 – 30 m and 0.06 - 1.5m in height.

Mega-ripples may be sub classified into two types. Type I develop at lower velocities (0.3 – 0.8 m/s) and are characteristically straight crested (Dalrymple *et al.*, 1978). Type II develop under velocities of 0.7 – 1.5m/s and are usually referred to as dunes (Dalrymple *et al.*, 1978). The dune crests are sinuous and their troughs appear as scour pits. Finally, sandwaves occur as very large bed-forms (that occur in high energy flow in deep water), such features are not seen in this study.

Previous studies in the local area

Eastwood (1977), investigated the Eden Estuary in terms of water circulation, facies distribution and morphological features. His measurements of velocity & salinity profiles revealed that there was an asymmetry, with ebb tidal velocities exceeding the flood velocities. Further, maximum salinity was coincident with high water (HW) in the middle estuary, whilst maximum salinity occurred before HW in the lower estuary and following HW in the upper estuary. Eastwood (1977) identified two tidal deltas; a flood delta composed of largely flood orientated sandwaves, yet with ebb orientated features also present and an ebb delta at the estuary mouth, composed of entirely ebb orientated sandwaves. At maximum rates of bed-form advance (0.41m/tide), bed-load transport was reported to be 316 kg/m per tide. Eastwood (1977) makes the first reference to the internal structures of the bed-forms, stating a prominent flood orientation within the sand waves, despite the variance in the outer shape, hence highlighting the importance of the flood tide in formation, but he also recognized that there was an ebb tide modification. This emphasizes the requirement to monitor these features over tidal & seasonal time scales. Eastwood (1977) extensively sampled the estuary for sediment grain size, composition and texture, which provided the first comprehensive map of sediment facies. He concluded that the distribution of sediments within the estuary may be explained by the importance of wave action to the South of the Eden channel and to flood tidal activity to the North.

Sediment transport in the outer Eden estuary was further investigated by Jarvis & Riley (1987) through the specific monitoring of water movement and sediment transport from a fixed platform at an intertidal location in the mouth of the estuary. Onshore movement of sediment was indicated by bed-load transport (determined from bed-form migration after Simons (1965). Average transport rates at the estuary mouth were reported to be $0.24\text{m}^{-1}\text{tide}^{-1}$. However, due to the position of the platform on West Sands, the contribution of wave sediment transport and potentially aeolian transport to the sediment flux is difficult to determine. Morphological changes in the estuary mouth over the three-year survey period were relatively small and indicated a stable environment.

Bates & Oakley (2004) built upon previously acquired knowledge of sediment and biotope distribution in the Eden from Eastwood (1977), using combined acoustic ground discrimination systems (AGDS) and remotely sensed satellite biotope mapping, facilitating the designation of the Eden as part of the Tay Estuary Special Area of Conservation (SAC). As part of the 2004 study, Bates & Oakley (2004) investigated the sedimentary features of the Tay estuary, evaluating sediment transport using current velocity data to calculate bed-form migration rates in the proximity of frontal systems through methods based on a modified Bagnold (Bagnold, 1966, Sternberg, 1972) equation. Coupling their velocity data with bathymetric bed-form data indicated asymmetry of bed-form features. Furthermore, the use of high-resolution sonar for long term modelling of sediment transport in estuaries was advocated due to the repeatable precision.

The methodology used in this study is an extension of the protocols used by Bates and Oakley (Bates and Oakley, 2004) to quantify bed-load transport, however further to calculating the celerity

of the bed-forms from average velocity data, this study also uses direct measurement of migration from elapsed time profiles via sequential bathymetric and hypsometry surveys.

Prior to acquiring the time lapse bathymetry data, a pilot direct measurement pin survey was undertaken to understand the relative timescales over which bed-forms were migrating, this was done with the aim that the interval in sequential bathymetric surveys would capture sufficient movement, yet confidence could be given to ensuring that the same bed-forms on subsequent profiles was being measured.

3.2.1. Time lapse hypsometry

Two pin surveys were undertaken during this study, one on the northern shore of the Eden estuary, located in the area previously studied by Eastwood (1977) and by McKie in (1985) where flood bed-forms dominate (labelled Flood Bed-form Zone, Figure 3-11, Figure 3-12 photograph). The second area studied here is located in the relatively newly formed surface channel that cuts across the spit on West Sands (labeled West Sands channel Figure 3-11).

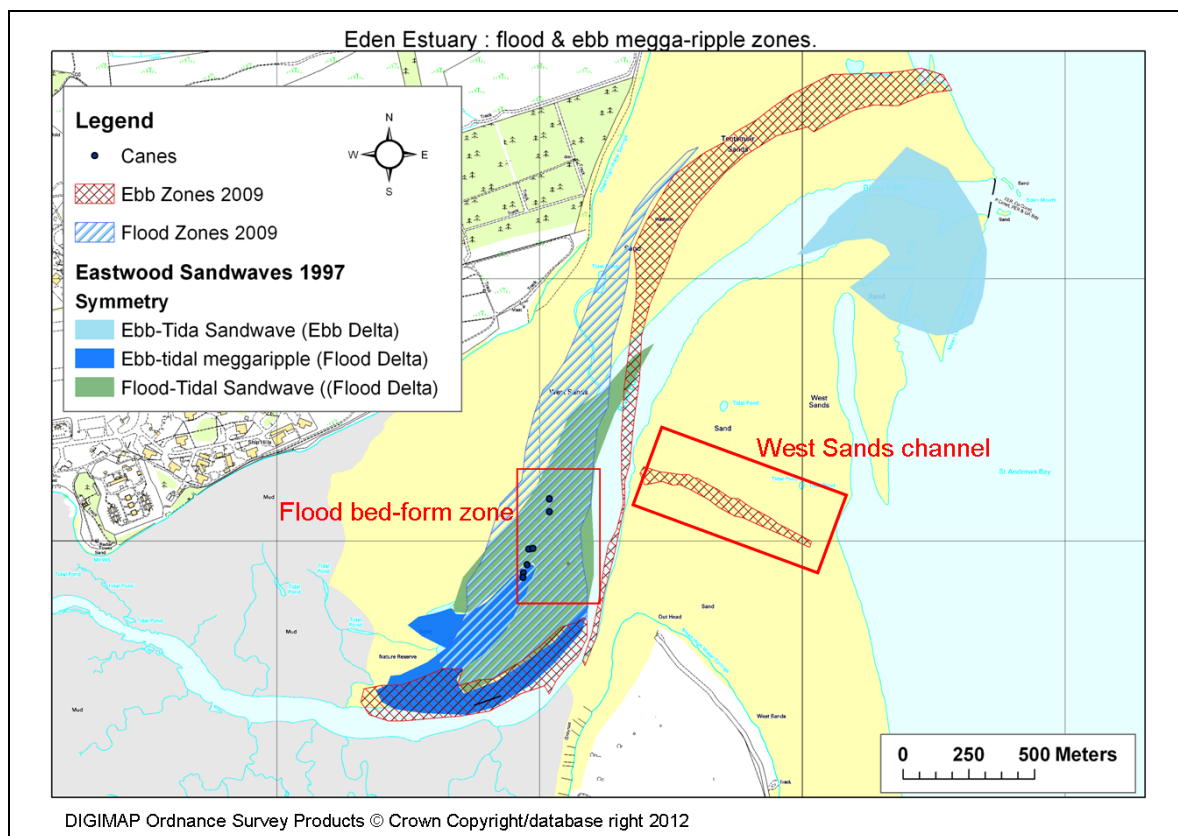


Figure 3-11: Presents the locations of the two hypsometry bed-form surveys (marked by red rectangles) which were undertaken on the inter-tidal zone, exposed at low water. Also highlighted, are the extents of historical and contemporary ebb and flood orientated bed-form complexes.



Figure 3-12: Photograph of a flood bed-form in the study area, which lies to the north of the Eden channel, forming part of the Flood Bed-form Zone identified in Figure.3-11. (sea-ward to left, landward to right).

3.2.1.1. Methodology

An initial pilot study was undertaken within the flood bed-form zone during April 2011 to understand approximate migration rates in the area, allowing the planning of later bathymetry time lapse surveys to image inaccessible submerged bed-form features.

Bamboo canes were sunk to approximately 0.75m into the front of a line of successive flood bed-forms marking the crest position (Figure.3-13). In the following days the canes were re-visited to record the magnitude of movement. In a total of nine days the bed-forms had travelled both in the flood and ebb direction depending on the tidal phase, resulting in a net flood movement of 0.66m.

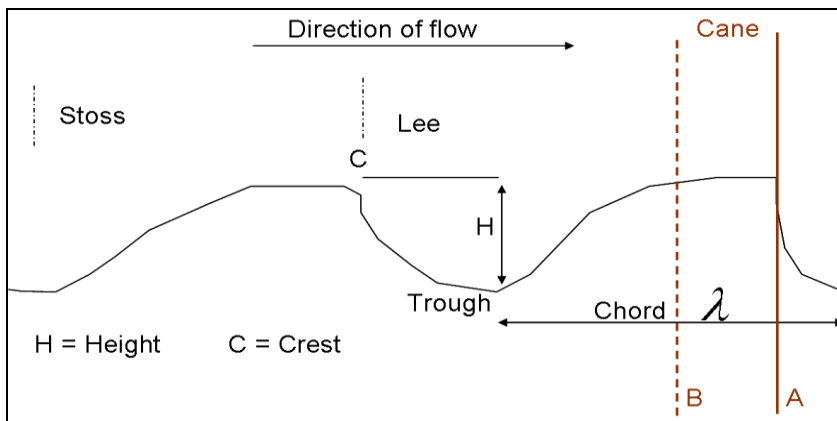


Figure 3-13: Diagram to illustrate the descriptive terminology of bed-forms.

Six bed-forms were monitored and measured and the data summarized as means; these data were used to parameterize the bed-form migration (equation 6) equation modified from Simons *et al* (1965) equation (4).

$$Q_{bf} = \alpha \cdot H \cdot \rho_s \cdot C_b (1 - \rho) \quad (\text{Jinchi, 1992, Hoekstra } et al., 2004) \quad (6)$$

Parameterized as follows;

α is a shape factor (see equation 5), H is the height (m) of the bed-form (trough to crest) ρ_s is the particle density (Kg m³), C_b is the migration rate (or celerity) (ms⁻¹), and ρ is sediment porosity.

Porosity was taken to be 0.4, as widely accepted for well sorted non cohesive sediments. Shape parameters were calculated from mean bed-form height and cross-sectional area and found to be overall 0.5, though feature shape altered during the reversal of bed-forms profiles remained approximately triangular.

For comparison of methodologies, the summary data were combined with average transport current velocities (recorded at the survey site) following Bates and Oakley (2004) using the Sternberg (1972) bed shear stress (τ_0) equation in combination with volumetric sediment transport and critical shear stress (τ_c) equation (Bagnold, 1966), and substituting the summary data into the following equations;

Bed-form celerity (c) was determined using equation 7;

$$c = \frac{2ib}{c_b H} \quad (7)$$

Where H is the bed-form height in meters and C_b is the bed-form volume (m³).

The rate of sediment transport is determined from equation 8;

$$ib = KW(\tau_0 - \tau_c)^{3/2} \quad (8)$$

K is a friction term and W is the width of the channel, however as the bed-forms do not span the width of the channel, W was set to 1m such that transport rate could be expressed in m³ and hence comparable to the Simmons' data. K is calculated as follows (equation 9);

$$K = 8/(\sigma - \rho)^{3/2} g \quad (9)$$

Where σ represents particle density (kgm³) and ρ is the density of the seawater (kgm³), g is gravitational acceleration and set at 9.81 ms⁻².

Fluid density may be empirically determined from average salinity (salinity here ranged between 25-31 PSU).

Boundary shear stress Sternberg (1972) equation.

$$\tau_0 = 3 \times 10^{-3} \rho \overline{U}_{50}^2 \quad (10)$$

U_{50} is the average current velocity (ms^{-1}) at 50cm above the sea bottom.

Critical shear stress is calculated from;

$$\tau_c = \theta_c (\sigma - \rho) g D_{50} \quad (11)$$

Where θ_c , is the dimensionless bed shear stress and is set to 0.045, which is representative for turbulent flow (Dyer, 1972, Bagnold, 1966). D_{50} is the Median particle size (however in this study modal particle size is used, representing the majority of sediment). This analysis provides two terms, C the celerity or migration rate (ms^{-1}) and I_b , which is the sediment bedload term ($\text{kgm}^{-1}\text{s}^{-1}$). The bedload value may then be converted to a rate per hour and multiplied by the duration for which the current velocity remains above the critical value for transport (for both ebb and flood flow) to give a net rate per tide.

Particle size was determined from surface sediment samples taken in the location of the study, to calculate the critical velocities for bed-load transport. Particle size analysis was carried out using a Coulter Counter LS230 following the method outlined in Chapter 3.11. The duration for which critical velocities were maintained were calculated from data recorded at the survey site (Valeport lightweight Model 106) following the methodology in Chapter 3.11.

The second intertidal pin survey followed the same methodology as the pilot study however following observations of the behaviour of the bed-forms to reverse the bed-forms were monitored each day for 14 days. Six representative replicates were monitored, which allowed for canes being lost due to the dynamic conditions. The replicate data were averaged to give daily means, which were analysed using equation (6) (Jinchi, 1992, Hoekstra *et al.*, 2004) for bed-form transport only, as velocity information for this area was not available.

3.2.1.2. Results

Area 1 – Flood bed-form zone

Table 3-5: Summary data for the pilot study pin survey on the flood bed-form field.

Largely Neap tides					Largely Spring Tides				
Date Range	Pin	Vs (m)	H (m)	length (m)	Date Range	Pin	Vs (m)	H (m)	length (m)
30/04/2011 08/05/2011 9 inc days	1	-0.485	0.29	11.17	16/05/2011 21/05/2011 6 inc days	1	-0.21	0.29	5.2
	2	0	0	0		2	-1.23	0.31	7
	3	-2.575	0.13	4.14		3	1.14	0.42	5.78
	4	1.475	0.67	10.05		4	2.67	0.54	4.56
	5	1.57	0.64	9.52		5	2.15	0.69	11.12
	6	1.13	0.615	12.28		6	2.22	0.61	12.39
	Mean	0.186	0.391	7.860		Mean	1.123	0.477	7.675
meters per day		0.02			meters per day		0.19		
meters per tide		0.01			meters per tide		0.09		

Data on the celerity or migration rate for the bed-forms (Table.3-5) were used to calculate the sediment transport rate $m^3/tide^{-1}$ and the mass of sediment transported (Table.3-6), using equation (6). The mean migration rate was calculated to be $0.005m/tide^{-1}$. More sediment particles were being transported over the larger spring tides than on neap conditions. Negative values are given where transport is out of the estuary when ebb flow is dominant. Generally on the smaller neap tides, it was observed that the bed-forms began to reverse from flood to ebb orientation, before resuming back to flood orientation on the larger spring tides.

Table 3-6: Summary data calculated from the bed-form migration equation.

cycle	m3/tide	Tonnes		1-p	Vs	H	Mass g/cm3	p
Neap	0.001	0.003		0.6	0.01	0.391	2.50	0.4
Spring	0.013	0.033		0.6	0.09	0.477	2.50	0.4
mean	0.0073	0.018						

The Calculated rate of sediment transport from the pilot study is $0.007m^3/tide^{-1}$, giving the mean mass in tonnes per $m^3/tide$ as 0.018.

Using the mean velocity required to calculate τ_0 (boundary shear stress) following Bates and Oakley (2004) the average of spring and neap durations of critical current velocities (Table3-7) was taken and substituted into the sediment transport equation (8) and the results are presented in Table.3-8.

Area 2 – West Sands channel

The summary data (Table 3-5) for the West Sands channel show that bed-forms are migrating at a net mean rate of $-0.73 \text{ m/tide}^{-1}$. Here the negative value denotes that the transport is in a seaward direction and that the ebb currents are dominating over the flood currents for mean conditions.

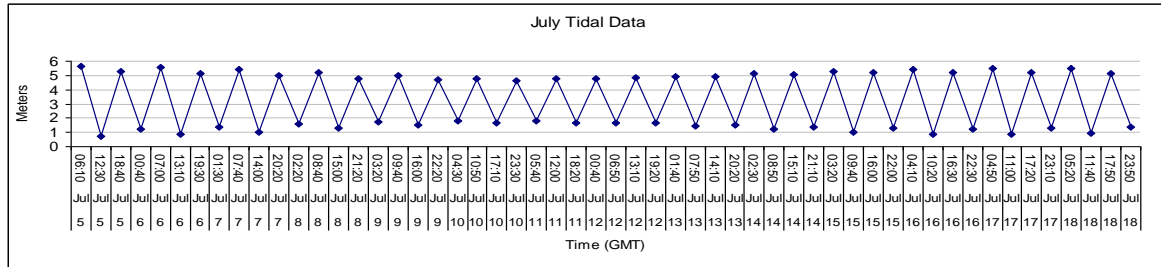


Figure 3-14: Tidal heights during the period 05/07/11 to 18/07/11.

However, it was observed (Table 3-5) that transport (thus bed-form movement) is in the flood direction as the tides progress towards the neap cycles (Figure 3-14), following the neap cycles transport changes to the ebb direction and rates increase approaching spring cycles. The heights of the bed-forms are smaller during the neap tidal cycles.

Table 3-9: Bed-form migration rates (m/tide), to be used in quantifying the volume and mass of the sediment being transported per tidal cycle.

Date	length	Height	cb (celerity)
05/07/2011	3.11	0.27	0.41
06/07/2011	3.61	0.26	0.33
07/07/2011	6.12	0.21	1.55
08/07/2011	3.69	0.19	1.62
09/07/2011	3.51	0.17	0.54
10/07/2011	3.18	0.17	0.36
11/07/2011	3.29	0.13	0.56
12/07/2011	3.27	0.16	0.38
13/07/2011	3.25	0.25	0.45
14/07/2011	3.40	0.13	0.45
15/07/2011	2.73	0.14	-0.34
16/07/2011	3.06	0.22	-1.65
17/07/2011	4.20	0.26	-2.49
18/07/2011	4.32	0.20	-3.63
mean	3.62	0.20	-1.46
negative = Ebb			Net movement
positive = Flood		per tide	-0.73

Substitution of the migration rate per tide (Table 3-9) into the equation for bed-form transport (6) results in net export of 0.043 m^3 per tidal cycle of sediment through the channel on West Sands, this represents $0.108 \text{ tonnes per m}^3$ per tidal cycle (Table 3-10).

No velocity data were available for this area hence the comparative velocity method for sediment transport was not undertaken.

Table 3-10: Volume and mass of sediment being transport per tidal cycle through the West Sands channel.

m ³ /tide	Tonnes		1-p	Vs	H	Mass g/cm ³	p
0.043	0.108		0.6	0.73	0.20	2.50	0.4

3.2.1.3. Discussion

For Area 1 flood bed-form zone, the current survey reports a mean transport of sediment bedload at a rate of 0.007m³/tide⁻¹, this equates to a mass transport of 0.018 tonnes m³/tide⁻¹(Table 3-6). Using a slightly different method for sediment transport, to compare methodologies (Bates and Oakley, 2004) a lower migration rate (celerity) of 0.022m/tide⁻¹ was calculated, compared to the 0.052m/tide⁻¹ from the bed-form equation (6). The difference may be expected, as the current velocity data were recorded within the flood bed-form zone, but closer to the main channel. The water depth difference between the location of the current meter compared to many of the bed-forms, may be sufficient to cause much spatial variation in velocities. Aeolian transport is also likely to contribute to bedform migration over the intertidal zone, at varying spatial and temporal rates driven by the availability of sand, its moisture content, the speed and angle of the approaching wind and from bedform development altering the local topography (Anthony *et al.* 2009, Wal and M^cmanus 1993). A local study (adjacent to the Eden Estuary) of aeolian transport rates by Wal and McManus (1993) observed maximum transport rates to have occurred in the middle beach zone, ranging from 0.01-0.3kg s⁻³ m⁻¹ for corresponding shear velocities of 0.2-0.46m s⁻¹. Clearly aeolian transport is an important contributor to intertidal sediment transport and may explain some of the disparity between the empirical current velocity estimate and the direct measurement methodologies.

The bed-form equation method may also capture saltating particle movement and similarly aeolian transport at low water.

In 1974 the bed-forms were surveyed (Eastwood, 1977) in a similar manner. Using the 1974 report data, the sediment transport rate was re-calculated using equation (6) to investigate trend changes. The 1974 mean data, for the two transects which most closely match the current hypsometry survey give a transport rate of 0.010m³/tide⁻¹, equating to 0.025 tonnes m³/tide⁻¹ or a difference of 2.7kg greater per tide than at present.

A further survey in 1985 (M^cKie) reports, for a transect most closely matching the position of the current survey, revealed a sediment transport rate of 0.017 m³/tide⁻¹, a volume slightly greater than recorded in 1974 and also to the current rate of transport.

Both the 1974 and the 1985 calculated rates of transport are greater than at present; this is consistent with the findings from Chapter 3.1.2 (estuary volume analysis) which similarly inferred that flood velocities were currently lower than during the 1970s.

The changes in the rate of flood driven bedload may be attributed to differences in sustained periods of NAO phases and particularly with the corresponding wind conditions. During the 1970s and 1980s, the percentage of offshore winds was below the long term mean conditions (Chapter 2.3, Figure 2-47), and thus received more onshore winds relative to the present. Under such conditions, the flood tide would have been assisted by the onshore wind and also the volume of water entering the estuary potentially would have been greater, with the sea piling against the coast (Pugh, 2004). Although the flood velocities would be enhanced, the duration of the flood cycle would be lengthened leading to a shortened ebb tide and hence increased ebb velocities against the wind, such that flood velocities likely would still exceed the ebb velocities. At low water onshore Aeolian transport would probably have enhanced onshore bed-form migration. By contrast, 2011 exhibited more dominance in westerly offshore winds which would have favoured less flood (landward) transport and greater offshore aeolian transport.

The data for Area 2 the West Sands channel indicate a net export of sediment at a rate of $0.043\text{m}^3/\text{tide}^{-1}$. This channel has developed relatively recently and hence there is no comparative data to assess for trend. These data may however offer supportive evidence for Coriolis and centrifugal force influencing ebb tidal currents in the outer estuary (chapter 2.3.2.2).

3.2.1.4. Summary

Current rates of bedload transport on the northern inter-tidal flood bed-form area are less now than during the 1970s and 1980s. The current rate of sediment transport is $0.007\text{m}^3/\text{tide}^{-1}$, equating to a mass of 0.018 tonnes $\text{m}^3/\text{tide}^{-1}$. The new inter-tidal channel which has developed across the spit at West Sands shows net ebb transport at a rate of $0.043\text{m}^3/\text{tide}$, equating to a mass of 0.108 tonnes m^3/tide .

3.2.2. Time lapse Bathymetry

3.2.2.1. Methodology

Sequential swath bathymetry datasets were acquired during March 2011 over two selected areas that were dominated by ebb and flood features respectively. Surveys were planned to span neap and spring tidal cycles, to accommodate differences in tidal current durations & velocities, thereby giving approximate average conditions, however ultimately surveys were weather and personnel dependant, thus approximated to spring and neap conditions. Data was acquired and processed using the same equipment and protocols outlined in chapter 2, section 2.3.3 (morphological change analysis). To maximise both precision and repeatability in the sequential surveying, a location was chosen that included a fixed marker-a metal structure that is a relic from war time protection. This structure is readily visible on the bathymetric surveys and is hence used for spatial referencing and

calibration. Data was acquired in transect lines running orthogonal to the bed-form features (Figure 3-15), forming swathes of data for each of the two locations.

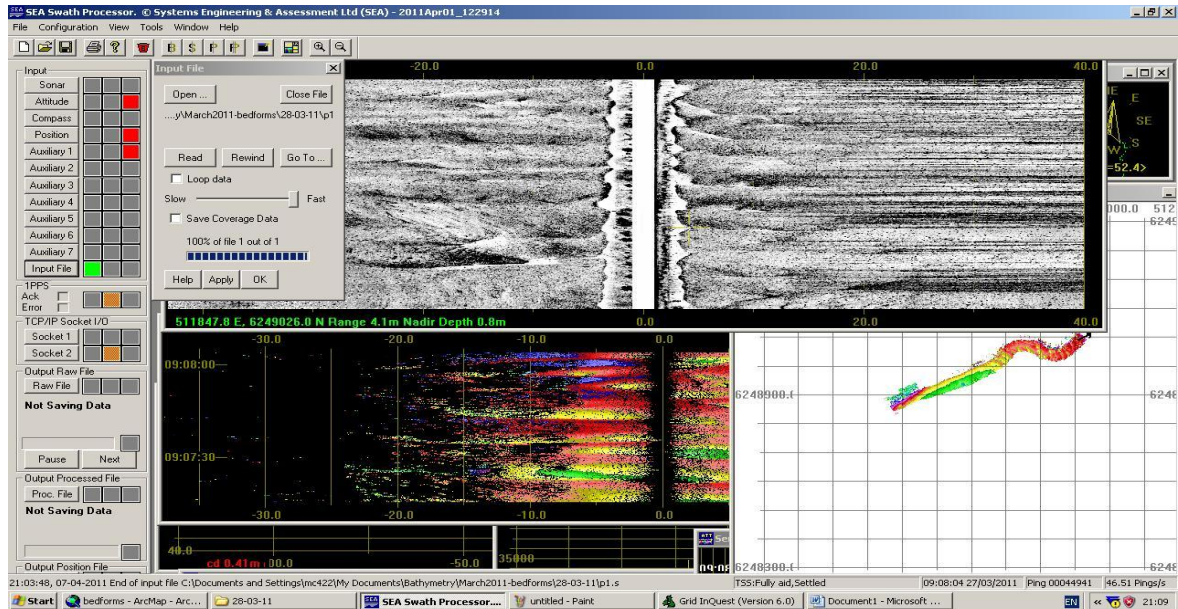


Figure 3-15: Screen image of data acquisition using Systems Engineering Software (SEA swath real time acquisition version 3.07.10).

Processed and edited data exported from Sea Grid Processor (SEA Inc. version 3.7.9.0) as point data, were converted from the recorded coordinate system UTM zone 30 to OSGB36, using Grid InQuest file conversion software (Geodetic Software Solutions Ltd.) before being loaded to ArcGIS (ESRI, © 1995–2008) for analysis. In ArcGIS the point data were converted to raster datasets using the spatial analyst to create an interpolated (Inverse distance weighted) digital elevation model (DEM) at 0.25m horizontal resolution (Figure 3-16). The vertical resolution was preserved from the acquisition DGPS centimetre scale.

Individual cross-sectional profiles were extracted from the DEM orthogonal to bed-form orientation (i.e. parallel to flow direction, Figure 3-16) and the data were output to Excel (Microsoft, 2003) for display and further analysis (Figure 3-17). The distance between corresponding crest positions and also the bed-form height was measured and used to calculate the migration rate. These data were then used to quantify bed-form transport in terms of volume of sediment per unit time, following (Jinchi, 1992, Hoekstra *et al.*, 2004) equation (6).

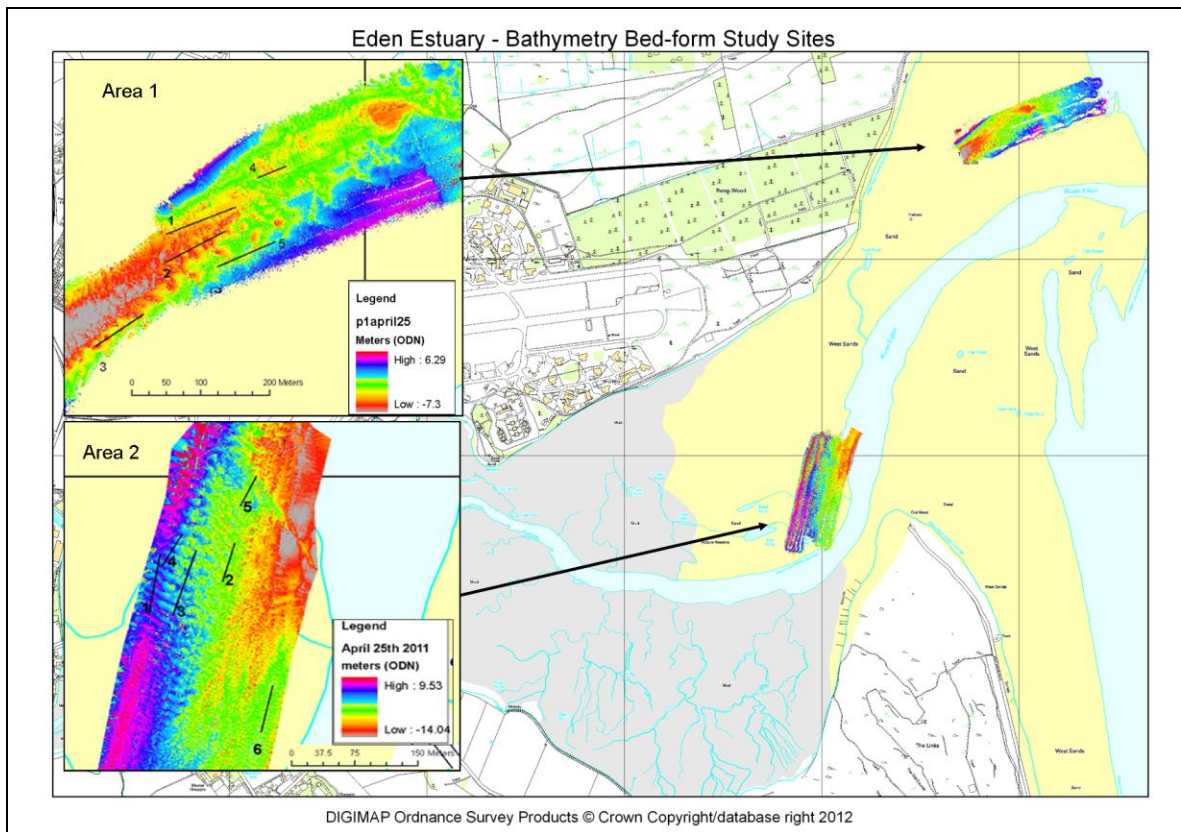


Figure 3-16: DEM of the study area, showing numbered profile transects orthogonal to bed-forms.

Additionally cross comparison using methods from Bates and Oakley (2004) calculated sediment transport based upon the duration and mean velocity for bedload transport.

Estuary wide up-scaling

Using the merged LiDAR and bathymetry DEM from chapter 2.3.3 (morphological change analysis), zones of flood and ebb dominated areas were mapped in ArcGIS (ESRI, © 1995–2008) and their relative area calculated, using the ‘calculate geometry’ option within the attribute table.

From each zone, representative cross-profile transects were extracted and bed-form geometry attributes measured. Mean attribute values were then used to calculate sediment transport rates and the mass of sediment movement to give an approximation of net estuary-wide bedload transport.

3.2.2.2. Results

Ebb bed-form (area 1)

Difficulties were experienced as data were acquired for both areas at the same time, in hindsight due to the dynamic nature of area 1 (at the very outer parts of the estuary which is influenced by wave action), the interval between successive surveys could have been shorter, as bed-form movement was not well captured. A repeat of the predominantly spring tidal regime was undertaken in May 2011, following the capture of an approximate neap tidal regime from 24/04/11 to 12/05/11.

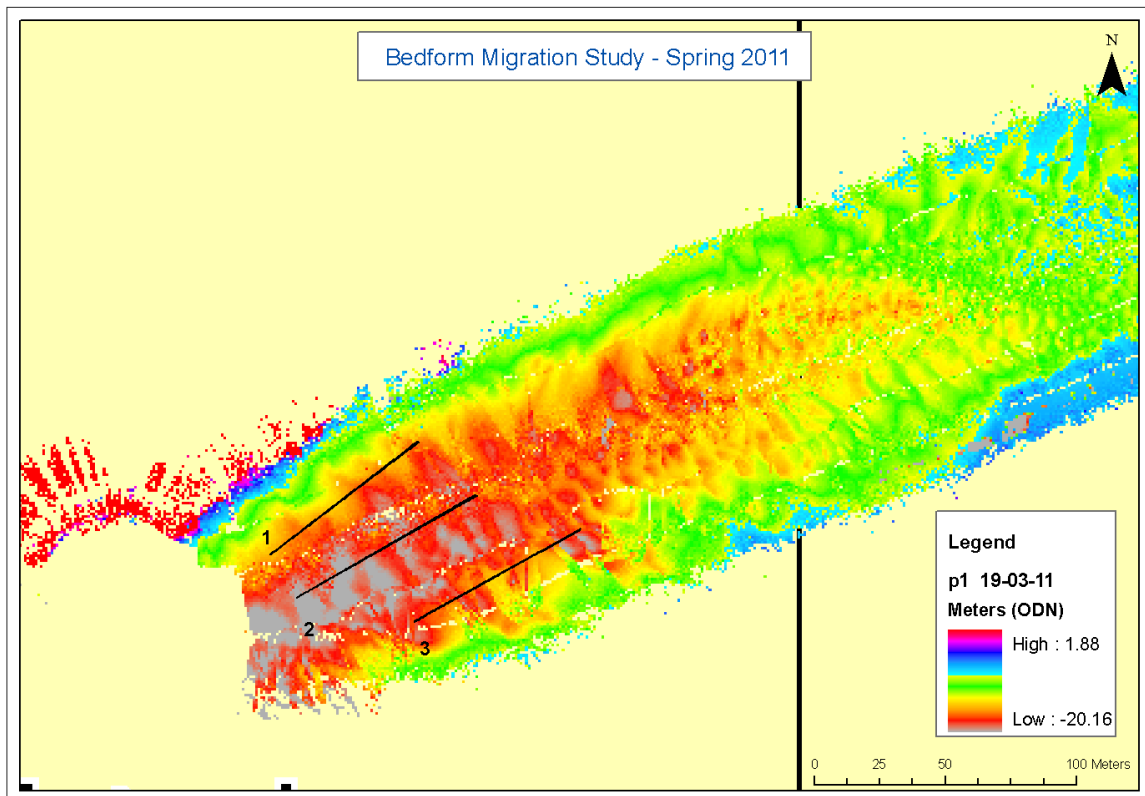


Figure 3.17: Area 1 DEM; bed-forms were clearly defined for 19/03/11 and three cross-sectional profiles extracted.

Unfortunately, the extracted cross-sectional profiles for the period 19/03/11 to 28/03/11 were of limited use in tracking bed-forms (Figure 3-18 and appendix 2 Figures 3 and 4), the interval between surveys being too long and interrupted by wave activity altering the characteristics of the bed-forms. In Figure 3-18 below, only the central bed-form is perhaps recognisable as ebb orientated, which had become much lower in profile rather than migrating any distance.

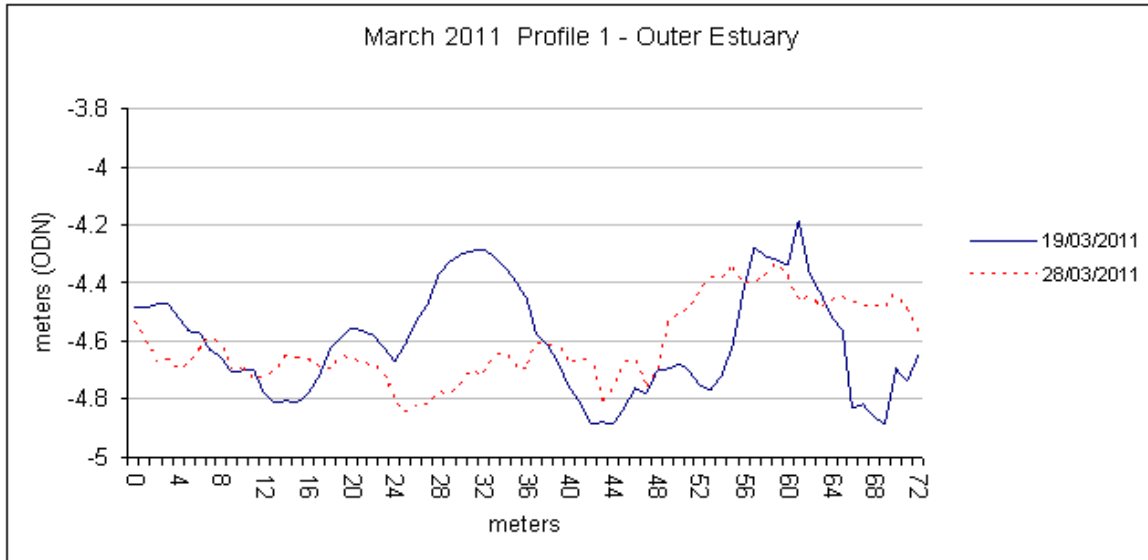


Figure 3-18: Cross-sectional profiles for March 2011; orientated left to right SW-NE, landward to sea-ward.

Table 3-11: Summary data for area 1, for both neap and spring cycles. Additionally the March Spring data are shown (included as total mean data). Rate is m/tide and heights are meters.

Ebb Bed-form Field						
Springs			Neaps			
	Mean Migration	12/05/2011 Mean Height	25/05/2011 Mean Height	Mean Migration	25/04/2011 Mean Height	12/05/2011 Mean Height
rate/period	-2.45	0.86	0.94	rate/period	2.63	0.94
rate/tide	-0.09			rate/tide	0.71	0.94
-0.30386	-0.39	0.32		rate/tide	0.07	0.82
	mean	0.90		mean		0.82
	SD	SD	SD	SD	SD	SD
	1.18	0.54	0.56	2.78	0.23	0.44
	mean rate per tide	-0.01		height	0.86	
	with march	-0.31			0.75	

The mean rate of bed-form migration was calculated to be 0.01m/tide⁻¹ (Table 3-11), and with the March data included, 0.31m/tide⁻¹. Movement is in a net ebb direction for both data sets.

.Flood Bed-form (area 2)

Extracted profiles are presented in appendix 2 figures 15 to 26. Over a period of ten days, the bed-forms migrated landward into the estuary under flood dominated tidal currents.

The bed-forms are predominantly triangular in cross-section (Figure 3-19 and appendix 2 profiles) however during reversal over the neap tidal cycle, the shape departs from triangular, which not only has implications to the shape factor used in equation (6), but also making measurement extremely difficult (particularly profiles 2, 3 and 5).

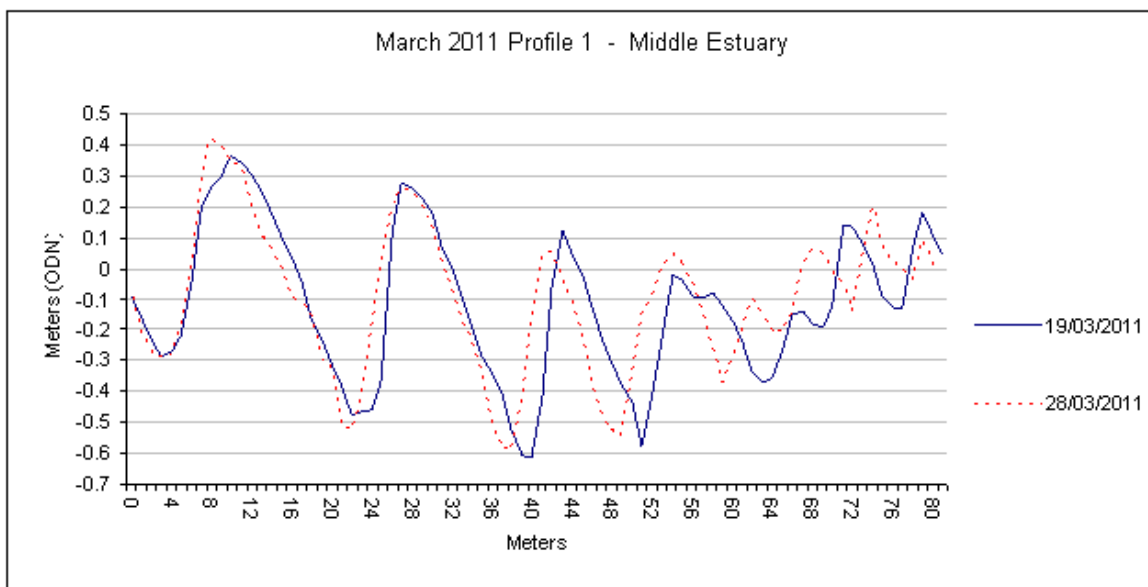


Figure 3-19: Orthogonal profile 1 taken from the flood bed-form field (19-03-11 & 28-03-11). Horizontal distance is in meters increasing seaward. The profile runs SW –NE from landward to sea-ward.

Despite the difficulties, a mean rate of transport was determined from summary data of bed-form height and migration rate; the rate of movement was calculated as 0.10m/tide^{-1} for bed-forms averaging 0.66m in height (Table 3-15)..

Estuary wide up-scaling

Cross-sectional profiles were extracted from mapped zones of characteristically ebb or flood dominated bed-forms, along transects which are identified in Figure 3-20. From these transects measurements were made of bed-form geometry; Mean heights for ebb and flood bed-forms were calculated as 0.75m and 0.53m respectively (Table 3-18), and using the mean migration rates from areas 1, 2 and the West Sands channel, the bed-form migration equation (6) was used to calculate volume of sediment transport (Table 3-19).

Table 3-18: Average bed-form height (m) and wavelengths (m) measured from cross-profile transects.

Ebb Orientated		Flood Orientated	
Height (m)	Length (m)	Height (m)	Length (m)
0.75	13.30	0.53	10.65

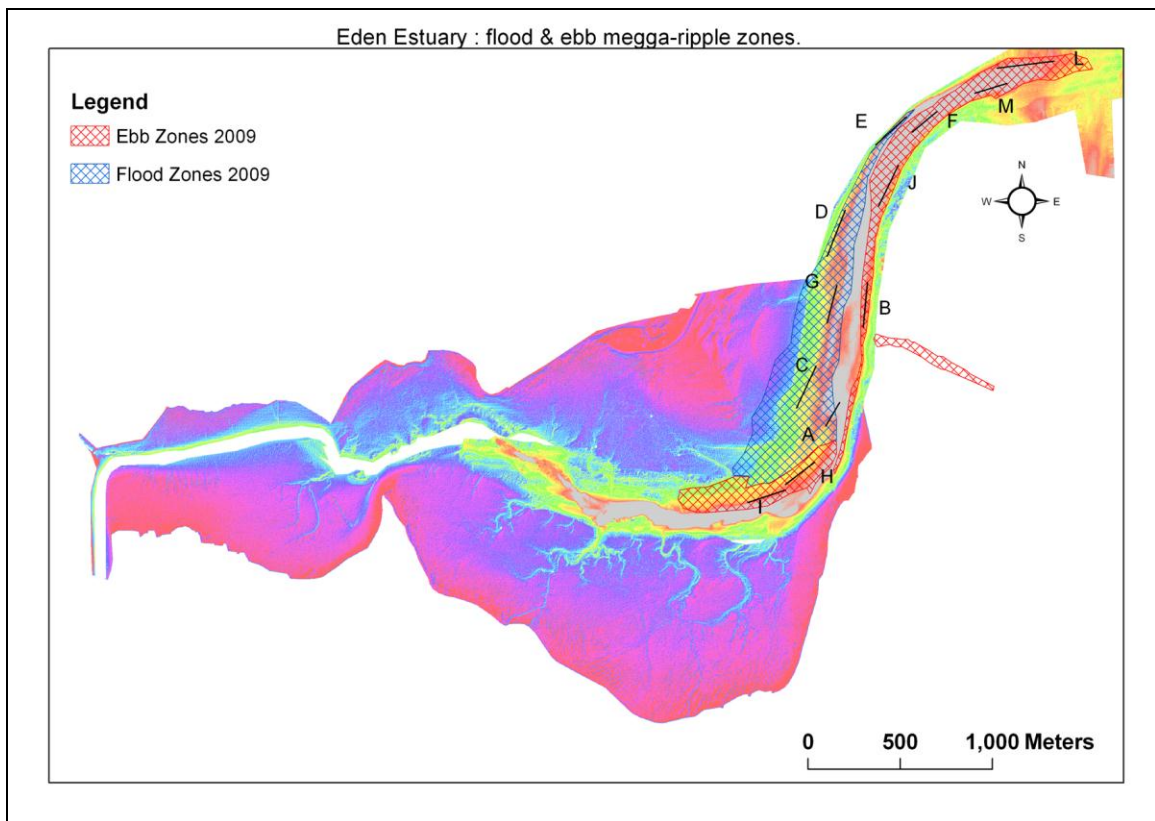


Figure 3-20: Locations of cross-sectional profiles used to calculate mean estuary-wide bed-form characteristics for estimation of net sediment transport.

Table 3-19: Volume of sediment transport calculated using bed-form equation (6) combined with average estuary wide measurements of height (Table 3-18) and migration rates calculated for area 1 and area 2 analyses.

cycle	m3/tide	Tonnes		1-p	Vs	H	Mass g/cm3	p
Ebb	0.002	0.006		0.6	0.01	0.750	2.50	0.4
cycle	m3/tide	Tonnes		1-p	Vs	H	Mass g/cm3	p
Flood	0.016	0.040		0.6	0.10	0.530	2.50	0.4

Assumptions had to be made to enable an estuary-wide estimate of net sediment transport, firstly that the modal particle size and porosity for the transport zones identified in Figure 3-20 roughly equated to the value used in the calculations and secondly that the mean rates of bed-form migration for each of the zones also roughly equated to the rate applied. The first assumption is likely, as particle size was measured within these main zones and varied little, apart from being more 'well sorted' towards the outer estuary. The second assumption is less certain, however bed-form geometry is known to be dependent on water depth (Dalrymple and Rhodes, 1995, Wewetzer and Duck, 1996), thus the outer estuary bed-forms should offset heights towards the middle estuary. To account for applying the measured migration rates from Area 1 and Area 2 to these mean geometry data, the volume/ tide values used in up-scaling are the mean from Areas 1 & 2 together with those calculated in Table 3-19 (since migration speed is a function of the height of the bed-form). The up-scaled net transport estimate is presented in Table 3-20.

Table 3-20: A quantitative estimate of sediment transport in the Eden estuary (per tidal cycle). Left includes the new channel which cuts across West Sands spit, right is with this zone excluded.

Location	Area (m ²)	m ³ /tide	Transport/Area	Location	Area (m ²)	m ³ /tide	Transport/Area
Main Ebb	229095	-0.012	-2749	Main Ebb	229095	-0.012	-2749
Main Flood	457068	0.017	7770	Main Flood	457068	0.017	7770
Ebb	121821	-0.012	-1462	Ebb	121821	-0.012	-1462
WWS Channel	31393	-0.108	-3390				
		Net m ³ /tide	169			Net m ³ /tide	3559
		Tonnes/tide	422			Tonnes/tide	8898

Two values for the net volume of sediment transport are calculated; inclusion of the West Sands channel produces a volume of 169 m³/tide-1 and thus flood directional transport of 422 tonnes of mobile sediment per tide. Excluding the West Sands channel gives a net flood directional transport of sediment at a rate of 3559m³/tide-1, equating to 8898 tonnes of mobile sediment. These values represent the total of mobile sand over the area identified in Figure 3-13 and not total volume of net import to the estuary.

3.2.2.3. Discussion

This study has highlighted the many problems involved with quantifying sediment transport within the confines of a small shallow estuary. The comparative assessment methods both experienced problems; the bed-form tracking method was susceptible to survey timing and data coverage issues during the neap tidal cycle, when the water depth was at times less than 2m. The mean duration for critical transport velocity method was found to be sensitive to the spatial variability of the current regime and would not have captured the contribution of aeolian transport during low water exposure; if the methodology had been found to be appropriate for the site it would have allowed inclusion of the bathymetry data, where there was ambiguity in identifying corresponding bed-forms.

Comparative differences in the results between methods may also be due to direct measurement methods capturing saltating and aeolian driven transport on the inter-tidal zone. This study has demonstrated that recorded velocities must be taken directly above the bed-forms being monitored.

The bathymetry bed-form data for the outer estuary (Area 1) are difficult to interpret, due to the problems with acquisition, however taking the conservative migration rate of 0.01m/tide is probably more realistic (based upon the March data having few replicate bed-forms); it is also likely that wave activity has impacted on transport in this zone adding to the difficulty in accurately quantifying transport.

Data for the middle estuary (bathymetry Area 2), give a time lapse bathymetry volume transport rate of $0.018\text{m}^3/\text{tide}^{-1}$, which relative to the hypsometry (hypsometry Area 1) data for the landward edge of the area ($0.007\text{m}^3/\text{tide}^{-1}$) is 0.011m^3 more per tide. This may be expected, as the number of replicates for the bathymetry data was greater compared with the pilot pin survey. Also, the bathymetry data covered a wider and more representative area for the flood bed-form field, having 4 times as many replicates.

In terms of historical comparison, the hypsometry data are likely to be more reflective of change that has occurred; since the methodologies and the spatial data collection are more closely matched to the historical methods, however the bathymetry data, being more representative of the bed-form field, will be a more accurate assessment of sediment transport within the bed-form field.

Migration rates are available within the research literature and examples are given for both sub-tidal and intertidal zones within a review paper by Wever (2004) for various measurement methodologies (Table 3-21).

Table 3-21: A comparison of bed-form migration rates (data from Wever, 2004).

Location	Method	Height	Migration rate	Literature Reference
Subtidal	Diver & Stakes	40 cm	40.5 cm/tide	Shephard & Hails 1984
	Current meter	30 cm	26.6 cm/tide	Bokuniewicz et al. 1977
	BRM	40 cm	20 cm/tide	Wever & Stender 2000
Inter-tidal	Direct measurement	24 cm	1.92 cm /day	Larcombe & Jago 1996
	Echosounder	81 cm	10.16 cm/tide	Dalrymple 1984
	Stakes	14 cm	32.64 cm/day	Terwindt & Brouwer 1986

Comparison between estuaries is difficult even for similar feature heights, as the tidal asymmetry of the estuary may be different, dependent upon river inflow, dominant wind direction and the tidal range, leading to reversals in transport etc. Similarly whilst bed-form height is proportional to water depth, velocities may vary due to morphology with increased velocities through more constrained channels, highlighting the importance of taking additional current meter readings. For intertidal areas, the direction of sustained periods of wind plays an important role, not only for tidal asymmetry, but having implications for aeolian transport, which may accentuate or counteract the net current velocity driven transport.

Whilst there is much spatial and temporal variability in sediment transport within the estuary, an attempt at the assessment of estuary-wide transport was made to provide additional supporting evidence of directional trend in terms of the estuary being more erosional or depositional. The result was very dependent upon the inclusion of the hypsometric data for the West Sands channel, for which very little is known of the source of sediment which is being transported sea-ward. It is known that long-shore drift is transporting sediment northwards along the shoreline (Ferentinos and McManus, 2009), which may contribute to the sediment source for the channel. The spit to sea-ward may provide additional sediment for this channel; during low water the extensive spit offers a long fetch for wind driven transport, whilst at high water wave activity over the area may redistribute the unconsolidated sands into the channel. Conversely, the estuary may too offer a source of sediment supply; under Coriolis ebb currents leaving the estuary are likely to exit along the southerly shore and through the channel, mobilizing sediment seaward. The elevation of the West Sands channel with respect to the main Eden channel is such that transport will be via the early to mid cycle ebb currents, thus there is uncertainty as to how much bedload transport from the immediate vicinity of the beach channel would occur, however inclusion of the hypsometric data for the West Sands channel gives a more realistic estuary-wide calculation of a $169\text{m}^3/\text{tide}^{-1}$, representing a net landward mobilization of sediment over a surface area of 807984m^2 , placing the estuary in a net depositional phase.

3.2.2.4. Summary

Bed-form tracking using time lapse bathymetry methods gave the present rate of sediment transport near the estuary bar to be a net ebb movement of $0.021\text{m}^3/\text{tide}^{-1}$. The transport rate for the middle estuary flood bed-form field was calculated to be $0.018\text{m}^3/\text{tide}^{-1}$. Up-scaling to estimate an estuary-wide net direction of mobile sediment bed-load transport, based on representative rates of transport for flood and ebb dominated zones respectively, gave a volume of flood mobilised sediment of $169\text{m}^3/\text{tide}^{-1}$ under present hydrodynamic conditions. This value is presented with the caveat that it is calculated on limited data and a much more detailed survey would be required to accurately capture of true rates.

3.3. Salinity

Contemporary data are used to elucidate present conditions, with the additional use of limited recent historical data to identify potential directional trends of change, correlating spatial changes with regime shifts. Salinity was chosen as it represents the transition regime between fresh and marine conditions, indicative of temperature, dissolved oxygen and PH conditions with respect to the contribution of river to seawater.

Aims

- Identify regime shifts in salinity.

3.3.1. Introduction

Few historical records exist that record salinity and temperature for the Eden estuary and hence it is difficult to assess accurately any long term changes or trends. However, two data sources have been identified for near bottom salinity profiles recorded over different tidal cycles and these are used to provide an indication of change. Eastwood (1977) presents mean data profiles for water depth, salinity and current velocities at various stations along the landward to sea-ward salinity gradient, whilst investigating propagation of the tidal wave and stratification in the estuary. Data was collected over a period of 6 months from June to November 1974. At the Guardbridge station, salinity was reported to have increased gradually throughout the flood tide, reaching surface salinities of $24 \text{ }^0/\text{00}$ (parts per thousand PPT³) and bottom salinities of $21 \text{ }^0/\text{00}$ over a tidal range of 0.90-2.80m. Following high water the surface salinities were reported to have dropped quite rapidly,

³ PPT roughly equates to Practical Salinity Units or PSU.

however the bottom salinities remained stable, indicating density separation of river and tidal waters. The average salinity over the period studied revealed stratification, with the surface salinity being 3 ‰ and bottom salinity 7 ‰.

A second study at Guardbridge was undertaken in 1990 (Loutit, 1991) during which salinity profiles were taken on two separate days, 20th September & 14th November 1990. These days were chosen to represent salinities at differing tidal heights corresponding to Springs and Neap cycles. The September profile revealed salinity to vary from 0 – 30 ‰ over a tidal range of 0.70 – 2.20 m and the November profile showed salinity to vary from 0 - 20 ‰ over a tidal range of 0.66 – 2.10 m. The tidal ranges were quite similar.

Plotting the predicted tides for 1990 (Figure 3-21, it can be seen that the selected days were not so different in their position in the tidal cycle however the data are still useful to compare with similar tidal ranges in contemporary data.

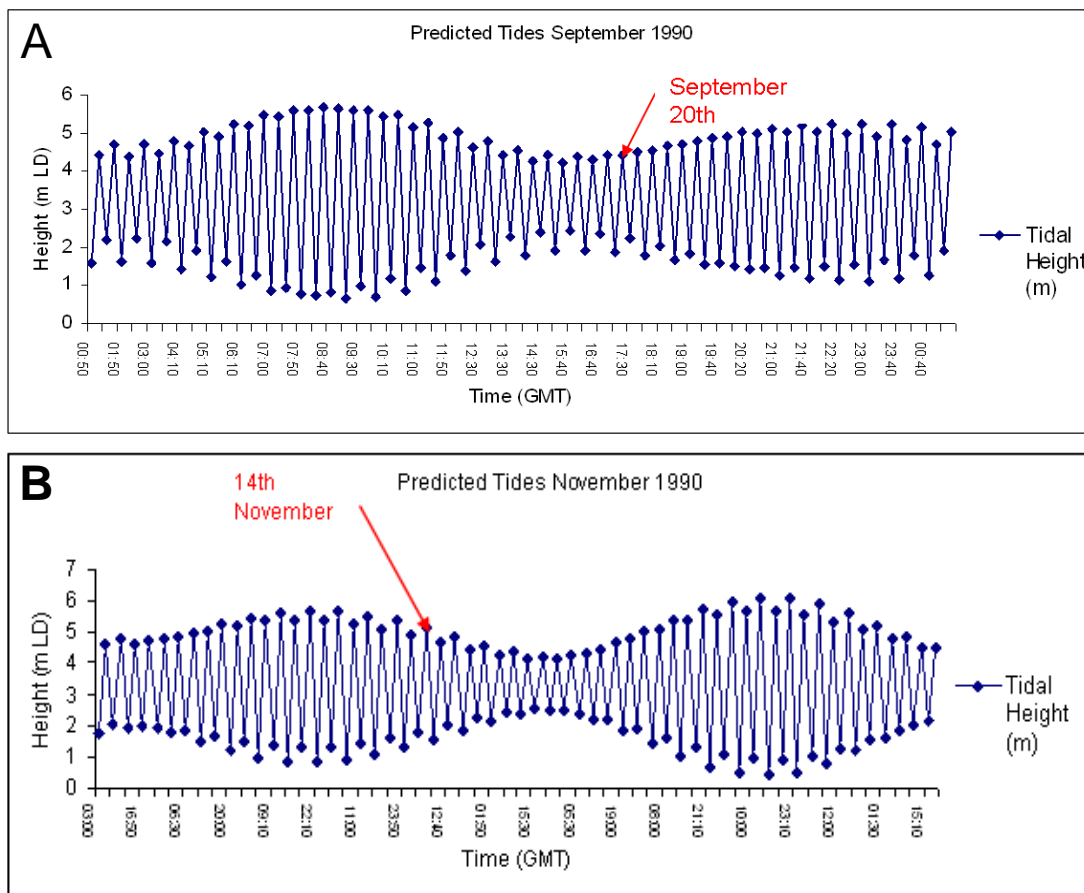


Figure 3-21: Predicted tidal heights, A are September 1990 tides and B are November 1990 tides (Neptune.Tides, 2011)

3.3.1.1. Methodology

Annual salinity and temperature data were recorded using a Solinst LTC junior logger located just seaward of the road crossing at Guardbridge. The logger recorded near bed conductivity ($\mu\text{S}/\text{cm}$) tidal level (m) and temperature ($^{\circ}\text{C}$), sampling at 15 minute intervals. The data were barometrically compensated (Solinst Barologger Gold) for changes in atmospheric pressure.

The recorded data were downloaded using Levellogger 3.4.0 software and exported as a text file for analysis and the conductivity values were subsequently converted to PPT for comparison with the historical data. R statistical software (CRAN, 2011) was used to present the data non-parametrically as box plots showing median, quartile and dispersion information.

Comparative tidal profiles were plotted in Excel for similar times of year and tidal ranges as the profiles by (Loutit, 1991) and the maximum and minimum salinity values were recorded.

3.3.1.2. Results

Annual data for 2010 (Figure 3-22) range from approximately 0 to 26 PPT over the year, with outlier values remaining below 30 PPT. Median salinity is reported as 10.79 PPT, whilst mean salinity is 6.11 PPT (Table 3-22). For these salinities, temperature ranges between 0.42°C and 22.76°C , with median and mean values 12.66°C and 11.36°C respectively.

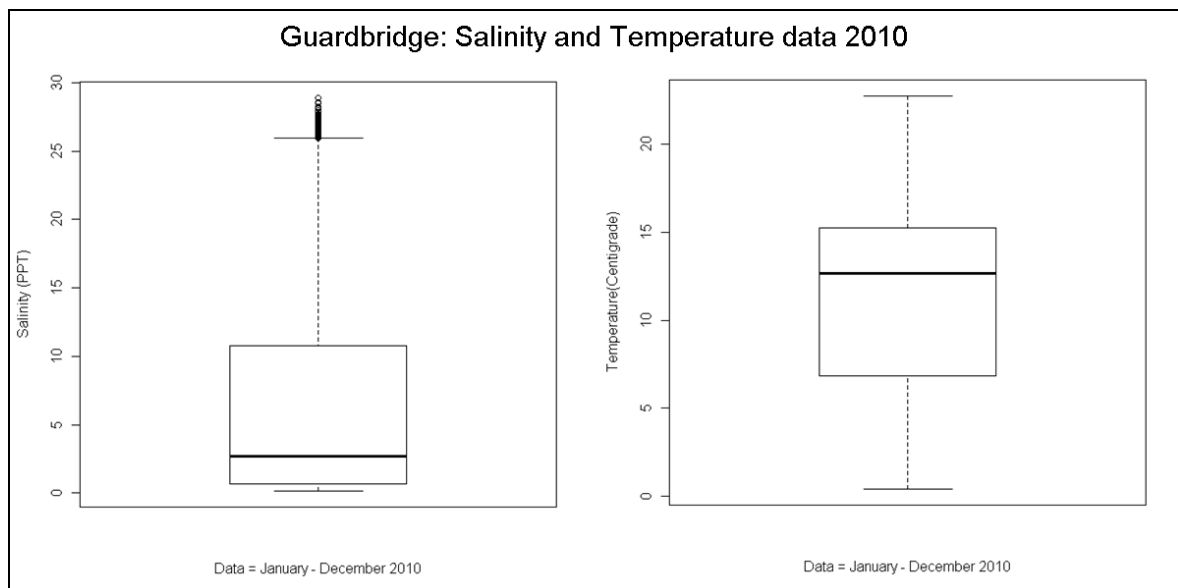


Figure 3-22: Annual data for salinity and temperature at Guardbridge (2010). Salinity - extreme of the lower whisker, the lower hinge, the median, the upper hinge and the extreme of the upper

whisker 0.16, 0.69, 2.71, 10.79 and 25.94 respectively. Similarly the statistics for temperature are 0.42, 6.85, 12.66, 15.26 and 22.76.

Table 3-22: Guardbridge annual summary data on salinity and temperature (2010).

	Salinity (PPT)	Temperature (°C)
Mean	6.11	11.36
Minimum	0.16	0.42
Maximum	28.89	22.76

Combined water depth and salinity profiles are presented for similar times of year and tidal states for comparison with Loutit (1991); the tidal amplitude range for 18th/19th September 2010 (Figure 3-23) which compares to Loutit (1991) September profile, is 1.61m and 1.88m, ebb and flood respectively and the salinity varies from 0.39-18.96 PPT. Temperature varies from 11.27°C to 13.30°C, with a mean of 12.38°C.

The second profile, presents data for the 11th/12th November 2010 (Figure 3-24); the amplitude rangws from 2.15m to 2.14m, ebb and flood tidal heights respectively and the salinity varies from 0.35-10.36 PPT. Temperature varies from 6.59°C to 7.20°C, with a mean of 6.85°C.

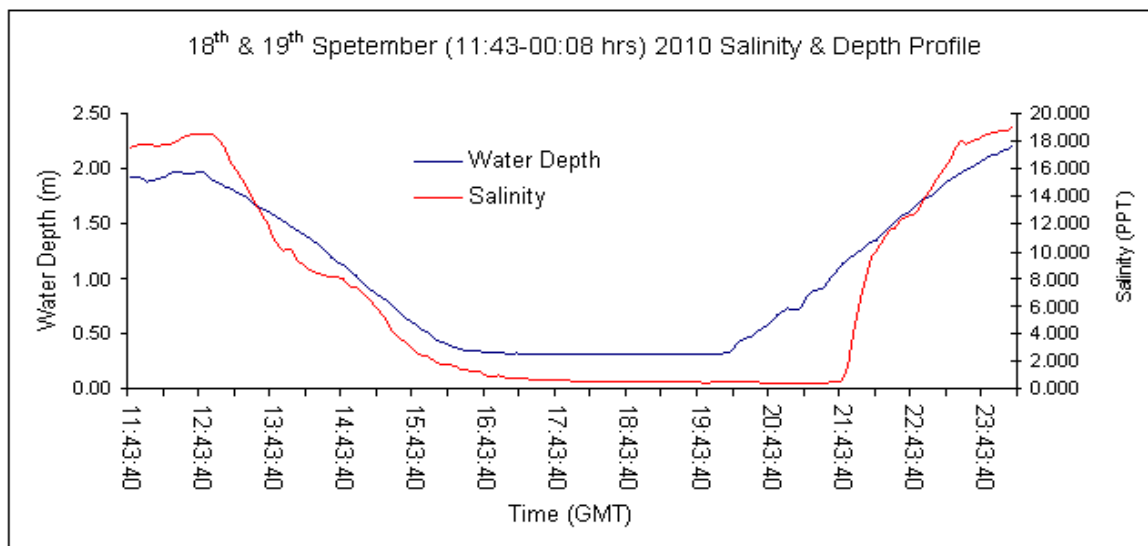


Figure 3-23: 2010 Salinity and tidal height profile for comparison with Loutit (1991) September 20th profile.

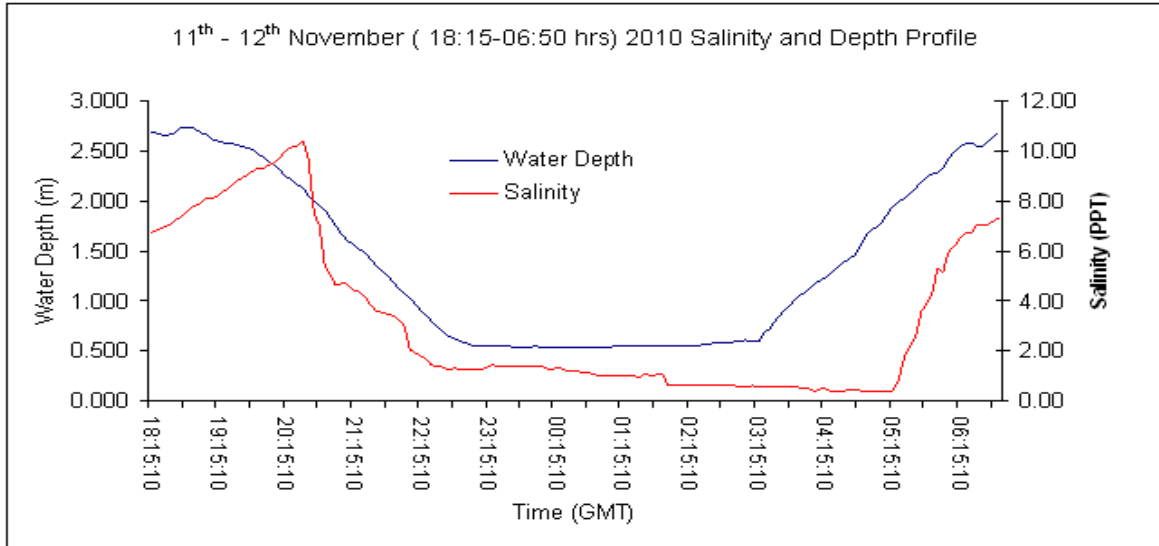


Figure 3-24: 2010 Salinity and tidal height profile for comparison with Loutit (1991) November 14th profile.

3.3.1.3. Discussion

The available historical data for comparative analysis was not only limited in quantity, but also was limited to recording a single spring and neap cycle, as a consequence, statistical correlation cannot be made, however the data are still valuable to infer broad trends or pattern over time. Changes to a salinity regime may be driven by increased river discharge or by changes to the tidal volume entering the estuary, through either sea level rise or changes to the estuary basin morphology. Short term shifts may also be driven by sustained onshore (offshore) winds, which pile water against (away from) the coast (Pugh, 2004) or from the passage of pressure systems (Pugh, 2004), deviating actual tidal heights from predicted ones.

Viewing the data in context with river discharge (Table 3-23) the observed differences in salinity range may be expected. Eastwood (1977) reports a mean salinity for June to November 1974 of 7.63 PPT, compared to the mean of 6.32 PPT for the same period in 2010, between these two periods there is an 82% increase in the total discharge.

Table 3-23: River Eden monthly total flow (cumecs) (Centre for Ecology & Hydrology, 2010)

	Jan	Feb	Mar	Apr	May	Jun	Jul	Aug	Sept	Oct	Nov	Dec	mean	Annua
1974	11.69	10.76	11.96	5.15	4.56	3.48	2.45	2.16	2.79	2.75	11.58	14.84	7.01	84.17
1990	20.43	25.61	11.86	6.06	4.61	4.03	5.87	2.97	2.22	9.24	8.46	11.76	9.43	113.12
2010	22.65	15.78	14.38	10.79	5.577	3.422	6.333	4.484	5.749	10.2	15.79	14.19	10.78	129.34

The magnitude of the salinity change does not fully reflect the magnitude of the increase in discharge, suggesting the influence of other drivers. In terms of changes to sea level, the Lunar nodal maximum was 5 years prior to the 1974 study and hence contributed only a small amount to increased sea level, however from the results of chapter 2, we can expect more onshore winds during negative NAO periods which are accompanied by below average flow (Figure 3-25). Onshore winds, the slight increase in sea level and the much lower river discharge may in combination help explain the relative differences in salinity between 1974 and 2010.

Comparing the two salinity depth profiles (Figures 3-23 and 3-24) with those of Loutit (1991) reveals the contemporary data having lower salinities for similar tidal ranges, whilst river discharges are higher for 2010, by 159% and 87% respectively. Temporal proximity to lunar nodal maximums, hence higher sea levels, is approximately the same (3 and 4 years post maximum) and therefore making little contribution to altered conditions. Offshore westerly winds were however greater in 2010 than 1990 (Chapter 2.2 Figure 2-36), which would have led to a shortened duration of the flood tide and lessened saline intrusion towards Guardbridge. Thus combined river discharge and offshore wind conditions may help to explain the large differences in salinities, however with just two profiles caution must be given to their interpretation. Similarly interpretation of temperature differences between these data is difficult; September data means are 10.32°C and 12.38°C and November data means are 8.64°C and 6.85°C (1990 & 2010 respectively). The increased ratio of fresh to seawater between 1990 and 2010 would perhaps infer lower mean water temperatures however for September this appears not to be the case. River temperatures largely change in response to atmospheric temperature and ground water conditions (Gosling, 2011, Conlan *et al.*, 2007), without air temperature data and with such limited historical records, conclusion are unable to be drawn.

Despite the restricted data, with knowledge of the periodic variability in sea level with respect to the lunar nodal cycle and patterns present in river discharge (Figure 3-25) associated with phases of the NAO, broad speculations may be made for salinity regime changes and to the concomitant effect of altered acidity with respect to the percentage of dissolved gasses, influencing the potential distribution of regime-limited species.

Approaching the lunar nodal maximum, salinity would be expected to shift in a landward direction with increasing sea level and conversely a seaward regime shift would be expected approaching the nodal minimum. Where these situations occur along with persistent NAO phases, river discharge becomes increasingly important in modifying the salinity regime.

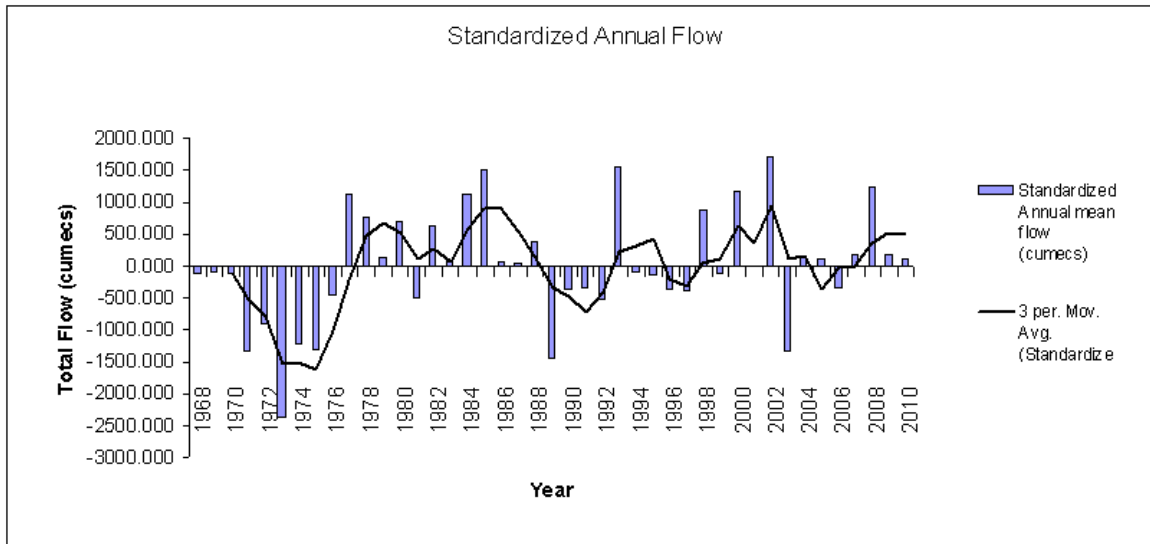


Figure 3-25: River Eden, Kembeck gauged data, presented as deviation from mean discharge conditions.

In NAO positive years generally there are more frequent and stronger westerly winds accompanied by cool summers and mild wet winters, however not only are there more and stronger westerly winds, but the passage of the depressions leads regionally to a rise in sea level due to the reduction in atmospheric pressure. Under such conditions, mean river discharge is likely to be high, water temperatures more stable over the seasons and although sea level may be increased under low atmospheric pressures, offshore westerly winds are likely to impede saline intrusion up the estuary. In contrast NAO negative years are characterized by fewer westerlies and much colder winters, with the passage of higher atmospheric pressure systems leading to a regional lowering of sea level. Thus during NAO negative years, less river discharge may be expected (with the exception of flash snow melt), more seasonal variation in temperature and a more landward shift in salinity under more on-shore wind conditions. The proportional impact of the passage of pressure systems to wind conditions will however be subject to the relative intensities of each; one may counter act the impact of the other or may dominate as a driving mechanism.

3.3.1.4. Summary

Assessment of the limited salinity and temperature data to identify regime shifts, highlighted the importance of the timing and volume of freshwater inflows, associated with persistent NAO phases and also the temporal proximity with the lunar nodal maximum to the resulting abiotic conditions.

Altering the river discharge will lead to shifts in salinity, stratification, water residence time and estuary mixing; influencing hydrodynamics with a feedback to the morphological development of the estuary and the spatial distribution of species. Changes to sea level are less widely consequential impacting on how far up the estuary salinity penetrates, which may also be driven by persistent up or down estuary wind.

Whilst differences were found, far greater variability is observed within and between tidal phases, inferring impacts from salinity changes are more likely to be in terms of alteration of estuary hydrodynamics than direct impacts to species and their distribution.

3.4. Chapter Discussion

Data from the tidal asymmetry analyses revealed a net import of coarser particles resulting from dominance in flood velocities and inferred an export of the finer suspended load resulting from both the dominance of the ebb tidal duration and the length of the low water slack period. Evaluating the estuary tidal volume similarly inferred flood dominance for coarser particle transport. The identification of zones of bed-forms displaying directional orientations to ebb and flood tides, highlighted the spatial variability in bedload transport within the estuary; quantifying the rates of transport for the characteristic zones and up-scaling these to make a rough estimate of net directional transport for the estuary as a whole revealed a net flood directional transport with respect to coarser particle transport. Placing the estuaries developmental stage within Dronkers classification (Dronkers, 1986) by morphology, would place the Eden as a Type II, having a central slot channel and higher intertidal flats. The residual flood transport (bedload) however infers a transition to a Type I stage, which is similarly inferred by the dominance of the low water slack, causing the movement of sediment from the intertidal to the sub-tidal, which has also been observed for the Dyfi estuary (Brown and Davies, 2010) and peak ebb velocities occurring closer to high water than during the 1970s, having implications to the removal of sediment from the intertidal area.

Limited data were available to assess regime shifts in salinity despite this the findings were broadly consistent with those of the tidal asymmetry and bed-form transport data. Changes to the salinity regime occur largely through either an increase in river discharge or from an increase in the tidal volume entering the estuary (resulting from changes to basin geometry or increased sea level), thus reflected by the tidal asymmetry.

Comparisons of the data from the three sections in this chapter inferred the estuary has transitioned between developmental stages; asymmetry analysis compared data with those of Eastwood (1977) recorded on the flood bed-form zone to the north of the channel, which inferred a greater flood asymmetry during the 1970s. Similarly comparison between tidal prisms suggested that Eastwood's (1977) tidal volume was smaller than at present, inferring a shallower estuary during that time (since river flow was less) reflecting higher flood tidal dominance. Bed-form migration data were also compared to Eastwood (1977), revealing a higher rate of transport for the northern flood bed-form zone than today and again leading to the conclusion of a higher intertidal area during that time than is present today. Although confidence in comparisons for the salinity data is low, coupled with information regarding the river discharge and wind regimes does allow more confidence in the data. Salinity profile data from Eastwood (1977) at Guardbridge suggested a landward shift in salinity

relative to the present (despite the smaller tidal prism calculated for that time) and similarly data from Loutit (1991) for Guardbridge also revealed higher salinities than at present. This regime shift in salinity was proposed to be dependent upon the volume of river inflow to the estuary and to both temporal proximity to persistent phases of the NAO and the lunar nodal cycle. Reviewing the historical trend in the salinity regime may also infer a reduction in the strength of the flood velocities over time, with increased river flow accentuating ebb velocities and consequential removal of finer particles as suspended load and the inhibition of flood velocities, limiting bedload transport into the estuary.

Tidal asymmetry analysis proved a useful indicator of climate driven change; river flow and wind regime may indicate potential directional change, however provide less information on the directional shift in erosional or depositional character and to the relative rates of net fine and coarse particle transport, though were import here to link the asymmetry shift to the patterns of climate variability.

The data from this chapter suggest that the estuary has become less depositional in character compared with data from the 1970s, over the period of approximately 30 years. Whilst the lunar nodal impacts to tidal volume perturb the asymmetry, the interval over which the basin morphology appears to be oscillating exceeds that of the 18.6 nodal period and thus eliminates it as a primary driving mechanism. Pethick (1994) attributes the dynamic oscillatory states as driven by morphological feedback mechanisms, however the morphological development is also driven by the tidal asymmetry, which in turn has been proposed here as being perturbed by patterns of river flow and sustained directional wind conditions.

3.5. Chapter summary

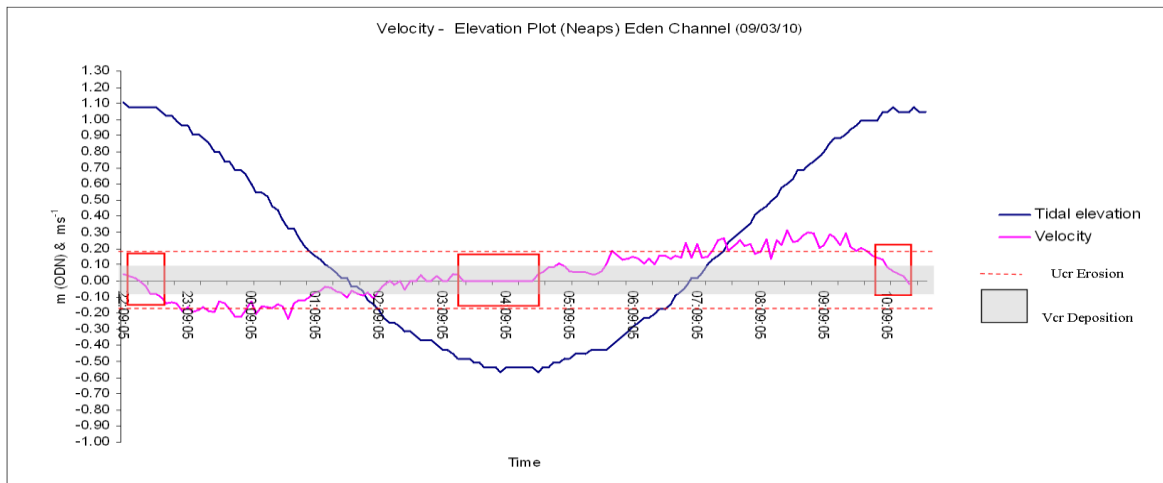
Tidal asymmetry analysis identified an overall net ebb dominance in the vertical tide (tidal duration), inferring export of finer particles, similarly the inequality identified in the duration of slack water also pointed towards the export of finer particles (longer low water slack period). Conversely, critical current velocities for the modal particle size were dominant on the flood tide, thus favouring the import of larger particles. The tidal asymmetry inferred deposition to be within and along the channel edges and potentially a lowering of the intertidal area under peak ebb velocities occurring closer to high water than during the mid 1970s.

Comparison of bedload transport and tidal prism data inferred the estuary to be deeper and less flood dominated than during the mid 1970s, this is consistent with the findings of estuary elevation analysis in chapter 2, however up-scaling of bed-form migration rates to give an estuary wide transport estimate, identified an overall net flood bedload transport, consistent with the tidal and

current velocity data and similarly with the elevation data which suggested deposition within the channel. Comparative salinity profile data similarly pointed towards less flood dominated conditions at present than during the mid 1970s. Patterns of river flow, coupled with sustained phases of the NAO and associated wind conditions are proposed to explain the regime shift in salinity.

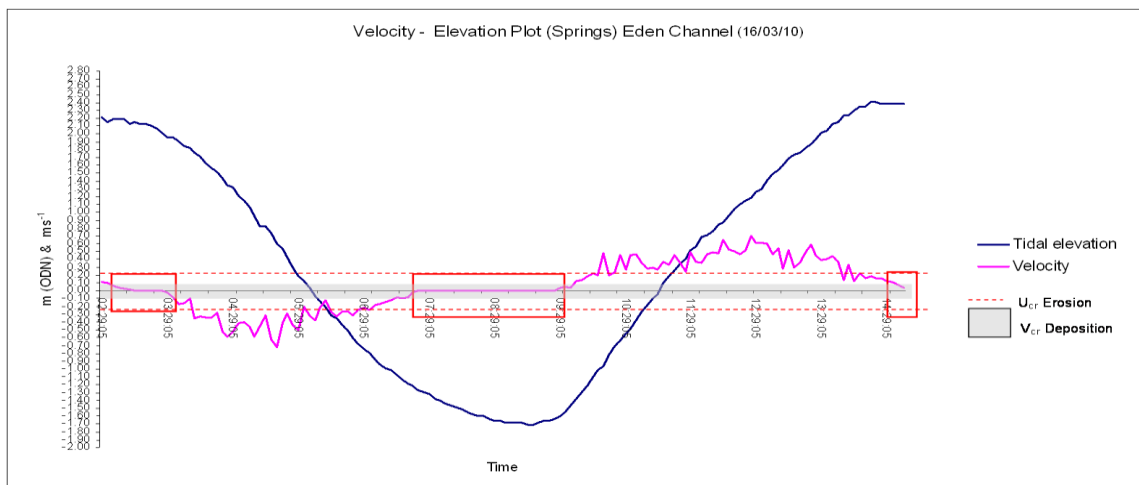
The chapter aim was to identify key abiotic influences which may be applied as indicators of climate driven change. Shifts in both tidal asymmetry and salinity are driven largely by either changes to river inflow or to the tidal volume and may be exacerbated by sustained patterns of directional wind; the data from this chapter infer the estuary has become less depositional in character through shifts in asymmetry and thus reflecting the impact of climatic variability between the 1970s and present. Tidal asymmetry has been demonstrated as a useful indicator of climate driven change; 'river flow' and 'wind regime' were also very useful indicators of directional change, however provided less information on the directional shift in erosional or depositional character and to the relative rates of net fine and coarse particle transport, though were important here to link the asymmetry shift to the patterns of climate variability.

3.6. Chapter 3: Appendices



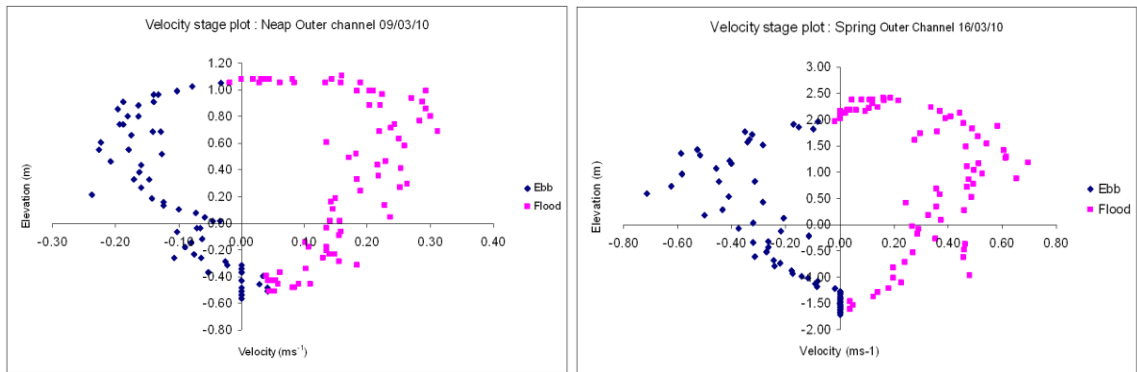
Chapter 3 appendix 1 Figure 1: Neap tidal elevation plot 09/03/10 Eden Outer Channel.

The neap elevation plot for 09/03/10 (Figure 1) reveals transport occurs mid cycle and the majority of deposition late ebb through to just after low water.



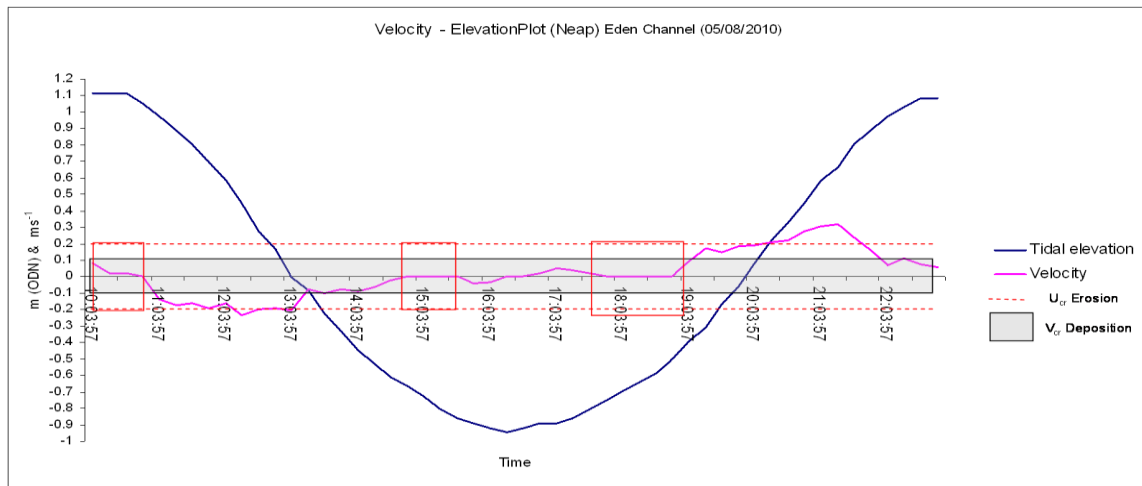
Chapter 3 appendix 1 Figure 2: Spring tidal elevation plot 16/03/10 Eden Outer Channel.

Figure 2 spring cycle for 16/03/10 also reveals transport occurs mid cycle and deposition is almost confined to the slack water periods, but to just after low water and shorter than during neaps.



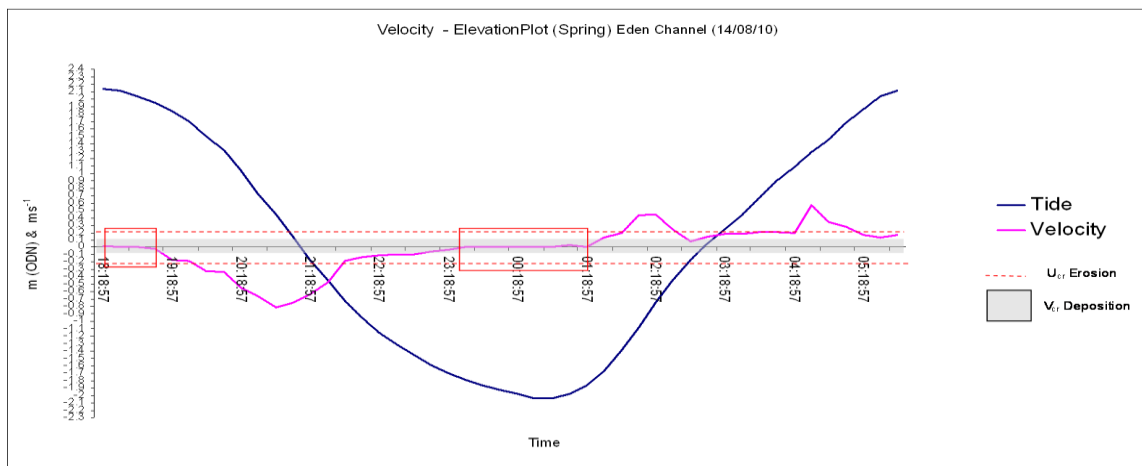
Chapter 3 appendix 1 Figure 3: Neap & Spring Velocity stage plots for the above elevation analyses.

The maximum velocities observed in Figure 3 for springs are almost double neap velocities.



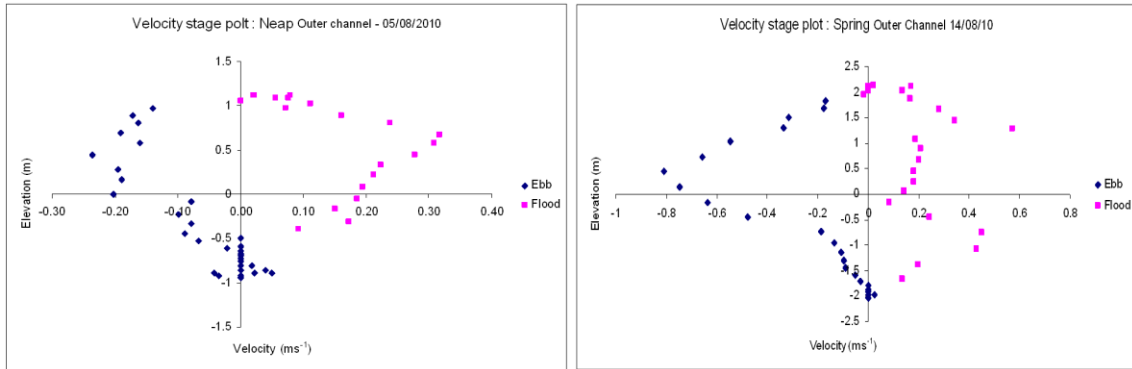
Chapter 3 appendix 1 Figure 4: Neap tidal elevation plot 05/08/10 Eden Outer Channel.

Figure 4 neap tidal cycle, for the 5th of August shows similar patterns of peak velocities mid cycle and the majority of deposition over the low water period.



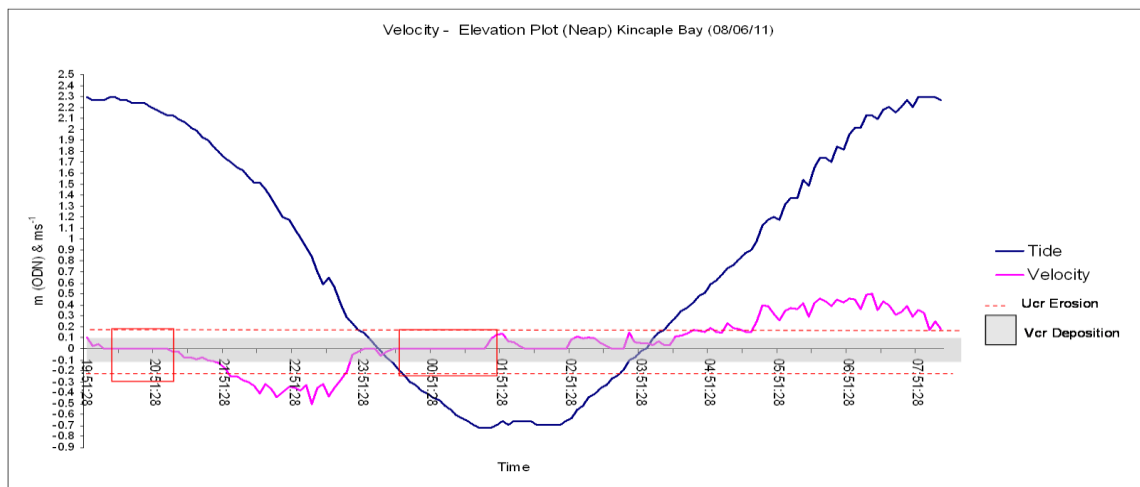
Chapter 3 appendix 1 Figure 5: Spring tidal elevation plot 14/08/10 Eden Outer Channel.

Figure 5 spring tidal cycle for the 14th of August shows peak velocities mid cycle and deposition confined to slack waters. The duration of deposition is less than during the neap cycle.



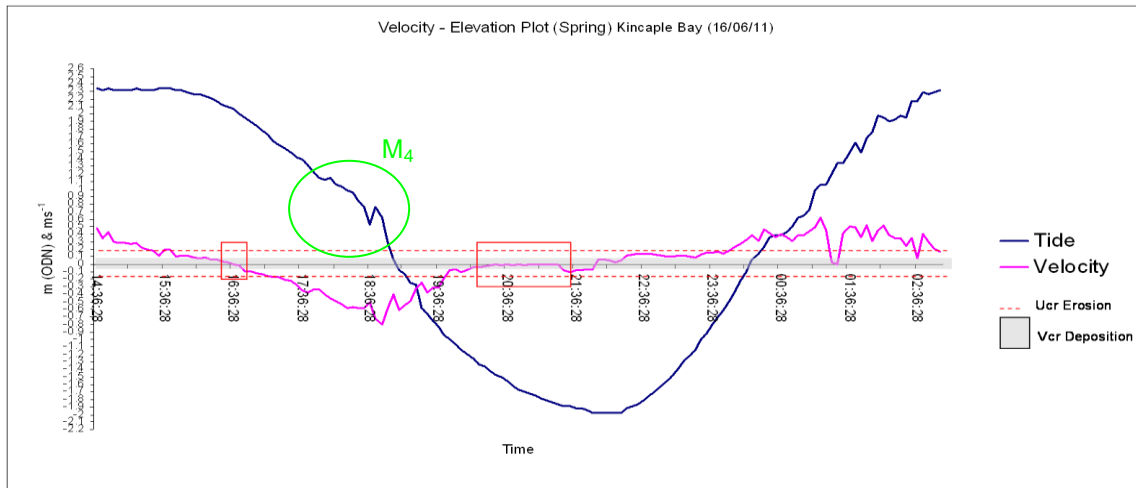
Chapter 3 appendix 1 Figure 6: Neap & Spring Velocity stage plots for the above elevation analyses.

Spring tidal cycle velocities seen in Figure 6 are more than double the neap velocities, however are leaning towards ebb & flood velocities being more symmetrical over the spring tides.



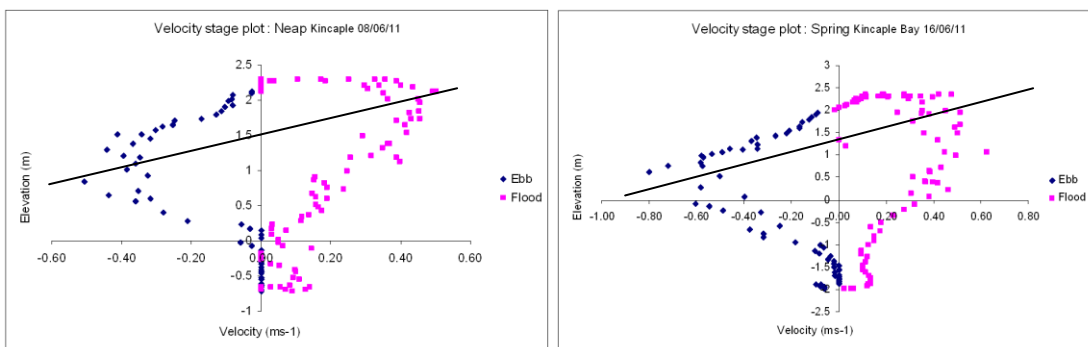
Chapter 3 appendix 1 Figure 7: Neap tidal elevation plot 08/06/11 Kincapple Bay Channel.

Figure 7 neap tidal cycle, the majority of deposition over the low water period. Peak ebb velocities are closer towards low water than at the Outer channel location and peak flood towards high water.

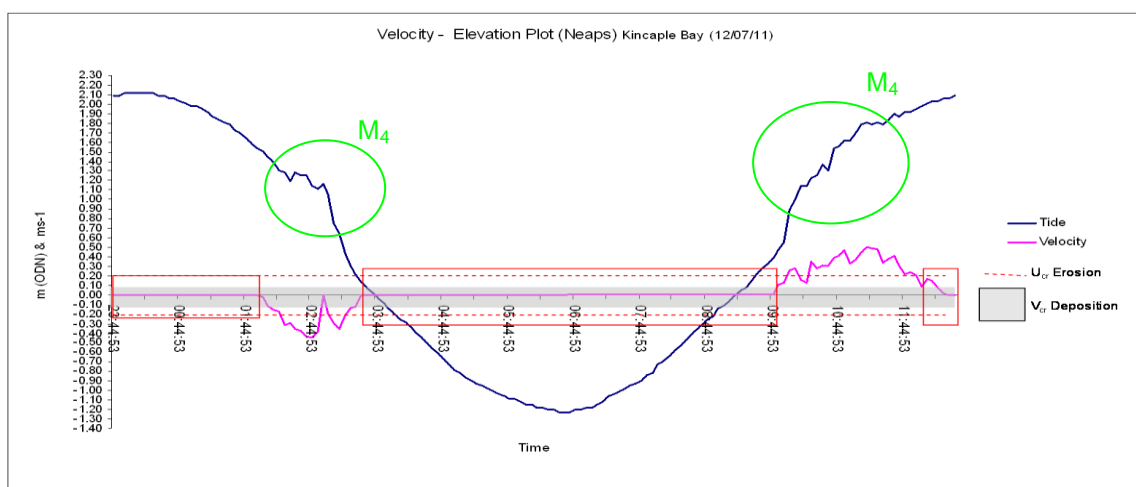


Chapter 3 appendix 1 Figure 8: Spring tidal elevation plot 16/06/11 Kincaple Bay Channel.

Figure 8 spring tidal cycle displays evidence of interaction with overtides (m_4 harmonic). The duration of deposition is seen to be greater at low water, though shorter than for the above neap cycle. The stage plots at Kincaple Bay (Figure 9) show a temporal shift in peak velocities, with peak ebb mid cycle and peak flood prior to high water.

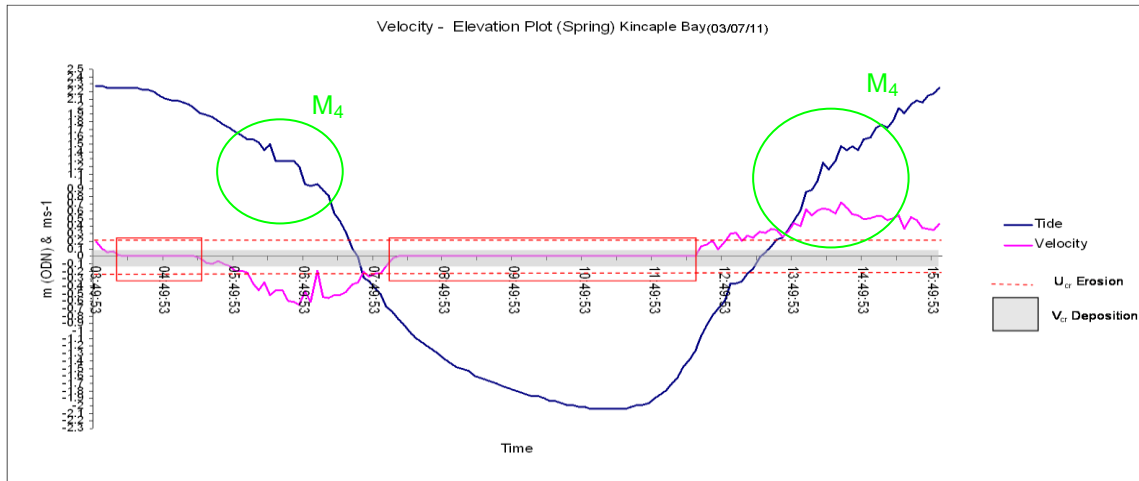


Chapter 3 appendix 1 Figure 9: Neap & Spring Velocity stage plots for Figure 8 elevation analyses.



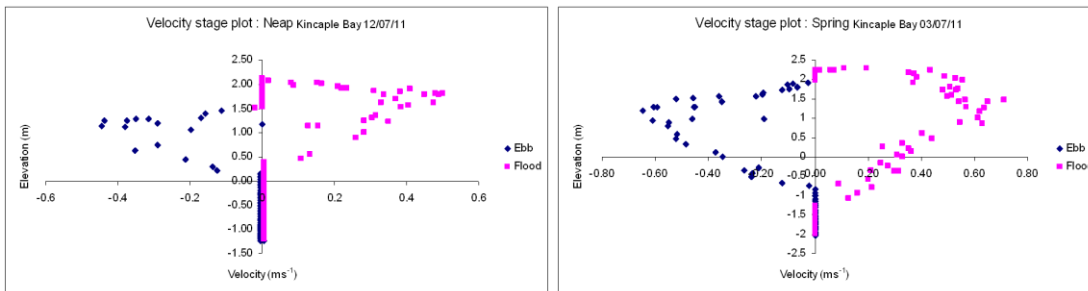
Chapter 3 appendix 1 Figure 10: Neap tidal elevation plot 12/07/11 Kincaple Bay Channel.

The influence of overtides is seen in Figure 10, which give rise to the peak current velocities.



Chapter 3 appendix 1 Figure 11: Spring tidal elevation plot 03/07/11 Kincaple Bay Channel.

Figure 11 shows a similar pattern of influence of overtides and peak velocities. The deposition phases are shorter for the spring cycle than the ebb and greatest at low water.

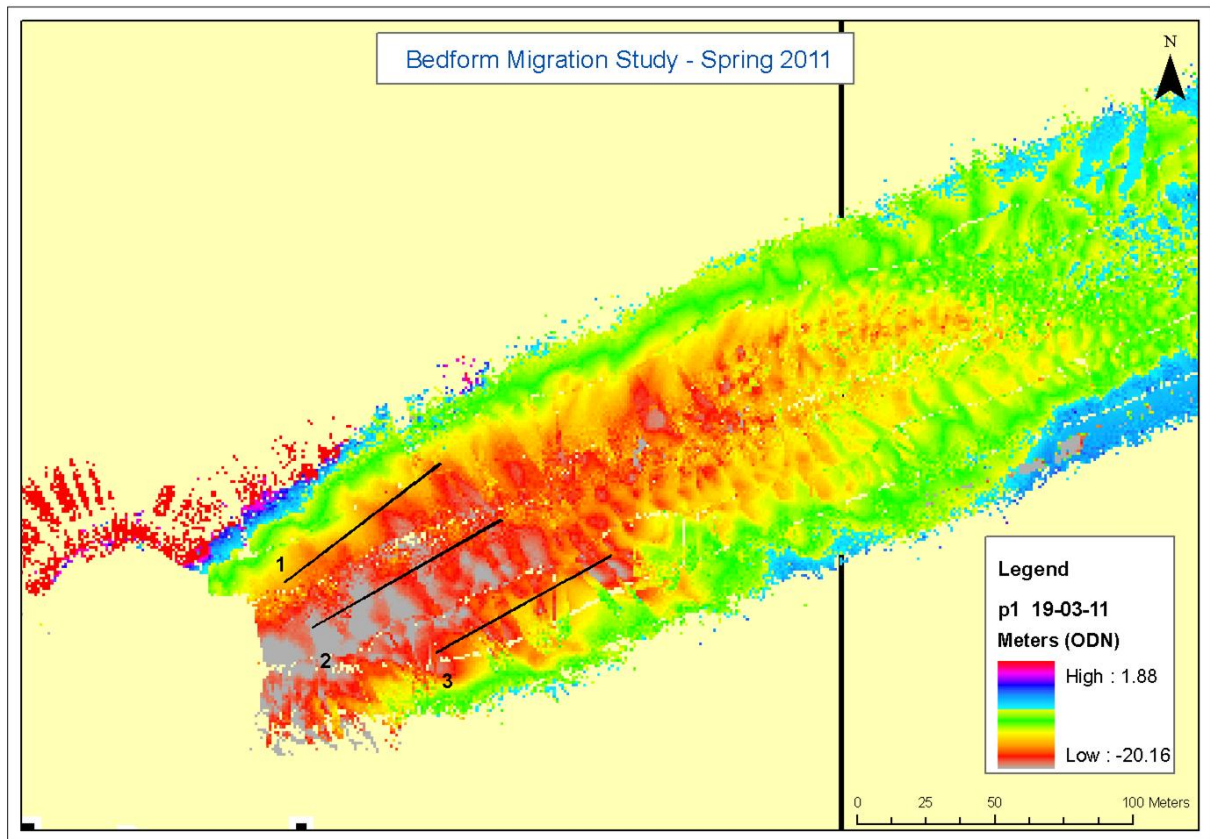


Chapter 3 appendix 1 Figure 12: Neap & Spring Velocity stage plots for the above elevation analyses.

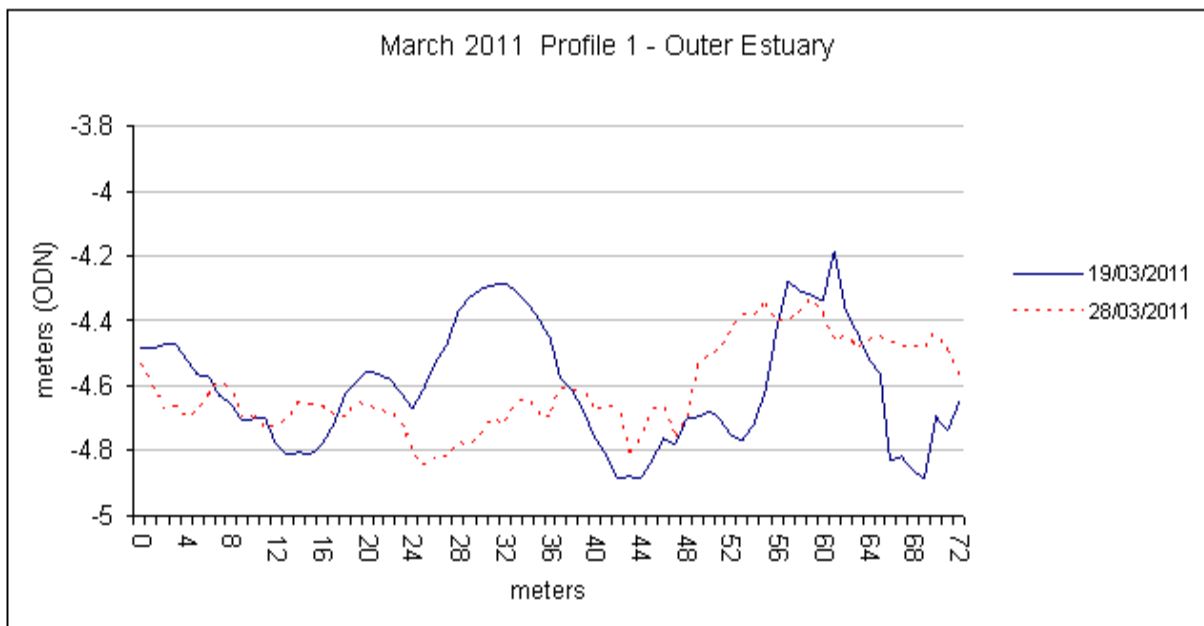
The velocity stage plots (Figure 12) show more symmetry for the spring cycle than the neap. Peak velocities are centred around the overtides, with flood velocities tending towards high water, especially on the neap cycle.

Appendix 2

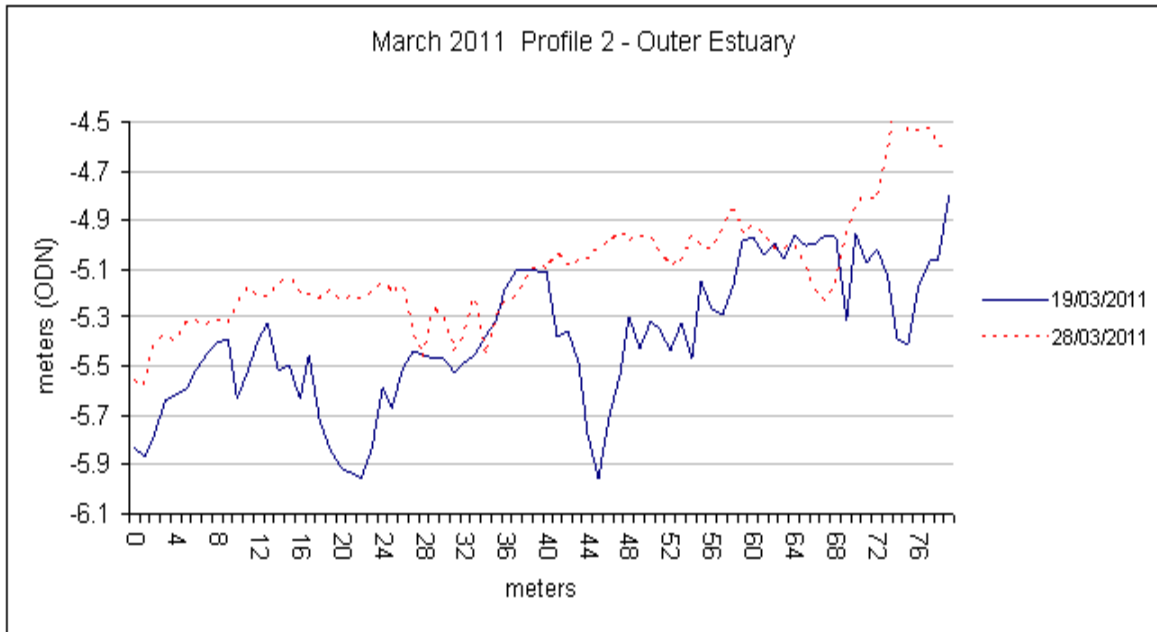
Outer Estuary Bed-form Tracking



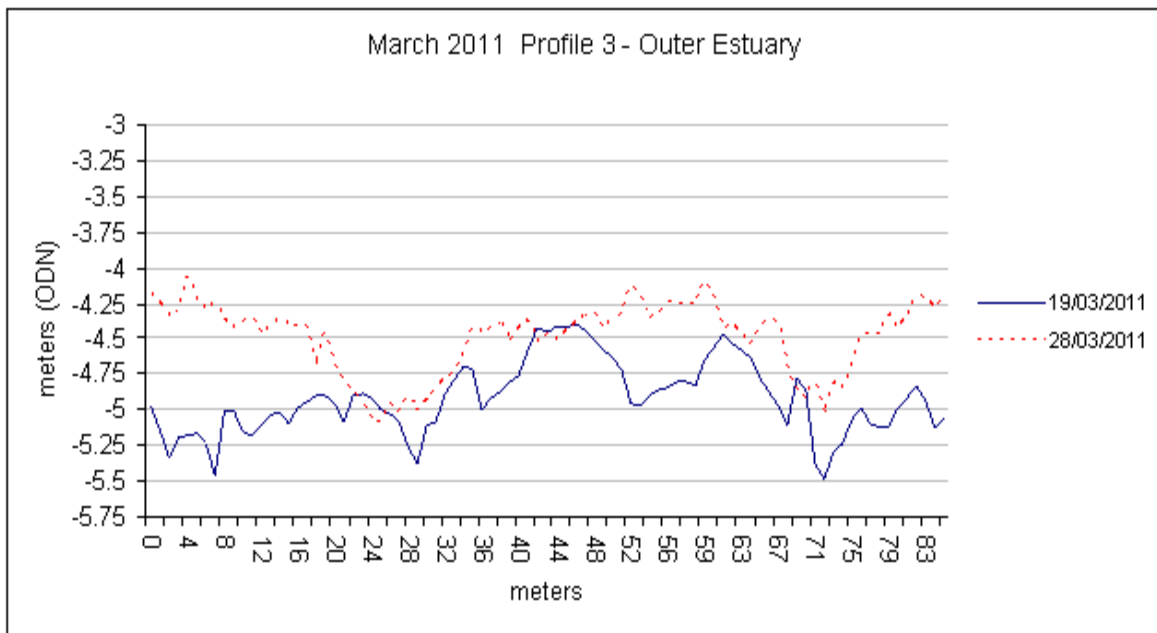
Chapter 3 appendix 2 Figure 1: Location of the cross-sectional profiles for March 2011.



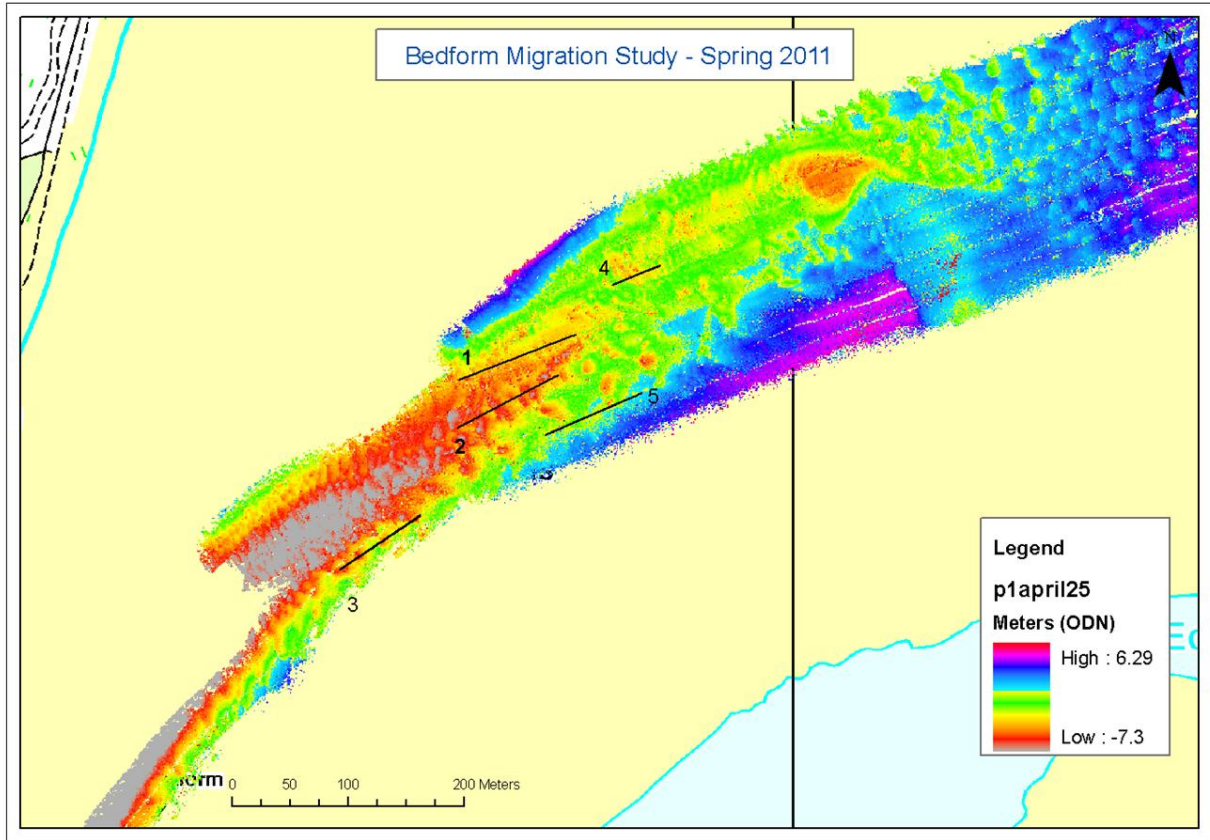
Chapter 3 appendix 2 Figure 2: Cross-sectional profile 1 for March 2011, showing the ambiguity between corresponding bed-forms. Left-right is SW-NE and landward to sea-ward respectively.



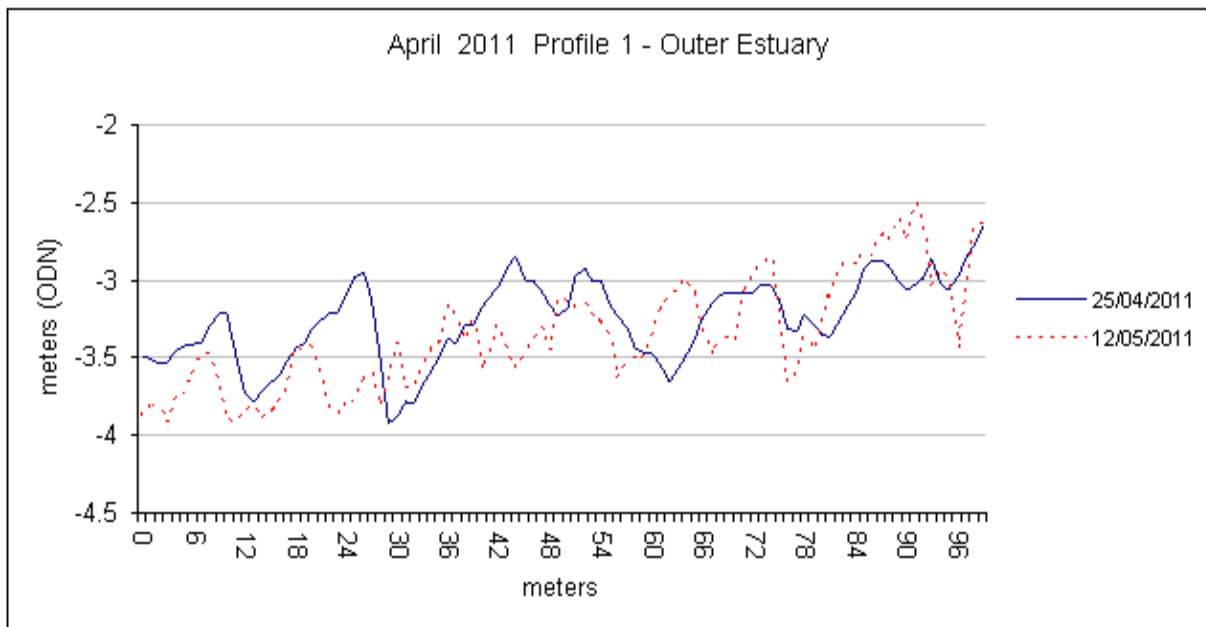
Chapter 3 appendix 2 Figure 3: Cross-sectional profile 2 for March 2011. Not used due to ambiguity.



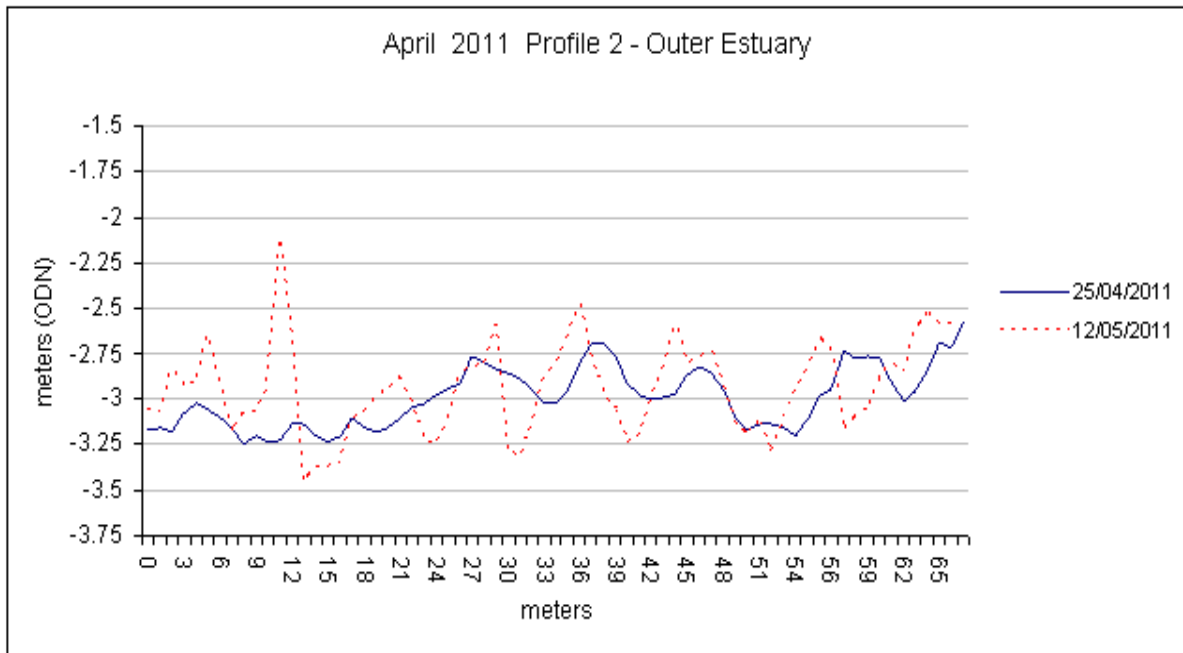
Chapter 3 appendix 2 Figure 4: Cross-sectional profile 3 for March 2011. Showing reversal in movement (data 28/03/11).



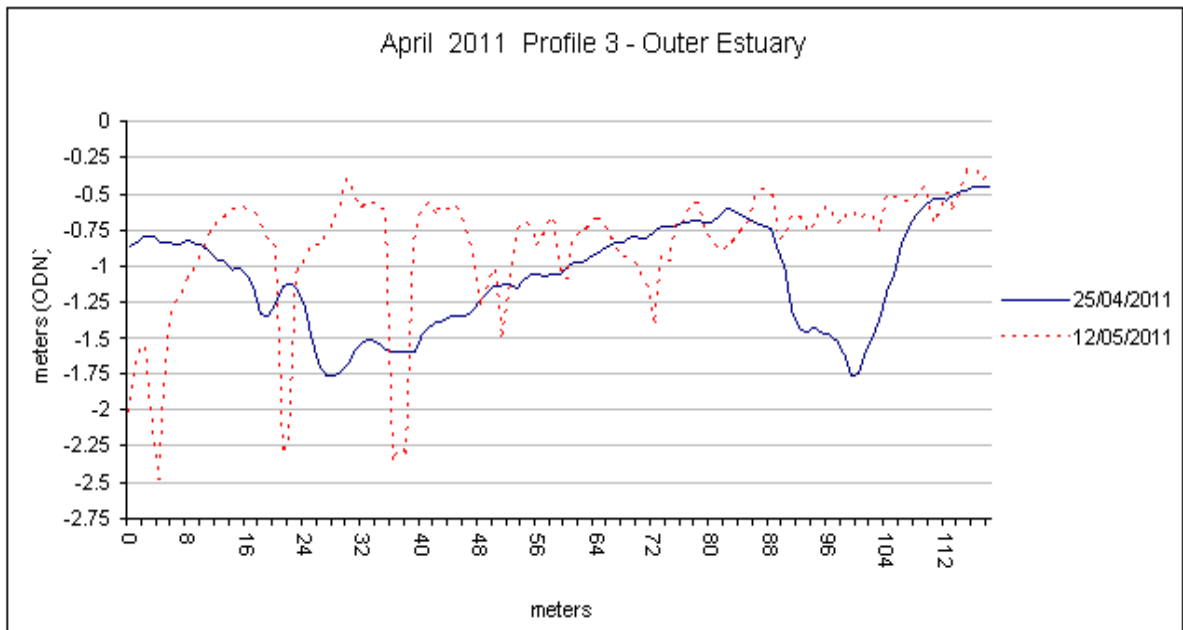
Chapter 3 appendix 2 Figure 5: Location of the cross-sectional profiles for 25/04/11 to 12/05/11.



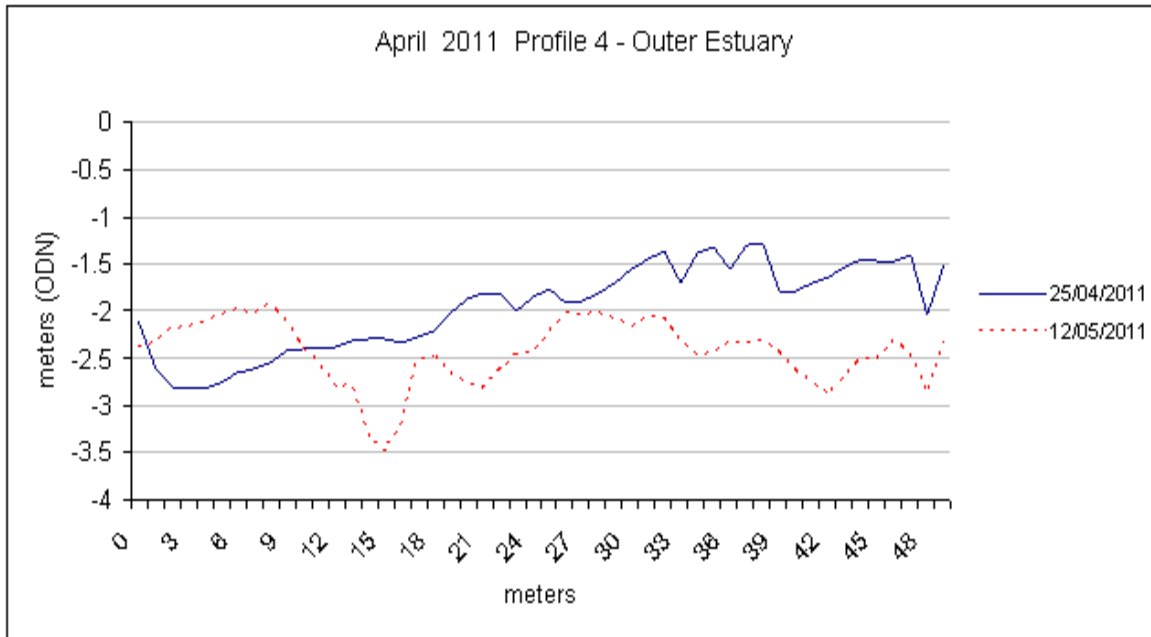
Chapter 3 appendix 2 Figure 6: Cross-sectional profile 1 for April/May 2011.



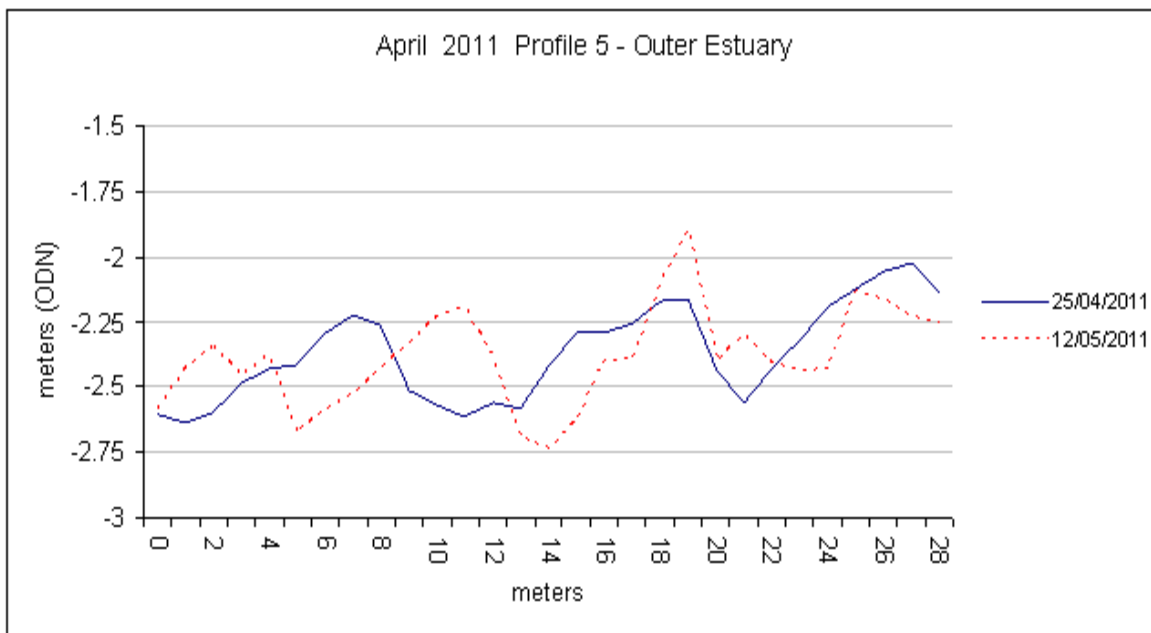
Chapter 3 appendix 2 Figure 7: Cross-sectional profile 2 for April/May 2011.



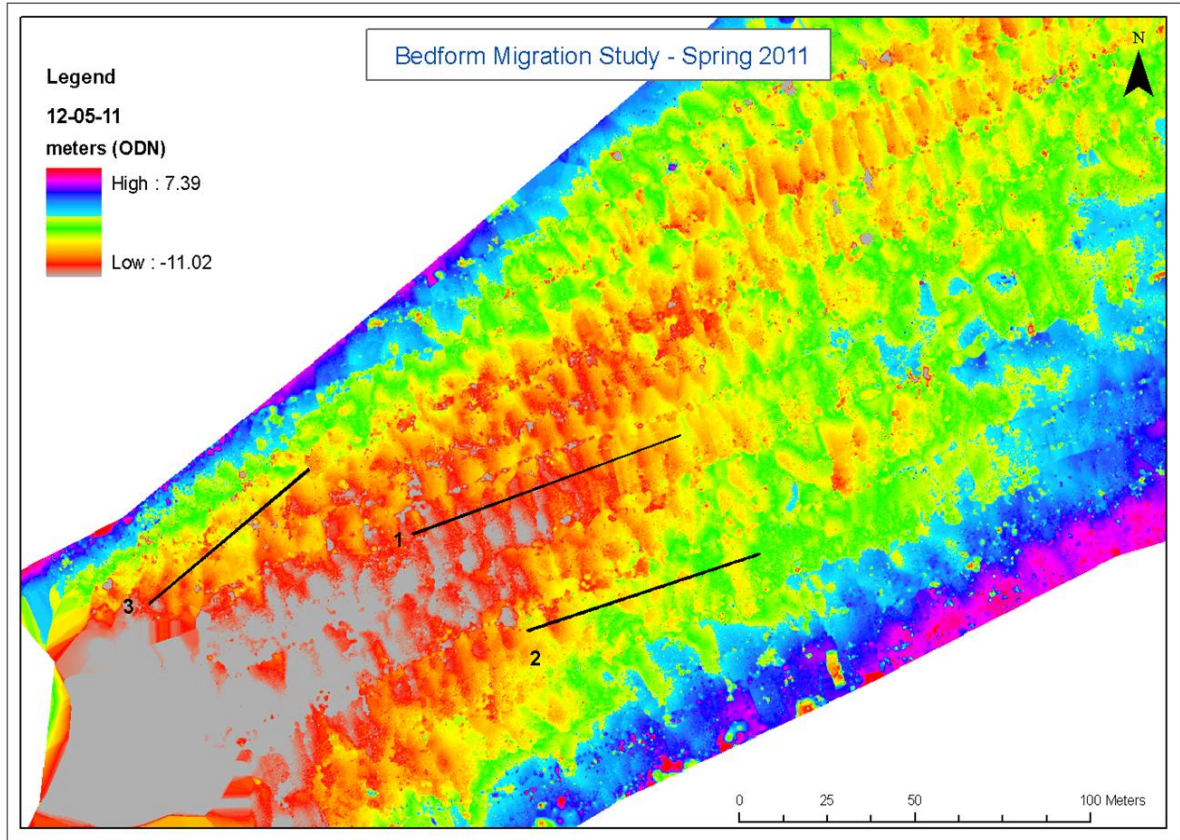
Chapter 3 appendix 2 Figure 8: Cross-sectional profile 3 for April/May 2011.



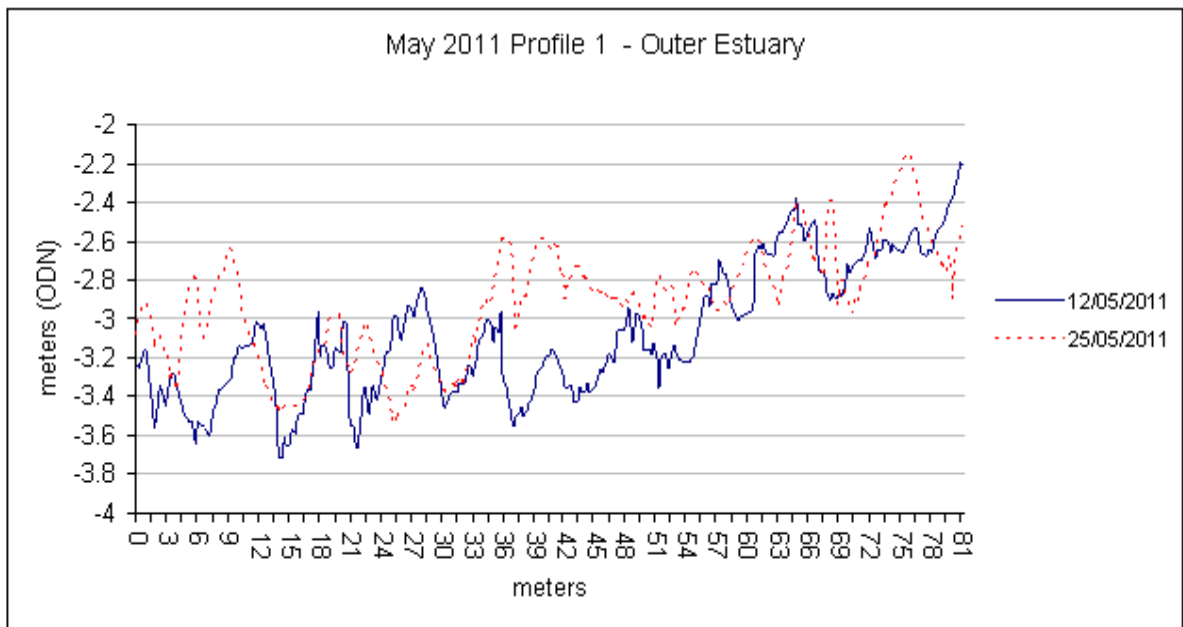
Chapter 3 appendix 2 Figure 9: Cross-sectional profile 4 for April/May 2011.



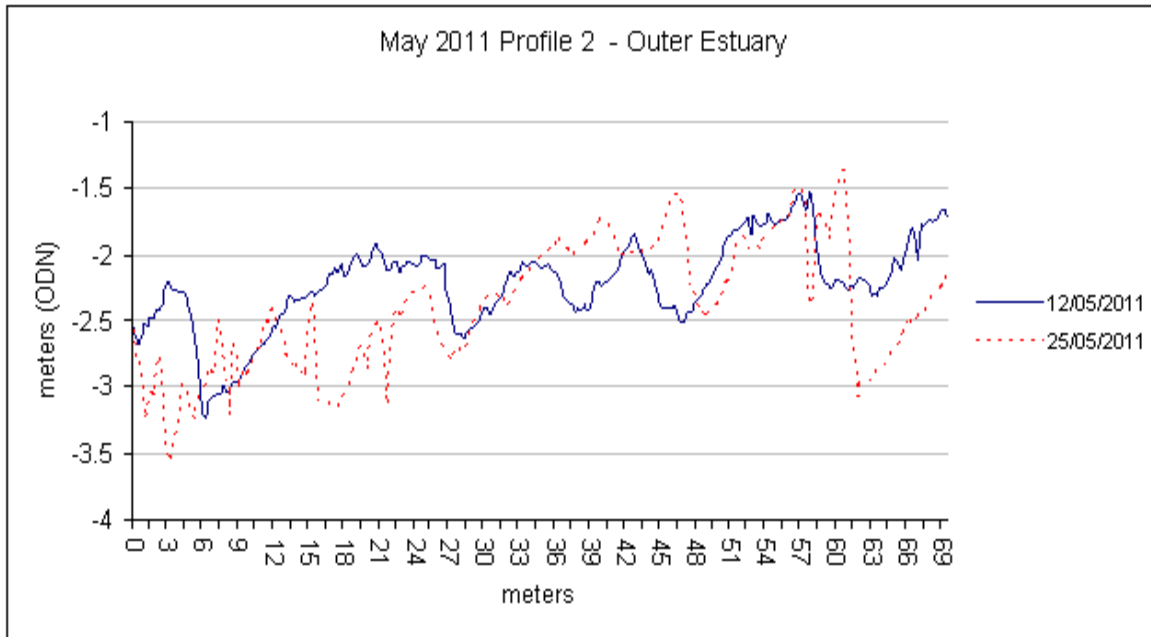
Chapter 3 appendix 2 Figure 10: Cross-sectional profile 5 for April/May 2011.



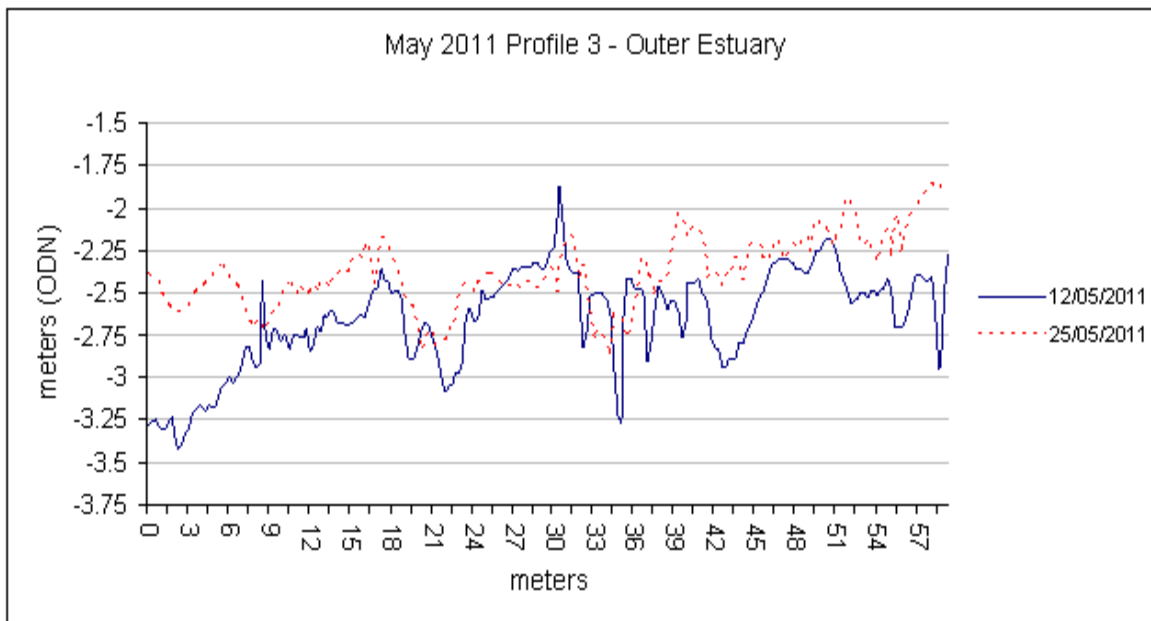
Chapter 3 appendix 2 Figure 11: Location of the cross-sectional profiles for 12/05/11 to 25/05/11.



Chapter 3 appendix 2 Figure 12: Cross-sectional profile 1 for 12/05/11 to 25/05/11.

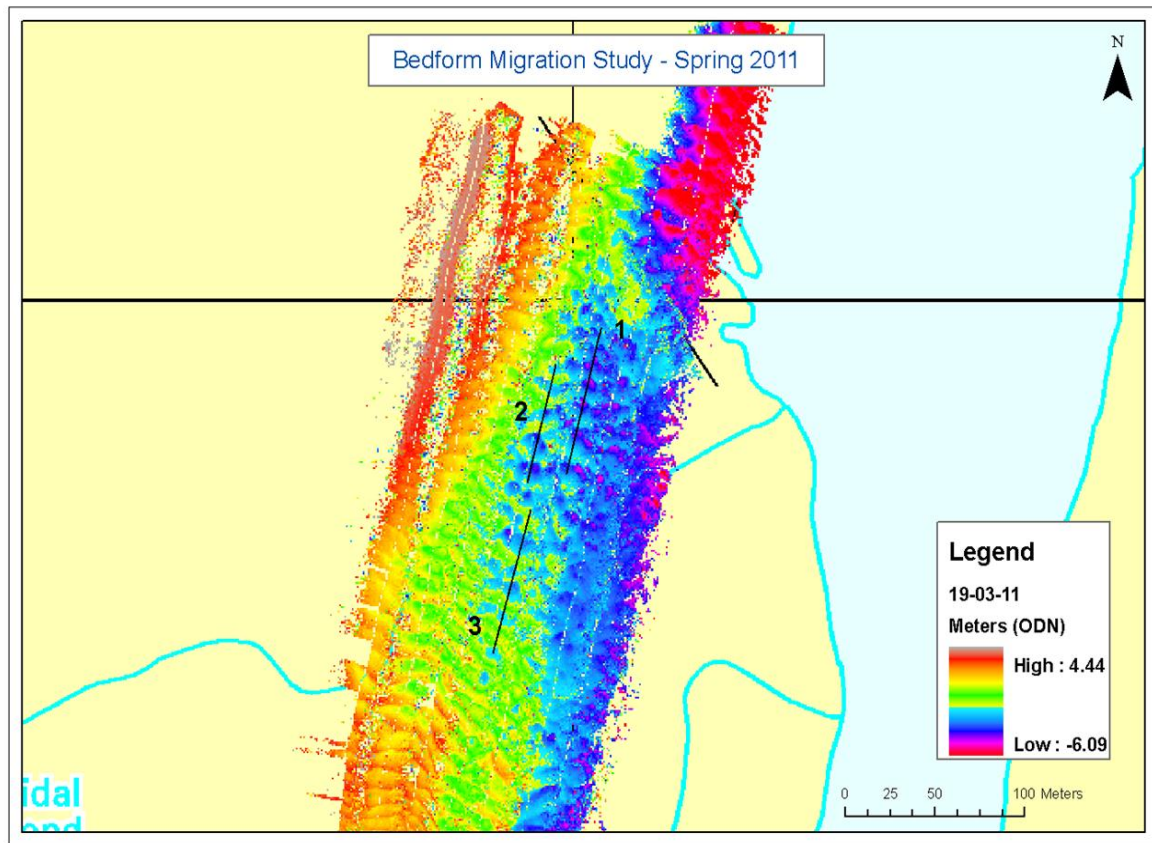


Chapter 3 appendix 2 Figure 13: Cross-sectional profile 2 for 12/05/11 to 25/05/11.

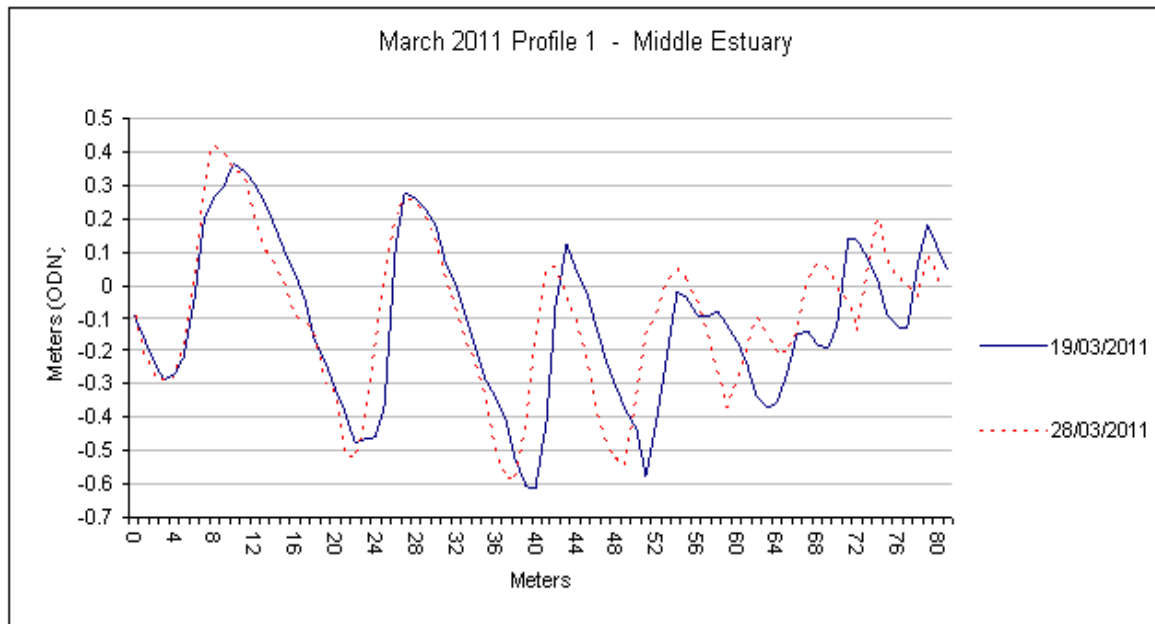


Chapter 3 appendix 2 Figure 14: Cross-sectional profile 3 for 12/05/11 to 25/05/11.

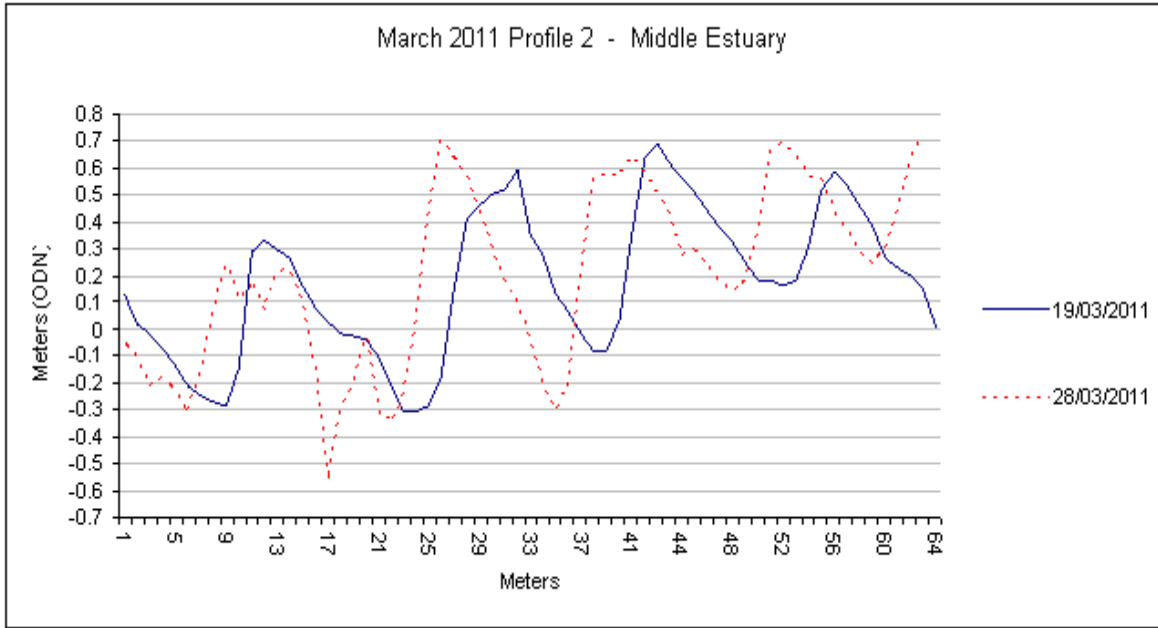
Middle Estuary Bed-form Tracking



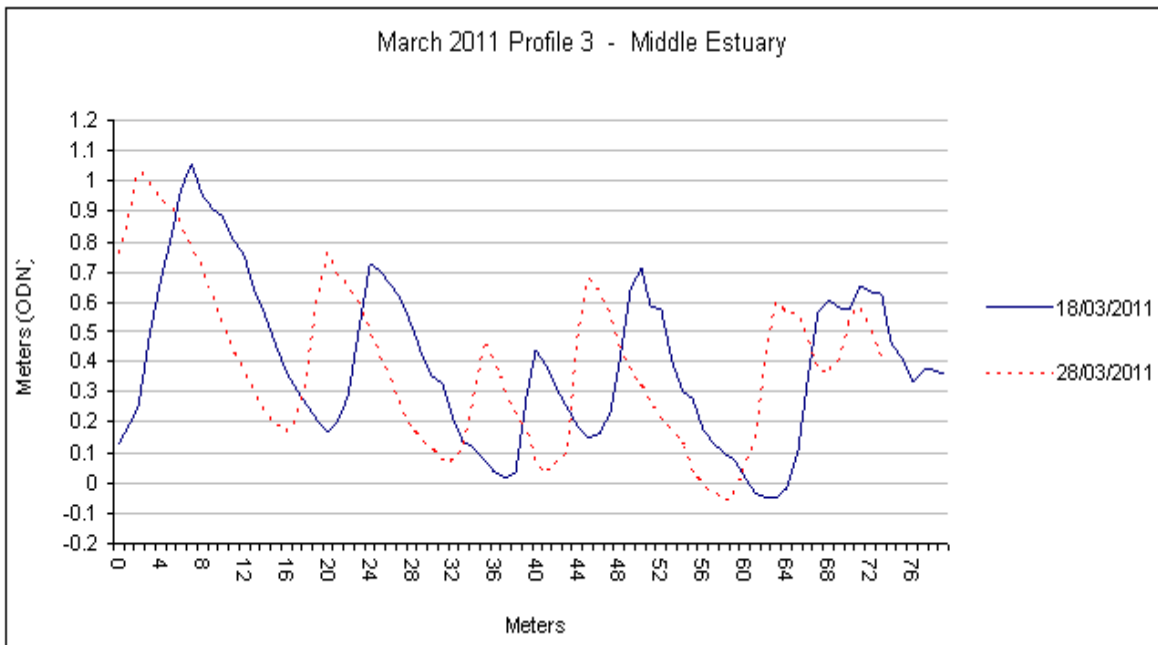
Chapter 3 appendix 2 Figure 15: Location of the cross-sectional profiles for 19/03/11 to 28/03/11



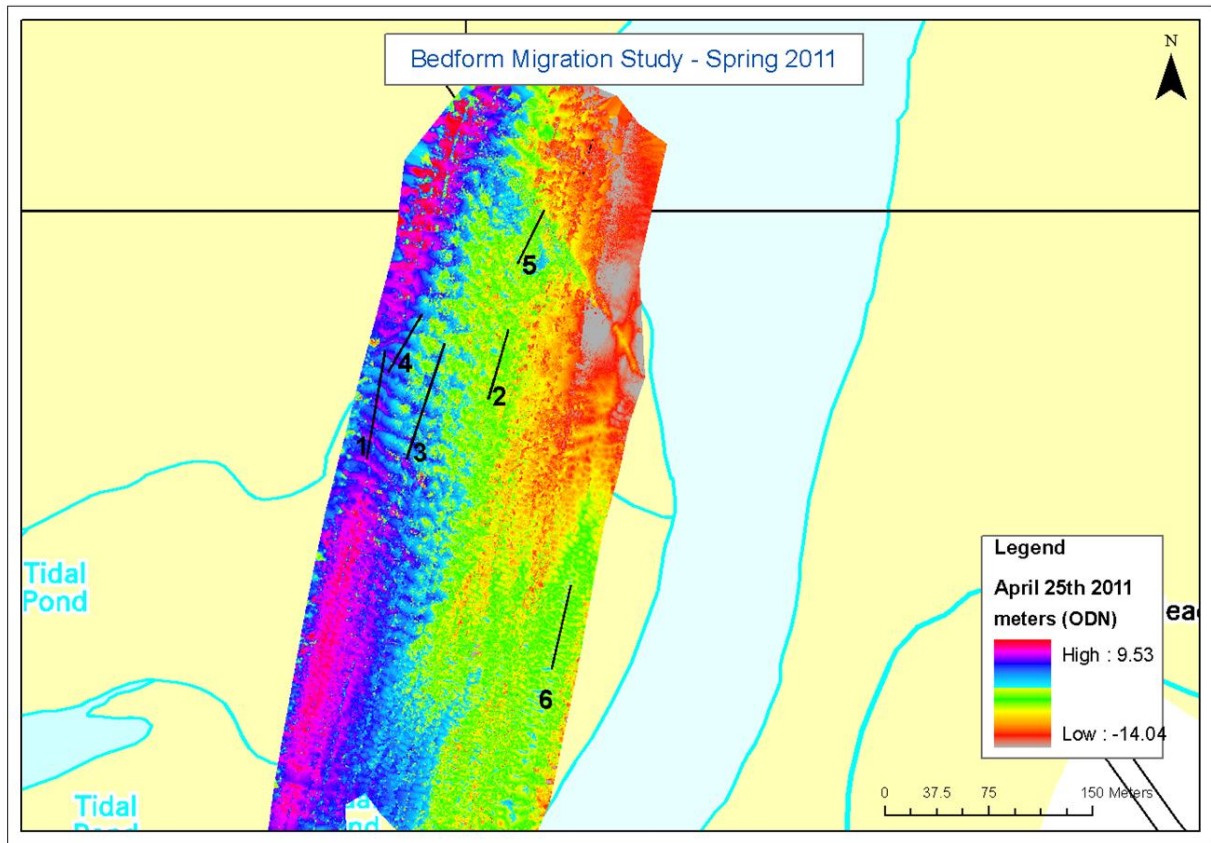
Chapter 3 appendix 2 Figure 16: Cross-sectional profile 1 for 19/03/11 to 28/03/11.



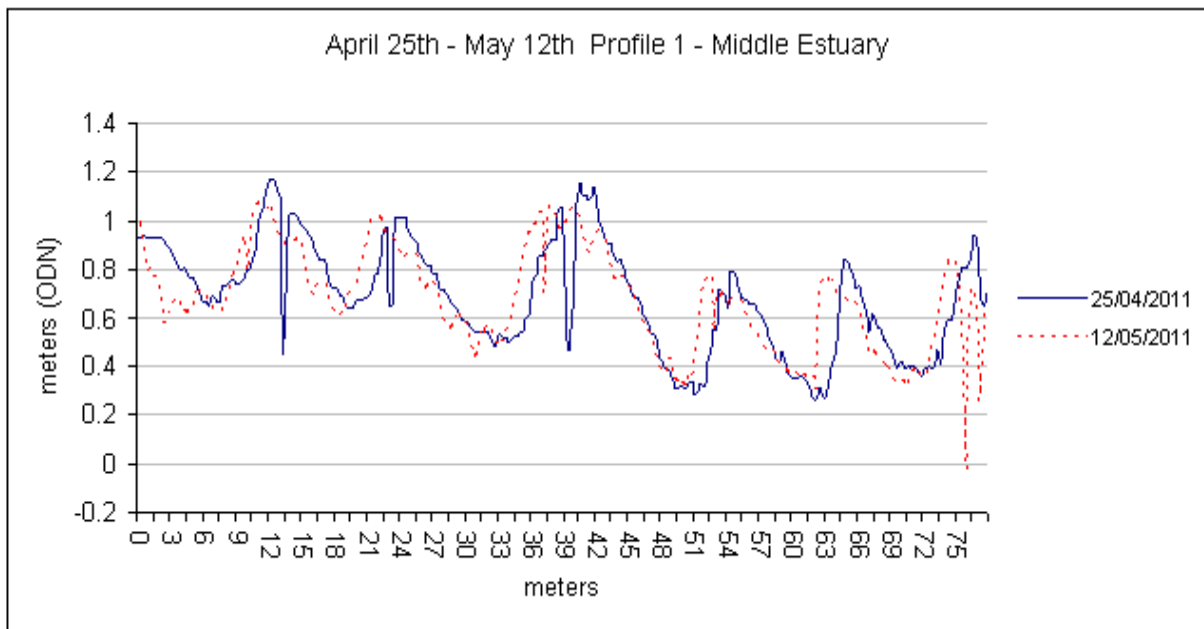
Chapter 3 appendix 2 Figure 17: Cross-sectional profile 2 for 19/03/11 to 28/03/11.



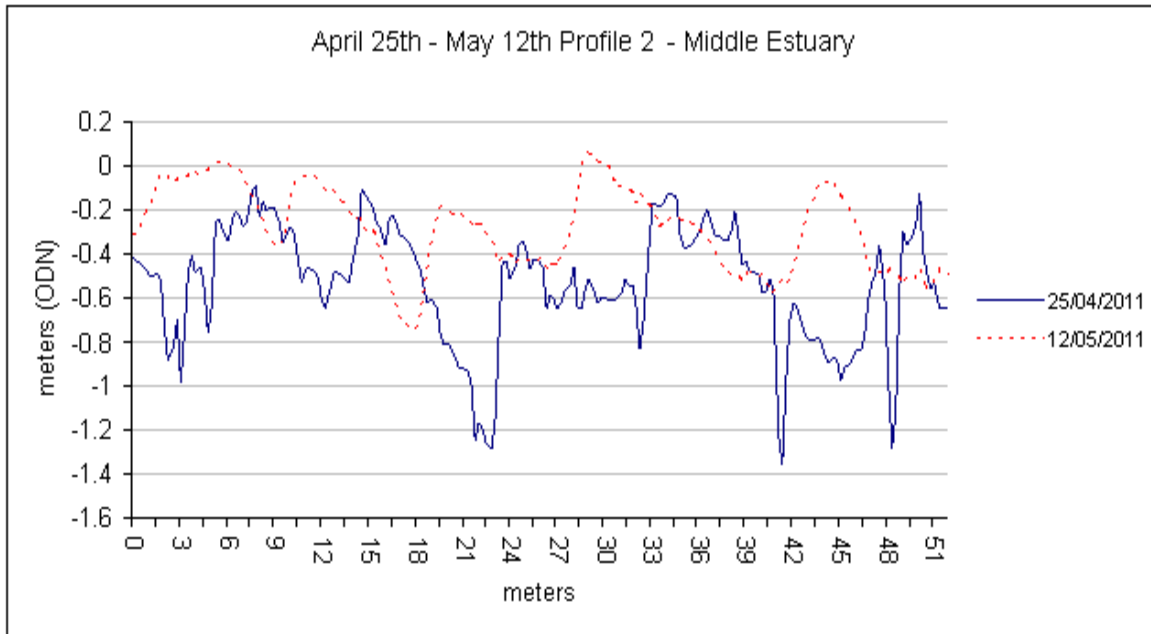
Chapter 3 appendix 2 Figure 18: Cross-sectional profile 3 for 19/03/11 to 28/03/11.



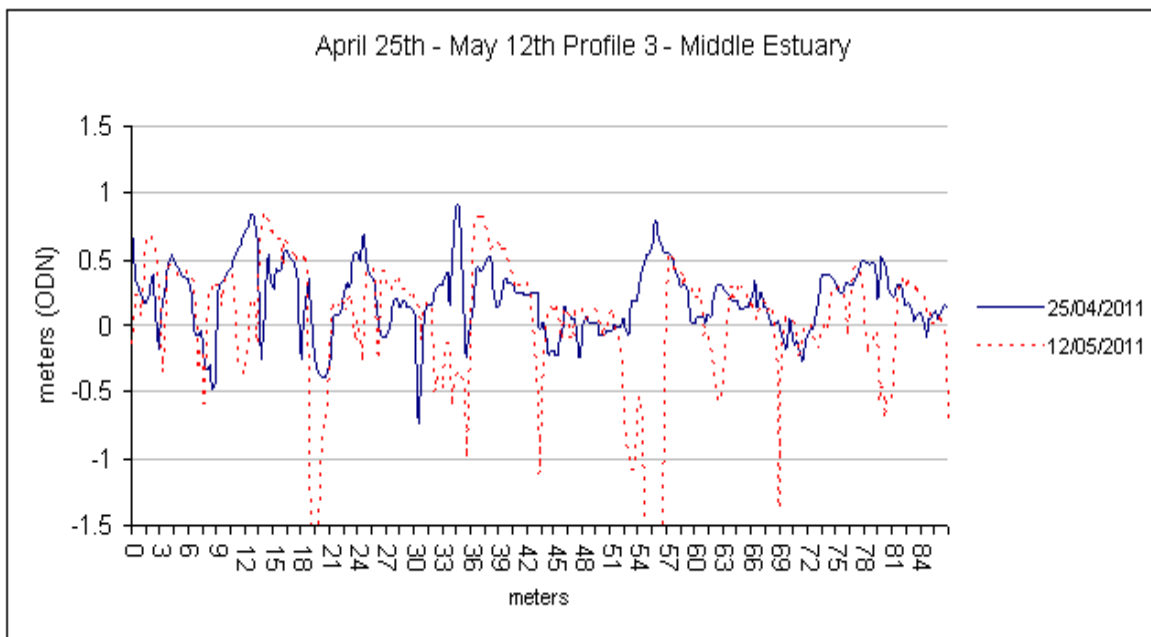
Chapter 3 appendix 2 Figure 19: Location of the cross-sectional profiles for 25/04/11 to 25/05/11.



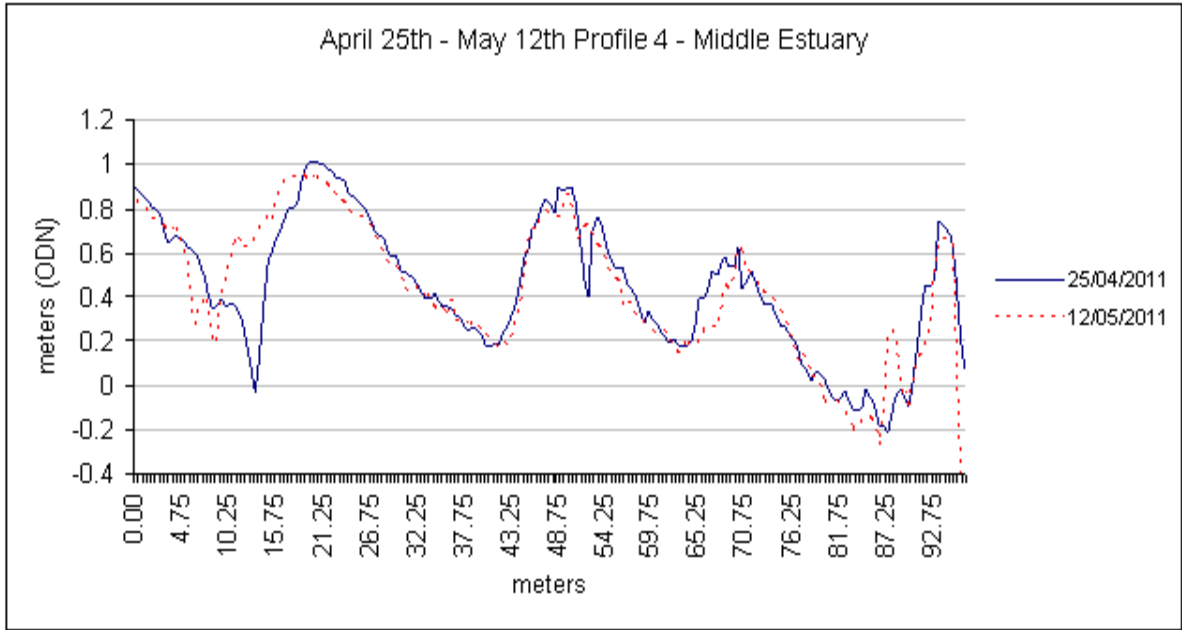
Chapter 3 appendix 2 Figure 20: Cross-sectional profile 1 for 19/03/11 to 28/03/11.



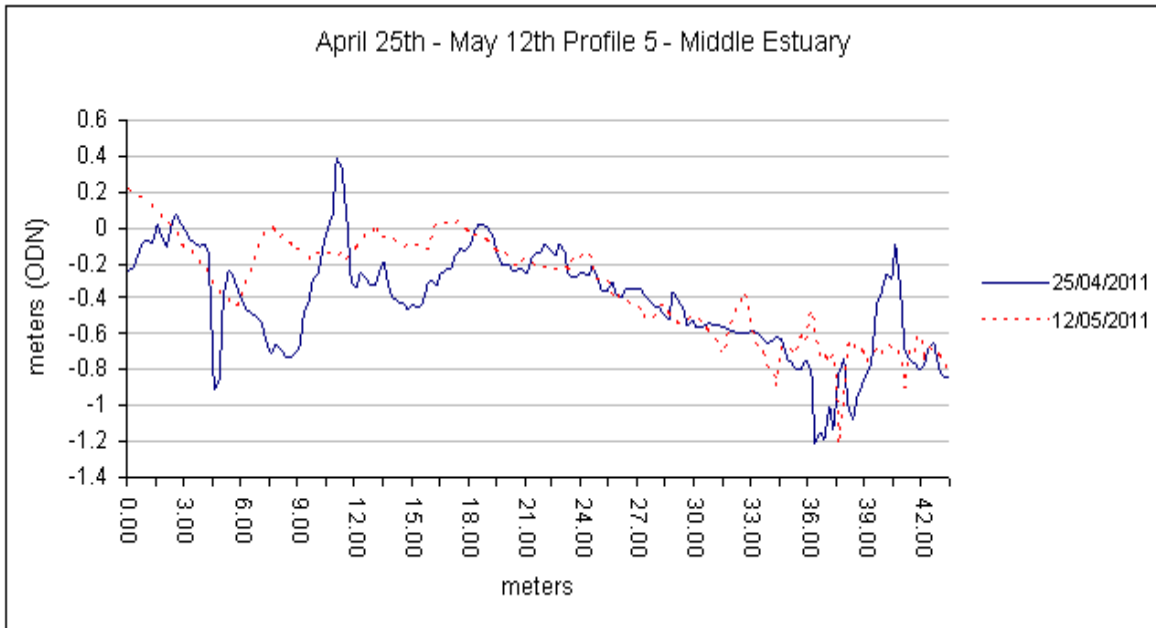
Chapter 3 appendix 2 Figure 21: Cross-sectional profile 2 for 19/03/11 to 28/03/11.



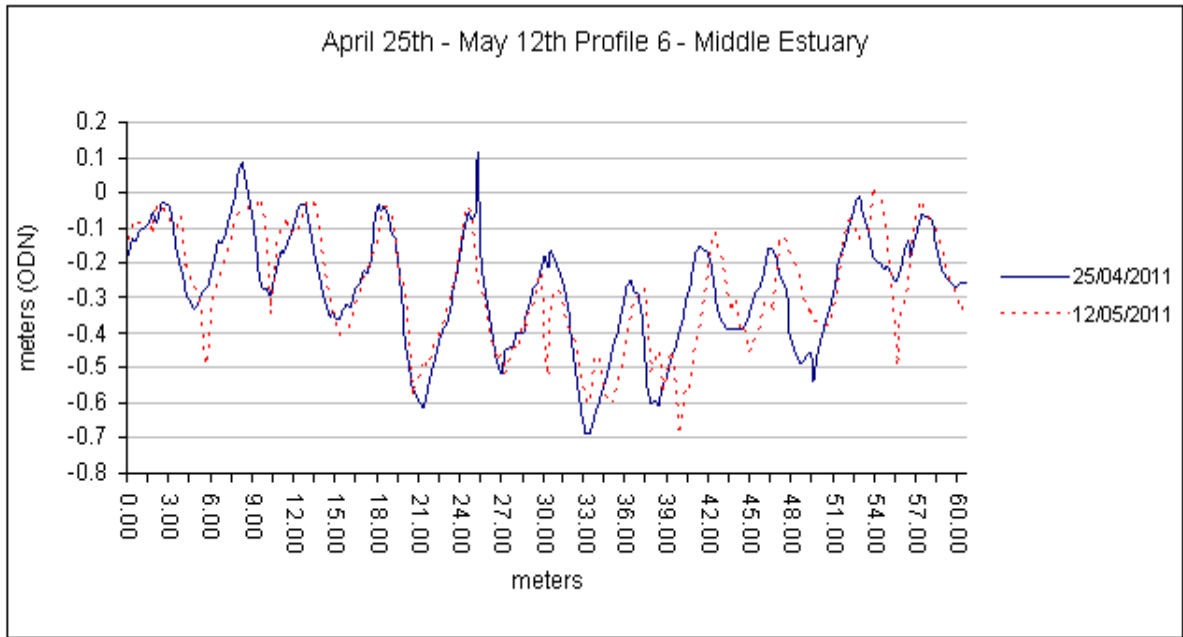
Chapter 3 appendix 2 Figure 22: Cross-sectional profile 3 for 19/03/11 to 28/03/11.



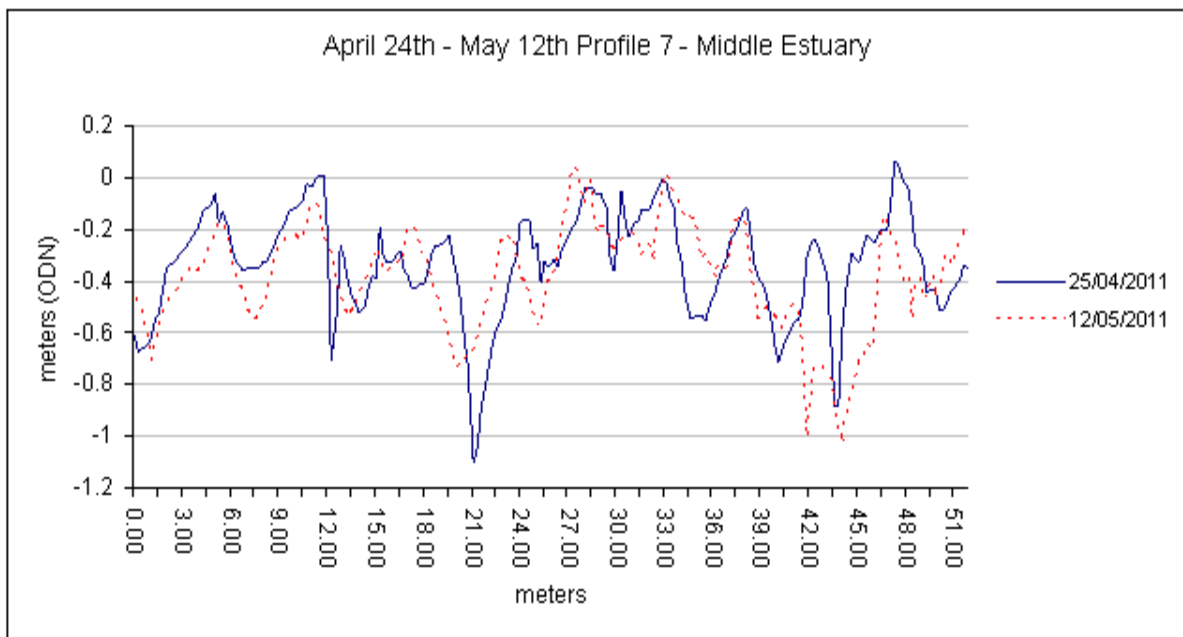
Chapter 3 appendix 2 Figure 23: Cross-sectional profile 4 for 19/03/11 to 28/03/11.



Chapter 3 appendix 2 Figure 24: Cross-sectional profile 5 for 19/03/11 to 28/03/11.



Chapter 3 appendix 2 Figure 25: Cross-sectional profile 5 for 19/03/11 to 28/03/11.



Chapter 3 appendix 2 Figure 26: Cross-sectional profile 5 for 19/03/11 to 28/03/13

3.6.1. References

Section 3.1 Tidal Asymmetry Analysis

- AL-Anezi, K., Somerfield, C., Mee, D. & Hilal, N. 2008. Parameters affecting the solubility of carbon dioxide in seawater at the conditions encountered in MSF desalination plants. *Desalination*, 222, 548-571.
- Attrill, M. J. & Rundle, S. D. 2002. Ecotone or Ecocline: Ecological Boundaries in Estuaries. *Estuarine, Coastal and Shelf Science*, 55, 929-936.
- Blatt, H., Middleton, G. & Murray, R. 1981. Origin of Sedimentary Rocks. Prentice-Hall, Englewood Cliffs, N. J.,.
- DEFRA 2008. Tidal Asymmetry analysis: Analysis and Modelling guide, V1.0 ©ABPmer.: DEFRA: Environment Agency, Marine Environmental Research.
- Dronkers, J. J. 1986. Tidal asymmetry and estuarine morphology. *Journal of Sea Research*, 20(2/3):.
- Dyer, K. R. 1995. Chapter 14 Sediment Transport Processes in Estuaries. *In: Perillo, G. M. E. (ed.) Developments in Sedimentology*. Elsevier.
- Eastwood, K. M. 1977. Some Aspects of the Sedimentology of the Superficial Deposits of the Eden Estuary, Fife, Scotland. PhD., University of St Andrews.
- Elliott, M., Whitfield, A. K., Potter, I. C., Blaber, S. J. M., Cyrus, D. P., Nordlie, F. G. & Harrison, T. D. 2007. The guild approach to categorizing estuarine fish assemblages: a global review. *Fish and Fisheries*, 8, 241-268.
- ESRI © 1995–2008. Environmental Systems Research Institute (ESRI), Inc. California. USA. ARCMAP Version 9.3.
- Friedrichs, C. T. & Aubrey, D. G. 1988. Non-Linear Tidal Distortion in Shallow Well-Mixed Estuaries - A Synthesis. *Estuarine Coastal and Shelf Science*, 27, 521-545.
- Friedrichs, C. T., Aubrey, D. G. & Speer, P. E. 1990. Impacts of relative sea-level rise on evolution of shallow estuaries.
- FSBI 2007. Climate change and the fishes of Britain and Ireland: Briefing Paper 4.: Fisheries Society of the British Isles, Granta Information Systems, 82A High street, Sawston, Cambridge, CB2 4h, UK.
- Jarvis, J. & Riley, C. 1987. Sediment transport in the mouth of the Eden estuary. *Estuarine, Coastal and Shelf Science*, 24, 463-481.
- Jenkins, G. J., Perry, M.C., and Prior, M.J. 2009. The climate of the United Kingdom and recent trends. Met Office Hadley Centre, Exeter, UK.
- Little, C. 2000. *The Biology of Soft Shores and Estuaries*, Oxford University Press, Oxford.
- Magnuson, J. J., Crowder, L. B. & Medvick, P. A. 1979. Temperature as an Ecological Resource. *American Zoologist*, 19, 331-343.

- MCKie. 1985. A Study of Bedform Migration in the Eden Estuary, North East Fife. M.A, St Andrews.
- Microsoft 2003. Microsoft Office Professional Edition Excel SP3.
- Mosley, L. M., Peake, B. M. and Hunter, K. A. 2010. Modelling of pH and inorganic carbon speciation in estuaries using the composition of the river and seawater end members. *Environmental Modelling & Software*, 25, 1658-1663.
- Mucha, A. P. & Costa, M. H. 1999. Macrozoobenthic community structure in two Portuguese estuaries: Relationship with organic enrichment and nutrient gradients. *Acta Oecologica*, 20, 363-376.
- Pugh, D. T. 2004. Changing sea levels. Effects of tides, weather and climate. *Cambridge University Press*, 280 pp.
- Robins, P. & Davies, A. 2010. Morphological controls in sandy estuaries: the influence of tidal flats and bathymetry on sediment transport. *Ocean Dynamics*, 60, 503-517.
- Wang, Z. B., Jeuken, C. & De Vriend, H. J. 1999. Tidal asymmetry and residual sediment transport in estuaries. A literature study and application to the Western Scheldt. WL delft hydraulics.

Section 3.2 Sediment Transport: Bedload

- Anthony, E. J., M.-H. Ruz, and S. Vanhee. 2009. Aeolian sand transport over complex intertidal bar-trough beach topography. *Geomorphology* 105: 95-105.
- Bagnold, R.A., 1966. An Approach to the Sediment Transport Problem From General Physics. in *Physiographic and Hydraulic Studies of Rivers: Geological Survey Professional Paper 422-I*, United States Government Printing Office, Washington.
- Bates, C.R. & Oakley, D.J., 2004. Bathymetric sidescan investigation of sedimentary features in the Tay Estuary, Scotland, *International Journal of Remote Sensing*, 25, 5089-5104.
- Besio, G., Blondeaux, P., Brocchini, M., Hulscher, S., Idier, D., Knaapen, M.A.F., Nemeth, A.A., Roos, P.C. & Vittori, G., 2008. The morphodynamics of tidal sand waves: A model overview, *Coastal Engineering*, 55, 657-670.
- Besio, G., Blondeaux, P., Brocchini, M. & Vittori, G., 2004. On the modeling of sand wave migration, *Journal of Geophysical Research-Oceans*, 109.
- Besio, G., Blondeaux, P. & Vittori, G., 2006. On the formation of sand waves and sand banks, *Journal of Fluid Mechanics*, 557, 1-27.
- Blatt, H., Middleton, G. & Murray, R., 1981. *Origin of Sedimentary Rocks*, pp. 1980, 1782 pp. Prentice-Hall, Englewood Cliffs, N. J.,.
- Boyd, R., Dalrymple, R. & Zaitlin, B.A., 1992. Classification of Clastic Coastal Depositional-Environments, *Sedimentary Geology*, 80, 139-150.

- Dalrymple, R.W., Knight, R.J. & Lambiase, J.J., 1978. Bedforms and their Hydraulic Stability Relationships in a Tidal Environment, Bay of Fundy, Canada, *Nature*, 275, 100-104.
- Dalrymple, R.W. & Rhodes, R.N., 1995. Chapter 13 Estuarine Dunes and Bars. in *Developments in Sedimentology*, pp. 359-422, ed. Perillo, G. M. E. Elsevier.
- Dinehart, R.L., 2002. Bedform movement recorded by sequential single beam surveys in tidal rivers, *Journal of Hydrology*, 258, 25-39.
- Dyer, K.R., 1972. 2 Sedimentation in Estuaries. in *The Estuarine Environment: The inaugural symposium of the Estuarine and Brackish-water Biological Association.*, pp. 10-32, eds. Barnes, R. S. K. & Green, J. Applied Science Publishers (London).
- Eastwood, K.M., 1977. Some Aspects of the Sedimentology of the Superficial Deposits of the Eden Estuary, Fife, Scotland., PhD., University of St Andrews.
- Engel, p. & lau, Y.L., 1980. Computation of Bed Load Using Bathymetric Data, pp. 369-380 *Journal of the Hydraulics Division*.
- ESRI, © 1995–2008. Environmental Systems Research Institute (ESRI), Inc. California. USA. ARCMAP Version 9.3.
- Ferentinos, G. & McManus, J., 2009. Nearshore Processes and Shoreline Development in St Andrews Bay, Scotland, U.K, edn, Vol., pp. Pages, Blackwell Publishing Ltd.
- Flemming, B.W., 2000. The role of grain size, water depth and flow velocity as scaling factors in: Trentesaux, A. *et al.* (Ed.) (2000). *Marine Sandwave Dynamics*, International Workshop, March 23-24 2000, University of Lille 1, France. Proceedings.
- Hoekstra, P., Bell, P., van Santen, P., Roode, N., Levoy, F. & Whitehouse, R., 2004. Bedform migration and bedload transport on an intertidal shoal, *Continental Shelf Research*, 24, 1249-1269.
- Idier, D., Ehrhold, A. & Garlan, T., 2002. Morphodynamics of an undersea sandwave of the Dover Straits, *Comptes Rendus Geoscience*, 334, 1079-1085.
- Jarvis, J. & Riley, C., 1987. Sediment transport in the mouth of the Eden estuary, *Estuarine, Coastal and Shelf Science*, 24, 463-481.
- Jinchi, H., 1992. Application of sandwave measurements in calculating bed load discharge Erosion and Sediment Transport Monitoring Programmes in River Basins. (Proceedings of the Oslo Symposium, August 1992) IAHS Publ. no. 210.
- Knaapen, M.A.F., Henegouw, C.N.V. & Hu, Y.Y., 2005. Quantifying bedform migration using multi-beam sonar, *Geo-Marine Letters*, 25, 306-314.
- McKie, 1985. A Study of Bedform Migration in the Eden Estuary, North East Fife., M.A, St Andrews.
- Microsoft, 2003. Microsoft Office Professional Edition Excel SP3.
- Nemeth, A.A., Hulscher, S. & de Vriend, H.J., 2002. Modelling sand wave migration in shallow shelf seas, *Continental Shelf Research*, 22, 2795-2806.

- Oakley, D.J., 2003. An acoustic investigation of the bedforms and their distribution in the middle and outer Tay Estuary. BSc. Honours Dissertation. University of St Andrews. School of Geography & Geosciences.
- Pugh, D.T., 2004. Changing sea levels. Effects of tides, weather and climate, Cambridge University Press, 280 pp.
- Rubin, D.M. & McCulloch, D.S., 1980. Single and Superimposed Bedforms - A Synthesis of San-Fansisco Bay and Flume Observations, *Sedimentary Geology*, 26, 207-231.
- Simons, D.B., Richardson, E.V. & Nordin Jr, C.F., 1965. Bedload equation for ripples and dunes, pp. 9US Geological Survey Profesional Paper 462H.
- Sternberg, R., 1972. Predicting initial motion and bedload transport of sediment particles in the shallow marine environment. in *Shelf Sediment Transport: Process and Pattern*, pp. 61-82Dowden, Hutchinson and Ross INC. Stroudsburg, Pennsylvania.
- Ten Brinke, W.B.M., Wilbers, A.W.E. & Wesseling, C., 1999. Dune growth, decay and migration rates during a large-magnitude flood at a sand and mixed sand-gravel bed in the Dutch Rhine river system, *Fluvial Sedimentology* Vi, 28, 15-32.
- Wal, A., and J. McManus. 1993. Wind regime and sand transport on a coastal beach-dune complex, Tentsmuir, eastern Scotland, p. 159-171. Geological Society.
- Wever, T.F., 2004. Bedforms and Bedform Migration:A Data Review. in *Marine Sandwave and River Dune Dynamics*, Enschede, the Netherlands.
- Wewetzer, S.F.K. & Duck, R.W., 1996. Side-scan sonograph from the middle reaches of the Tay Estuary, Scotland, *International Journal of Remote Sensing*, 17, 3539-3540.

Section 3.3 Salinity

- Centre for Ecology & Hydrology 2010. NERC. National River Flow Archive: 18011- Forth at Craigforth.
- Conlan, K., Wade, T., Ormerod, S., Lane, S., Durance, I. & Yu, D. 2007. Preparing for climate change impacts on freshwater ecosystems (PRINCE) Science Report: SC030300/SR. © Environment Agency, Rio House, Waterside Drive, Aztec West, Almondsbury, Bristol, BS32 4UD. Tel:01454 624400 Fax: 01454 624409.
- CRAN 2011. R Statistical Software <http://cran.r-project.org/>. **R version 2.13.2** ed.
- Dronkers, J. J. 1986. Tidal asymmetry and estuarine morphology. *Journal of Sea Research*, 20(2/3):.
- Eastwood, K. M. 1977. Some Aspects of the Sedimentology of the Superficial Deposits of the Eden Estuary, Fife, Scotland. PhD., University of St Andrews.
- Gosling, R. 2011. The impact of climate change on water temperature and ecological health in Scottish rivers, .

Loutit, S. 1991. Water Circulation and Sedimentation within the Upper Eden Estuary, N.E Fife, Scotland. BSc. Geology Honours Dissertation. St Andrews University, Department of Geology.

Pethick, J. 1994. Estuaries and Wetlands - Function and Form. *Wetland Management*, 75-87.

Pugh, D. T. 2004. Changing sea levels. Effects of tides, weather and climate. *Cambridge University Press*, 280 pp

Section 3.4 Chapter Discussion

Brown, J. M. & Davies, A. G. 2010. Flood/ebb tidal asymmetry in a shallow sandy estuary and the impact on net sand transport. *Geomorphology*, 114, 431-439.

Dronkers, J. J. 1986. Tidal asymmetry and estuarine morphology. *Journal of Sea Research*, 20(2/3):.

Eastwood, K. M. 1977. Some Aspects of the Sedimentology of the Superficial Deposits of the Eden Estuary, Fife, Scotland. PhD., University of St Andrews.

Loutit, S. 1991. Water Circulation and Sedimentation within the Upper Eden Estuary, N.E Fife, Scotland. BSc. Geology Honours Dissertation. St Andrews University, Department of Geology.

Pethick, J. 1994. Estuaries and Wetlands - Function and Form.. *Wetland Management*, 75-87.

CHAPTER 4

4. BIOTIC RESPONSES

Chapter aim

This chapter aims to capture a relative trajectory of 'estuary health' through a broad overview of;

- Ecosystem function within 'asymmetry sensitive zones', estimated through macrofaunal community diversity.
- Adaptation/Acclimatisation: a focus on the response of the keystone species *Zostera noltii*.

Estuarine ecosystems are complex mosaics of interacting habitats within which biophysical and biochemical processes support nutrient cycling and energy flow processes. Spatial variability not only the in benthic habitat but also in terms of salinity, current velocities and nutrient gradients within the water column are responsible for the spatial distribution of populations of phytoplankton, fish and swimming crustaceans, which support a wealth of higher consumers including seals, porpoise, wildfowl, raptors, foxes and man. Estuaries represent valuable habitats not only as a source for food, but as breeding and nursery grounds for wildfowl, fish, seals and as a refugia during harsh weather.

The stability and functioning of ecosystem processes is dependent upon a balanced and stable structure within the food web, loss of species within or across trophic levels may alter key processes that sustain ecosystem health; loss on local scales is thought to be one of the major drivers of environmental change (Cardinale 2012; Hooper *et al.* 2012). Species losses may occur in response to changes in nutrient supply or retention, water circulation, regime shifts in salinity or temperature, energy levels and the spatial extents and distribution of habitat types.

In the preceding chapter, potential changes to abiotic variables were identified in response to climate driven variability through shifts in the asymmetry between river flow and the tidal prism. Altered asymmetry has consequences for energy levels, turbidity, water temperature, salinity and dissolved gasses. Of these, salinity has been identified as an important controlling variable within estuaries for benthic organisms (Attrill and Rundle, 2002) and the relationship between the hydrodynamic regime (defining salinity) with the spatial heterogeneity of benthic organisms explained by observed associations with sediment characteristics (Bolam, 2003, Warwick and Uncles, 1980, Jones, 1950). Additionally though, with predicted changes in seasonality of precipitation, decreased summer rainfall may lead to reduced runoff carrying suspended nutrients, particulate organic matter (POM) and mineral particles into the estuary. With the decreased

freshwater contribution to tidal volume, an increased residence time may be expected before the tide flushes seaward. Conversely during winter, increased precipitation may lead to greater suspended loads being carried into the estuary, although the residence time may be reduced due to tidal dispersion and advection (FSBI, 2007). Pulses of increased nutrient and particulate organic matter input drive benthic primary and secondary production (Boschker *et al.*, 2005, Hopkinson *et al.*, 1999, Hopkinson *et al.*, 1997). The variability in the delivery of nutrients and POM into the estuary and their residence has impacts both in terms of promoting biomass and exerting a bottom up control on heterotrophic production but also in changing the community biodiversity through the dominance of a particular species (e.g. macroalgal mats)

Sustained abiotic changes drive the reorganization of habitats and in turn may lead to the following biological responses: physiological changes or adaptations, shifts in ecological timing/phenology, loss of species near their ecological limits, perturbation of inter species relationships and changes to the spatial distribution and also the connectivity of communities (Day *et al.*, 2008, FSBI, 2007, Hicks *et al.*, 2011, Montoya and Raffaelli, 2010, Walther *et al.*, 2002). Whilst spatial distribution shifts are often the initial response of mobile species (Parmesan and Yohe, 2003), not all organisms are able to relocate in line with the rate of change and thus biodiversity may be reduced with implications for the maintenance of ecosystem processes.

This chapter focuses on identifying change(s) to species distribution patterns, temporally and/or spatially, with the aim of linking the patterns found with those of shifts in the abiotic regimes and evaluating ecosystem health through the maintenance of ecosystem function.

4.1. Ecosystem Function, Community Composition and Species Diversity

Aim

- Identify temporal change(s) in species community composition and hence function.

Ecosystem functioning is defined here as the cumulative biophysical and biochemical ecosystem processes which are driven and are maintained by species with differing functional roles or traits.

Within communities, there is often overlap in functional roles that enables the community to buffer against environmental stochasticity or perturbation. The loss of species without loss of community function is known as the functional redundancy hypothesis; the remaining species forming groups with overlapping functional roles, thus maintaining ecosystem services. Loss of dominant species, ecological engineers or those with a disproportional effect on their environment compared to their abundance (keystone species), however, may lead to a reduction in ecosystem function, through de-coupling of facultative or mutualistic interactions (Thrush *et al.*, 2008), for example between grazers and downward conveyors or epiphytes and sea grasses etc. In some systems, only 20-50% of diversity is required to maintain ecosystem function (Schwartz *et al.*, 2000).

High levels of ecosystem functioning and having a range of species that respond differently to different environmental perturbations insures a stable provision of ecosystem goods and services, such as nutrient cycling, pollution buffering, sediment stability, energy flow & carbon cycling. In light of current climate predictions (Jenkins, 2009, IPCC, 2007), there is increasing importance to gauge the impact of observed climate variability on the physical and biological processes operating within estuaries and the implications towards the continued levels of ecosystem functioning.

A number of studies have investigated the inter-relationship between ecosystem function, species diversity and functional diversity and the majority found a strong correlation between species diversity and functional diversity (Hewitt *et al.*, 2008, Bremner *et al.*, 2003, Hooper *et al.*, 2005). In this study species diversity was assessed using a range of diversity measures as a rough proxy to gauge a level of ecosystem health and function. Additionally the similarity in sample groupings was quantified to identify distinct community assemblages, from which it was then possible to compare losses or gains in functional roles, enabling the community buffering capacity for service provision to be assessed.

The diversity of a community and the number/variety of ecological traits may be expressed by a number of measures. No single measure can fully capture the multitude of facets of biodiversity within an ecosystem however the most common two measures of alpha diversity used are species richness and species evenness. 'Richness', is simply the number of species that are present, whereas 'evenness' is a measure of the relative abundance of the different species which are present, representing the equitability of the community structure. Many other measures are available to capture various attributes of local, regional or global facets of biodiversity; 'genetic' (phenotypic), 'species composition', 'species interaction', higher taxon' (phylogenetic distinction) or beta diversity along gradients.

In this study, species richness, species evenness and species composition are used to assess biodiversity; matching the addition or loss of species with that of traits required to maintain community functional processes. Intertidal macroinvertebrates are frequently used to assess biodiversity because they are largely sessile organisms and they are responsive to environmental perturbations and are also used in this study for their importance within the tropic web.

Two macrofaunal surveys were available for historical comparison of potential species community changes in response to shifts in environmental regimes driven by natural and/or anthropogenic pressures. The first survey was Bioparis, a multi partner European project that began in 1998, investigating anthropogenic and natural change in sensitive coastal zones. It was designed to maximize information on intertidal systems obtained from Remotely Sensed data integrated with ground-truthing. The deliverables were mapped spatial distributions of sediment types and their infaunal assemblages.

The second survey was undertaken by the University of St Andrews, Heriot-Watt University and the University of Edinburgh on behalf of the Scottish Natural Heritage (SNH) in 2002, to assess the

Firth of Tay and Eden estuary as candidates for the designation of Special Area of Conservation (SAC). The project aim was to map the littoral and sublittoral communities, generating a record of biotic and sedimentological characteristics using ground-truthing and remotely sensed data.

4.1.1.1. Methodology

Macrofaunal cores were collected at two locations within the Eden Estuary for comparison with historical surveys undertaken for BIOPTIS in 1999 and SNH in 2002 (Figure 4-1). Sample acquisition followed the original protocols for each respective survey and standard protocols for benthic macrofaunal sampling (Worsfold and Hall, 2010). The core size to match with the Bioptis survey was a 19cm diameter stovepipe (0.028m²) to a depth of 15cm. The comparative core for the SNH survey was a 0.1m² box core to a depth of 15cm. The location of each sample point was determined using a Garmin eTrex hand held GPS. In addition to each macrofaunal single core taken at each station, subsamples of sediment were taken for particle size and organic content analysis. The macrofaunal core samples were sieved through a 500 µm mesh and the screenings fixed with a 10% buffered saline-formalin solution, containing Rose Bengal stain to aid identification. Following a 72 hour fixing period, taxonomic identification was (where possible) taken to species level and the number of species per core recorded for diversity analysis

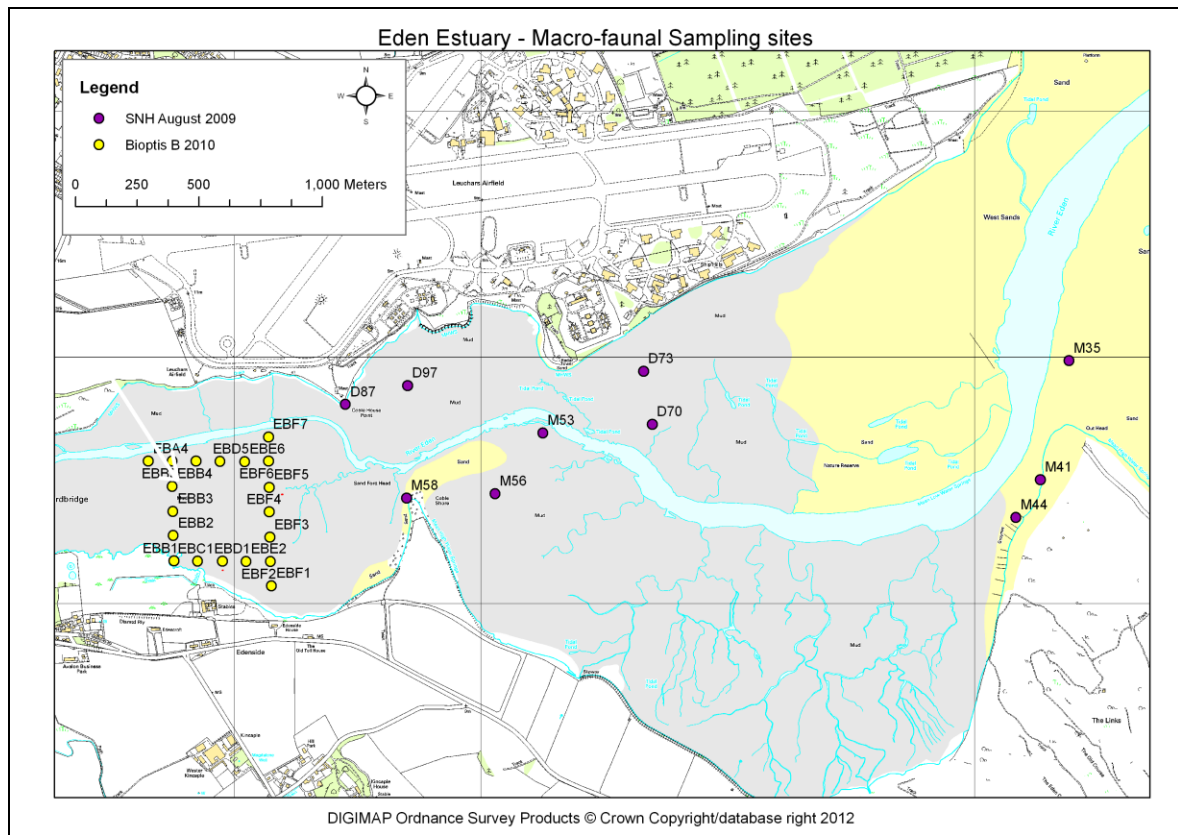


Figure 4-1: Eden estuary macrofaunal core sampling sites.

Particle size analysis was carried out using a Coulter Counter LS230. A small sub-sample of raw sediment from each macrofaunal core location was mixed with water and added to the LS230 machine through a 2 mm sieve until the obscuration reached approximately 12%. Each sample was sonicated for approximately 30 seconds before analysis commenced. Data and the sample statistics were output to Excel for analysis.

For organic content analysis, replicate samples were dried at 50 °C until a constant weight was achieved, the sediment was homogenised and approximately 2 g placed into porcelain crucibles and actual dry weights (DW) were recorded. The crucibles were placed into a muffle furnace at 450°C overnight then allowed to cool in a dessicator for one hour before re-weighing to measure the ash-free dry weight (AFDW): the difference between DW and AFDW is used to calculate the percentage of organic content.

In Excel (Microsoft, 2003), a species matrix was constructed, tabulating both survey time samples together with environmental information (granulometry, organic content etc), this table was used as input to Primer for statistical analysis (Appendix 1 Figures 8 to 11).

The statistical analysis was performed using Primer multivariate ecological software (Clarke and Gorley, 2006) to compare the community structure between successive time periods, cross-correlating patterns found with available environmental data.

Various diversity indices were calculated on the tabulated data before pre-treatment and multivariate analysis. Pre-treatment of the tabulated biotic data matrix used a square root transformation, to accommodate for the dominance in the abundance of a small number of species compared to the majority within the matrix, such that similarities in less abundant species were not masked. The environmental data matrix was pre-treated by normalization to account for the different variables having non comparable measurement scales.

Following pre-treatment a Bray Curtis species resemblance matrix was constructed, taking pairs of recorded variables and comparing them for similarity (similarity, dissimilarity or distance) and nMDS applied to display the pairwise similarities matrix, once a reasonable stress coefficient had been achieved. The standardised environmental resemblance matrix was similarly processed to nMDS, after which the biotic variables were cross-matched with the environmental variables using the BIO-ENV procedure to find the 'Best' matching subsets of environmental variables to the assemblage patterns

Cluster analysis was then performed on the biotic data to identify natural groupings, using the hierarchical method to construct a visual representation of the cluster in the form of a dendrogram.

The 2D-MDS was then linked to the cluster analysis, overlaying the clusters and superimposing circles representing species or environmental variables (bubble plots), which help to explain the division of the clusters.

Anosim, (Analysis of Similarity) the non-parametric multivariate analysis of the variance in Beta diversity could not be performed, due to lack of replicates for the data.

4.1.1.2. Results

Bioptis 1999 – 2010 Data

The transformed Bray Curtis similarity matrix was subjected to cluster analysis, to identify natural groupings of data, and presented as a dendrogram (Figure 4-2).

From the dendrogram analysis, at 46% similarity all of the samples for the 1999 data can be distinguished from all of the samples from the 2010 data. However, slicing the dendrogram at 50% similarity, three clusters can be identified, with a further division separating sample 10EBE2 with the remaining 2010 data samples.

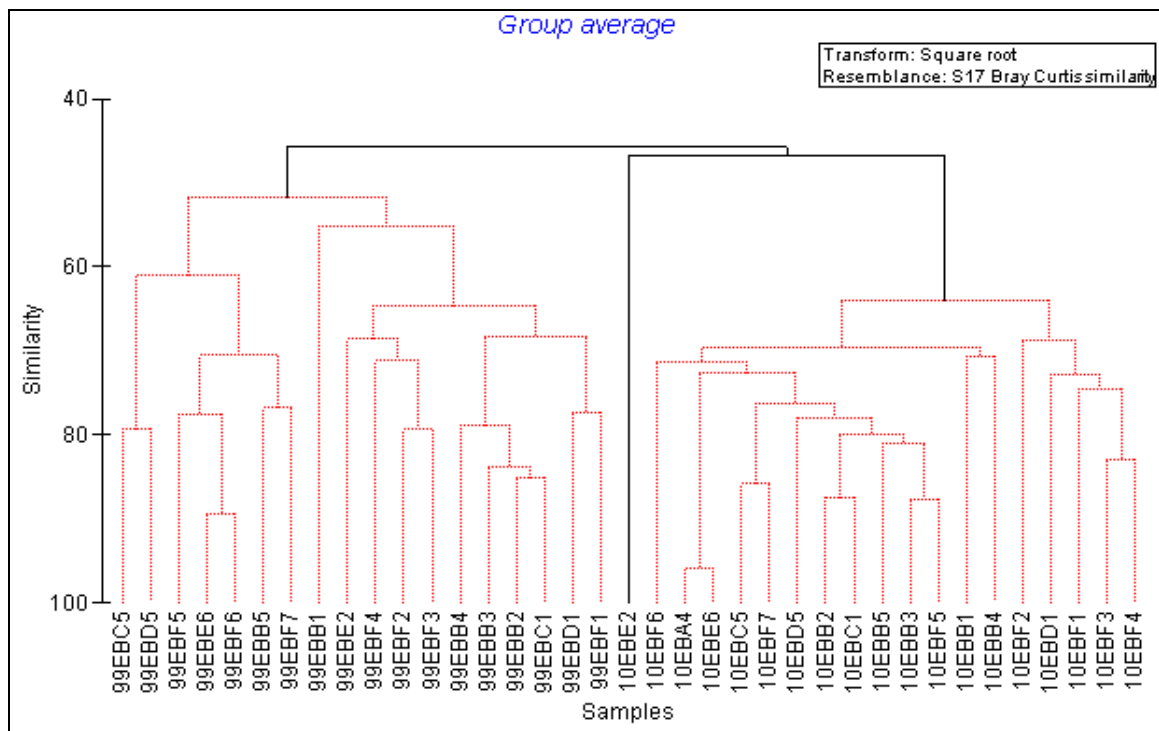


Figure 4-2: Dendrogram resulting from the cluster analysis of square root transformed species abundance data. The matrix used the s17 Bray–Curtis similarity index at the 5% level of significance. Samples are prefixed by the year in which they were surveyed. Dashed lines represent group structure for which the SIMPROV test has found no evidence of dissimilarity. Conversely solid black lines have been identified as statistically similar by SIMPROV.

Displaying the same resemblance matrix data (used to create the dendrogram) as a 2d nMDS Ordination plot (Figure 4-3), the relative Euclidian distances, which were calculated from the similarity rankings of the resemblance matrix, now represent how similar the samples are. Thus

samples that are plotted close together are very similar and points far apart are dissimilar. Following 29 iterations, a minimum stress of 0.15 was achieved. This stress level denotes a reasonable ordination, providing confidence for the interpretation (Clarke and Gorley, 2006).

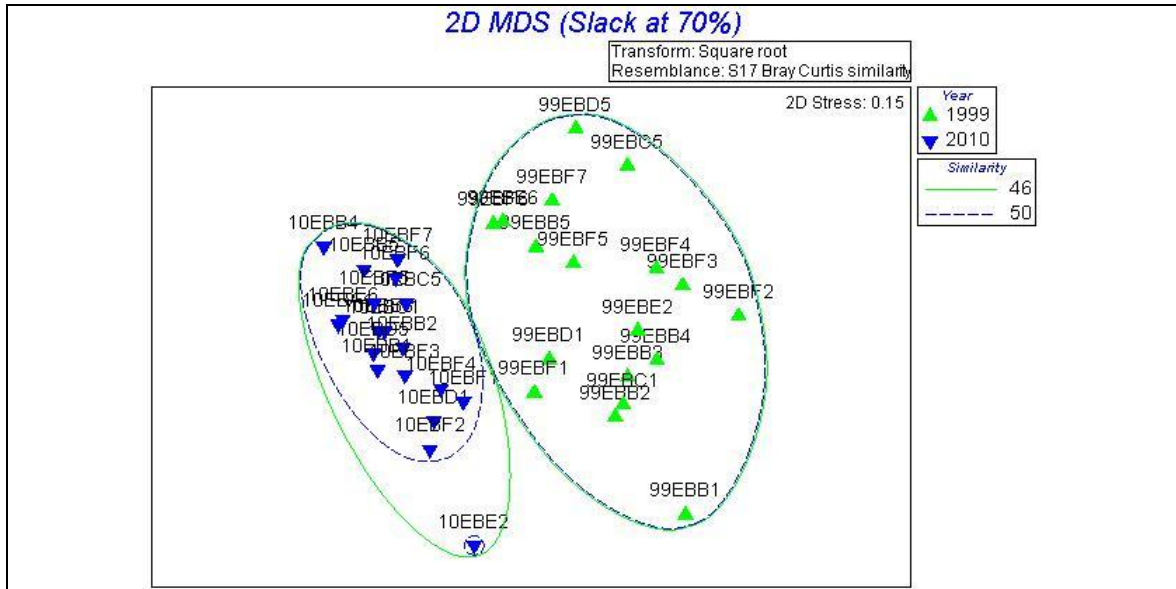


Figure 4-3: 2D nMDS (Minimum stress: 0.15), with overlays of Bray Curtis similarity of 46% and 50% (blue dashed line) (slack 70%) identified by the SIMPROF analysis and displayed in the dendrogram.

Taking the two percentage thresholds of similarity obtained from the SIMPROF analysis and superimposing these on the MDS, enables overlays of each of the species or environmental attributes and thus a method of identifying which attribute helps to explain the distinguished groupings (Figures 4-4 to 4-6).

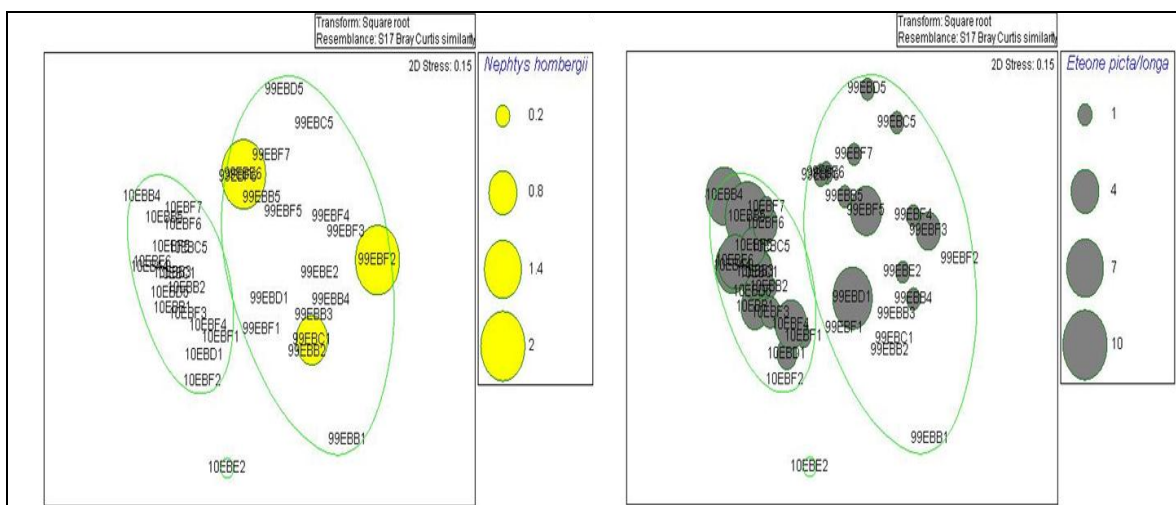


Figure 4-4: Bubble plot species 'overlays' of *Nephtys hombergii* and *Eteone sp.* The bubble size represents the scale for the number of individuals within each sample.

The 2010 samples can be distinguished from the 1999 samples by the absence of both *Nephtys hombergii* and *Corophium volutator* (Figures 4-4 and 4-5). There are also higher numbers of *Hydrobia*, *Eteone picta*/ *E. longa*, *Oligochaetes* and *Cerastoderma edule* in the 2010 survey. The later were almost absent in 1999. Sample 10EBE2 may be distinguished from the remaining 2010 data by the absence of *Eteone longa*.

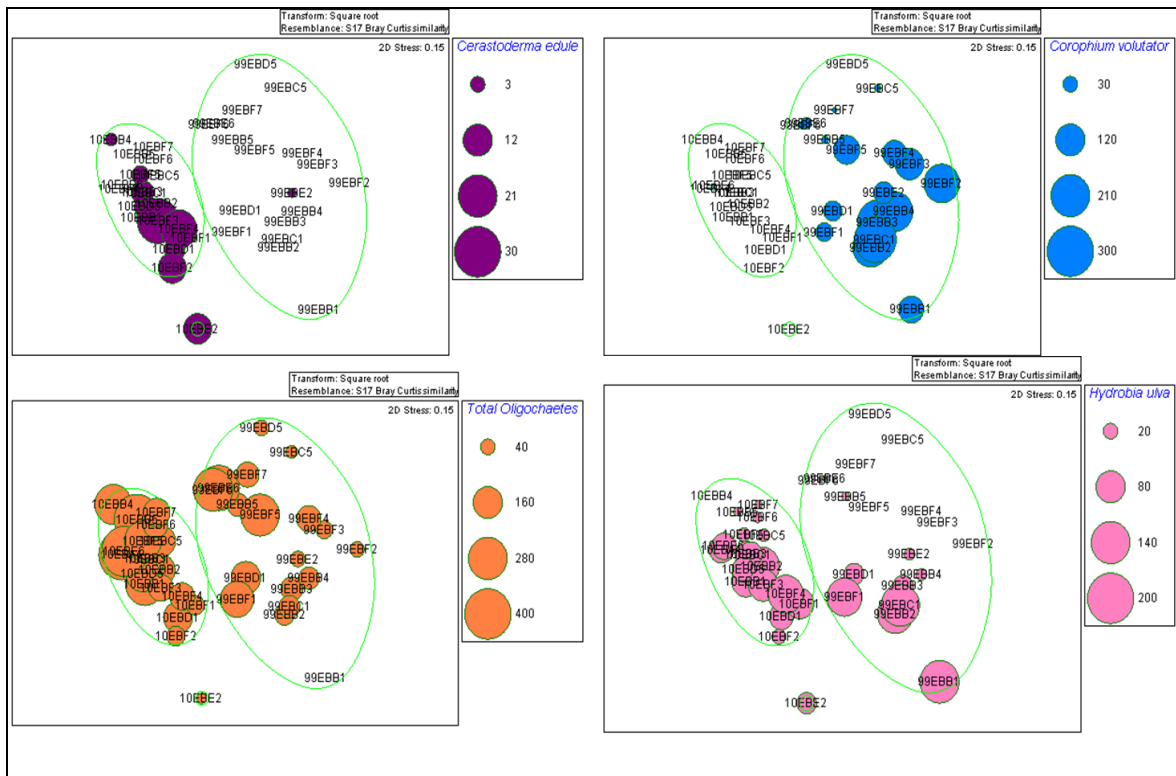


Figure 4-5: Bubble plot ‘overlays’ of *Cerastoderma edule*, *Corophium volutator*, total *Oligochaetes* and *Hydrobia ulvae*.

The environmental 2D nMDS ordination (Figure 4-6) shows the 2010 environmental data to be more homogeneous than the 1999 data, having slightly more tightly grouped samples. When displayed with overlays at the biological divisions of 46% and 50% Bray Curtis Similarity, there is little evidence of any relationship between the species abundance clusters and the similarities of the collective environmental data. For the percentage of particles less than 63 μm (Figure 4-7), however, a trend may be seen where the 2010 samples display a generally higher percentage of finer mud particles than in 1999.

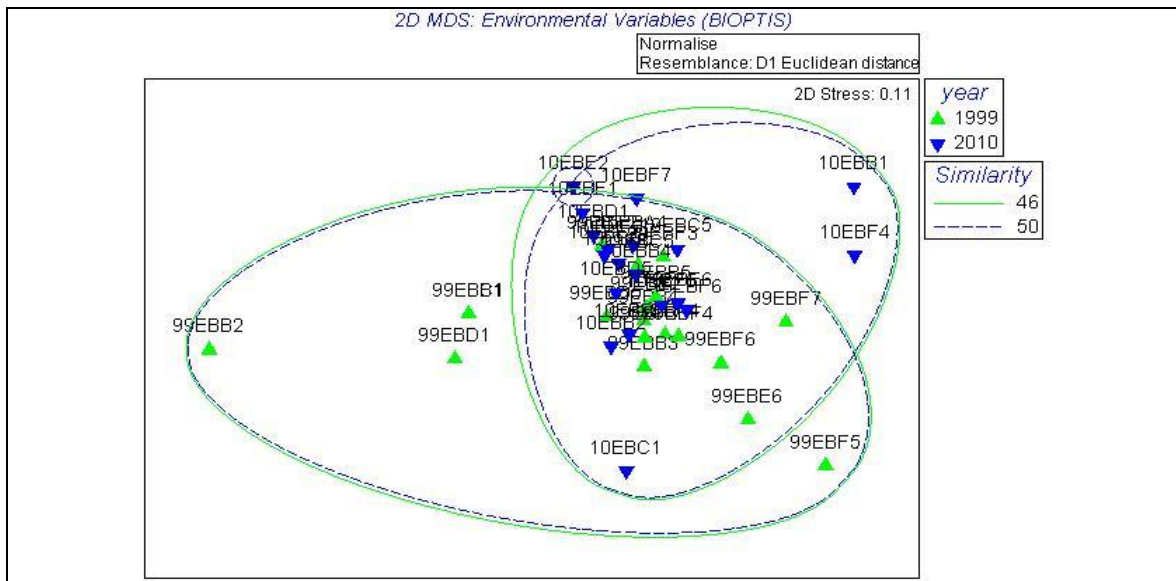


Figure 4-6: 2D nMDS ordination for the normalised environmental variables (stress 0.11). Overlain are the 46% and 50% Similarity divisions which were identified through SIMPROV for the biological data, thus showing that the distinction between the two survey periods observed in the biological data is not explained by the environmental variables.

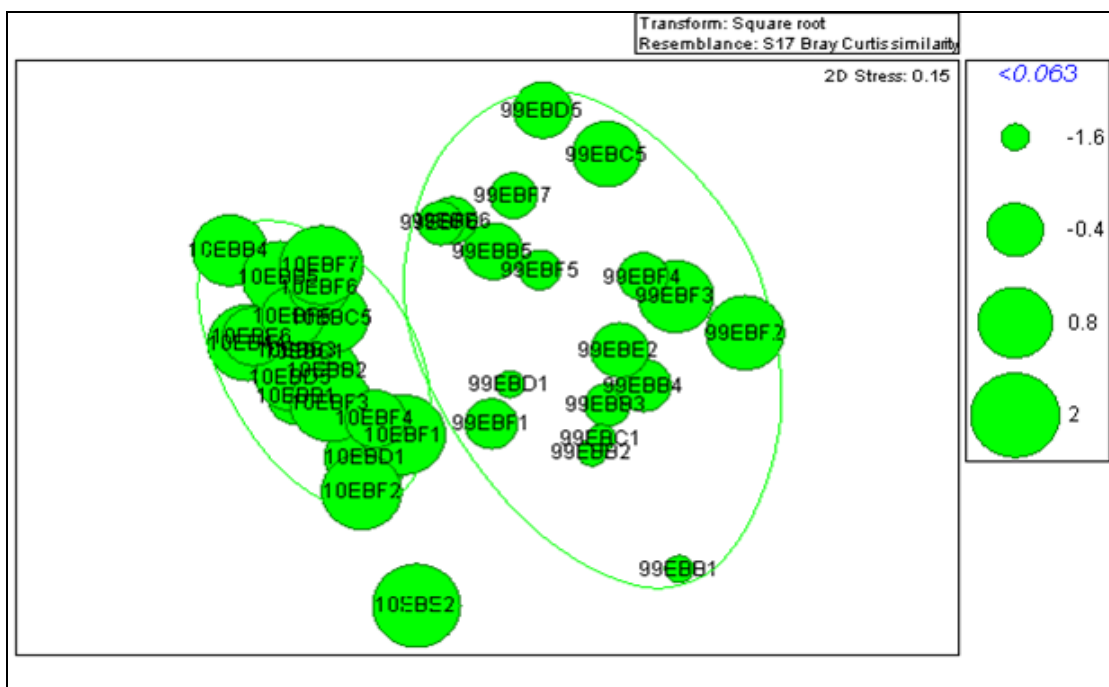


Figure 4-7: Mud content nMDS; the percentage of <63 µm particle size retained in sieve.

The results for particle size analysis (Figure 8) indicate a shift from relatively poorly sorted samples in 1999, showing a broad range of sizes from less than 63 µm up to 2 mm. Conversely the 2010

samples show increased sorting, with particles ranging from less than 63 µm up to 0.5 mm. The modal sizes in Table 4-1 are displayed in red and represent the sediment retained at the given mesh aperture. In general and for the modal particle size, there is a shift towards finer grains in 2010.

Table 4-1: Particle size categories. Modal size class is shown in red and missing data as N/A.

Sample	1999 Data						2010 Data					
	2mm	1mm	0.5mm	0.25mm	0.063mm	<0.063mm	2mm	1mm	0.5mm	0.25mm	0.063mm	<0.063mm
EBB5	0.809	0.027	0.233	2.885	67.324	28.722	0.000	0.000	0.000	2.581	44.980	52.386
EBC5	0.119	0.074	0.157	1.545	56.978	41.126	0.000	0.744	0.744	7.140	45.290	46.842
EBD5	0.170	0.023	0.064	0.916	70.789	28.037	0.000	0.000	0.679	8.600	47.290	45.435
EBF6	2.182	0.313	0.651	2.488	80.990	13.375	0.000	0.000	0.437	10.680	59.950	29.913
EBB1	N/A	N/A	N/A	N/A	N/A	N/A	0.000	2.310	1.192	15.400	53.650	27.425
EBC1	N/A	N/A	N/A	N/A	N/A	N/A	0.000	0.000	0.556	28.190	53.140	18.088
EBD1	N/A	N/A	N/A	N/A	N/A	N/A	0.000	0.000	0.446	4.380	30.820	64.333
EBF2	0.021	0.036	0.187	0.794	43.205	55.756	0.000	0.000	0.366	4.870	35.910	58.832
EBF1	0.793	0.084	0.346	4.398	73.945	20.435	0.000	0.000	0.000	1.296	32.660	66.040
EBE2	0.458	0.298	0.666	2.289	69.765	26.524	0.000	0.000	0.000	0.660	26.570	72.765
EBF3	0.405	0.462	1.118	4.161	41.798	52.057	0.000	0.000	0.102	4.390	34.590	60.934
EBF4	0.115	0.244	0.591	2.579	78.781	17.690	0.000	1.373	2.570	10.530	55.590	29.945
EBF5	4.744	0.770	0.896	3.309	80.424	9.856	0.000	0.000	0.330	6.460	60.300	32.884
EBF7	0.120	0.304	1.722	14.680	67.991	15.183	0.000	0.000	0.067	4.480	30.020	64.443
EBE6	4.165	0.168	0.410	3.798	74.875	16.584	0.000	0.000	0.656	10.150	57.630	31.529
EBA4	0.000	0.209	0.371	2.832	78.419	18.169	0.000	0.000	0.603	8.020	31.990	59.450
EBB4	0.060	0.016	0.304	4.268	71.737	23.614	0.000	0.000	0.819	8.820	40.630	50.492
EBB3	0.000	0.023	0.133	4.650	82.266	12.929	0.000	0.000	0.363	11.670	57.080	30.877
EBB2	N/A	N/A	N/A	N/A	N/A	N/A	0.000	0.000	0.067	11.760	56.370	31.767

Diversity

The individual sample diversity graphs are available in Chapter 4 Appendix.1. Since replicate data were not available, the standard deviation calculated for each survey (which is likely to be larger than if calculated on individual replicates due to heterogeneity) is used here to indicate differences.

Two indices were calculated for 'Evenness', Pielou's index and the Simpson index, for the former, EBD1, EBF2 and EBF6 were different (1 survey standard deviation), with EBD1 being more diverse in 1999 and EBF2, EBF6 were more diverse in 2010. Simpson's index similarly identified EBF2 and EBF6 as more diverse in 2010, however identified EBB5 as being more diverse in 1999. The two methodologies differ in that Pielou's index is a development of Simpson's index. Simpson's index is weighted towards abundance and therefore indicates dominance and is less sensitive to 'Richness'

Assessing 'Richness', again two indices were used; the Shannon Diversity index and Margalef's index. The Shannon index identified EBF2 and EBF6 as more diverse in 2010 and sample EBB5 as more diverse in 1999. The Margalef index identified EBB2 and EBF1 as 'Richer' in 2010.

The number of species found, in the following samples were all greater in 2010; EBB1, EBB2, EBB3, EBC1, EBD5, and EBF1. For the number of individuals present, EBB5 contained more individuals in 2010.

Grouping the diversity data by survey (Figure 4-8), mean values for all diversity indices were higher in 2010 however the values lie within the variability of the 1999 data. It was not possible to run t-tests for significant differences, as by grouping the data each survey had a single sample.

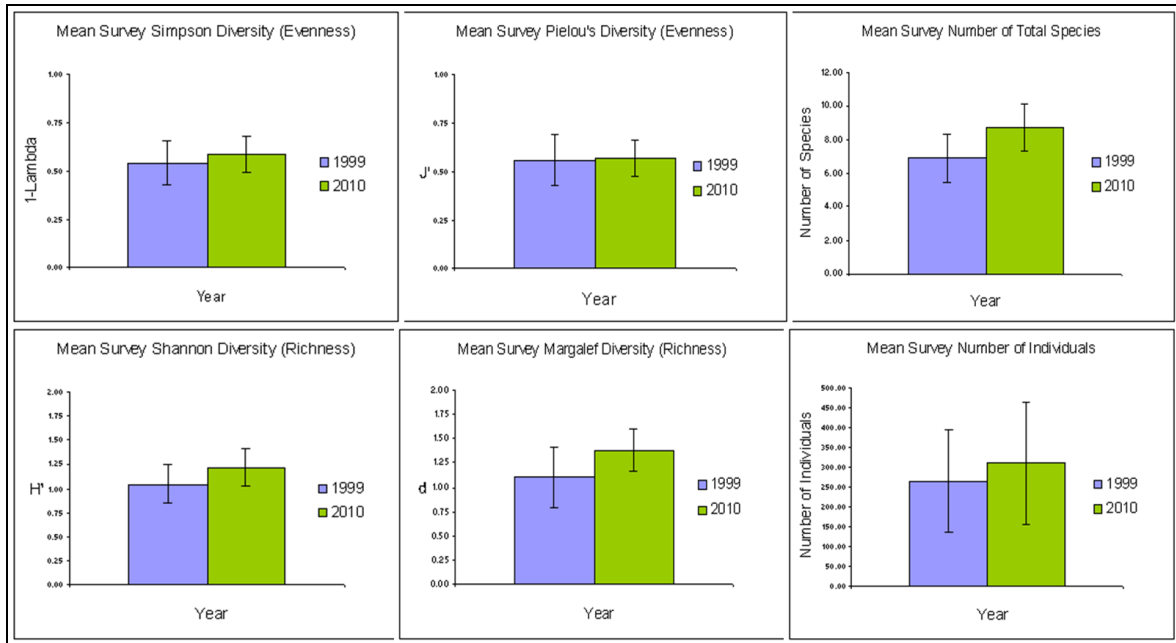


Figure 4-8: Diversity indices composite for 'between' survey comparison. Error bars are 1 standard deviation.

SNH 2002 - 2009 Data

The transformed Bray Curtis similarity matrix was subjected to cluster analysis, to identify natural groupings of data and is presented as a dendrogram (Figure 4-9).

From the SIMPROV analysis, 20% Bray-Curtis similarity for 5% significance identifies two clusters within the data, sample 2002M53 and the remaining samples. However, slicing the dendrogram at 25% similarity (also a level of significant grouping identified by SIMPROV), three clusters can be identified, with the further division separating samples 2009M53 and 2002 D97 from the main group.

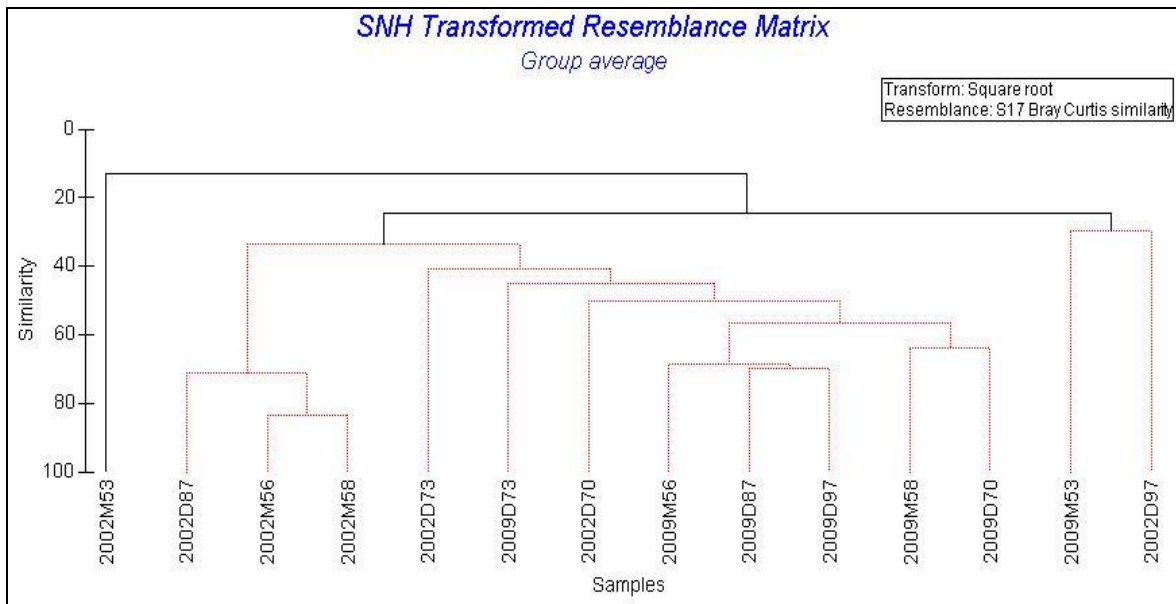


Figure 4-9: Dendrogram resulting from the cluster analysis of square root transformed species abundance data. The matrix used the s17 Bray–Curtis similarity index at the 5% level of significance. Samples are prefixed by the year in which they were surveyed. Dashed lines represent group structure for which the SIMPROV test has found no evidence of dissimilarity. Conversely solid black lines have been identified as statistically similar by SIMPROV.

The same resemblance matrix data was used to create a 2d MDS Ordination plot (Figure 4-10), to represent how similar or dissimilar the samples were to each other; following 32 iterations, a minimum stress of 0.11 was achieved, providing a good level of confidence for the interpretation of the displayed results (Clarke and Gorley, 2006). Taking the two percentage thresholds of Bray–Curtis similarity obtained from the SIMPROF analysis, and overlaying these on the ordination plot enables the relative Euclidian distances and the groupings to be visualized (Figure 4-10).

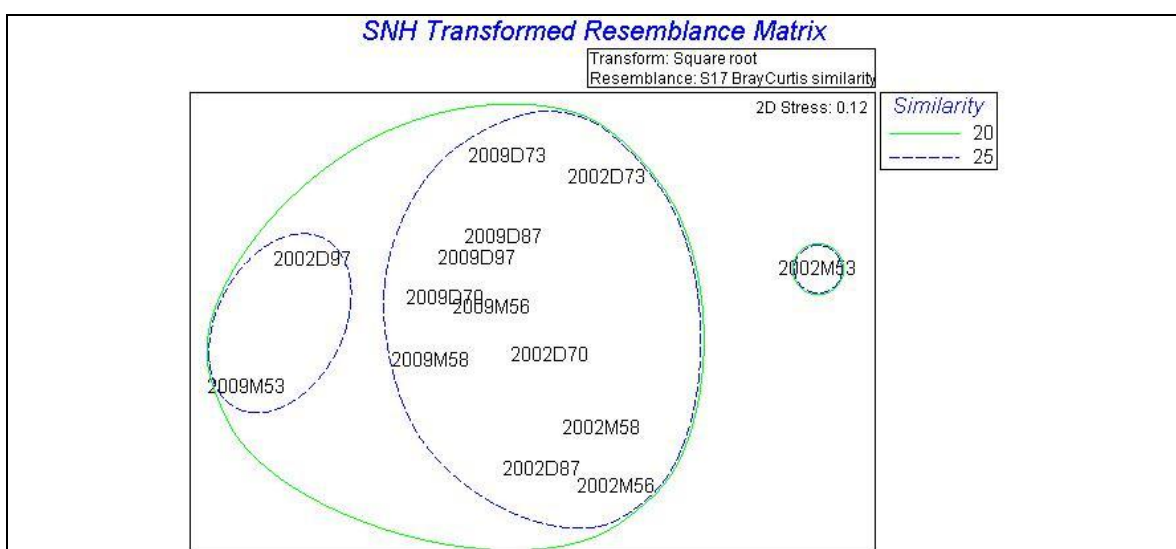


Figure 4-10: 2D MDS of species data (2-d: Minimum stress: 0.11 occurred 32 times), with overlays of Bray Curtis similarity at 20% and 25% (slack 70%) identified from the Dendrogram.

Repeating Figure 4-10 with overlays of each of the species or environmental variables, enabled the identification of which attribute(s) most contributed to explaining the distinguished groupings (Figures 4-11, 4-12 and 4-14).

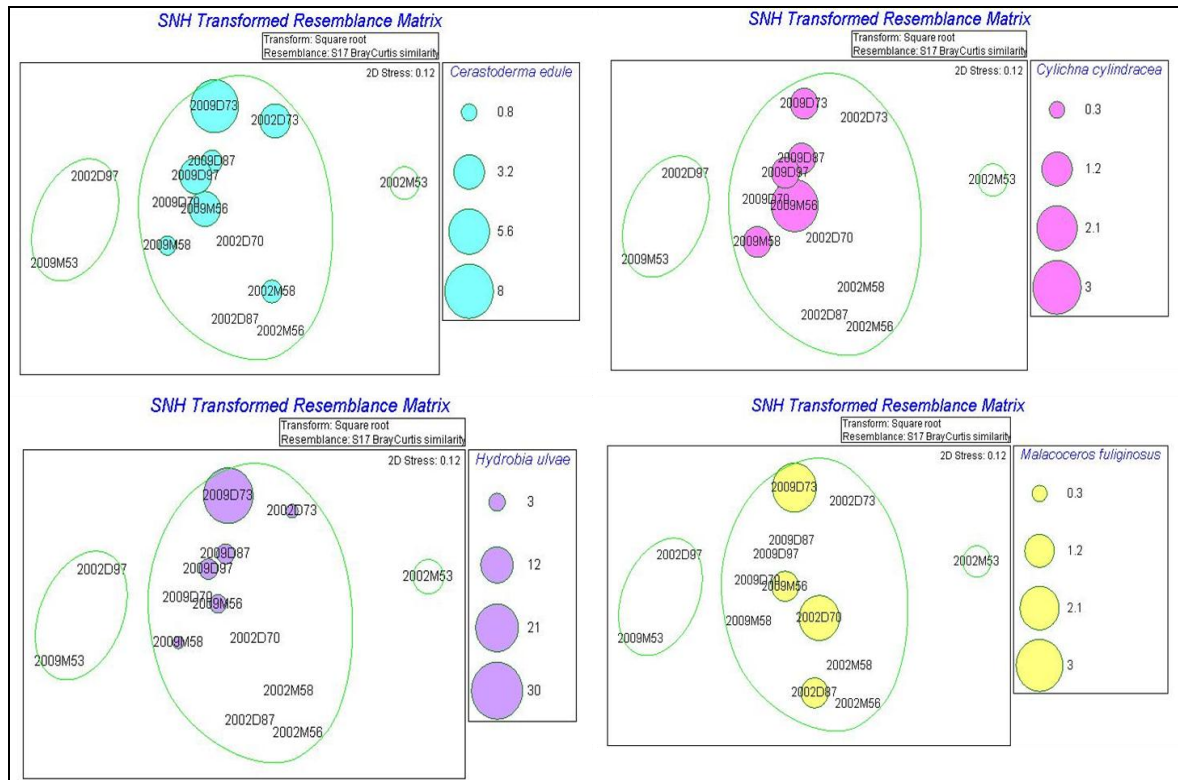


Figure 4-11: Overlay 'Bubble plots' representing defining species for the 25% Bray Curtis similarity partition. *Cerastoderma edule*, *Cylichna cylindracea*, *Hydrobia ulvae* and *Malacoceros fuliginosus*.

From the biological overlays (Figures 4-11 and 4-12), the main central grouping of samples, identified at 25% similarity (Figure 4-10), may be distinguished from the other two groups by the presence of five species; *Cerastoderma edule*, *Cylichna cylindracea*, *Hydrobia ulvae*, *Malacoceros fuliginosus* and *Eteone longa/picta*.

Samples 2002M53 is further distinguished from 2002D97 and 2009M53 by the presence of two species; *Pygospio elegans* and *Corophium volutator* and the absence of *Tubificoides benedii*.

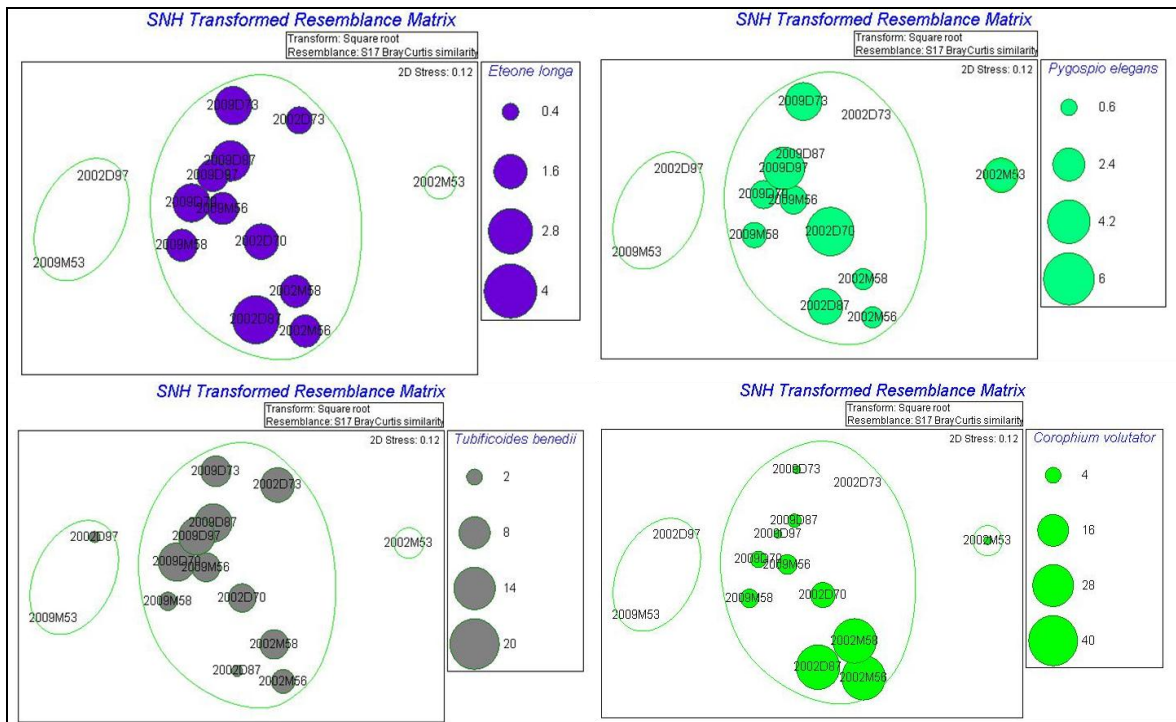


Figure 4-12: Overlay 'Bubble plots' representing defining species for the 25% Bray Curtis similarity partition; *Eteone longa/picta*, *Pygospio elegans*, *Tubificoides benedii* and *Corophium volutator*.

The environmental 2D MDS ordination (Figure 4-13), when displayed with overlays at the biological clustering of 20% and 25% Bray Curtis Similarity, indicates that the available environmental variables only explain the distinction of sample 2002M53.

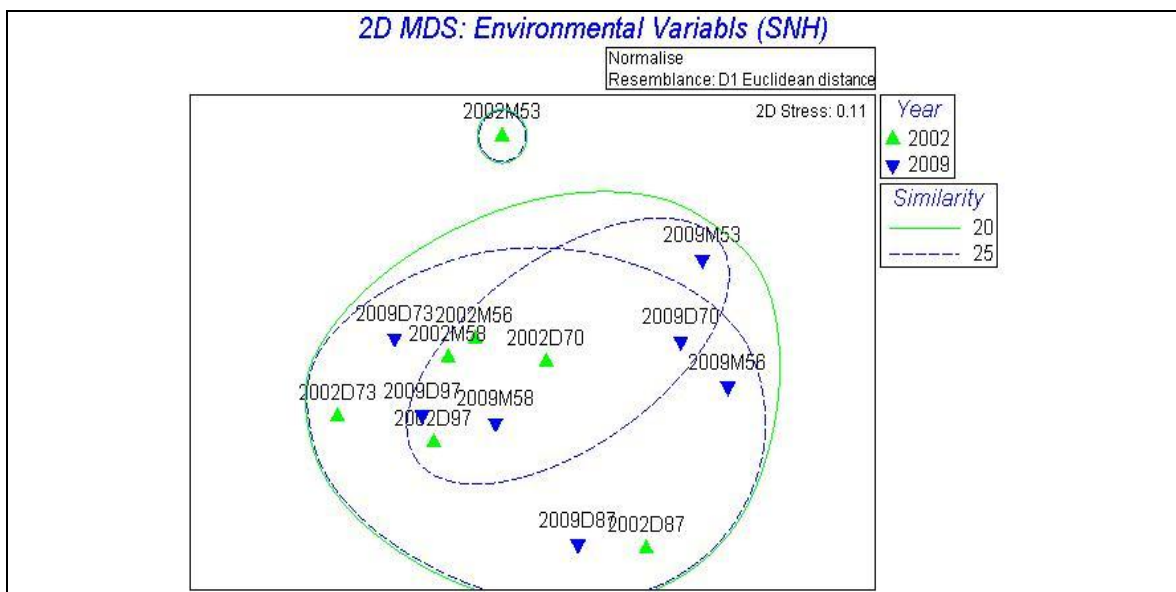


Figure 4-13: 2D MDS ordination for the normalised environmental variables (stress 0.11).

Plotting the overlays of each environmental variable however gave no clear indication of a single driving attribute. A combined trend may be seen (Figure 4-14) with the percentage of organic content and the percentage of particles retained in a 0.125 mm sieve.

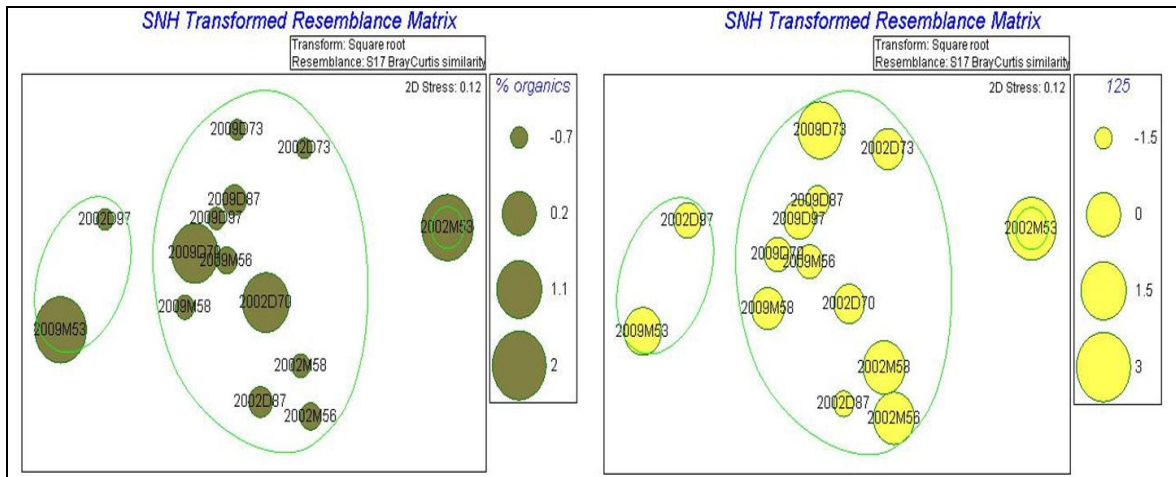


Figure 4-14: nMDS of the environmental variables; % Organic content and Particles retained in 0.125 mm sieve.

The results for particle size analysis (Table 4-2) indicate there is a small general shift towards finer grains, with the absence of the >2000 µm size class and a reduction of samples containing ≥1000 µm particles in 2009. Sample M58 has become bimodal in distribution in 2009.

Table 4-2: Particle size categories. Modal size class is shown in red.

2002									
Core	Sorting	Skew	>2000µm	1000µm	500µm	250µm	125µm	63µm	<63µm
D70	0.73	1.50	0.00	0.00	3.60	16.50	27.50	16.60	35.80
D87	0.70	3.97	0.00	0.70	3.30	6.70	12.50	14.60	62.20
M53	0.71	0.75	0.00	0.03	0.06	3.87	67.86	20.60	7.58
M56	0.97	1.03	0.00	0.04	0.23	29.32	47.66	14.22	8.52
M58	0.80	0.87	0.00	0.87	2.93	31.84	49.47	9.56	5.34
D77	0.59	1.01	0.59	11.04	36.19	21.65	0.96	0.74	2.03
D73	1.58	0.20	0.00	0.00	4.40	59.80	30.01	0.93	4.86
D97	0.77	0.47	0.00	0.00	4.90	38.20	22.60	8.20	26.10
2009									
Core	Sorting	Skew	>2000µm	1000µm	500µm	250µm	125µm	63µm	<63µm
D70	9.88	3.91	0.00	1.59	1.41	10.00	21.58	15.88	49.54
M56	15.92	3.61	0.00	2.69	2.25	14.60	20.71	20.73	39.02
D87	0.41	1.14	0.00	0.00	0.01	13.33	17.07	23.16	46.43
M53	13.91	3.35	0.00	3.10	4.15	24.25	39.78	13.18	15.54
M58	-0.83	0.32	0.00	0.00	0.09	27.43	30.79	13.11	28.57
D73	0.76	-0.06	0.00	0.00	0.16	28.40	56.58	4.09	10.77
D77	-0.28	0.20	0.00	0.00	0.17	28.14	43.48	10.85	17.35
D97	-0.30	0.16	0.00	0.00	2.89	47.17	28.19	6.92	14.83

Diversity

The individual sample diversity results are presented in Appendix.1. Two measures were calculated for 'Evenness', Pielou's index and the Simpson index. Pielou's index indicated samples M56, D87 and D97 were more diverse in 2009 than 2002. Similarly the same three samples were also identified by the Simpson's index as being more diverse in 2009 than 2002.

'Richness' was investigated using both the Margalef index and also the Shannon index. The Margalef index indicated that M53, M56 and D87 were more diverse in 2009 than 2002. The Shannon measure of Richness identified the same three samples and additionally D97 as more diverse in 2009.

The total number of species found and also the total number of individuals found was greater only in sample D73 for 2009.

Grouping the diversity data by survey (Figure 4-15); mean values for all diversity indices were higher in 2009 than 2002, however the values lie within the variability of the 2002 data. It was not possible to run t-tests for significant differences having combined the data for each survey only one sample remained per survey.

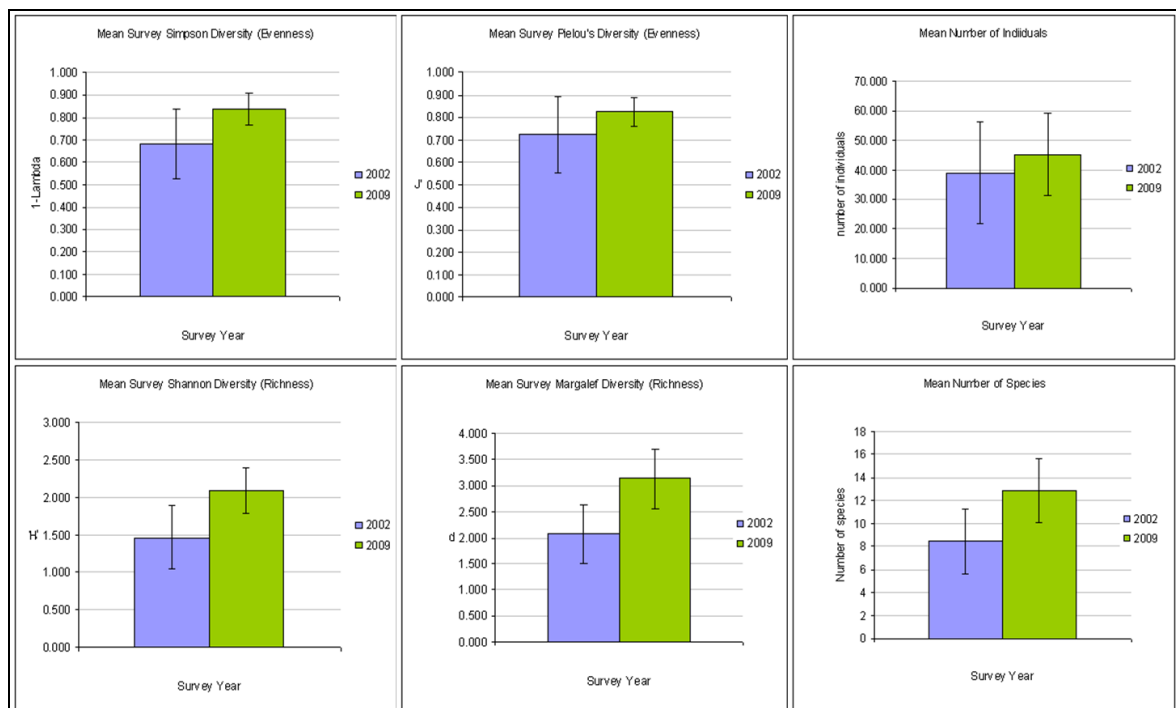


Figure 4-15: Diversity indices composite for 'between' survey comparison. Error bars are 1 standard deviation.

4.1.1.3. Discussion

Bioptis 1999 – 2010 Data

The 2D MDS ordination, with overlays of species abundance, identified all of the 2010 samples to be dissimilar to the 1999 samples at a Bray Curtis similarity of 46%. Two species were identified as no longer present in the 2010 samples. These were *Nephtys hombergii* and *Corophium volutator*. The environmental data identified the 2010 samples as being generally a little more homogeneous and with increased numbers of samples having modal particle sizes below 63 μ m and a reduction of particles above 500 μ m. It is known that *N. hombergii* has a preference for finer sediment and although it can be found in sediment with both high and low mud content, abundance generally increases as mud content increases and is a dominant species under low oxygen concentrations (Bellan, 2011). It therefore seems unlikely that change to the modal particle size would have forced change in the spatial distribution between 1999 and 2010. *N. hombergii* is a burrowing predator, mainly feeding on invertebrates, juvenile molluscs and other polychaetes. However it also scavenges and grazes on detritus and diatoms (Bellan, 2011). With *N. hombergii* having a diverse strategy for feeding, it seems unlikely that the concomitant absence of *C. volutator* would have caused the disappearance of *N. hombergii*, however with the increasing presence of *E. longa* competition may have had a contributory role to spatial reorganization of species. The salinity tolerance of *N. hombergii* is from approximately 18 to 30 Practical Salinity Units (PSU) (Hayward and Ryland, 1995), although pore-water salinity was not recorded in the original survey, it was however taken in 2010 (GMH 3430 Greisinger digital conductivity meter) following the method of Johnson *et al.* (1979) to compare historically with other surveys over the same area. Salinity was found to be generally lower in 2010 (Appendix.1) than values reported for the late 1970s. Coupled with the observed increase in river flow (1999 total 121.4 cumecs/yr⁻¹, 2010 total 131.7 cumecs/yr⁻¹) a lowering of salinity may have been a contributory factor for the absence of *N. hombergii*.

Corophium volutator was similarly investigated for substrate preference, although they are often found in muddy sand and mud (Hayward and Ryland, 1995), experiments by Meadows (1964a, 1964b) found that fine to coarse sand were favoured and over a variety of anaerobic to aerobic conditions (reflecting the amount of organic matter present). Within the sediment, *C. volutator* occupies semi-permanent U-shaped burrows, deposit feeding on organic detritus, bacteria and diatoms raked into the burrow by its second antennae. It is also a suspension feeder on small particles and grazes on the microphytobenthos. *C. volutator* can tolerate a wide range of salinities from nearly full seawater salinity to almost fresh water (Neal and Avent, 2006), however in the Ythan estuary, *C. volutator* were found migrating in and out of areas depending on salinity driven by seasonal rainfall and river flow (McLusky, 1970). There is little indication of why *C. volutator* is no longer present in the 2010 samples, but this may just be a combination of over predation and changes in salinity.

Although two species were absent from the 2010 samples, higher abundances (Analysis of Similarity) is a non-parametric (randomization-based) method of multivariate analysis of *Hydrobia*

ulvae, *Eteone longa/picta*, total oligochaetes and *Cerastoderma edule* was observed. In terms of maintenance of ecosystem processes, it is important to identify if there is an overlap in the functional traits between the lost species and those that remain. Initially assessment of change to diversity, though a number of measures was undertaken to identify samples where there potentially may have been significant change. Statistically three sample standard deviations are required to identify significant differences between samples, however due to the original survey sampling scale, no replicates were available. Thus the standard deviation for the whole survey was used to identify differences; due to the natural heterogeneity of infauna this should provide a conservative measure of difference.

For individual abundances, only one sample had potentially significantly more individuals (EBB5) and for the number of species, there were 7 samples which potentially (with respect to the variability) contained more species in 2010, inferring there may be greater capacity for maintenance of ecosystem processes with concomitant increased buffering capacity for change.

Assessing the diversity indices for each of the samples was more complicated. In terms of evenness, both indices identified 1 sample to be less diverse and two samples to be more diverse. More evenness within a community enables recovery from perturbation and increases productivity (Hewitt *et al* 2008). Similarly for richness, the Shannon index indicated that 1 sample was less diverse and 2 were more diverse, whilst the Margalef index identified 5 samples as being more diverse in 2010. Increased richness potentially helps a community to buffer against change, through the increased overlap in functional traits. These results perhaps reflect the heterogeneity of the macrofauna and prove the requirement for replicate samples is necessary to give greater confidence in interpretation. In light of the lack of replicates, assessing the difference between the two surveys as a whole, the combined data infer a trend for increased diversity over all indices, which suggest ecosystem processes have at least been maintained and may potentially indicate an increased redundancy.

SNH 2002 - 2009 Data

The 2D MDS ordination, for the SNH data samples shows no clear separation between surveys over the time interval, inferring no remarkable change has occurred. At 25% similarity three groups may be distinguished, where samples 2002D97 & 2009M53 form one separate group and sample 2002M53 forms another. The 2D MDS ordination (stress 0.11) of the environmental data identified 2002M53 as being dissimilar from all other samples, for both the 20% and 25% Bray Curtis species similarity groupings. Particle size analysis for M53 (Table.15) identifies a shift towards being less well sorted, with a greater proportion of particles from 250 m – 1000 m. Between 2002 and 2009, M53 has also shown a species compositional change, with the loss of *Nereis diversicolor* and *Pygospio elegans* from 2002 to 2009 and with the addition of *Scoloplos armiger*, *Mytilus edulis* and total oligochaetes. *N. diversicolor* and *P. elegans* both have a wide salinity tolerance ranging from approximately 2 to 30 PSU and both are found in sand, muddy sand and in mud. Both variables are

within the ranges for each of the surveys and thus do not explain the absence of the species in 2009.

P. elegans has several feeding strategies, dwelling within a mucus lined sand tube, it is able to filter-feed by building a mucus net, it can also use its palps for suspension-feeding on plankton and is a selective deposit-feeder (Bolam and Fernandes, 2003). *N. diversicolor* is perhaps one of the most diverse feeders: it has been observed as an omnivore, scavenger, predator, surface deposit feeder and it is able to switch to suspension and filter feeding by spinning a funnel shaped mucus net to trap suspended particles and phytoplankton (Nielsen *et al.*, 1995, Costa *et al.*, 2006). Evidence of both carnivorous and herbivorous feeding was observed from specimens found in samples from this current survey (Figure 4-16). Since both species have such versatile feeding abilities, a change in spatial distribution driven by food source seems unlikely, however positive correlations between *N. diversicolor* and *P. elegans* abundances (Morgan, 1997), coupled with the ephemeral nature of the opportunistic *P. elegans* (Bolam and Fernandes, 2003) may explain the absence of the two species from the 2009 samples.

In terms of continued ecosystem functioning *P. elegans* and *N. diversicolor* have relatively similar functional roles. *P. elegans* is a sediment stabilizer and ecosystem engineer, forming biogenic mounds when tube densities are very high (Bolam and Fernandes, 2003). *N. Diversicolor* also stabilizes sediment through lining its U shaped burrows with mucus. The functional traits of the replacing species (*S. armiger*, *M. edulis* and *Oligiochaetes*) do not fully overlap with *P. elegans* and *N. diversicolor*. *S. armiger* and *Oligiochaetes* bioturbate sediment whilst burrowing and feeding on sub-surface detritus. In relatively high densities, however *M. edulis* is a bioengineer, stabilizing surface sediment and reducing near-bed flow velocities (Widdows *et al.*, 2002). The total number of species in 2002M53 was only 3, which in 2009 increased to 10, this increase in the number of species (increase in diversity) infers the 2009 community have a greater potential for the maintenance of ecosystem functioning.



Figure 4-16: *Nereis diversicolor* feeding (left) on a *Tubificoides benedii* and (right) on organic debris, found within the 2009 samples.

In Sample D97, *Capilella* spp. were no longer present in 2009. Capitellidae are opportunistic deposit feeding polychaetes with a wide environmental tolerance, enabling them to dominate in polluted or hypoxic conditions (Riley and Bilewitch, 2009). Their population can rapidly explode then crash following a breach of the carrying capacity when food supply becomes limiting (Chesney and Tenore, 1985). Instead, *P. elegans*, *C. edule* and *H. ulvae* appeared as relatively numerous at that station from 2002 to 2009; representing overall a change from 10 to 15 species present. The particle size analysis indicates a shift towards increased sorting and a modal size range 250 μ m, together with reduced mud content, representing a sediment type preferable to *C. edule*.

Assessing individual abundances for all samples; only one sample had potentially significantly more individuals in 2009 (D73). Similarly the number of species contained in sample D73 potentially was significantly higher in 2009, inferring a greater capacity for maintenance of ecosystem processes in this locality.

Both diversity indices for 'evenness' identified three samples as having potentially significant differences: M56, D87 and D97 were more even in 2009, inferring a likelihood for higher productivity and a resilience to change. In terms of richness, the Margalef index identified M53, M56 and D87 to have greater richness in 2009, whilst the Shannon index additionally identified D97. Bearing in mind the spatial heterogeneity for macrofaunal samples and the variation in sediment character, combining samples for the whole survey shows a trend towards increased evenness and richness in 2009.

Changes in the sediment characteristics indicate that there has been a change in the hydrodynamic conditions since 1999 and 2002 respectively. The inner estuary shows a shift towards finer particles and the salinity data reflect lower salinities for the contemporary survey, inferring a greater contribution of river water (including POM, fine sediment and nutrients) to the estuarine volume. Supporting data for a greater contribution of river flow is given by data for the 5 years preceding 1999 (Table 4-3), when river flow per month averaged 10.35 cumecs and by 2010 this had risen to 11.16 cumecs. Towards the middle estuary (SNH data), a general shift to an increased percentage of finer particles is also seen, whilst other samples are less well sorted reflecting the variability in circulation.

Table 4-3: Eden river flow: statistics for 5 years preceding each survey (Johnston 1978 – salinity measurements were taken in August)

Period	Mean monthly flow (cumecs)	Mean annual flow (cumecs)	Survey
1973-1978	8.83	105.93	Johnston 1978
1994-1999	10.35	124.18	BIOPTIS 1999
1997-2002	11.98	143.76	SNH 2002
2004-2009	11.17	134.08	SNH 2009
2005-2010	11.16	133.91	BIOPTIS 2010

No clear differences between surveys 2002 and 2009 were observed, perhaps reflecting similar river flow inputs. Changes in the circulation in the middle estuary may however have been driven by altered tidal asymmetry during the period (see Chapter 3).

Changes in species distribution may also have been influenced by moderation of catchment nutrient inputs. In 1992, a treatment plant was installed at the Paper Mill at Guardbridge, resulting in a considerable reduction of suspended solids entering the Eden estuary (Clelland, 1997). Nitrogen inputs from agricultural runoff, however, increased from 1980-1994, which is thought to have contributed to growth of *Enteromorpha* mats potentially causing local anoxia (Cardoso *et al.*, 2004). Despite this, algal mat growth was found not to exceed OSPAR assessment limits for surveys in 2000 and 2006 (CFAS, 2007), although in 2006 the average wet weight biomass for 29 macroalgal samples was $1,098 \pm 844 \text{ g/m}^2$, a value that exceeded the OSPAR criterion of 500 g/m^2 (due to the standard deviation). Potentially the extent of the algal mats could have caused spatial changes in community composition through development of anoxic conditions.

Due to the time limitations of this thesis and the scale of the available historical surveys, single core samples were taken at each of the stations to match the original surveys. Whilst these data provide an inference of trends which may be present, no significant conclusions may be drawn. The data are however valuable in giving a baseline for more in depth targeted research. The biodiversity results for the two comparative surveys 'infer' an increase in richness and evenness. As a result, there is an increased potential for overlap of functional traits, providing resilience to change and sustainable maintenance of ecosystem processes. For the areas studied, the estuary appears not to have been negatively affected, in terms of ecosystem health, by abiotic changes to the estuary.

4.1.1.4. Summary

In the inner estuary, comparison was made between community composition from 1999 and 2010. Data quality was limited by the sampling method, which took single cores at each station in line with the original survey protocols; without replicate data no significant conclusions could be made. Despite this, an effort was made to identify potential trends in the data.

2D MDS ordination identified a significant temporal shift in community composition between 1999 and 2010. Two species were identified as no longer present, while others were more abundant. Diversity indices for evenness and richness displayed a trend for increased diversity for the survey. The total number of species in 7 samples was greater than in 1999. Particle size analysis and 2D MDS at 46% Bray Curtis similarity identified a trend for increased mud content in the 2010 samples. Compositional change in the inner estuary seems most likely to have been driven by changes to river flow altering the salinity regime, coupled with moderations made to suspended solids released to the estuary from Guardbridge.

For the middle estuary comparison was made between 2002 and 2009; no clear differentiation was seen between the surveys. Three groupings were identified by 2D MDS ordination at 25% Bray Curtis similarity, containing 3, 10 and 15 species respectively. The group containing only 3 species was also identified by 2D MDS ordination of the environmental data as being distinct and is located in a zone historically colonized by algal mat. Combined survey diversity indices for evenness and richness similarly displayed a trend for increased diversity since the original survey. The total number of species was greater only in one sample location (D73) than in 2002 and this sample also revealed an increase in the number of individuals and displayed a shift towards finer sediment content. Generally the middle estuary shows little change between the two survey periods in response to subtle changes to sediment characteristics.

There is no evidence from these two surveys that observed and predicted climate change (Jenkins, 2009) has had negative effects on the macrofaunal communities of the inner and middle Eden estuary. Although abiotic changes have taken place, community evenness and richness appear to have improved and infer that ecosystem functioning and services are stable. Management of anthropogenic inputs, particularly suspended solids, has likely improved ecosystem functioning, allowing a more even community composition from which greater secondary production is achieved through better utilization of niche resources.

4.2. Biotic Responses

4.2.1. Species Adaptation / Acclimatisation

Acclimatization is the suite of reversible physiological/ structural changes that an organism undergoes in response to sustained natural environmental stresses, and it is distinct from adaptation which includes irreversible genetic changes that occur enabling increased productivity (Sultan, 2000). *Zostera* species, along with other sea-grasses, are known to adapt to a number of environmental stresses; responding to changes in salinity (Benjamin *et al.*, 1999, Murphy *et al.*, 2003), temperature (Ralph *et al.*, 2007) , turbidity/ light regime (Ralph *et al.*, 2007) and energy regimes (Peralta *et al.*, 2005). In chapter 2.3 (Species distribution patterns) *Zostera noltii* was observed to have changed in spatial distribution since the 1970s, spreading to a wider area throughout the inner estuary and extending in range to more seaward locations. With the extension in its range, *Z. noltii* is now growing within different environmental pressures; this short study investigates what morphological changes *Z. noltii* has undergone to enable it to flourish.

Aims

- To identify morphological changes to the eelgrass *Z. noltii*.
- To identify potential driving mechanisms for morphological changes observed.

4.2.1.1. Methodology

In August 2009 blade length, blade width, number of blades and within patch stem density measurements were taken for replicate patches of *Zostera noltii* at locations ranging from the inner, to outer Eden estuary (Figure 4-17) and from similar elevations on the high intertidal zone. At each location 3 replicates were taken from three patches to represent each of the locations. At the time of sampling, surface water salinity was measured (using a GMH 3430 digital conductivity meter, Greisinger electronics) and sediment samples were taken for particle size analysis and also for percentage organic content. Additionally, samples of surface water were collected for ammonium (NH_4^+) analysis (for each patch only due to processing costs). The ammonium surface water samples were filtered through a 0.45um syringe filter and stored at -80°C for transportation to Aberdeen University Analytical Services, Scotland, where nutrient analysis was performed using a FIA Star 5010 analyser. Spectrophotometer readings were converted to parts per million (ppm) by

cross calibration with standards of the same salinity as the samples. Particle size analysis and the percentage of organic content within the sediment followed the methodologies outlined in section 4.1.1.

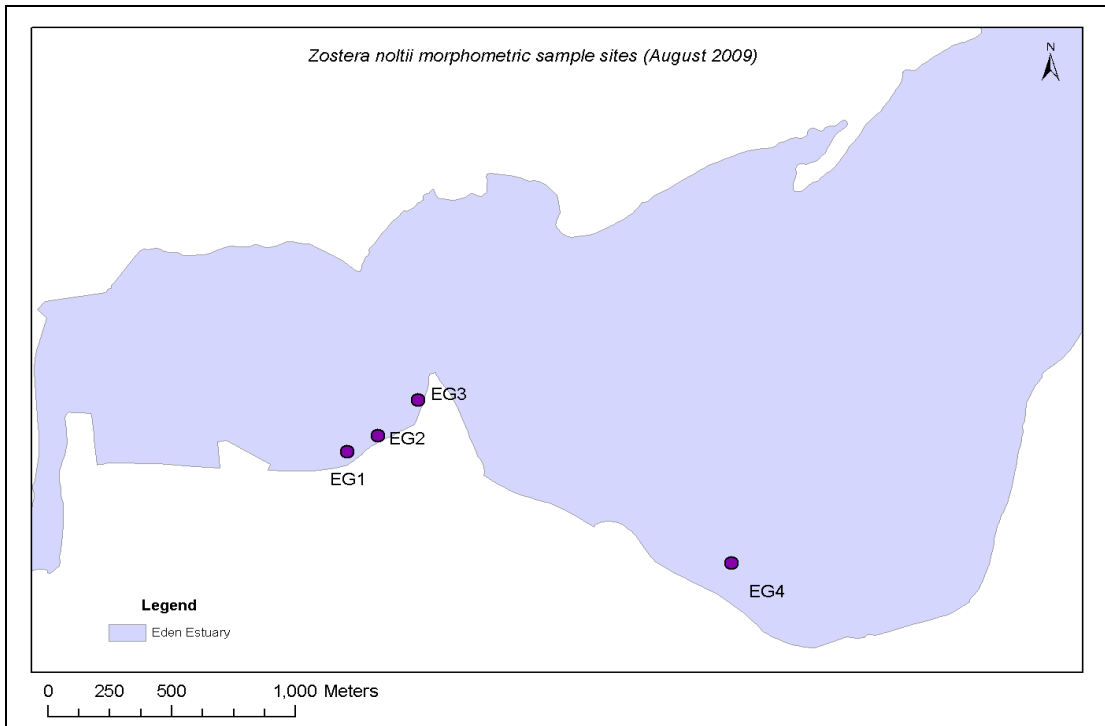


Figure 4-17: *Zostera noltii* sample locations (August 2009).

For accurate measurement of the leaf width, the blades were photographed on a graticule (Figure 4-18), the photographs were subsequently loaded to UTHSCSA Image Tool (Wilcox *et al.*, 2002) where the image was enlarged and measured, using the measuring tool, following calibration against the graticule in the image.



Figure 4-18: *Zostera noltii* blades laying over a centimetre scale graticule (small divisions are mm) used to calibrate the 'measurement tool'.

'Length of Blade', was determined by taking the longest leaf from each stem, since this represented the oldest and most fully grown blade (mean length per stem was extremely variable due to extent of growth of the youngest blade).

The 'within patch' density of stems was evaluated in the field by quadrat; initially a 1m² quadrat was trialled, however a 25cm by 25cm quadrat (Figure 4-19) was found to be more appropriate due to the size of the patches and the density of the stems. The resulting area measured was 0.0625m².



Figure 4-19: *Zostera noltii* patch and 0.0625m² quadrat for evaluation of stem density.

Exploratory data analysis used R statistical software (CRAN, 2011) to display comparative data on stem density, blade length and blade width as box plots, providing information on sample minimum, lower quartile, median, upper quartile and sample maximum.

Data for surface water ammonium (NH₄⁺) content were graphically displayed in Excel (Microsoft, 2003) as mean values with respect to salinity. Data were grouped by similar salinities (for this plot only), rather than by location as two patches were influenced by runoff and revealed reduction in salinity relative to ambient levels.

Tabulated data for each patch (blade measurements, % organic content, salinity and modal particle size) was used for Principal Component Analysis (PCA), projecting the ordinations between the potentially related variables to identify which variable/s most explained the data.

4.2.1.2. Results

The 'within patch' density of stems (Figure 4-20) followed a broad trend for increased density moving from landward to seaward. Location EG3 displays considerable variability in density however the median value follows the overall trend. At location EG2 the variability is far less, although outliers are present. One-way analysis of variance found no significant differences between any locations.

More variation was found between the EG1 (landward sample location) and the rest of the sample locations, than between any of the other locations.

Mean density per m² was also calculated for each patch (Table 4-4), and similarly displays only the landward and seaward samples are greatly different.

Table 4-4: Zostera noltii mean density expressed per m²

	EG1	EG2	EG3	EG4
Mean	6181	7477	7353	8274
STDEV	53	54	117	20

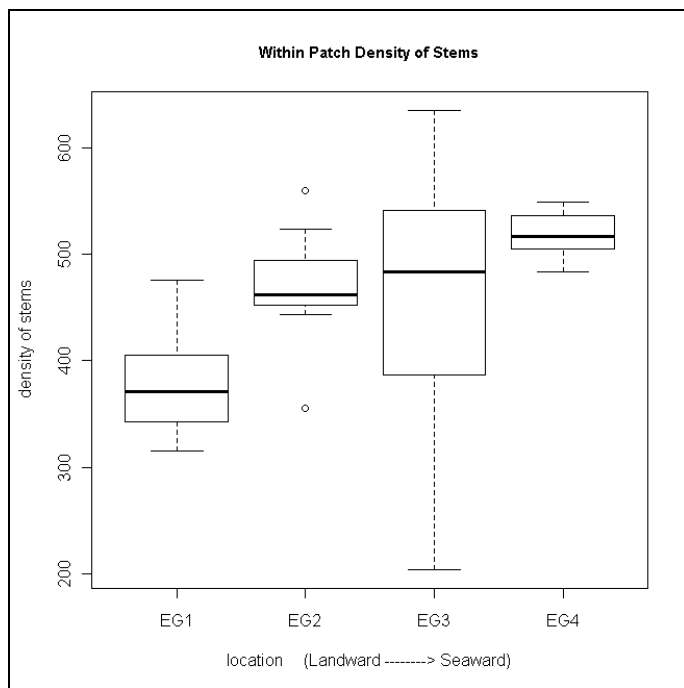


Figure 4-20: Eden estuary Figure 4: Zostera noltii mean density expressed per m²

Blade width (Figure 4-21) displays a trend for decreasing width moving from the inner towards the outer estuary. Variability in 'width' is fairly uniform, though EG4 (the most seaward location) displays least variability. Little difference is was found between the median values for EG3 and EG4. One-way analysis of variance found no significant differences between samples for the four locations.

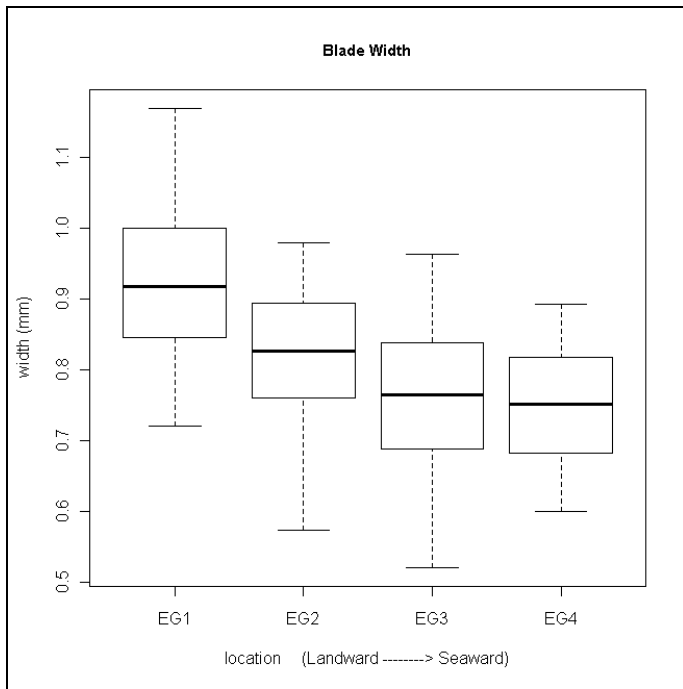


Figure 4-21: *Zostera noltii* blade width (mm).

Length of blade (Figure 4-22) displays a trend for increasing length moving from the inner estuary towards the outer estuary. There is considerable variability in the range of values for EG2 and the median differs little from EG3. The two extremities (EG1 & EG4) were most different in median values; one-way analysis of variance gave a 5% significant difference (One-way ANOVA F crit. 7.71) between these locations.

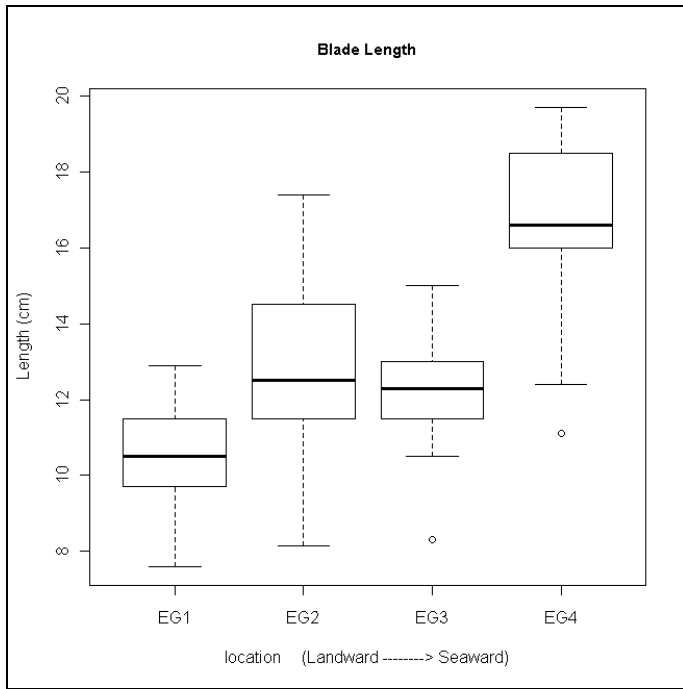


Figure 4-22: Eden estuary *Zostera noltii* blade length (cm).

Ammonium (NH_4^+) data was grouped by similar salinities and the mean values plotted (Figure) against increasing salinity (PSU). A relationship was found between increasing ammonium content in the seawater, with increasing salinity. The gradient in the relationship became steeper above 20 PSU.

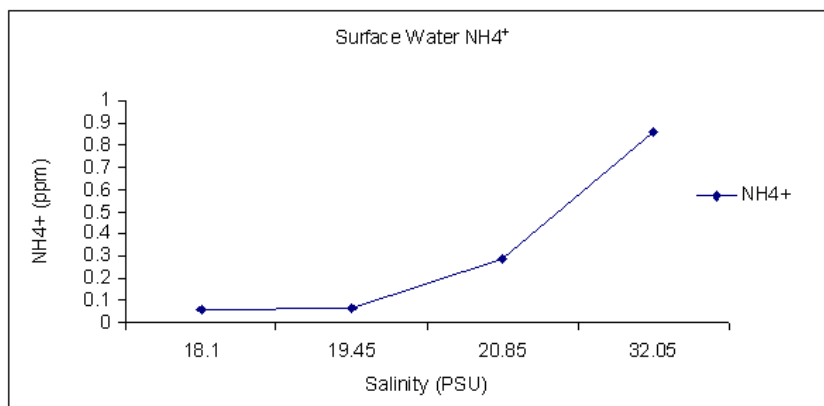


Figure 4-23: Surface water ammonium (NH_4^+) levels recorded against mean salinities for the inner, middle and both outer estuary locations.

The morphometric measurements and environmental variables were tabulated (Table 4-5) and input to PCA (Figure 2-24) to identify the attributes which explained the greater proportion of variance.

Table 4-5: Tabulated data used for as input to the PCA

Replicate	Sample	Salinity (ppt)	NH4 ⁺ (ppm)	Stem density (0.0625m ²)	% organics	length (cm)	width (mm)	Modal particle size
EG1-1	1	17.6	0.08	431	0.08	10.80	0.74	194.2
EG1-2	2	18.2	0.03	362	0.07	9.31	0.89	194.2
EG1-3	3	18.3	0.04	366	0.13	11.36	0.97	194.2
EG2-3	4	18.3	0.08	456	0.08	14.25	0.82	213.2
EG2-2	5	18.7	0.10	420	0.09	10.78	0.81	213.2
EG2-1	6	20.2	0.04	526	0.06	12.86	0.98	213.2
EG3-3	7	20.7	0.11	454	0.07	13.70	0.77	234.1
EG4-3	8	20.7	0.11	516	0.05	17.64	0.77	194.2
EG3-2	9	20.8	0.82	558	0.06	12.23	0.76	234.1
EG3-1	10	21.2	0.10	366	0.05	10.88	0.75	234.1
EG4-1	11	31.6	1.46	512	0.10	18.46	0.74	194.2
EG4-2	12	32.5	0.26	524	0.05	13.36	0.73	194.2

Principal component analysis identifies stem density, salinity (psu), blade length and NH₄⁺ as having strong positive effects on PC1, whilst blade width has strong negative effect on PC1.

Particle size has a strong positive effect on PC2 and the percentage of organic content has strong negative effect on PC2.

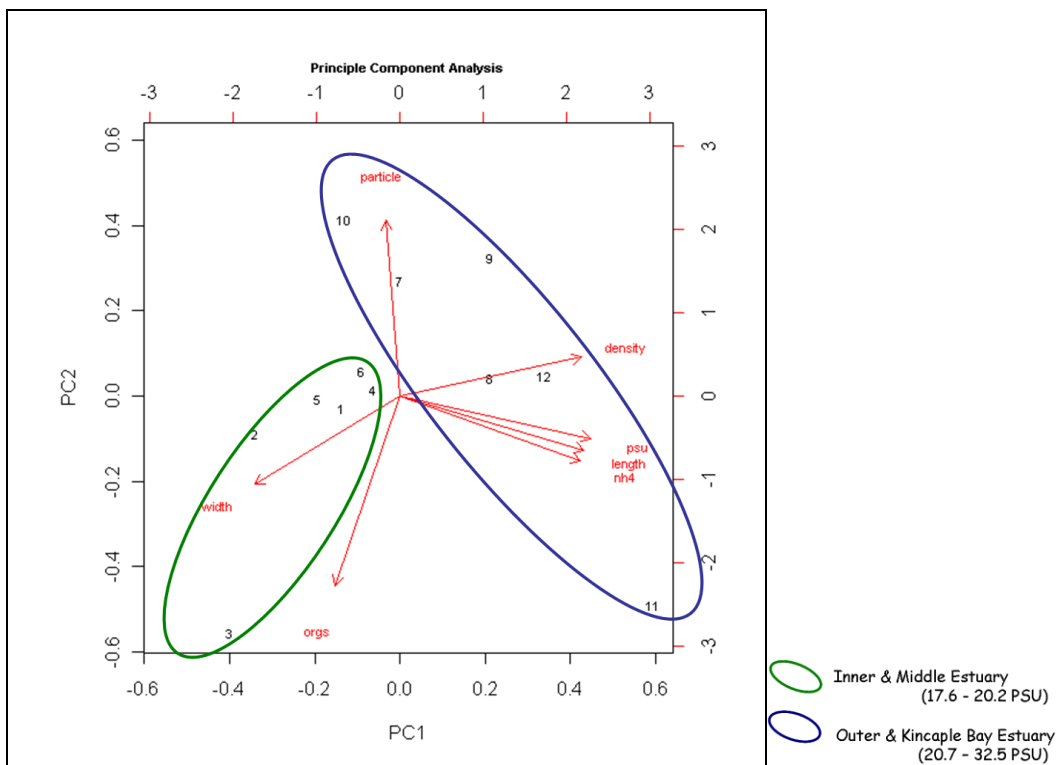


Figure 4-24: Principal component analysis of *Zostera noltii* morphometrics and environmental attributes.

Output from the principal component analysis (Figure 4-25) indicates that 43% of variance is explained by PC1 and 23% of the variance is explained by PC2.

Importance of components:							
	PC1	PC2	PC3	PC4	PC5	PC6	PC7
Standard deviation	1.7392	1.2613	0.9010	0.8624	0.64925	0.51264	0.38030
Proportion of Variance	0.4321	0.2273	0.1160	0.1062	0.06022	0.03754	0.02066
Cumulative Proportion	0.4321	0.6594	0.7753	0.8816	0.94180	0.97934	1.00000

Figure 4-25: Principal component analysis output statistics.

4.2.1.3. Discussion

Changes to the size and density of *Z. noltii* plants was observed between the inner and outer estuary intertidal locations; plants exhibited trends for longer and thinner blades and a higher density of stems to seaward and trends for shorter, wider and lower density of stems in the landward direction. Significant differences in morphodynamics were not found in this study; this is perhaps because samples could only be collected from available patches of *Z. noltii* plants (having similar elevations and littoral positions), these patches were actually not very far from each other, thus the conclusions that can be drawn are limited. Principal component analysis identified a positive interaction with increasing stem density and length of blades corresponding to increasing salinity and ammonium in the surface pore water, which reflects the landward seaward estuarine salinity gradient. The second principal component identified a gradient moving from high organic content through to increased particle size, reflecting the gradient between river born higher organic deposition in the lower energy inner estuary and increasing particle size moving seaward to higher energy conditions. Although it may be expected that particle size would co-vary with salinity in response to increasing energy conditions seaward, circulation within the bays coupled additional sediment contribution from erosion (of glacial sands) at the high water mark may add to the non linear salinity-particle size relationship.

From the PCA, samples 7,9,10 are from EG3 and appear to have closer associations to particle size than sample 8, 11 and 12 (EG4) which are more associated with salinity and ammonium. This may suggest that the level of energy (wave and current velocities) also plays an important role determining plant morphology additional to salinity. Peralta *et al.* (2005) observed that under severe storm conditions *Z. noltii* changed morphology, forming shorter and narrower leaf blades in response to elevated wave activity. Narrower leaves would seem preferential in higher energy conditions, reducing the drag against the currents and lessening the chance of uprooting.

The PCA identified a close relationship between salinity and ammonium (Figure 4-23); Salinity is known to impact on NH₄⁺ adsorption, with a greater efflux of NH₄⁺ from the sediment with increased salinity (Rysgaard *et al.*, 1999). *Zostera* species preferentially utilize ammonium as an

inorganic nitrogen source (Alexandre *et al.*, 2010, Hemminga *et al.*, 1994), both from the water column and from the sediment pore water, using both leaves and roots (Hemminga, 1998), although the leaves have been identified as the primary reducing sites during assimilation (Alexandre *et al.*, 2010). The narrowing of blade width whilst growing in saline and high energy conditions (an environment causing a greater efflux of NH_4^+) should not require lengthening of the leaf blade to preserve the total surface area; inferring blade lengthening is not likely to be the result of NH_4^+ acquisition alone. In terms of preserving surface area for photosynthesis, variation in P_{max}^B for different leaf morphotypes was observed by Peralta *et al.* (2000), with small leaf morphotypes of *Z. noltii* (located on the channel edge) having a higher P_{max}^B than larger leaved morphotypes (growing within the channel). Variation was attributed to the high surface to volume ratio in the smaller leaves allowing chlorophyll to be distributed more evenly and giving an inverse relationship between blade size and photosynthetic capacity.

It therefore seems unlikely that lengthening of blades in the current survey is to preserve blade surface area for an equal level of photosynthesis compared to other morphotypes. Conversely, photosynthetic activity in *Zostera marina* decreases linearly with decreasing salinity (Biebl and McRoy, 1971) largely due to the decrease in bicarbonate ions (Hellblom and Bjork, 1999) rather than the reduction in salinity, thus the shorter inner estuary *Z. noltii* blades may have developed wider blades to maximize photosynthetic activity.

Since both the shorter wider and longer thinner morphotypes of *Z. noltii* had the same surface area, uncertainty still remains as to why the seaward plants were greater in length. The first principal component identified density as a strong positive factor; growing close to a plant's ecological tolerance limit causes a high energy demand, impacting on metabolic and growth rates (Biebl and McRoy, 1971). Peralta (1999) observed small morphotypes to produce internodes every 3.5 days, whilst large morphotypes required 5 days and having shorter intermodal length, thus producing a higher density of stems. With increased density, self-shading is likely to impact on photosynthetic capacity, therefore an increase in blade length may be a method to overcome low irradiance and by positioning higher up the canopy (Spence *et al.*, 1973).

Data acquisition for this survey was limited by the designation of the Eden estuary as a SSSI, SPA and SAC and by *Z. noltii* being a UKBAP priority species and Habitat. The study aimed to cause as little impact to the *Zostera* beds as possible, thus below ground metrics and total biomass were not recorded. The study also lacks information on the photosynthetic activity of the plants, which in hindsight would have aided interpretation of the results. Despite these shortcomings, the study has identified morphometric plasticity in the *Z. noltii* within the Eden estuary, which would appear to result from variability in growth rates and photosynthetic capacity resulting from salinity, bicarbonate ion availability and or changes to tidal/wave energy stress.

4.2.1.4. Summary

In August 2009 the eelgrass *Zostera noltii* was investigated for morphological changes; blade length, blade width, number of blades and within patch stem density measurements were taken for replicate patches at locations ranging from the inner, to outer Eden estuary and all plants were located at similar elevations on the high intertidal zone. Plants growing at more landward locations exhibited a trend for shorter, wider and less dense growth of stems, whilst the trend for seaward plants was for longer thinner and more dense growth of stems. Overall there were no significant differences in leaf blade area, likely due to the patches being separated by only small distances. Changes exhibited by the *Z. noltii* may result from variability in growth rates and photosynthetic capacity in response to salinity, bicarbonate ion availability and or changes to tidal/wave energy stress. Data for total biomass, photosynthetic activity and below ground metrics would have aided interpretation of the results.

4.3. Chapter Discussion

The aim of this chapter was to identify temporal change in ecosystem function, through changes to macro-faunal species community composition and through the spatial distribution of the keystone species, *Zostera noltii*, and investigate regime shifts brought about by changes to the local and regional climate. Macro-fauna are often used to indicate a level of “ecosystem health” and functioning (Borja *et al.*, 2008, Borja *et al.*, 2004). The diversity of community structure represents a number of functional roles which maintain an array of ecosystem processes. Thus the loss of species with high sensitivity levels can cause potential functional change. Macrofauna also, have a limited range of mobility and thus reflect responses to the localized ambient environmental conditions and importantly they are relatively long lived and thus are able to reflect gradual trends in physicochemical conditions (Borja *et al.*, 2000, Fano *et al.*, 2003). The estuarine zone targeted for macro-faunal analysis in this study spanned between the relatively low salinity inner estuary and the estimated front of the tidal intrusion. Climate driven regime shifts were anticipated to impact in this zone, through changes to the volume of river flow causing a seaward shift in the tidal asymmetry and relative sea level rise under the influence of the lunar nodal cycle causing a landward shift in asymmetry. Altered asymmetry will impact on the hydrodynamic regime and energy levels, turbidity, water temperature, salinity and the quantity of dissolved gasses in the water. Additionally, increased runoff has the potential to elevate nutrients, dissolved and suspended organic matter and sediment input to the estuary, whilst increased estuarine volumes reduce their residence times. Sustained abiotic changes drive the reorganization of habitats and may lead to biological responses in terms of physiological changes or adaptations within species. This component of climate driven change was the focus for the second part of the chapter that investigated the spatial distribution changes by *Z. noltii*. As a keystone species supporting a wealth of other organisms; a reduction in *Z. noltii* potentially could impact on network of other organisms, from primary producers to higher heterotrophs with consequences to the maintenance of ecosystem processes. Of the anticipated

abiotic regime changes, salinity was expected to be the most challenging environmental stressor for *Z. noltii*; in maintaining osmolality, in regulating growth rates and hence for productivity.

Data from this study, for the inner estuary, suggest a shift towards increased mud content in the sediment and a trend for increased community diversity; additional salinity data infer that salinities have lowered over the survey area for the inner estuary since the late 1970s, all these data point towards a seaward shift in the asymmetry likely driven by increased river inflow and a reduction in the tidal range following the lunar nodal maximum in 2006. Data for the middle estuary are less conclusive, displaying little change over time in both overall sediment characteristics and macro-faunal community composition, although a trend for increased community diversity was observed. Changes to the middle estuary survey location would appear to be driven more by management of nutrient and suspended solids input to the estuary than by change to the asymmetry; mean riverine and 'discharge' nitrogen loadings to the estuary reduced by approximately 0.5mg/l between 1997 and 2000 and by a further 1mg/l by 2005 (CFAS, 2007), which probably contributed to a reduction in macro-algal cover present today.

The keystone species *Z. noltii*, and associated epiphytes, as primary producers are particularly sensitive to variation in nutrient and light availability (Fano *et al.*, 2003), but since light is not limiting for high intertidal species they are perhaps more vulnerable to competition by opportunistic macro-algae which thrive on eutrophic pulses. The morphological changes exhibited by *Z. noltii* are likely driven by a combination of hydrodynamics (particularly wave exposure) and by salinity causing metabolic stress, impacting on growth rates and photosynthetic capacity. *Z. noltii* has increased in both area and range, increasing habitat availability and therefore potentially greater species diversity.

Despite the limitations of these surveys, the data may tentatively point towards a trend for increased ecosystem health through generally greater evenness and richness of community diversity and the expansion in range of the keystone species *Z. noltii*, supporting a hierarchy of other organisms. As early as the 1850s, Charles Darwin recognized that diversity of species increased ecosystem functioning through adaptation to different environmental conditions, species utilized different niches evolving complementary communities which increased both utilization of resources and productivity (Hector, 2009, Hector and Hooper, 2002). The changes both to the macro-faunal community and to the eelgrass *Z. noltii* infer increased community diversity and hence may be interpreted as able to support an increased level of ecosystem functioning and provision of services despite the abiotic changes that have occurred.

4.4. Chapter summary

Estuary health was estimated through changes to macro-faunal community diversity as a proxy measure of ecosystem function and the response of the keystone species *Z. noltii* to regime changes brought about by local and regional climate change. The community composition displayed

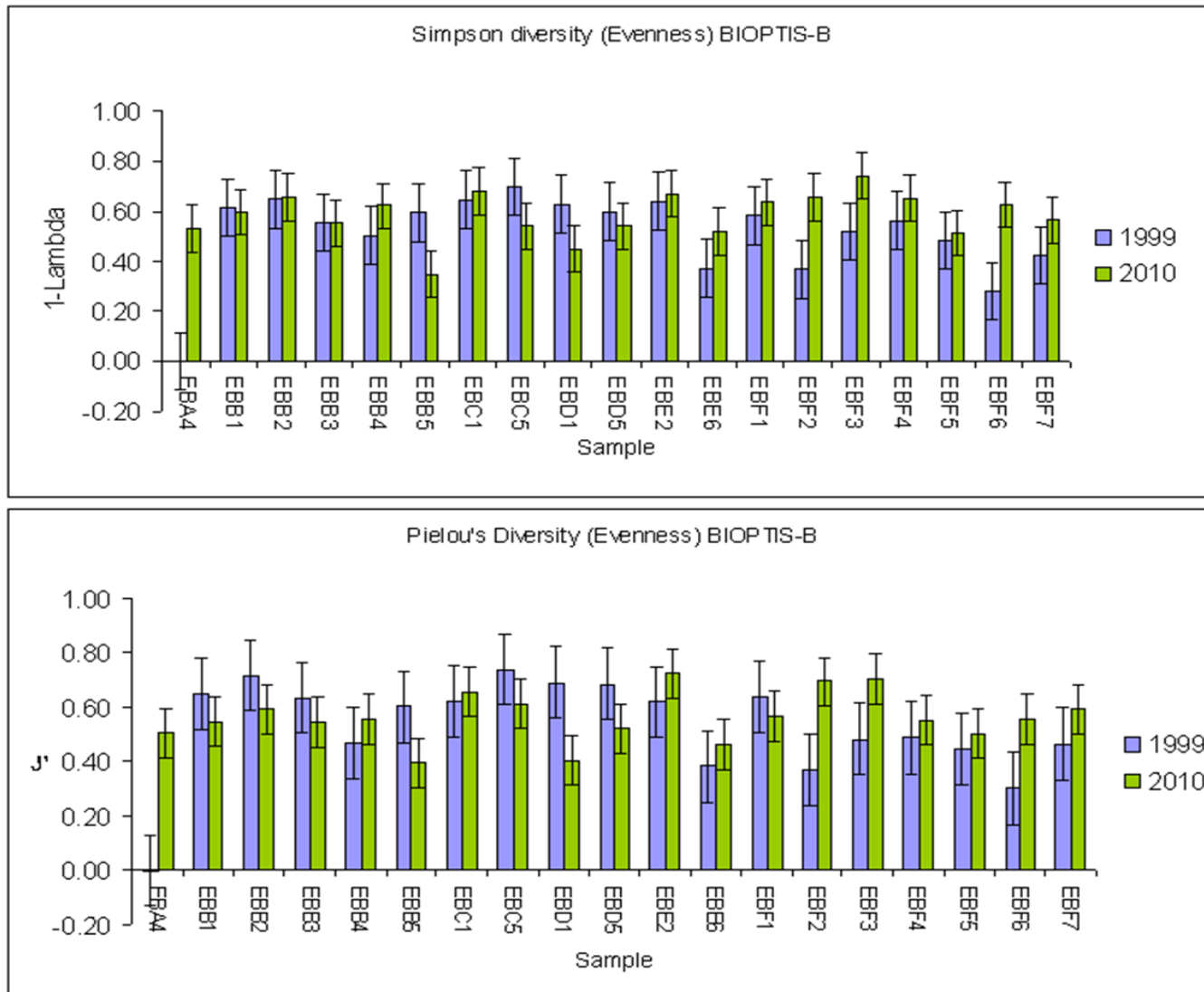
a trend for increasing diversity in the inner estuary between 1999 and 2010; less change was evident for the middle estuary between 2002 and 2009. All of the inner estuary samples for community composition from 1999 were significantly different to those of 2010 (Bray Curtis similarity at 46%, stress 0.15). A shift in particle size towards increased mud content was accompanied by increased river flow during the sample interval, inferring a seaward shift in salinity, consistent with the findings of chapter 3. Additional interstitial salinity data similarly displayed a lowering of salinity for the sample zone. Interpretation of the middle estuary data was less clear, where only 2 samples were significantly different between surveys, although an overall trend for increased diversity was observed. Middle estuary trends may have resulted from changes to macro-algal cover.

Acclimatization by the keystone species *Z. noltii* gave rise to morphological variations with inner estuary forms having a trend for shorter and wider blades, with lower density of stems and seaward forms having a trend for longer and thinner blades with a higher density of stems. Length of blades for the landward most blades was significantly different to length in seawards most blades (at 5% level of significance). Both the area and range of *Z. noltii* has increased since the late 1970s through acclimatization and hence a concomitant increase in habitat availability. For greater certainty in the trends found within this study, further targeted research involving replicate samples is required, however this study does give an overview of the current state of 'estuary health' and indicates a level of functioning that has kept pace with local and regional climate/ environmental changes.

Appendix 1

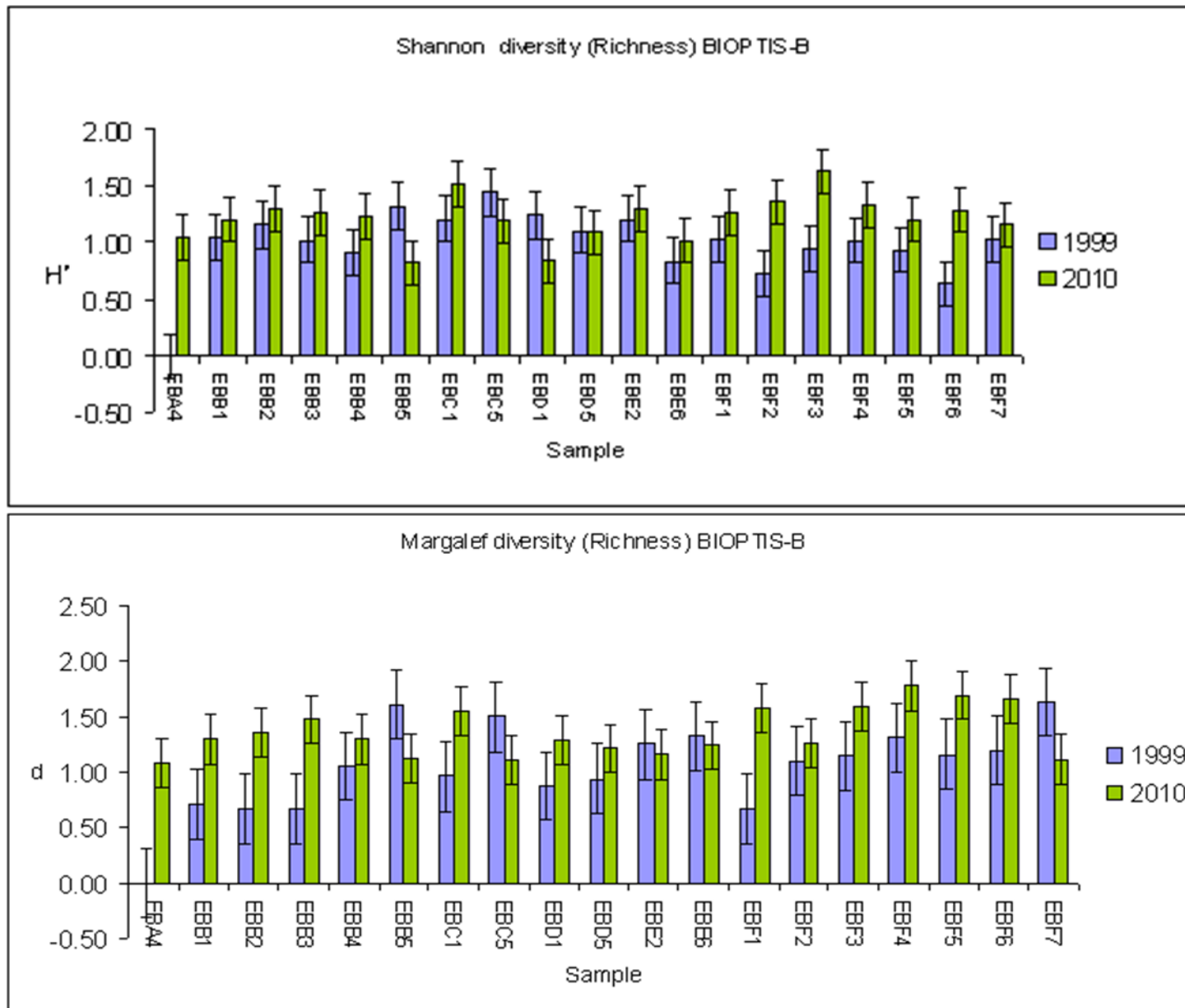
4.5. Chapter 4: Appendices

Diversity analysis of individual samples -BIOPTIS



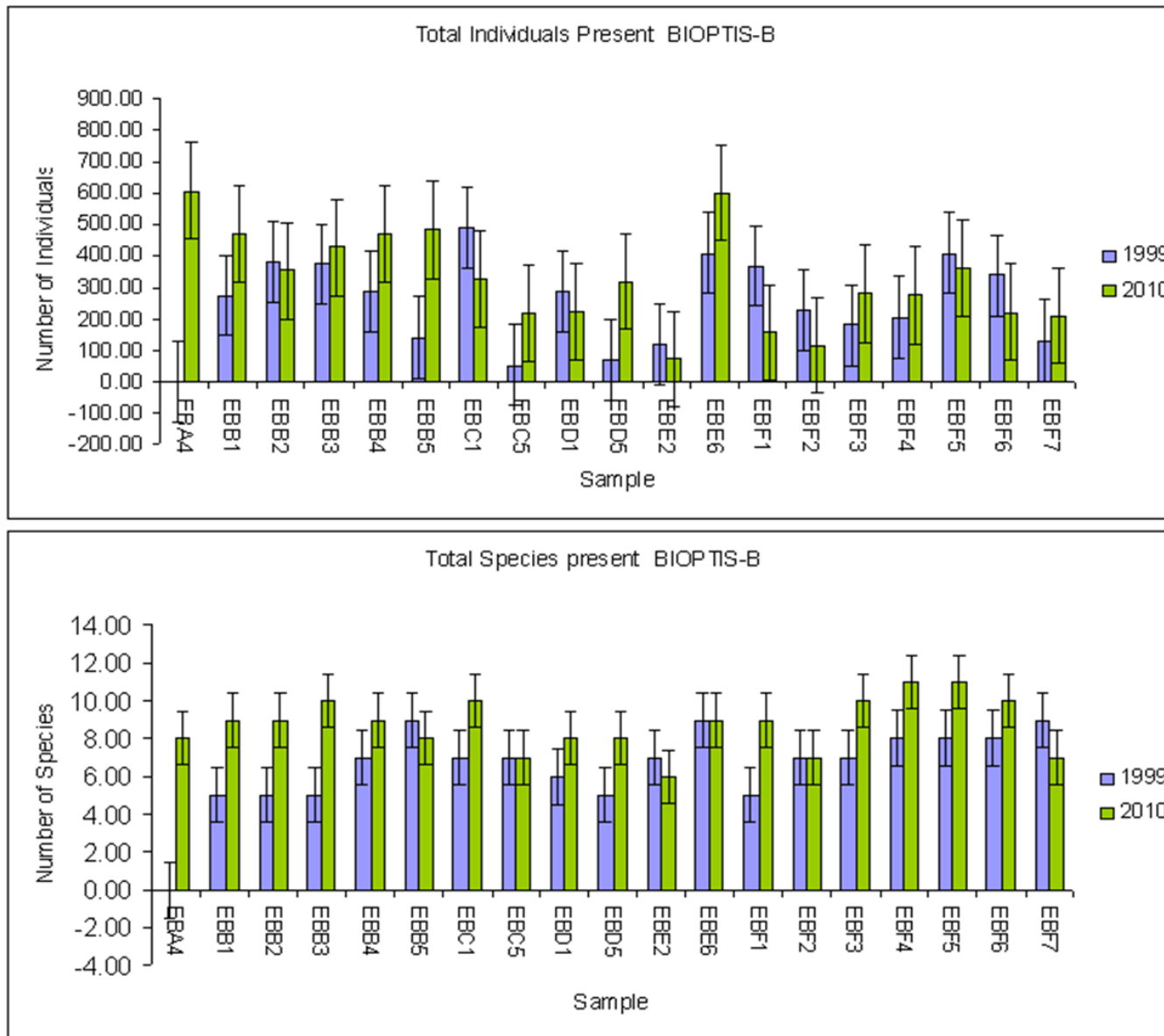
Chapter 4 appendix 1 Figure 1: Evenness diversity indices for the individual samples, error bars are 1 standard deviation of the survey total.

Appendix 1



Chapter 4 appendix 1 Figure 2: Richness diversity indices of the individual samples, error bars are 1 standard deviation of the survey total

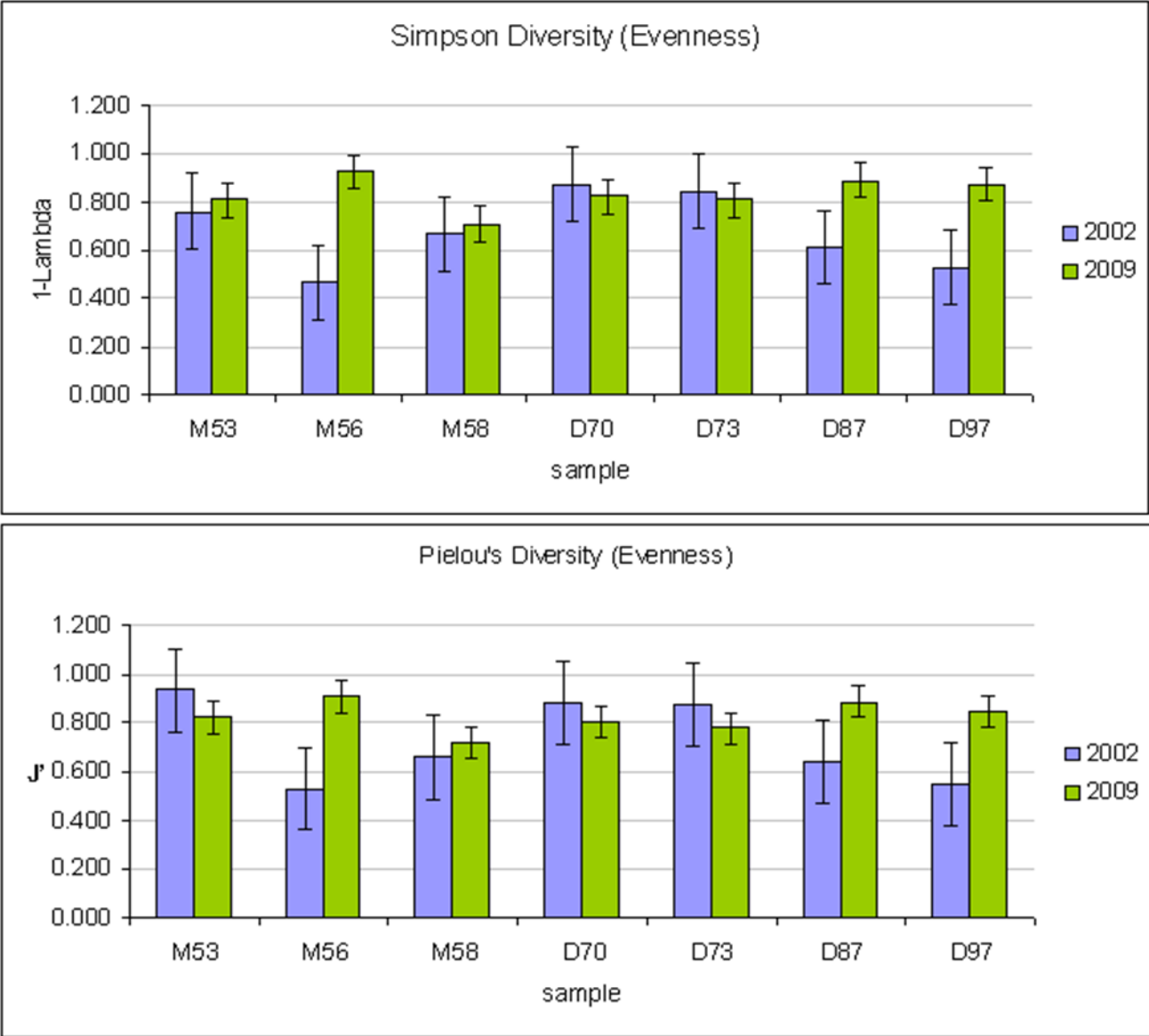
Appendix 1



Chapter 4 appendix 1 Figure 3: Total number of individual counts and total number of species counts for the individual samples, error bars are 1 standard deviation of the survey total.

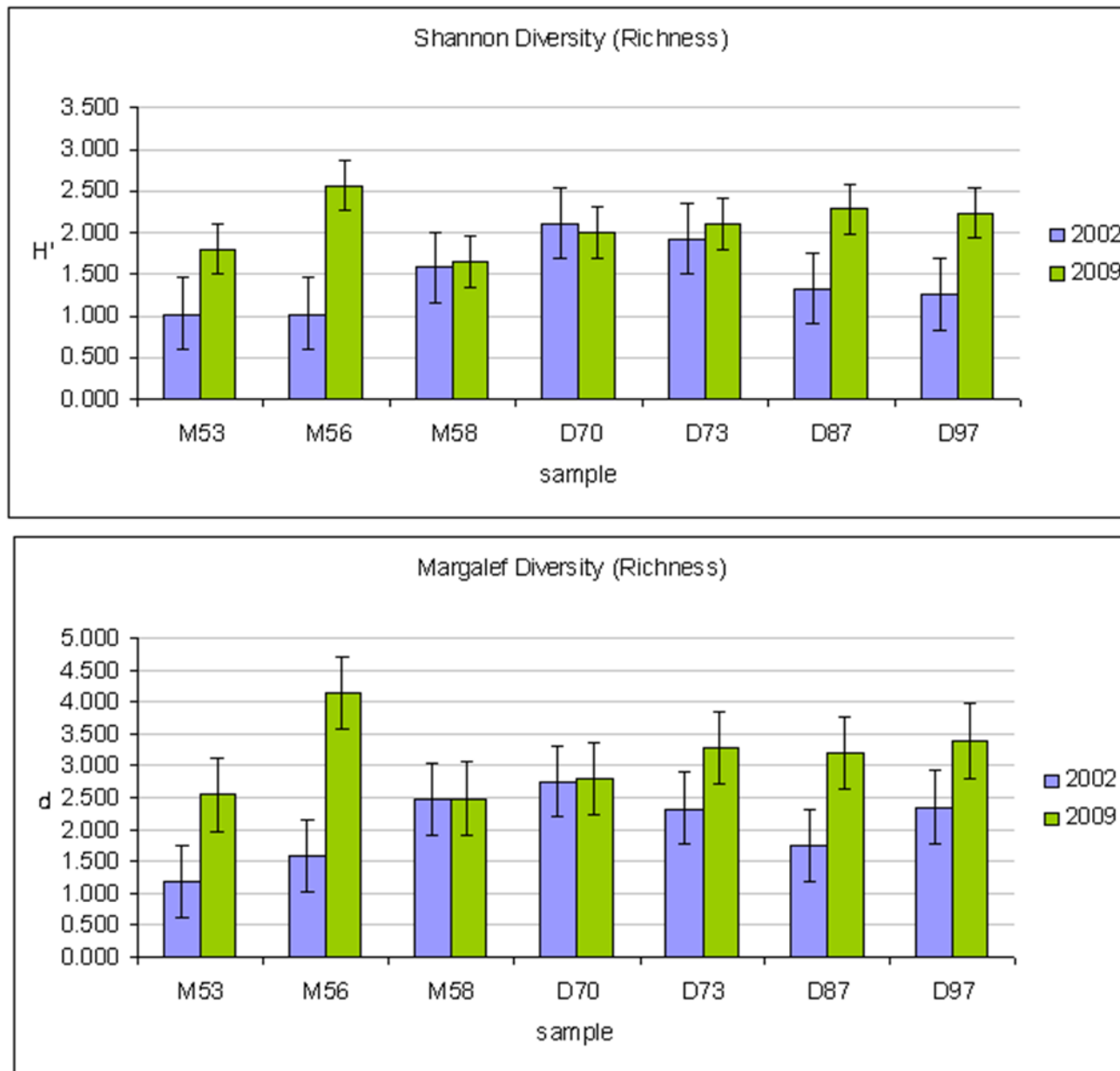
Appendix 1

Diversity analysis of individual samples - SNH



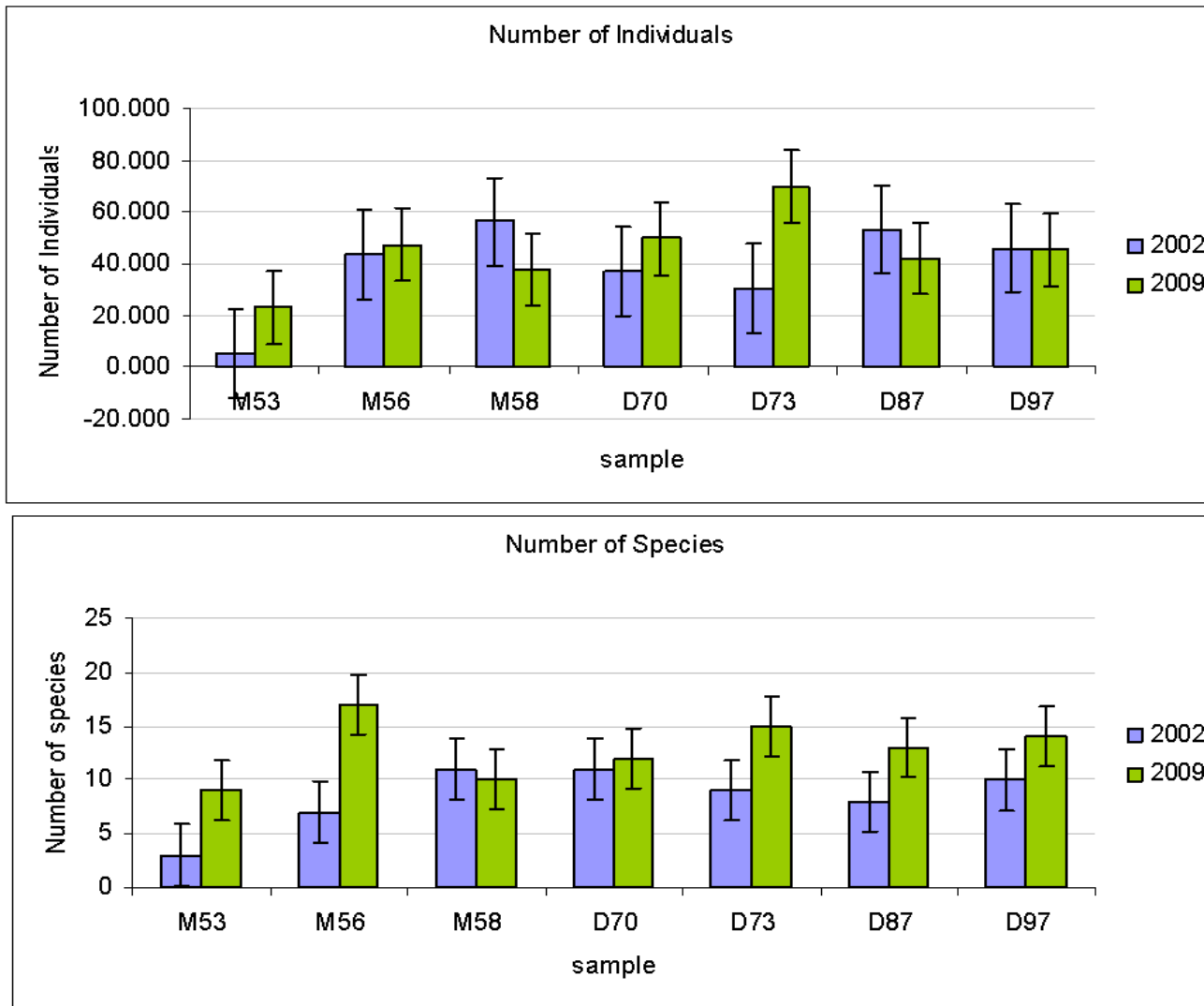
Chapter 4 appendix 1 Figure 5: Evenness diversity indices for the individual samples, error bars are 1 standard deviation of the survey total.

Appendix 1



Chapter 4 appendix 1 Figure 6: Richness diversity indices for the individual samples, error bars are 1 standard deviation of the survey total.

Appendix 1



Chapter 4 appendix 1 Figure 7: Total number of individual counts and total number of species counts for the individual samples, error bars are 1 standard deviation of the survey total.

Appendix 1

Core	Organic carbon (%)	2	1	0.5	0.25	0.063	<0.063	%>60um	dist	elev mm
99EBA4	2.815	0.000	0.209	0.371	2.832	78.419	18.169	81.831	339.6	-577.08
99EBB3	1.923	0.000	0.023	0.133	4.650	82.266	12.929	87.071	156.48	1105.59
99EBB4	3.396	0.060	0.016	0.304	4.268	71.737	23.614	76.386	244.75	834.79
99EBB5	4.729	0.809	0.027	0.233	2.885	67.324	28.722	71.278	366.4	-284.53
99EBC5	5.086	0.119	0.074	0.157	1.545	56.978	41.126	58.874	388.93	-67.73
99EBD5	3.795	0.170	0.023	0.064	0.916	70.789	28.037	71.963	45.65	47.54
99EBE2	4.365	0.458	0.298	0.666	2.289	69.765	26.524	73.476	136.79	974.91
99EBE6	2.846	4.165	0.168	0.410	3.798	74.875	16.584	83.416	464.01	49.54
99EBF1	3.395	0.793	0.084	0.346	4.398	73.945	20.435	79.565	91.38	1059.05
99EBF2	5.412	0.021	0.036	0.187	0.794	43.205	55.756	44.244	174.56	980.53
99EBF3	3.488	0.405	0.462	1.118	4.161	41.798	52.057	47.943	263.66	829.58
99EBF4	2.590	0.115	0.244	0.591	2.579	78.781	17.690	82.310	360.6	752.87
99EBF5	0.000	4.744	0.770	0.896	3.309	80.424	9.856	90.144	450.06	535.50
99EBF6	3.291	2.182	0.313	0.651	2.488	80.990	13.375	86.625	542.88	167.65
99EBF7	2.382	0.120	0.304	1.722	14.680	67.991	15.183	84.817	636.09	-199.99
10EBA4	4.227	0.000	0.000	0.603	8.020	31.990	59.450	44.839	339.600	-561.500
10EBB1	3.026	0.000	2.310	1.192	15.400	53.650	27.425	75.578	14.980	1528.500
10EBB2	1.932	0.000	0.000	0.067	11.760	56.370	31.767	70.129	67.020	1298.500
10EBB3	2.220	0.000	0.000	0.363	11.670	57.080	30.877	71.333	156.480	1088.500
10EBB4	3.913	0.000	0.000	0.819	8.820	40.630	50.492	54.183	244.750	738.500
10EBB5	4.393	0.000	0.000	0.000	2.581	44.980	52.386	51.954	366.400	-341.500
10EBC1	1.888	0.000	0.000	0.556	28.190	53.140	18.088	83.774	30.160	1338.500
10EBC5	5.081	0.000	0.744	0.744	7.140	45.290	46.842	59.000	388.930	-141.500
10EBD1	5.143	0.000	0.000	0.446	4.380	30.820	64.333	40.790	92.890	1138.500
10EBD5	3.904	0.000	0.000	0.679	8.600	47.290	45.435	60.473	45.650	-71.500
10EBE2	6.941	0.000	0.000	0.000	0.660	26.570	72.765	34.171	136.790	1058.500
10EBE6	3.154	0.000	0.000	0.656	10.150	57.630	31.529	71.590	464.010	68.500
10EBF1	5.999	0.000	0.000	0.000	1.296	32.660	66.040	39.955	91.380	1048.500
10EBF2	4.715	0.000	0.000	0.366	4.870	35.910	58.832	45.861	174.560	958.500
10EBF3	4.463	0.000	0.000	0.102	4.390	34.590	60.934	43.546	263.660	838.500
10EBF4	2.856	0.000	1.373	2.570	10.530	55.590	29.945	72.919	360.600	728.500
10EBF5	2.748	0.000	0.000	0.330	6.460	60.300	32.884	69.837	450.060	518.500
10EBF6	2.924	0.000	0.000	0.437	10.680	59.950	29.913	73.992	542.880	728.500
10EBF7	5.036	0.000	0.000	0.067	4.480	30.020	64.443	39.603	636.090	-321.500

Chapter 4 appendix 1 Figure 9: BIOPTIS survey environmental variables matrix.

Appendix 1

Species	2002M53	2009M53	2002M56	2009M56	2002M58	2009M58	2002D70	2009D70	2002D73	2009D73	2002D87	2009D87	2002D97	2009D97
Arenicola marina									2	1			1	1
Capitella spp			1	1				14	3	4		8	18	
Eteone longa			2	2	2	2	3	4	1	4	10	5		2
Fabricia sabella		1		1								16		6
Glycera capitata														
Malacoceros fuliginosus				1			5			7	1			
Mediomastus fragilis				7								1	1	
Nereis diversicolor	3		10	2	23	5	6	2	53	5		1	1	1
Nereis virens							2	2		1				
Neptis hombergii			1											
Nephtys longostosa														
Pygospio elegans	7		1	3	1	2	27	3		10	8			16
Scoloplos amiger		17		1	1			1						1
Spiophanes bombyx														
*Ploynoidae (polynoinae)				1										
Ampharete grubei (baltica?)													4	
Chironomidae:Diptera														1
nemertean sp.					2						3			
Chaetozone setosa								1						
Oligochaeta spp		91		58		392	20	288		21	100	29	1000	119
Enchytraeidae														
Tubificidae spp					1	2	1						1	
Tubificoides benedii			20	44	46	7	39	133	87	55	1	128	1	117
Tubificoides pseudodagaster		1												
Bathyporeia sarsi														
Corophium volutator	1		1000	39	1000	30	100	18		1	1000	9		1
Crangon crangon					3				6				1	
Leptomysis gracilis														
Pontopliulus trispinosus										4				
Semibalanus balanoides														
Halyciclops sp.														
Abra abra		1					1							
Buccinum undatum		1												
Cerastoderma edule				11	2	1			10	59		2		12
Chamelea gallina														
Cylichna cylindracea				8		1				1		1		1
Hydrobia ulvae				10		2			3	798		14		16
Macoma baltica		1		19	17		2	13	6	15	4	18	5	6
Mytilus edulis		7		1				2				1		

Chapter 4 appendix 1 Figure 10: SNH survey species matrix.

Appendix 1

Core	% organics	Sorting	Skew	>2000	1000	500	250	125	63	<63	elev mm
2002M53	24.698598	0.71	0.75	0	0.03	0.06	3.87	67.86	20.6	7.58	-1145
2009M53	24.698598	13.9063	3.35316	0	3.097848	4.146832	24.25274	39.77992	13.17856	15.54411	688.5
2002M56	2.5821915	0.97	1.03	0	0.04	0.23	29.32	47.66	14.22	8.52	649.62
2009M56	2.5821915	15.9179	3.60854	0	2.686001	2.246843	14.60249	20.71062	20.72963	39.02442	688.5
2002M58	1.6176073	0.8	0.87	0	0.87	2.93	31.84	49.47	9.56	5.34	986.56
2009M58	1.6176073	-0.8328	0.321662	0	0	0.094079	27.42662	30.79431	13.11471	28.57028	878.5
2002D70	19.69275	0.725	1.496	0	0	3.6	16.5	27.5	16.6	35.8	-308.29
2009D70	19.69275	9.8782	3.91338	0	1.591463	1.408006	9.99621	21.57986	15.88216	49.54229	-471.5
2002D73	0.6913551	1.576	0.195	0	0	4.4	59.8	30.01	0.93	4.86	769.12
2009D73	0.6913551	0.755597	-0.06491	0	0	0.159636	28.40094	56.57748	4.094161	10.76778	528.5
2002D87	3.7723014	0.699	3.968	0	0.7	3.3	6.7	12.5	14.6	62.2	2056.08
2009D87	3.7723014	0.412605	1.14031	0	0	0.013009	13.33441	17.07091	23.15582	46.42585	2208.5
2002D97	0.9288136	0.772	0.474	0	0	4.9	38.2	22.6	8.2	26.1	377.75
2009D97	1.1335593	-0.29522	0.163538	0	0	2.88975	47.17306	28.18806	6.918391	14.83074	198.5

Chapter 4 appendix 1 Figure 11: SNH survey environmental variables matrix.

4.6. References

Section 4.1 Ecosystem Function

- Attrill, M.J. & Rundle, S.D., 2002. Ecotone or Ecocline: Ecological Boundaries in Estuaries, *Estuarine, Coastal and Shelf Science*, **55**, 929-936.
- Bellan, G., 2011. *Nephtys hombergii* Savigny in Lamarck, 1818. In Read, G.; Fauchald, K (Ed) World Polychaeta database. Accessed through: World Register of Marine Species.
- Bolam, S.G., 2003. Estuary Process Research Project (EstProc). Spatial patterns of estuarine macrobenthic assemblages: relationships with hydrodynamic regime. Report No: FD1905/CEFAS Laboratories, Remembrance Ave, Burnham-on-Crouch, Essex, CM0 8HA.
- Bolam, S.G. & Fernandes, T.F., 2003. Dense aggregations of *Pygospio elegans* (Claparede): effect on macrofaunal community structure and sediments, *Journal of Sea Research*, **49**, 171-185.
- Boschker, H.T.S., Kromkamp, J.C. & Middelburg, J.J., 2005. Biomarker and carbon isotopic constraints on bacterial and algal community structure and functioning in a turbid, tidal estuary, *Limnology and Oceanography*, **50**, 70-80.
- Bremner, J., Rogers, S.I. & Frid, C.L.J., 2003. Assessing functional diversity in marine benthic ecosystems: a comparison of approaches, *Marine Ecology-Progress Series*, **254**, 11-25.
- Cardinale, B. J. 2012. Biodiversity loss and its impact on humanity (vol 486, pg 59, 2012). *Nature* **489**: 326-326.
- Cardoso, P.G., Pardal, M.A., Raffaelli, D., Baeta, A. & Marques, J.C., 2004. Macroinvertebrate response to different species of macroalgal mats and the role of disturbance history, *Journal of Experimental Marine Biology and Ecology*, **308**, 207-220.
- CFAS, 2007. OSPAR eutrophication assessments: SEPA comprehensive procedure 2008 - Eden.DEFRA: Environment Agency, Marine Environmental Research.
- Chesney, E.J. & Tenore, K.R., 1985. Oscillations of Laboratory Populations of the Polychaete *Capitella-capitata* (TYPE-I) - Their Causes and Implications for Natural-Populations, *Marine Ecology-Progress Series*, **20**, 289-296.
- Clarke, K.R. and R.N, Gorley, 2006. PRIMER v6: User Manual/Tutorial.PRIMER-E. Ltd, 3 Meadow View, Luton, Ivybridge, Plymouth, PL21 9RH, UK.
- Clelland, B.E., 1997. The Eden estuary: a review of its ecological and conservation interest, with particular reference to water quality. in *The estuaries of central Scotland.*, Edinburgh.
- Costa, P.F.E., Oliveira, R., F & Cancela Da Fonseca, L., 2006. Feeding Ecology of *Nereis diversicolor* (O.F. Muller) (Annelida, Polychaeta) on Estuarine and Lagoon Environments in the Southwest Coast of Portugal, *Pan-American Journal of Aquatic Sciences*, **1**, 114-126.

- Day, J.W., Christian, R.R., Boesch, D.M., Yanez-Arancibia, A., Morris, J., Twilley, R.R., Naylor, L., Schaffner, L. & Stevenson, C., 2008. Consequences of climate change on the ecogeomorphology of coastal wetlands, *Estuaries and Coasts*, **31**, 477-491.
- FSBI, 2007. Climate change and the fishes of Britain and Ireland: Briefing Paper 4. Fisheries Society of the British Isles, Granta Information Systems, 82A High street, Sawston, Cambridge, CB2 4h, UK.
- Hayward, P.J. & Ryland, J.S., 1995. *Handbook of the marine fauna of North-West Europe*, edn, Vol., pp. Pages, Oxford University Press, Oxford.
- Hewitt, J.E., Thrush, S.F. & Dayton, P.D., 2008. Habitat variation, species diversity and ecological functioning in a marine system, *Journal of Experimental Marine Biology and Ecology*, **366**, 116-122.
- Hicks, N., Bulling, M.T., Solan, M., Raffaelli, D., White, P.C.L. & Paterson, D.M., 2011. Impact of biodiversity-climate futures on primary production and metabolism in a model benthic estuarine system, *BMC Ecology*, **11**, 7.
- Hooper, D.U., Chapin, F.S., Ewel, J.J., Hector, A., Inchausti, P., Lavorel, S., Lawton, J.H., Lodge, D.M., Loreau, M., Naeem, S., Schmid, B., Setälä, H., Symstad, A.J., Vandermeer, J. & Wardle, D.A., 2005. Effects of biodiversity on ecosystem functioning: A consensus of current knowledge, *Ecological Monographs*, **75**, 3-35.
- Hooper, D. U. and others 2012. A global synthesis reveals biodiversity loss as a major driver of ecosystem change. *Nature* **486**: 105-U129.
- Hopkinson, C.s., Allen, D., Buchsbaum, R., Deegan, L., Dionne, M., Giblin, A., Hobbie, J., Morris, J., Peterson, B., Vallino, J. & Voronismarty, C., 1997. Plum Island Sound Comparative Ecosystem Study (PISCES): Effects of changing land cover, climate and sea level on estuarine trophic dynamics.
- Hopkinson, C.S., Jr., Giblin, A.E., Tucker, J. & Garritt, R.H., 1999. Benthic Metabolism and Nutrient Cycling along an Estuarine Salinity Gradient, *Estuaries*, **22**, 863-881.
- IPCC, 2007. Climate Change 2007: Synthesis Report. Contribution of Working Groups I, II and III to the Fourth Assessment Report of the Intergovernmental Panel on Climate Change, pp. 104, eds Pachauri, R. K. & Reisinger, A. IPCC, Geneva, Switzerland.
- Jenkins, G.J., Perry, M.C., and Prior, M.J., 2009. The climate of the United Kingdom and recent trends Met Office Hadley Centre, Exeter, UK.
- Johnston, J.P., Cobb, J.L.S. & Bell, B., 1979. Survey of Shorebird Feeding Distribution and Movements on the Eden Estuary NE Fife, Including a Study of the Invertebrate Food Source. *in Report for the Nature Conservancy Council, . South East Scotland Region*.
- Jones, N.S., 1950. MARINE BOTTOM COMMUNITIES, *Biological Reviews*, **25**, 283-313.
- McLusky, D.S., 1970. Salinity Preference in *Corophium Volutator*, *Journal of the Marine Biological Association of the United Kingdom*, **50**, 747-752
- Meadows, P.s., 1964a. Experiments on Substrate Selection by *Corophium* Species: Films and Bacteria on Sand Particles, *Journal of Experimental Biology*, **41**, 499-511.

- Meadows, P.S., 1964b. Substrate Selection by Corophium Species: The Particle Size of Substrates, *Journal of Animal Ecology*, **33**, 387-394.
- Microsoft, 2003. Microsoft Office Professional Edition Excel SP3.
- Montoya, J.M. & Raffaelli, D., 2010. Climate change, biotic interactions and ecosystem services, *Philosophical Transactions of the Royal Society B-Biological Sciences*, **365**, 2013-2018.
- Morgan, T.S., 1997. The formation and dynamics of Pygospio elegans tube-beds in the Somme Bay, France., Ph.D., Southampton University, UK.
- Neal, K. & Avent, P., 2006. Corophium volutator. A mud shrimp. Marine Life Information Network: Biology and Sensitivity Key Information Sub-programme [on-line]. Plymouth: Marine Biological Association of the United Kingdom.
- Nielsen, A.M., Eriksen, N.T., Iversen, J.J.L. & Riisgard, H.U., 1995. Feeding, Growth and Respiration in the Polychaetes *Nereis diversicolor* (Facultative Filter-Feeder) and *N. virens* (Omnivorous) - A Comparative Study, *Marine Ecology-Progress Series*, **125**, 149-158.
- Parnesan, C. & Yohe, G., 2003. A globally coherent fingerprint of climate change impacts across natural systems, *Nature*, **421**, 37-42.
- Riley, K. & Bilewitch, J., 2009. Capitella capitata. Gallery worm. Marine Life Information Network: Biology and Sensitivity Key Information Sub-programme [on-line]. Plymouth: Marine Biological Association of the United Kingdom.
- Schwartz, M.W., Brigham, C.A., Hoeksema, J.D., Lyons, K.G., Mills, M.H. & van Mantgem, P.J., 2000. Linking biodiversity to ecosystem function: implications for conservation ecology, *Oecologia*, **122**, 297-305.
- Thrush, S.F., Coco, G. & Hewitt, J.E., 2008. Complex positive connections between functional groups are revealed by neural network analysis of ecological time series, *American Naturalist*, **171**, 669-677.
- Walther, G.R., Post, E., Convey, P., Menzel, A., Parmesan, C., Beebee, T.J.C., Fromentin, J.M., Hoegh-Guldberg, O. & Bairlein, F., 2002. Ecological responses to recent climate change, *Nature*, **416**, 389-395.
- Warwick, R.M. & Uncles, R.J., 1980. Distribution of Benthic Macrofauna Associations in the Bristol Channel in Relation to Tidal Stress, *Marine Ecology - Progress Series*, **3**, 97-103.
- Widdows, J., Lucas, J.S., Brinsley, M.D., Salkeld, P.N. & Staff, F.J., 2002. Investigation of the effects of current velocity on mussel feeding and mussel bed stability using an annular flume, *Helgoland Marine Research*, **56**, 3-12.
- Worsfold, T.M. & Hall, D.J., 2010. Guidelines for processing marine macrobenthic invertebrate samples: a Processing Requirements Protocol: Version 1.0. Unicmarine Report NMBAQCMbPRP to the NMBAQC Committee, pp. 33, ed O'Reilly, M.

Section 4.2 Biotic Responses

- Alexandre, A., Silva, J. & Santos, R., 2010. Inorganic nitrogen uptake and related enzymatic activity in the seagrass *Zostera noltii*, *Marine Ecology-an Evolutionary Perspective*, **31**, 539-545.
- Benjamin, K.J., Walker, D.I., McComb, A.J. & Kuo, J., 1999. Structural response of marine and estuarine plants of *Halophila ovalis* (R.Br.) Hook. f. to long-term hyposalinity, *Aquatic Botany*, **64**, 1-17.
- Biebl, R. & McRoy, C.P., 1971. Plasmatic resistance and rate of respiration and photosynthesis of *Zostera marina* at different salinities and temperatures., *Marine Biology*, **8**, 48-&.
- Borja, A., Bricker, S.B., Dauer, D.M., Demetriades, N.T., Ferreira, J.G., Forbes, A.T., Hutchings, P., Jia, X., Kenchington, R., Marques, J.C. & Zhu, C., 2008. Overview of integrative tools and methods in assessing ecological integrity in estuarine and coastal systems worldwide, *Marine Pollution Bulletin*, **56**.
- Borja, A., Franco, J. & Muxika, I., 2004. The biotic indices and the Water Framework Directive: the required consensus in the new benthic monitoring tools, *Marine Pollution Bulletin*, **48**, 405-408.
- Borja, A., Franco, J. & Perez, V., 2000. A marine Biotic Index to establish the ecological quality of soft-bottom benthos within European estuarine and coastal environments, *Marine Pollution Bulletin*, **40**, 1100-1114.
- CFAS, 2007. OSPAR eutrophication assessments: SEPA comprehensive procedure 2008 - Eden.DEFRA: Environment Agency, Marine Environmental Research.
- CRAN, 2011. R Statistical Software <http://cran.r-project.org/>.
- Fano, E.A., Mistri, M. & Rossi, R., 2003. The ecofunctional quality index (EQI): a new tool for assessing lagoonal ecosystem impairment, *Estuarine Coastal and Shelf Science*, **56**, 709-716.
- Hector, A., 2009. Charles Darwin and the Importance of Biodiversity for Ecosystem Functioning, *Vierteljahrsschrift der Naturforschenden Gesellschaft in Zuerich*, **154**, 69-73.
- Hector, A. & Hooper, R., 2002. Ecology - Darwin and the first ecological experiment, *Science*, **295**, 639-640.
- Hellblom, F. & Bjork, M., 1999. Photosynthetic responses in *Zostera marina* to decreasing salinity, inorganic carbon content and osmolality, *Aquatic Botany*, **65**, 97-104.
- Hemminga, M.A., 1998. The root/rhizome system of seagrasses: an asset and a burden, *Journal of Sea Research*, **39**, 183-196.
- Hemminga, M.A., Koutstaal, B.P., Vansoelen, J. & Merks, A.G.A., 1994. The nitrogen supply to intertidal eelgrass (*Zostera-marina*), *Marine Biology*, **118**, 223-227.
- Microsoft, 2003. Microsoft Office Professional Edition Excel SP3.

- Murphy, L.R., Kinsey, S.T. & Durako, M.J., 2003. Physiological effects of short-term salinity changes on *Ruppia maritima*, *Aquatic Botany*, **75**, 293-309.
- Pearce, A., Boyle, J. & Goater, T., 2006. An assessment of the ecological health of the sediment of the Eden Estuary, Fife, in relation to opportunistic macroalgal cover. MR 02/06.Scottish Environment Protection Agency (SEPA).
- Peralta, G., Brun, F.G., Hernandez, I., Vergara, J.J. & Perez-Llorens, J.L., 2005. Morphometric variations as acclimation mechanisms in *Zostera noltii* beds, *Estuarine Coastal and Shelf Science*, **64**, 347-356.
- Peralta, G., Perez-Llorens, J.L., Hernandez, I., Brun, F., Vergara, J.J., Bartual, A., Galvez, J.A. & Garcia, C.M., 2000. Morphological and physiological differences between two morphotypes of *Zostera noltii* Hornem. from the south-western Iberian Peninsula, *Helgoland Marine Research*, **54**, 80-86.
- Ralph, P.J., Durako, M.J., Enríquez, S., Collier, C.J. & Doblin, M.A., 2007. Impact of light limitation on seagrasses, *Journal of Experimental Marine Biology and Ecology*, **350**, 176-193.
- Rysgaard, S., Thastum, P., Dalsgaard, T., Christensen, P.B. & Sloth, N.P., 1999. Effects of salinity on NH₄⁺ adsorption capacity, nitrification, and denitrification in Danish estuarine sediments, *Estuaries*, **22**, 21-30.
- Spence, D.H.N., Campbell, R.M. & Chrystal, J., 1973. Specific leaf areas and zonation of freshwater macrophytes., *Journal of Ecology*, **61**, 317-328.
- Sultan, S.E., 2000. Phenotypic plasticity for plant development, function and life history, *Trends in Plant Science*, **5**, 537-542.
- Wilcox, D., Dove, B., M^cDavid, D. & Greer, D., 2002. UTHSCA Image Tool for Windows.The University of Texas Health Science Center. San Antonio, Texas.

CHAPTER 5

5. THESIS DISCUSSION & FUTURE IMPLICATIONS

5.1. Discussion

This thesis aimed to take a holistic 'whole ecosystem approach' to investigating the changes an estuary undergoes in response to climate variability. There are both advantages and disadvantages to this methodology, whilst a broad overview has the advantage of considering how the estuary responds as a dynamic system, capturing interacting physical, biological and chemical processes at multiple spatial scales, linking and placing these in context within regional scale changes affecting estuary driving mechanisms, the breadth of the study inevitably leads to a loss of resolution and data quality due to time and effort limitations in terms of data collection. Interpreting data from much of this thesis has been challenging, since in many cases rigorous statistical analysis could not be performed in the absence of replicate samples, despite this the data are valuable for inferring a directional trend of ecosystem change and provide a starting point for more targeted higher resolution research.

The organizational structure of previous chapters was designed to collate results from the composite sections and form them into chapter discussions which linked together the various facets of the estuary being investigated. This final chapter will bring together the chapter discussions, aiming to tie and integrate the findings across the different avenues of investigation. It also will discuss the relative contribution of different driving mechanisms on a global scale and their links to the local responses in the estuary

Chapter 2 aimed to identify trend or pattern present within the chronologies of selected estuarine driving mechanisms and also within the consequential spatial changes to the estuary. Having identified the presence of pattern an additional aim was to propose potential causal links for these drivers of change, attempting to directly link variability in estuarine dynamics with the northern hemisphere climate patterns. Several potential sources of influence were identified for which it was difficult to rank their overall relative importance due to close interrelationships and feedback mechanisms between them and the way in which they impacted on different facets of the estuaries dynamics. The following paragraph revisits the chapter results which identified associations with potential driving mechanisms, and continues to discuss their interrelationships.

Analysis of the river flow and wind direction data for the Eden revealed significant periodicity corresponding to known periods of solar and orbital cycles (lunar and planetary), inferring both thermal and gravitational influences to local patterns of precipitation, wind regime and

morphological change, however what remained unclear was if these were direct influences, or if the periodicity identified had been transferred by an intermediary mechanism for example the NAO.

Data for the smoothed annual river flow and the wind direction counts were found to significantly cross-correlate with the annual smoothed NAOI and similarly spatial changes to shoreline and channel alignment were also observed to closely match patterns in both the NAOI and the concomitant wind regime. These cross-correlations therefore pointed towards the NAO having an important role in the local climate regime. Autocorrelation analysis of both the wind direction and river flow data additionally identified significant influences coincident with episodes of volcanic activity during which ash and sulphate aerosols were released into the lower stratosphere causing 'NAO like' climatic circulation; identifying a further mechanism for climate perturbation and reinforcing the link between the NAO and local climate.

In assessing the multiple influences (Chapter 2, table 2-7), it was noticed that the periodicity present within the data are not consistently present across the potential driving mechanisms and thus no singular driver was responsible. It was originally hypothesised that solar activity was the major driving mechanism for the NAO, which subsequently caused the variability observed in the local Eden data, however although periodicity approximate to the 11 year Schwabe cycle was observed in the NAOI, periods corresponding to the ~22 year Hale magnetic cycle were not, yet both of these solar periods were present in the wind direction data and river flow time series for three rivers, suggesting the data are not solely influenced (or potentially driven) by the NAO.

Absence of the Hale cycle within the NAOI might be expected, since the NAO is largely structured by inequality of equator to pole solar heating of the atmosphere (Ruzmaikin & Feynman 2002) and hence magnetic polarity reversals, which do not reflect irradiance changes, are unlikely to directly influence the NAOI time series. This then raises the question of by what mechanism the ~22 year cycle influences the wind direction and river flow data. Presence of the ~22year periodicity may be explained by the 22 year Hale magnetic cycle superimposing on the terrestrial magnetic field, altering the rotational period of the Earth through modulations of the electromagnetic coupling between the Earth's mantle and core (Hoeppner and Bittner 2007) speeding up or slowing down of the rotational period will apply changes to the frictional torque between the rotating Earth and the atmosphere and consequently impacting on wind regimes as a bottom up response i.e. from Earth to Atmosphere driven change. Changes in the length of day have similarly been reported by several authors investigating ENSO events (Dickey *et al.* 2007; Mazzarella 2008; Mazzarella *et al.* 2010; Zheng *et al.* 2003) although in terms of a 'top down' (Atmosphere to Earth) response; as a thermally driven atmospheric angular momentum (AAM)~ocean coupling causing a change to the Earth's rotational speed. Although the interrelationship between both these mechanisms (top down & bottom up) isn't fully understood, together they help explain the presence of the ~11 year cycle in the NAOI and both the ~11 and ~22 year cycle in the wind data and precipitation data through wind driven evaporation of the North Atlantic. Cross correlation of annual smoothed data for river flow and wind direction data with the NAOI revealed an approximate periodicity of 34 years (2.1 Fig. 2-17 and 2.2 Fig.2-37), which was only significant for the wind data; since this frequency is not

present in the individual monthly time series it must represent a modulation, perhaps reflecting a feedback between the NAO on the wind regime.

Chapter 2 highlighted changes to shoreline alignment and the unusual occurrence of westerly winds for 2009 and 2010, despite the strongly negative NAOI. This anomaly has also been investigated in the literature by Jung *et al* (2011), attributing the anomaly to internal atmospheric dynamical processes; it was also noted in chapter 2 that a number of volcanic eruptions occurred between 2008 & 2009, projecting ash and aerosols into the stratosphere mimicking NAO like conditions. However it is also interesting to note that 2009 marked the solar minimum and the onset of a new Hale magnetic cycle and thus anomalous wind may at least be partly attributed to the previously discussed bottom up frictional response of the Hale cycle between the Earth's rotation and the atmosphere.

Understanding these combined influences which shape the patterns of estuary dynamics provides the first step towards identifying driving mechanisms. Whilst significant relationships and close associations to solar, orbital and to internal climate patterns of the NAO were identified, without direct modelling this study is only able to postulate on the drivers and their combined affect to the patterns identified.

In chapter 3 key abiotic influences to the estuary were identified which were linked to climate driven change on contemporary scales, placing short term directional change within context of much longer term variability. The fundamental hypothesis proposed was that climate variability would apply shifts to the tidal asymmetry (the balance between river inflow and the tidal volume) which determines whether the estuary is in a largely erosional or depositional phase. This hypothesis was investigated through the analysis of tidal data, to identify net ebb or flood dominance, by analysis of bed-form migration, to quantify net directional bedload transport and by analysis of salinity data to capture the current variability in salinity regime.

Tidal asymmetry analysis identified a net ebb dominance in the vertical tide (tidal duration) and a dominance in the low water slack, both inferring an export of finer particles. Critical velocities for transport on the horizontal tide however inferred a net import of coarser particles. Overall the asymmetry data pointed towards deposition within and along the channel margins and with peak ebb velocities occurring near high water, there was a removal of finer sediment from the intertidal flats. Although the bedload transport data similarly revealed a net flood dominance in coarser particle transport, comparison with data from the mid 1970s suggested that the current rate of sediment import to the estuary was lower. A conclusion also drawn by patterns of salinity, reflecting a seaward regime shift, inferring increased river inflow dominance.

The abiotic data coupled with elevation analysis indicates that the estuary has become deeper since the mid 1970s and further so since 2002, inferring a seaward shift in asymmetry between 1974 and 2009 (~35 years). Analysis of river flow data revealed strong evidence for a positive monotonic trend ($p=0.01$) in annual mean flow for the Eden, which is consistent with the proposed

seaward shift in asymmetry during the sample period. However the monotonic trend was not present for the longer time series of the rivers Tay and Thames, inferring the monotonic trend to be an artifact of the short time series, rather than a persistent long term trend. Patterns of variability in flow were also identified within the mean annual flow data; cross-correlating the smoothed annual flow data with the NAOI identified a significant relationship between the two over several lags, though also revealing an underlying non significant periodicity of approximately 35 years. In terms of developmental stage (Dronkers 1986), the infilling of the channel coupled with a lowering of the intertidal flats infers the peak Type II 'deep channel with high intertidal flats' has been achieved at some point after the 1970s, followed by a shift in asymmetry towards Type I conditions thereafter.

A relative direction of ecosystem health was estimated through the analysis of macrofaunal community diversity in selected 'asymmetry sensitive zones' and by investigating the response (through adaptation / acclimatization) of the keystone species *Z. noltii* to the regime changes brought about by local and regional variability in climate. Data were limited, such that significant conclusions could not be drawn, however potential trends were identified, which may form the basis for future research. In the inner estuary, community composition displayed a trend for increased species diversity between 1999 and 2010, with the 2010 data being significantly distinct (Bray-Curtis 95% significance at 46% similarity) from the 1999 data. The increase in community diversity was accompanied by an increase in river discharge during the sample interval and a shift in particle size towards a finer particle content. Interstitial salinity data for the inner estuary site supported the evidence of increased river flow and the observed increase in finer particles and together provide supportive evidence for a shift in asymmetry indicated by the abiotic data.

At the middle estuary location, the two sample periods could not be significantly distinguished by community diversity, however species diversity was generally increased. River flow was lower in 2009 than 2002 and despite this the finer particle contribution was increased, perhaps reflecting the significant positive monotonic trend in river flow since 1968 identified in chapter 2.

Although the two surveys identified increased fines between 1999-2010 and is therefore contradictory to the inferences of increased finer particle export by the tidal asymmetry data for 2009, in fact both scenarios may be correct and although greater tidal flushing of fines is occurring, the increase in the rate of delivery to the estuary by the increased river discharge may lead to some deposition at the high water slack and reflect residence time. Difference in the methodologies used for particle size analysis between the survey protocols may also contribute to the resulting patterns; the original surveys (Bates *et al.* 2004) categorized classes by sieving, which may over estimate the sizes for the smaller fractions as air drying may result in flocculation. Evidence for greater deposition of finer particles historically is given by Coulter Counter data from Hamilton (1993) which reveals a much higher organic content for both sites at that time.

Estimation of relative ecosystem health, from species diversity over the 'asymmetry sensitive zone', inferred a potential trajectory towards increased health and functioning. The estimation was based largely on community composition, although the functional roles for species which had altered either

temporally or spatially were investigated in terms of their contribution to service provision. Given more time Taxonomic Similarity coupled with 'functional role traits', identifying distinct taxa which may use resources differently (Woodward 2009), may have improved the estimation of ecosystem functioning however an apparent general positive trend was identified. It is proposed that the observed changes to community composition result largely from the limitation of nutrient inputs, constraining the growth of the opportunistic macro-algae (which may cause anoxic sediment conditions) rather than due to the regime shifts in environmental conditions. However there are implications to shifts in the asymmetry; net ebb asymmetry in the vertical tide leading to the export of finer particles may have implications to the distribution of larval settlement, thus leading to more seaward distribution of certain species. Similarly dominance of flood or ebb tidal velocities may impact on swimming behavior; for example *C. volutator* were observed to swim on the flood of each tide, in the Ems Estuary of the Wadden Sea, leading to a net landward movement of the population (Essink *et al.* 1989), whilst Holmstrom and Morgan (1983) observed individuals of *C. volutator* from the rivers Dee and Dovey swimming mainly on the ebb of spring tides, just after high tide thus moving seaward. The reduction in presence of *C. volutator* from the inner estuary site may reflect the ebb asymmetry coupled with dispersal and swimming behavior however many other factors may equally have contributed to their demise, including predation by polychaetes, fish and migratory birds which occupy the estuary, or poor recruitment for the sampling year.

The keystone species *Z. noltii* was observed to have morphological variations, displaying a trend for shorter wider blades with a lower density of stems in the inner estuary and longer thinner less dense forms more seaward. The variation is proposed to result from a coupled response to increased salinity and energy levels causing metabolic stress with consequences to growth rates and photosynthetic capacity. Increase in the number and extent of stands, providing greater habitat availability, infers a potential for increased functioning and service provision. Changes to the asymmetry do not appear to have had negative consequences to *Z. noltii* in fact ebb asymmetry may have had positive influences contributing to the seaward dispersion of the species.

5.2. Future implications for the Estuary

In terms of future predicted climate change, recent global and local climate models for medium/ high emissions scenarios suggest the east coast of Scotland will experience increased seasonality in precipitation with concomitant seasonality of river flow, increases in relative sea level and a decrease in average wind speeds accompanied by greater storminess (IPCC 2007; Jenkins 2009).

The implications to the estuary regarding sea level rise predictions are that the tidal asymmetry will be shifted landward due to the increased volume of water entering the estuary, accompanied by a change in the vertical tide towards being more ebb dominated with increased export of finer particles, whilst the horizontal tide will show less asymmetry shifting to less flood orientated and

thus resulting in reduced import of coarser particles. Under such conditions the estuary moves towards a more Type I developmental stage (Dronkers 1986). However with wind speeds predicted to be lower, the extent to which wind assisted shifts to asymmetry will impact on the estuary is likely to be reduced, thus asymmetry will largely be driven by the relative contributions of river inflow and tidal volume. Whilst no change was predicted for annual levels of precipitation, the predicted changes to seasonality were not observed in the river flow, although a positive monotonic trend in flow for the rivers Tay and Thames was revealed, thus future asymmetry is likely to be more dependent upon the tidal contribution to asymmetry dynamics. In terms of estuary health, under the predicted climate change the increased ebb asymmetry will be accompanied by an increase in tidal flushing, depending upon the balance between nutrient delivery from river flow and the rate of tidal flushing primary productivity may become more limited. Estuary wide, the impact of storminess tends to be transient however the extent of the impact is largely dependent on coincident circumstances, i.e. with the passage of storms occurring at spring high tides coupled with particularly low pressure systems and certain wind directions. Under these circumstances, the high water zone is most vulnerable to wave erosion and has been observed to realign where unrestricted by mitigation measures.

Controversy persists as to the cause of global climate change since the 1960s (the beginning of the 1961-1990 baseline used by the IPCC for trend comparison, and integral to the design of GCMs) such that there is much recent research investigating links to the contribution of external driving mechanisms (Davis and Brewer 2011; Foukal 2012; Gray *et al.* 2012; Hood and Soukharev 2012; Ineson *et al.* 2011; Kodera 2002; Qu *et al.* 2012; Scafetta 2010; Scafetta 2012a; Scafetta 2012b; Shaviv 2008; Swingedouw *et al.* 2011; Weng 2012). Much of the recent research focuses on the contribution of the various components of solar activity on influencing climate patterns. Whilst this thesis identified significant influence consistent with solar periodicity, the analyses were insufficient to capture the nature of the relationship and further modelling is proposed to attribute causal mechanisms. If however the solar connection is correct, then the present position within the solar Gleissberg cycle (~90 years length) at Schwabe cycle 24 (2012) is moving towards a Gleissberg minima, which could be expected to occur in the mid 2000s and the level of solar activity likely to be observed is similar to levels in the late 1800s – early 1900s (chapter 2.2, Figure 2-41). Observing the long term pattern of the NAOI since 1825; patterns of positive and negative phases are likely to persist as the phases oscillate around a long term mean. This presumably occurs as short term (Schwabe) thermal changes to the atmosphere cause pressure differentials between the Azores high and the Icelandic low, however over a much longer term (Gleissberg) the atmosphere cools slowly allowing both pressure centres to change equally yet retain the ~11 year variability. Further implications for atmospheric circulation are; with a general cooling of the atmosphere it may be expected that the thermally driven Hadley circulation, arising from the poleward gradient of tropical temperature, is likely to slow causing a weakening of the easterly trade winds accompanied by a warming of sea surface temperatures (with implications to CO₂ dissolution), as observed in association with ENSO events (Wang and Fiedler 2006), and thus a reduction in evaporation. Consequentially wind recordings may be expected to reduce in number (and strength), returning to

levels observed in the Eden during the 1930s and 1940s (chapter 2.2, Figure 2-29), accompanied potentially by a reduction in precipitation and hence river flow. Under a 'lower solar activity climate', reduced wind and river inflow infers greater tidal dominance in asymmetry and a landward shift in the salinity regime. Changes to the erosional / depositional stage will largely be dependent upon the temporal position within the lunar nodal cycle coupled with rates of sea level rise (SLR), which depend largely upon ocean (and air) temperatures. It may be anticipated therefore that the estuary will oscillate around a more stable equilibrium which infers less environmental stress being transferred to the biota.

In summary, there is a close relationship proposed between solar activity, patterns of the NAOI and patterns of local climate, which are consistent with observed variability in the historical time series data for the Eden and in the abiotic responses to shifts in tidal asymmetry. Whilst causal mechanisms can only be proposed, these observations form a baseline for future targeted modelling.

5.3. References

- Bates, C. R., C. G. Moore, T. Malthus, J. M. Mair, and E. Karpouzli. 2004. Broad scale mapping of habitats in the Firth of Tay and Eden Estuary, Scotland. Scottish Natural Heritage Commissioned Report No. 007 (ROAME No. F01AA401D).
- Davis, B. A. S., and S. Brewer. 2011. A unified approach to orbital, solar, and lunar forcing based on the Earth's latitudinal insolation/temperature gradient. *Quaternary Science Reviews* **30**: 1861-1874.
- Dronkers, J. J. 1986. Tidal asymmetry and estuarine morphology. *Journal of Sea Research* **20(2/3)**:
- Essink, K., H. L. Kleef, and W. Visser. 1989. On the Pelagic Occurance and Dispersal of the Benthic Amphipod tentative. *Journal of the Marine Biological Association of the United Kingdom* **69**.
- Foukal, P. 2012. A New Look at Solar Irradiance Variation. *Solar Physics* **279**.
- Gray, L. J. and others 2012. Soalr Influences on Climate (vol 50, RG1006, 2012). *Reviews of Geophysics* **50**.
- Hamilton, L. C. 1993. An Analysis of the Fine-Grain Sediments of the Eden Estuary. St Andrews University.
- Hoepfner, K., and M. Bittner. 2007. Evidence for solar signals in the mesopause temperature variability? *Journal of Atmospheric and Solar-Terrestrial Physics* **69**.
- Holmstrom, W. F., and E. Morgan. 1983. Variation in the Naturally-Occuring Rhythm of the Estuarine Amphipod, *Corophium volutator* (Pallas). *Journal of the Marine Biological Association of the United Kingdom* **63**.
- Hood, L. L., and B. E. Soukharev. 2012. The Lower-Stratospheric Response to 11-Yr Solar Forcing: Coupling to the Troposphere-Ocean Response. *Journal of the Atmospheric Sciences* **69**.
- Ineson, S. and others 2011. Solar forcing of winter climate variability in Northern Hemisphere. *Nature Geoscience* **4**: 753-757.
- Ippc. 2007. Climate Change 2007: Synthesis Report. Contribution of Working Groups I, II and III to the Fourth Assessment Report of the Intergovernmental Panel on Climate Change, p. 104. *In* R. K. Pachauri and A. Reisinger [eds.]. IPCC, Geneva, Switzerland.
- Jenkins, G. J., Perry, M.C., and Prior, M.J. 2009. The climate of the United Kingdom and recent trends. Met Office Hadley Centre, Exeter, UK.
- Kodera, K. 2002. Solar cycle modulation of the North Atlantic Oscillation: Implication in the spatial structure of the NAO. *Geophysical Research Letters* **29**.
- Qu, W., J. Zhao, F. Huang, and S. Deng. 2012. Correlation Between the 22-Year Solar Magnetic Cycle and the 22-YEAR Quasicycle in the Earth's Atmospheric Temperature. *Astronomical Journal* **144**.

- Scafetta, N. 2010. Empirical evidence for a celestial origin of the climate oscillations and its implications. *Journal of Atmospheric and Solar-Terrestrial Physics* **72**: 951-970.
- . 2012a. A shared frequency set between the historical mid-latitude aurora records and the global surface temperature. *Journal of Atmospheric and Solar-Terrestrial Physics* **74**.
- . 2012b. Multi-scale harmonic model for solar and climate cyclical variation throughout the Holocene based on Jupiter-Saturn tidal frequencies plus the 11-year solar dynamo cycle. *Journal of Atmospheric and Solar-Terrestrial Physics* **80**.
- Shaviv, N. J. 2008. Using the oceans as a calorimeter to quantify the solar radiative forcing. *Journal of Geophysical Research-Space Physics* **113**.
- Swingedouw, D., L. Terray, C. Cassou, A. Voltaire, D. Salas-Melia, and J. Servonnat. 2011. Natural forcing of climate during the last millennium: fingerprint of solar variability. *Climate Dynamics* **36**: 1349-1364.
- Wang, C., and P. C. Fiedler. 2006. ENSO variability and the eastern tropical Pacific: A review. *Progress in Oceanography* **69**.
- Weng, H. 2012. Impacts of multi-scale solar activity on climate. Part I: Atmospheric circulation patterns and climate extremes. *Advances in Atmospheric Sciences* **29**: 867-886.
- Woodward, G. 2009. Biodiversity, ecosystem functioning and food webs in fresh waters: assembling the jigsaw puzzle. *Freshwater Biology* **54**.